INTERACTIVE EFFECTS OF NON-STRUCTURAL ELEMENTS ON THE BEHAVIOUR OF TALL BUILDING STRUCTURES

by
Regina Gaiotti

A Thesis submitted to the Faculty of Graduate Studies and Research in partial fulfilment of the requirements for the Degree of Doctor of Philosophy

Department of Civil Engineering
and Applied Mechanics
McGill University, Montreal
March 1990

ISBN 0-315-63485-5

INTERACTIVE EFFECTS OF NON-STRUCTURAL ELEMENTS ON THE BEHAVIOUR OF TALL BUILDING STRUCTURES

by
Regina Gaiotti

Abstract

The lateral stiffening effects of cladding and partition walls, which are usually unaccounted for in a building structure's design, are investigated in this research project. Direct and iterative, linear elastic finite element analyses of representative modules of these components and their supporting primary structure were performed. These were used to study their general lateral load behaviour, and to establish their modes of interaction and induced forces. As a result, new and practical analogous strut models have been devised to allow their incorporation in, and the analysis of, the total building structure. The strut models permitted the effects of the non-structural elements' interaction on the static and dynamic responses of tall building structures to be studied. The ultimate objective of this work has been to contribute towards the development of new procedures of analysis and design of building structures braced by precast concrete cladding panels and non-loadbearing concrete blockwork walls.

EFFETS DE L'INTERACTION DES ELEMENTS NON-STRUCTURAUX SUR LE COMPORTEMENT DES STRUCTURES MULTI-ETAGEES

par
Regina Gaiotti

Résumé

La plupart du temps négligée lors du dimensionnement, la contribution du revêtement extérieur et des cloisons internes à la résistance latérale d'un édifice est étudiée dans ce projet de recherche. Des modules représentatifs de ces composantes non-structurales et la structure primaire les supportant ont été analysés par éléments finis, en utilisant des méthodes directes et itératives assumant des déformations élastiques linéaires. Ces analyses ont permis d'étudier leur comportement sous charges latérales, et d'établir les modes d'interaction et les forces induites. Conséquemment, de nouveaux modèles pratiques d'éléments diagonaux équivalents ont été développés pour permettre l'incorporation de ces composantes et l'analyse de la structure complète les incluant. Ces modèles permettent d'étudier les effets de l'interaction des éléments non-structuraux sur le comportement statique et dynamique d'édifices multi-étagés. L'objectif principal de ce projet est de contribuer au développement de nouvelles procédures d'analyse et de dimensionnement de structures contreventées par des panneaux de revêtement en béton préfabriqué et par des murs non-porteurs en blocs de béton.

ACKNOWLEDGEMENTS

The author gratefully acknowledges the time and effort that her research supervisor, Prof. B. Stafford Smith, has spent on this research work, and his guidance and assistance throughout the writing of the thesis. In particular, the author greatly appreciates Prof. Stafford Smith's advice and encouragement throughout the progress of her studies at McGill University. It has been a privilege to have worked with him.

The author wishes to acknowledge the valuable discussions held on specific topics with Prof. P. Léger and Prof. D. Mitchell, as well as the consultations with local structural engineers, architects, masons, and precast concrete producers, in particular the following: Nandor Huszar, Schokbeton Québec Inc.; Joe Gallacchio, Quinn-Dressel Associates; Tony Di Miele, Tolchinsky and Goodz Architects; Franz Knoll, Nicolet-Chartrand-Knoll; Ermanno Romanese, Maconnerie Trois Etoiles Ltée.

The author is forever grateful to her loved ones for their support, encouragement and understanding.

Finally, the author expresses her appreciation to Natural Sciences and Engineering Research Council of Canada for the financial support given to this study.

CONTENTS

LIST OF TABLES

LIST OF FIGURES

CHAPTER 1

GENERAL INTRODUCTION

The stiffening effect of non-structural elements in a building has been recognized for many years, but it has generally been neglected in design procedures due to a lack of understanding of the interaction between these elements and the building's primary structure.

It has been observed in studies of building structures that the measured lateral stiffnesses and natural periods of vibration can deviate significantly from the values determined from analyses of mathematical models of the structures. For example, from an experimental study of the Empire State Building, Rathbun (1938) concluded that the non-structural masonry increased the stiffness of the steel frame by four and a half times. In another study (Wiss and Curth 1970), the measured stiffness of a 56-storey building was found to be four times that calculated by the design engineer. Further, Ellis (1980) reported that the measured frequencies of many buildings could be as much as twice those predicted by computer analyses. Undoubtedly, these major discrepancies are caused, to a large extent, because the structural analysis is based on a bare model of the primary structure, while the stiffness provided by such non-structural elements as cladding and partition walls is neglected.

Wind analyses of building structures that neglect the stiffening effects of the non-structural components will result in overestimated deflections, which may lead to a conservative, less economic design of the primary structure. Further, such analyses do not reveal the altered behaviour of the structure due to its interaction with the non-structural elements, nor do they reveal the critical fact that these elements may be subjected to forces that in all probability exceed those for which they were designed. In the case of earthquake loading analyses, however, neglecting the effects of the non-structural elements on the structure's behaviour can lead to underestimated design forces that lead to an unconservative, unsafe design for both the primary structure and the non-structural elements.

Cladding and partition walls are the two major items usually unaccounted for in contributing to the lateral stiffness of a building structure. There are other neglected non-structural items that contribute to a lesser degree and which will not be studied here; these include, for example, the stair systems, fire protection and the mechanical services.

The purpose of the project has been to determine the interaction of the primary moment resisting frame with, firstly, cladding, and secondly, blockwork infills.

The ultimate aim of the work has been to contribute towards the development of new and practical methods of design that provide for the stiffening effects of these two major types of non-structural components. As a result, the designs of the building structures should be more economical in the case of wind loading governing their design, and safer in the case of seismic loading being critical. On the way towards achieving the final objective, a new understanding has been gained of the modes of interaction between the non-structural components and the primary structure, and of the nature and magnitude of the forces that the interaction induces in the components and the frame. New and efficient modelling techniques for representing the elements in the total structures have been developed from the acquired understanding of the modes of interaction. Consequently, the effects of the non-structural components' interaction on the static and dynamic lateral load behaviour of representative types of tall building structures have been revealed.

To the best of the writer's knowledge the results of the research described in this thesis make an original contribution to understanding the interactive effects of cladding panels and non-loadbearing blockwork infills, and, in her opinion, they form the basis of feasible and practical design methods for incorporating these components as parts of the structure. In support of this belief, the writer considers it appropriate to refer to an unsolicited proposal, and a offer of funding, made by the Executive Committee of the Canadian Prestressed Concrete Institute, for her to extend the research in order to consolidate the findings relating to precast concrete panels, and to write for them a design manual.

The thesis is written in two parts, the first relating to the effects of cladding, and the second to non-loadbearing blockwork infills. Each part includes its own introduction, literature review, research objectives, and descriptive review of the respective non-structural components. A proposed procedure for analysing the total building structure braced by the non-structural component is given to conclude each part.

The research work presented herein is based on an entirely elastic approach, direct and iterative, for the reason that it offers the most promising and direct generalized information on the interactive behaviour between non-structural elements and a building's primary structure. As a logical sequel to this study, future research should include nonlinear analyses which would give a more realistic indication of the interactive behaviour.

PART I

THE STIFFENING EFFECT OF CLADDING

CHAPTER 2

INTRODUCTION AND LITERATURE REVIEW

2.1 Introduction

2.1.1 General

It has been tacitly recognized for many years that some cladding systems contribute significantly to the lateral stiffness of buildings. Despite this, the effect is generally neglected in the design of building structures due to the lack of understanding of the interaction between cladding and the building's primary structural system. It is also evident that the interaction causes loads in cladding and its connections for which they are not designed.

Numerous cladding failures (ENR 1980) have indicated that the cladding is not non-structural in function as normally assumed by designers. Possible failures in the cladding system could entail a risk of injury to the public. In addition, repairs to the cladding system can increase the eventual cost of the building facade considerably from its already expensive initial cost of 10 to 20 percent of the building's total cost.

As an example, in a study of the seismic response of a twelve-storey reinforced concrete frame structure severely damaged during the 1985 Mexico earthquake, damage to the cladding system was investigated (El-Gazairly and Goodno 1989). The street face of the structure was clad with heavy precast concrete spandrel panels. Additional cladding was used to enclose the columns at the front corners of the building. The precast concrete column cover panels were severely cracked at the location of the connections (weld plates attached to plate inserts). The cracks were visible on the front face of the building at almost every level, but fortunately none of the panels fell from the structure to the ground. A linear dynamic analysis of the structure, with and without the cladding, confirmed that the exterior facade was a participating structural element, despite its design assumption to the contrary, and the forces at the column cladding locations grossly exceeded the connections' capacity.

2.1.2 Scope of the Investigation

The increase in lateral stiffness that the cladding may provide is dependent on its form and its material properties, and especially on the method by which the cladding system is connected to the main structural framing system. The types of cladding considered in this study are aluminum curtain walling and precast concrete panels. However, emphasis is placed on the stiffening effect of architectural precast concrete cladding panels.

Detailed finite element analyses were performed to study the interaction between a typically connected, representative precast concrete cladding panel and its supporting structural frame. The significant parameters and their relative importance in influencing the structure's racking stiffness were also determined.

On the basis of a study of results from detailed analyses of the cladding panel interacting with a frame, the panels were modelled in example moment-resisting frame and wall-frame structures by diagonal bracing struts. Static and dynamic analyses of three-dimensional models of the example structures, with and without the stiffening effects of the panels, were performed. The capabilities of the panels and their connections of withstanding the induced loads were also investigated.

The objectives of this study are as follows:

1. To determine the mode of behaviour of a typically-connected representative precast concrete panel within a moment-resisting frame.
2. To evaluate the sensitivity of the structure's racking flexibility to the flexibilities of the panel, its connections, and the frame members.
3. To estimate the magnitude of the stiffening influence of the panel and its connections.
4. To develop an analogous spring model to simulate the actions involved when the frame with the panel and its connections are subjected to a horizontal load.
5. To formulate an equivalent strut model to represent the panel and its connections in the overall structure analyses.
6. To examine the effect of the precast concrete cladding panels on the static and dynamic responses of a moment-resisting frame structure and a wall-frame structure.
7. To check the resulting forces in the connections and the resulting stresses in the panels against the ultimate capacity of the connections and the allowable stresses in the panel, respectively.
8. To determine the effect of varying the connection stiffnesses on the stiffening influence of cladding panels.
9. To determine the influence of rigid beam-ends on the behaviour of a clad moment-resisting frame.

10. To present an analysis procedure for the analysis of building structures braced by precast concrete cladding panels.

2.2 Literature Review

2.2.1 Contribution of Cladding to Lateral Load Resisting System

Cladding systems are usually assumed as non-structural in function, and provisions are made for the supporting auxiliary system or for the connection methods in attempting to avoid the cladding's interaction with the structure. It has been suggested or concluded in a number of studies, however, that some cladding systems contribute significantly to the lateral stiffness of a structure.

The frequencies and modes of vibration of four tall buildings were measured from their wind-induced vibrations and compared with computed frequencies obtained from simple theoretical models (Crawford and Ward 1964, Ward and Crawford 1966). The models were based on assumptions such as, that the girders are flexurally rigid, and that the elevator cores do not contribute to the stiffness of the buildings. In some cases the discrepancy between the measured and theoretical values of the fundamental periods was as large as 73 percent, and was attributed to non-structural effects such as the cladding. The present author believes that the studies are, unfortunately, inconclusive because the theoretical models used in the investigations were over-simplified.

To study the dynamic behaviour of a clad building, experimental and analytical tests were performed on an existing 25-storey building clad with precast concrete panels (Goodno and Will 1978, Palsson et al. 1984). Computed frequencies of the building structure without including the effect of the cladding were smaller than the experimental results of the real structure, by 16 percent in one translational direction, 32 percent in the other, and 73 percent in torsion. The discrepancies were attributed to the stiffening influence of the precast concrete cladding panels. From a linear dynamic analysis of the structure with the stiffening effect of the cladding included, it was concluded that it might not always be conservative to neglect the additional stiffening contribution of heavyweight cladding systems (Palsson et al. 1984). In addition, as part of the on-going study, a program of experimental testing and analytical modelling has been initiated to provide quantitative information about the performance of connection designs common to West Coast US practice (Craig et al. 1988, Goodno et al. 1988, Palsson and Goodno 1988, Pinelli and Craig 1989), since properly conceived and designed connections are essential to assure the satisfactory performance of precast concrete panels.

Henry and Roll (1986) investigated the behaviour of the cladding-frame interaction for reinforced concrete structures by developing two computer programs which incorporated the exterior facade and its connections into linear elastic static and linear dynamic analyses. The authors concluded that neglecting the cladding system will not always lead to conservative results, the connections may attract large forces for which they were not designed, and the type of connections used will affect the structural response of the building.

The influence of precast concrete cladding panels on the modal response of a steel frame test structure was investigated by Rihal (1989). A preliminary study of the results of the shaking tests indicated that the addition of cladding decreased the fundamental mode frequency by approximately 16 percent. Additionally, tests on flexible precast concrete cladding connections, which are common in West Coast US practice, were performed to investigate their strength and behaviour. Cyclic in-plane racking tests of a precast concrete cladding panel and its connections were also carried out.

A full-scale test on a one-storey single-bay structural assemblage, which consisted of a steel moment-resisting frame with two precast concrete panels, attached by typical connection arrangements, performed well when tested by subjecting it to a recorded earthquake (Sack et al. 1989). Analytical results showed that the full-scale test assemblage with cladding had a 17 percent greater lateral stiffness than the bare frame. Also, some basic connections were tested experimentally to obtain static stiffness properties and a limited amount of low-cycle fatigue data.

Two examples of tall structures which make use of the cladding to provide stiffness are now described. The structural system of the 54-storey One Mellon Bank Centre in Pittsburgh employs an exterior framed steel tube with an unique exposed steel stressed skin as both a structural bracing system and the facade (Tomasetti et al. 1986). The tower framing was first analysed without accounting for the facade panels. The drift ratio produced by the analysis was H/290. In the second analysis, the model included the tower framing as well as the facade panels. The panels were modelled using a fine-mesh of uniform membrane elements. The building drift ratio with facade panels was found to be H/590, a considerable difference from the previous analysis. A significant cost-saving was achieved with this design.

In a building in Montreal, architectural precast concrete panels were used successfully as bracing members in a 15-storey steel frame building (Martineau 1989). The accumulated shears were transferred directly from one precast concrete panel to the next below with appropriate and easy to execute connections. It was concluded that probably some savings were achieved by using the panels as bracing members.

2.2.2 Methods of Accounting for Cladding in Analytical Models

In this section a brief review of some of the methods of accounting for cladding in the analytical models is given.

Weidlinger (1973) concluded that great economies can be obtained if the entire shear carrying component of a tall building is replaced by reinforced concrete panels. In his study, a finite element program was adapted for the static analysis of spandrel panels of various configurations attached *continuously* to the columns of the exterior frame. A model to represent the panels in a wind analysis of a structure, consisting of two diagonal cross bracing struts, whose properties can be determined using the results of the finite element analyses, is discussed.

In a paper by Gjelsvik (1974), an elastic-plastic method of analysis of the interaction of precast concrete panel walls with steel frames was presented. It was assumed that the panels were rigid and weightless, and panel-frame interaction occurred only through four bolts connecting the panel to the beams. The study demonstrated that positive use can be made of the panels as part of the lateral load resisting system.

A dynamic analysis of the Transamerica Building in San Francisco (Stephen et al. 1974) was performed to assess the influence of several parameters on the lateral stiffness of the structure. Of the several parameters, the exterior precast concrete panels were modelled and approximated by diagonal bracing in the frame. However, the bracing was assigned a very low stiffness, because the exterior panels were detailed so as to avoid providing significant lateral stiffness. Therefore, in this analysis the stiffening effect of the cladding was negligible.

In an on-going study of the effect of heavyweight precast concrete cladding on the dynamic response of a building structure (Goodno and Will 1978, Palsson et al. 1984, Goodno and Palsson 1986), stiffness matrices for the cladding and the exterior framing were developed and incorporated into a three-dimensional computer model of the building. The interstorey shear stiffness representing the lateral stiffness provided by the cladding panels was selected so as to obtain a close correlation of the analytical and experimental values.

Henry et al. (1989) developed a mathematical model consisting of beam elements to represent precast concrete cladding as a lateral load resisting building component. The box frame model, Fig. 2.1, is composed of four box-like frames called panel-boxes assembled at adjacent corners to form a single cladding panel and is connected to the columns of the building frame at the four panel corners. Each panel-box consists of four beam elements that are rigidly connected. The panel-box horizontal beams are used primarily to model the panel's flexural characteristics and the vertical beams model the panel's shear characteristics. The cross-sectional area and moment of inertia for the beam elements represent the corresponding properties of the cladding panel. The comparison of the structural responses predicted by the box frame model were within the design limits of the responses obtained by a finite element model.

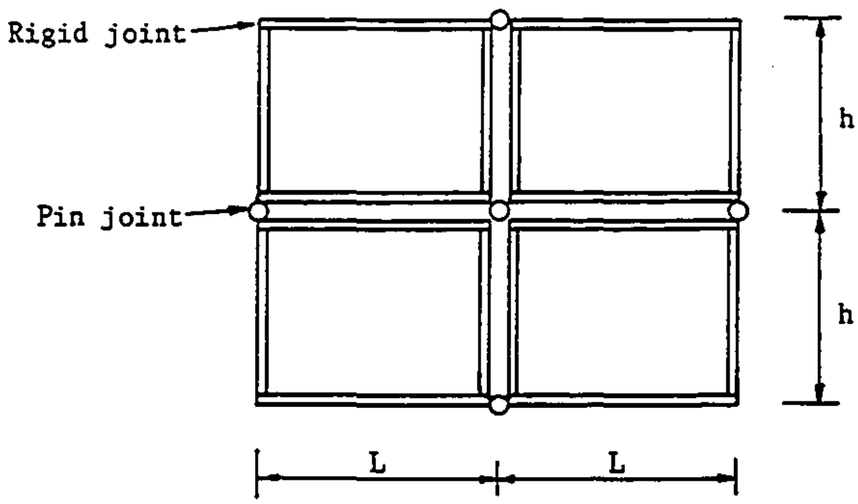

Figure 2.1: Box Frame Model (Henry et al. 1989)

CHAPTER 3

TYPES OF CLADDING SYSTEMS

The degree to which cladding will contribute to the lateral load resisting system of the building structure is a function of the form and material properties of the cladding, and the method by which the cladding system is connected to the primary structural framing system. Among the many types of exterior building skins, such as curtain wall, precast concrete, masonry, preformed panels, concrete, composite systems, etc. (Green 1982), curtain walling and precast concrete cladding are the most widely used in tall buildings.

3.1 Curtain Walls

Curtain walls are lightweight non-loadbearing panels, usually suspended in front of the structural frame, with their deadweight, wind loading and self-weight seismic forces transferred to the structural frame through anchor points. Curtain walling is most commonly associated with a rectangular grid of vertical and horizontal frame members with infill panels of glass or a combination of glass and some other lightweight sheeting (Brookes 1983). Because of its extensive use, the following discussion will focus on aluminum curtain walling. The multiplicity and diversity of aluminum curtain walls does not allow them to be easily categorized; however, they may be broadly classified according to their method of installation. The majority of aluminum curtain walls built to date may be identified as one of the following five different systems: 1) the stick system, 2) the unit system, 3) the unit-and-mullion system, 4) the panel system, and 5) the column-cover-and-spandrel system (Aluminum Curtain Wall Design Guide Manual 1979).

In the stick system, Fig. 3.1, the component parts of the wall are assembled on site piece by piece. Usually the mullion members are installed first, followed by the horizontal rail members, the panels, if any, and finally the glazing or window units. The stick system has been, and still is, in wide use. Many manufacturers consider it to be superior to other systems because of the relatively low shipping and handling costs, and the fact that it offers some degree of dimensional adjustment to site conditions.

The curtain wall in the unit system, Fig. 3.2, is composed of large framed units pre-assembled at the factory, complete with spandrel panels, if any, and sometimes pre-glazing. The units are joined together, with the units themselves becoming the frame. This system

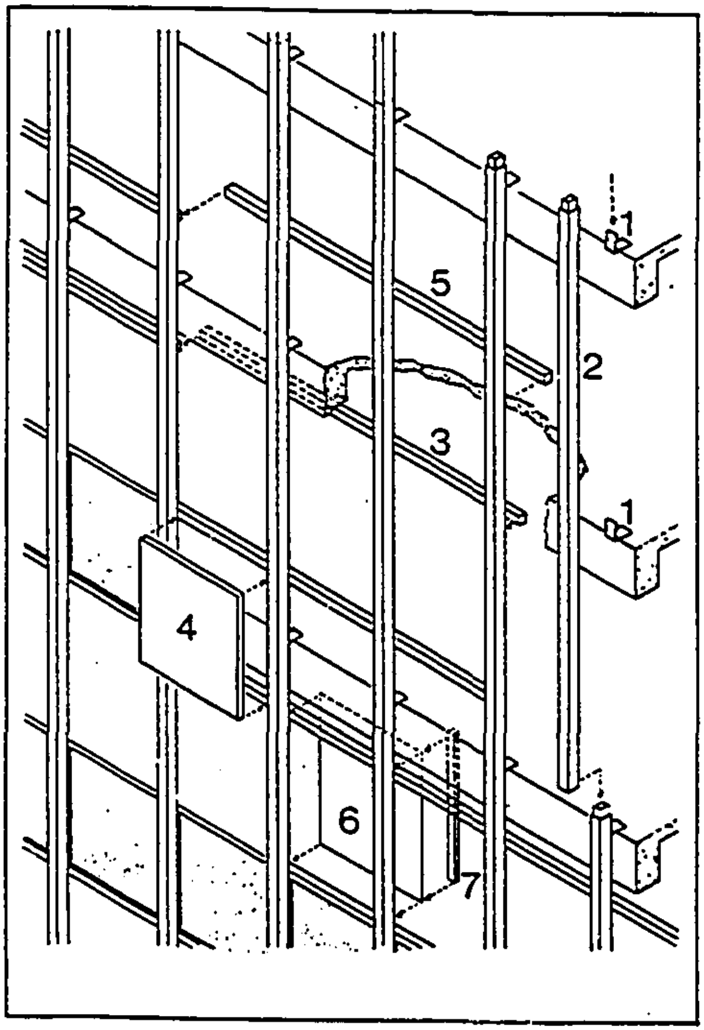

STICK SYSTEM—Schematic of typical version

1: Anchors. 2: Mullion. 3: Horizontal rail (gutter section at window head). 4: Spandrel panel (may be installed from inside building). 5: Horizontal rail (window sill section). 6: Vision glass (installed from inside building). 7: Interior mullion trim.

Other variations: Mullion and rail sections may be longer or shorter than shown. Vision glass may be set directly in recesses in framing members, may be set with applied stops, may be set in sub-frame, or may include operable sash.

Figure 3.1: The Stick System (Aluminum Curtain Wall Design Guide Manual 1979)

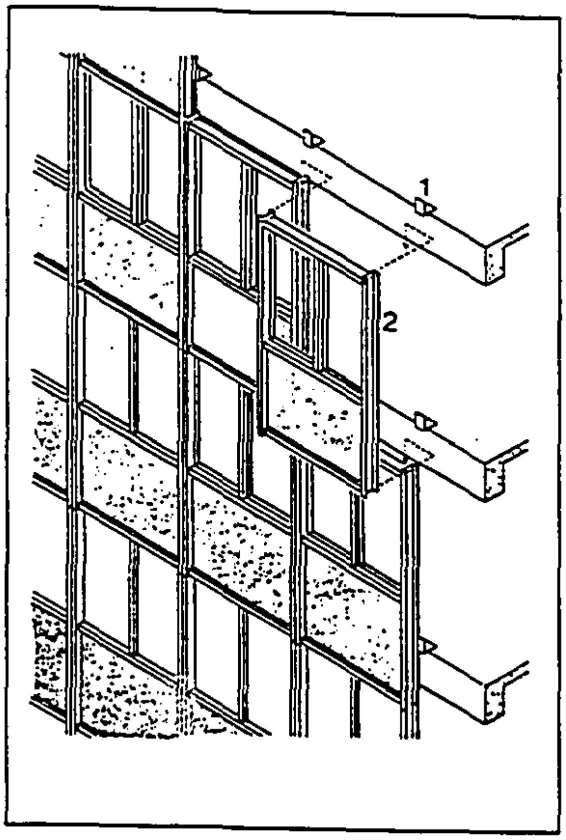

UNIT SYSTEM—Schematic of typical version
1: Anchor. 2: Pre-assembled framed unit.

Figure 3.2: The Unit System (Aluminum Curtain Wall Design Guide Manual 1979)

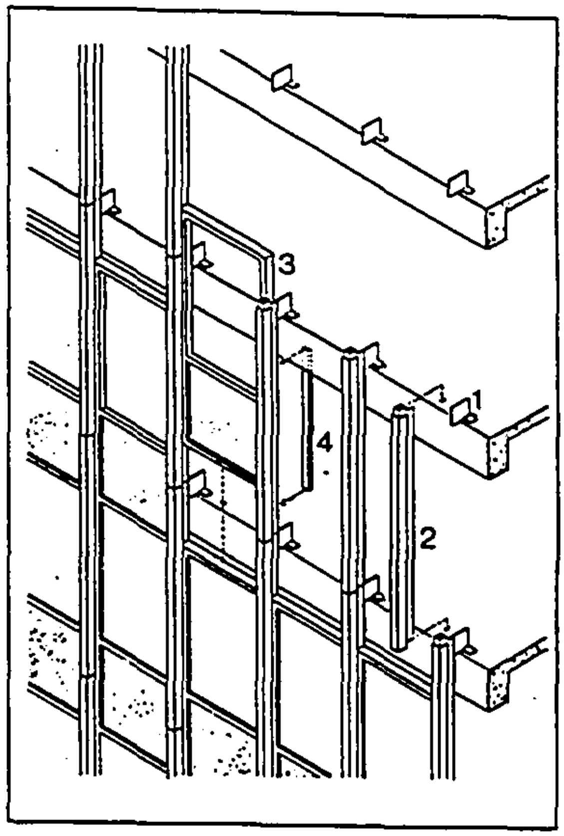

UNIT-AND-MULLION SYSTEM—Schematic of typical version
1: Anchors. 2: Mullion

Figure 3.3: The Unit-and-Mullion System (Aluminum Curtain Wall Design Guide Manual 1979)

is advantageous in that the units are entirely assembled in the factory under careful supervision, and on-site installation is rapid in requiring minimum field labor. However, the units are bulky and require more space for shop assembly, shipping and on-site storage.

The unit-and-mullion system, Fig. 3.3, is a combination of the two previous systems. First, the mullion members are installed on site, then pre-assembled framed units are placed between them. The system is often used when the mullion sections are unusually deep or large in cross section, making it impractical to include them as part of the pre-assembled unit.

In the panel system, Fig. 3.4, the panels are not pre-assembled framed units as in the unit system, but are instead homogeneous units formed from sheet metal or as castings. The panel system is usually employed when it is desired to suppress the grid pattern caused by the framework of the previous systems.

The column-cover-and-spandrel system, Fig. 3.5, as its name suggests, consists of column cover sections, long spandrel units which span between the column covers, and infill glazing units.

In the stick system, the unit system and the unit-and-mullion system, the window mullions are the principal members of the grid. The horizontal members rarely form the support for curtain walls. The mullions, which span from floor to floor, must withstand the axial stresses caused by the panels' deadweight and the bending stresses caused by the wind and earthquake loads. It is in the transverse direction that the mullion must have greatest stiffness and strength. The depth of the mullion is thus dependent on its span and the area of glazing it is required to carry. Manufacturers offer a range of mullion sections to cope with a variety of vertical spans. Figs. 3.6, 3.7, and 3.8 illustrate just a few.

Of vital importance in determining the stiffening influence of a cladding system is its method of connection to the structural frame. For aluminum curtain walling various types of mullion-to-structure connections are used. Figs. 3.9 and 3.10 present several examples of attachments to different types of structural frames. Each of the connections can be classified generally as either fixed or movable. A fixed connection is one that is firmly attached to both the mullion and the building structure, acting generally as a pinned connection. It is designed to resist both wind and dead loads. A movable connection is designed to resist only lateral wind loading while permitting some vertical movement.

The above brief description of the curtain wall and its components allows for a better understanding of its interaction with the building's structural system. A sketch of a curtain wall (the mullion) attached to a building's structure is illustrated in Fig. 3.11a, while in Fig. 3.11b the equivalent structural model is shown. In the structural model, the connections of the wall to the slab are shown as pin connections while the expansion joints can be represented as connections allowing vertical movement. From Fig. 3.11b, it can be seen that the structural system cannot pick up vertical forces from vertical displacements of the slabs, therefore no restraint or stiffening effect is expected to develop. Although the connections may in practice have some vertical bending resistance, hence will not be true pin connections, no significant stiffening influence can be expected from the aluminum curtain

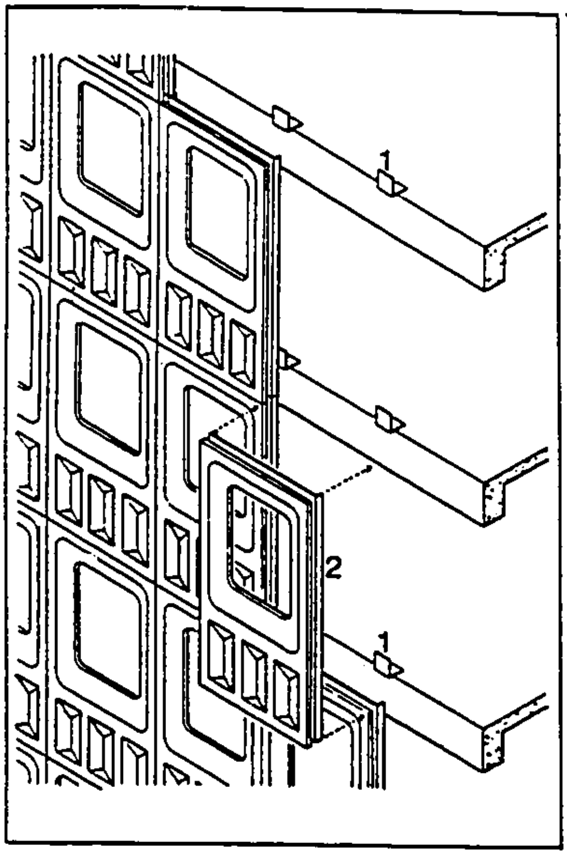

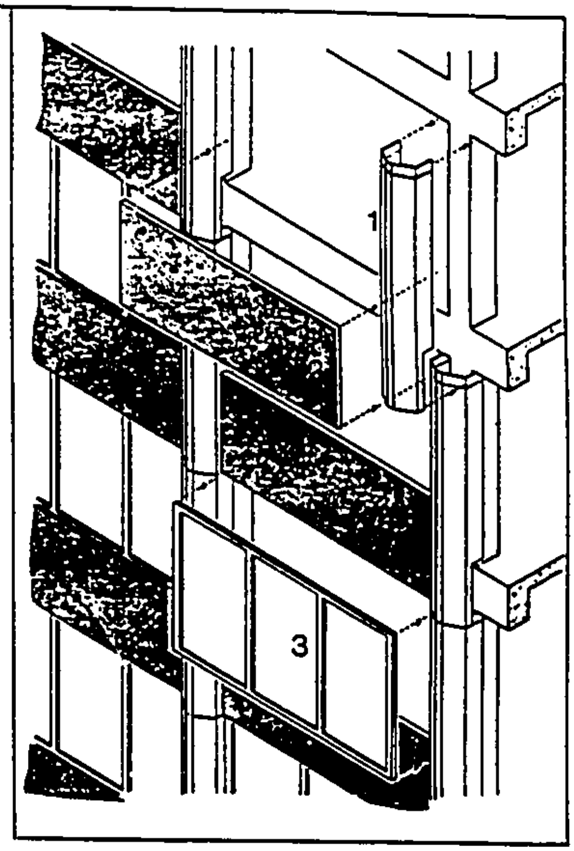

Figure 3.4: The Panel System (Aluminum Curtain Wall Design Guide Manual 1979)

Figure 3.5: The Column-Cover-and-Spandrel System (Aluminum Curtain Wall Design Guide Manual 1979)

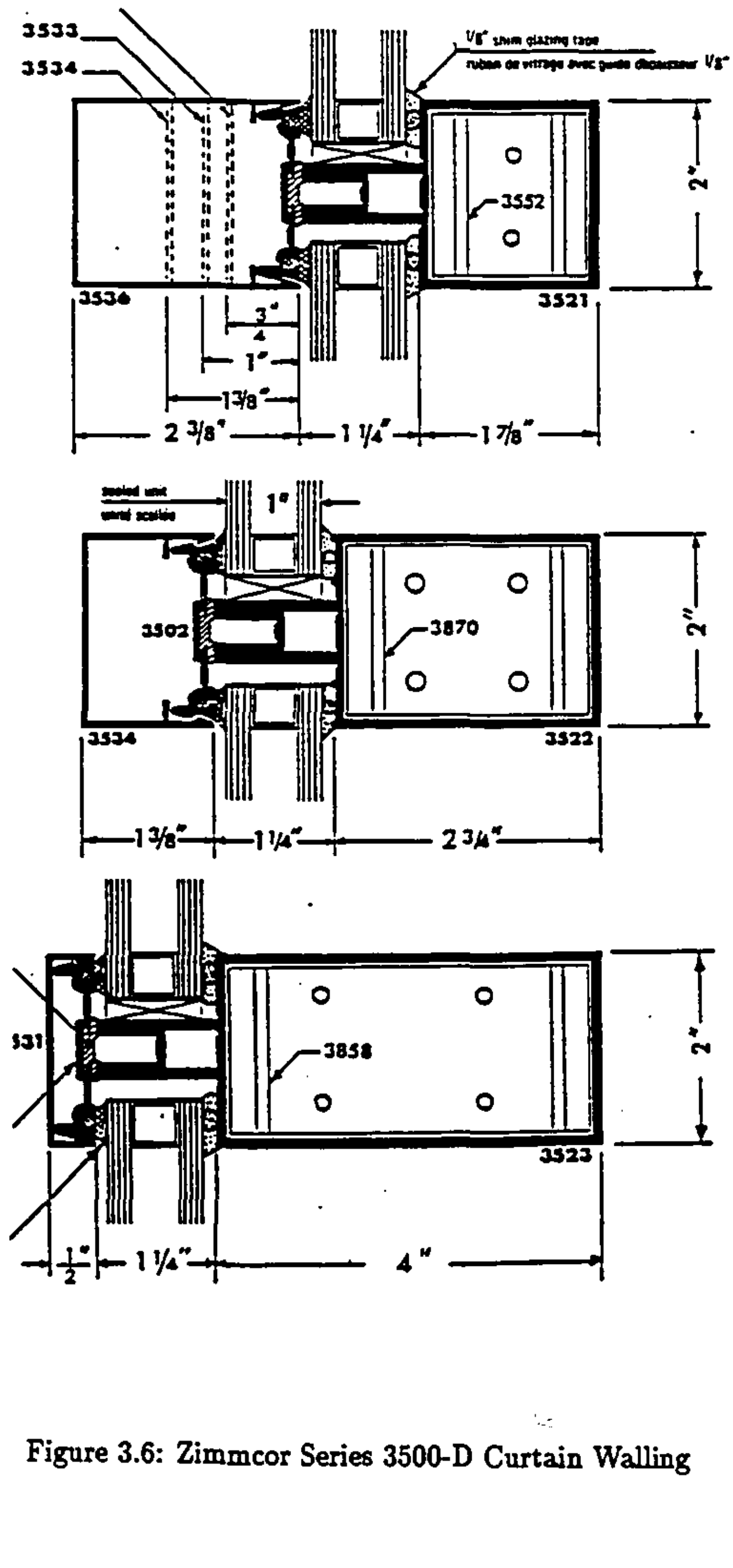

Figure 3.6: Zimmcor Series 3500-D Curtain Walling

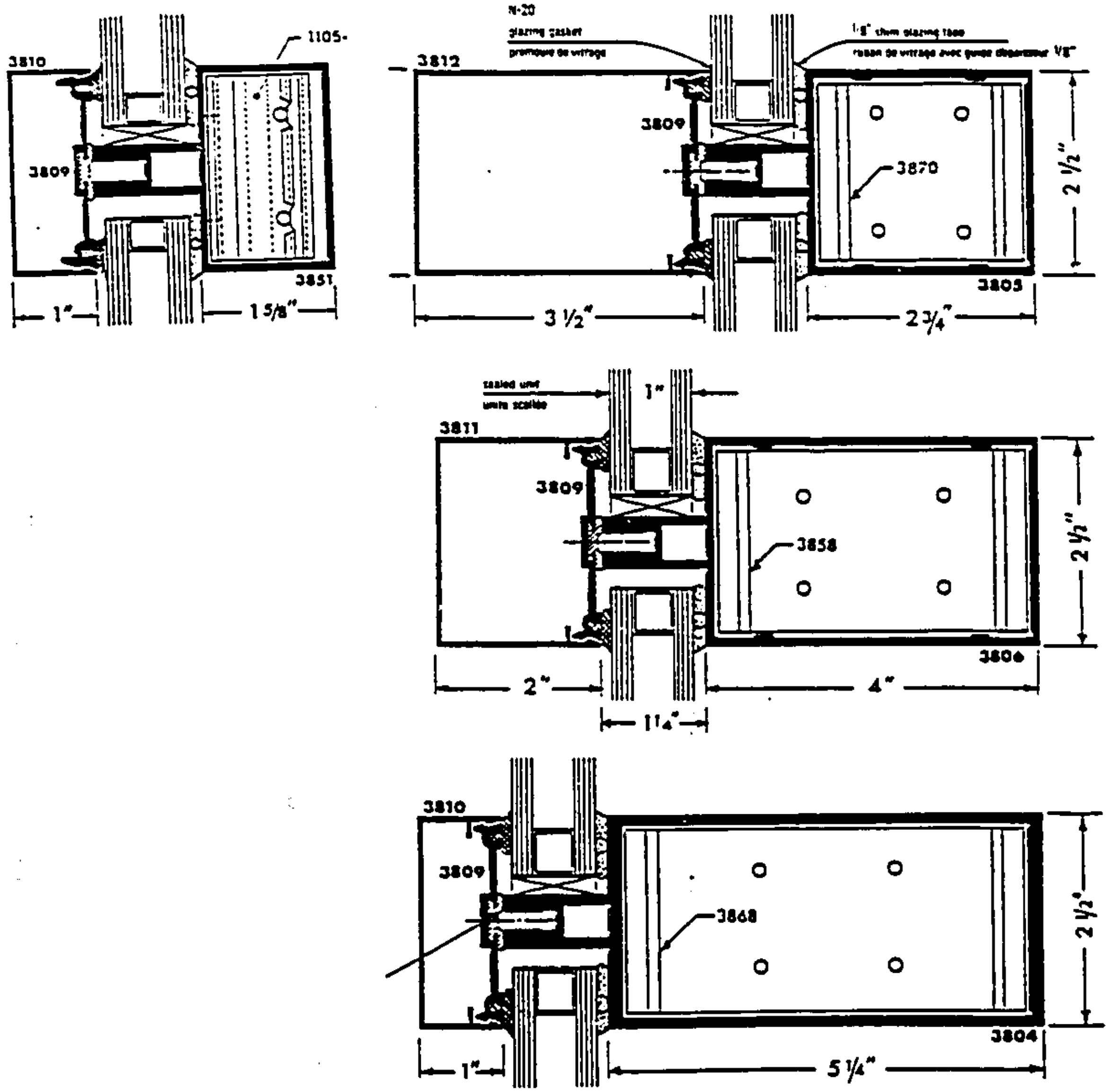

Figure 3.7: Zimmcor Series 3800-S Curtain Walling

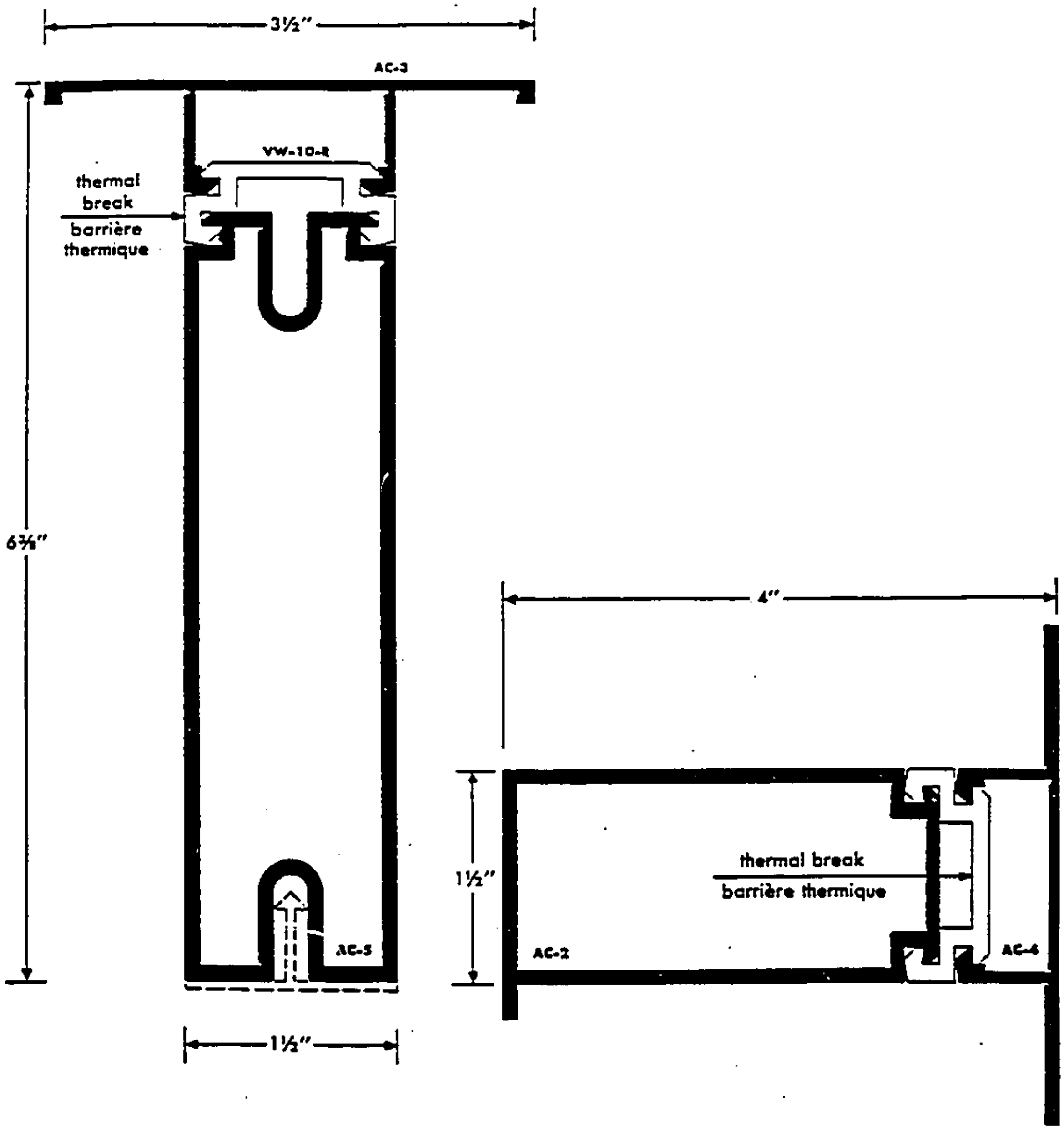

Figure 3.8: Zimmcor Series 2000 Curtain Walling

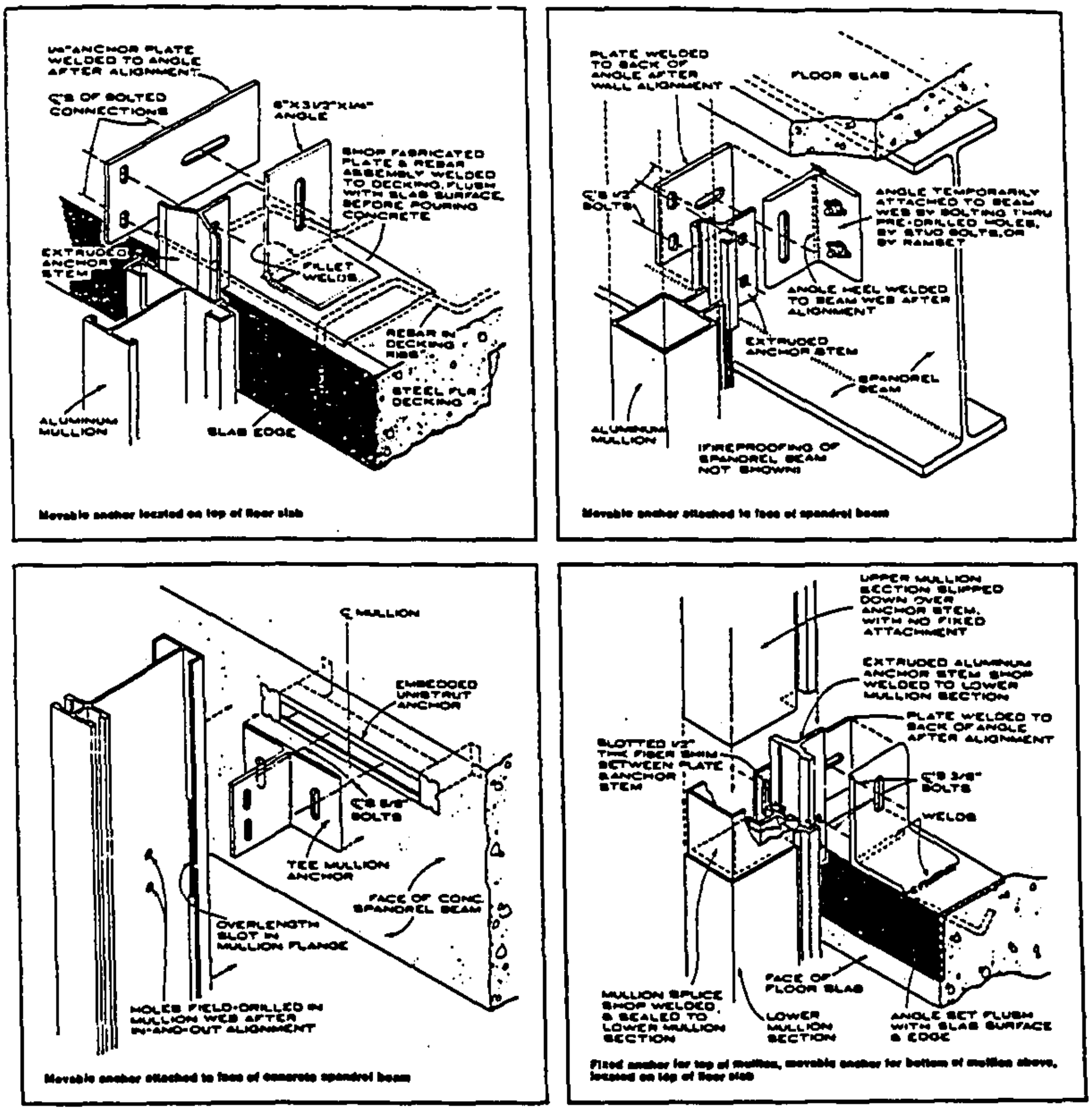

Figure 3.9: Examples of Mullion-to-Structure Connections (Aluminum Curtain Wall Design Guide Manual 1979)

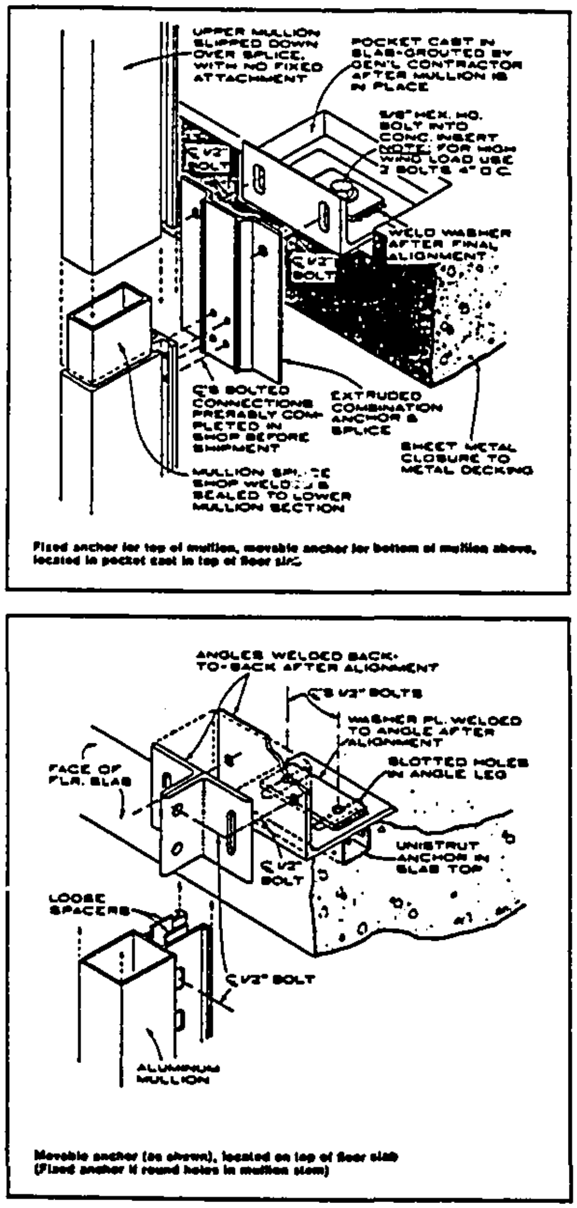

Fixed anchor for top of mullion, movable anchor for bottom of mullion above, located in pocket cast in top of floor slab.

Movable anchor (as shown), located on top of floor slab (Fixed anchor if round holes in mullion stem)

Figure 3.10: Examples of Mullion-to-Structure Connections (Aluminum Curtain Wall Design Guide Manual 1979)

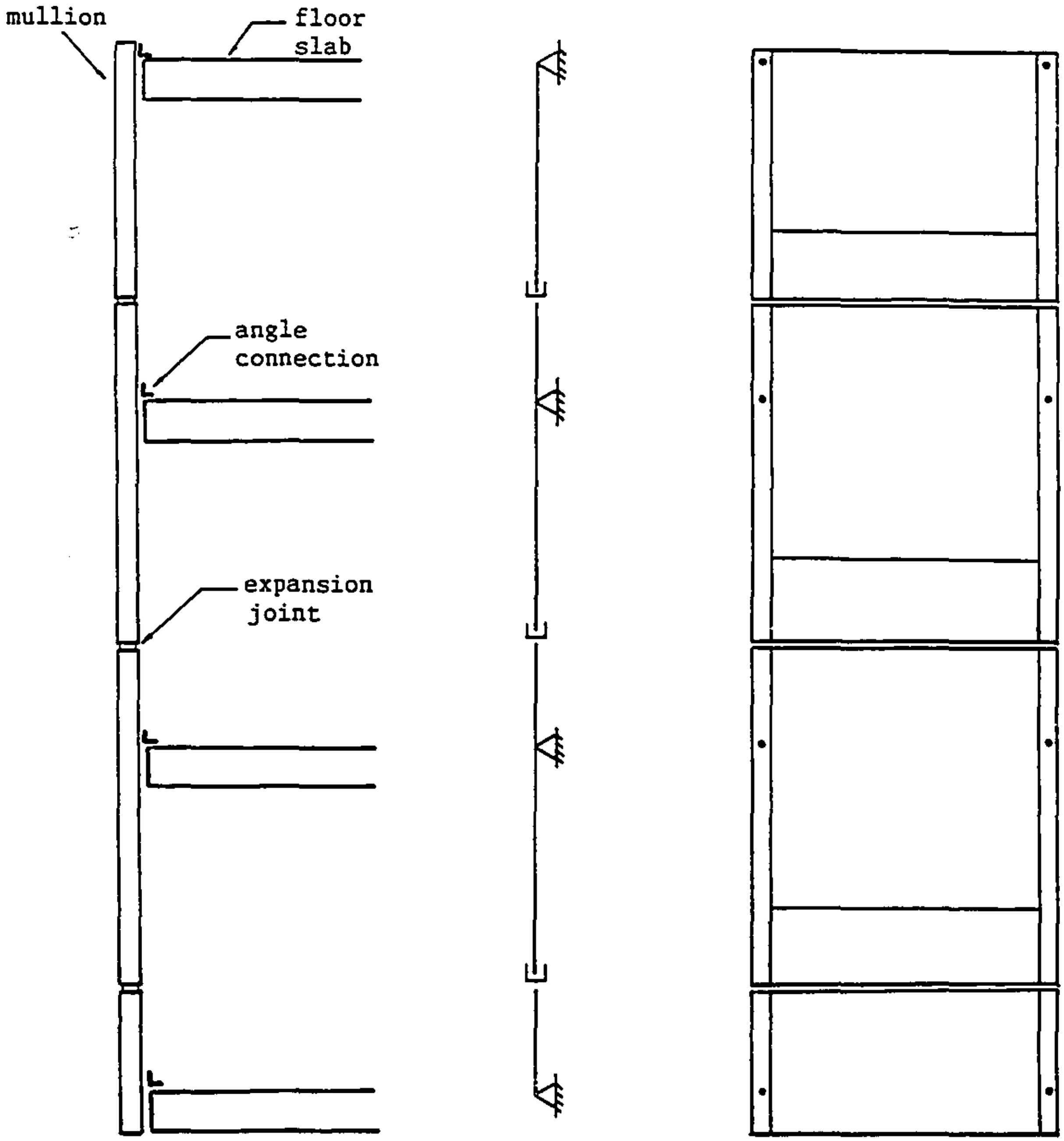

(a) (b) (c)

Figure 3.11: Location and Restraint Conditions of Curtain Wall Connections

walls since the aluminum mullions themselves are not very stiff. In Fig. 3.11c an elevation view of the panel is shown with the location points of the connections. Because the panel is suspended at the top by angle connections and no lateral restraints are provided at the bottom, the curtain wall will not provide additional lateral stiffness to the structural frame.

3.2 Precast Concrete Panels

Precast concrete cladding allows considerable freedom of architectural expression while advantage can be taken of the economies of mass production of the precast elements. Precast concrete panels can be produced with a concrete face in a variety of colours and textures, with exposed aggregate architectural finishes, and with hammered and sculptured faces. Also available are precast concrete panels faced with various other materials such as granite, marble, brick, stone and glazed ceramic tiles (Green 1982).

The precast concrete panels considered in this study are non-loadbearing panels; that is, they are not intended to contribute to the gravity and lateral load resistances of the structure. They are designed to resist only their transfer of deadweight to the supports, wind forces, seismic forces generated by their mass, forces due to restraint of volume changes, and handling forces. The manufacturing, transportation and erection forces will normally govern the panel design, while the forces resulting from earthquake loads may govern the connection design.

Properly conceived and designed connections are vital to the satisfactory performance of precast concrete panels. In choosing their number, location and degrees of restraint, the Metric Design Manual for Precast and Prestressed Concrete by the Canadian Prestressed Concrete Institute, CPCI, (1987) recommends that:

(a) a system of connections should be statically determinate to permit a more accurate determination of forces,

(b) the internal stresses should be minimized,

(c) the panel should be allowed to move in its plane to accommodate storey drift and volume changes,

(d) torsional moments on supporting beams should be minimized, and

(e) contact between the structural frame and the cladding should be prevented during an earthquake.

The typical arrangement of connections suggested by the CPCI manual is shown in Fig. 3.12. The number and spacing of connection points is influenced by the type and size of panel. The Prestressed Concrete Institute, PCI, manual for Structural Design of Architectural Precast Concrete (1977) provides greater details of the locations and restraint conditions for various practical panel sizes, Fig. 3.13. Generally, the load support connections are located near the bottom of the panel. In some cases, however, units may be suspended at the top, and tied with lateral connections at the bottom.

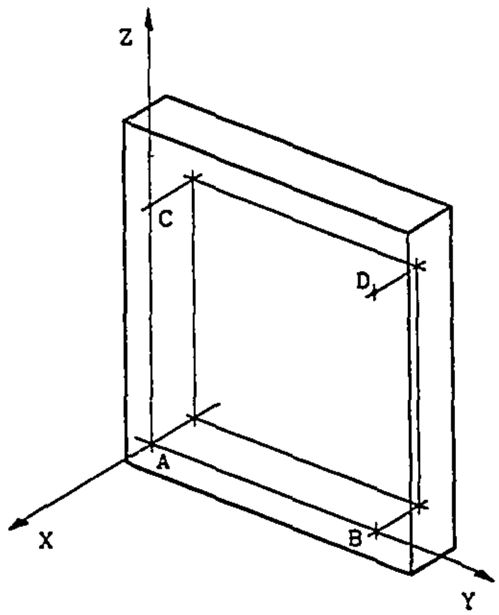

Connection	Restraint*		
	X	Y	Z
A	1	1	1
B	1	0	1
C	1	1	0
D	1	0	0

*Restrained = 1
Free = 0

Figure 3.12: CPCI Typical Connection Arrangement

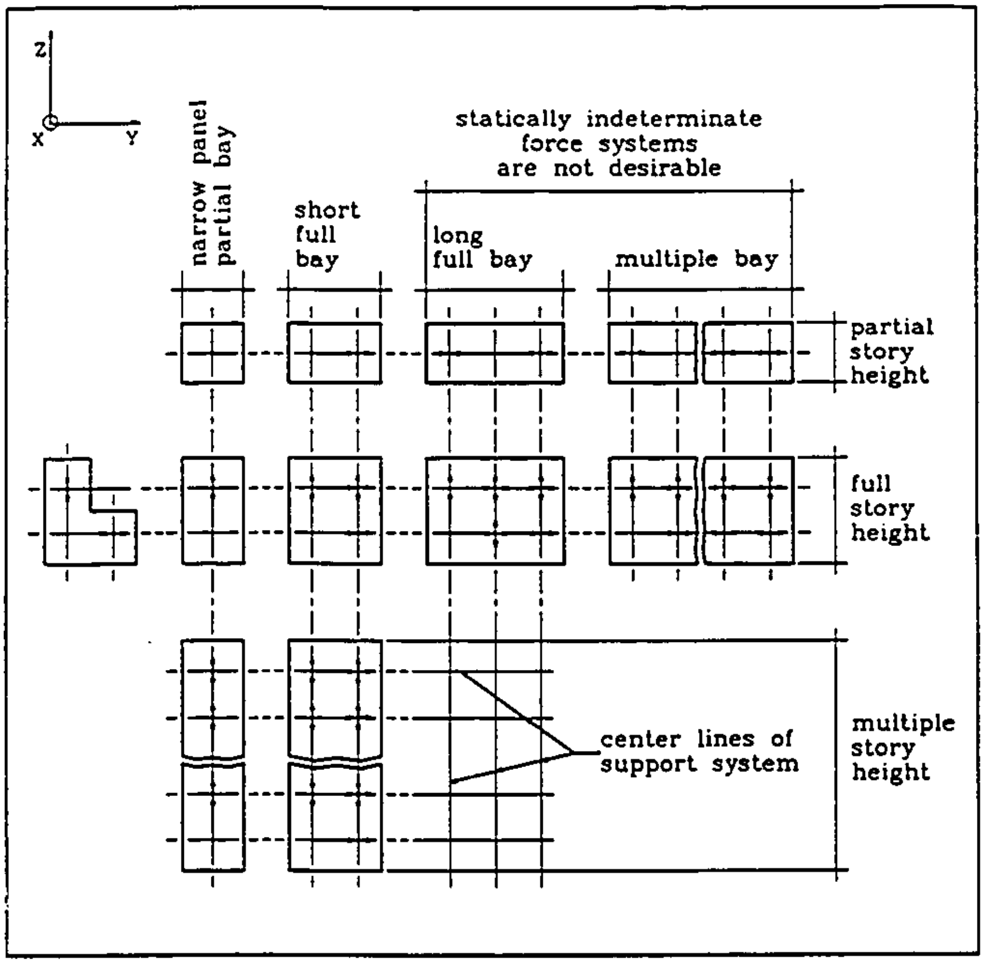

Symbol	Force Transfer Possible In Direction Of X	Y	Z	Designation Of Connection
+	•	•	•	X-Y-Z connection
+	•	•		X-Y Connection
+	•		•	X-Z Connection
+	•			X Connection

Arrow indicates direction in which movement is possible or desirable without restraint.

Figure 3.13: PCI Typical Connection Arrangements

Since panels vary considerably in size, shape and weight, from one building to another, the panel connections are often detailed for the particular building. They can be broadly categorized, however, as either loadbearing, tie-back or alignment connections (PCI Manual 1985). For completeness and further reference a brief description of several connections will follow. Fig. 3.14 illustrates some typical direct loadbearing connections. The load transfer is usually through shims as shown in (a). In (b) and (c) rods or bolts in inserts are used in the upper panel and grouted into holes in the lower panel or support. In (d) through (g) some welding arrangements are shown. An anchor bolt projecting from the supporting member is shown in (h). In (i) and (j) reinforcing bars projecting from the panel are grouted into sleeves. While in (k) a drilled-in expansion anchor is employed.

Typical steel or concrete haunch loadbearing connections are shown in Fig. 3.15. In (a) a cladding panel cast with a typical concrete corbel to support it is shown. Various types of rolled steel section as haunches are illustrated in (b) through (f). The steel haunches can be embedded in the panel as in (c), (d) and (e), or welded on after stripping the formwork as in (b) and (f). Steel and concrete haunch connections are economical solutions for connections subjected to significant vertical bending.

Illustrated in Fig. 3.16 are several of the wide variety of angle seat bearing connections. As shown in (c), the angle may require to be stiffened if the load is large. Figs. (b), (d), (e) and (f) show confinement reinforcement around embedded studs to add ductility to the connection.

In addition to the loadbearing connections, most precast panels require tie-back connections. In Fig. 3.17 several examples of the use of a welded plate or flat bar in tie-back connections are shown, while in Fig. 3.18 angles are employed instead of plates. Fig. 3.19 illustrates how bolts into inserts can be used. Threaded rods are used instead of bolts in Fig. 3.20. Fig. 3.21 shows how both bolting and welding are often used. It should be noted that when bolts are used, slots or oversize holes should be provided to permit adjustments during erection.

Figs. 3.22 and 3.23 illustrate typical examples of alignment connections used to align adjacent panels. In Fig. 3.22 the connections are welded, while in Fig. 3.23 they are bolted. With bolted connections, slotted holes are used to allow adjustments and panel movement.

Unless there are other local governing codes which impose special requirements for exterior elements and their connections, such as the Structural Engineers Association of California seismic code (1988), the general guidelines presented above are those used in practice in the many parts of North America.

Due to the material properties of precast concrete panels and to the nature and location of their connections, the possibility of precast concrete panels providing additional lateral stiffness to a building's structural framing system cannot be disregarded. However, a more detailed investigation of the panels and their interaction with a structural frame is required before drawing any conclusions.

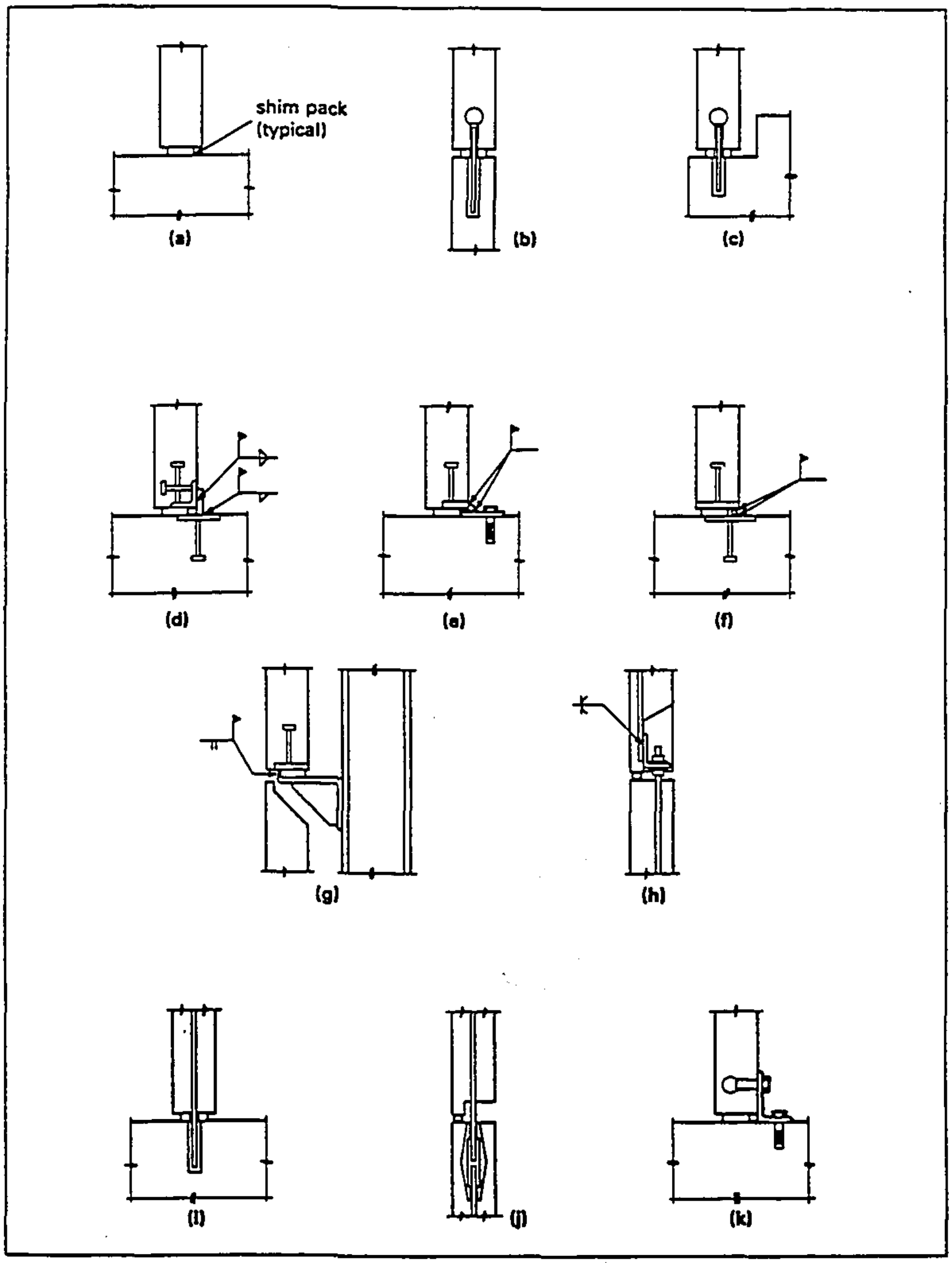

Figure 3.14: Examples of Direct Loadbearing Connections (PCI Manual 1985)

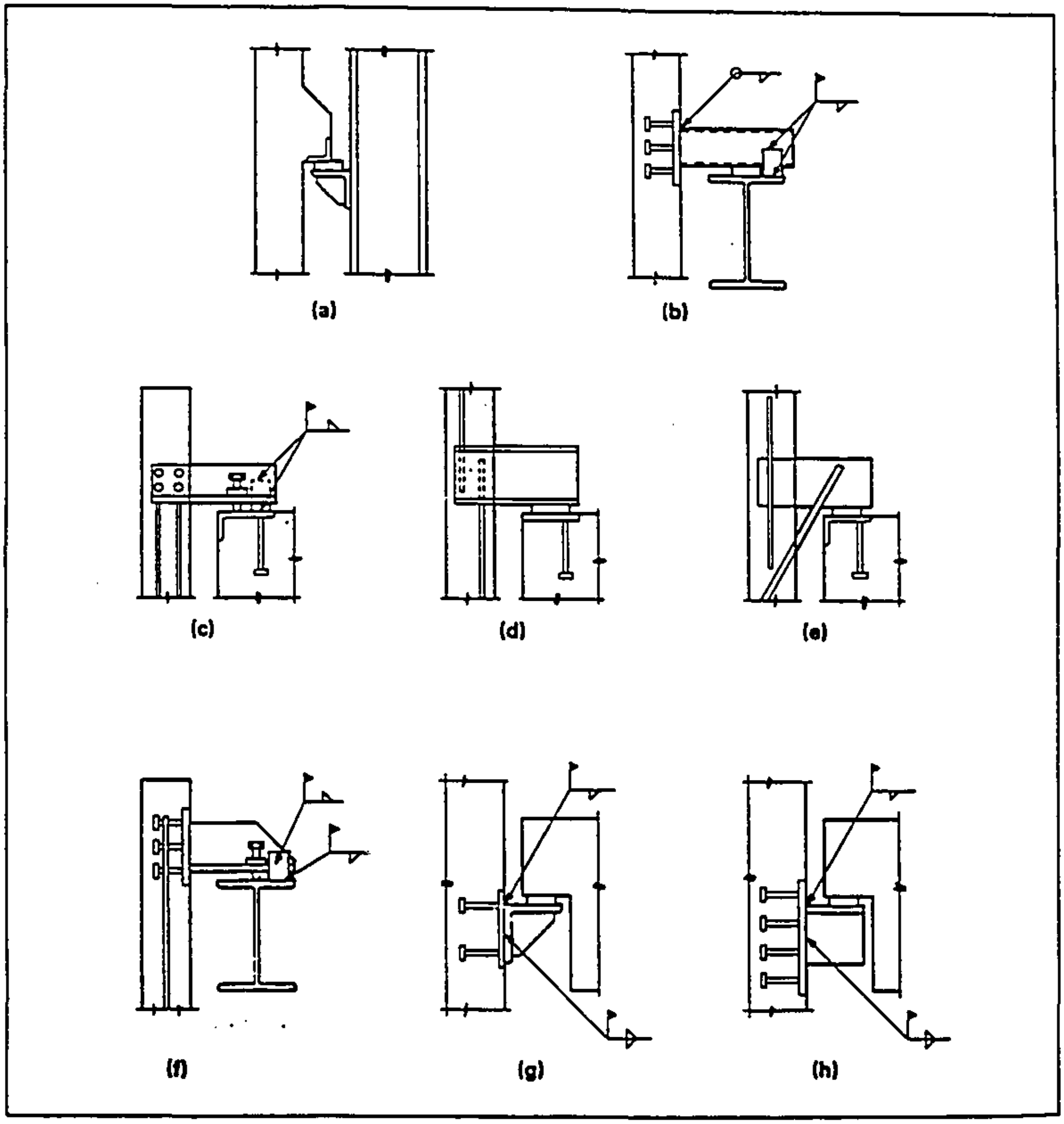

Note: Use of shims vs. levelling bolts depends on local practice or preference.

Figure 3.15: Typical Haunch Loadbearing Connections (PCI Manual 1985)

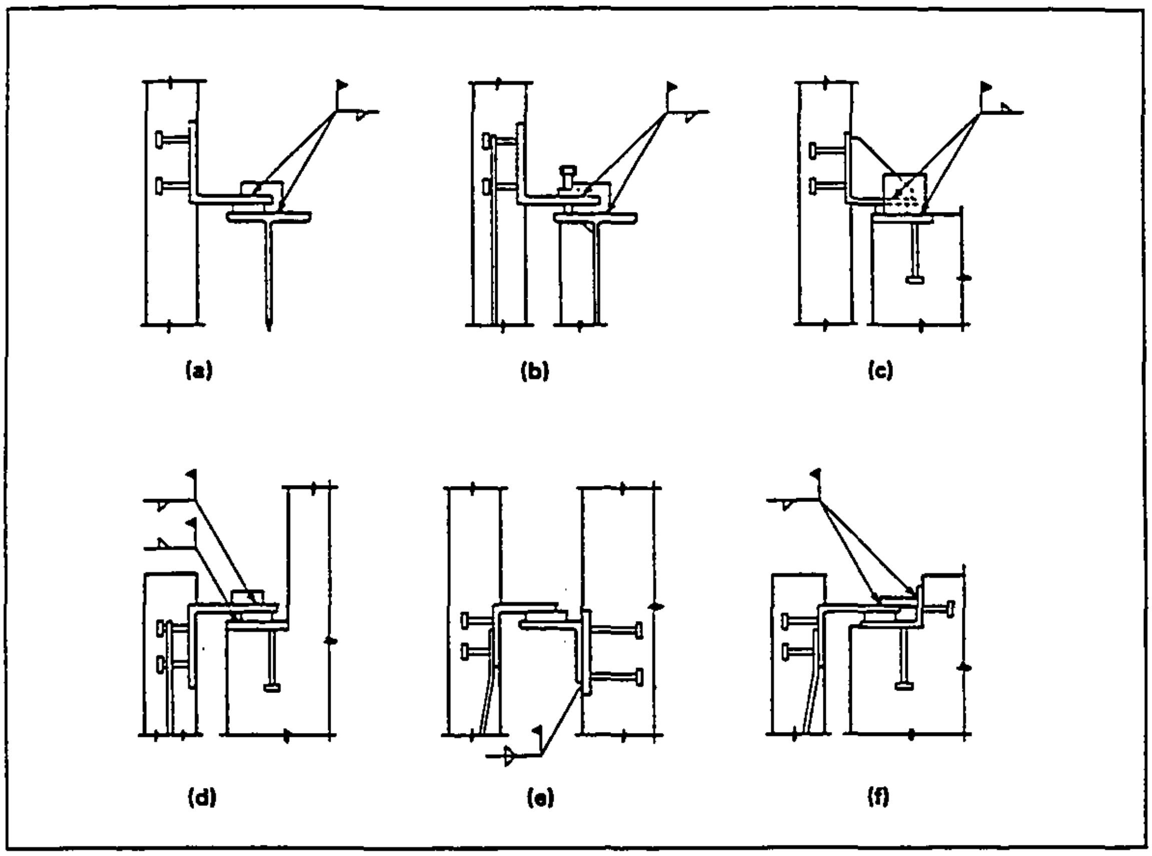

Note: Use of shims vs. levelling bolts depends on local practice or preference.

Figure 3.16: Angle Seat Bearing Connections (PCI Manual 1985)

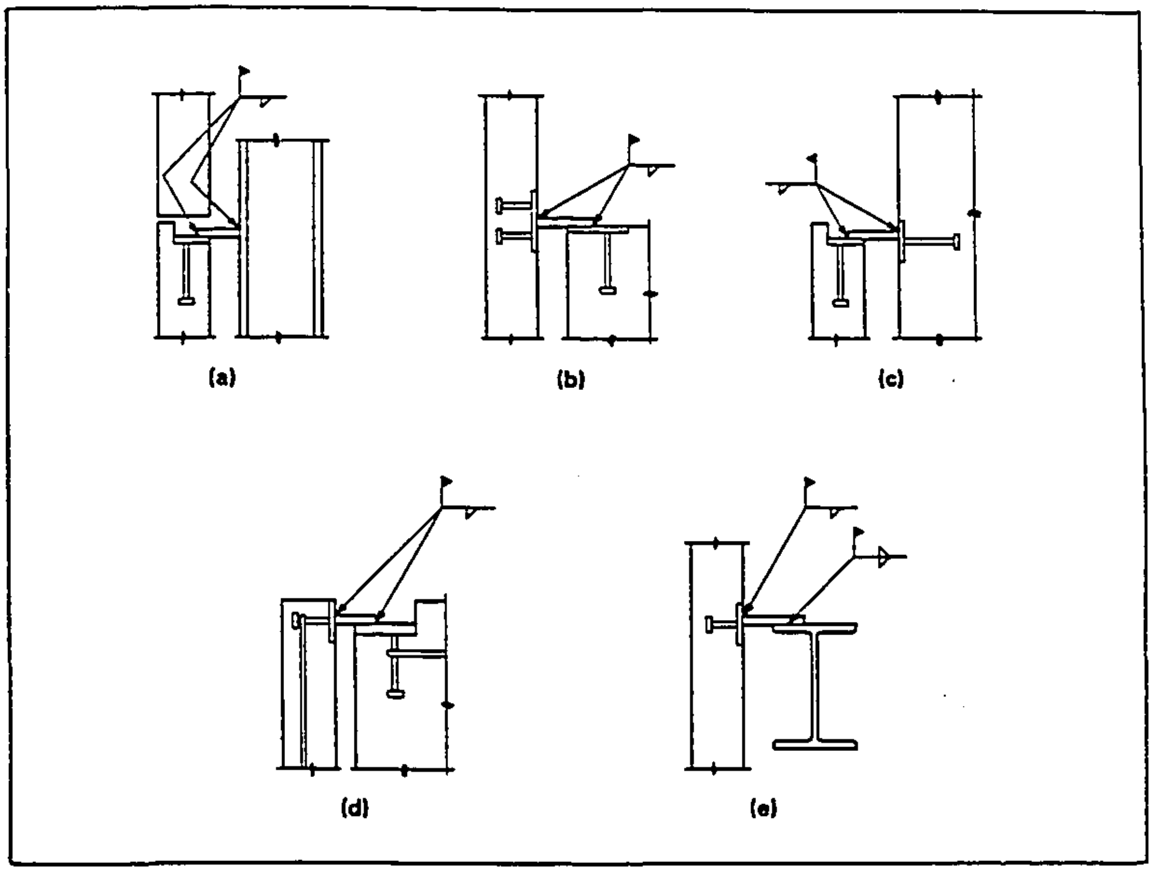

Figure 3.17: Welded Plate or Flat Bar Tie-Back Connections (PCI Manual 1985)

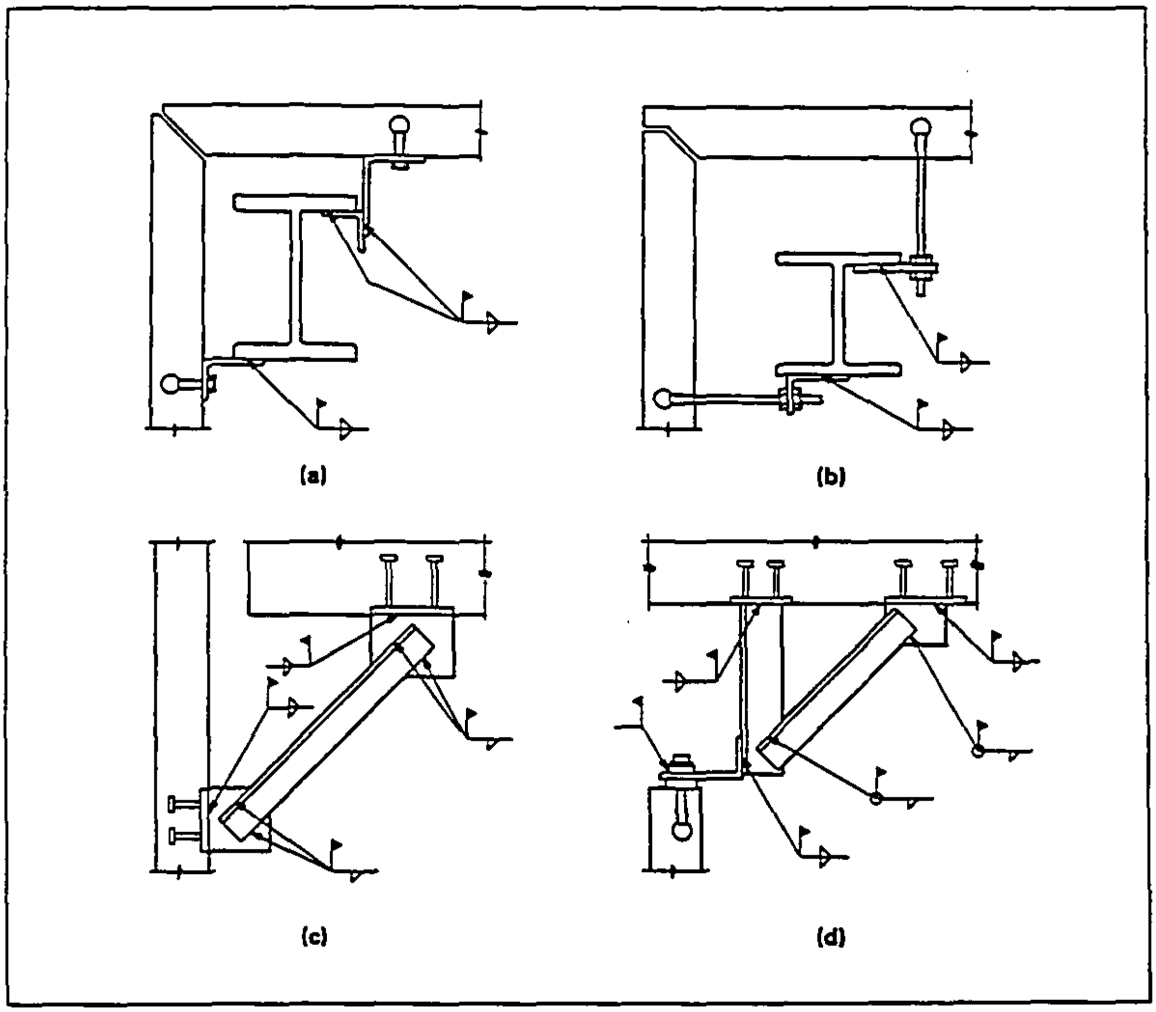

Figure 3.18: Welded Angle Tie-Back Connections (PCI Manual 1985)

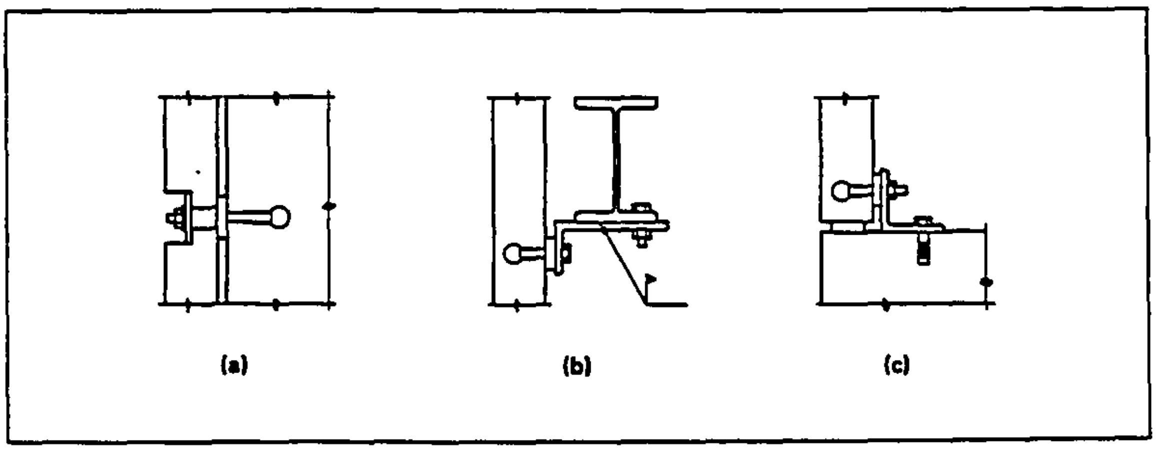

Figure 3.19: Bolted Angle Tie-Back Connections (PCI Manual 1985)

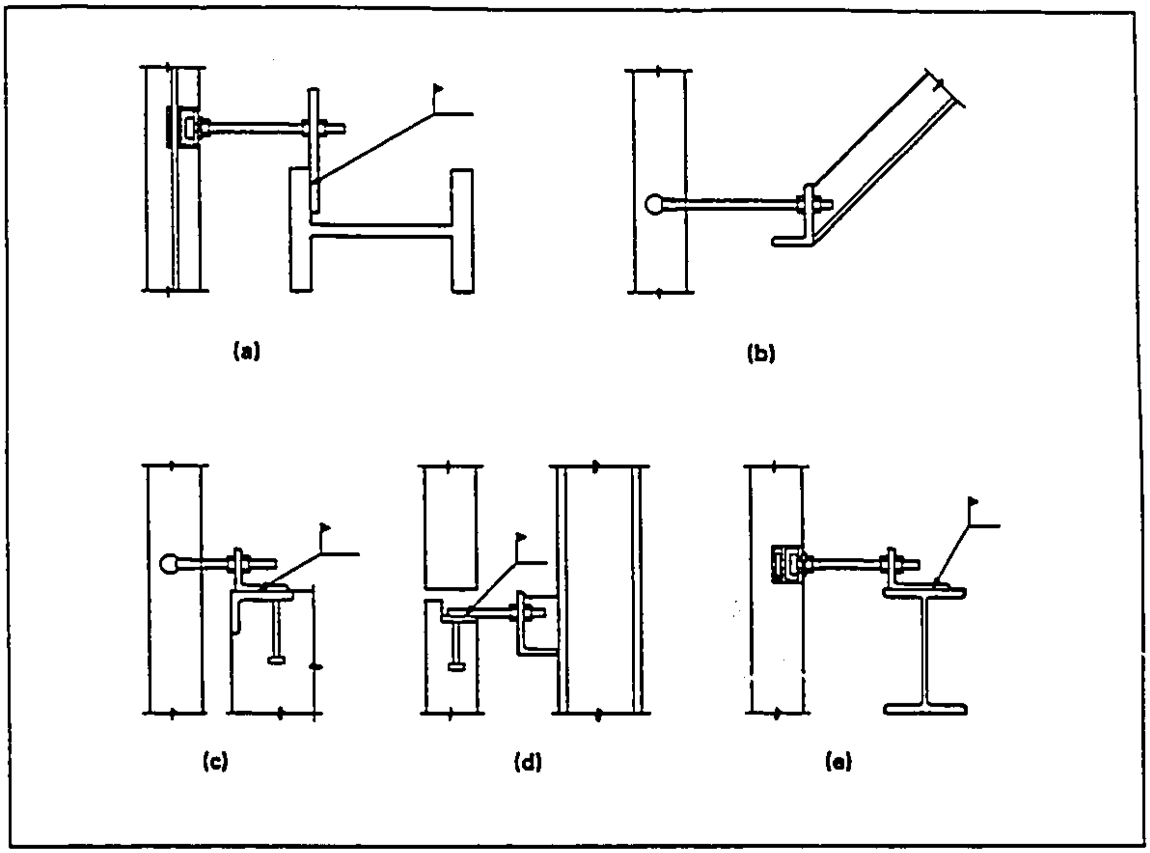

Figure 3.20: Angle Tie-Back Connections Using Threaded Rods (PCI Manual 1985)

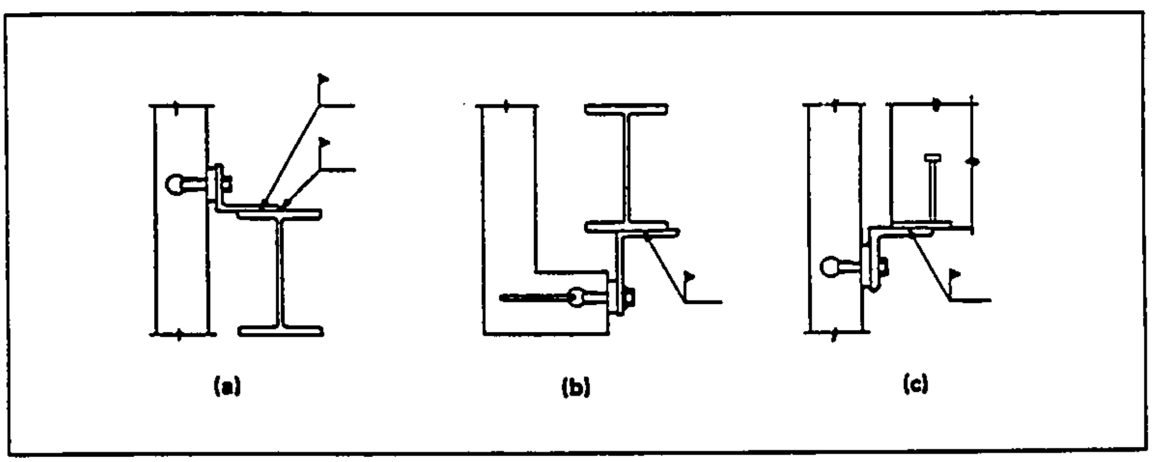

Figure 3.21: Bolted and Welded Angle Tie-Back Connections (PCI Manual 1985)

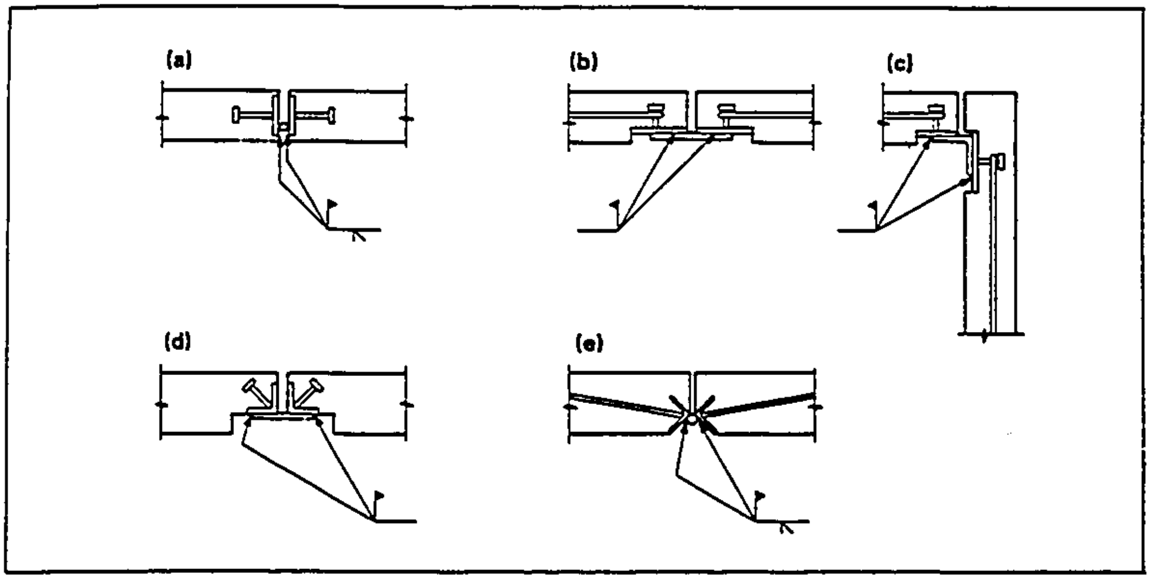

Figure 3.22: Welded Alignment Connections (PCI Manual 1985)

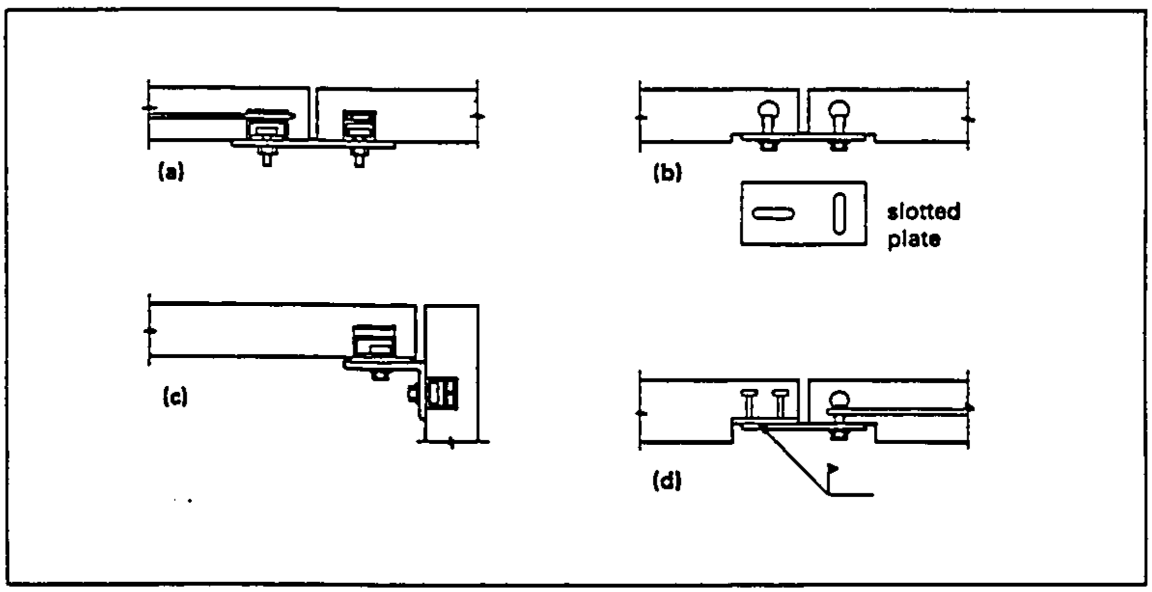

Figure 3.23: Bolted Alignment Connections (PCI Manual 1985)

CHAPTER 4

ANALYSIS OF A REPRESENTATIVE PRECAST CONCRETE CLADDING PANEL

In order to assess the approximate amount of stiffening contributed by cladding panels, an analytical study was performed of a laterally loaded moment-resisting frame, with and without cladding panels. The number of panel types used in building construction, with their variations in height-to-length proportions, their number, sizes and shapes of window openings, their planar and non-planar form, and their locations and detailing of connections, is virtually infinite. Therefore, a relatively simple representative planar panel, as used commonly in eastern North American building construction, is described as well as two typical types of building structures to which the panel is attached.

Rather than analysing a multi-storey multi-bay structure, a single-storey module, which was designed to behave as a typical end-bay-width storey of the frame, and simulating the effects of panels above and below and on one side, was investigated. Several lateral load analyses were performed to obtain a better understanding of the interactive behaviour between the panel and the frame.

4.1 Description of the Representative Example Structures and Panels

The selected example structures, with the floor plans shown in Figs. 4.1 and 4.2, are typical of many medium-rise building structures, being twenty stories tall and of reinforced concrete. In the wall-frame structure, Fig. 4.1, the core and the moment-resisting framing in combination provide the lateral force resistance. The other structure, Fig. 4.2, differs from the first in that the structural core is omitted and the primary, moment-resisting, framing is designed to provide all the required lateral force resistance. As in many medium-rise reinforced concrete buildings, the floor system is a two-way flat plate supported by columns, some of whose sections reduce up the height at levels 5 and 12, as recorded in the column schedule presented in Fig. 4.3. In every storey, two precast concrete cladding panels are attached to each exterior face of the structures.

The representative cladding panel is of precast concrete faced with polished granite, and is of a type manufactured by Schokbeton Quebec, Inc. The panel, Fig. 4.4, comprises a 125

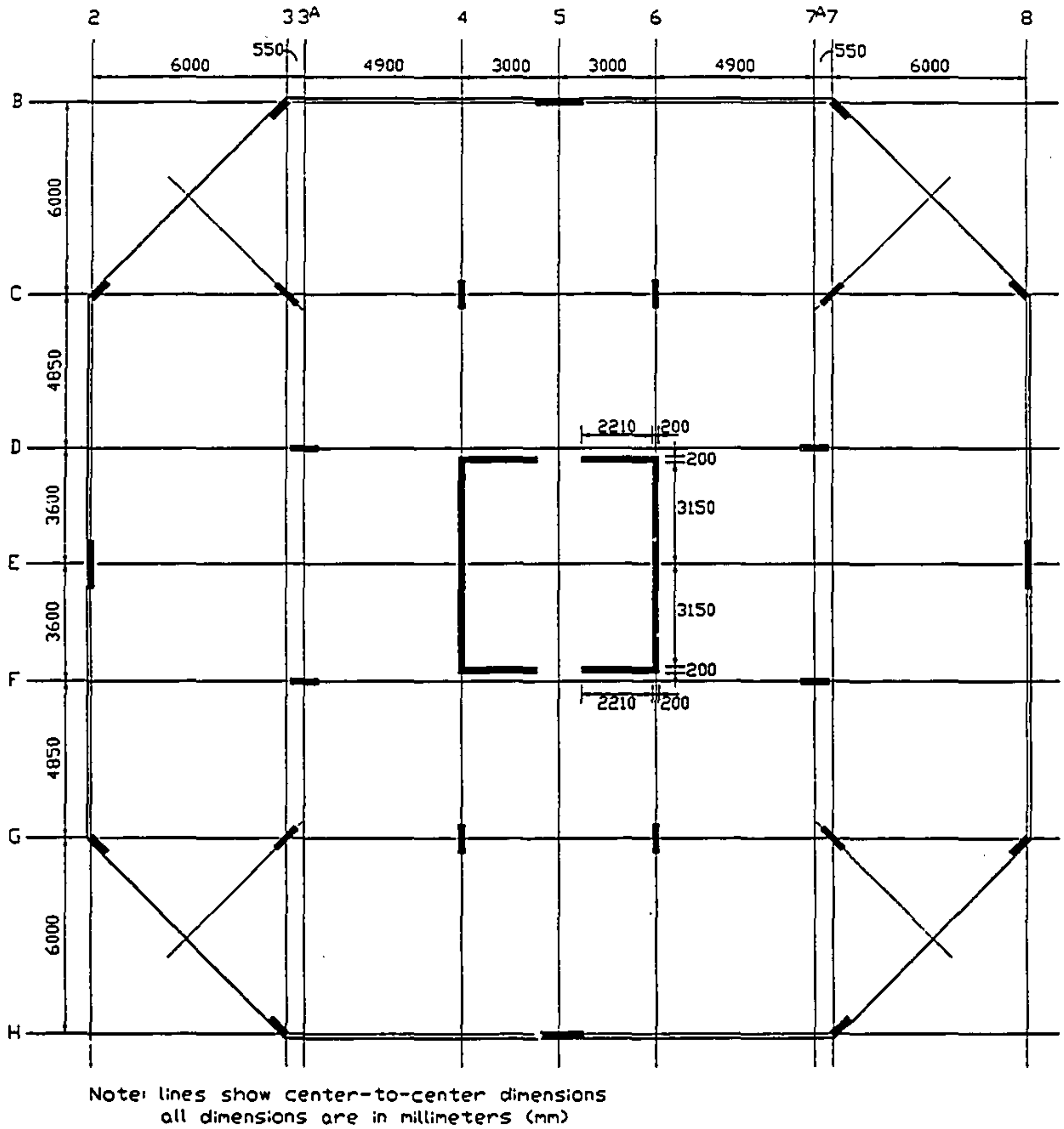

Figure 4.1: Floor Plan of Example Wall-Frame Structure

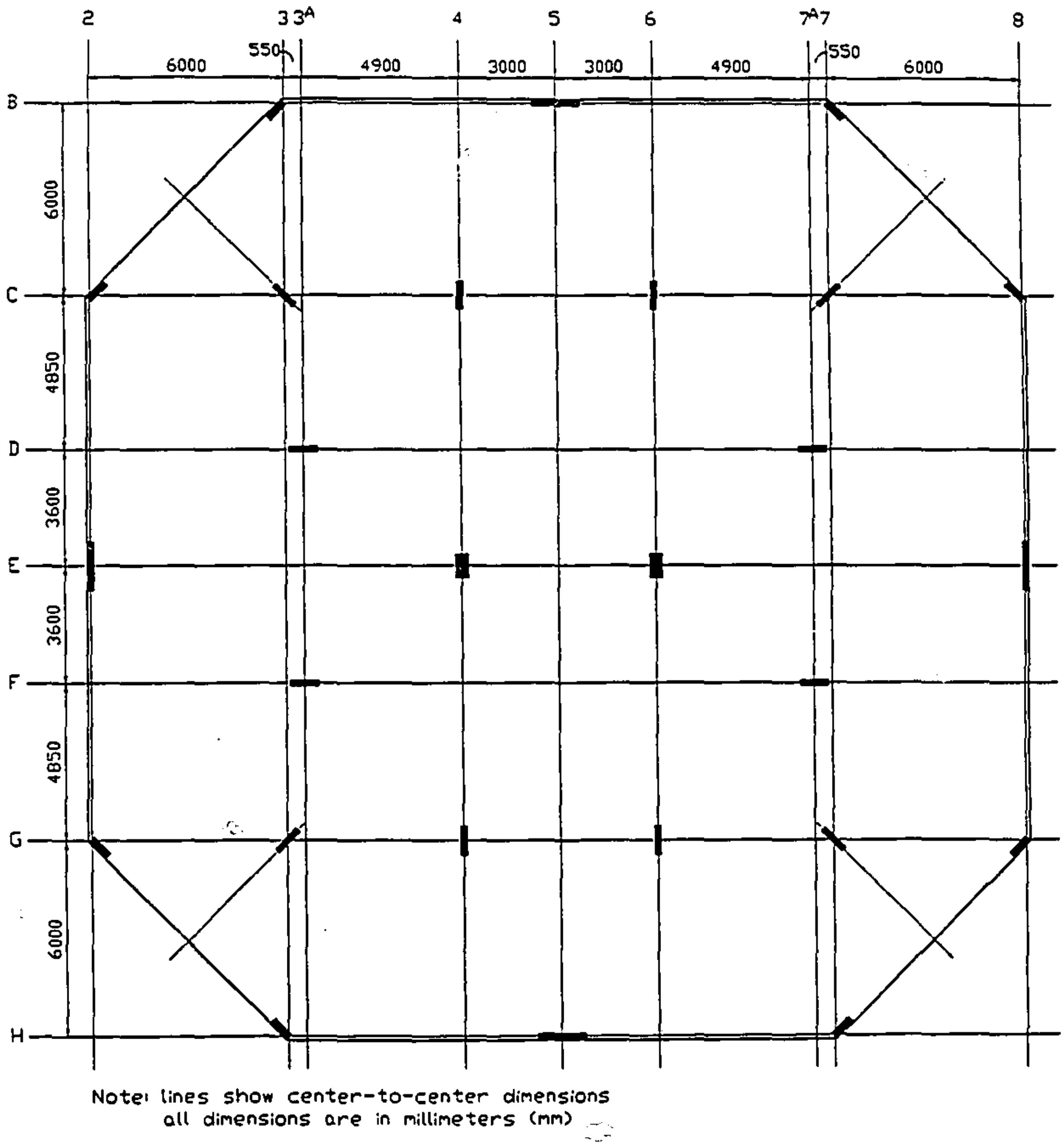

Figure 4.2: Floor Plan of Example Moment-Resisting Frame Structure

20 @ 2540 = 50800

	C3,C4,C6,C7 G3,G4,G6,G7	$D3^A$,$D7^A$ $F3^A$,$F7^A$	B5,H5 E2,E8	B3,B7,C2,C8 H3,H7,G2,G8	E4,E6
Roof					
20th					
19th					
18th					
17th	200 X 600	200 X 600			
16th					
15th					
14th					
13th					
12th					
11th			200 X 1500	220 X 720	400 X 750
10th					
9th	200 X 750	200 X 750			
8th					
7th					
6th					
5th					
4th					
3rd	200 X 900	200 X 900			
2nd					
Gr.fl.					

Note: all dimensions are in millimeters (mm)

Figure 4.3: Column Schedule for Example Structures

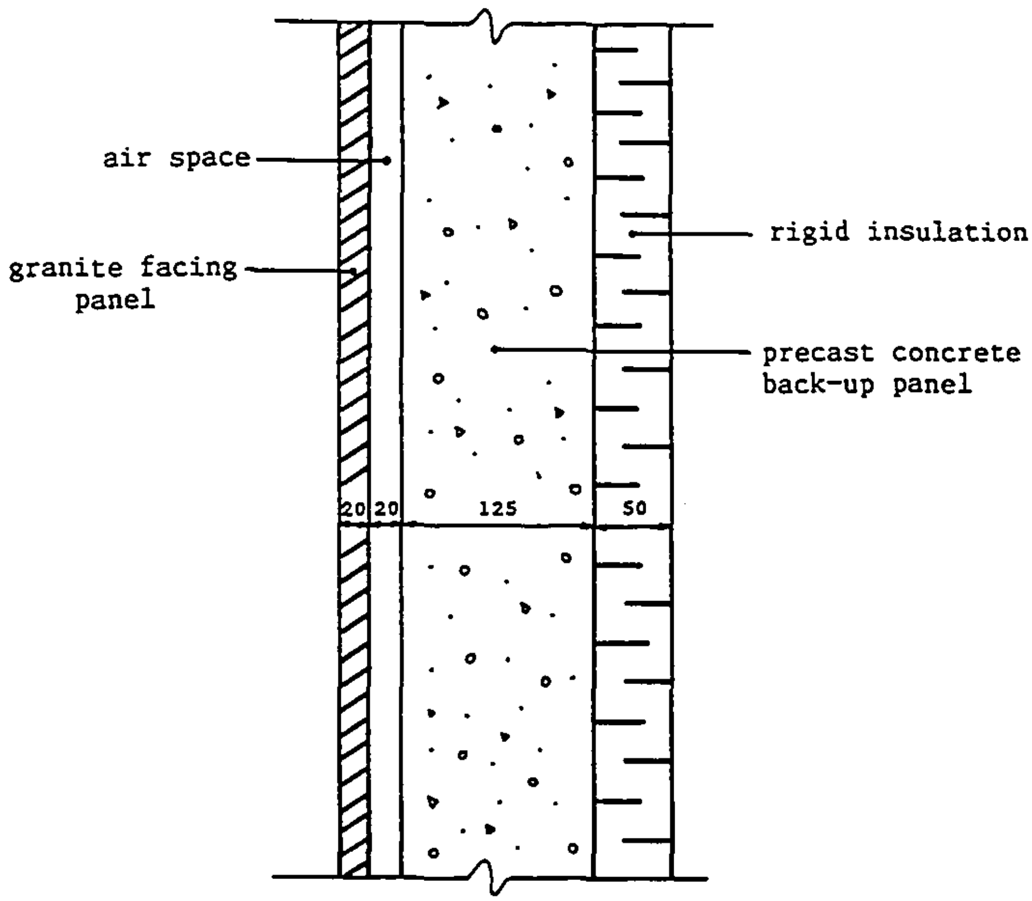

Note: dimensions are in (mm)

Figure 4.4: Cross-Section of Representative Cladding Panel

mm-thick precast concrete panel, to the face of which is secured a 20 mm-thick polished granite panel separated by a 20 mm.-wide air space. Rigid, 50 mm.-thick insulation is attached to the back of the panel. The air space behind the exterior facing eliminates water leakage. It does so by equalizing the pressure on the two sides of the exterior facing, hence preventing water from being forced in. This is known as the rain screen principle (Brookes 1983).

The panel is a full-storey high and a full-bay long, and it has two window openings, Fig. 4.5. It is lightly reinforced to prevent cracking, to provide strength for transportation and erection, and to support the panel in use.

Although the connections are designed to transmit only the loads resulting from the weight and mass of the panel, as referred to in Chapter 3, in fact they also serve to carry the forces that result from the interaction of the frame and panel as the structure deflects under lateral load. The types and stiffnesses of the connections, therefore, influence the panel's stiffening effect; hence, the connections are explained in some detail. Referring to Fig. 4.5, the panel is connected to the structural frame by two loadbearing connections, 1 and 5, near the bottom of the panel, and four angle tie-back connections, 2, 3, 4 and 6. Details of each connection are shown in Figs. 4.6, 4.7, and 4.8. Loadbearing connection 1 also constrains lateral displacement of the panel in its plane, while connection 5 differs in allowing lateral movement, by means of neoprene pads placed on each side of the HSS section, Fig. 4.8 (section A-A). In connections 2, 3, and 4, which are identical, vertical movement is allowed by the oversize hole in the angle, with the vertical slot in the attached plate; however, in-plane lateral displacements are restrained. The elongated hole in the angle leg welded to the slab permits adjustment during erection. The angle in connection 6 is the same as in 2, 3 and 4, except that the plate has a horizontal slot to permit in-plane lateral motion.

The connections described are typical of those used in Montreal and other eastern cities, and conform in their design, location and restraint conditions with the recommendations of the design manuals referred to in Section 3.2.

4.2 Behaviour of a Clad Moment-Resisting Frame

When an unclad moment-resisting frame is subjected to lateral loading, its stiffness is a function of the bending resistance of the columns, girders and joints, and of the axial rigidity of the columns. The horizontal shear is resisted by shear in the columns which causes the columns to bend in double curvature with points of contraflexure at approximately mid-storey-height levels. The moments applied to a joint from the columns above and below are resisted by the attached girders, which also bend in 'forward' double curvature, with points of contraflexure at approximately mid-span. These deformations of the columns and girders allow racking and horizontal deflection of the frame, Fig. 4.9.

When a moment-resisting frame, similar to the above, is clad with precast concrete panels that are attached in any of the recommended ways shown in Figs. 3.12 and 3.13, the

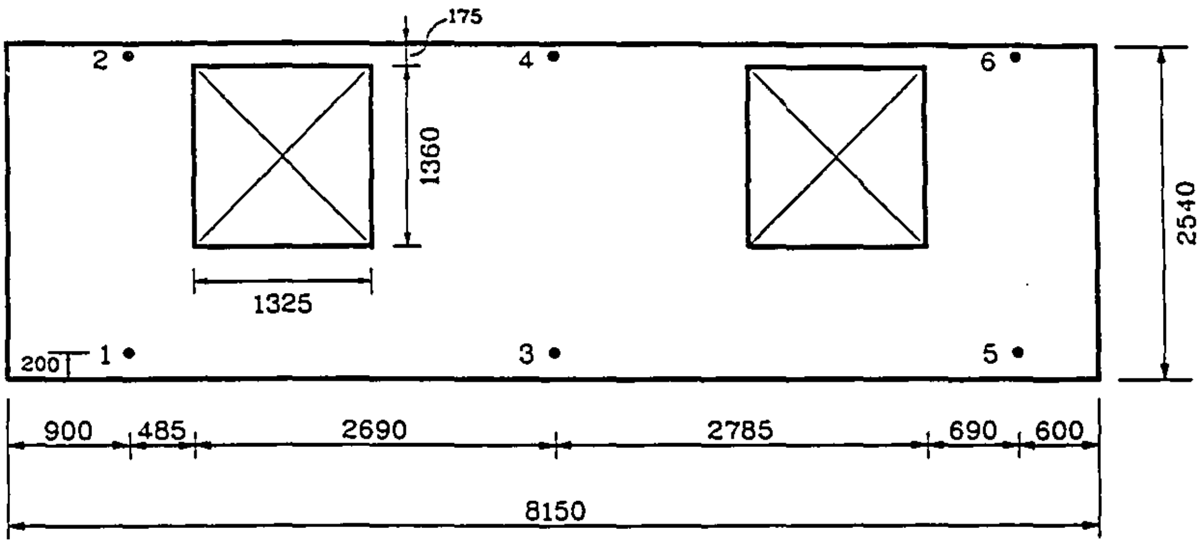

Note: all dimensions are in millimeters (mm)

Figure 4.5: Location of Connections in Representative Panel

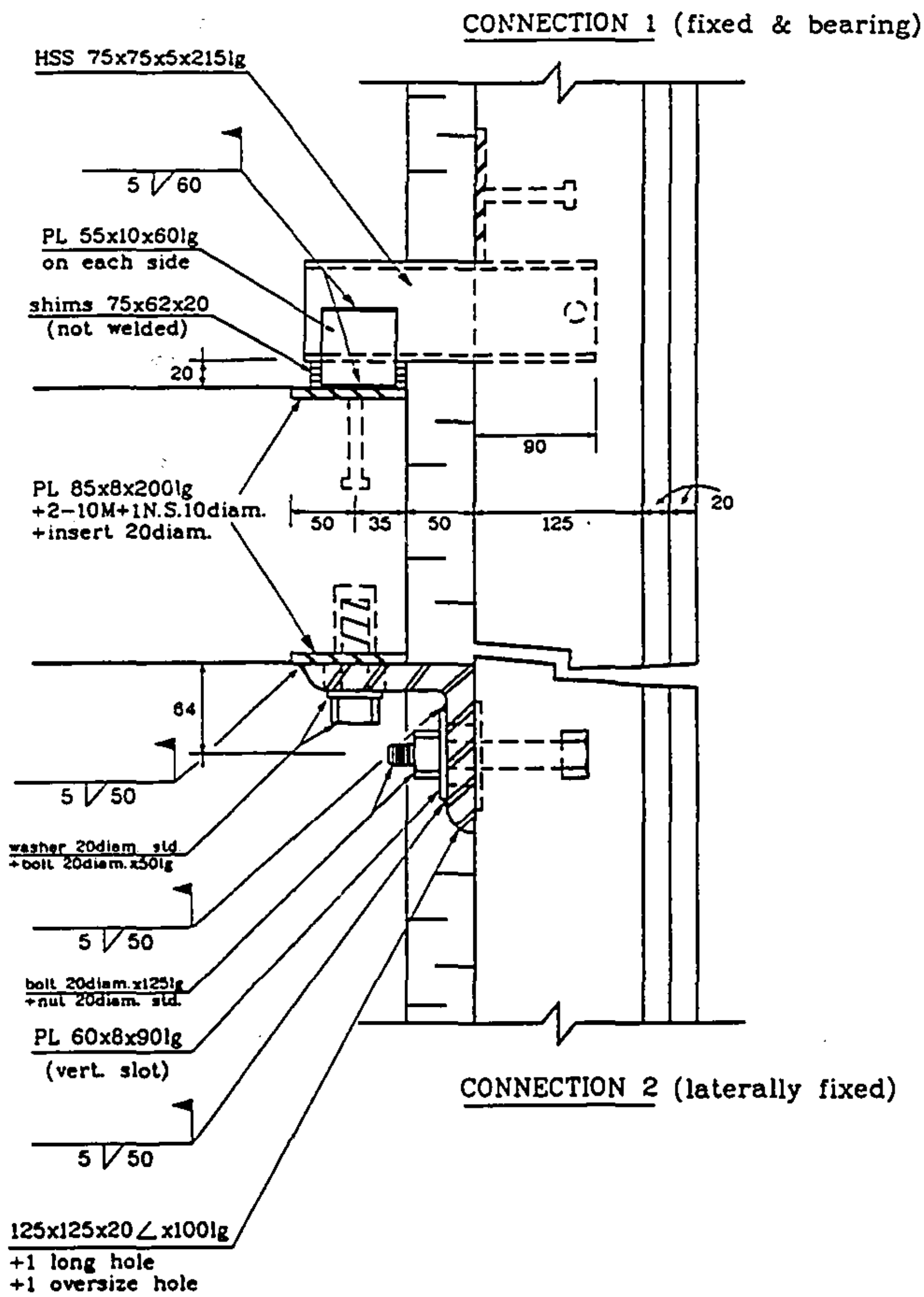

Figure 4.6: Details of Connections 1 and 2

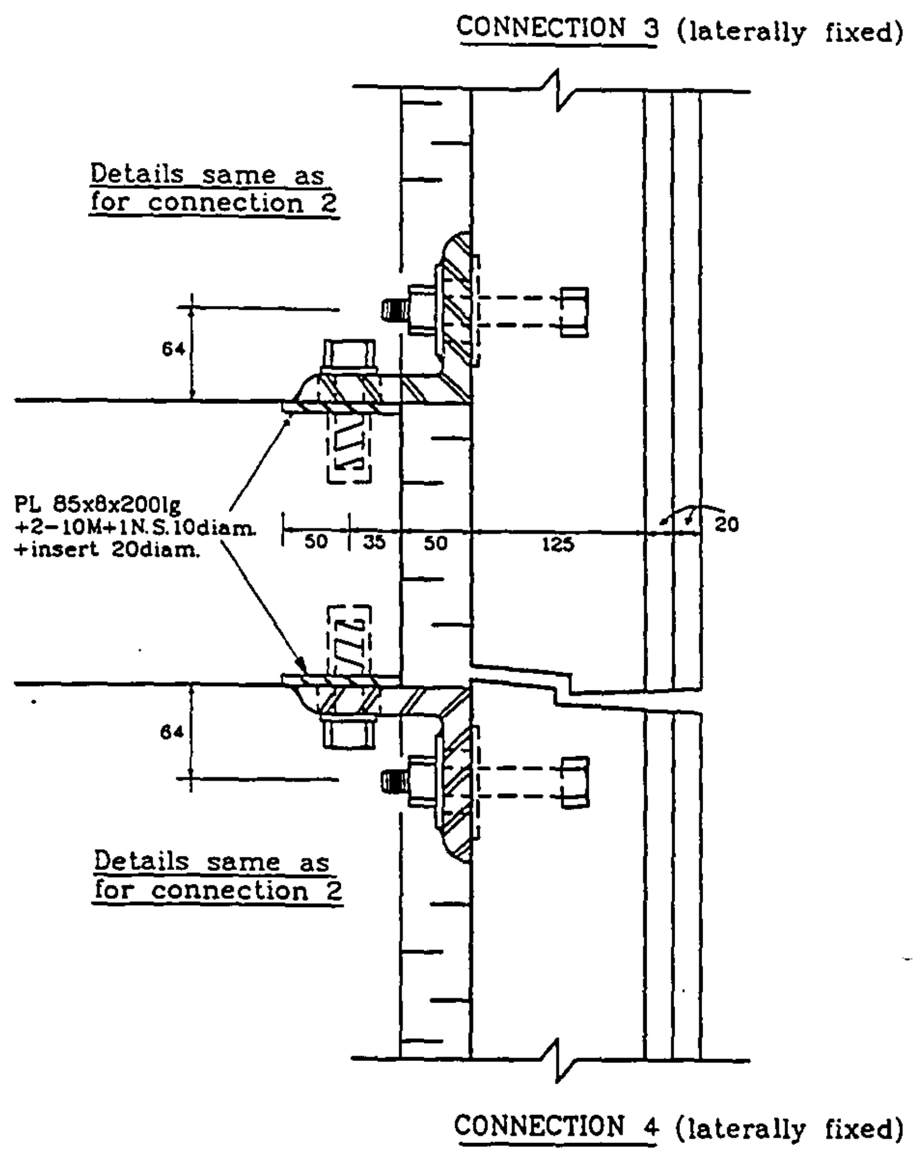

Figure 4.7: Details of Connections 3 and 4

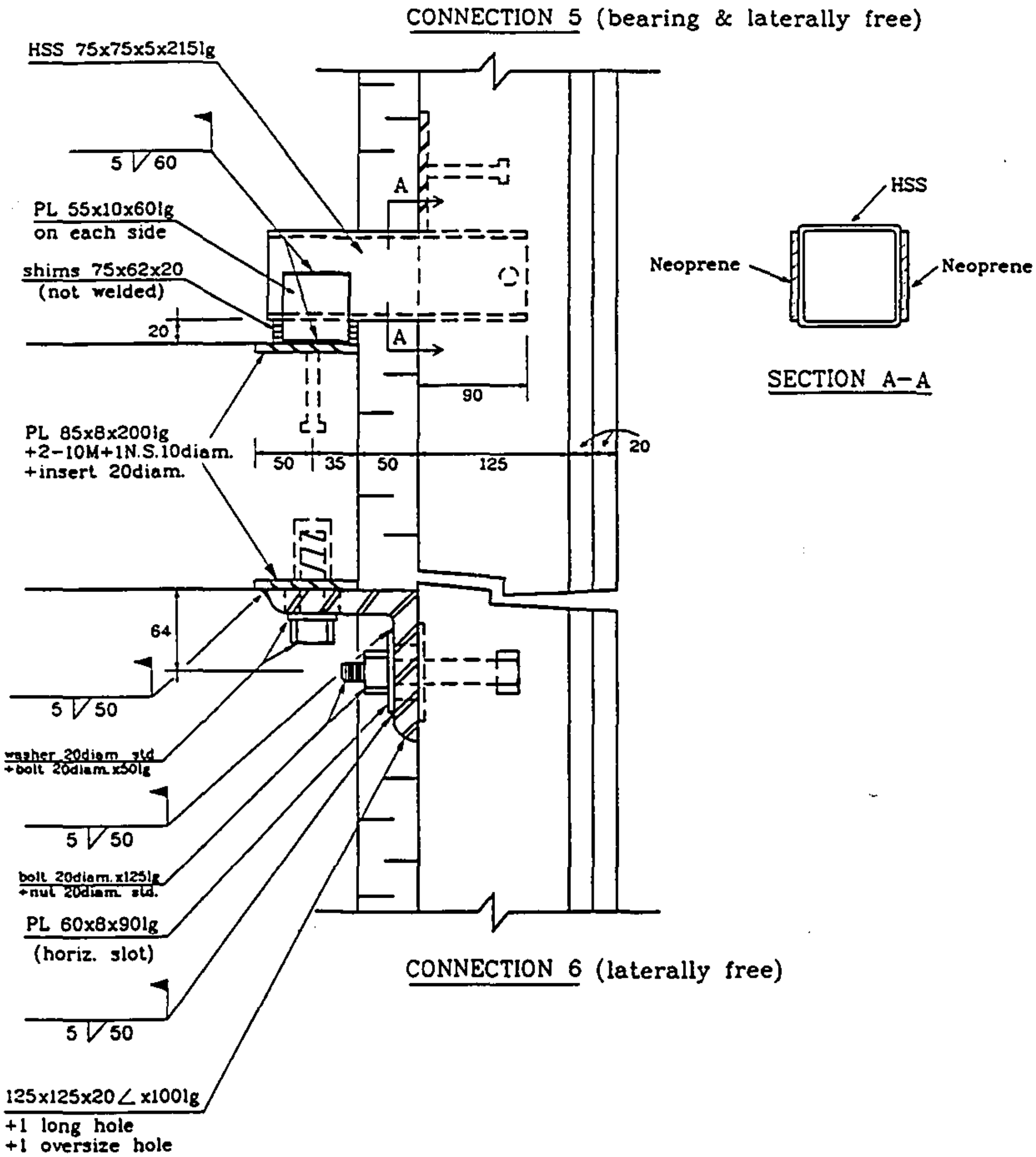

Figure 4.8: Details of Connections 5 and 6

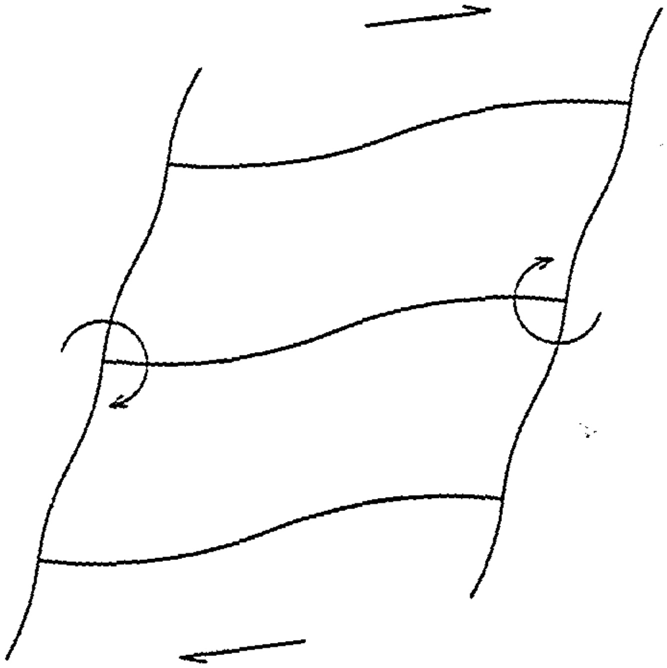

Figure 4.9: Racking of a Moment-Resisting Frame

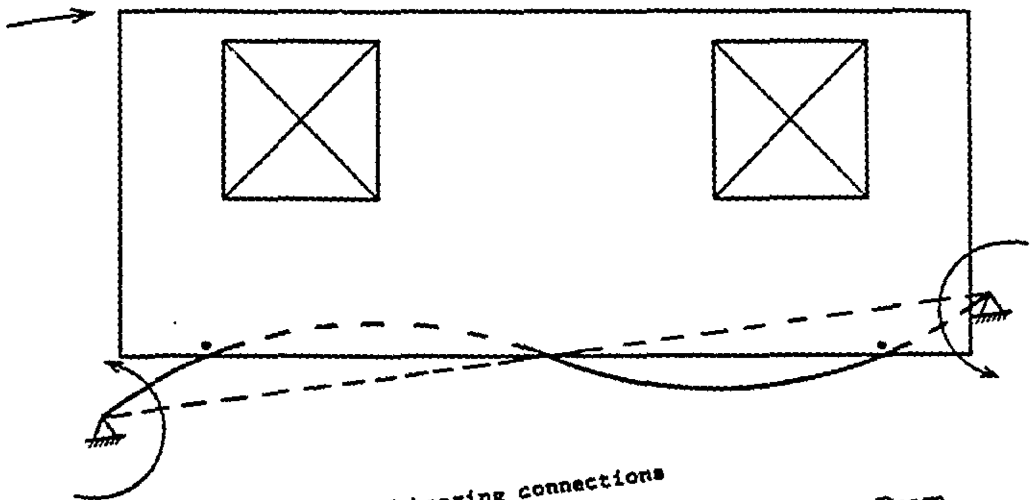

Figure 4.10: Laterally Loaded Panel Supported by Beam

lateral load behaviour of the structure is considerably altered.

As a means to understanding the behaviour of the clad moment-resisting frame, first consider a panel supported by only a beam and laterally loaded in its plane, as in Fig. 4.10. The panel deforms in shear as well as rotating with a corresponding 'backward' double-curvature bending of the beam. Considering next a typical storey of the frame with the panel attached and the structure subjected to shear. The resulting interaction between the frame and panel is a combination of the actions shown in Figs. 4.9 and 4.10, with opposing 'forward' and 'backward' double-curvature bending deformation of the beam, tending to cause a quadruple-curvature bending of the beam. The important net effect of this is to significantly stiffen the assembly. The degree to which the 'backward' double-curvature bending of the beam (associated with the in-plane rotation of the panel) counters its 'forward' double-curvature bending (associated with racking of the frame) determines the lateral stiffening of the structure. It is believed that the extent of the stiffening is also significantly dependent on the span-wise locations of the loadbearing connections.

In a typical storey of the panel-clad frame, the horizontal shear is carried mainly by the panel and the remainder by the columns, Fig. 4.11. The couple acting on the panel, resulting from the horizontal shear applied to the top of the panel and the horizontal reaction at the bottom, is resisted by the opposite couple due to the vertical reactions from the panel's loadbearing connections, which causes the beam to bend with the 'backward' double curvature. The horizontal shear carried by the columns is transferred as moments to the ends of the beams, causing them to bend in 'forward' double curvature.

4.3 Modelling the Slab as an Equivalent Beam

Flat plate structures under horizontal loading behave similarly to moment-resisting frames. The columns bend in double curvature and the slab deforms out of its plane in a three-dimensional form of double-curvature bending. If the columns are on a regular orthogonal grid, the response of the structure can be studied by considering a line of columns in the direction of loading, and the associated portion of slab, replaced by an equivalent moment-resisting frame bent. For the analysis, the slab is replaced by an equivalent beam with the same double-curvature bending stiffness as the slab. The flexural stiffness of the equivalent beam depends mainly on the width-to-length spacing of the columns and on the dimension of the columns in the direction of drift. Curves and equations based on these parameters are available to obtain an equivalent beam (Coull and Wong 1981).

In the example representative structures in which the precast concrete panels are supported by the slabs, the deformation of the slabs is more complex than described above. Therefore, the available curves for obtaining an equivalent beam are inappropriate for the portions of the slabs to which the panels are connected. When the structure is laterally loaded, the panel rotates in its plane, pulling the slab upwards by its bearing connection at the windward end and pushing the slab down by its bearing connection at the other end. Since the panel is supported at only two points and is not subjected to any other vertical force, the forces with which the panel pulls up and pushes down are equal in magnitude.

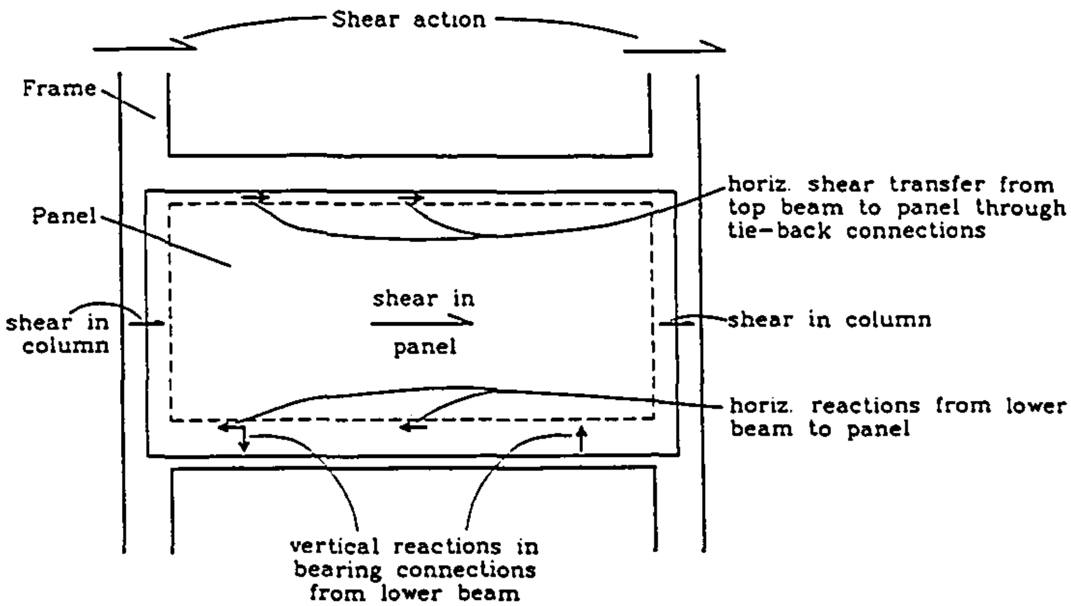

Figure 4.11: Transfer of Shear in a Typical Storey of a Panel-Clad Frame

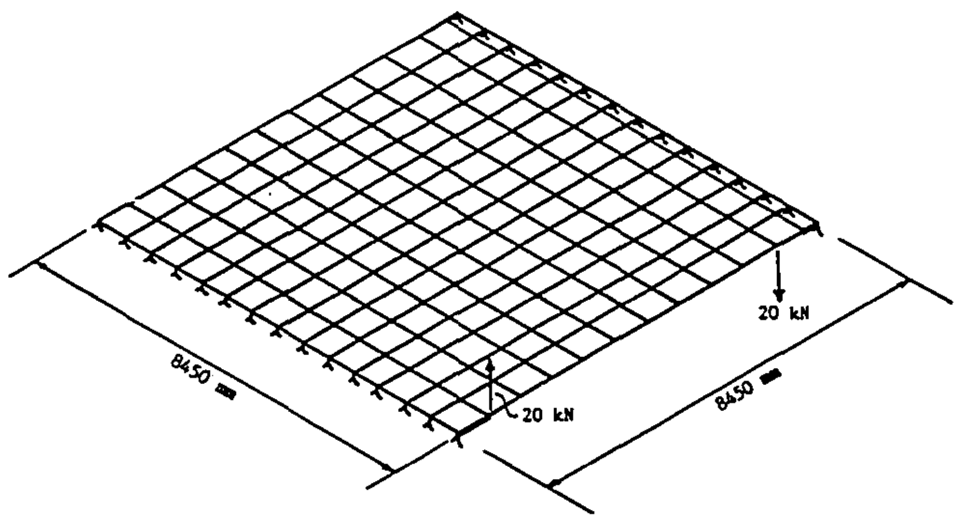

Figure 4.12: Mathematical Model of Slab Subjected to Equal and Opposite Vertical Forces

The vertical forces from the panel cause the slab to bend in double curvature, Fig. 4.10, in a direction, however, opposite to the double-curvature bending of the slab due to the racking of the frame, Fig. 4.9. Therefore, to obtain an equivalent beam for the slab subjected to this second mode of deformation, a finite element analysis of the slab was required.

A slab of both length and width equal to the length of one bay was analysed, Fig. 4.12. The side edges were assumed simply supported, while the end edges were assumed free. The rigid joint zones of the columns (AA' and BB' in Fig. 4.13) were represented by rigid arms at the exterior end edge. Vertical 20 kN loads were applied in opposite directions at the approximate points of location of the loadbearing connections. The slab was modelled by 168 plate bending elements, and a computer analysis was performed.

Using the moment area method of analysis and the results from the computer analysis, the flexural inertia of the equivalent beam was determined. The shear force and bending moment diagrams, and the elastic curve of the equivalent beam, are shown in Fig. 4.13. From the results of the slab analysis, the tangential deviation of point B on the elastic curve from the tangent through point A can be obtained, Fig. 4.13c,

$$| t_{B/A} | = .286143 + \frac{8150}{750}(.443613) = 5.10674 \tag{4.1}$$

The same tangential deviation can be determined using the moment area method, Fig. 4.13b,

$$\begin{aligned} t_{B/A} &= \frac{1}{EI}[0.5(-12071)(3090.9)(3709.1 + 600 + 0.667(3090.9)) \\ &\quad +0.5(14485)(3709.1)(600 + 0.333(3709.1)) \\ &\quad + 0.5(9656.6)(600)(0.667(600)) + (4828.4)(600)(300)] \\ &= \frac{-6.7469X10^{10}}{EI} \\ | t_{B/A} | &= \frac{6.7469X10^{10}}{EI} \end{aligned} \tag{4.2}$$

By equating the two tangential deviations, Eqs. 4.1 and 4.2, and using E = 20 kN/mm^2 (20000 MPa), the flexural inertia of the equivalent beam was found to be $6.6059X10^8$ mm^4.

It should be noted that the deformation of the slab is negligible at a perpendicular distance greater than half the length of the slab from the line of the applied loads, Fig. 4.14.

4.4 Mathematical Model of the Single-Storey Module of the Panel-Clad Frame

To study the interactive behaviour of the frame and panel, and to estimate the resulting lateral stiffening effect, structural analyses of a number of panel-frame modules were per-

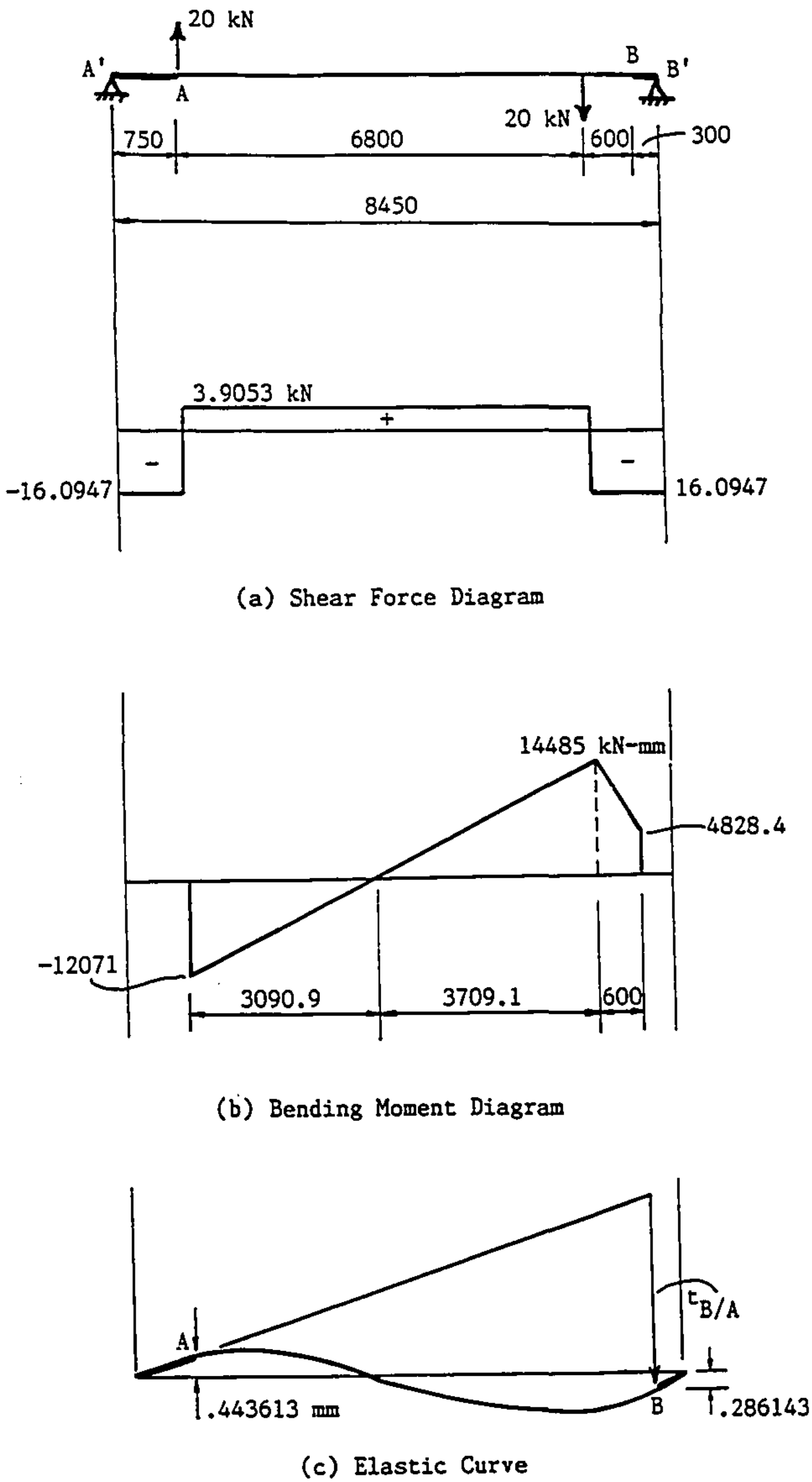

Figure 4.13: Force Diagrams and Elastic Curve of Equivalent Beam

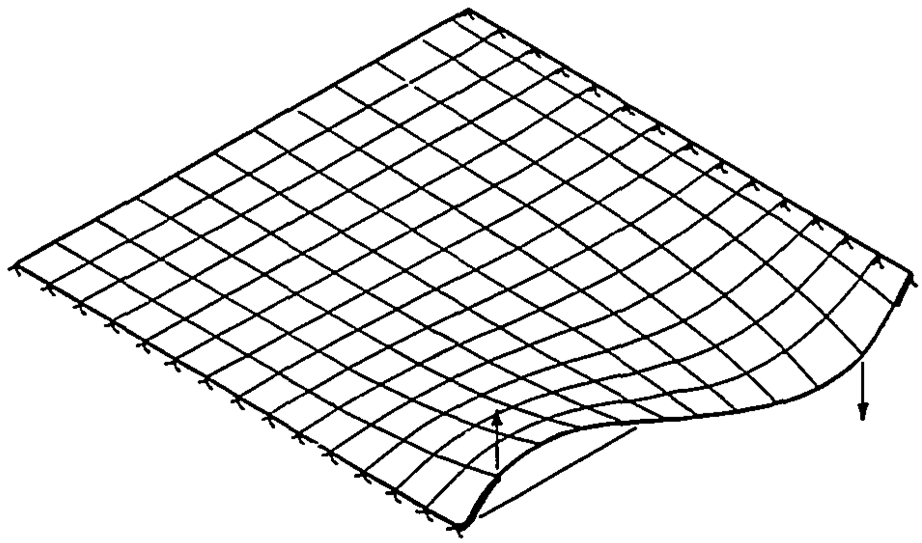

Figure 4.14: Deflected Shape of Slab

formed. A typical storey-height end-bay-width unit of the panel-clad frame was modelled as shown in Fig. 4.15. The moment-resisting frame to which the panel is connected is the same for each example structure, therefore, only one model was required.

To account for the panel's actual interaction with a full-sized beam, and for the effects of panels above and below and to one side of the considered module, a modified single-storey frame module was devised. It consisted of:

(a) a half-inertia column, $I = 2.8125X10^{10}\ mm^4$, at the left side of the bay, adjacent to the next clad bay,

(b) a full-inertia column at the right side, transformed to allow for its section being aligned at 45° to the panel plane, $I = 3.741X10^9\ mm^4$,

(c) a full-inertia beam at the bottom, as determined in the previous section, with rigid arms at the ends to represent the rigid joint zone of the columns, and

(d) an axially rigid three-part link at the top, whose purpose was to cause the tops of the columns and top connections of the panel to the frame to translate identically.

To neglect axial deformations in the frame members, the column and beam elements were assigned very large sectional areas. In addition, the top and bottom of the left column and, separately, the top and bottom of the right column were constrained to rotate identically. This provided a representation of the effects on the considered module of the clad modules above and below. The frame members were assigned a modulus of elasticity of 20 kN/mm^2 (20000 MPa).

The panel was modelled by a mesh of 240 membrane plane stress elements, having the thickness and modulus of elasticity of the precast concrete panel, that is, 125 mm and 20 kN/mm^2 (20000 MPa), respectively. The mesh was not uniform due to the asymmetric locations of the window openings, and of the connections of the panel to the structural frame.

The restraining connections were represented in the model by vertical and horizontal links with assigned axial stiffnesses equal to the separately calculated stiffnesses of the connections in the restrained directions. The vertical stiffness of the bearing connections, 1 and 5, was obtained by taking the inverse of the vertical flexibility of the connection. Referring to Fig. 4.16, the vertical flexibility of the connections can be expressed as

$$f_{1v} = f_{5v} = \left(\frac{L^3}{3EI}\right)_{HSS\ in\ flex.} + \left(\frac{L}{GA}\right)_{HSS\ in\ shear} + \left(\frac{L}{AE}\right)_{comp.\ plates} \qquad (4.3)$$

Other factors such as bending of the steel section in the concrete, rotational restraint due to the side plates at the outer end of the steel section, and local deformation of the panel were not considered in calculating the stiffnesses of the bearing connections 1 and 5. These were found to virtually compensate each other as is shown in Table 4.1, where the stiffness of a cantilever with an effectively longer length decreases, but if its free end is restrained against rotation, the stiffness increases considerably. An approximate flexibility

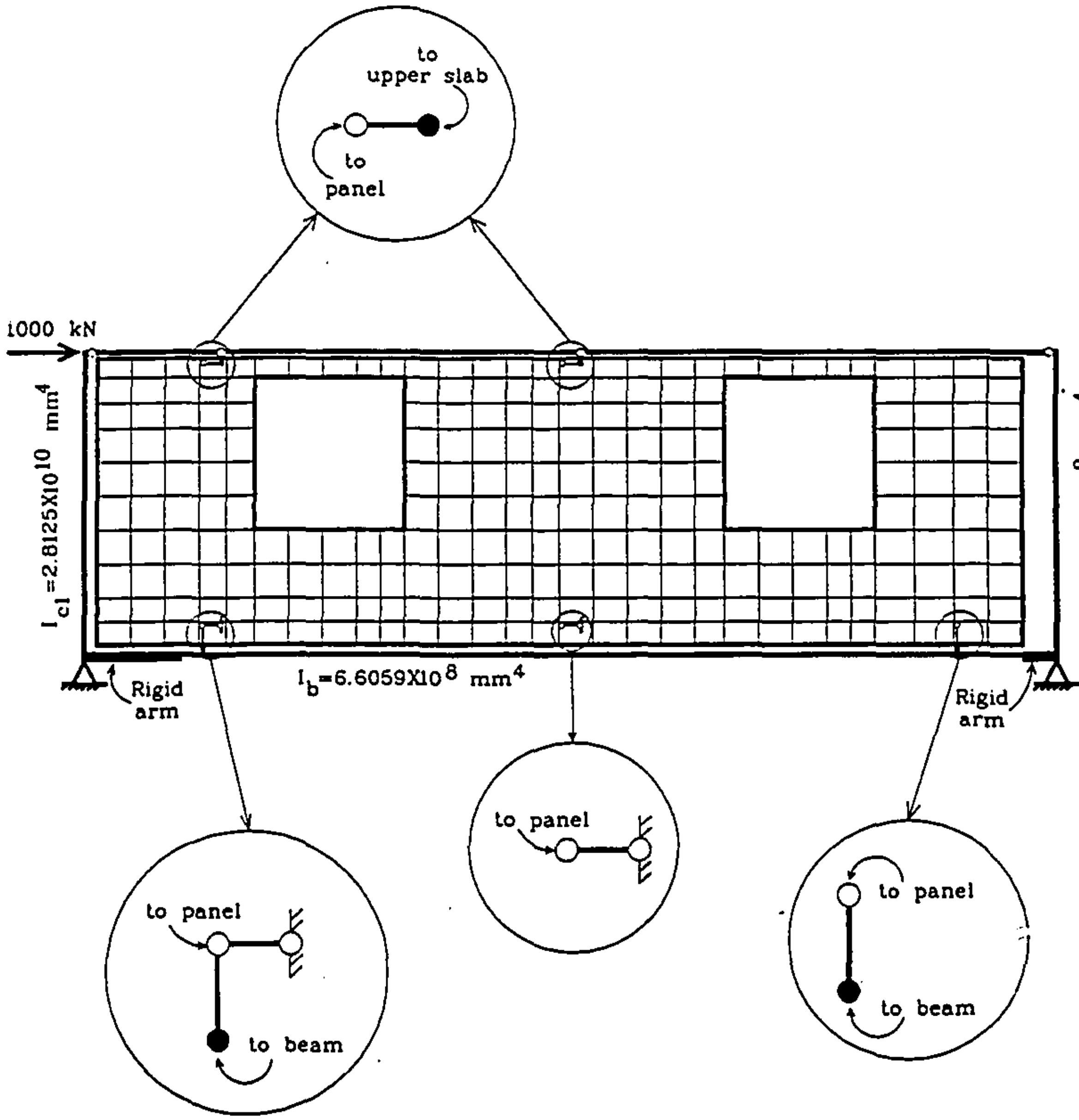

Figure 4.15: Mathematical Model of Panel-Clad Frame

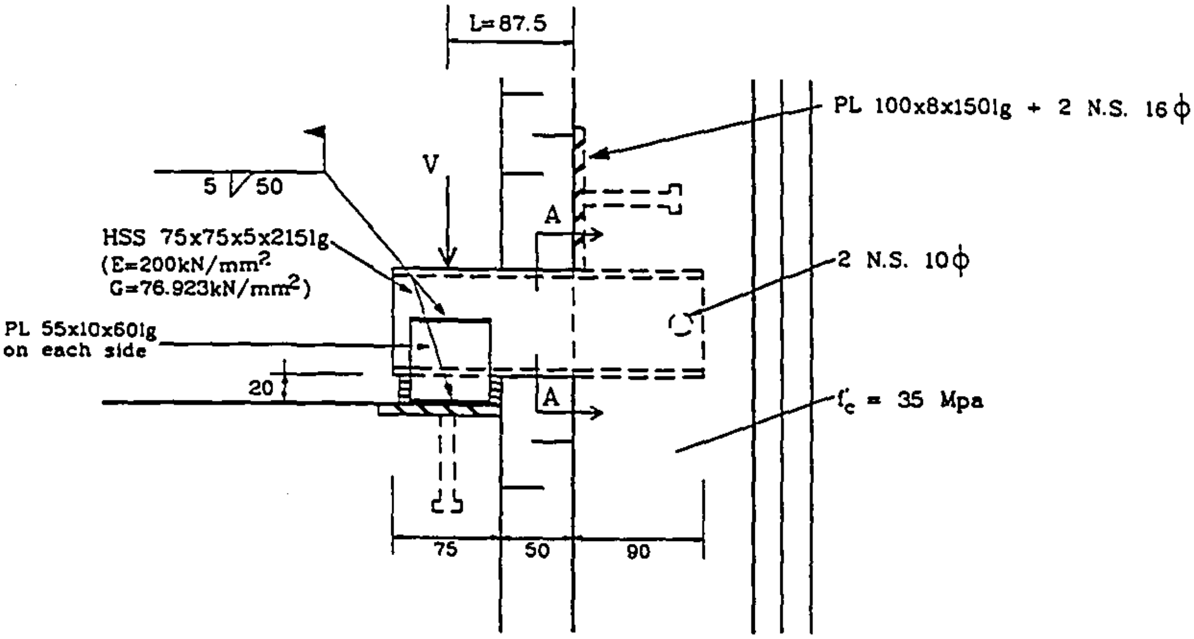

Figure 4.16: Details of Steel Haunch Bearing Connection

	STIFFNESS* (kN/mm)
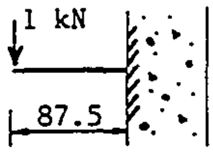	526.0
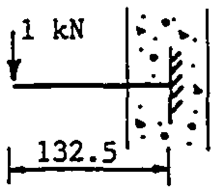	203.9
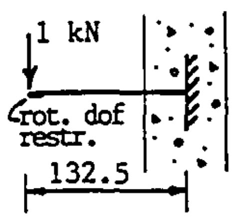	452.3

*Does not include axial flexibility of plates

Table 4.1: Influence of the HSS's Effective Length and End Condition on the Overall Connection Stiffness

of the connections, as given in Eq. 4.3, was considered to be adequate for the model due to the large number of variables that would be involved in computing this more exactly. Therefore, substituting numerical values for the variables in Eq. 4.3 and inverting the resulting flexibility produced an approximate value of 450 kN/mm for the vertical stiffness of the connection. The fictitious equivalent vertical link was 200 mm long and was assumed to be of steel (E = 200 kN/mm^2 or 200000 MPa), hence its axial area was found to be 450 mm^2.

Connection 5 does not provide any restraint in the lateral direction, therefore no horizontal link was provided at its location. However, connection 1 was designed to prevent lateral movement, hence a horizontal link with an axial stiffness equivalent to the lateral stiffness of the connection was provided. The flexural stiffness of the side plates as well as the stiffness of the HSS in flexure, shear and torsion were used to compute the overall lateral stiffness of the connection. The deformation of the plates subjected to lateral loading is shown in Fig. 4.17. The lateral stiffness of the plates can be approximated by

$$k_{plates} = \left(\frac{12EI}{L_{AB}^3}\right)_{plate\ 1} + \left(\frac{12EI}{L_{DE}^3}\right)_{plate\ 2} \tag{4.4}$$

The lateral flexibility of the HSS, Fig. 4.18, is

$$f_{HSS} = \left(\frac{L^3}{3EI}\right) + \left(\frac{L}{GA}\right) + \left[\frac{L}{GJ}(lever\ \ arm)^2\right] \tag{4.5}$$

Substituting numerical values for the variables in Eqs. 4.4 and 4.5, adding the inverse of Eq. 4.4 to Eq. 4.5, and inverting the result produced an approximate value for the lateral stiffness of connection 1 equal to 200 kN/mm. Assuming the horizontal link to be 150 mm long and also made of steel, the axial area for the link was taken as 150 mm^2.

Connections 2, 3 and 4 were modelled by horizontal links only, since these connections permit movement in the vertical direction. The lateral flexibility of each of these connections can be approximated by adding the shear flexibilities of the legs of the angle, Fig. 4.19, that is

$$f_{2H} = f_{3H} = f_{4H} = \left(\frac{h}{GA}\right)_{leg\ 1} + \left(\frac{h}{GA}\right)_{leg\ 2} \tag{4.6}$$

The inverse of Eq. 4.6 gives the lateral stiffness of the connection. Therefore, substituting the relevant numerical values in Eq. 4.6, and inverting the result produced a value of 1167 kN/mm for the lateral stiffness of connections 2, 3 and 4. The axial area for 150 mm long steel horizontal links was, thus, found to be 875 mm^2.

Connection 6 does not restrain the panel from moving in either the lateral or vertical directions; therefore, no links were provided at the location.

A summary of the estimated stiffnesses of the connections and the factors used in their

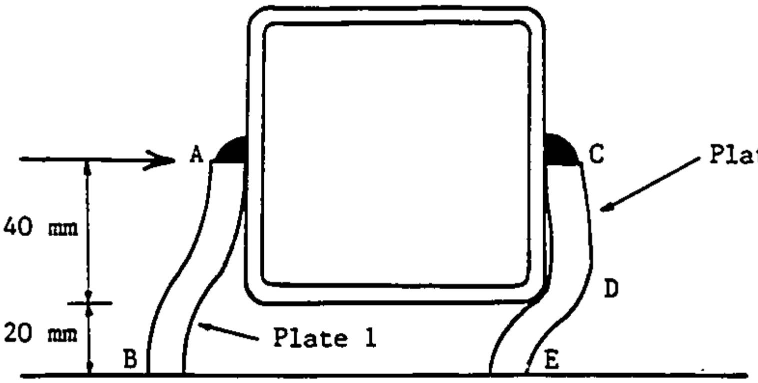

Figure 4.17: Elastic Deformation of Side Plates Under Lateral Loading

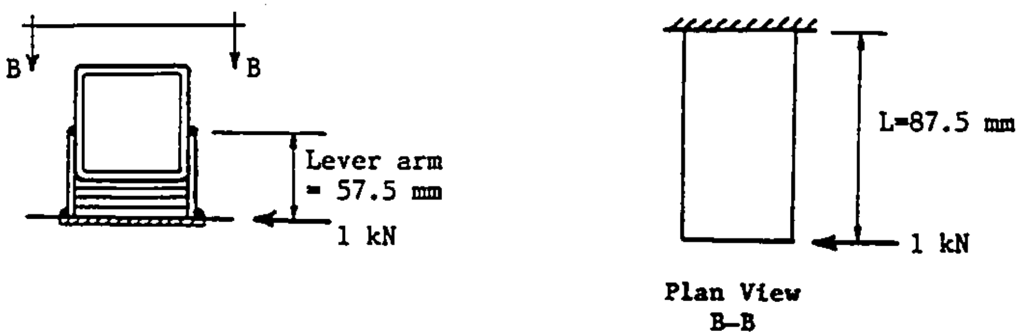

Figure 4.18: HSS Section Subjected to Lateral Load

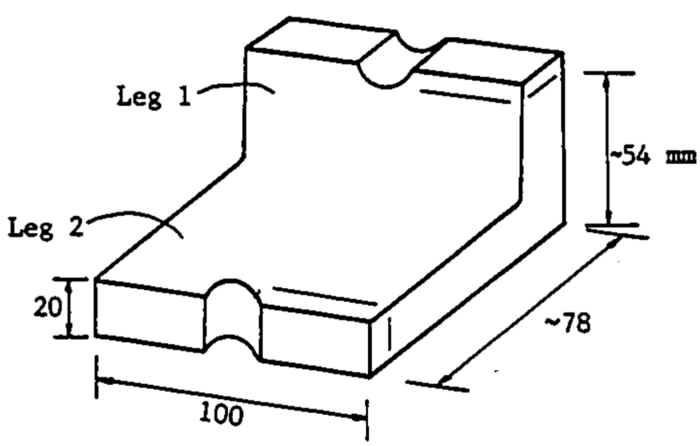

Figure 4.19: Dimensions of Angle Required to Calculate its Flexibility

determination are given in Table 4.2. The arrangements of the links in the model are shown encircled in Fig. 4.15.

4.5 Lateral Load Analyses of the Single-Storey Module

The first step to estimating the lateral stiffening effect of the cladding panel was to perform a lateral load analysis of the structural frame without any cladding panels attached to it. Considering the unclad frame, the moments from the columns cause the slab to deform in double-curvature bending as described in the first paragraph of Section 4.2. Hence an equivalent beam with properties based on the width-to-length spacing of the columns, and on the dimensions of the columns, was determined. The effective slab width ratio, for $b/Y' > 1$, is given as (Coull and Wong 1981)

$$\frac{Y_e}{Y} = \frac{h}{Y} + \frac{Y'}{Y}\left[1 - 0.4\left(\frac{b}{Y'}\right)^{-1}\right] \tag{4.7}$$

where h = wall or column thickness,
Y = bay width,
$Y' = Y - h$, and
b = clear span between walls or columns.

The effective width of an end bay is taken to be 45 percent of the corresponding interior value, given by Eq. 4.7. This is slightly less than half the value for a full interior bay because it is less restrained against transverse rotation than an interior bay. By substituting b = 7400 mm, Y = 6000 mm, and h = 200 mm into Eq. 4.7, an effective width of 4182 mm was calculated. Taking 45 percent of this value for the end span, the flexural inertia for the equivalent beam was obtained as $I_b = 1.2545X10^9\ mm^4$.

The frame was analysed for a lateral load of 1000 kN, Fig. 4.20. For further reference, this will be denoted as analysis I. The complete module, Fig. 4.15, with the panel and its connections modelled as described in Section 4.4, was then analysed (analysis II) for the 1000 kN load. A series of analyses of the panel-frame module with the components in various states of attachment and rigidity was performed. The purposes of the analyses were as follows:

(a) to determine the individual effects of the flexibilities of the panel, horizontal connections, and vertical connections;

(b) to determine the mode of interaction between the panel and frame;

(c) to determine the order of the increase in stiffness of the frame with cladding over that of the unclad frame, and

(d) to compare the sensitivity of the panel-clad frame's lateral flexibility to the flexibility of the panel and its connections, with the sensitivity of the same structure's flexibility to the flexibility of the beam.

Connection No.	Restraint Directions	Factors Affecting Flexibility of Connections in Restraint Directions	Approx. Stiffness Values (kN/mm)
1	Horizontal: Vertical: Out-of-plane:	Plates-flex., HSS-flex., shear, tors. HSS in flex. & shear, comp. of plates (not relevant)	200 450
2	Horizontal: Out-of-plane:	Sum of shear flexibilities of legs (not relevant)	1167
3	Horizontal: Out-of-plane:	Sum of shear flexibilities of legs (not relevant)	1167
4	Horizontal: Out-of-plane:	Sum of shear flexibilities of legs (not relevant)	1167
5	Vertical: Out-of-plane:	HSS in flex. & shear, comp. of plates (not relevant)	450
6	Out-of-plane:	(not relevant)	—

Table 4.2: Stiffness Values of Connections

Descriptions, and references to figures, of the analyses performed to achieve the above objectives and their salient results are given in Table 4.3.

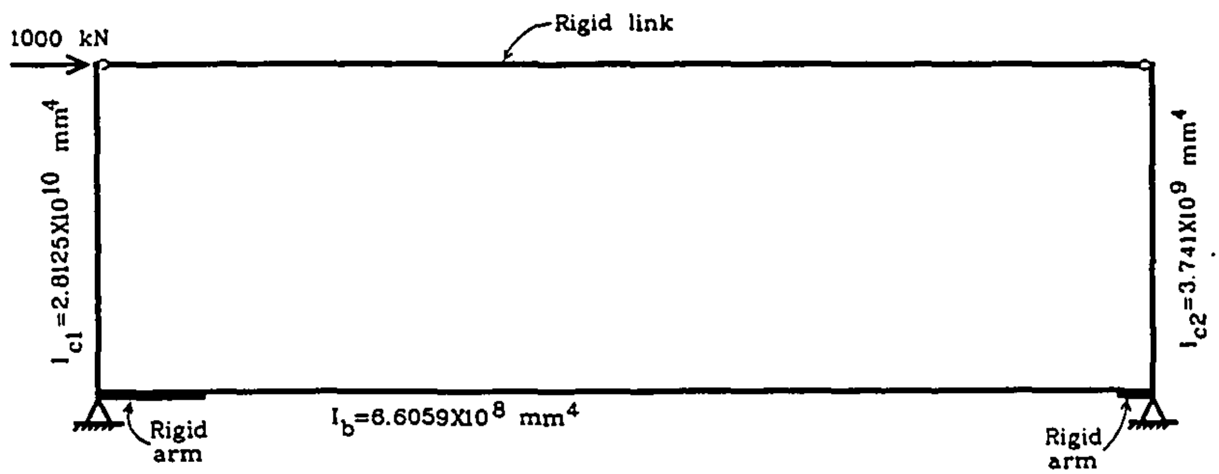

Figure 4.20: Mathematical Model for Unclad Frame (Analysis I)

Analysis No.	Description	Ref. Figure	Top Displ. (mm)	Flexibility (mm/kN)
I	Structural frame alone without panels	4.20	126.35	$126.35X10^{-3}$
II	Complete module, that is, panel connected to actual frame	4.15	3.62	$3.62X10^{-3}$
III	Panel and horizontal connections only and supported vertically at the locations of bearing conn.	4.21	4.17	$4.17X10^{-3}$
IV	Complete module, but effectively without columns i.e assigning these a very small inertia, and with the beam assigned to be effectively rigid	4.22	4.71	$4.71X10^{-3}$
V	Complete module, but effectively without columns	4.23	17.08	$17.08X10^{-3}$
VI	Complete module, but with panel and connections assigned to be effectively rigid	4.24	0.52	$0.52X10^{-3}$
VII	Complete module, but with beam assigned to be effectively rigid in flexure	4.25	1.51	$1.51X10^{-3}$

Table 4.3: Description of Analyses and their Salient Results

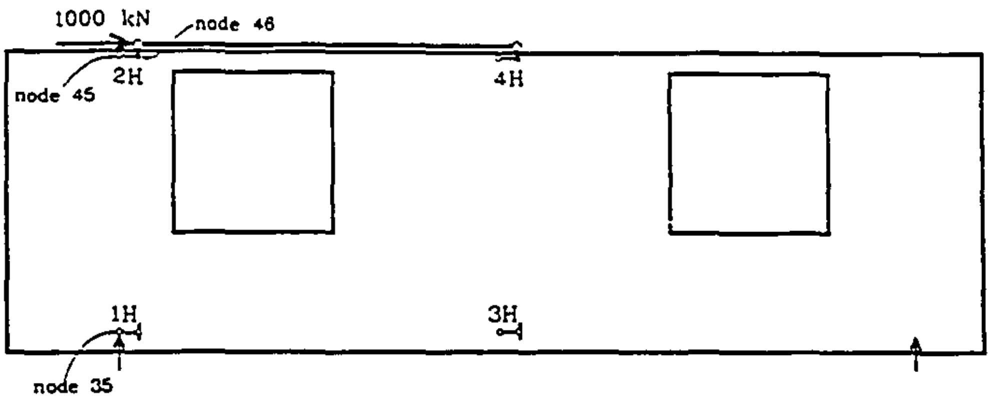

Figure 4.21: Model for Analysis III

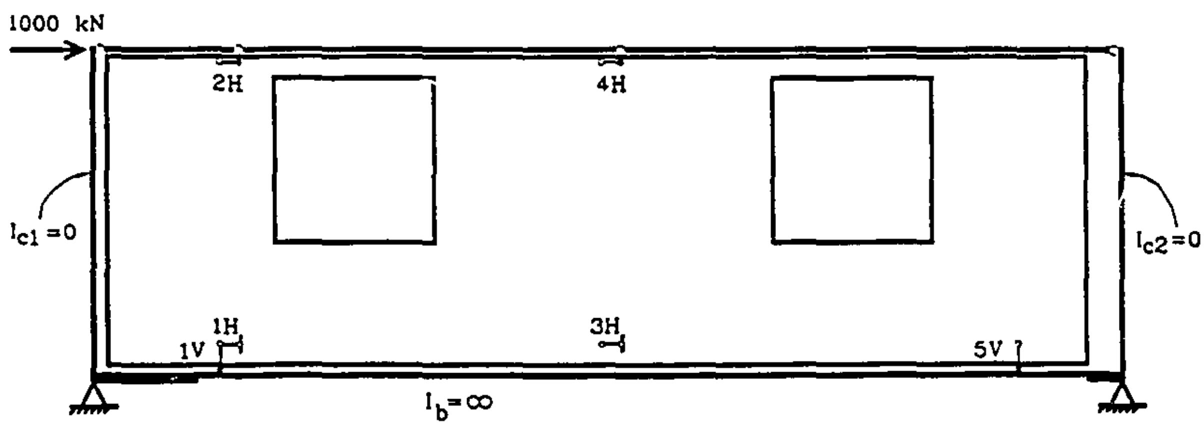

Figure 4.22: Model for Analysis IV

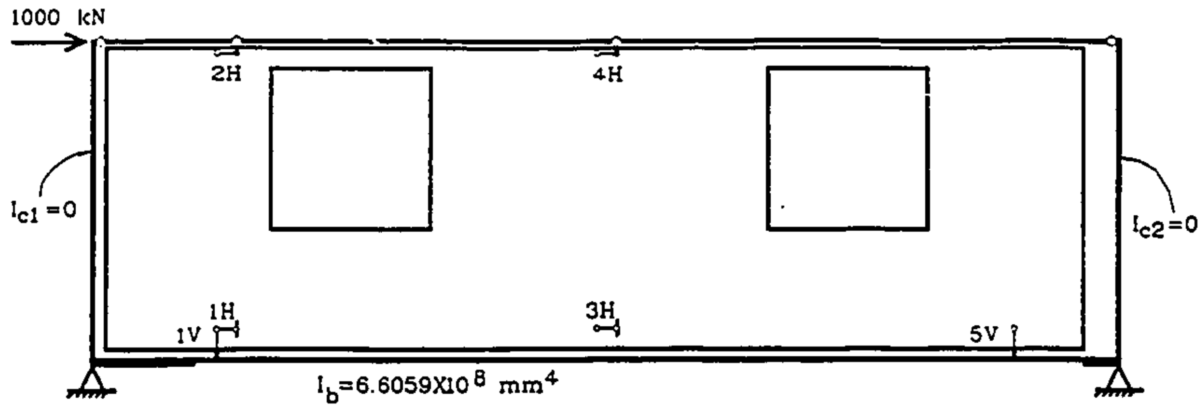

Figure 4.23: Model for Analysis V

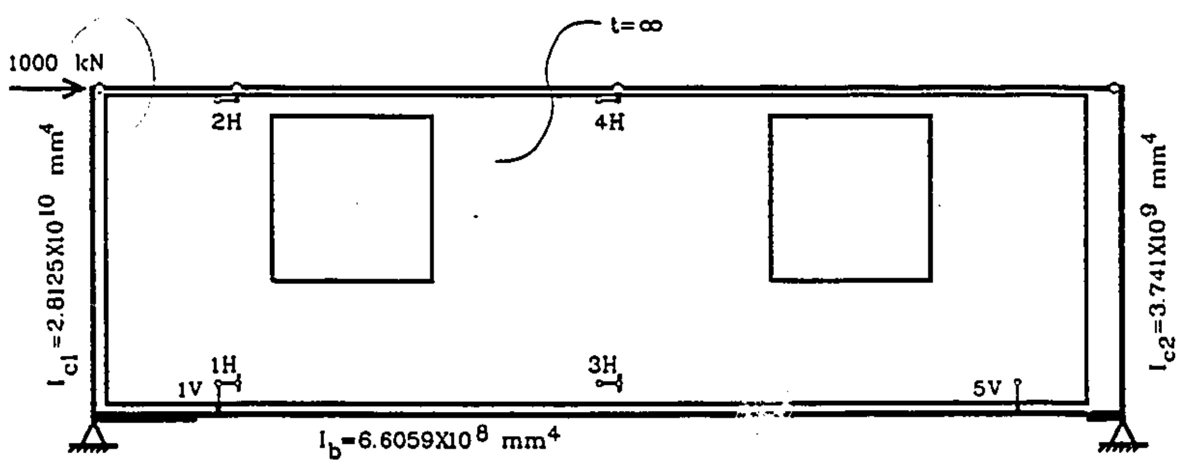

$A_{1H}=A_{2H}=A_{3H}=A_{4H}=A_{1V}=A_{5V}=\infty$

Figure 4.24: Model for Analysis VI

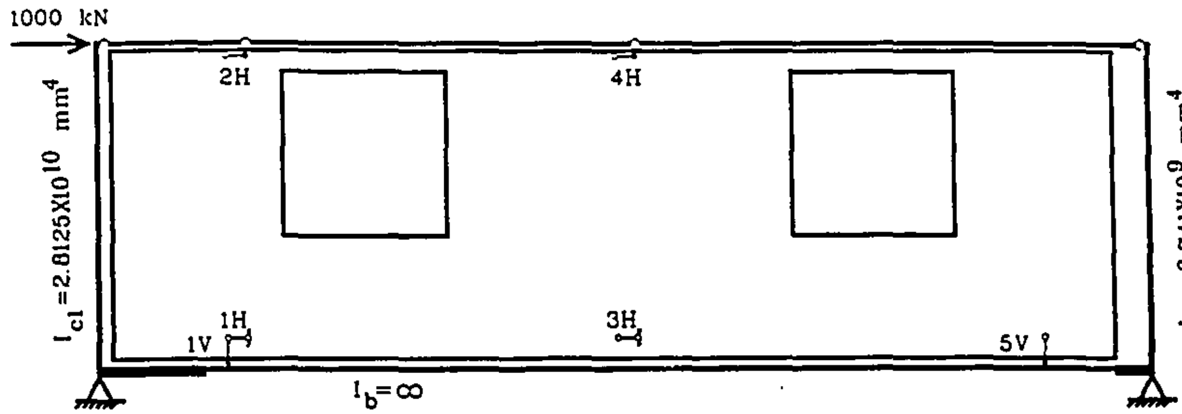

Figure 4.25: Model for Analysis VII

CHAPTER 5

DISCUSSION OF RESULTS FROM ANALYSES OF A SINGLE-STOREY MODULE

The results obtained from the lateral load analyses of the previous section were studied in detail to determine the behaviour of the structural frame with the precast concrete panel attached to it. In an attempt to generalize the structural problem, so as to allow a clearer understanding of its complex behaviour, a spring model of the frame and the panel with its connections has also been developed. The conclusions drawn, although for only one particular type of precast concrete panel, are extended to other possible types of panels.

5.1 Discussion of Results

5.1.1 Individual Flexibilities of the Panel and its Connections

In interpreting the results of the analyses, it was convenient to consider the flexibilities of the panel and the components, and their individual effects on the lateral flexibility at the top of the single-storey module. From these a good indication of the relative participation of the various components in the lateral flexibility and stiffness of the structure was obtained.

From analysis III, the effect of the panel's and the horizontal connections' flexibilities on the lateral flexibility of the module was obtained. Referring to Fig. 4.21, the effect of the panel's flexibility was obtained by taking the difference between the displacements of nodes 45 and 35, and dividing by the applied load, giving $f_p = 3.0014X10^{-3}$ mm/kN. The effect of the horizontal connections' flexibilities was obtained by summing the displacement of node 35 with the difference in displacements of nodes 46 and 45, and dividing the result by the applied load, giving $f_{hc} = 1.1701X10^{-3}$ mm/kN. This flexibility, f_{hc}, represents the total effect of the individual flexibilities of the horizontal connections. The load carried by the horizontal connections is shared between the individual horizontal connections according to the spring model in Fig. 5.1. The flexibility f_{hc} could have been obtained, alternatively, by substituting the calculated stiffness values of each horizontal connection, Section 4.4, into Fig. 5.1.

In analysis IV the beam was effectively rigid, and the influence of the vertical connections was accounted for, in addition to the panel and horizontal connections. Therefore, the

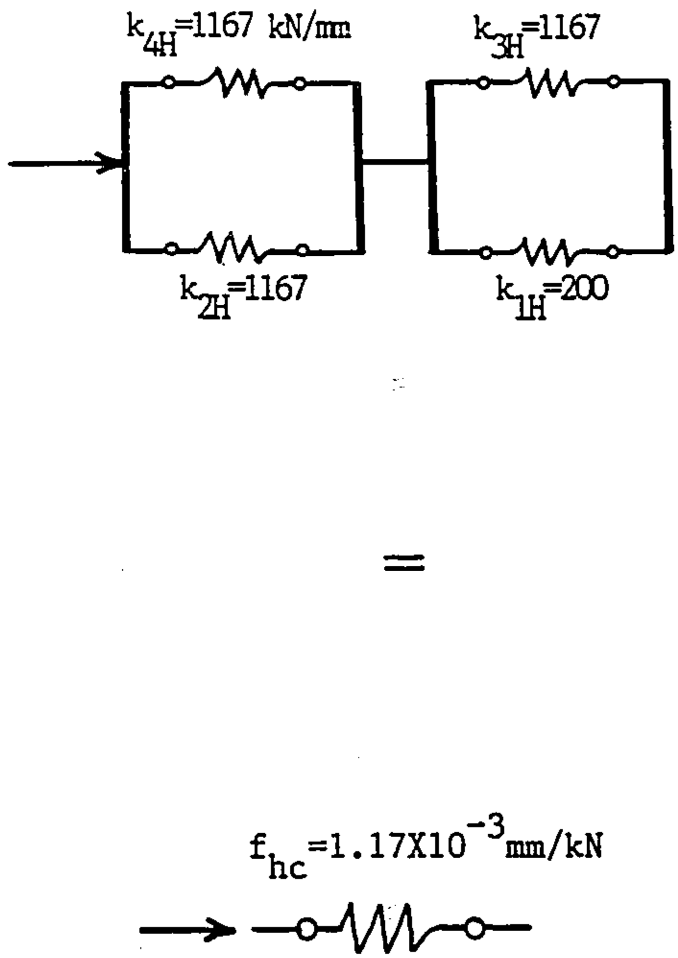

Figure 5.1: Spring Model for Effect of Flexibilities of Horizontal Connections

effect of the flexibility of the vertical connections is the difference between the flexibilities of analyses III and IV, that is, $0.54X10^{-3}$ mm/kN.

5.1.2 Interactive Behaviour of Panel and Frame

The modes of deformation for the load applied to the frame alone (Analysis I), for the panel supported by the beam (Analysis V), and for the panel-clad frame (Analysis II) are presented in Fig. 5.2.

Now consider superimposing the effects of the racking unclad frame and the panel's forward rotation. The combined interactive behaviour of the 'forward' double-curvature bending of the beam due to racking of the frame, Fig. 5.2a, and the 'backward' double-curvature bending caused by the panel's forward rotation, Fig. 5.2b, results, in this particular structure, in a net deformation of the beam resembling a downward-displaced 'forward' quadruple-curvature bending, Fig. 5.2c. The net downward displacement appears to be due to having a longer rigid arm at the windward end of the beam which, as it rotates, imposes a larger downward displacement on the beam at that end. This downward displacement modifies the quadruple-curvature bending deformation imposed on the beam by the combined behaviour, and it also causes the unsymmetrical mode of deformation of the structure.

It can be observed in Fig. 5.2c that a significant part of the rotation of the windward vertical edge of the panel, which is larger than the overall rotation of its lower horizontal edge, can be attributed to the panel deforming in shear, especially in the regions of the window openings where the panel is significantly more flexible in shear. The effective shearing stiffness of the panel can be considered as resulting from the deformations of a five-part shear block assembly in which the middle and end blocks are very much stiffer in shear than the two blocks at the window openings.

5.1.3 Stiffening Effect of Panel-Clad Frame

By comparing the results of analyses I and II, Table 4.3, it is found that the shearing stiffness of the storey-height module with the panel attached is 35 times that of the bare frame. It is very evident from this that the precast concrete panel, even though connected to the frame in the recommended way, gives rise to a high degree of composite action between it and the frame, and significantly stiffens the structure against lateral loading. The previously described 'backward' and 'forward' double-curvature modes of bending of the beam, which interact to cause a quadruple-curvature mode of deformation involve a much greater amount of strain energy, thereby causing the increase in stiffness of the structure.

The interaction and deformations described above can be more simply represented by the mechanism in Fig. 5.3 with the panel, through its connections, significantly restraining the lateral in-plane displacements of the clad frame relative to those of the unclad frame, and where the flexibility of the panel around the window openings is modelled as a flexible beam.

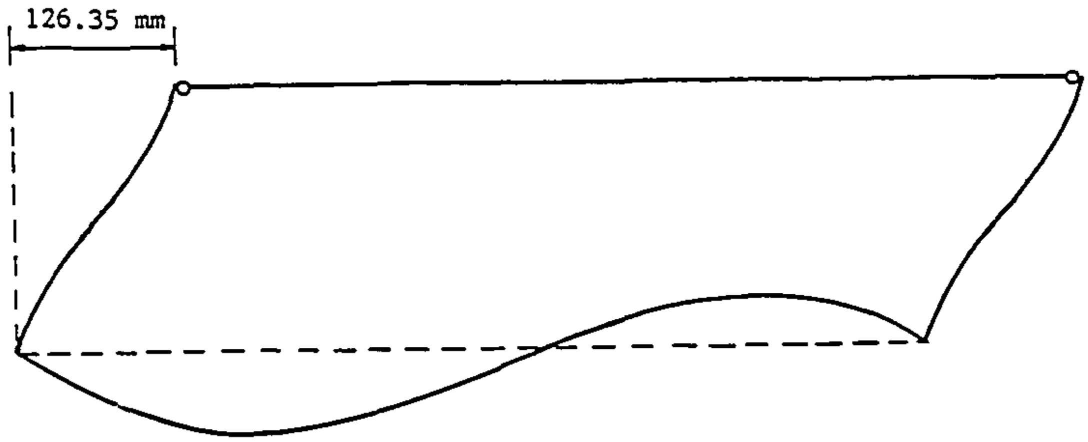

(a) Unclad Frame (Analysis I)

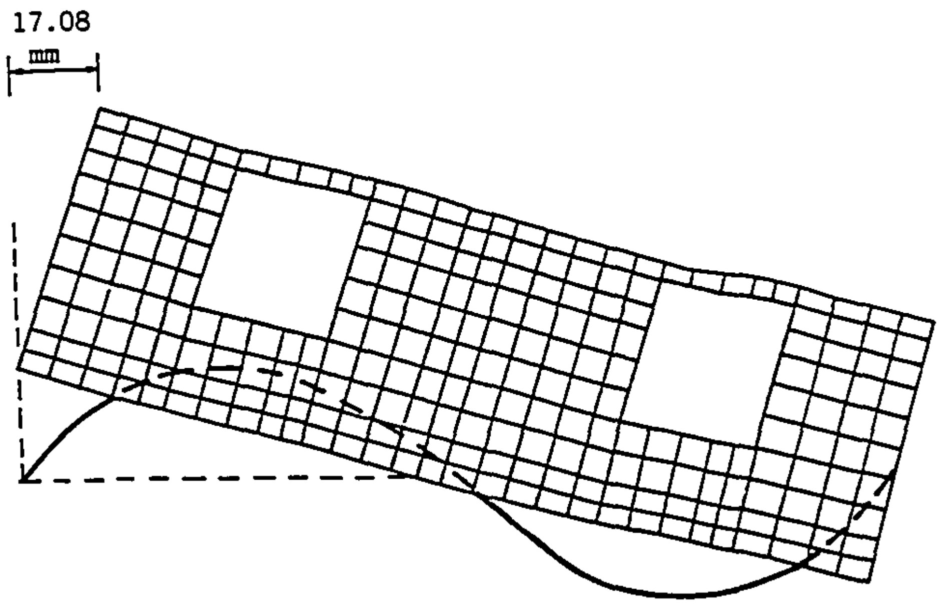

(b) Panel Supported by Beam (Analysis V)

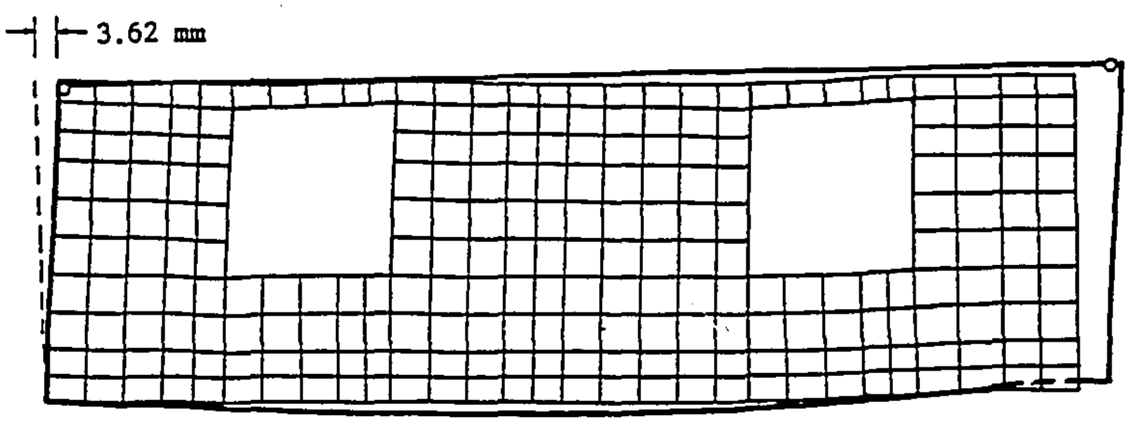

(c) Complete Module (Analysis II)

Figure 5.2: Modes of Deformation of the Frame and Panel

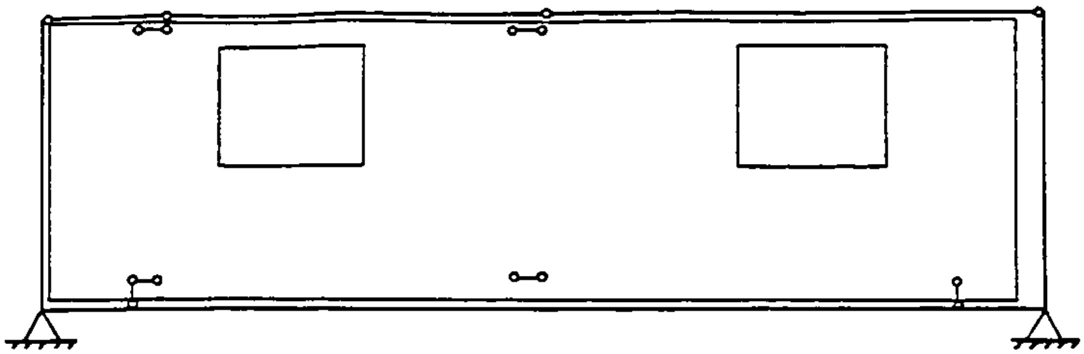

(a) Actual Panel-Clad Frame Module

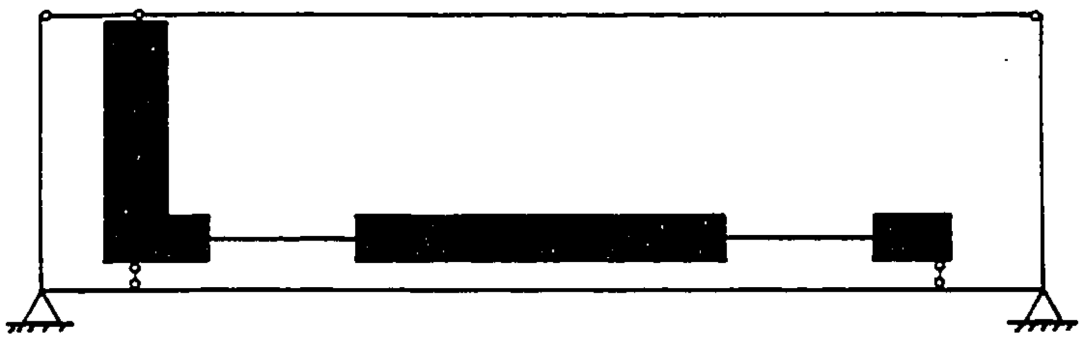

(b) Representative Mechanism

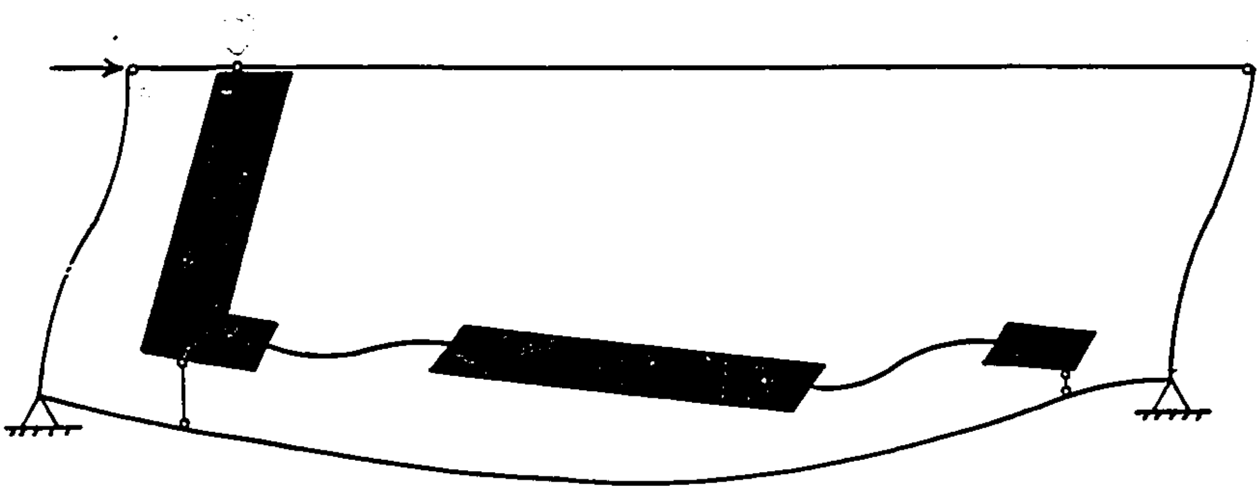

(c) Deflected Shape of Representative Mechanism

Figure 5.3: A Representative Mechanism of the Panel-Clad Frame

5.1.4 Relative Sensitivity of Structure's Lateral Flexibility to Beam, Panel and Connections Flexibilities

In contrast to an unclad moment-resisting frame, whose lateral flexibility can easily be apportioned between the flexibilities of its columns and girders, the lateral flexibility of a clad moment-resisting frame is much more complex. The changed mode of deformation of the frame due to its interaction with the panel, and the intricate modes of deformation of the panel and its connections, preclude the possibility of a simple analysis to determine the sensitivity of the frame's flexibility to those of the individual components. Hence the need arose to undertake a series of detailed analyses of a specific example in which the different modes of deformation were decomposed.

To assess the sensitivity of the structure's lateral flexibility to the flexibility of the panel with its connections, the flexibility obtained from the analysis of the complete module, but with the panels and connections assigned to be rigid (analysis VI) was subtracted from the result of the analysis of the complete module (analysis II). The value obtained was $3.10X10^{-3}$ mm/kN.

Similarly, to determine the sensitivity of the structure's lateral flexibility to that of the beam, the flexibility obtained from the analysis of the complete module, but with the beam assigned to be rigid (analysis VII) was subtracted from the result of the analysis of the complete module (analysis II). The value obtained in this case was $2.11X10^{-3}$ mm/kN.

Evidently, the sensitivity of the structure's lateral flexibility to the flexibility of the panel with its connections in this particular structure was approximately 50 percent greater than it was to the flexibility of the beam.

Referring to Table 4.3, the flexibility of the panel connected to the beam alone, analysis V, is large, $17.08X10^{-3}$ mm/kN. However, when the stiffnesses of the columns are reintroduced into the model, as they are in analysis II, the interaction between the panel and the frame is mobilized. The resulting flexibility of the structure is $3.62X10^{-3}$ mm/kN. The moment-resisting frame's racking action severely constrains the rotation of the panel, by the action described in Section 5.1.2; therefore, the contribution of the beam's bending to the lateral flexibility of the structure is significantly diminished by the composite action.

The major point of note from this section is that the sensitivity of the structure's racking flexibility to the flexibility of the panel with its connections can be of the same order as it is to the beam's flexural flexibility.

5.2 An Analogous Spring Model

An analogous spring model has been developed to better visualize the actions involved when the moment-resisting frame with the panel and its connections are subjected to a horizontal load. The spring model is presented in Fig. 5.4. It includes springs which represent the flexibilities of the three major components: the panel with its connections, f_p, f_{hc}, f_{vc}; the columns, f_c, and the beam, comprising three components, f_{b1}, f_{b2}, f_{b3}. The rigid bar

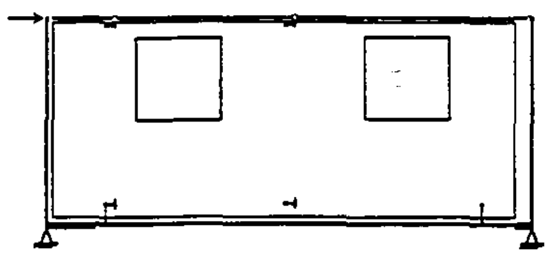

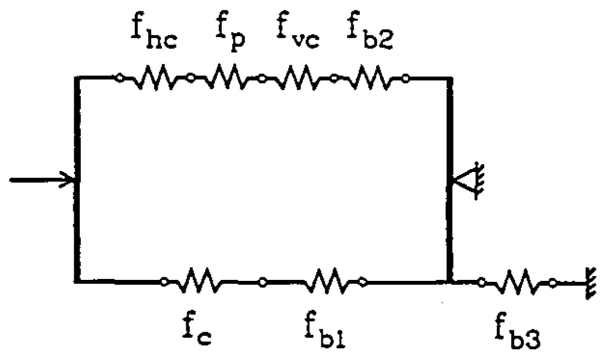

Figure 5.4: Analogous Spring Model of Panel-Clad Frame

at the left, which represents the top of the frame where the load is applied, can translate but not rotate. The rigid bar at the right, which allows for the 'forward' and 'backward' double-curvature bending of the beam, pivots about a rigid support at its centre.

The effects of the flexibilities of the panel, and the horizontal and vertical connections were obtained in Section 5.1.1. The stiffnesses of the columns are added together, that is,

$$k_c = \left(\frac{12EI}{h^3}\right)_{left\ col.} + \left(\frac{12EI}{h^3}\right)_{right\ col.} \tag{5.1}$$

and inverted to give the flexibility of the columns equal to $2.143X10^{-3}$ mm/kN.

5.2.1 Determination of Beam Flexibilities f_{b1}, f_{b2}, f_{b3}

The flexibilities representing the beam, f_{b1}, f_{b2}, and f_{b3}, are unknown; hence, three equations were required to solve for these. The equations were determined using the results from analyses II and V, and those of an additional analysis.

The additional lateral load analysis required was that of the structural frame alone as in analysis I, but with the beam assigned the inertia value as in the complete module analysis, that is, $6.6059X10^8\ mm^4$, as opposed to that found in the first paragraph of Section 4.5. When subjected to a lateral load of 1000 kN, the bare frame displaced 235.70 mm at the top. For completeness, this will be denoted as analysis VIII.

Considering the above case of the unclad moment-resisting frame subjected to lateral load, this is equivalent in the spring model to assigning an infinite flexibility, or a zero stiffness, to the springs f_p, f_{hc}, and f_{vc}. In this case f_c represents the flexibility of the columns bending and f_{b1} and f_{b3} represent the 'forward' double-curvature bending flexibility of the beam due to the moment the columns apply at the beam-column joint, Fig. 5.5. An expression relating f_{b1} and f_{b3} was obtained using the displacement result of analysis VIII, Δ_1, and the spring model. The flexibility of the spring model in Fig. 5.5 is

$$\frac{\Delta_1}{Q} = f_c + (f_{b1} + f_{b3}) \tag{5.2}$$

Substituting the results of analysis VIII and the flexibility of the columns, previously calculated, an expression representing the flexibility of the beam due to racking was obtained,

$$(f_{b1} + f_{b3}) = 233.557X10^{-3}\ \ mm/kN \tag{5.3}$$

In analysis V, the panel with its connections connected to the flexible beam was subjected to lateral loading. This is equivalent to assigning an infinite flexibility, or zero stiffness, to the columns represented by the spring f_c. The deformations of the panel and the horizontal and vertical connections are represented by f_p, f_{hc} and f_{vc}, respectively,

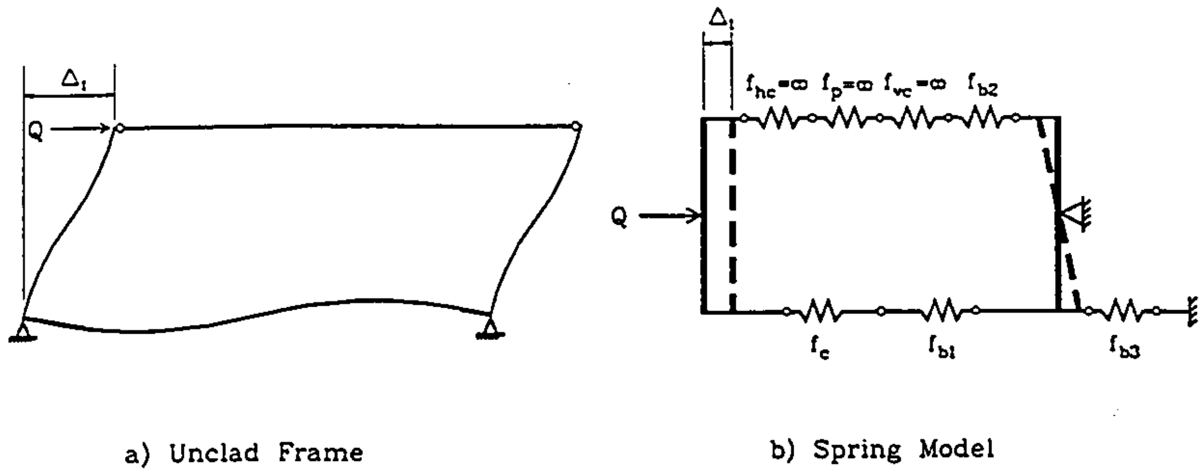

Figure 5.5: Spring Model Representation of Unclad Frame

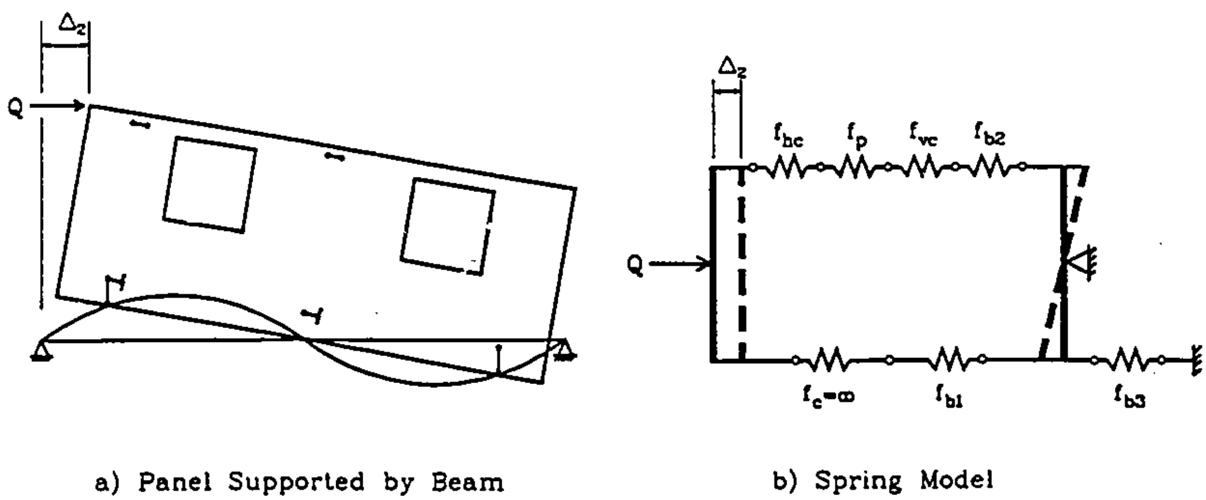

Figure 5.6: Spring Model Representation of Panel Supported by Beam

while f_{b2} and f_{b3} represent the 'backward' double-curvature bending of the beam due to the panel's forward rotation, Fig. 5.6. From the result of analysis V and the spring model just described, a relationship between the flexibilities f_{b2} and f_{b3} was derived. The flexibility of the spring model in Fig. 5.6 is given as

$$\frac{\Delta_2}{Q} = (f_{hc} + f_p + f_{vc}) + (f_{b2} + f_{b3}) \tag{5.4}$$

Substituting the results of analysis V and the flexibilities of the panel and its connections, obtained in Section 5.1.1, into Eq. 5.4, the flexibility of the beam due to 'backward' double-curvature bending was found to be

$$(f_{b2} + f_{b3}) = 12.37X10^{-3} \quad mm/kN \tag{5.5}$$

A third equation was obtained from the lateral load analysis of the complete module (Analysis II), and its corresponding spring model, Fig. 5.7a. From the free-body diagram of the left rigid bar, Fig. 5.7b, the following expression for the horizontal force equilibrium can be written

$$P_1 + P_2 = Q \tag{5.6}$$

where

$$P_1 = k_1\delta_1 = \frac{(\Delta_3 + x)}{(f_{hc} + f_p + f_{vc}) + f_{b2}} \tag{5.7}$$

and

$$P_2 = k_2\delta_2 = \frac{(\Delta_3 - x)}{f_c + f_{b1}} \tag{5.8}$$

Equilibrium of the free-body diagram of the right rigid bar, Fig. 5.7c, is achieved, if and only if

$$2P_1 + P_3 = Q \tag{5.9}$$

that is,

$$x = \frac{f_{b3}[Q(f_{hc} + f_p + f_{vc} + f_{b2}) - 2\Delta_3]}{(2f_{b3} + f_{hc} + f_p + f_{vc} + f_{b2})} \tag{5.10}$$

Substituting Eq. 5.10 into Eqs. 5.7, 5.8 and 5.6, an expression for the flexibility of the complete module in terms of f_{b1}, f_{b2}, and f_{b3} was found

$$\frac{\Delta_3}{Q} = \frac{f_c(f_{b2} + f_{b3}) + (f_{hc} + f_p + f_{vc})(f_c + f_{b1} + f_{b3}) + f_{b1}(f_{b2} + f_{b3}) + f_{b2}f_{b3}}{(f_c + f_{b1} + f_{b3}) + (f_{hc} + f_p + f_{vc} + f_{b2} + f_{b3}) + 2f_{b3}} \tag{5.11}$$

Substituting the results of analysis II and the flexibilities of the columns and the panel with its connections into Eq. 5.11, the following equation was obtained

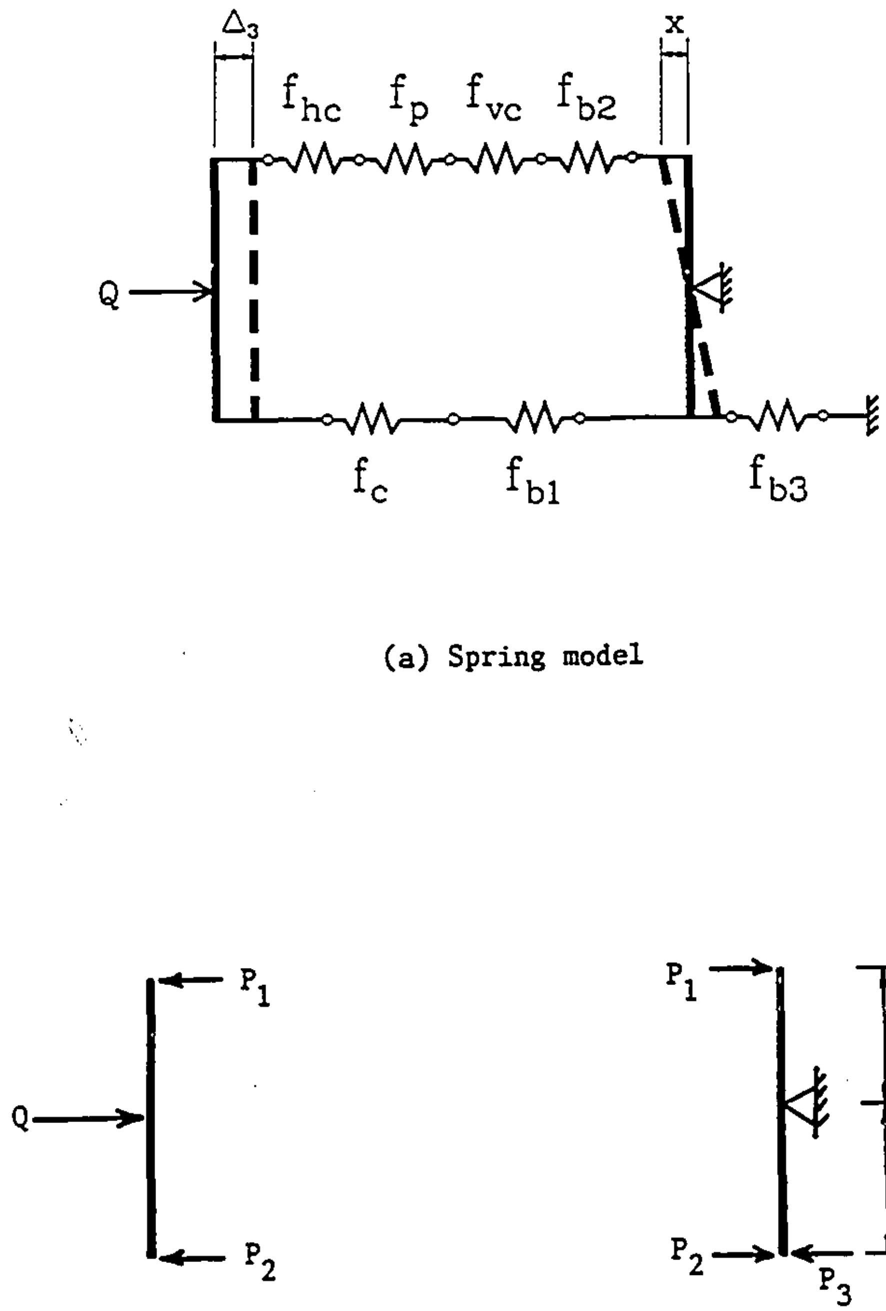

(a) Spring model

(b) Left bar

(c) Right bar

Figure 5.7: Free-Body Diagrams Associated with Analogous Spring Model of Panel-Clad Frame

$$f_{b2}f_{b3} + 12.37X10^{-3}f_{b1} - 7.24X10^{-3}f_{b3} + 2.21941X10^{-4} = 0 \qquad (5.12)$$

Solving Eqs. 5.3, 5.5, and 5.12 simultaneously, the values for f_{b1}, f_{b2}, and f_{b3} were determined:

$$f_{b1} = 181.28X10^{-3}, f_{b2} = -39.91X10^{-3}, f_{b3} = 52.28X10^{-3} \quad mm/kN \qquad (5.13)$$

or,

$$f_{b1} = 293.07X10^{-3}, f_{b2} = 71.88X10^{-3}, f_{b3} = -59.51X10^{-3} \quad mm/kN \qquad (5.14)$$

5.2.2 Validity and Purpose of Spring Model

To verify that the model properly represents the frame and the panel with its connections, both solution sets were checked in a manner similar to above against the results of analysis VI. Although, mathematically, both solution sets are correct, physically, the first solution set gives the best results because the sense of the displacements of the right rigid bar that it produces are logically correct.

By representing the panel-clad frame by an analogous spring model, the interactive mode of behaviour of the panel with the frame can be better visualized. The accuracy of the spring model was confirmed using the results of the detailed finite element analyses. The spring model can be further used to develop in algebraic terms an expression for the flexibility of the complete panel-clad frame module as a function of the flexural inertias of the frame members, the flexibilities of the panel and its connections, the storey height, and the relative distance of the vertical connections from the column-beam joint to the length of the beam, Appendix A. This algebraic expression offers the potential of representing the sensitivity of the structure's racking flexibility to the flexibilities of the frame, panel and connections. This is proposed as a topic for further research.

5.3 Bracing Effects of Other Types of Precast Concrete Cladding Panels

The discussion presented applies to one particular, but representative, precast concrete panel. Therefore, the lateral stiffening influence of other types of precast concrete panels will depend on the particular values of such parameters as the size of the panel, the thickness of the panel, the number and size of window openings, the stiffnesses of the connections, and the stiffnesses of the structural frame members. However, in Section 5.1.3 it was concluded that the 'backward' and 'forward' double-curvature modes of bending of the beam, which interact to cause a quadruple-curvature mode of deformation involve a much greater amount of strain energy, thereby causing the increase in stiffness of the structure. The composite action may be perceived in an alternative simpler way, in which the lateral stiffening is caused by the high rigidity of the panel being transferred to the frame through the laterally fixed connections at the top and bottom of the panel. This action restrains the top and bottom of the frame from moving relatively in the lateral direction, while the vertical connections restrain the panel from rotating within the frame. Recalling the recommendations for locating the connections in all types of practical panel sizes, as outlined by the CPCI and PCI design manuals (1987, 1977), Figs. 3.12 and 3.13, it can be observed that all of the panels have laterally fixed connections at the top and bottom, and two loadbearing connections restraining vertical movement at each end of the panel at the bottom. Therefore, with the present recommendations for connections, all types of panels designed according to the CPCI and PCI design manuals will have a restraining effect when the structure is subjected to lateral loading.

CHAPTER 6

MODELLING CLADDING PANELS IN THE OVERALL STRUCTURE ANALYSES

Having concluded from the detailed finite element analyses of the single-storey panel-clad frame module that typically connected precast concrete cladding panels have a significant stiffening effect, it was necessary to develop practical techniques to model these in the analyses of the total structure. Several equivalent strut models are presented and evaluated on the basis of their accuracy in correctly representing the interactive behaviour of a moment-resisting frame and a cladding panel with its connections, and on the basis of their practical value. From the behaviour of the most accurate model, a clearer understanding of the panel-frame interaction was obtained.

6.1 Model 1 - Simple, Single-Diagonal

In the simple, single-diagonal strut model, Fig. 6.1, the diagonal bracing strut is assigned a cross-sectional area to give a horizontal stiffness equivalent to the effect of the representative panel and its connections in the structural frame. To obtain the horizontal stiffness of the struts, the lateral stiffness obtained from the single-storey bare-frame analysis (analysis I) was subtracted from the lateral stiffness determined from the complete module analysis (analysis II). In other words, to model a panel and its connections in a building by using a simple, single diagonal, it is required to make a lateral load analysis of a single-storey model of the bare frame, as well as a detailed lateral load analysis of the panel and its connections within the frame.

Referring to Fig. 6.1, the horizontal stiffness of a single-diagonal braced frame is given as

$$k = \frac{AE\cos^2\theta}{d} \tag{6.1}$$

where A = cross-sectional area of diagonal,
E = modulus of elasticity of diagonal (panel),
d = length of diagonal, and
θ = slope of diagonal.

stiffening is caused by the high rigidity of the panel being transferred to the frame through the laterally fixed connections at the top and bottom of the panel. This action restrains the top and bottom of the frame from moving relatively in the lateral direction, while the vertical connections restrain the panel from rotating within the frame. Recalling the recommendations for locating the connections in all types of practical panel sizes, as outlined by the CPCI and PCI design manuals (1987, 1977), Figs. 3.12 and 3.13, it can be observed that all of the panels have laterally fixed connections at the top and bottom, and two loadbearing connections restraining vertical movement at each end of the panel at the bottom. Therefore, with the present recommendations for connections, all types of panels designed according to the CPCI and PCI design manuals will have a restraining effect when the structure is subjected to lateral loading.

CHAPTER 6

MODELLING CLADDING PANELS IN THE OVERALL STRUCTURE ANALYSES

Having concluded from the detailed finite element analyses of the single-storey panel-clad frame module that typically connected precast concrete cladding panels have a significant stiffening effect, it was necessary to develop practical techniques to model these in the analyses of the total structure. Several equivalent strut models are presented and evaluated on the basis of their accuracy in correctly representing the interactive behaviour of a moment-resisting frame and a cladding panel with its connections, and on the basis of their practical value. From the behaviour of the most accurate model, a clearer understanding of the panel-frame interaction was obtained.

6.1 Model 1 - Simple, Single-Diagonal

In the simple, single-diagonal strut model, Fig. 6.1, the diagonal bracing strut is assigned a cross-sectional area to give a horizontal stiffness equivalent to the effect of the representative panel and its connections in the structural frame. To obtain the horizontal stiffness of the struts, the lateral stiffness obtained from the single-storey bare-frame analysis (analysis I) was subtracted from the lateral stiffness determined from the complete module analysis (analysis II). In other words, to model a panel and its connections in a building by using a simple, single diagonal, it is required to make a lateral load analysis of a single-storey model of the bare frame, as well as a detailed lateral load analysis of the panel and its connections within the frame.

Referring to Fig. 6.1, the horizontal stiffness of a single-diagonal braced frame is given as

$$k = \frac{AE\cos^2\theta}{d} \tag{6.1}$$

where A = cross-sectional area of diagonal,
E = modulus of elasticity of diagonal (panel),
d = length of diagonal, and
θ = slope of diagonal.

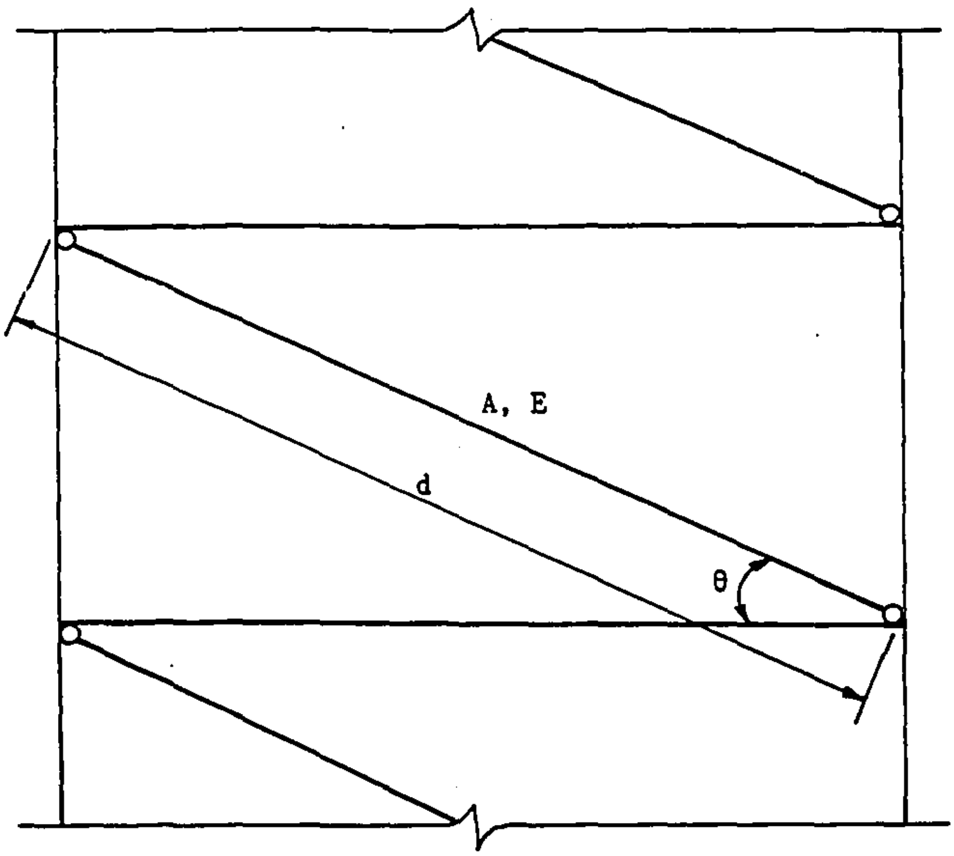

Figure 6.1: Model 1 - Simple, Single-Diagonal

To check the accuracy of this model, and the other models to follow, the top lateral displacement and the frame-member moments obtained from the lateral load analysis of a single-storey representation of the modelled frame were compared with those obtained from a detailed finite element analysis of a single-storey model of the panel-clad frame subjected to a horizontal load. The representative panel and its connections were the same as in the previous chapters; however, to simplify the model, a symmetrical frame without rigid beam-ends was used, Fig. 6.2. Similar to Section 4.4, the frame was represented by a column element at each side of the panel, and a beam element at the bottom of the panel. The column elements were assigned a flexural inertia of $1.5X10^{10}$ mm^4 and an infinitely large axial area. The beam element was assigned a flexural inertia of $5.334X10^8$ mm^4 and an infinitely large axial area. The panel was anchored to the supporting beam, while the tops of the columns were connected to the panel by rigid horizontal links, to constrain the tops of the frame and panel to translate identically. To obtain the behaviour of a typical storey, it was necessary to constrain the top and bottom of the left column to rotate identically, and to constrain similarly the top and bottom of the right column. A 1000 kN lateral load analysis was performed on the model. The resulting top lateral displacement was 6.2553 mm and the frame-member moments are presented in Fig. 6.3.

To calculate the area of the diagonal bracing strut, the lateral stiffness of the symmetric bare frame was required. From a lateral load analysis of the frame, Fig. 6.4, its stiffness was determined to be 2.336 kN/mm. The horizontal stiffness of the diagonal was obtained by subtracting the stiffness of the bare frame from the stiffness of the complete frame and panel, that is

$$\begin{aligned} Horiz.\ stiff.\ of\ equiv.\ strut &= \frac{1000}{6.2553} - 2.336 \\ &= 159.864 - 2.336 \\ &= 157.528\ kN/mm \end{aligned} \tag{6.2}$$

By equating the expression in Eq. 6.1 to the value obtained in Eq. 6.2, and setting d equal to 8823.5 mm, θ equal to 16.73°, and the modulus of elasticity, E, equal to 20.0 kN/mm^2 (20000 MPa), the axial area of the diagonal was calculated to be 75777 mm^2.

As a check, a lateral load analysis was then performed on the simple, single-diagonal braced frame model, Fig. 6.5. The top lateral displacement was 6.2553 mm which was identical, as expected, to the detailed finite element analysis of the panel-clad frame. However, the resulting frame-member moments, Fig. 6.6, were grossly underestimated compared with those obtained from the detailed analysis of the panel-clad frame. The errors in the frame-member moments were of a large magnitude because the model does not allow vertical forces to be applied to the beam at the locations of the bearing connections as in the detailed analysis of the panel-braced frame.

Therefore, the single-diagonal strut model gives the correct lateral displacements, provided that a detailed finite element analysis of the panel and its connections within the

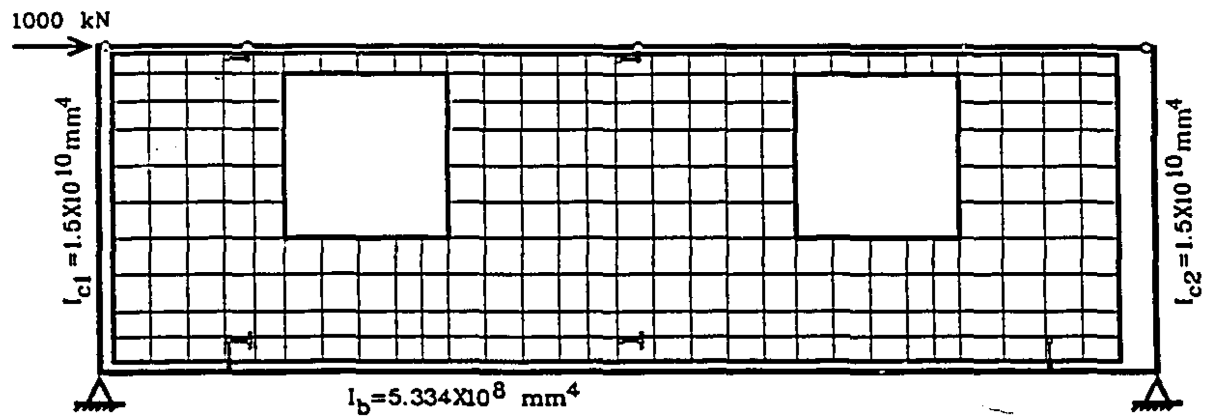

Figure 6.2: Mathematical Model for Detailed Analysis of Representative Symmetrical Panel-Clad Frame

Figure 6.3: Frame-Member Moments from Detailed Analysis of Symmetrical Panel-Clad Frame

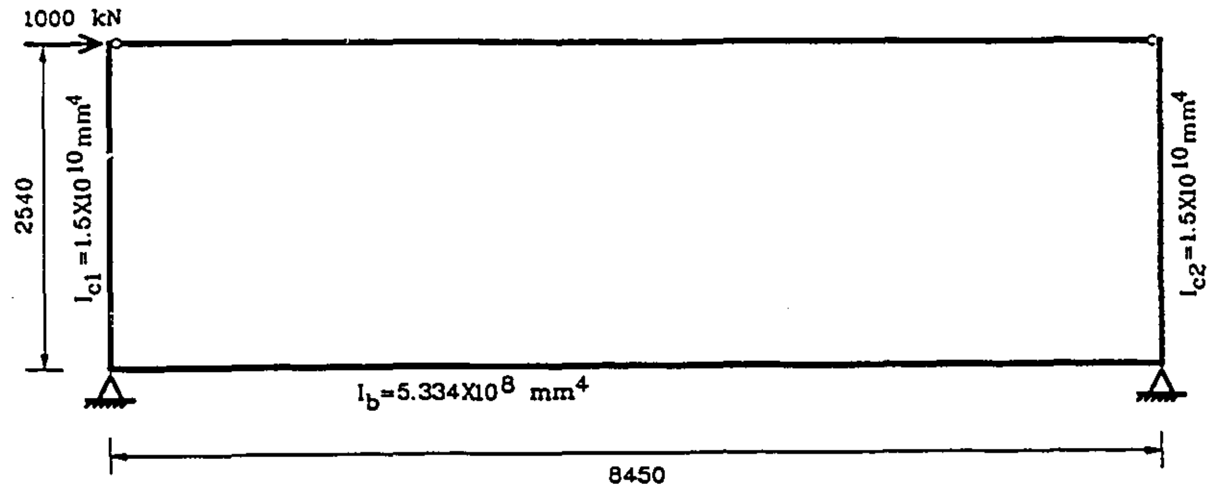

Figure 6.4: Mathematical Model of Symmetrical Moment-Resisting Frame

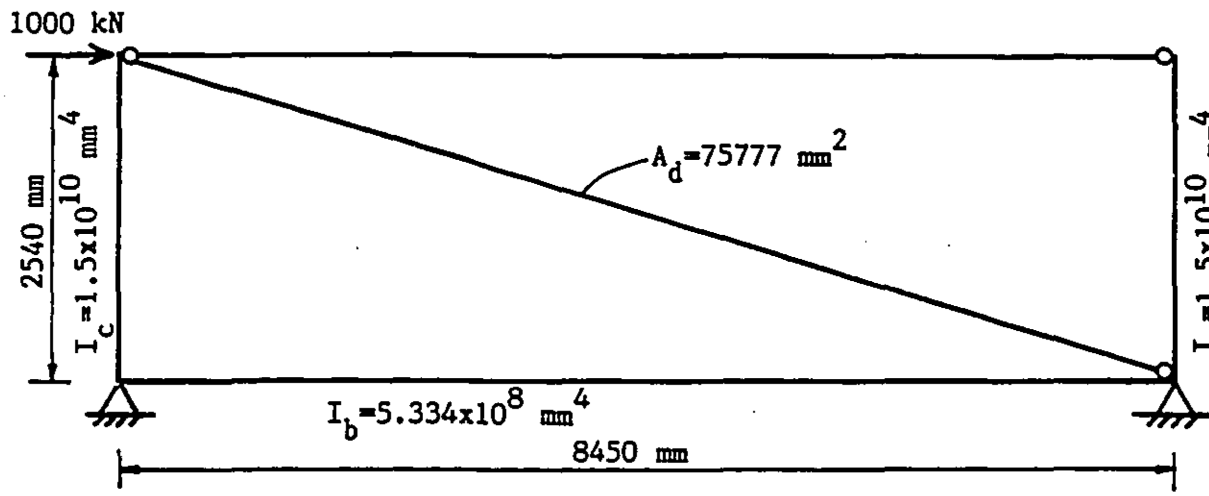

Figure 6.5: Simple, Single-Diagonal Braced Frame Model

—— detailed finite element analysis

– – – simple, single-diagonal strut model

Note: values shown for strut model only,
for detailed analysis values see Fig. 6.3

Figure 6.6: Frame-Member Moments for Simple, Single-Diagonal Braced Frame Model

frame has been performed first to obtain the correct sectional area for the diagonal. It has the advantages of extreme simplicity in concept and in use for analysis. It has a major disadvantage, however, in that it does not produce the correct frame-member moments.

6.2 Model 2 - Double-Diagonals to Corners

The more sophisticated Model 2, Fig. 6.7, consists of two diagonal bracing struts, one extending from the top-left corner of a storey and ending at the right bearing connection to the lower beam of the storey, while the other extends from the left bearing connection of the panel to the upper beam and ends at the bottom-right corner of the storey. By this arrangement, the vertical components of the forces in the struts act transversely to the beams, causing them to bend as in the detailed analysis of the panel-clad frame.

The areas of the two diagonal bracing struts were determined by equating their combined horizontal stiffnesses to the lateral stiffness of the panel and connections supported by a rigid beam. The stiffening effect of the panel and its connections on a rigid beam is equal to the stiffening effect of the panel and its connections within a flexible frame. This results because the lateral stiffening effect of the panel and its connections, thus the stiffness of the diagonal strut, is dependent on the lateral displacement of the panel and on the vertical forces in the bearing connections. Therefore, provided that the diagonal struts have the correct axial area to give the correct lateral displacement, by equilibrium the vertical forces acting transversely to the beam will be the same whether the beam is rigid or flexible. The validity of this argument is proven in Appendix B.

The horizontal stiffness of one strut, Fig. 6.7, is as given in Eq. 6.1. The stiffness of the panel and connections supported by a rigid beam was obtained in analysis IV, Table 4.3. By equating the expression in Eq. 6.1 to half of the stiffness value of analysis IV, and setting d equal to 7965.81 mm, θ equal to 18.594° and the modulus of elasticity, E, equal to 20.0 kN/mm^2 (20000 MPa), the axial area of each strut was determined to be 47066 mm^2.

A lateral load analysis was then performed on a single-storey representation of Model 2 with half-stories above and below, Fig. 6.8. The top four nodes were constrained to translate identically in the horizontal direction, while the bottom four nodes were restrained against any lateral displacement. The nodes at the cut ends of the diagonals were constrained to displace in the vertical direction identically to the corresponding centre nodes of the diagonals in the full storey. The resulting interstorey drift was 4.6205 mm, which is 74 percent of that obtained from the finite element analysis of the panel and frame. The resulting frame-member moments for a single-storey representation of the frame are shown in Fig. 6.9. The moments at the ends of the beams and columns were only 54 percent of those obtained from the finite element analysis, Fig. 6.3. These results indicate that Model 2 does not give a good representation of the actual panel and frame behaviour. The reason the model is too stiff is because, at one end, the struts are acting at the corners; therefore, the vertical forces are being transferred to axially rigid columns, while in the actual case the panel is being supported at both bearing connections by a flexible beam.

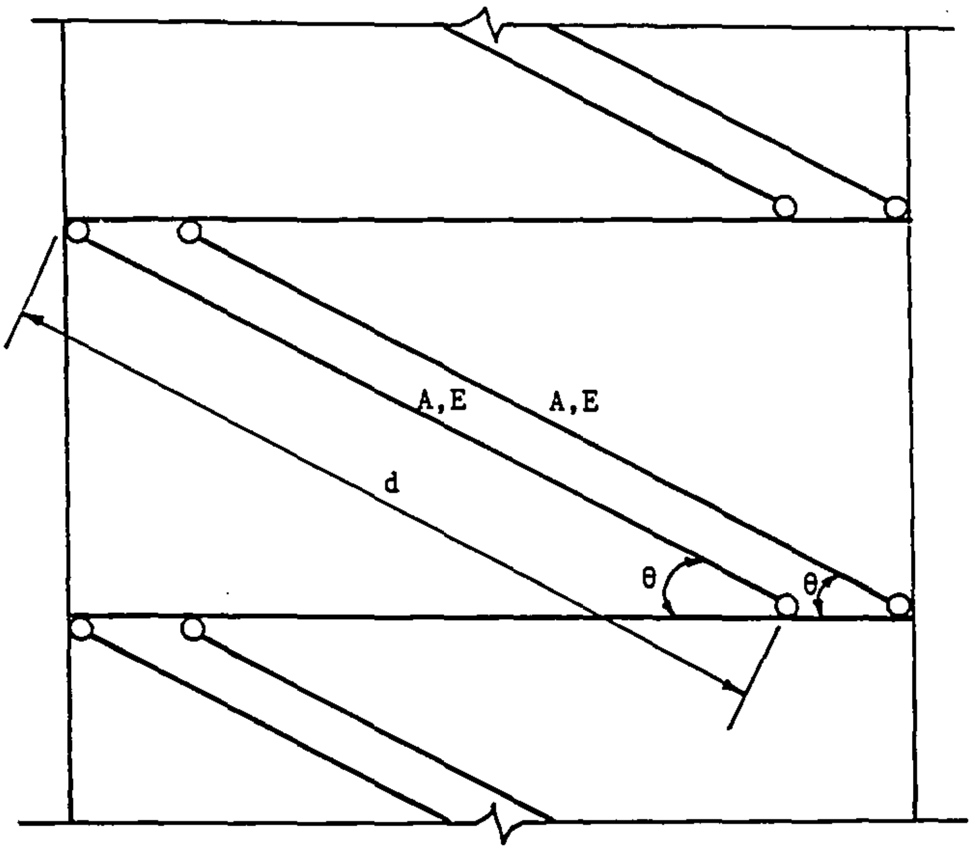

Figure 6.7: Model 2 - Double-Diagonals to Corners

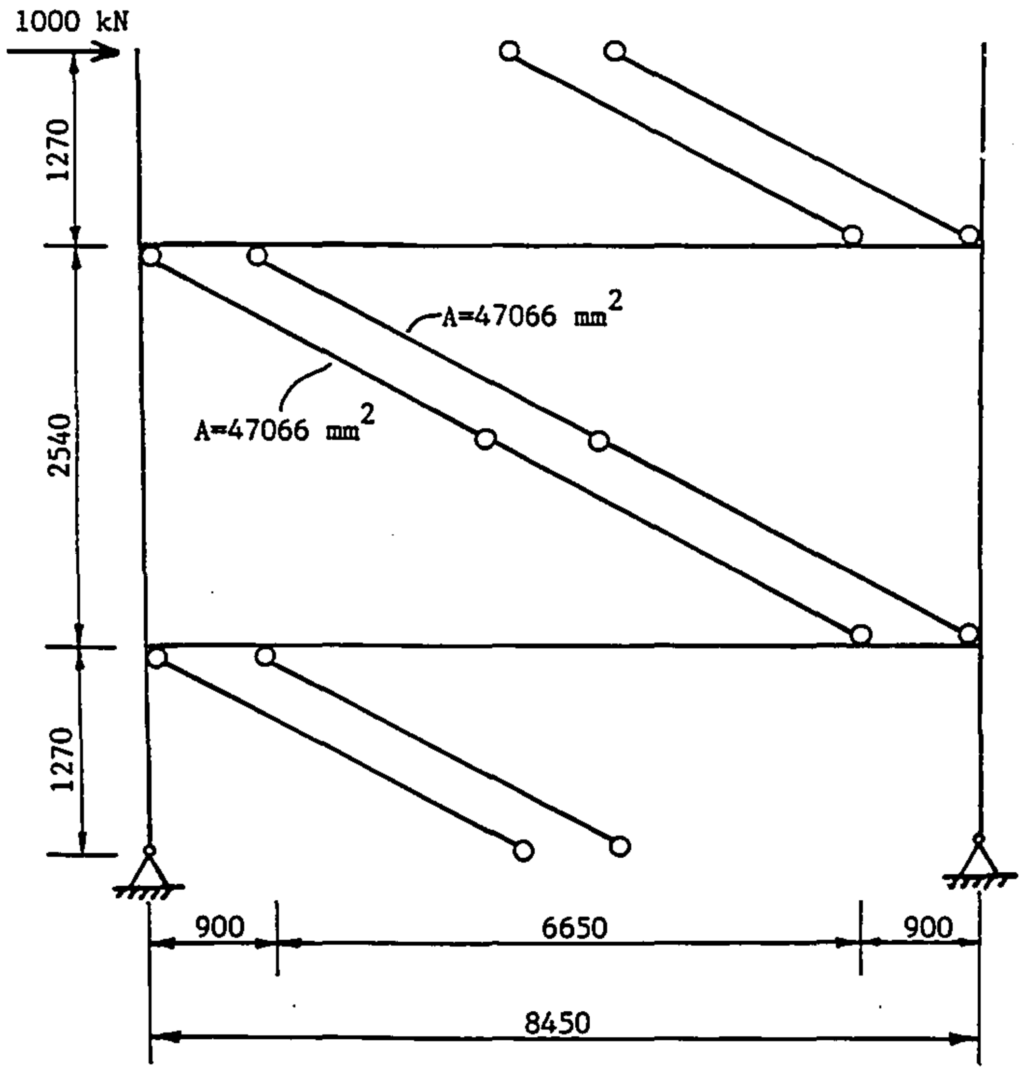

Figure 6.8: Single-Storey Representation of Model 2 with Half-Stories Above and Below

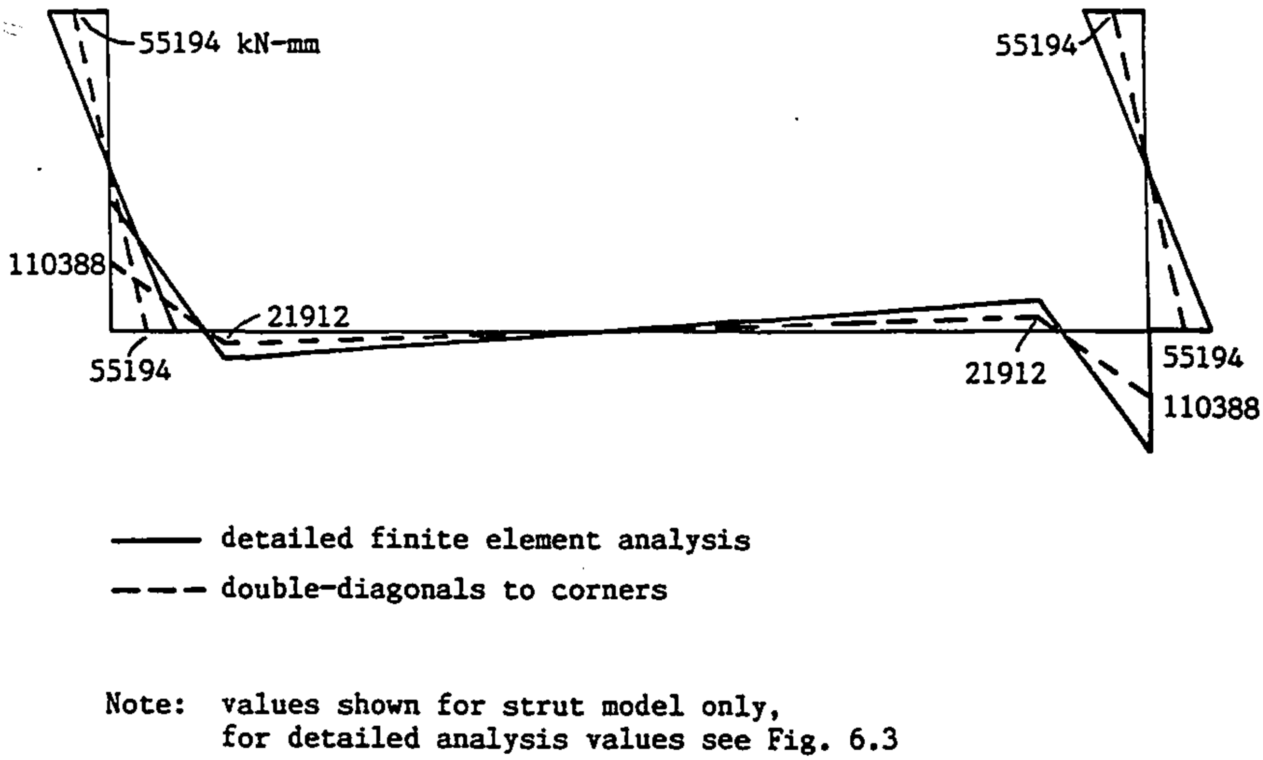

Figure 6.9: Frame-Member Moments for Double-Diagonals to Corners Braced Frame Model

6.3 Model 3 - Double-Diagonals to Centres

In Model 3, Fig. 6.10, as in Model 2, the panel and connections are represented by two diagonal bracing struts. In Model 3, however, one of the struts extends from the left bearing connection on the beam above to the centre of the beam below, and the other strut extends from the centre of the beam above to the right bearing connection on the beam below. As in Model 2, the vertical components of the forces in the struts act transversely to the beams causing them to displace as in the detailed analysis of the panel-clad frame. This model differs from Model 2 in that the slope of the struts is greater; therefore, the bending it imposes on the beam per unit lateral displacement is less, or the energy involved per unit displacement is less, that is, Model 3 is more flexible than Model 2.

Similarly to Model 2, the areas of the two diagonal bracing struts were obtained by equating their combined horizontal stiffnesses to the lateral stiffness of the panel and connections supported by a rigid beam.

By equating the expression in Eq. 6.1 to half of the stiffness value of analysis IV, Table 4.3, and setting d equal to 4184.16 mm, θ equal to 37.3766° , and the modulus of elasticity, E, equal to 20.0 kN/mm^2 (20000 MPa), the axial area of each strut was found to be 35168 mm^2.

From a lateral load analysis of a single-storey representation of Model 3 with half-stories above and below, Fig. 6.11, and with constraint conditions similar to those used in the analysis of Model 2, the interstorey drift was 6.0565 mm. This is 97 percent of that obtained from the finite element analysis of the panel-clad frame. The resulting frame-member moments in a single-storey representation of the frame are shown in Fig. 6.12. The moments at the ends of the beams and columns were only 6 percent greater than those obtained from the finite element analysis of the panel and frame. The results obtained from this model agree very closely with those of the finite element analysis. As in the case of the previous model, to determine the cross-sectional areas of the struts, a detailed finite element analysis of a panel and its connections supported by a rigid beam is necessary to properly represent the stiffening effect of the flexibility of the panel with its connections.

6.4 Model 4 - 'Improved' Single-Diagonal

Model 4, Fig. 6.13, consists of a single-diagonal bracing strut which extends from the left bearing connection in the beam above, to the right bearing connection on the beam below. Similarly to Model 3, the vertical components of the forces in the struts act transversely to the beams, causing them to displace as in the detailed analysis of the panel-clad frame, and the model is more flexible than Model 2 since the strut has a greater slope and is supported by the beam. However, this model is simpler in concept and more efficient to use in analysis than Model 3.

As in the previous two models, the area of the diagonal bracing strut was obtained by equating its horizontal stiffness to the lateral stiffness of the panel and connections

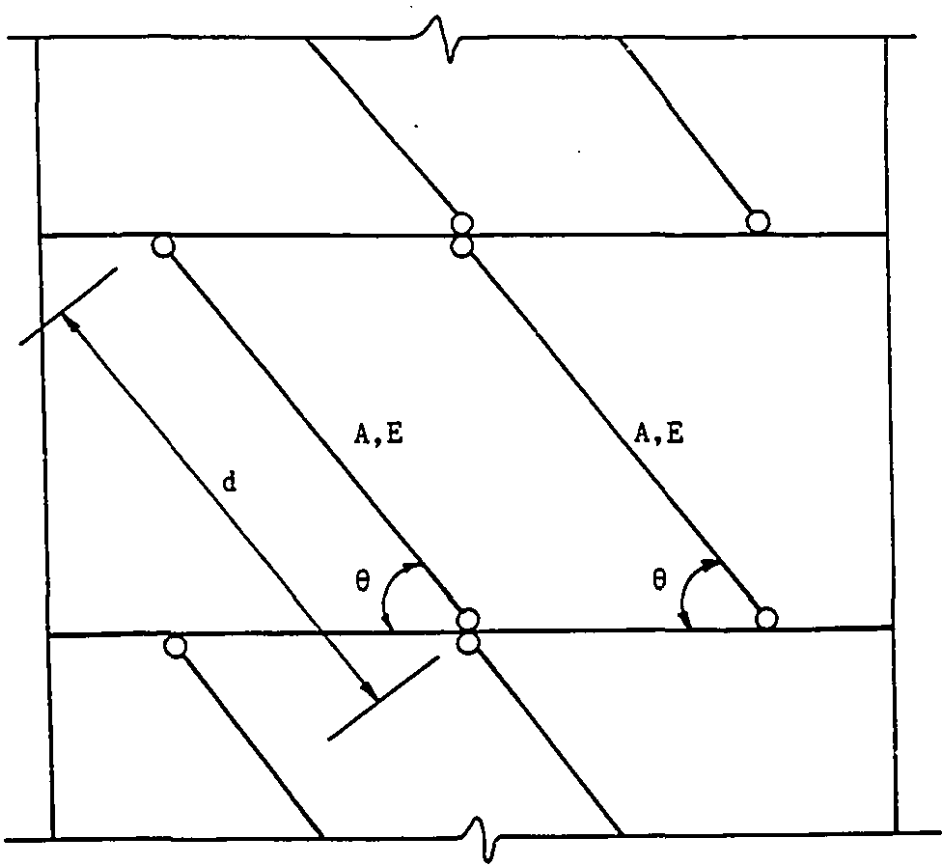

Figure 6.10: Model 3 - Double-Diagonals to Centres

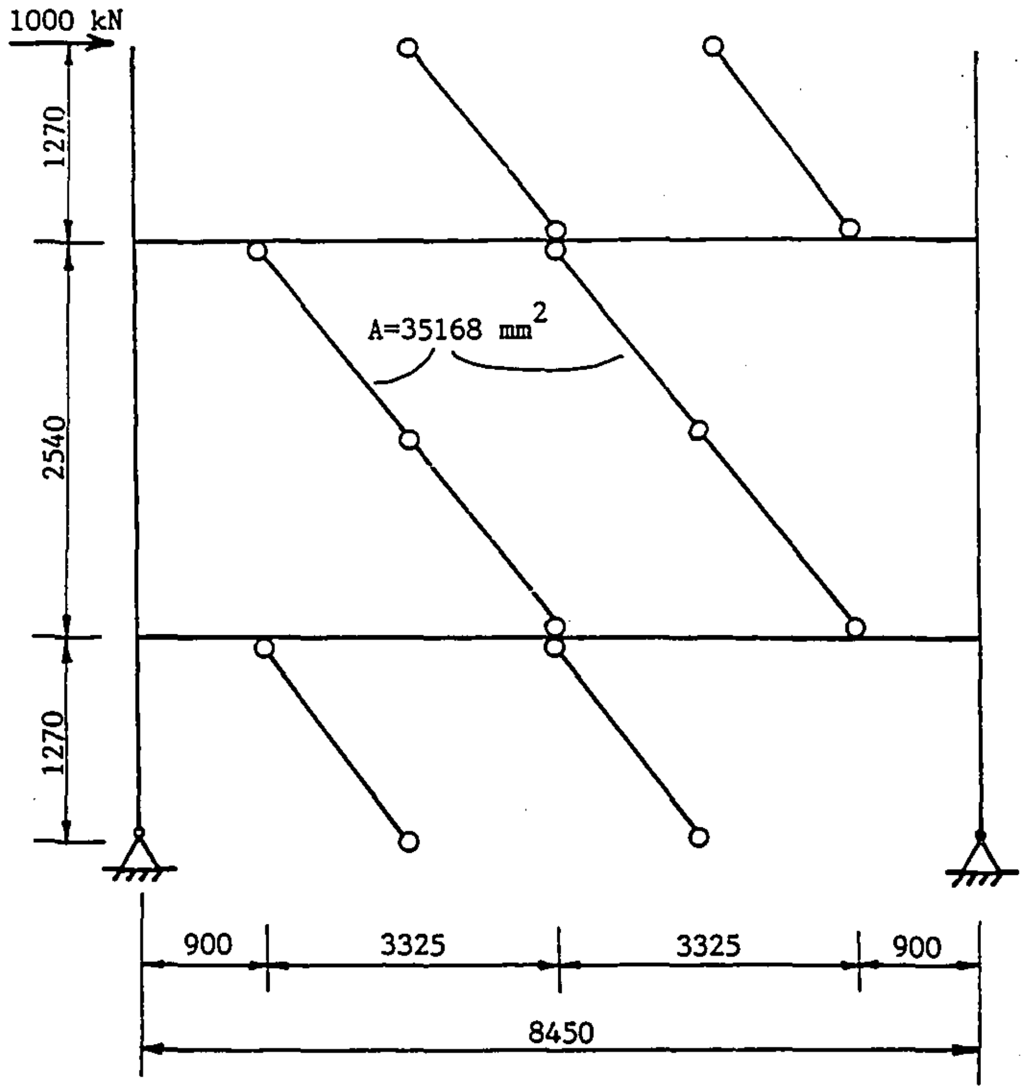

Figure 6.11: Single-Storey Representation of Model 3 with Half-Stories Above and Below

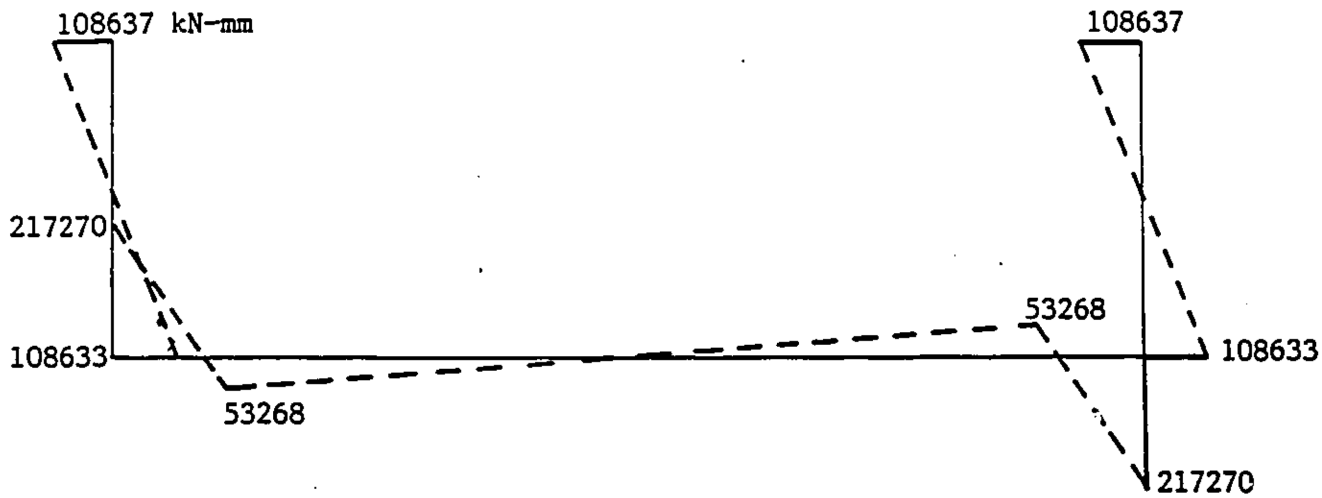

Figure 6.12: Frame-Member Moments for Double-Diagonals to Centres Braced Frame Model

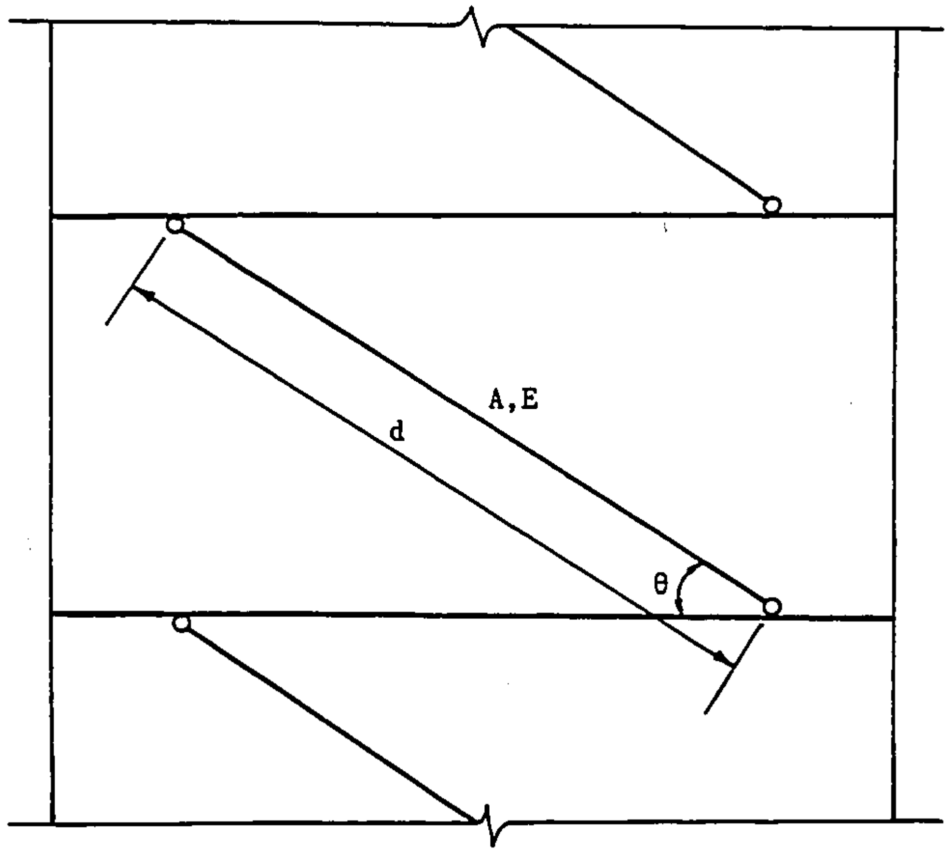

Figure 6.13: Model 4 - 'Improved' Single-Diagonal

supported by a rigid beam.

By equating Eq. 6.1 to the stiffness value of analysis IV, and setting d equal to 7118.57 mm, θ equal to 20.9046° and the modulus of elasticity, E, equal to 20.0 kN/mm^2 (20000 MPa), the axial area of the strut was determined to be 86592 mm^2.

A single-storey representation of Model 4 with half-storeys above and below, Fig. 6.14, and with similar constraint conditions as in the previous two analyses was analysed for an applied horizontal load of 1000 kN. The resulting interstorey drift was 6.0565 mm which was exactly the same as that obtained from Model 3. The resulting frame-member moments were also identical to those found from Model 3. Hence, Model 4, like Model 3, predicts very good results for the behaviour of the laterally loaded panel connected within a frame, but it is a much simpler representation than Model 3. As in the other models previously described, a finite element analysis of a panel and its connections supported by a rigid beam is initially necessary to determine the cross-sectional area of the diagonal bracing strut. However, the analysis has the advantage that it is independent of the frame's members stiffnesses.

6.5 Further Understanding of the Panel-Clad Frame Interaction

A clearer understanding of the structural frame's behaviour can be gained from Model 4, the 'improved' single-diagonal, which best represents the panel connected within the frame in its usually recommended way.

A braced bent under horizontal loading behaves as a vertical cantilever truss. The columns act as the chords in carrying the external load moment, and the diagonals and girders serve as the web members in carrying the horizontal shear. For the braced frame shown in Fig. 6.13, which best represents the panel-clad frame behaviour, the member actions that contribute to its shear displacement are axial deformations in the diagonals and beams, and bending in the beams as shown in Fig. 6.15.

Since the beam's axial deformations between the locations of the loadbearing connections are contributing to the shear displacement of the frame, the model used for the analyses of Chapter 4, Fig. 4.15, in which the beam's axial area was assigned a large value to make it effectively rigid, does not accurately represent the panel-frame system.

To assess the contribution of the beam's axial deformations to the shear displacement of the panel-clad frame, the resulting forces in the horizontal connections were examined. From the locations of the panel's connections, Fig. 4.15, the portion of beam that would be subjected to axial deformations is between the left horizontal connection and the middle horizontal connection. From Fig. 8.1, the approximate axial force applied to the beam is the difference between the load carried by the top-left horizontal connection and the bottom-left horizontal connection (or the difference between the top and bottom middle horizontal connections), that is, 86.03 kN. The beam's length over which this force would be applied is 3175 mm, and its actual area is 198200 mm^2. The resulting axial deformation of the

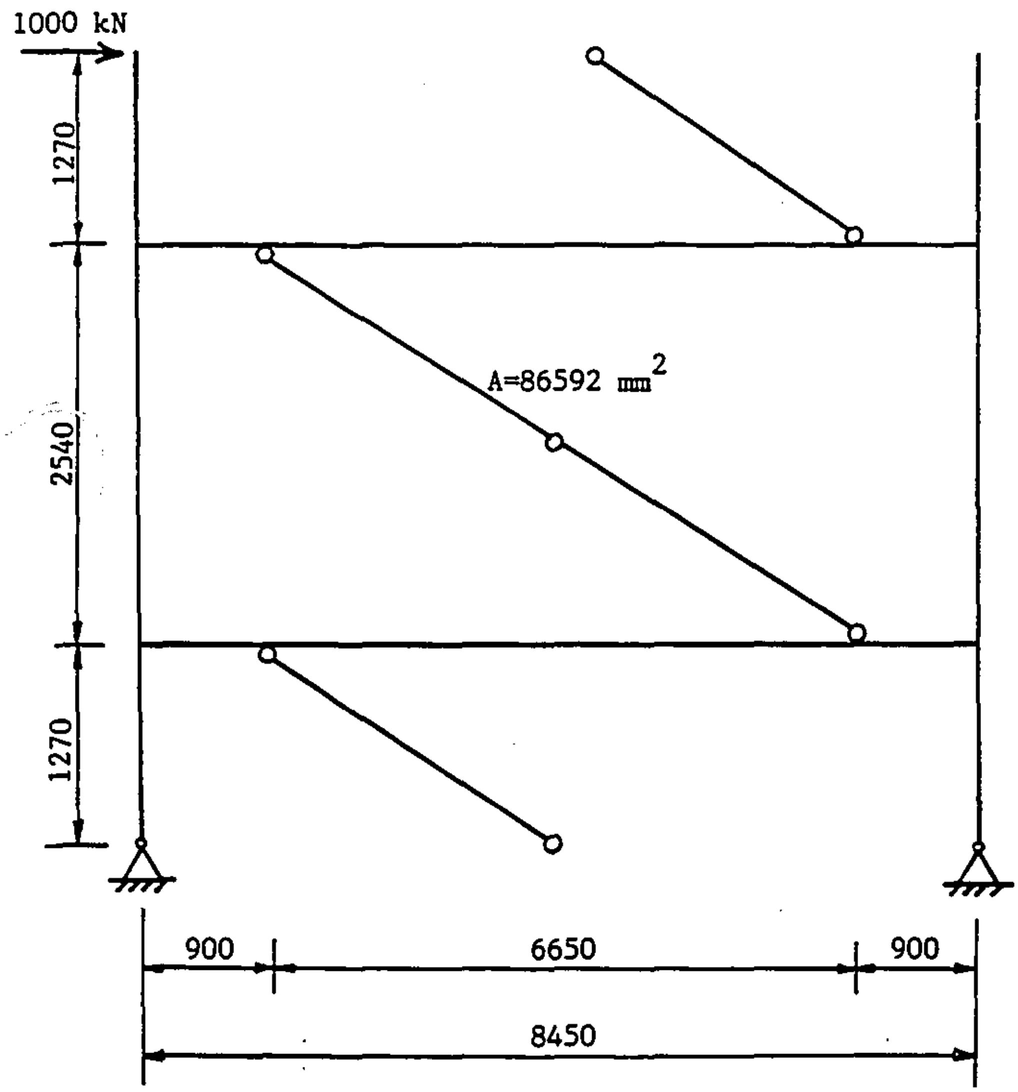

Figure 6.14: Single-Storey Representation of Model 4 with Half-Storeys Above and Below

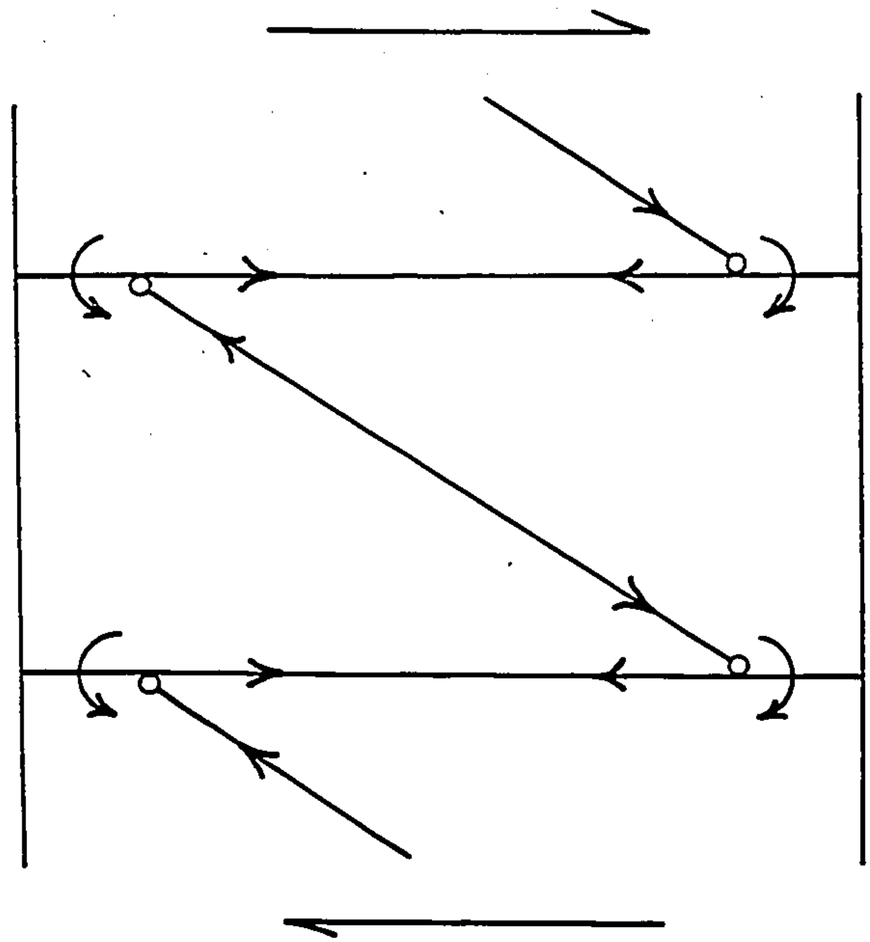

Figure 6.15: Member Actions Contributing to Model's 4 Shear Displacement

beam would, thus, be 0.0689 mm, which is only 1.9 percent of the panel-clad frame's top displacement of 3.62 mm. Therefore, by assuming the beam to be axially rigid a very small error was introduced in the lateral displacement. It is concluded that the axial deformations in the beam are negligible for the representative panel-clad frame analysed and, therefore, the analyses performed in Chapter 4 are sufficiently accurate for the purpose of this study.

CHAPTER 7

THE EFFECT OF PRECAST CONCRETE CLADDING PANELS ON THE STATIC WIND LOAD RESPONSE OF STRUCTURES

The effect of the precast concrete cladding panels on the static wind load response of the two types of structures described in Section 4.1 was explored. The effects of the panels in the total structures were represented by the 'improved', single-diagonal equivalent strut model described in the previous chapter. Static wind load analyses of the example moment-resisting frame and wall-frame structures, with and without the equivalent diagonal struts, that is, with and without the effects of the panels, were performed and the results compared.

7.1 The Effect of Panels on the Static Wind Load Response of a Moment-Resisting Frame Structure

7.1.1 Modelling the Example Structure and the Panels

To study the building's static response, a three-dimensional analysis of the example moment-resisting frame structure was required. Because of the structure's plan double-symmetry, it was possible to reduce the problem to the analysis of a quarter-plan model, subjected to a quarter of the loading. A plan view of the computer model is shown in Fig. 7.1. The columns were represented by beam-type elements. They were assigned their corresponding flexural inertias and sectional areas. The rigid joint zone of the columns on the exterior faces of the building were represented by rigid arms. The slabs were replaced by equivalent beams with appropriate effective widths (Coull and Wong 1981). The effective width of an end bay was taken to be 45 percent of the corresponding interior full-bay value. The beams were assigned a horizontal axis inertia of

$$I_b = \frac{Y_e t^3}{12} \tag{7.1}$$

where Y_e = effective width of the equivalent beam, and
t = thickness of the slab.

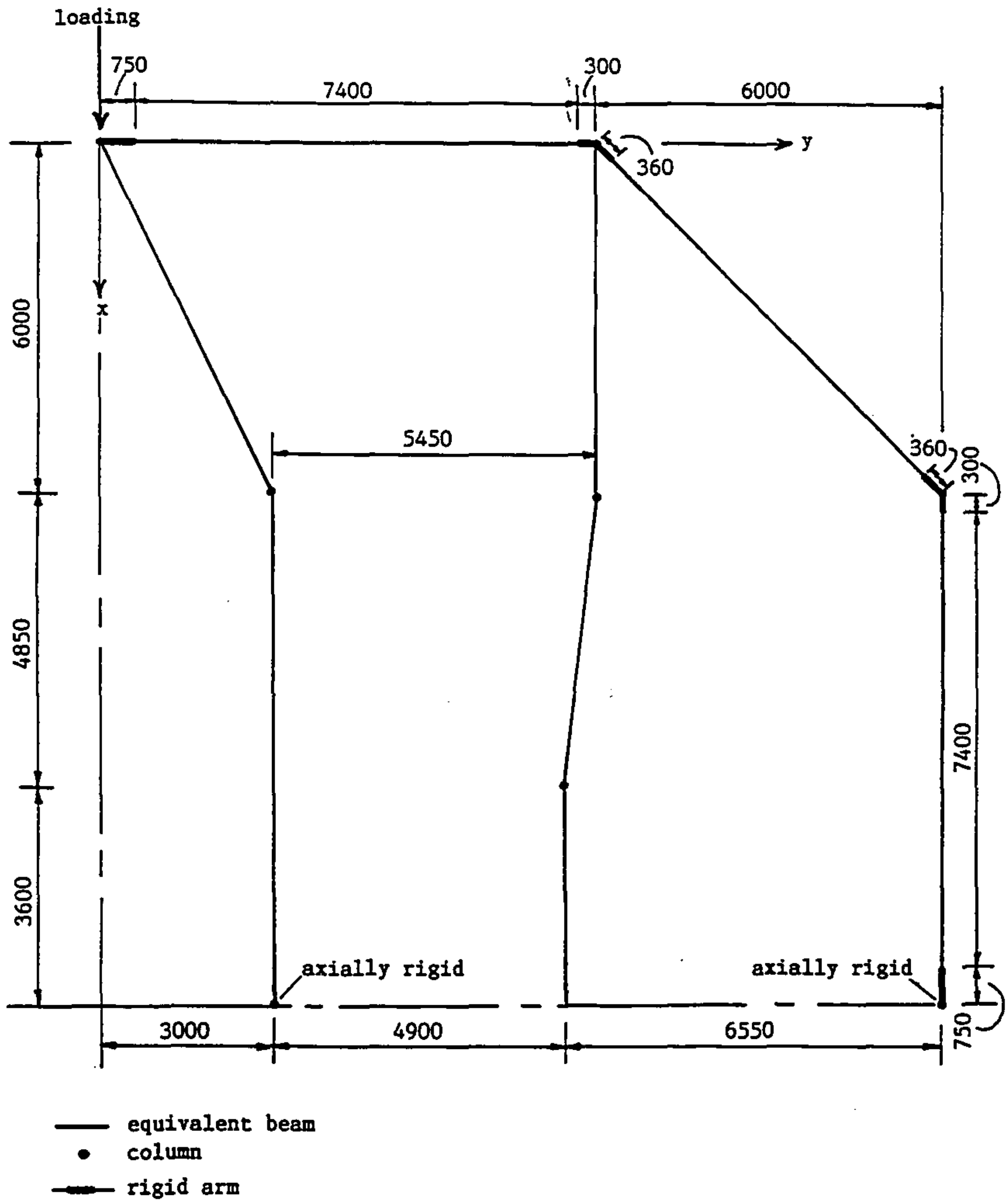

Figure 7.1: Typical Floor of the Mathematical Model for the Example Moment-Resisting Frame Structure

Eq. 7.1 was applied to every bay except in the cases of the example structures in which the stiffening effect of the cladding panels was included. In these cases, the flexural inertia of the equivalent beam supporting the cladding panels was taken from a specific analysis, Chapter 4, Section 4.3, to account for the vertical forces that the panel's bearing connections applies to the slab. The values assigned to the sectional areas of the beams were not important since the nodes at every floor were constrained to move identically in the direction of loading. To obtain the conditions of symmetry required for use of the quarter-plan model of the structure, the horizontal translation of all the nodes in the plane perpendicular to the direction of the loading was restrained, and the ends of the columns on the line of symmetry were restrained against rotation about the axis of loading. The structure behaves anti-symmetrically about the axis of symmetry perpendicular to the axis of loading. Hence, the structure was constrained against vertical displacement along the line of anti-symmetry by assigning an effectively rigid axial area to the columns on this axis, and by restraining the cut end of the beam against vertical displacement at every floor. A uniformly distributed lateral load of 1.268 kN/m^2 was used to simulate the wind loading. For the quarter-plan model of the structure, the loading was 9.1614 kN/m, and it was applied as equivalent concentrated loads at the floor levels.

The precast concrete panels which are located on the exterior faces of the structure at every storey, were modelled by the 'improved' single-diagonal bracing struts with assigned sectional areas to provide a horizontal stiffness component equal to the predetermined stiffness of the example panel and its connections. The example panel stiffness was determined separately, from a finite element analysis of a storey-height, bay-width module of the panel and its connections supported by a flexurally and axially rigid beam. The lateral stiffness of the panel and connections supported by a rigid beam was obtained from analysis IV, Table 4.3. The cross-sectional area of the strut was determined to be 86592 mm^2 in Chapter 6, Section 6.4, and this value is valid for the representative panel with its connections, regardless of the stiffnesses of the frame members.

7.1.2 Analyses and Results

The structure was analysed first without cladding panels, that is without the equivalent diagonal struts. The resulting top deflection of 98.377 mm, gave a drift index of 1/516 which would satisfy the acceptable drift limit range of between approximately 1/300 to 1/500. The overall deflected shape of the structure, Fig. 7.2, indicates the predominantly shear mode of displacement of a moment-resisting frame with a small overall flexural component of displacement due to the axial deformations in the columns and to their moment fixity at the base.

The structure with cladding panels, that is including the equivalent diagonal struts, was then analysed. The resulting top displacement was 31.061 mm, corresponding to a drift index of 1/1635. The top displacement was 68.4 percent less than that of the structure without cladding panels, indicating the panels' very significant overall stiffening effect. The deflected shape of the structure, Fig. 7.2, represents a combination of flexural and shear behaviour. By adding the struts, the shear rigidity of the moment-resisting frame structure

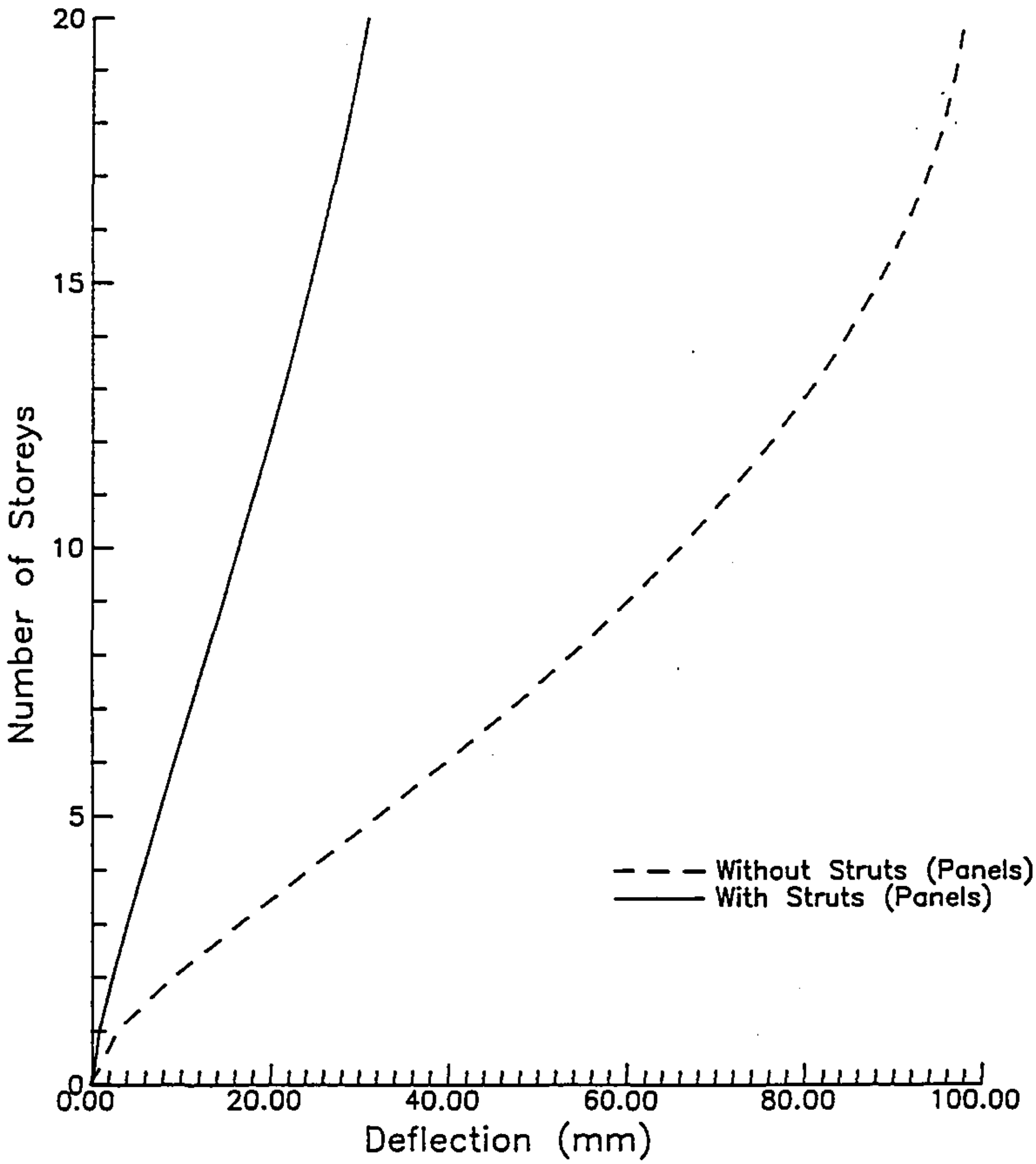

Figure 7.2: Deflected Shapes of the Example Moment-Resisting Frame Structure

was increased, while its overall flexural rigidity was reduced. This reduction was a result of the significantly increased axial deformations in the columns adjacent to the panel arising from the vertical components of the forces in the struts. Fig. 7.3 shows the distribution of the axial stresses in the columns adjacent to the cladding panels for the analyses of the example structure with and without panels. The column between the two adjacent cladding panels did not deform axially because it is on the building's line of symmetry, but the axial stress in the column at the other side of the panel increased by a factor of 6.8 when the effect of the panels was added.

The deflected shape of the example moment-resisting frame structure without bracing consisted of a small flexural component and a large shear component, giving a predominantly shear configuration, Fig. 7.4. The deflected shape of the example moment-resisting frame structure with bracing, however, was composed of a larger flexural component and a smaller shear component, giving rise to a flexural profile in the lower part of the structure, and a shear profile in the upper part, Fig. 7.5.

Except for the beam supporting the cladding panel, the frame-member moments in the lower storeys of the clad moment-resisting frame structure were reduced by approximately 50 to 70 percent from those of the unclad frame structure.

7.2 The Effect of Panels on the Static Wind Load Response of a Wall-Frame Structure

7.2.1 Modelling the Example Structure and the Panels

To determine the static response of the example wall-frame structure, a three-dimensional analysis of the building was required. The wall-frame structure differs from the moment-resisting frame structure in that it has a structural core. Using a simple wide-column model, the core was represented by an equivalent column located at the centroidal axis of the wall aligned in the direction of the loading. The equivalent column was assigned the flexural rigidity EI of one-half of one of the cores. The wide-column effect of the wall on its interaction with the connecting beam, and the condition that plane sections of the wall remain plane, was incorporated by means of stiff arms located at the connecting beam levels, spanning between the effective column and the external fibre of the wall. The rest of the model, and the loading, was identical to that of the example moment-resisting frame structure. A plan view of the computer model for the wall-frame structure is illustrated in Fig. 7.6.

The precast concrete cladding panels were represented by the 'improved' single-diagonal bracing struts with axial areas identical to those in the example moment-resisting frame structure, Section 7.1.1.

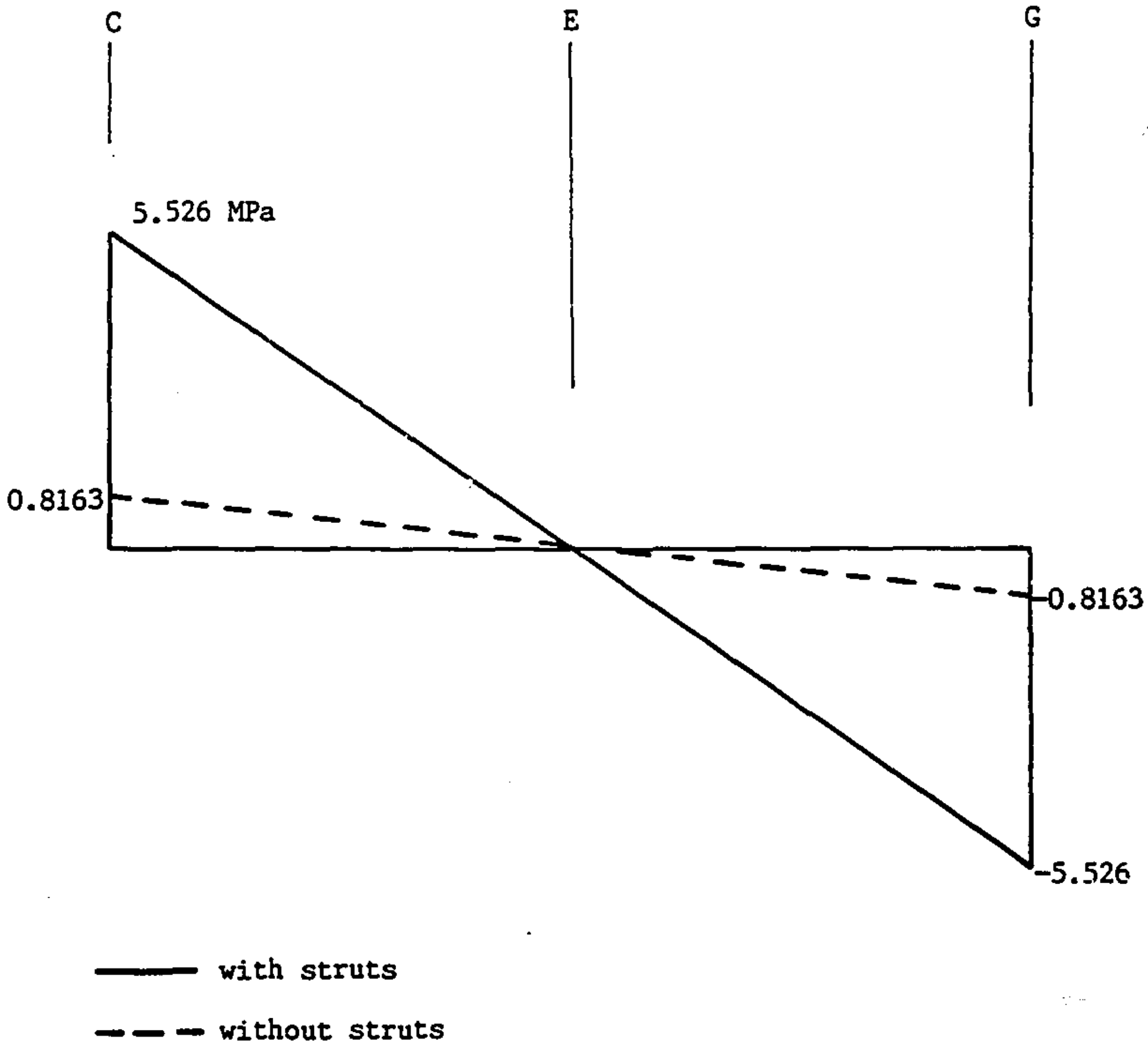

Figure 7.3: Distribution of Axial Stresses in Columns Adjacent to the Cladding Panels

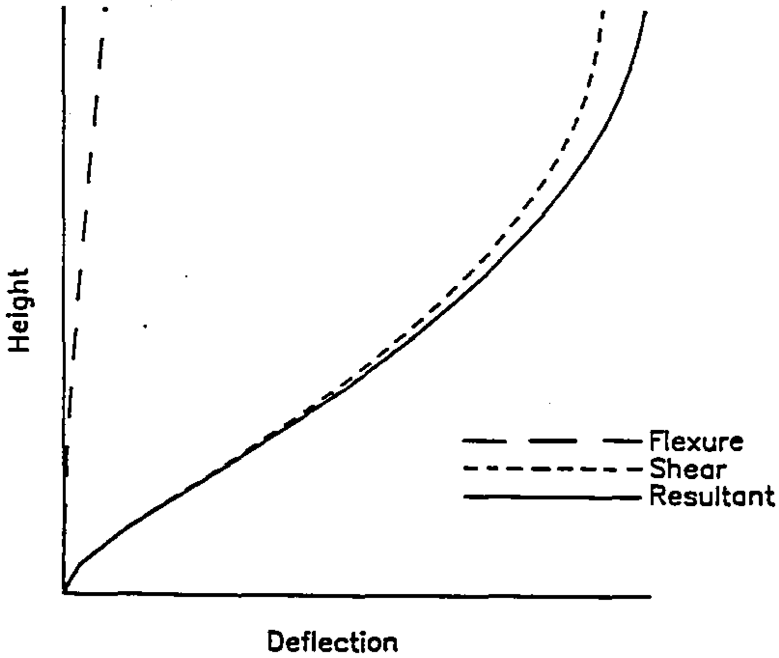

Figure 7.4: Deflected Shapes of the Example Moment-Resisting Frame Structure Without Bracing

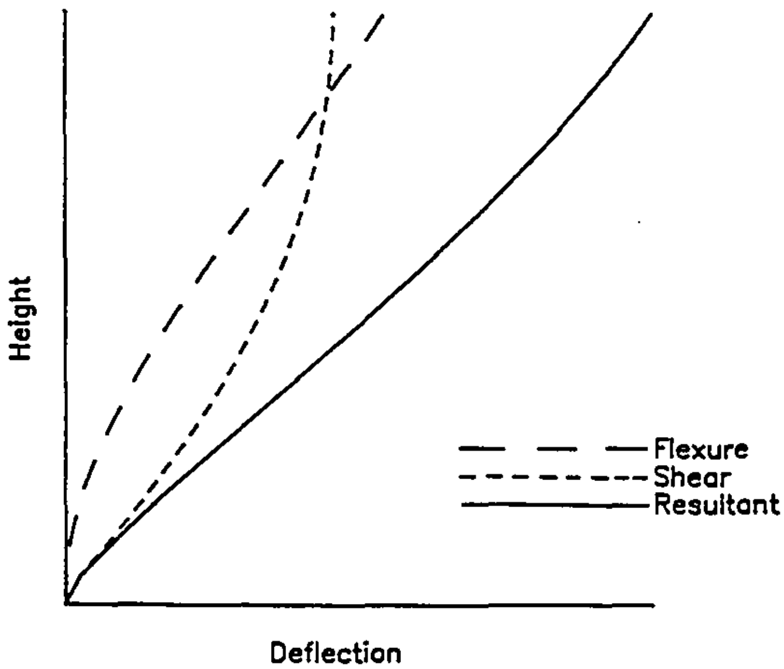

Figure 7.5: Deflected Shapes of the Example Moment-Resisting Frame Structure With Bracing

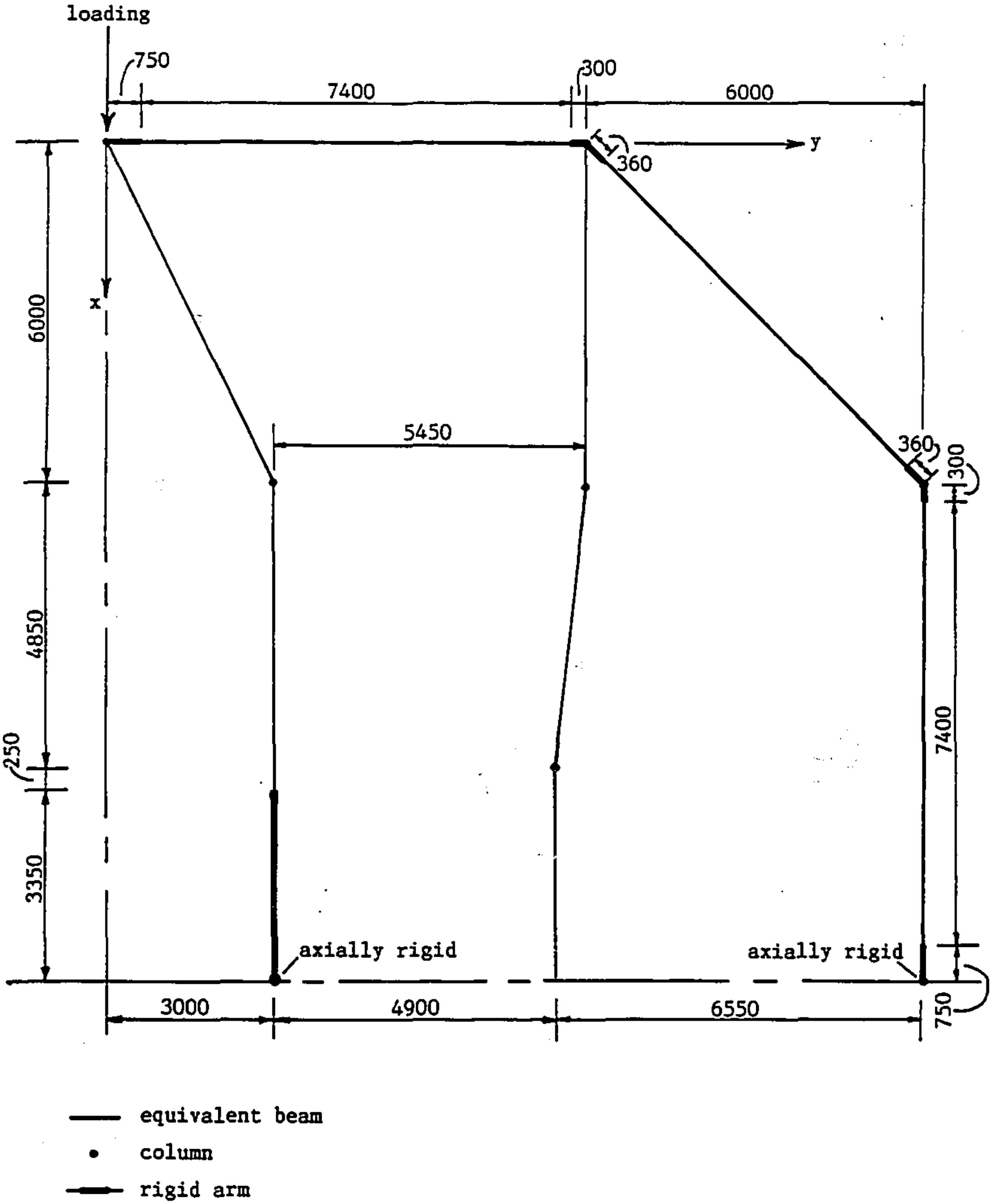

Figure 7.6: Typical Floor of the Mathematical Model for the Example Wall-Frame Structure

7.2.2 Analyses and Results

The wall-frame structure was analysed first without including the effect of the cladding panels, that is without the equivalent diagonal struts. The resulting top displacement of 25.579 mm, gave a drift index of 1/1986, that is well within the acceptable limit. Typically, the deflected shape of a wall-frame structure has a flexural profile in the lower part, and a shear profile in the upper. In this case, the overall deflected shape of the structure, Fig. 7.7, has a predominantly flexural configuration which is due to the high rigidity of the core, with a slight shear profile in the top part of the structure.

The wall-frame structure with the cladding panels, that is including the equivalent diagonal struts, was then analysed. The resulting top deflection was 16.370 mm, corresponding to a drift index of 1/3103. The effect of the cladding panels was to decrease the top displacement of the unclad structure by 36.0 percent. The deflected shape of the structure, Fig. 7.7, is similar to that of the structure without the panels. However, if the deflected shape of the wall-frame structure without the struts is normalized to have a top displacement equal to that of the structure with the struts, Fig. 7.8, it can be observed that relatively greater shear deformation was present in the structure with the bracing. Adding the bracing to the wall-frame structure, increased the shear rigidity, GA, of the structure, but did not alter the bending rigidity of the walls, EI. Therefore, the α-parameter ($= \sqrt{GA/EI}$) was increased. In accordance with wall-frame theory (Heidebrecht and Stafford Smith 1973), as α increases, the point of contraflexure of the deflected shape of a wall-frame structure is lowered. This corresponded with the greater shear configuration of the clad structure.

The frame-member moments in the lower storeys of the clad wall-frame structure, except for the beam supporting the cladding panel, were approximately 25 to 30 percent less than those of the unclad wall-frame structure.

Although significant, the stiffening effect of the cladding was less for the wall-frame structure than for the moment-resisting frame structure. This was because the unclad wall-frame structure is a much stiffer structure than the unclad moment-resisting frame structure.

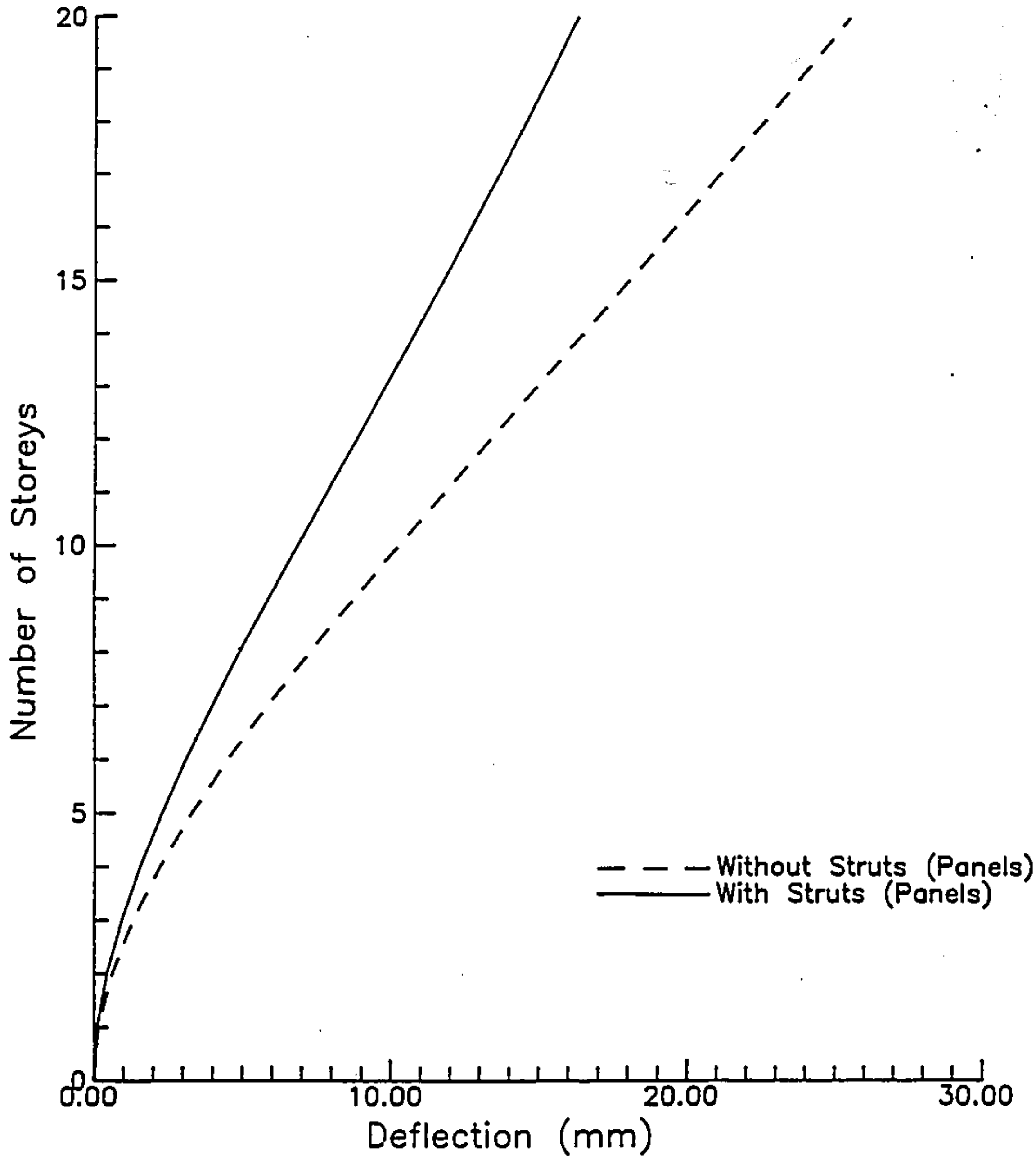

Figure 7.7: Deflected Shapes of the Example Wall-Frame Structure

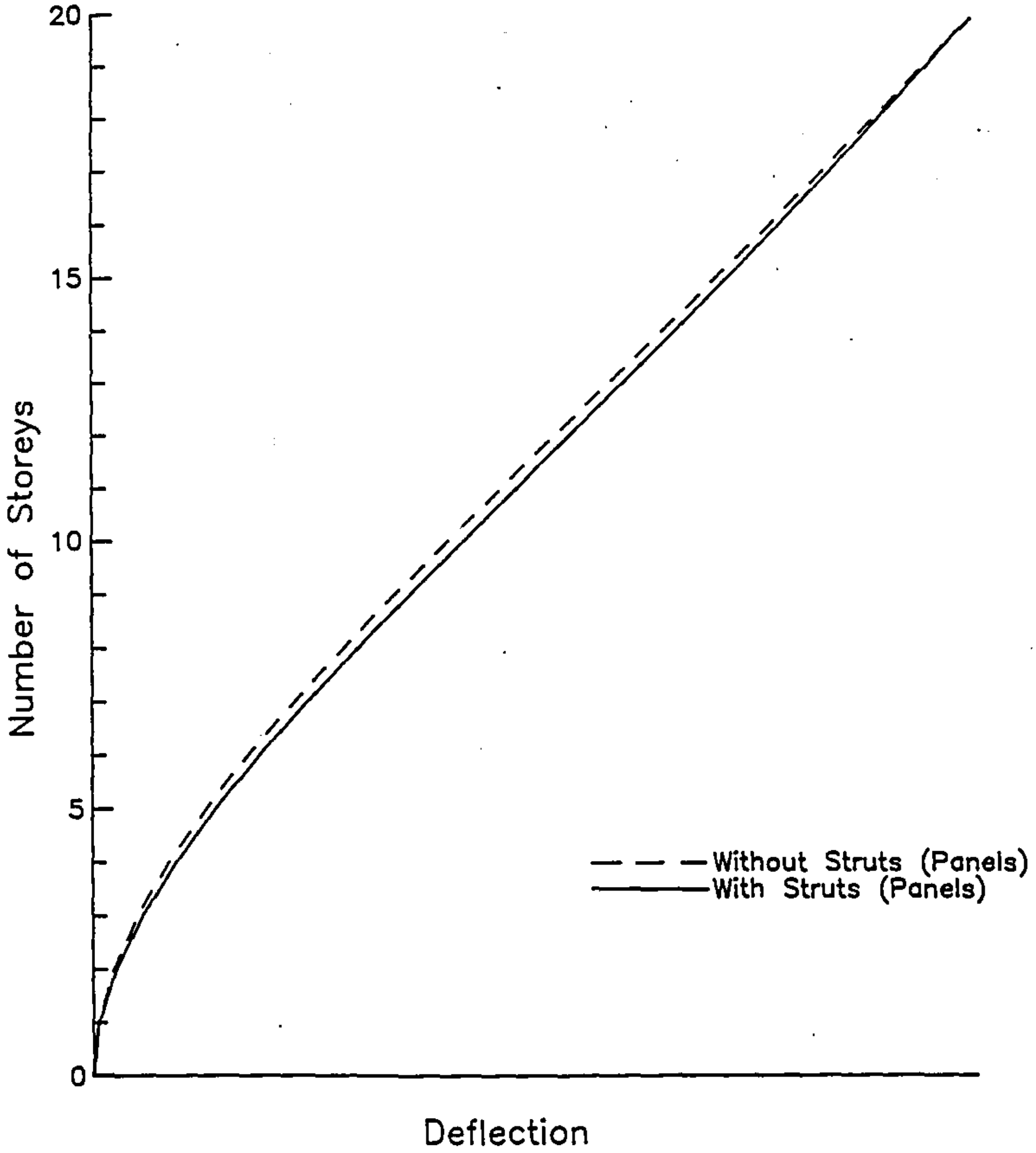

Figure 7.8: Normalized Deflected Shapes of the Example Wall-Frame Structure

CHAPTER 8

RESULTING FORCES IN CONNECTIONS AND STRESSES IN PANEL

It is necessary to consider that, while on the one hand the precast concrete cladding panels provide additional stiffness to the structure, on the other hand they attract loads to themselves which may exceed those for which they were designed. Therefore, it should be verified that the panel and the connections are capable of withstanding the loads to which they are 'inadvertently' subjected. To achieve this, the resulting forces in the diagonal bracing struts of the analysed modelled structure must be converted to forces in the connections for checking against their ultimate capacity, and to stresses in the panel for checking against their allowable values.

8.1 Resulting Forces in the Connections

An estimate of the resulting vertical forces in the bearing connections can be made by taking the vertical component of the force in the 'improved' single-diagonal strut.

In the analysis of the example moment-resisting frame, with bracing to represent the panels, the largest diagonal force occurred in the second storey and had a value of 299.85 kN. The diagonal struts were at an angle of 20.9046° to the horizontal, Section 6.4. Therefore, by taking the vertical component of the diagonal force, the vertical forces in the bearing connections were determined to be 106.99 kN.

Having determined the vertical forces in the bearing connections, the corresponding horizontal forces in the tie-back and left side bearing connections can be obtained. This can be achieved by scaling the horizontal forces resulting from the detailed analysis of the storey-height panel-frame module, analysis II, by the ratio of the vertical forces in the bearing connections obtained above to the vertical forces from the detailed analysis.

The forces in the connections obtained from the analysis of the storey-height panel-frame module subjected to a horizontal load of 1000 kN, analysis II, are presented in Fig. 8.1. The factor necessary to scale the forces in the horizontal connections is thus 0.37718.

The resulting maximum forces that would occur in the connections of the precast concrete panels in this laterally loaded, 20-storey, clad moment-resisting frame example struc-

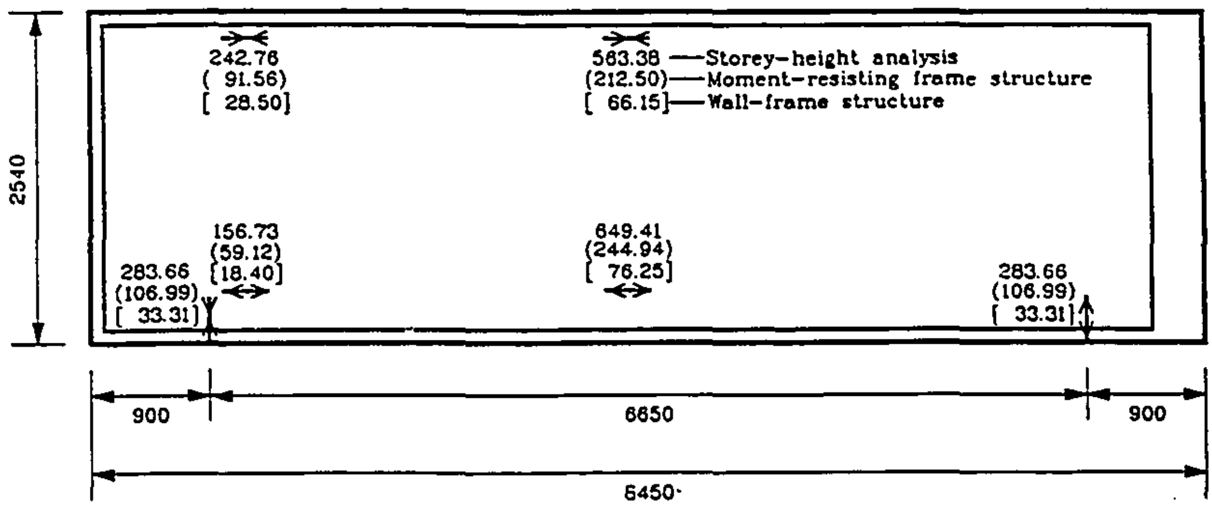

Figure 8.1: Resulting Maximum Forces in Connections

ture are shown in Fig. 8.1.

The resulting forces in the connections of the precast concrete panels in the example wall-frame structure were obtained similarly. The largest diagonal force in the bracing struts representing the panels in the example wall-frame structure was 93.35 kN, and it occurred in the sixth storey. By taking the vertical component of the diagonal force, the vertical forces in the bearing connections were computed to be 33.3085 kN. Hence, the scaling factor for the forces in the horizontal connections is 0.11742.

The resulting maximum forces that would occur in the connections of the precast concrete panels from the lateral load analysis of the example wall-frame structure are also shown in Fig. 8.1. These are only 31 percent of the magnitude of those in the connections of the panels in the moment-resisting frame structure.

8.2 The Ultimate Capacities of the Connections

The ultimate capacities of the two types of connection were checked for their worst loading condition:

(a) the steel haunch bearing connection, subjected to either a vertical force, lateral force, or to both simultaneously, and

(b) the tie-back connection, subjected to the largest lateral force.

The factored and service loads which the steel haunch and the tie-back panel connections must resist are summarized for the example moment-resisting frame and wall-frame structures in Tables 8.1 and 8.2, respectively. Details of the steel haunch bearing connection are shown in Fig. 4.16. The connection was checked for the concrete bearing capacity in two directions, the flexural and shear resistances of the steel section, and the maximum tensile stress in the steel section due to biaxial bending.

An estimate of the concrete bearing capacity is based on theory presented by Marcakis and Mitchell (1980). In Fig. 8.2, the analytical model to predict the ultimate capacity of the connection is presented. The model assumes a linear strain distribution in the concrete with a maximum strain of 0.003 at the front face of the panel. The CSA (1984) stress block factors are used to calculate the stress resultant at the front part of the connection, while a parabolic stress-strain curve is assumed in calculating the stress resultant at the rear part of the connection. The neutral axis depth is determined in a way so that equilibrium of the forces and the moments on the steel member is achieved. The contribution of the shear connectors to the concrete bearing capacity of the connection was neglected.

The resulting equilibrium conditions for the connection at the ultimate load condition are expressed as:

$$V_r = C_f - C_b$$

	Force (kN)	Critical Factored Resistance (kN)	Exceedance
<u>Steel Haunch Connection</u>:			
Vertical Load	198[1]	48.6	307%
Horizontal Load	89[2]	48.6	83%
<u>Tie-Back Connection</u>:			
Unfactored Shear	245	40	513%
Factored Shear	367	105	250%

[1] $= 1.25D + 1.5L$
[2] $= 1.5L$
where D = weight of half a panel; L = load resulting from wind load analysis

Table 8.1: Maximum Design Loads and Factored Resistances for Panel Connections in Moment-Resisting Frame Structure

	Force (kN)	Critical Factored Resistance (kN)	Deviation from Resistance
<u>Steel Haunch Connection</u>:			
Vertical Load	87[1]	48.6	+79%
Horizontal Load	28[2]	48.6	-42%
<u>Tie-Back Connection</u>:			
Unfactored Shear	76	40	+90%
Factored Shear	114	105	+9%

[1] $= 1.25D + 1.5L$
[2] $= 1.5L$
where D = weight of half a panel; L = load resulting from wind load analysis

Table 8.2: Maximum Design Loads and Factored Resistances for Panel Connections in Wall-Frame Structure

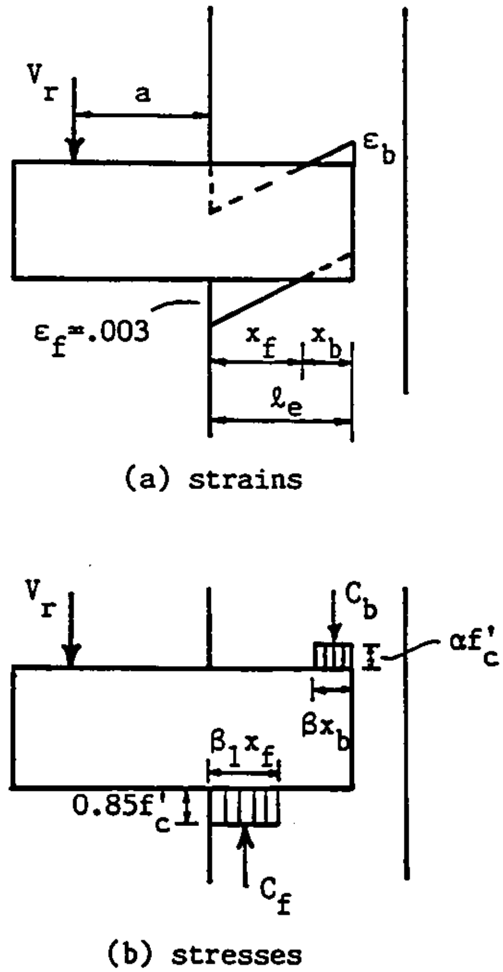

Figure 8.2: Analytical Model to Predict Ultimate Capacity of Connection

$$= 0.85\phi_c f_c' b \beta_1 x_f - \alpha \phi_c f_c' b \beta x_b \tag{8.1}$$

Taking moments about the front face of the panel gives,

$$\begin{aligned} V_r a &= C_b\left(\ell_e - \frac{\beta x_b}{2}\right) - C_f\left(\frac{\beta_1 x_f}{2}\right) \\ &= (\alpha\phi_c f_c' b \beta x_b)\left(\ell_e - \frac{\beta x_b}{2}\right) - (0.85\phi_c f_c' b \beta_1 x_f)\left(\frac{\beta_1 x_f}{2}\right) \end{aligned} \tag{8.2}$$

where V_r = factored resistance of the connection,
C_f = resultant compressive force at the front of the steel member,
C_b = resultant compressive force at the back of the steel member,
f_c' = specified compressive strength of concrete,
b = effective width of the connection (a maximum width equal to 2.5 x width of embedded member was assumed),
β_1 = CSA stress block factor $\left(= 0.85 - 0.08\left(\frac{f_c'-30}{10}\right) \not< 0.35 \not> 0.85\right)$,
x_f = depth of the strain distribution from the front of the connection,
x_b = depth of the strain distribution from the back of the connection ($x_f + x_b = \ell_e$),
ℓ_e = effective length of the connection,
$\alpha\beta = \frac{\varepsilon_b}{\varepsilon_o} - \frac{1}{3}\left(\frac{\varepsilon_b}{\varepsilon_o}\right)^2$,
$\beta = \frac{4-\frac{\varepsilon_b}{\varepsilon_o}}{6-\frac{2\varepsilon_b}{\varepsilon_o}}$,
ε_o = strain at maximum concrete stress assumed to be 0.002,
ε_b = strain at the back of the connection ,
a = distance from the front face of the connection to the resultant of the vertical loads,
ϕ_c = material factor for concrete (= 0.60).

For a given loading configuration the two unknowns, x_f and V_r, are found by solving Eqs. 8.1 and 8.2 simultaneously. A simplified expression for the concrete bearing capacity of the connection, however, has been developed (Marcakis and Mitchell 1980) and has been adopted by the CPCI design manual (1987):

$$V_r = \frac{0.85\phi_c f_c' b \ell_e}{1 + \frac{3.6e}{\ell_e}} \tag{8.3}$$

where $e = a + \frac{\ell_e}{2}$.

By substituting the values for the given example, Fig. 4.16, into Eq. 8.3, the concrete bearing capacity was calculated to be 48.6 kN. It should be noted that the computed concrete bearing capacity is conservative since the effect of the shear connectors was neglected.

The flexural and shear resistances of the steel section were also checked. The flexural resistance of the embedded structural member is (CPCI Design Manual 1987, Handbook of Steel Construction 1982)

$$M_r = \phi_a Z_s f_y \tag{8.4}$$

or,

$$M_r = V_r a + \frac{0.5V_r^2}{0.85\phi_c f_c' b} \tag{8.5}$$

where ϕ_a = material factor for steel (=0.90),
Z_s = plastic section modulus of steel section, and
f_y = yield strength of steel section.

The capacity of the steel section in shear (Handbook of Steel Construction 1982) is given by

$$V_r = \phi_a 0.55 f_y h t \tag{8.6}$$

where h = depth of steel section, and
t = thickness of section.

For the steel section in Fig. 4.16, M_r, Eq. 8.4, was determined to be 10.84 kN-m. By substituting this into Eq. 8.5, the flexural resistance of the steel section was calculated to be 105.2 kN. The shear resistance of the steel section, on the other hand, was found to be 126.2 kN, Eq. 8.6.

For the steel haunch bearing connection subjected to a vertical load, a comparison of the concrete bearing capacity (48.6 kN) with the flexural (105.2 kN) and shear (126.2 kN) resistances of the steel section, showed that the concrete bearing capacity was critical. Using this criterion, the factored vertical load acting on the steel haunch bearing connection of the panel in the clad moment-resisting frame structure, Table 8.1, exceeded the resistance of the connection by 307 percent. While the factored vertical load acting on the connection of the panel in the wall-frame structure exceeded the resistance of the connection by 79 percent.

For the steel haunch section subjected to a horizontal load, the concrete bearing capacity was again more critical than the flexural and shear resistances of the steel section. A comparison of the factored horizontal loads resulting from the analyses of the clad structures, with the concrete bearing capacity in the lateral direction, 48.6 kN, indicated that the capacity of the connection was sufficient to resist this for the panels in the wall-frame structure, Table 8.2, but not for those in the moment-resisting frame structure, Table 8.1.

For the simultaneous application of the horizontal and vertical loading on the steel haunch connection, the maximum tensile stress in the steel section due to the biaxial bending was verified. Referring to Fig. 8.3, and using the resulting factored moments, the maximum

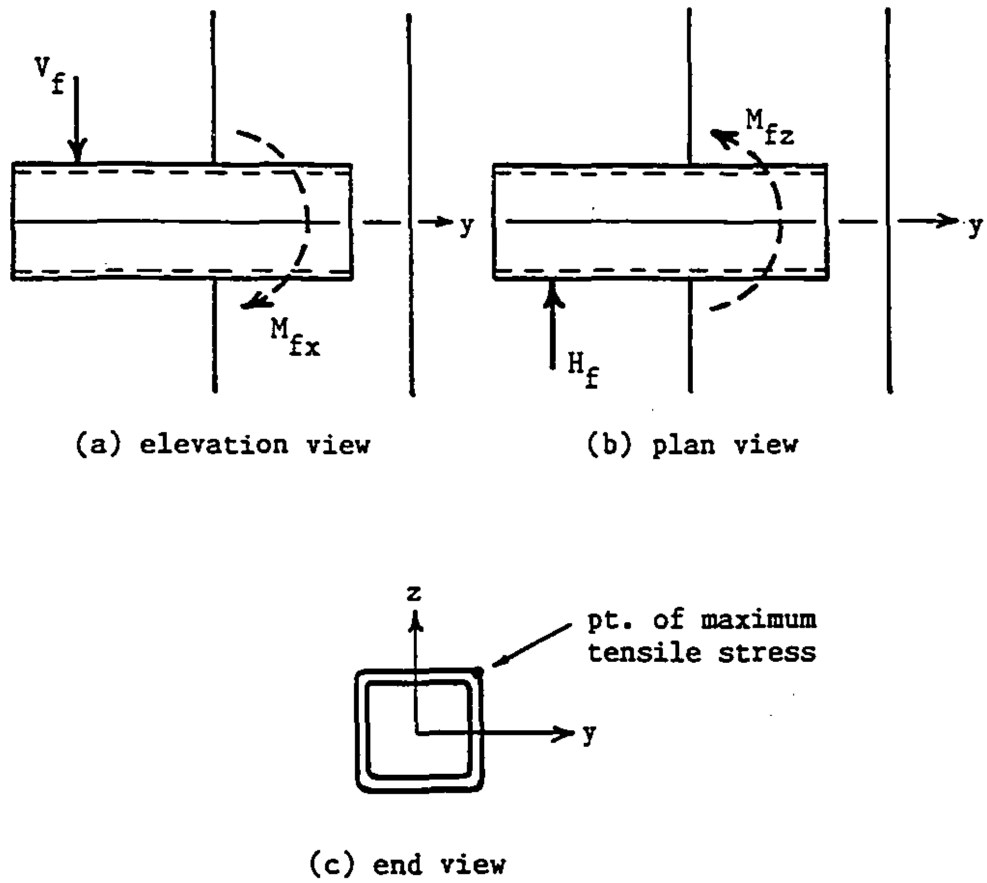

Figure 8.3: Biaxial Bending of the HSS Section

tensile stress is given by

$$\sigma_{max} = \frac{M_{fx}z}{I_x} + \frac{M_{fz}x}{I_z} \tag{8.7}$$

The factored moments due to the vertical and horizontal loads acting on the bearing connection of the panel in the clad moment-resisting frame were 17.3 kN-m and 7.79 kN-m, respectively. For the bearing connection of the panel in the clad wall-frame, the factored moments as a result of the vertical and horizontal loads were 7.61 kN-m and 2.45 kN-m. By substituting these values and the appropriate properties of the steel section into Eq. 8.7, the maximum tensile stress in the steel section was determined. In the case of the clad moment-resisting frame, the maximum tensile stress in the steel section, 885 MPa, exceeded the 350 MPa yield stress of the HSS section by 153 percent. In the case of the clad wall-frame structure, the maximum tensile stress, 355 MPa, exceeded very slightly the yield stress of the section.

It was also necessary in checking the capacity of the steel haunch connection to verify the shear and flexural resistances of the side plates which are welded to the HSS section, Fig. 4.17. The flexural and shear resistances of only plate DE was checked, since it is stiffer than plate AB; and, therefore, will attract the greater load. The stiffnesses of plates AB and DE were determined to be 0.255E and 6.875E, respectively, Eq. 4.4. The factored horizontal loads acting on the bearing connections, Tables 8.1 and 8.2, were assumed to be shared between the plates according to their stiffnesses to give the resulting factored shear and factored moment in plate DE. The factored flexural and shear resistances of plate DE were calculated using Eqs. 8.4 and 8.6, respectively. In the analysis of the clad moment-resisting frame, the available shear resistance of the plates was sufficient for the shear force resulting in the connections, but the resulting moment was 98 percent greater than the flexural resistance. The available resistances of the plates were sufficient for the loads in the connections of the panels attached to the wall-frame structure.

Considering the tie-back connection subjected to an in-plane lateral load, the shear resistance and the factored shear resistance of the bolts connecting the angle to the slab and to the panel were checked. Both these bolts are standard 20-mm diameter bolts with a shear resistance of V_s = 40.0 kN, and a factored shear resistance of V_r = 105 kN. The factored and unfactored shears acting on these connections from the clad moment-resisting frame analysis, Table 8.1, exceeded the resistances of the bolts by 250 and 513 percent, respectively. Only the bolts in the panels of the top five storeys of the moment-resisting frame would be capable to carry the induced unfactored shear. From the clad wall-frame analysis, the exceedances were 9 and 90 percent for the unfactored and factored shears, respectively, Table 8.1.

To summarize, it is evident that the example moment-resisting frame structure, and for the intensity of the applied horizontal loading, in which the panels reduced the top lateral displacement by 68.4 percent, the most heavily loaded connections would not withstand the loads to which they would be subjected. For the example wall-frame structure, in which the panels reduced the top lateral displacement by 36.0 percent, the connections would require a slight increase in strength to be adequate.

8.3 Resulting and Allowable Stresses in the Panel

The resulting stresses in the precast concrete cladding panels of the example structures can be obtained by multiplying the stresses found from the lateral load analysis of the single-storey panel-frame module by the same scaling factor as used for the horizontal forces in the tie-back connections. The maximum and minimum principal stresses in the panel were determined by multiplying the corresponding stresses of analysis II by 0.37718 for the moment-resisting frame structure, and by 0.11742 for the wall-frame structure.

Contour plots for the resulting maximum and minimum principal stresses in the panel of the moment-resisting frame structure are presented in Figs. 8.4a and 8.4b, respectively. For the wall-frame structure, these are shown in Figs. 8.5a and 8.5b, respectively. In general, local stress concentrations occur in the panels at the corners of the window openings, with tensile stresses at the corners of the leading diagonal, and at the locations where the connections inject concentrated loads into the panel. These are in accordance with the general understanding that stress concentrations occur around re-entrant corners and at points of concentrated load application. Away from these areas of local stress concentration, the panel is relatively lightly stressed.

The stress distributions are similar for the panels in the moment-resisting frame and wall-frame structures, except that the stresses in the panel of the moment-resisting frame structure are scaled by a larger factor than those in the panel of the wall-frame structure. Referring, in passing, to the contour plots of the maximum principal stresses, Figs. 8.4a and 8.5a, the largest stresses occur where the horizontal link at the top centre connects to the panel. The computed largest tensile stress for a panel in the moment-resisting frame structure was approximately 5.6 MPa, while that for a panel in the wall-frame structure was approximately 1.7 MPa. These values, however, are not meaningful, since they result from an applied force that is modelled as concentrated at a point, which does not represent what actually occurs at the location of the connection in the panel.

The permissible tensile stress for the concrete in the panel can be taken as the modulus of rupture (Collins and Mitchell 1987), that is,

$$f_r = 0.6\sqrt{f'_c} \quad \text{for normal density concrete} \tag{8.8}$$

Since the specified compressive strength of the panel's concrete is 35 MPa, the permissible tensile stress from Eq. 8.8 is 3.55 MPa. Away from the areas of stress concentration, the tensile stresses in the panels of both example structures are well within the permissible limit. Although only a hypothetical consideration, because of the inaccuracy of the stresses adjacent to points of load application, the values of stress in the regions of stress concentration are greater than the permissible stress in the panels of the moment-resisting frame structure, while those in the panels of the wall-frame structure are less than the permissible stress.

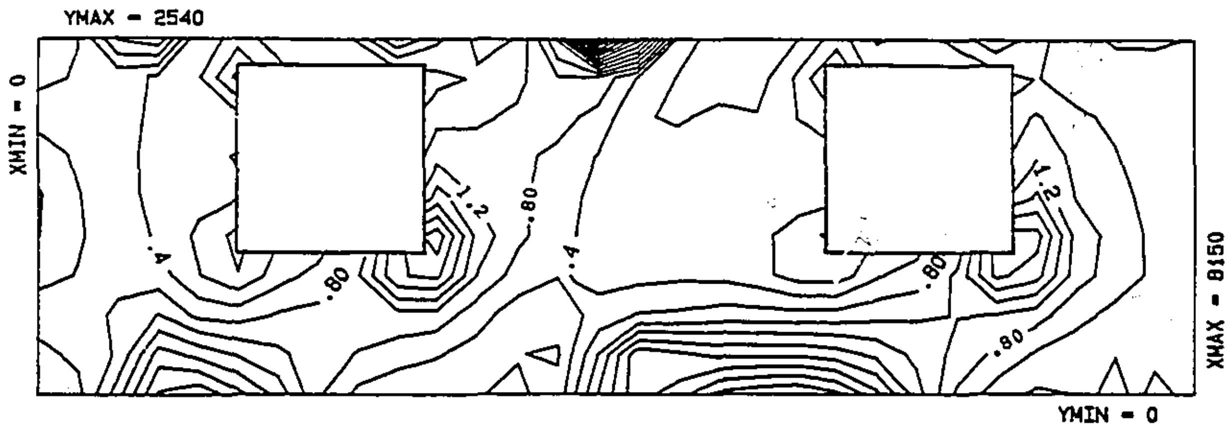

(a) Maximum Principal Stresses

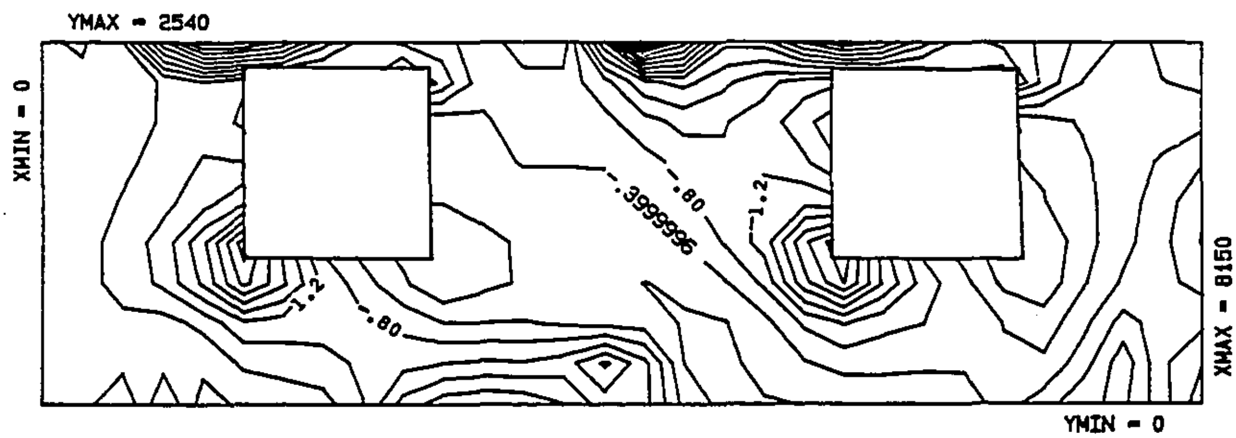

(b) Minimum Principal Stresses

Figure 8.4: Resulting Stresses in Worst Loaded Panel of Clad Example Moment-Resisting Frame Structure

(a) Maximum Principal Stresses

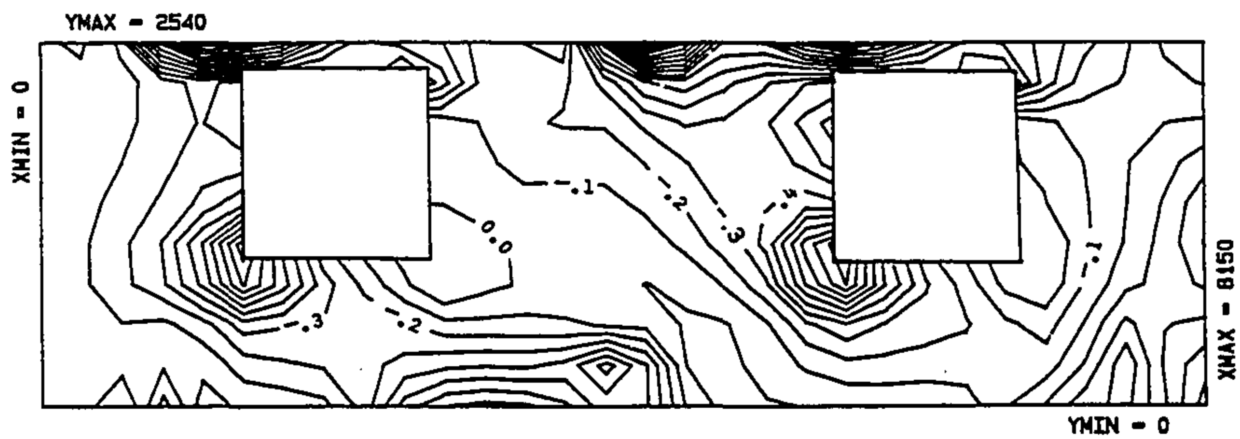

(b) Minimum Principal Stresses

Figure 8.5: Resulting Stresses in Worst Loaded Panel of Clad Example Wall-Frame Structure

Referring to the contour plots of the minimum principal stresses, Figs. 8.4b and 8.5b, the computed largest compressive stresses also occur at the locations of local concentrated stress. Taking the permissible compressive stress of concrete as $0.6f_c'$ (CSA 1984), that is, 21 MPa for the panels in question, this limit is satisfied even at the locations of stress concentration, Figs. 8.4b and 8.5b.

The analysed stresses were calculated by taking an average of the element stresses from the different membrane finite elements attached to a common node. Because of the high stress gradients in some regions, at certain joints the stress from one element was as much as 200 times greater than that given by an adjacent element. To obtain more accurate results, an analysis using a much finer mesh would have been required. However, for the purposes of this study, the size of mesh gave results sufficiently accurate to give an idea of the panel's stiffness, its stress distribution and the approximate magnitude of the stresses.

The stresses obtained from the analyses are intended primarily to give an indication of the stress distribution and where additional reinforcement would be required. It appears from the analyses that the panels in the wall-frame structure were adequate to withstand the loads to which they would be subjected, but additional reinforcement in critical areas of the panels in the moment-resisting frame structure would be necessary.

CHAPTER 9

THE EFFECT OF PRECAST CONCRETE CLADDING PANELS ON THE SEISMIC RESPONSE OF STRUCTURES

The effect of the precast concrete cladding panels on the seismic response of the two types of structures described in Section 4.1 was explored. A brief description of the background required and the approach used for the dynamic analyses is presented. Eigenvalue analyses and linear elastic response spectrum analyses of the example moment-resisting frame and wall-frame structures, with and without the stiffening effects of the panels, were performed and the results were compared. The purpose of these dynamic analyses was to make a comparison between the resulting dynamic properties and design quantities of the example structure, with and without the stiffening effect of the cladding panels, rather than an investigation of their absolute values. As in the static wind load analysis, the panels were modelled by the 'improved' single-diagonal bracing struts.

9.1 A Background to the Approach Used for the Seismic Analyses of Structures

Once the mathematical model of a structure has been developed, the first step in a seismic analysis is to determine the dynamic properties of the structure; that is, the natural periods of vibration and the mode shapes. In the linear elastic dynamic analyses, these are the most important properties governing structural response. The mode shapes dictate the distribution of the design quantities over the height of the building, and the natural periods, being related to the spectral amplitudes, govern the magnitudes of these design quantities.

The undamped free vibration mode shapes and frequencies of a structure are found from an eigenvalue analysis. This involves the solution of the following generalized eigenvalue problem

$$[K]\,[\Phi] = [M]\,[\Phi]\,[\omega^2] \tag{9.1}$$

where $[K]$ = stiffness matrix,

$[M]$ = diagonal mass matrix,
$[\omega^2]$ = diagonal matrix of eigenvalues, and
$[\Phi]$ = matrix of corresponding eigenvectors.

The eigenvectors are the mode shapes of the structure, and the eigenvalues are the circular frequencies squared. For each of the example structures an eigenvalue analysis, using the SAP80 (1986) computer program, was performed to investigate the influence of the cladding panels on the dynamic properties of the structure.

The next objective is to perform response spectrum dynamic analyses to evaluate the effect of the cladding panels on the overall design quantities. Although a full nonlinear time history analysis would be required for a theoretically 'correct' analytical result, it is rarely used in design practice, because it is difficult to employ and interpret, and it is also time-consuming and costly. The response spectrum method is computationally much more efficient, and with appropriate modal combination rules can yield results that show very good comparison with time history analysis (Neuss et al. 1983). Furthermore, the response spectrum is based on a range of possible earthquake ground motions, rather than a unique earthquake excitation, which may not predict the future seismic ground motions that may occur at a given site during the useful life of a structure. Response based on elastic periods will 'accurately' represent force levels from earthquakes of moderate intensity and will reflect at least the initial response to a very severe earthquake.

Before the dynamic analyses can be performed, a design spectrum must be chosen to represent the earthquake ground motion. Usually, the design response spectrum used in Canada for a seismic analysis is that provided by the National Building Code of Canada (1985). The design spectrum presented in the 1985 NBCC was derived from a response spectrum for 5 percent damping and was based on the assumption that the acceleration-related seismic zone factor is equal to the velocity-related seismic zone factor. It has also been derived to be used in conjunction with the periods of vibrations given by the code formulae, which include safety factors to account for non-structural effects, different types of overlying soils, etc., and to maintain a certain level of safety. Several other design spectra which represent response envelopes based on an entire variety of earthquake motions have been developed, for example, Newmark and Hall (1973), and Newmark et al. (1973). The design spectrum that must be used in a dynamic analysis is also dependent on the type of structure that will be excited; for this reason building codes for different types of structures have developed their own design response spectra, such as the American Petroleum Institute (API) (1981), the Nuclear Regulation Commission (NRC) (1973), the Veterans Administration (VA) (1973), etc. In this study, the Newmark and Hall (1973) elastic spectrum, Fig. 9.1, for 5 percent damping and scaled to 0.04g was used in the seismic analyses. It provides a better representation of actual earthquake spectra than many other spectra (Neuss et al. 1983); it is well-known, it reflects an upperbound envelope of actual spectrum curves, it is normalized with respect to the three ground motion parameters (acceleration, velocity, and displacement), and it covers long-period structures well. For the generalized and comparative purpose of this study, the maximum ground acceleration of 0.04g, chosen according to the 1980 NBCC for the Montreal region, was considered acceptable.

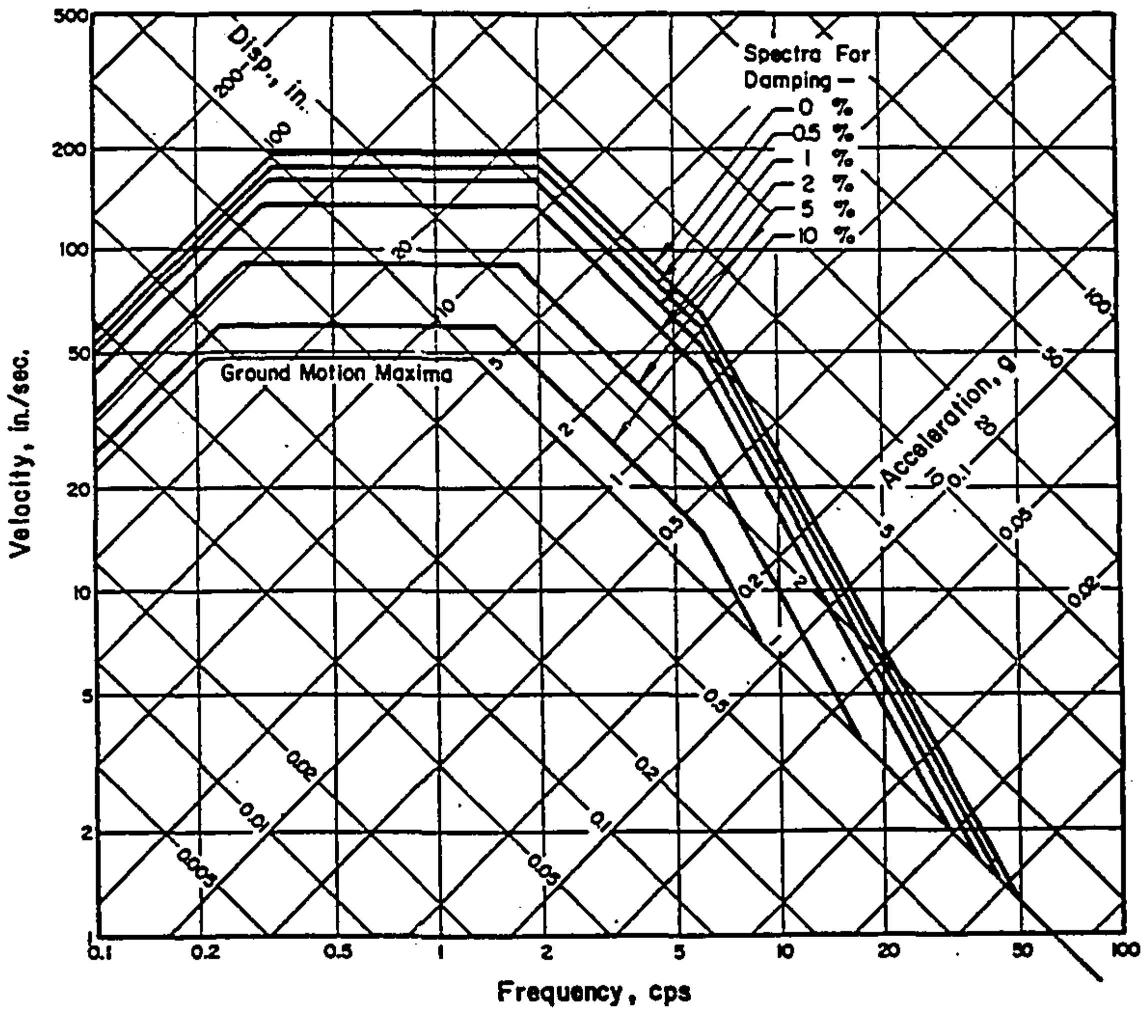

Figure 9.1: Newmark and Hall Design Spectrum (Newmark and Hall 1973)

To determine the seismic response quantities; that is, the resulting force and displacement quantities, the mode-superposition procedure (Clough and Penzien 1975) was used. It is not necessary, however, to include all the higher modes of vibration in the superposition process. A rule of thumb is to consider a sufficient number of modes so that an effective modal mass of at least 90 percent of the total mass is represented by the modes chosen. The effective modal mass, e, of the structure is that part of the total mass responding to the earthquake, and it is given by the following expression

$$e = \frac{\sum_{i=1}^{j} \frac{p_i^2}{m_i^*} \times 100}{\underline{r}^T[M]\underline{r}} \tag{9.2}$$

where $p_i \ = \underline{\Phi}_i^T[M]\underline{r}$
$m_i^* = \underline{\Phi}_i^T[M]\underline{\Phi}_i$
$\underline{r}$ = unit influence vector,
$[M]$ = diagonal mass matrix,
$\underline{\Phi}_i$ = mode shape vector i, and
j = number of retained modes.

Having determined the design response spectrum, and the number of modes to retain for the solution, a response spectrum seismic analysis was then performed by the SAP80 computer program to extract participation factors, spectral accelerations, and spectral displacements. Using these values, the overall building design quantities of primary concern including peak storey shears, peak storey overturning moments, peak storey deflections, and peak interstorey drifts were computed. To determine peak storey shears and overturning moments, it is necessary to calculate the equivalent external forces, $\overline{F}_{i,max}$, for each mode i, acting on the structure, that is,

$$\overline{F}_{i,max} = [M]\underline{\Phi}_i\gamma_i S_{ai} \tag{9.3}$$

where $[M]$ = diagonal mass matrix,
$\underline{\Phi}_i$ = mode shape vector i,
γ_i = participation factor for mode i, and
S_{ai} = spectral acceleration for mode i.

The peak storey shear, $V_{i,max}$, and peak storey overturning moment, $M_{i,max}$, for mode i, at any level k can be computed as follows

$$V_{i,max,k} = \sum_{j=k}^{N} F_{i,max,j} \tag{9.4}$$

and

$$M_{i,max,k} = \sum_{j=k+1}^{N} h_j \cdot F_{i,max,j} \tag{9.5}$$

where h_j is the height of the j^{th} floor above the k^{th} floor and N is the total number of storeys. The peak storey deflections, $\overline{\Delta}_{i,max}$, for mode i, are simply given by the following expression

$$\overline{\Delta}_{i,max} = \Phi_i \gamma_i S_{di} \tag{9.6}$$

where S_{di} is the spectral displacement for mode i. The peak interstorey drift, $\delta_{i,max}$, for mode i, at any level k, can then be calculated by taking the difference between the deflections of the floors above and below, that is,

$$\delta_{i,max,k} = \Delta_{i,max,k} - \Delta_{i,max,k-1} \tag{9.7}$$

An envelope of peak responses for each design quantity is calculated over the height of the building based on the square-root-of-the-sum-of-the-squares (SRSS) modal combination method. The SRSS method gives accurate response predictions for regular buildings, that is buildings in which the centres of stiffness and mass coincide, and for structures which do not have modes with closely spaced periods dominating the response (Maison et al. 1983). Its mathematical form is given by

$$R_{max} = \sqrt{\left(\sum_{i=1}^{n} R_i^2\right)} \tag{9.8}$$

where R_{max} = estimated maximum response for quantity R,
R_i = maximum response of quantity R in mode i, and
n = number of modes considered.

Other methods such as the absolute sum (ABS) rule yield responses that are too conservative and not appropriate for design purposes, while the complete quadratic combination (CQC) (Wilson et al. 1981) method is a recent development to provide good examples for irregular buildings and buildings having modes with closely spaced periods.

In addition to illustrating the influence of the cladding panels on the magnitudes of design quantities, the relative contribution of the various modes to the complete responses are also investigated to gain a better understanding of the dynamic response of each building. Because the SRSS modal combination method is used to compute peak responses for the seismic analyses performed, the contribution of each mode to peak response can be represented as a ratio of the square of the mode's peak response to the total sum of the squares of all modal peak responses (Neuss et al. 1983). That is, the contribution of mode 'n' to total peak response is represented by the ratio

$$\frac{(R_n)^2}{\sum_{i=1}^{N}(R_i)^2} \tag{9.9}$$

where R_i = peak response in mode i, and
N = total number of modes.

In this calculation, the square of the response is used, so that the sum of the modal contribution ratios will equal one.

9.2 The Effect of Panels on the Seismic Response of the Moment-Resisting Frame Structure

9.2.1 The Influence of Panels on the Dynamic Properties

Using the same mathematical model as for the case of the static wind load analysis, except its having mass values assigned at every floor level, the natural periods of vibration and mode shapes for the example moment-resisting frame structure, with and without the stiffening effect of the cladding panels, were extracted from an eigenvalue analysis using the SAP80 (1986) computer program. At a typical floor, a mass was assigned to the translational degree of freedom in the direction of the loading, corresponding to the mass of one-quarter of the structure plus the mass of two panels, that is, 0.113 $kN \cdot s^2/mm$. At the top, the mass was assigned a value of only one-quarter of the mass of the slab, that is, 0.0895 $kN \cdot s^2/mm$.

The first four translational mode shapes are presented in Fig. 9.2 for the cases with and without the stiffening effect of the cladding panels, that is modelled by the 'improved' single diagonal struts. In the case without bracing, the first mode shape verifies the predominantly shear mode of deformation of the moment-resisting frame structure, while in the case with the bracing the first mode shape illustrates a greater flexural profile in the lower part of the structure with a shear profile in the upper part. By adding the struts, the shear rigidity of the moment-resisting frame structure was increased, while its overall flexural rigidity was simultaneously reduced. This reduction was due to the significantly increased axial deformations in the columns adjacent to the braced panel arising from the vertical components of the forces in the struts. In both cases, the first mode shape compares with the deflected shape obtained from the static wind load analysis. The second, third and fourth mode shapes changed only slightly when the effect of the cladding panels were added. The nodes (i.e. neutral points) occurred at approximately the same locations in the braced and unbraced cases, and the anti-nodes (i.e. points of maximum displacements) occurred at similar locations with approximately the same values.

In Table 9.1, the natural periods of vibration for the two models are presented and compared. Significant variations in natural periods resulted when the stiffening effect of the cladding panels was added. The fundamental period for the case with the bracing was 2.1042 sec, or 46 percent smaller than the fundamental period for the case without the bracing of 3.9097 sec. From Eq. 9.1, the deviation could only have been due to the increase in stiffness since the mass matrix was the same in both cases. The higher modes showed even greater variations, that is, greater stiffening, with the largest difference resulting in the third mode. The cladding had an appreciable stiffening effect which was reflected in

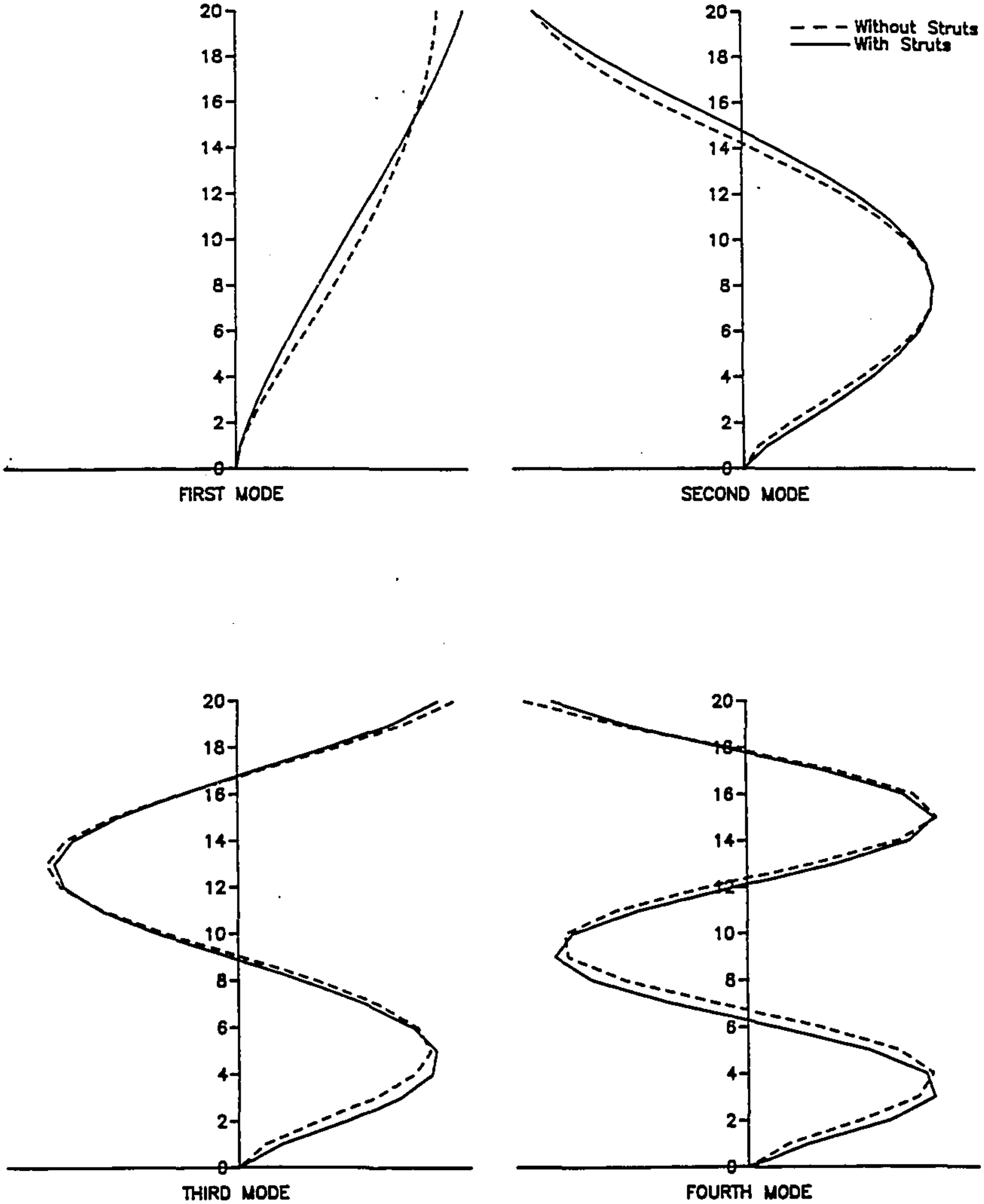

Figure 9.2: Mode Shapes for the Example Moment-Resisting Frame Structure

Mode Shape	Period Without Effect of Panels (s)	Period With Effect of Panels (s)	Deviation
1	3.9097	2.1042	-46%
2	1.2731	0.6278	-51%
3	0.7123	0.3255	-54%
4	0.4745	0.2232	-53%

Table 9.1: Natural Periods of Vibration for Example Moment-Resisting Frame Structure

No. of Modes	Without Effect of Panels	With Effect of Panels
1	77.26%	72.33%
2	87.55%	88.91%
3	91.44%	93.22%
4	93.60%	95.24%

Table 9.2: Effective Modal Mass for Example Moment-Resisting Frame Structure

the natural periods of vibration of the structure.

9.2.2 The Influence of Panels on the Response Quantities

Response spectrum dynamic analyses were performed on the moment-resisting frame structure, with and without the stiffening effect of the cladding panels, to determine the effect of the panels on the resulting design forces and displacements. The Newmark response spectrum, for 5 percent damping, scaled to 0.04g was used as the earthquake excitation. In Table 9.2, the cumulative effective modal mass percentages for the moment-resisting frame structure, with and without the panels, are presented. For each model, the SRSS combination of four analytical modes, which account for approximately 94 percent of the total effective mass, was used to calculate the peak storey shears, peak storey overturning moments, peak storey deflections, and peak interstorey drifts.

The peak storey shears for the example moment-resisting frame structure, with and without the effect of the cladding panels, are presented in Fig. 9.3a. The shape of the shear envelope changed slightly when the effect of the panels was included, because the mode shapes, in particular the first mode shape, changed somewhat when the struts representing the panels were added. The peak storey shears increased substantially throughout the height of the structure when the effect of the cladding panels was added. As the lateral stiffness was increased by including the struts, the natural periods decreased, Table 9.1, resulting in larger spectral accelerations, since for this structure the modes lie in the zone of increasing accelerations with decreasing periods of the Newmark response spectrum. Therefore, larger inertia forces and storey shears resulted. The value of base shear for the example moment-resisting frame in which the stiffening effect of the cladding panels was not included was 261.2 kN. When the effect of the panels was added, the resulting base shear was 567.6 kN, representing a very significant increase of 117 percent over the model without the effect of the panels.

Peak storey overturning moments for both models are shown in Fig. 9.3b. The overturning moments exhibit trends similar to those for the storey shears. The base overturning moment for the case in which the effect of the panels was included was 15525 kN-m, which is 103 percent greater than the value of 7661 kN-m obtained for the case without the effect of the panels.

In Fig. 9.4a, the peak storey deflections for the example moment-resisting frame structure, with and without the stiffening effect of the panels, are shown. As expected, smaller deflections resulted with a stiffer model. As was noted in the fundamental mode shape response, the deflected shape of the structure without the struts representing the panels exhibited primarily a shear mode configuration, while the deflected shape of the structure with the struts illustrated a greater cantilever response with a slight shear profile in the upper part of the structure. The fundamental mode shape contributed significantly to the overall combined response, since the deflected profiles of the structures closely resembled the first mode shape. It can be noted that smaller variations resulted in the total deflection than in storey shears or storey overturning moments. The top displacement for the model

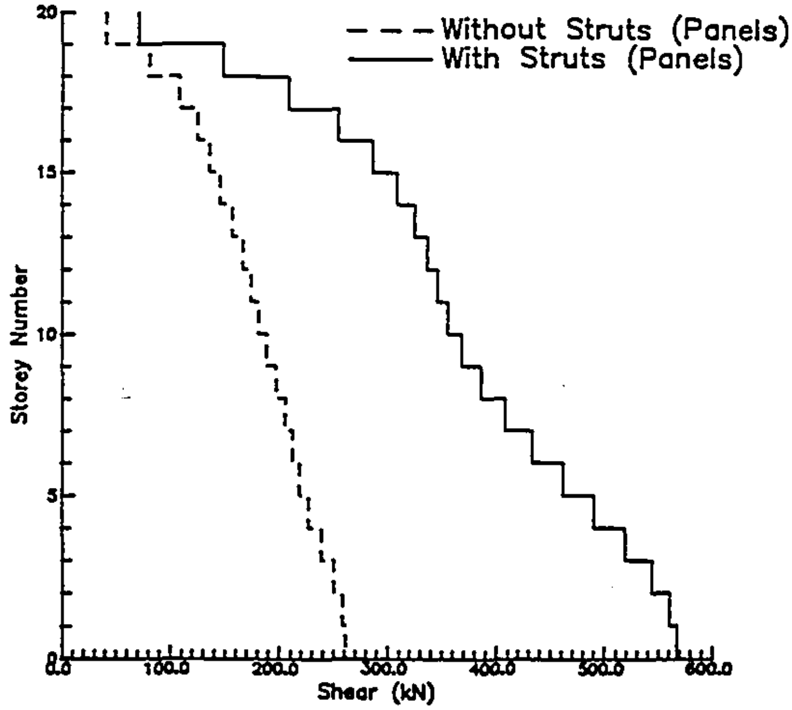

a) Peak Storey Shears

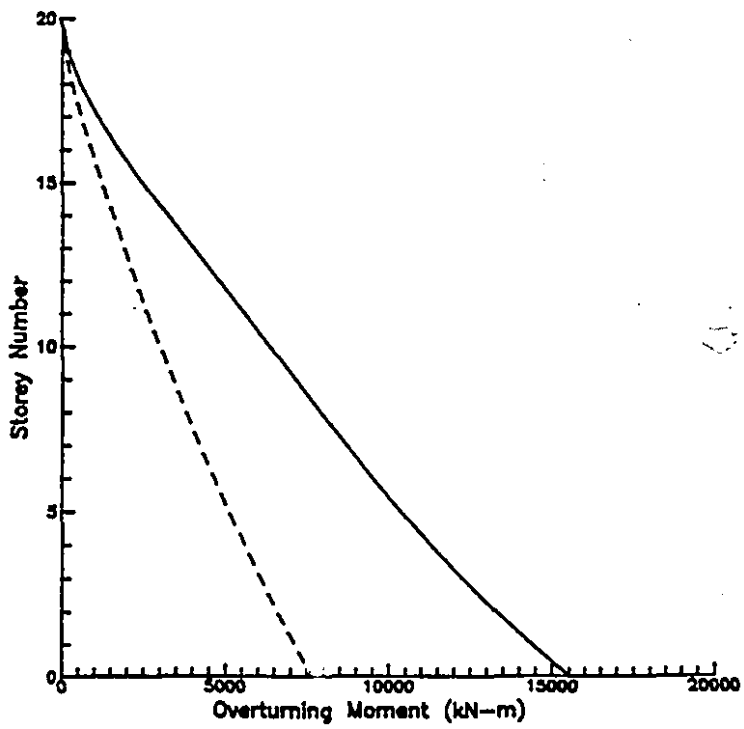

b) Peak Storey Overturning Moments

Figure 9.3: Influence of Panels on Storey Force Quantities for Moment-Resisting Frame Structure

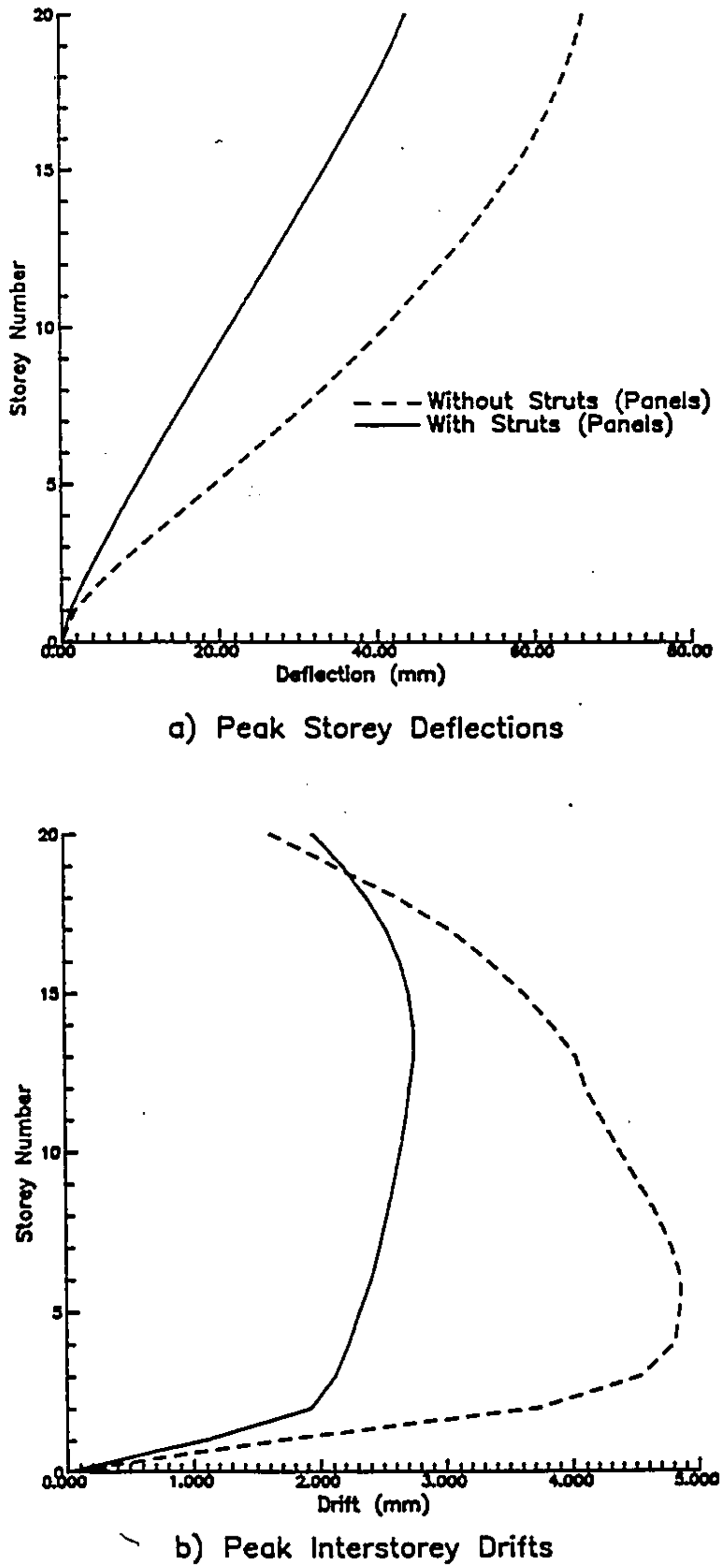

Figure 9.4: Influence of Panels on Storey Displacement Quantities for Moment-Resisting Frame Structure

with the effect of the panels was 44.1 mm, which is 34 percent less than the top displacement of 66.6 mm for the model without the panels. The largest deviation occurred at the sixth floor where the displacement of the structure with the panels was 11.9 mm, or 51 percent smaller than the displacement of the structure without the panels, 24.2 mm.

The deflection response is illustrated in the peak interstorey drift response plotted in Fig. 9.4b. For the structure in which the stiffness of the panels was neglected, the interstorey drift increased with increasing height until the seventh storey, indicating a flexural response due to the fixity of the base. From the seventh storey to the top of the structure, the interstorey drift decreased with increasing height, due to shear deformation. On the other hand, for the structure with the bracing struts, the interstorey drift increased with increasing height up to the fourteenth storey, indicating a greater flexural response than for the case of the structure without the bracing. The maximum interstorey drift occurred at the thirteenth floor for the structure with the effect of the panels, and its value was 2.763 mm, which is 43 percent smaller than the largest interstorey drift of 4.864 mm, occurring at the sixth floor, for the structure without the effect of the panels. It was also found that the interstorey drift in the top two stories was greater for the structure with the bracing than for the structure without the bracing. A purely shear-deforming fixed-base structure subjected to a distributed lateral loading is characterized by a small interstorey drift at the top, but, when the effect of the cladding panels was included, a flexural component was added to the deflected shape of the structure, as explained above, thus increasing the interstorey drift in the top part of the structure. Since the deflected shape of the structure without cladding panels already had a small flexural component, this effect was limited only to the very top floors.

9.2.3 The Relative Influence of Various Modes of Vibration on the Seismic Response

To demonstrate the relative influence of the various modes on the total combined response, the modal contributions of the first four modes to the total response are shown in Fig. 9.5 for the structure without the effect of the panels, and in Fig. 9.6 for the structure with the effect of the panels. At any storey level, the relative contribution is represented as the square of the individual modal contribution divided by the total sum of the squares of all twenty modal contributions. The modal contribution ratios for the forces at the base, the top deflection, and the maximum interstorey drifts are also recorded for the structures without and with the bracing struts in Tables 9.3 and 9.4, respectively.

For the structure without the effect of the cladding panels, Figs. 9.5a and 9.5b indicate that the higher translational modes, the second, third and fourth, contributed more to the peak storey shears and the peak storey overturning moments in the upper five or six stories of the building. Near the building's mid-height, the peak shear response was dominated by the fundamental mode only, but the peak overturning moment response still had a significant contribution from the second mode. At the base, the higher modes contributed more significantly to the shear response than they did near the mid-height of the building,

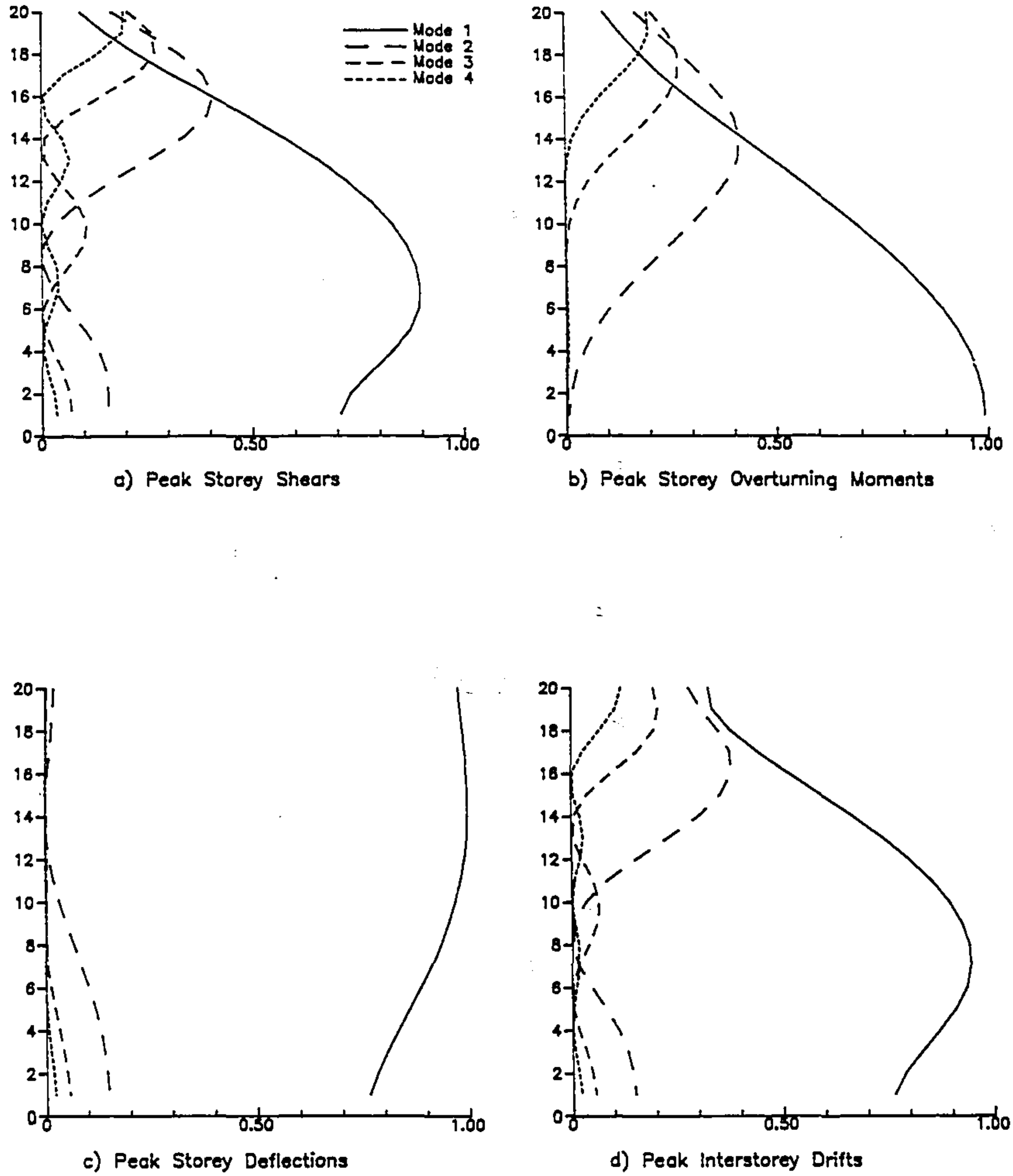

Figure 9.5: Modal Contributions to Response Quantities for Moment-Resisting Frame Structure Without the Effect of Cladding Panels

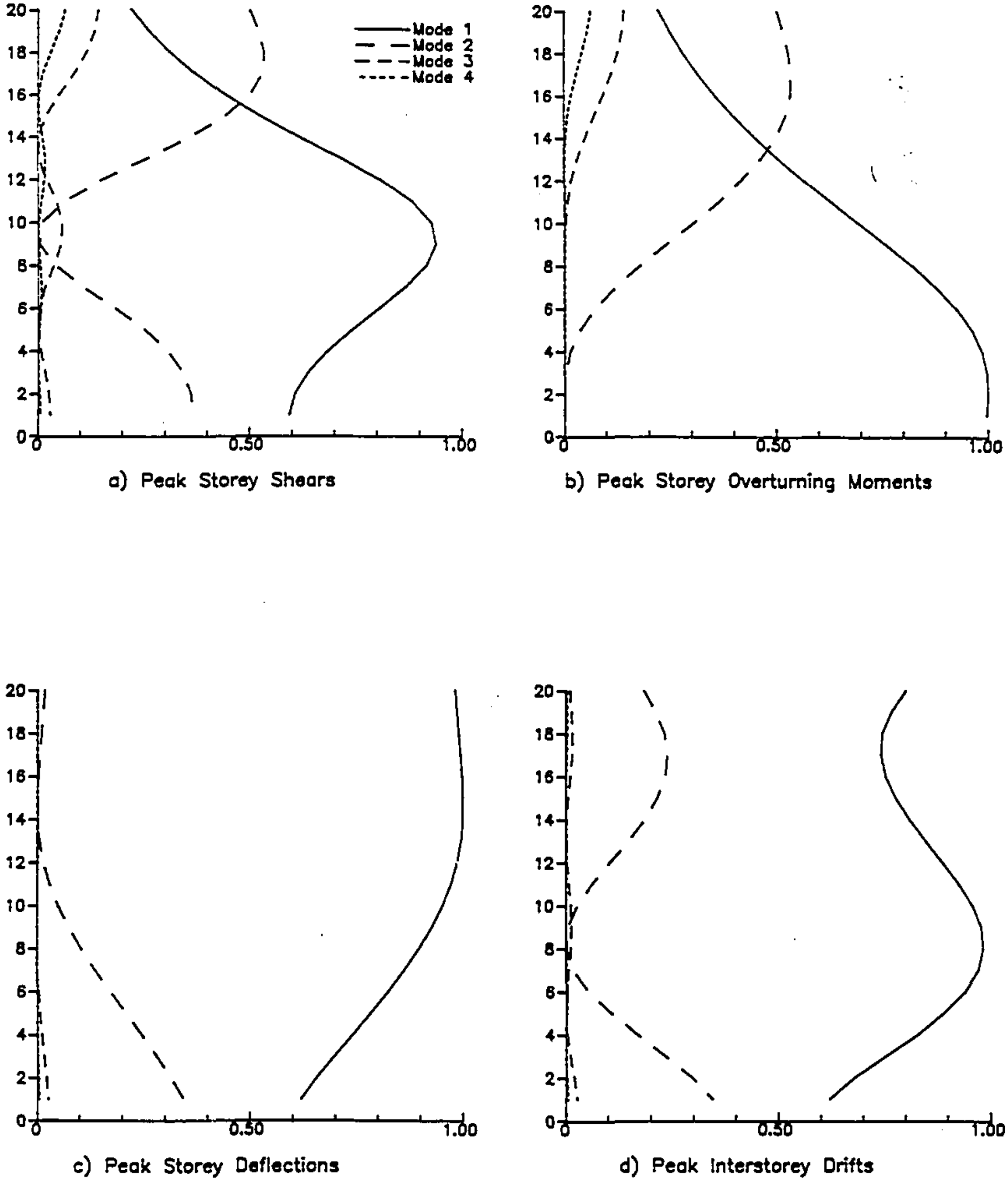

Figure 9.6: Modal Contributions to Response Quantities for Moment-Resisting Frame Structure With the Effect of Cladding Panels

Response Quantity	Modal Contribution Ratios					
	Mode 1	Mode 2	Mode 3	Mode 4	Higher Modes	Total
Base Shear	.705	.158	.070	.035	.032	1.000
Base O.M.	.991	.003	.005	.000	.001	1.000
Top Defl.	.978	.020	.002	.000	.000	1.000
Max. I.D.	.935	.047	.001	.011	.006	1.000

O.M. = Overturning Moment
Defl. = Deflection
I.D. = Interstorey Drift

Table 9.3: Modal Contribution Ratios for Example Moment-Resisting Frame Structure Without Effect of Panels

Response Quantity	Modal Contribution Ratios					
	Mode 1	Mode 2	Mode 3	Mode 4	Higher Modes	Total
Base Shear	.592	.368	.030	.007	.003	1.000
Base O.M.	.994	.005	.001	.000	.000	1.000
Top Defl.	.982	.018	.000	.000	.000	1.000
Max. I.D.	.850	.147	.000	.002	.001	1.000

Table 9.4: Modal Contribution Ratios for Example Moment-Resisting Frame Structure With Effect of Panels

with the second mode contributing 16 percent to the total sum of the squares of the base shear values, Table 9.3. The first mode dominated the base peak overturning moment, with its contribution being 99 percent, Table 9.3. In Fig. 9.5c, the higher modes are seen to generally contribute negligibly to the peak storey deflections, except near the base, where the second mode contributes 15 percent to the total sum of the squares of the deflections. Fig. 9.5d illustrates the modal contributions to interstorey drift, which resembled those to the shear response, except that in this case the fundamental mode contributed more than each of the higher modes. Similar to the shear response, the greatest contribution of the higher modes was near the top and the base of the structure.

For the structure with the cladding panels, that is, including the equivalent diagonal struts, the modal contributions to the peak storey shear and peak storey overturning moment responses are presented in Fig. 9.6a and 9.6b, respectively. Near the top of the building the higher modes contributed significantly to the shear response and overturning moment response, as they did in the case of the building without panels; however, in this case, the second mode dominated the response near the top. The second mode also contributed a considerable amount, 37 percent, to the base shear, Table 9.4. As for the structure without the panels, the fundamental mode dominated the base overturning moment response with the higher modes being insignificant, Table 9.4. In Fig. 9.6c, the significance of the higher modes are seen to contribute negligibly to the peak storey deflections in the upper region, as for the structure without the bracing. At the base, however, the second mode contributed 35 percent to the total sum of the squares value. Similar to the shear response, the modal contributions to the interstorey drifts in Fig. 9.6d show the greatest contribution of the second mode to be near the top and base of the structure, while the first mode was the largest contributor to the interstorey drift at all levels of the building.

9.3 The Effect of Panels on the Seismic Response of the Wall-Frame Structure

9.3.1 The Influence of Panels on the Dynamic Properties

As for the example moment-resisting frame structure, the natural periods of vibration and the mode shapes for the example wall-frame structure, with and without the stiffening effect of the cladding panels, were found from an eigenvalue analysis, using the SAP80 (1986) computer program. The mathematical model used for the wall-frame structure was the same as that used for the static wind load analysis, while the values of the masses were identical to those used for seismic analyses of the moment-resisting frame structure.

The first four translational mode shapes are presented in Fig. 9.7 for both cases; that is, with and without accounting for the cladding panels. In both cases, the fundamental mode shape verified the behaviour predicted from the static wind load analysis of the wall-frame structure. That is, the structure had a significant degree of cantilever type response, which was due to the high rigidity of the core, with a very slight shear beam response in the top part of the structure. The first mode shape of the structure with the bracing struts had

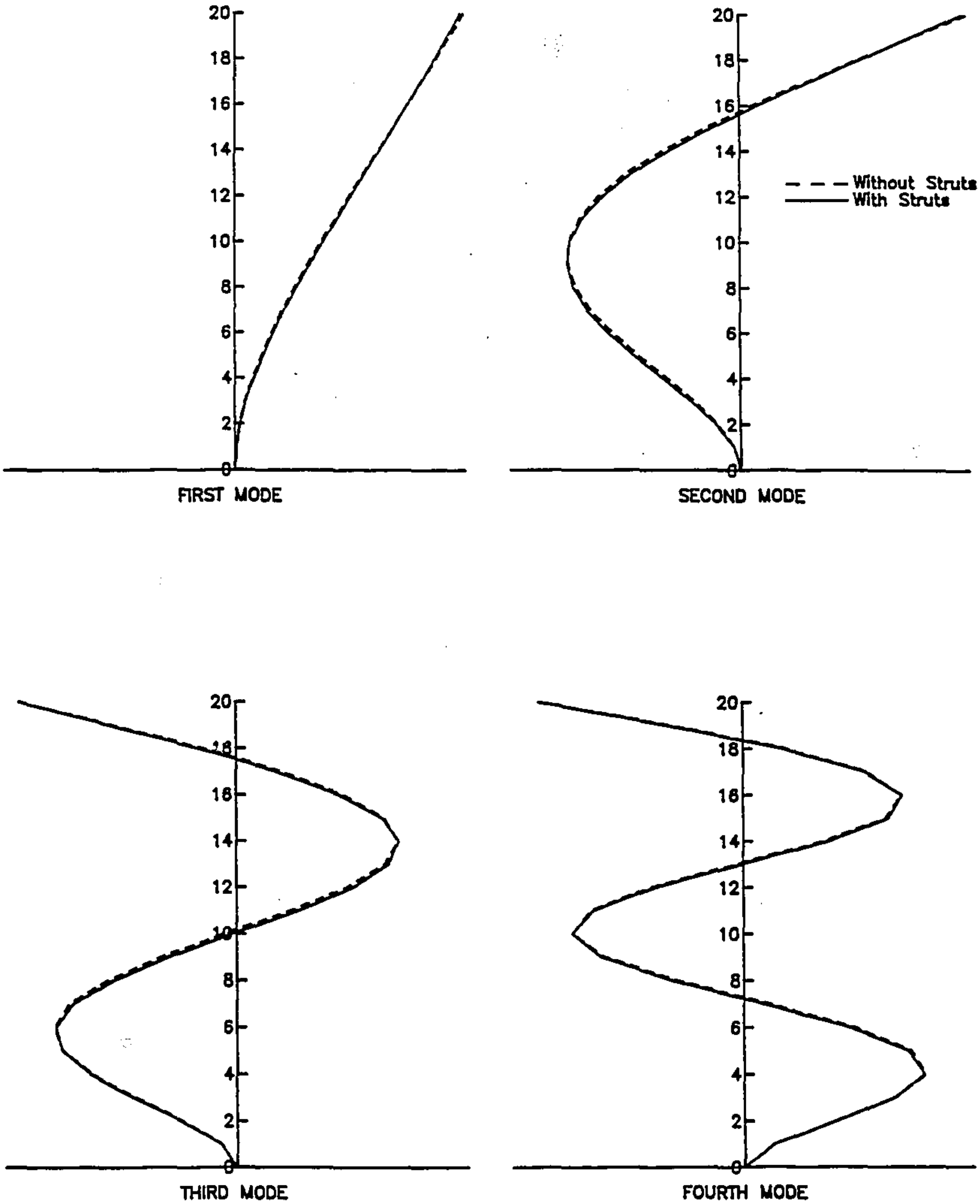

Figure 9.7: Mode Shapes for the Example Wall-Frame Structure

a slightly greater shear effect at the top of the structure than the first mode shape of the structure without bracing. This is in accordance with wall-frame theory, because by adding the bracing to the structure the shear rigidity of the structure increased, while the bending rigidity of the walls did not change; therefore, the point of contraflexure of the deflected shape of the structure was lowered. However, the mode shapes changed only very slightly when the struts representing the panels were added, indicating that the mode shapes were relatively insensitive to the modelling variation. The nodes and anti-nodes were similar for both cases. The invariance of the mode shapes probably resulted because the struts incorporated, did not basically, change the type of structure; that is, the shear rigidity of the structure increased, but the structure retained its wall-frame behaviour.

In Table 9.5, the natural periods of vibration for the two models are presented and compared. Although the mode shapes did not change significantly when the bracing struts were added, a significant variation in the natural periods resulted. The fundamental period of the structure with the cladding panels, that is including the equivalent bracing struts, was 1.4920 sec, or 20 percent smaller than the fundamental period of the structure without the panels, of 1.8571 sec. The stiffening influence of the cladding panels in the wall-frame structure resulted in the period shortening, but to a lesser degree than in the moment-resisting frame structure. Unlike for the moment-resisting frame structure, the higher modes showed smaller variations; that is, less stiffening due to the panels.

9.3.2 The Influence of Panels on the Response Quantities

Response spectrum dynamic analyses were performed on the wall-frame structure, with and without including the stiffening effect of the cladding panels, to evaluate the effect of the panels on the resulting design forces and displacements. As for the moment-resisting frame structure, the Newmark response spectrum, for 5 percent damping, scaled to 0.04g, was used as the earthquake excitation. The cumulative effective modal mass percentages for the wall-frame structure, with and without the bracing, are shown in Table 9.6. For each case, the SRSS combination of four analytical modes, which account for 92 percent of the total effective mass, was used to calculate the peak storey shears, overturning moments, deflections, and interstorey drifts.

In Fig. 9.8a, the predicted peak storey shears for the wall-frame structure, with and without the bracing struts, are presented for the full height of the building. The storey shears increased with the stiffer model, that is, the model including the effect of the panels. The shape of storey shear envelope curves were similar for both cases, because the mode shapes for the two models, Fig. 9.7, did not change significantly. Therefore, the distribution of the design quantities for the models can be expected to be similar. The values of base shear for the structures with and without the panels were 704.4 kN and 612.6 kN, respectively. The effect of the cladding panels was to increase the base shear by 15 percent. The largest deviation, however, occurred at the eleventh storey, where the shear increased from 377.4 kN to 449.7 kN, a 19 percent increase. Like the static analysis, and the eigenvalue analysis, the stiffening effect of the cladding panels on the wall-frame structure was not as great as on the moment-resisting frame structure.

Mode Shape	Period Without Effect of Panels (s)	Period With Effect of Panels (s)	Deviation
1	1.8571	1.4920	-20%
2	0.3833	0.3319	-13%
3	0.1455	0.1340	-8%
4	0.07559	0.07221	-4%

Table 9.5: Natural Periods of Vibration for Example Wall-Frame Structure

No.of Modes	Without Effect of Panels	With Effect of Panels
1	65.14%	65.97%
2	82.48%	83.13%
3	88.88%	89.13%
4	92.21%	92.34%

Table 9.6: Effective Modal Mass for Example Wall-Frame Structure

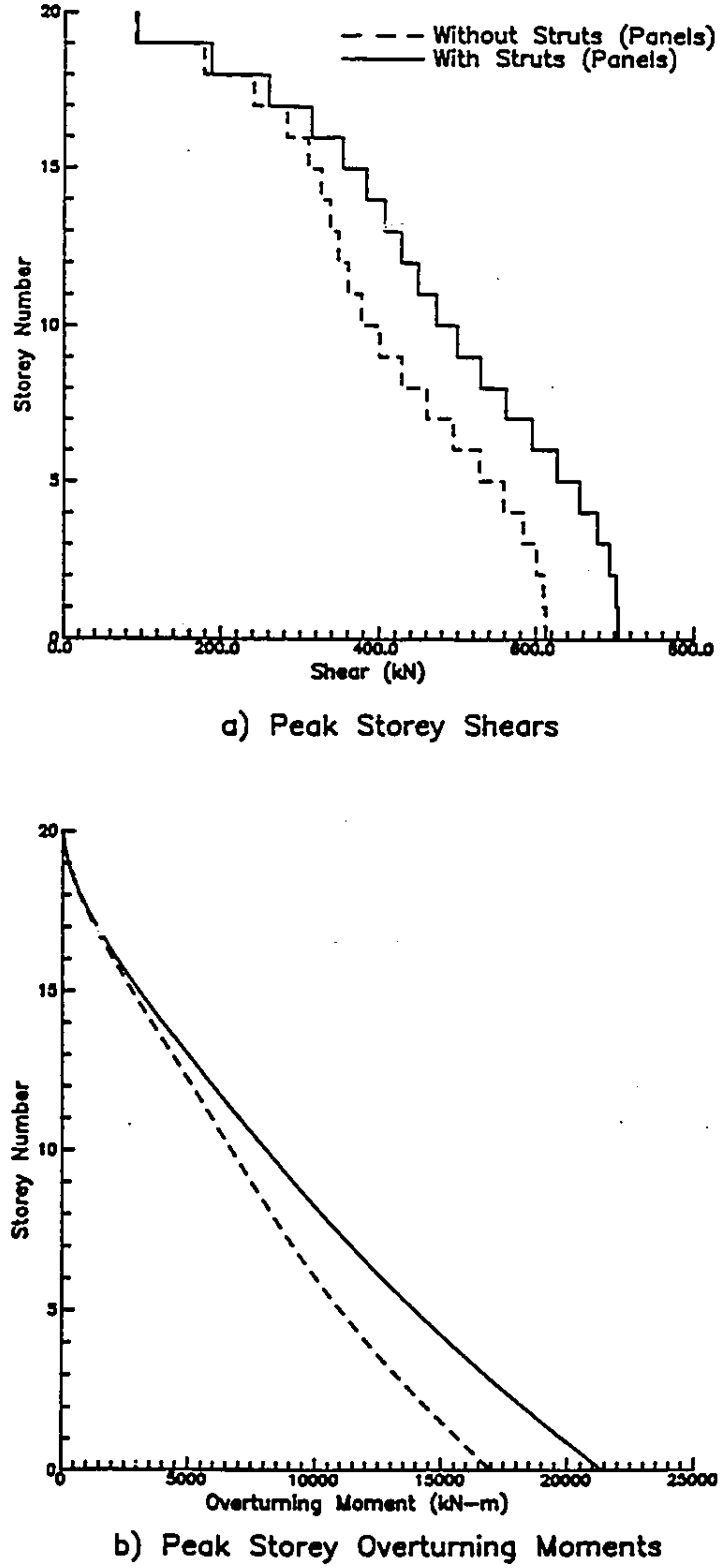

Figure 9.8: Influence of Panels on Storey Force Quantities for Wall-Frame Structure

The peak storey overturning moments are presented in Fig. 9.8b for both models. The overturning moment variations along the height of the structure, due to the stiffening effect of the panels, resembled the variations in the peak storey shears, except that at the base, the change in the peak overturning moment was slightly greater than that in the peak base shear. The 17004 kN-m base overturning moment of the model without the struts increased to 21395 kN-m, resulting in an increase of 26 percent.

In Fig. 9.9a, the peak storey deflections for the wall-frame structure, for both cases, are illustrated. As expected, the stiffer model gave smaller deflections. The top displacement for the case in which the stiffening effect of the cladding panels was not included was 40.7 mm. The top displacement for the structure with bracing was 32.9 mm, or 19 percent less than that without the effect of the panels. The peak storey deflection curves for both cases had a similar shape, for the same reason that the peak storey shears and the other response quantities did. The deflected shape of the building, in both cases, was similar to the fundamental mode shape, having a significant degree of flexural response, which was due to the high rigidity of the core, with a very slight shear beam response in the top part of the structure. The lower point of contraflexure in the model with the cladding panels was not as evident as it was in the fundamental mode shape, because the deflections were not normalized.

Peak interstorey drifts are shown in Fig. 9.9b. The interstorey drifts, as expected, decreased for the structure in which the stiffening effect of the cladding panels was accounted for. The interstorey drifts were more affected by the stiffening influence of the panels than were the deflections. This was probably because the higher modes contributed more to the interstorey drifts than to the deflections. The cantilever mode of deformation in the lower part of the structure was evident by the increasing interstorey drift with increasing height; whereas, in the upper part of the building, the interstorey drift decreased slightly with increasing height, reflecting a shear mode of deformation. In both cases the shapes were similar, except that in the model without the bracing struts, the interstorey drift began to decrease between the sixteenth and seventeenth floors, while in the model with the bracing, the interstorey drift began to decrease at a lower storey, between the fourteenth and fifteenth floors. As a result, the largest interstorey drift in the structure without accounting for the stiffening effect of the panels occurred at the sixteenth floor with a value of 2.639 mm; whereas, the largest interstorey drift in the building with the bracing occurred at the fourteenth floor, with a value which is 21 percent less than that without the bracing, that is, 2.0880 mm. Another deduction which can be drawn from Fig. 9.9b is that the interstorey drifts are proportionately more greatly reduced in the upper stories than in the lower ones. This results because the deflected shape has a greater shear configuration for the braced structure; that is, as explained earlier, in accordance with wall-frame theory the point of contraflexure has been lowered due to the bracing.

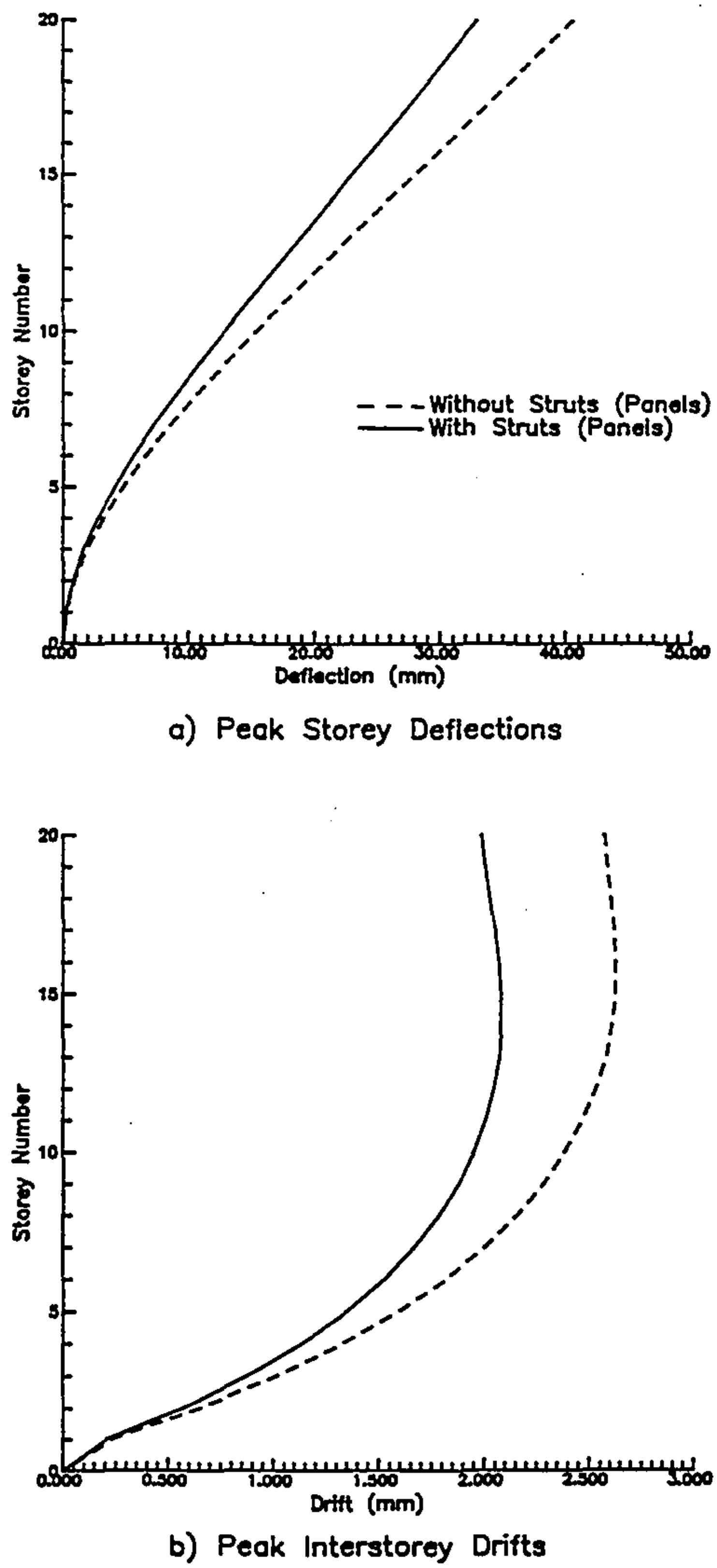

Figure 9.9: Influence of Panels on Storey Displacement Quantities for Wall-Frame Structure

9.3.3 The Relative Influence of Various Modes of Vibration on the Seismic Response

As for the moment-resisting frame structure, the relative modal contributions of the first four modes to the total combined response was studied to obtain a better understanding of the dynamic behaviour of the wall-frame structure. Because the relative modal contributions to the total response quantities were similar for both models - that is, with and without accounting for the stiffening effect of the cladding panels - the modal contributions to the peak storey shears, overturning moments, deflections, and interstorey drifts are only presented for the structure with the stiffening effect of the cladding panels in Fig. 9.10. At any level of the building, the relative contribution was represented as the square of the individual modal contribution divided by the total sum of the squares of all twenty modal contributions. The modal contribution ratios for the forces at the base, the top deflection, and the maximum interstorey drift are also shown in Table 9.7.

Similarly to the moment-resisting frame structure, the higher modes, that is, the second, third and fourth, were found to contribute substantially to the peak shear and the peak overturning moment responses in the upper stories of the structure, Fig. 9.10a and 9.10b. For the wall-frame structure, the second mode prevailed in the peak storey shears and the peak storey overturning moments in the top three and four stories, respectively. Near the building's mid-height, the shear response was dominated by the fundamental mode, but the overturning moment response still had a considerable contribution from the second mode. At the base, the second mode contributed substantially, 31 percent, to the total sum of the squares of the base shears, while the first mode prevailed in the overturning moment response, 98 percent, with higher modes being negligible, Table 9.7. Fig. 9.10c illustrates that the peak storey deflections were influenced predominantly by the first mode throughout most of the height of the structure. The second mode contributed 10 percent to the total sum of the squares of the peak deflection at the base. Similarly to the shear response, the modal contributions to the peak interstorey drifts in Fig. 9.10d showed the greatest contribution of the second mode near the top and base of the building. However, unlike the shear response the fundamental mode was the greatest contributor to the interstorey drift at all levels of the structure, for example 97 percent at the level of maximum interstorey drift, Table 9.7. Modes higher than the second contributed negligibly to peak storey deflections and peak interstorey drifts.

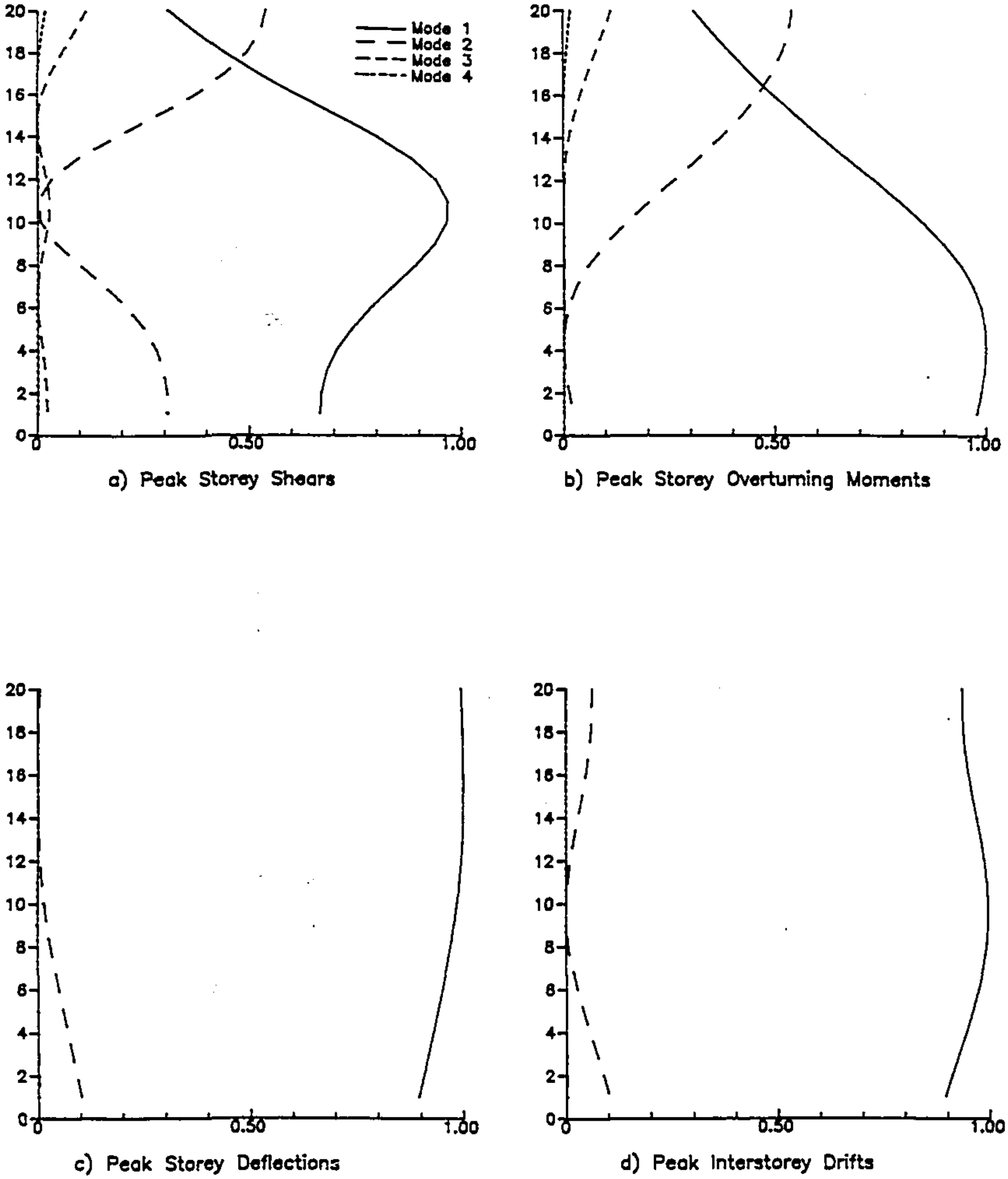

Figure 9.10: Modal Contributions to Response Quantities for Wall-Frame Structure With the Effect of Cladding Panels

Response Quantity	Modal Contribution Ratios					
	Mode 1	Mode 2	Mode 3	Mode 4	Higher Modes	Total
Base Shear	.664	.308	.024	.002	.002	1.000
Base O.M.	.976	.023	.001	.000	.000	1.000
Top Defl.	.996	.004	.000	.000	.000	1.000
Max. I.D.	.971	.029	.000	.000	.000	1.000

O.M. = Overturning Moment
Defl. = Deflection
I.D. = Interstorey Drift

Table 9.7: Modal Contribution Ratios for Example Wall-Frame Structure With Effect of Panels

Response Quantity	Modal Contribution Ratios					
	Mode 1	Mode 2	Mode 3	Mode 4	Higher Modes	Total
Base Shear	.664	.308	.024	.002	.002	1.000
Base O.M.	.976	.023	.001	.000	.000	1.000
Top Defl.	.996	.004	.000	.000	.000	1.000
Max. I.D.	.971	.029	.000	.000	.000	1.000

O.M. = Overturning Moment
Defl. = Deflection
I.D. = Interstorey Drift

Table 9.7: Modal Contribution Ratios for Example Wall-Frame Structure With Effect of Panels

CHAPTER 10

THE EFFECT OF VARYING CONNECTION STIFFNESSES ON THE STIFFENING INFLUENCE OF CLADDING PANELS

In Chapter 4, the stiffnesses of the connections were estimated on the basis of approximate calculations of their flexibilities in the restrained directions. Due to uncertainties in the exact behaviour of the connections and the number of variables involved in computing the flexibilities, the approximate stiffnesses were considered sufficiently accurate for the model. However, the actual stiffnesses of these same connections may be significantly different. Therefore, it was necessary to determine the effect of the connection stiffnesses on the stiffness response of the panel-clad frame. Using connections of different stiffnesses, lateral load analyses were performed on the single-storey panel-frame module and the example clad moment-resisting frame structure. The results were compared with those obtained in Chapters 4, 5, 7, and 8.

10.1 The Effect of Connection Stiffnesses on the Behaviour of the Single-Storey Panel-Frame Module

To study the effect of the connection stiffnesses on the clad frame, a lateral load analysis of the single-storey panel-frame module, Fig. 4.15, but with reduced connection stiffnesses was performed. The panel and frame members were modelled exactly as in Fig. 4.15, but the links representing the connections were assigned stiffnesses equal to one-tenth of those recorded in Table 4.2.

The complete module, with the connections modelled as described above, was analysed for the 1000 kN load. The lateral displacement at the top was 13.31 mm. The shearing stiffness of the storey-height module with the panel is, therefore, 9.5 times that of the bare frame (Analysis I, Table 4.3) compared with 35 times in the original case (Analysis II).

The resulting deflected shape of the frame with the panel and its connections is illustrated in Fig. 10.1. The combined interactive behaviour of the 'forward' double-curvature bending of the beam due to racking of the frame, and the 'backward' double-curvature bending caused by the panel's forward rotation resulted, in this particular structure, in a greater

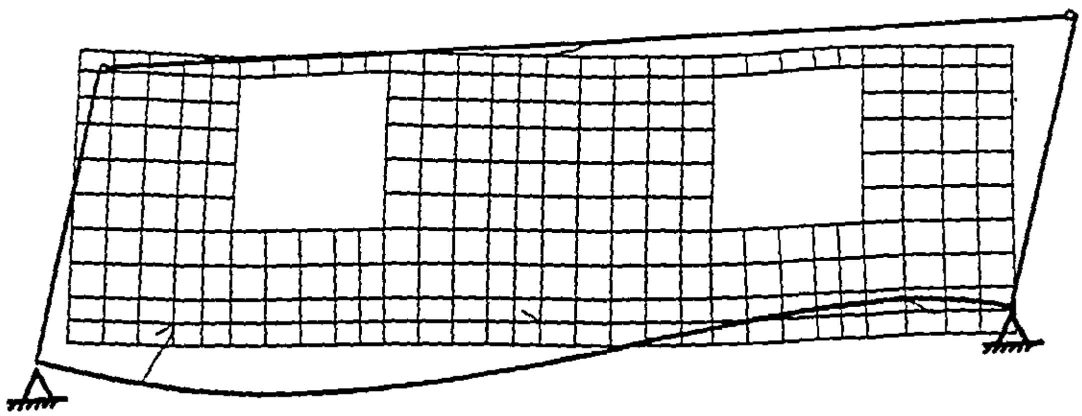

Figure 10.1: Deflected Shape of Panel-Clad Frame with Reduced Connection Stiffnesses

'forward' double-curvature bending component of the beam than in the original structure, Fig. 5.2c. This occurred because of the smaller forces in the bearing connections due to the reduced connection stiffnesses; therefore, significantly decreasing the 'backward' double-curvature bending component of the beam, and increasing the 'forward' double-curvature bending component of the beam as a result of the greater shear carried by the columns. The longer rigid arm at the windward end of the beam imposed a greater downward displacement on the beam at that end, and caused an unsymmetrical mode of deformation of the structure.

It is interesting to note that although the panel with reduced connection stiffnesses had a significantly smaller stiffening effect than the panel with the original connection stiffnesses, it carried a major proportion, 77 percent, of the external load as did the panel with the original connection stiffnesses, 81 percent.

10.2 The Effect of Connection Stiffnesses on the Static Wind Load Response of the Example Panel-Braced Moment-Resisting Frame Structure

10.2.1 Modelling the Structure and the Panels

To determine the effect of the connection stiffnesses on the static response of the example moment-resisting frame structure described in Chapter 4, a three-dimensional analysis of the building was performed. The mathematical model of the structure was identical to that of the example structure in Chapter 7, Fig. 7.1, and it was subjected to the same wind loading.

As in Chapter 7, the precast concrete cladding panels were modelled by the 'improved' single-diagonal bracing struts, but with assigned sectional areas to provide a lateral stiffness component equal to the stiffness of the example panel with its reduced connection stiffnesses. To determine the example panel stiffness with the stiffnesses of the connections reduced to one-tenth of their original values, a finite element analysis of a storey-height bay-width module of the panel and its connections, supported by a flexurally and axially rigid beam, was performed. The model was identical to that of analysis IV, Fig. 4.22, except with the connection stiffnesses reduced. The structure was subjected to a horizontal load of 1000 kN at the top, and the resulting displacement was 20.28 mm, giving a stiffness of 49.31 kN/mm. By equating the expression for the horizontal stiffness of the 'improved' single-diagonal strut, Eq. 6.1, to the stiffness value of the panel and the connections just determined, the axial area of the strut was found to be 20112 mm^2. This is 23 percent of the axial area of the strut used in Chapter 7.

10.2.2 Analyses and Results

The structure with the cladding panels having reduced connection stiffnesses, that is, with the equivalent diagonal struts computed in the previous section, was analysed. The resulting top displacement was 49.166 mm, corresponding to a drift index of 1/1635. The top displacement was 50 percent less than that of the structure without the cladding panels, Section 7.1.2, indicating the panels' very significant overall stiffening effect even though the connection stiffnesses were reduced to one-tenth of their original values. It should be recalled that the top displacement of the structure with cladding panels having the original connection stiffnesses was 68.4 percent less than that of the structure without the cladding panels.

The deflected shape of the structure, Fig. 10.2, represents a combination of flexural and shear deformations. By adding the struts, the shear rigidity of the moment-resisting frame structure was increased, while its overall flexural rigidity was reduced. This is also evident when comparing the deflected shapes of the structure with bracing, Fig. 10.3, with those of the structure without bracing, Fig. 7.4. A comparison of Fig. 10.3 and Fig. 7.5, however, indicates that reducing the stiffnesses of the connections significantly increased the overall flexural rigidity of the structure. This resulted because the less stiff struts induced smaller vertical forces in the columns, thereby reducing the axial deformations in the columns adjacent to the panels. The axial stress in the columns adjacent to the cladding panels increased by a factor of 5.2 when the effect of the panels with reduced connection stiffnesses was added, whereas in the original case, Section 7.1.2, the axial stresses in the panels' adjacent columns increased by a factor of 6.8.

The frame-member moments in the lower stories of the clad frame structure, except for the beams supporting the cladding panels, were approximately 40 percent less than those of the unclad frame structure. Recalling the original case of the clad frame structure, the corresponding moments were 50 to 70 percent less than those of the unclad structure.

10.2.3 Resulting Forces in Connections and Stresses in Panel

The resulting forces in the connections and stresses in the panel for the structure having panels with reduced connection stiffnesses were briefly examined.

An estimate of the resulting vertical forces in the bearing connections was made by taking the vertical component of the force in the 'improved' single-diagonal strut. The largest diagonal force occurred in the third storey and had a value of 205.03 kN. By taking the vertical component of this diagonal force, the vertical forces in the bearing connections were determined to be 73.16 kN. These are approximately 68 percent of those found in the original case, Chapter 8.

Having determined the vertical forces in the bearing connections, the corresponding horizontal forces in the tie-back and left bearing connections, and the stresses in the panel can be found. As described in Chapter 8, this can be achieved by scaling the horizontal forces and stresses resulting from the detailed analysis of the storey-height panel-frame module

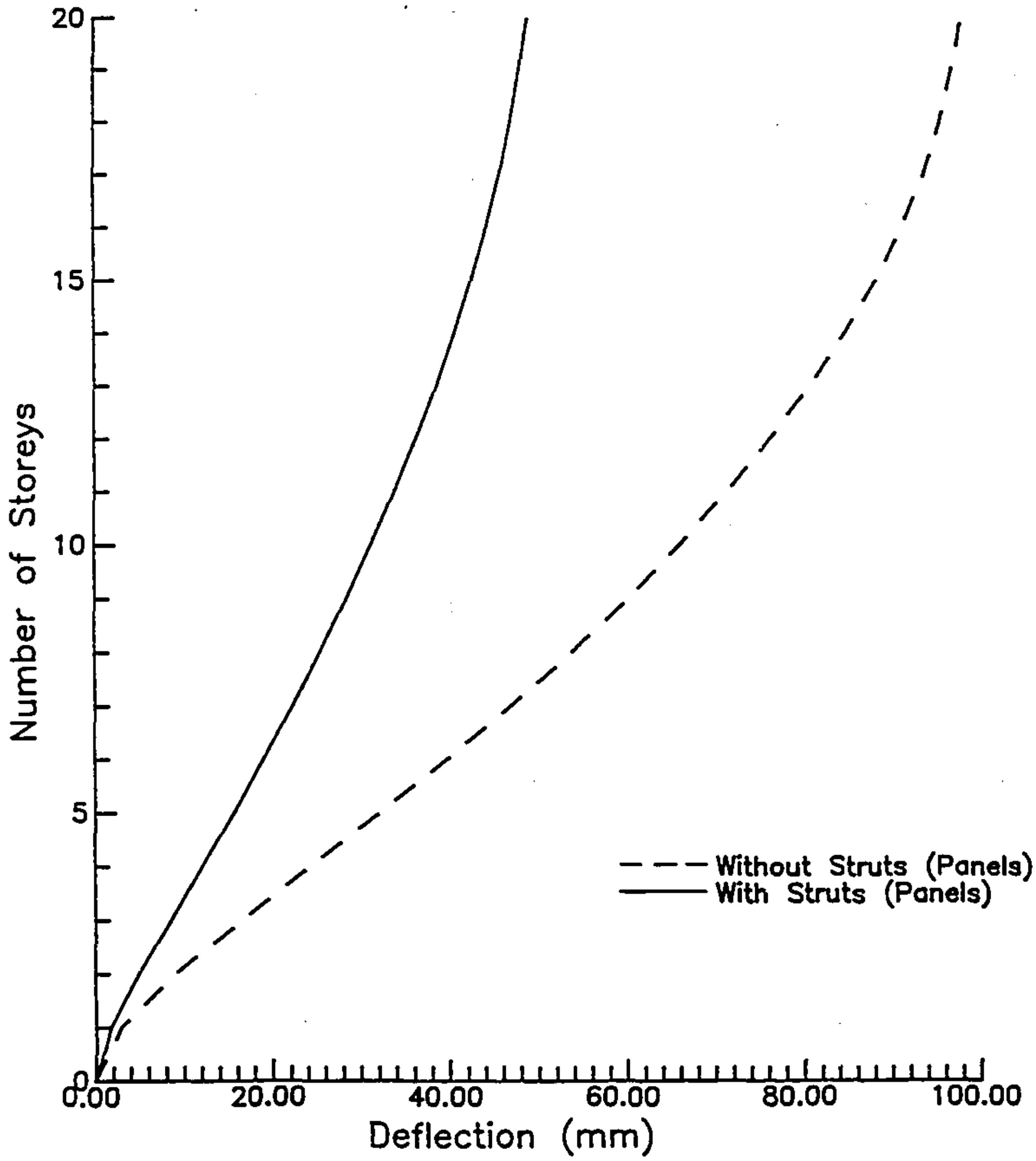

Figure 10.2: Deflected Shapes of Moment-Resisting Frame Structure (Reduced Connection Stiffnesses Case)

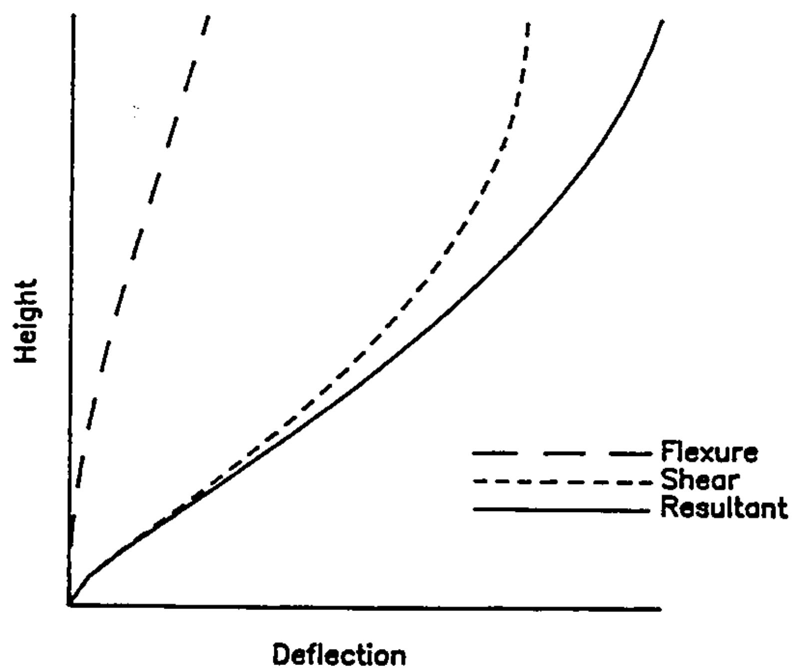

Figure 10.3: Deflected Configuration of Example Moment-Resisting Frame with Low-Stiffness Bracing

performed in Section 10.1, by the ratio of the vertical forces in the bearing connections determined above to the vertical forces from the detailed analysis.

The forces in the connections obtained from the detailed analysis in Section 10.1 are shown in Fig. 10.4. Therefore, the factor necessary to scale the forces in the horizontal connections and the stresses in the panel is 0.26916. The resulting maximum forces that would occur in the connections of the precast concrete panels, if their actual stiffnesses were reduced by a factor of ten, in the laterally loaded 20-storey clad moment-resisting frame structure are also presented in Fig. 10.4. The largest horizontal force is 72 percent of that obtained in the analysis of the example structure with cladding panels having the original connection stiffnesses.

Comparing the maximum design loads in the connections, based on the above results, with the resistances of the connections calculated in Chapter 8, it is evident, as in the original case, that the most heavily loaded connections would not withstand the loads to which they would be subjected.

The maximum and minimum principal stresses in the panel resulting from the detailed analysis of the storey-height panel-frame module were scanned. The largest stresses occurred in areas of local stress concentration, such as the corners of the window openings, and the points of concentrated load application. The largest tensile stress, when scaled by the appropriate factor obtained above, was approximately 3.7 MPa, which is slightly greater than the permissible tensile stress of 3.55 MPa calculated in Chapter 8. As in the original case, the maximum compressive stress was well within the acceptable limit.

It can be concluded that in a clad single-bay structure, although a reduction in stiffness of the connections may significantly reduce the stiffening effect of the cladding panel, it does not cause as large a reduction of the forces in, and therefore the strength requirements of, the connections. On the other hand, in a clad overall structure in which the lateral load resisting system also consists of components other than the clad frame, the reduction in the stiffening effects caused by a decrease in connection stiffnesses is not as significant as in a clad single-bay structure. In addition, the resulting reduction in the connection forces due to the decrease in the connection stiffnesses is greater than in the single-bay structure.

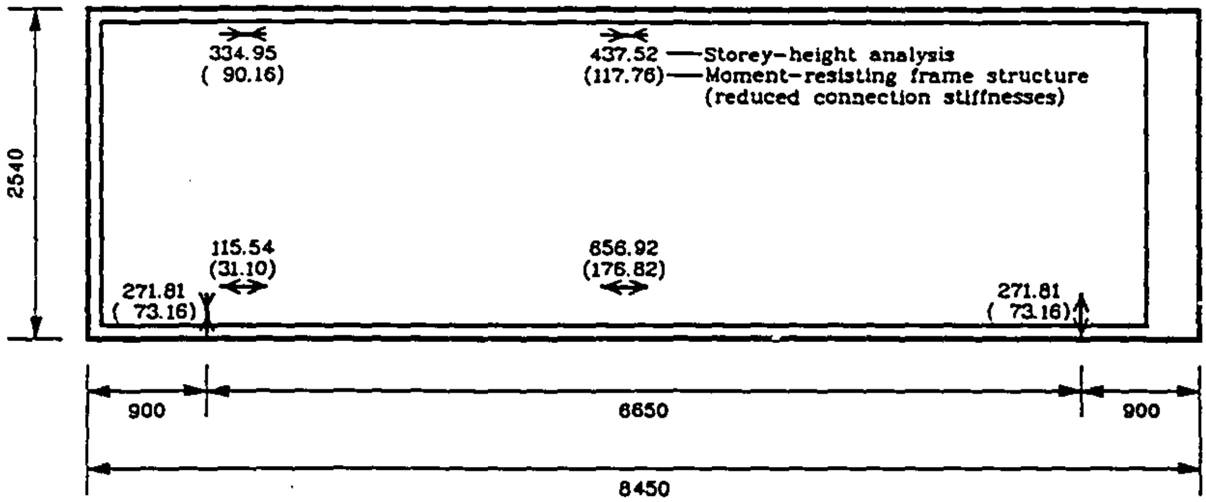

Figure 10.4: Resulting Maximum Forces in Connections (Reduced Connection Stiffnesses Case)

CHAPTER 11

THE EFFECT OF RIGID BEAM-ENDS ON THE BEHAVIOUR OF THE SINGLE-STOREY PANEL-FRAME MODULE

The representative panel-clad frame studied thus far has been a relatively complex one, with the frame being unsymmetric in that the columns had unequal stiffnesses, and the beam had unequal rigid arms at its ends. To obtain a clearer understanding of the behaviour of the structural frame with the precast concrete cladding panel attached to it, the effect of the rigid beam-ends on the behaviour of the single-storey panel-frame module was studied. Three cases were investigated:

(a) the beam with no rigid arms at the ends,

(b) the beam with equal, but short, rigid arms at the ends, and

(c) the beam with equal, but long, rigid arms at the ends.

In all these cases, the frame was still unsymmetric in that the columns had unequal stiffnesses.

The behaviour obtained from the representative panel-clad frame, where the rigid beam-ends were unequal, was then compared with the results of the study.

11.1 Case (a): No Rigid Beam-Ends

A series of lateral load analyses were performed on a single-storey bay comprising the structural frame and the panel with its connections, Fig. 11.1. This structure differs from the previous structure presented in Section 4.4 in that the beam has no rigid arms at the ends; that is, the flexural inertia of the beam extends to the supports. The frame was still unsymmetric in that the columns had unequal stiffnesses.

The first analysis performed was that of the complete model, but with the columns assigned a very small inertia to eliminate the moment-resisting frame action, Fig. 11.2. The resulting top lateral displacement was 17.95 mm and the displaced shape is shown in Fig. 11.3. The panel, as expected, deforms in shear as well as rotating forward in its plane

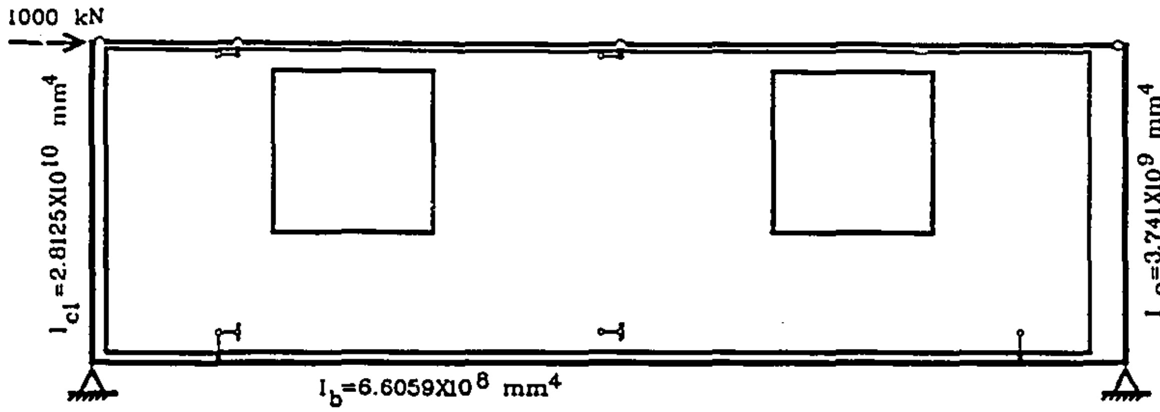

Figure 11.1: Model for Complete Panel-Clad Frame Module - Case (a)

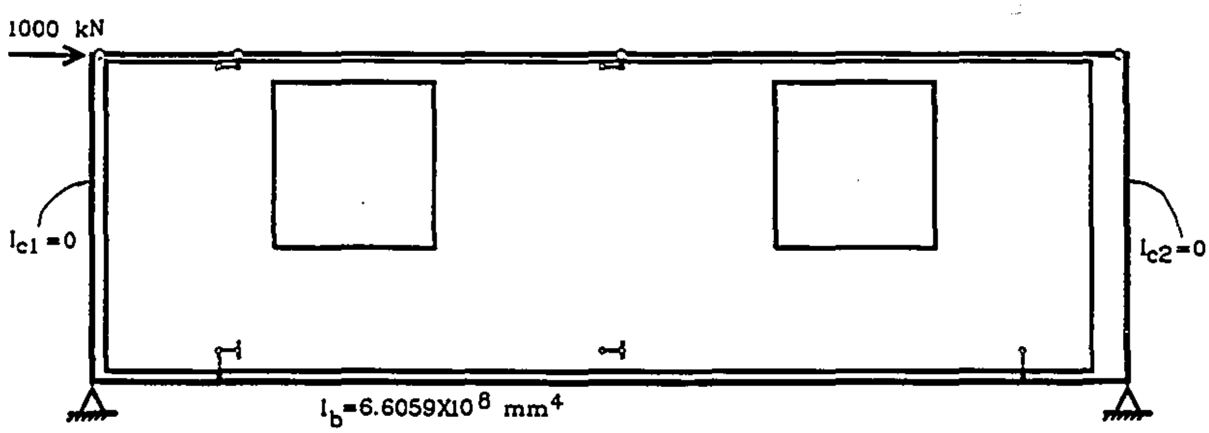

Figure 11.2: Model for Complete Module, but Effectively without Columns - Case (a)

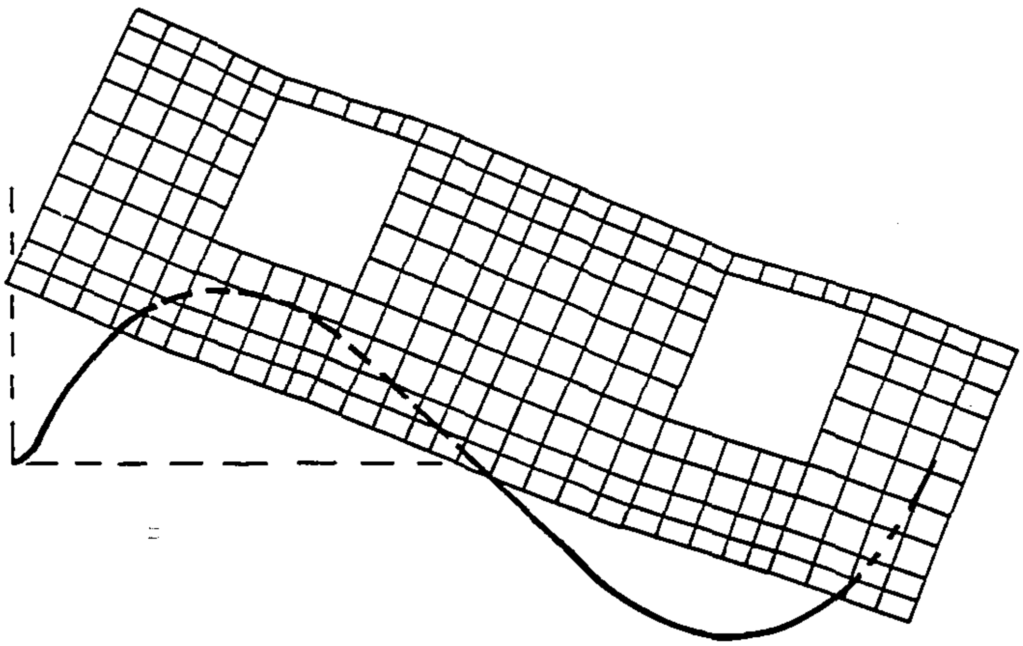

Figure 11.3: Deflected Shape for Panel Supported by Beam - Case (a)

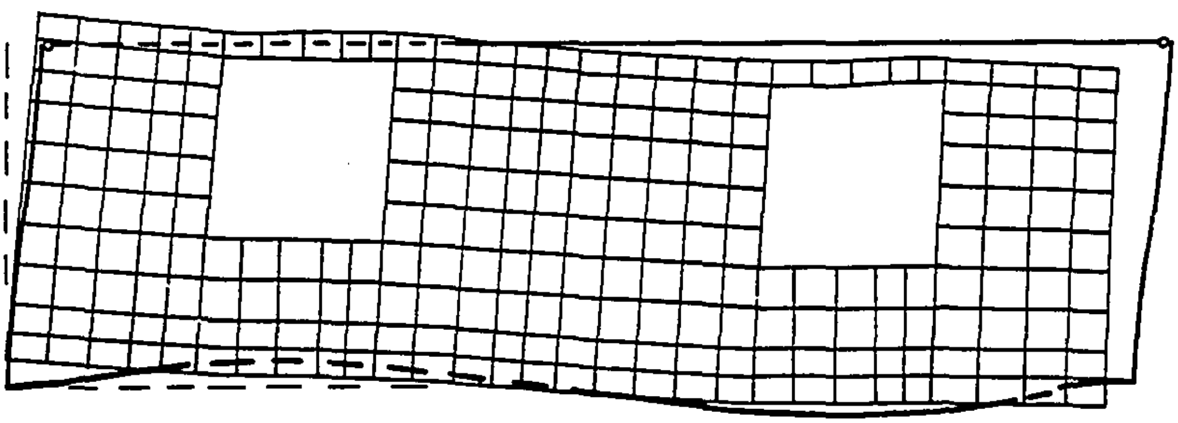

Figure 11.4: Deflected Shape for Complete Module - Case (a)

with a corresponding 'backward' double-curvature bending of the beam.

The complete model as presented in Fig. 11.1, that is, including the effect of the columns, was then analysed. The lateral displacement at the top due to the 1000 kN load was 5.39 mm, which was only 30 percent of that from the analysis without the effect of the columns. When the stiffnesses of the columns are reintroduced into the model, the interaction between the panel and the frame is mobilized. The moment-resisting frame's racking action severely constrains the rotation of the panel. This is also evident from the deflected shape of the panel-clad frame presented in Fig. 11.4.

To assess the sensitivity of the structure's lateral flexibility to the flexibilities of the beam, and the panel with its connections, several analyses were examined. In analysis VII of Section 4.5, the complete model was analysed, but with the beam assigned to be effectively rigid in flexure. To determine the sensitivity of the structure's lateral flexibility to that of the beam, the flexibility of analysis VII, Table 4.3, was subtracted from the result of the analysis of the complete analysis above. The value obtained was $3.88X10^{-3}$ mm/kN.

Similarly, to assess the sensitivity of the structure's lateral flexibility to the flexibility of the panel with its connections, it was necessary to perform a lateral load analysis of the frame, with no rigid beam-ends, with a rigid panel attached to it by rigid connections, Fig. 11.5. The resulting top lateral displacement was 2.04 mm. The deflected shape of the structure is shown in Fig. 11.6. If the panel and connections were infinitely flexible, the beam deflections would all correspond to 'forward' double-curvature bending. However, as the panel and connections would be stiffened, the forces carried by the panel would increase, as well as the vertical forces in the bearing connections, which would give rise to increased 'backward' double-curvature bending deformations in the beam. When the panel and connections were assigned to be completely rigid, the vertical forces in the bearing connections were at their maximum; therefore, the 'backward' double-curvature bending deformations of the beam were greater than for the complete analysis, in which the panel and the connections were flexible. To determine the sensitivity of the structure's lateral flexibility to the flexibility of the panel with its connections, the flexibility obtained from this analysis of the complete module, but with the panel and connections assigned to be rigid, was subtracted from the result of the analysis of the complete module. The value obtained in this case was $3.35X10^{-3}$ mm/kN.

In this particular case of no rigid beam-ends, the sensitivity of the structure's racking flexibility to the flexibility of the panel with its connections was approximately 14 percent less than it was to the flexibility of the beam.

11.2 Case (b): Equal, but Short Rigid Beam-Ends

In this case, the structure to be analysed differs from the previous case, in that the beam has 300 mm rigid arms at each of its ends, Fig. 11.7.

The complete module, but with the columns assigned a very small inertia to eliminate the moment-resisting frame action, was first analysed for an applied horizontal load of

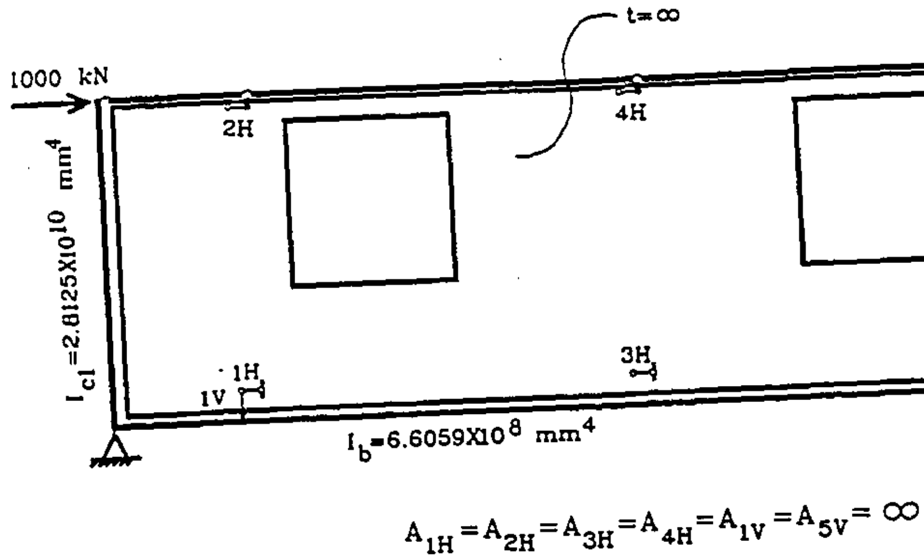

Figure 11.5: Model for Complete Module, but with Panel and Connections Rigid - Case (a)

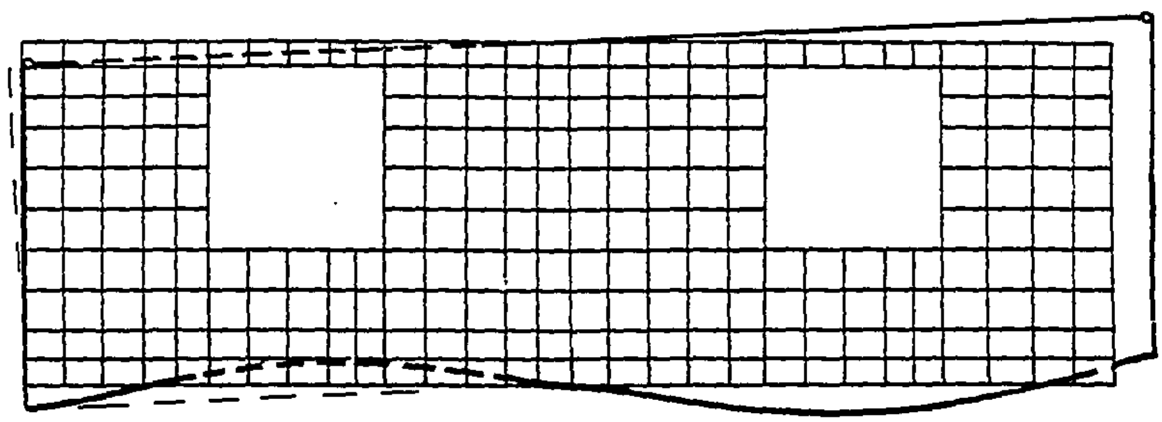

Figure 11.6: Deflected Shape for Frame with Rigid Panel and Connections - Case (a)

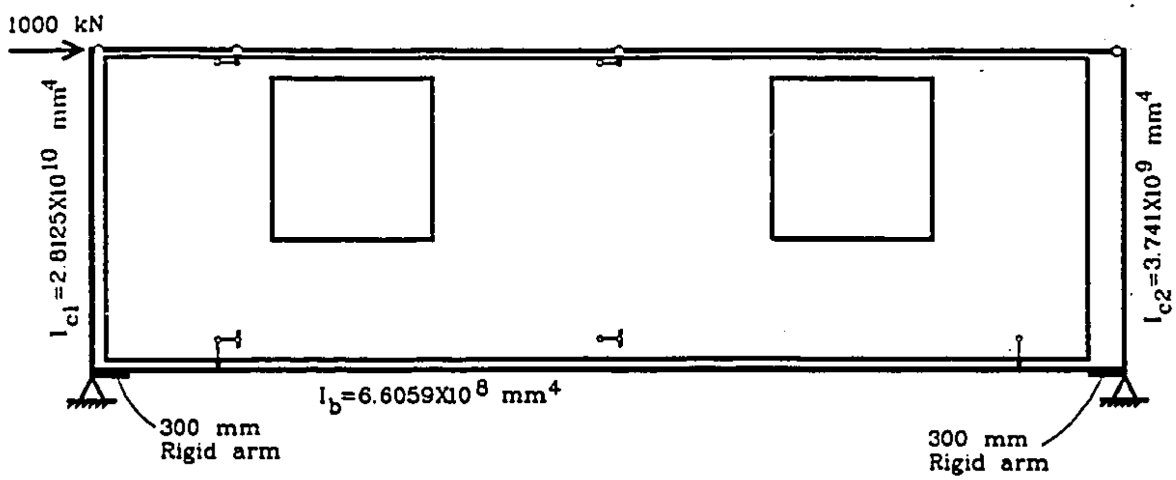

Figure 11.7: Model for Complete Panel-Clad Frame Module - Case (b)

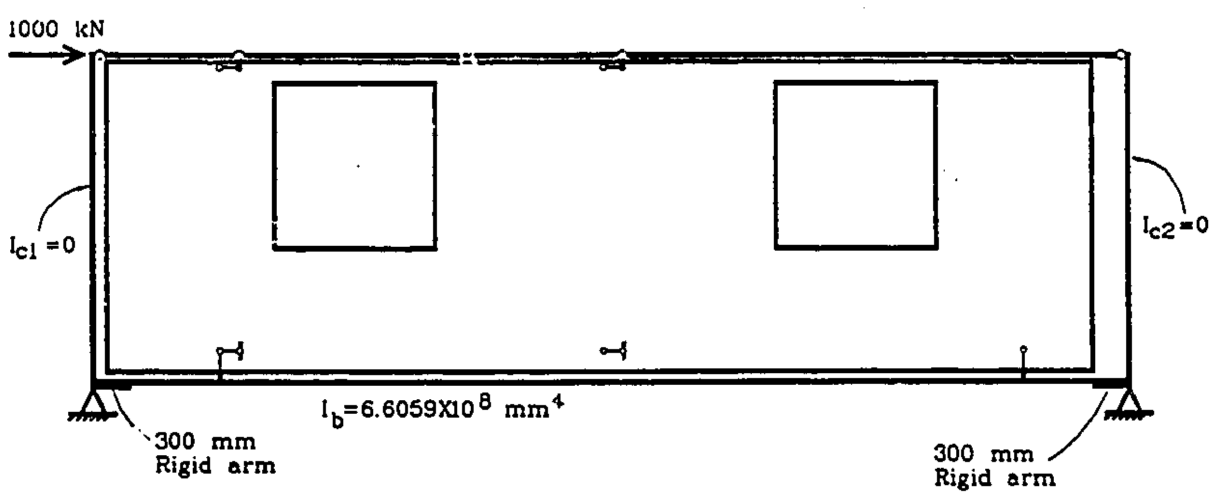

Figure 11.8: Model for Complete Module, but Effectively without Columns - Case (b)

1000 kN, Fig. 11.8. The tops of the frame and panel translated 17.85 mm in the horizontal direction and the displaced shape is shown in Fig. 11.9. As in case (a), the 'backward' double-curvature bending in the beam caused by the panel's forward rotation is evident.

Then the complete model, Fig. 11.7, including the effect of the columns was analysed. The top lateral deflection was 3.97 mm, which was only 22 percent of that of the analysis without the effect of the columns. The displaced shape of the panel and frame is presented in Fig. 11.10. By introducing the stiffnesses of the columns, the panel's rotation was reduced, and the 'forward' double-curvature bending of the beam due to racking of the frame reduced considerably the 'backward' double-curvature bending of the beam caused by the panel's forward rotation.

Comparing these results with those of case (a), where the beam had no rigid ends, it is clear that the rigid beam-ends increases the lateral stiffness of the structure. The lateral displacement from the complete analysis was 74 percent of that from the previous case. Further, the effect of the rigid beam-ends was to increase the 'forward' double-curvature bending of the shorter length beam; therefore, reducing, in a greater proportion, the 'backward' double-curvature bending of the beam caused by the panel rotating.

Similarly to the previous case, to determine the sensitivity of the structure's lateral flexibility to that of the beam, the flexibility obtained from analysis VII, Table 4.3, where the beam was assigned to be rigid and the rest of the components were flexible, was subtracted from the flexibility of the complete analysis presented above. The value obtained was $2.46X10^{-3}$ mm/kN.

A lateral load analysis of the complete model, but with the panel and connections assigned to be effectively rigid, Fig. 11.11, was performed. The top lateral displacement was small, that is, 0.79 mm. To assess the sensitivity of the structure's racking flexibility to the that of the panel with its connections, the flexibility of the model in Fig. 11.11, in which the frame was flexible, but the panel and connections assigned to be rigid, was subtracted from the result of the analysis of the complete module. The value obtained in this case was $3.18X10^{-3}$ mm/kN.

It is evident that in this case, unlike case (a), the sensitivity of the structure's lateral flexibility to the flexibility of the panel with its connections was greater, by 29 percent, than it was to the flexibility of the beam. Therefore, the effect of the rigid beam-ends was also to decrease more significantly the sensitivity of the structure's lateral flexibility to that of the beam.

11.3 Case (c): Equal, but Long Rigid Beam-Ends

The panel-clad frame structure in this case, is different from the previous case in that the beam has longer rigid arms at its ends, that is, 750 mm, Fig. 11.12.

When a lateral load analysis of the complete model, but with the columns assigned a very small inertia, Fig. 11.13, was performed, the tops of the frame and panel displaced

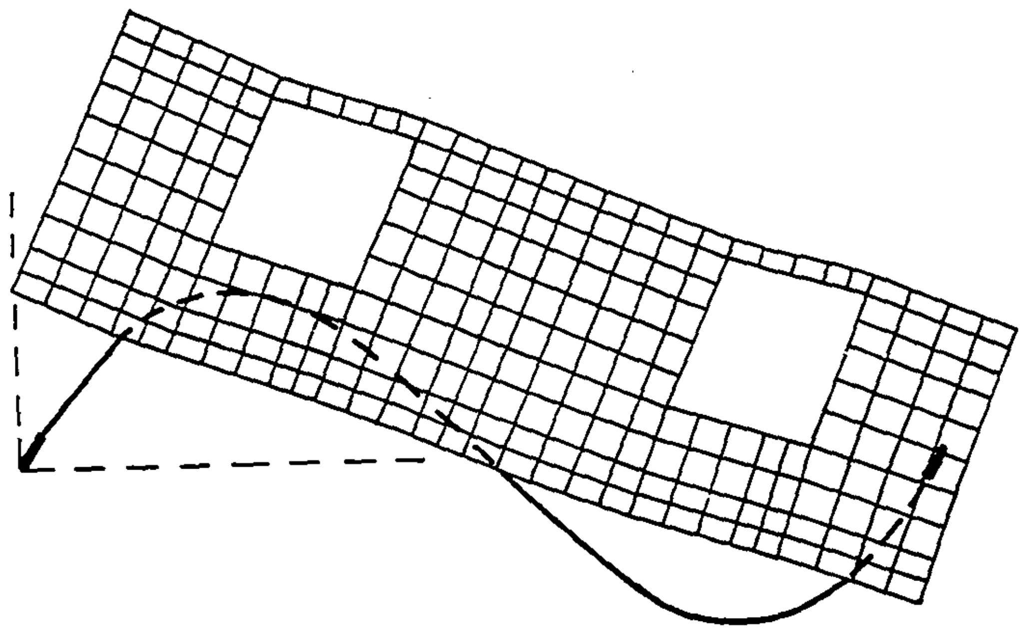

Figure 11.9: Deflected Shape for Panel Supported by Beam - Case (b)

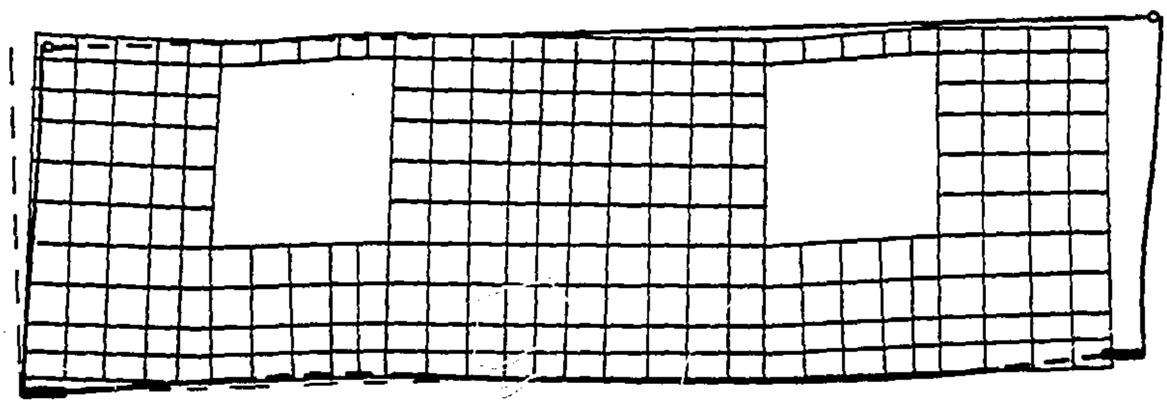

Figure 11.10: Deflected Shape for Complete Module - Case (b)

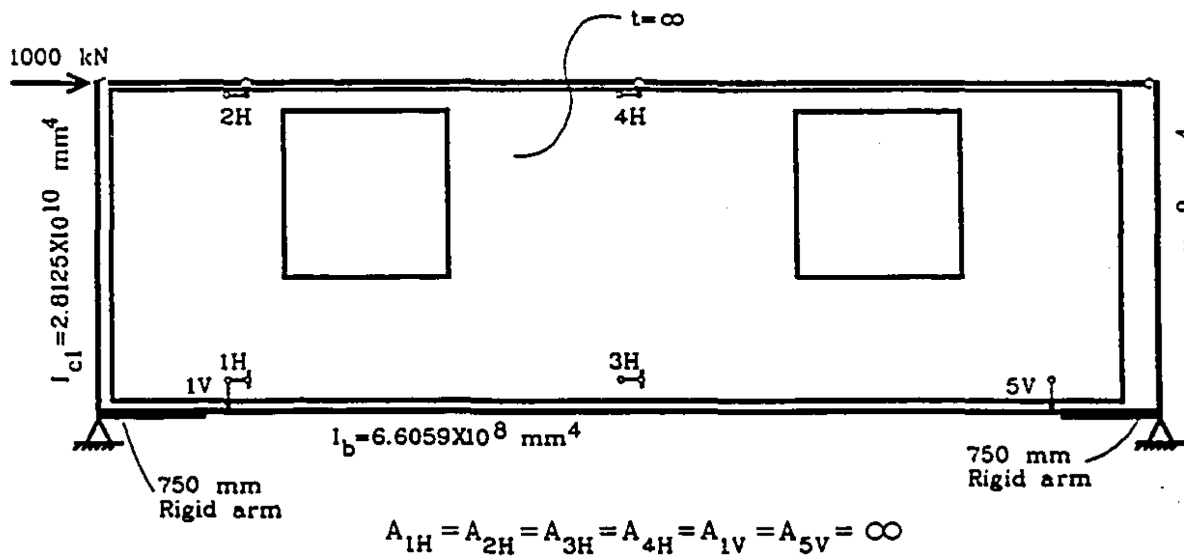

Figure 11.11: Model for Complete Module, but with Panel and Connections Rigid - Case (b)

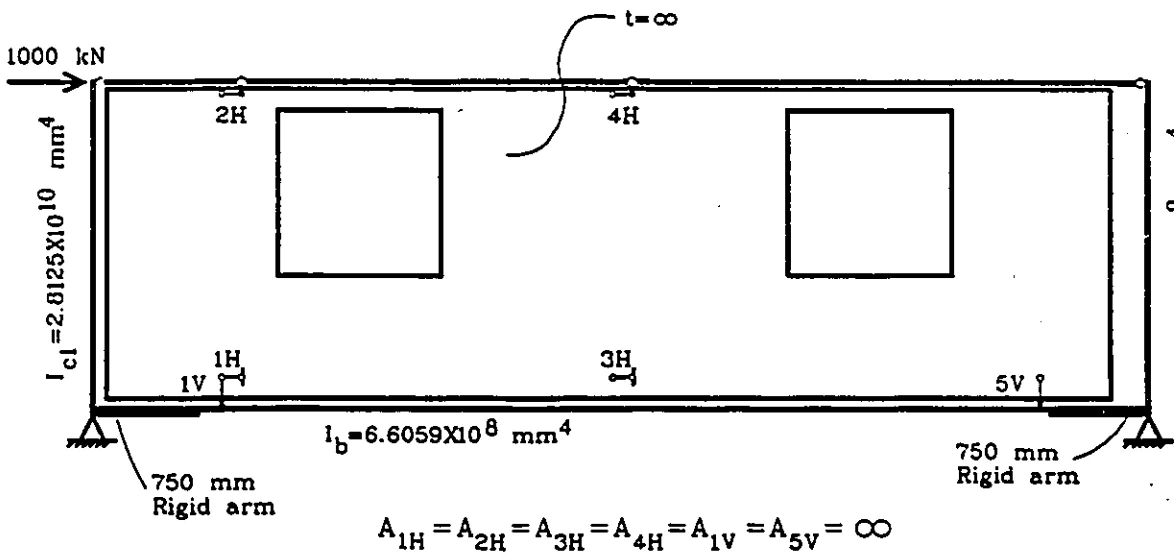

Figure 11.11: Model for Complete Module, but with Panel and Connections Rigid - Case (b)

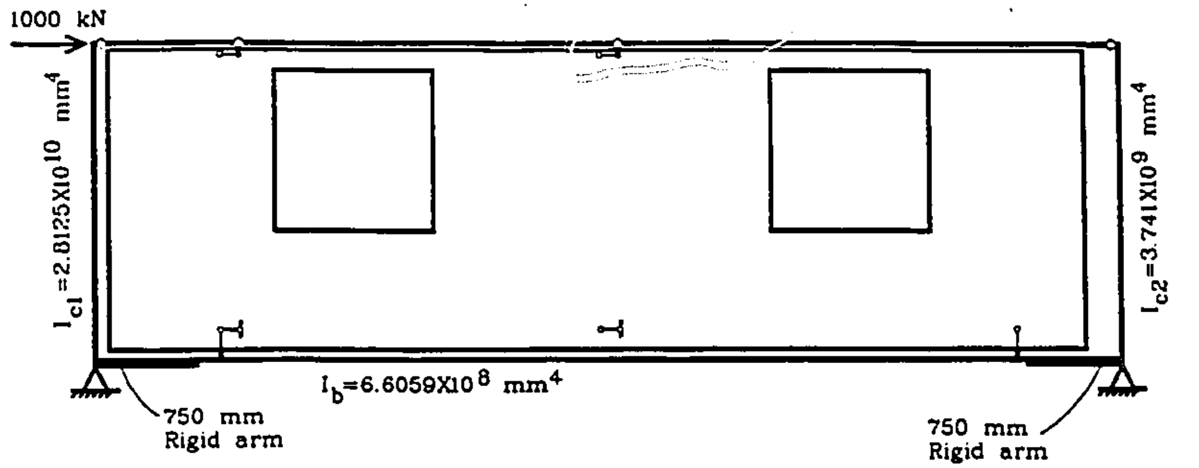

Figure 11.12: Model for Complete Panel-Clad Frame Module - Case (c)

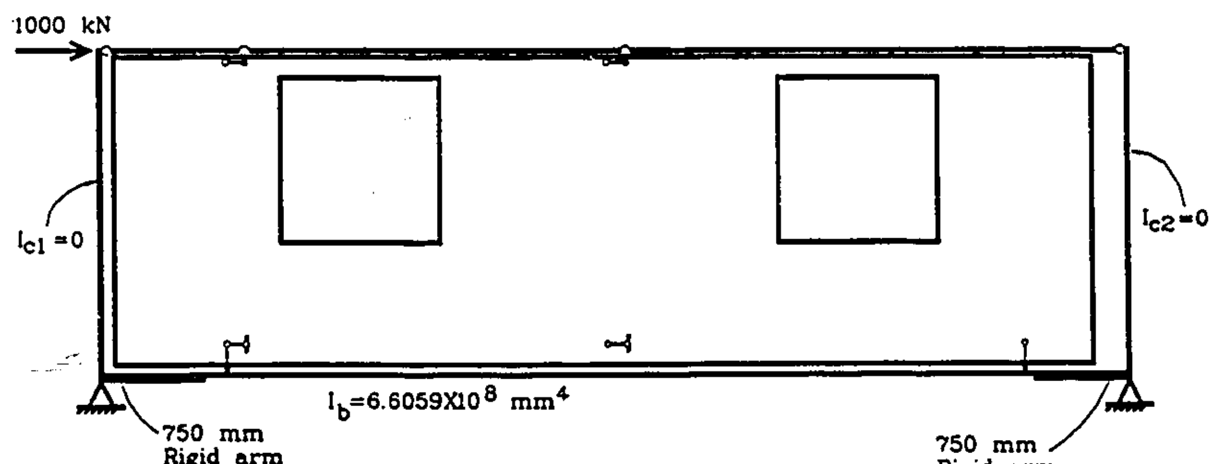

Figure 11.13: Model for Complete Module, but Effectively without Columns - Case (c)

16.32 mm in the horizontal direction. As can be seen from the deflected shape of the structure, Fig. 11.14, without the stiffnesses of the columns there is no moment-resisting frame action present, and the beam bends only in 'backward' double curvature, due to the panel's forward rotation.

An analysis of the complete module, Fig. 11.12, subjected to a horizontal load of 1000 kN was then performed. The top lateral deflection was 3.22 mm, which was only 20 percent of that of the analysis without the effect of the columns. Also, this displacement was only 60 percent of that obtained from the analysis without the rigid beam-ends, indicating that these contribute significantly to the stiffening response of the structure. The deflected shape of the complete module, Fig. 11.15, illustrates that by reintroducing the stiffnesses of the columns, the panel's forward rotation was reduced substantially and that, with longer rigid beam-ends, the moment-resisting frame's racking action changed the mode of deformation of the beam from 'backward' double-curvature bending to 'forward' double-curvature bending. Therefore, the longer the rigid beam-ends, the greater the 'forward' double-curvature bending of the shorter length beam and, since this action opposes the 'backward' double-curvature bending of the beam due to the panel rotating, the greater the stiffening effect.

Similarly to the other cases, to assess the sensitivity of the structure's lateral flexibility to that of the beam, the flexibility computed from analysis VII was subtracted from the flexibility of the complete analysis presented above. The resulting value was $1.71X10^{-3}$ mm/kN.

From a lateral load analysis of the complete module, but with the panel and its connections assigned to be effectively rigid, Fig. 11.16, the top displacement in the horizontal direction was found to be very small, that is, 0.21 mm. To determine the sensitivity of the structure's lateral flexibility to the flexibility of the panel with its connections, the flexibility of this analysis, in which the frame was flexible, while the panel and the connections were assigned to be rigid, was subtracted from the flexibility of the complete analysis. The resulting value in this case was $3.01X10^{-3}$ mm/kN.

In case (c), the sensitivity of the structure's racking flexibility to that flexibility of the panel with its connections was 76 percent greater than it was to the beam's flexibility. In comparison with case (b), the longer rigid beam-ends considerably reduced the sensitivity of the structure's lateral flexibility to the beam's flexibility.

11.4 A Comparison of the Representative Panel-Clad Frame With the Previous Cases

The representative panel-clad frame presented in Chapter 4, Fig. 4.15, differed from the hypothetical cases (a) to (c), in that the representative beam had a 750 mm long rigid arm at the windward end, and a 300 mm long rigid arm at the leeward end.

In Chapter 4, a lateral load analysis of the complete module, but with the columns assigned a very small inertia was performed, Analysis V. The resulting top lateral displace-

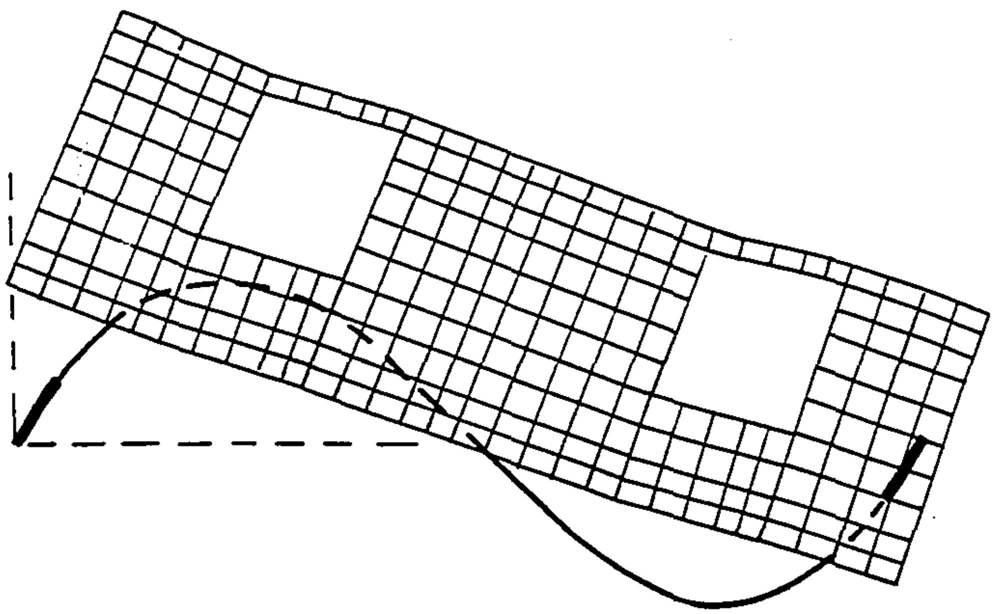

Figure 11.14: Deflected Shape for Panel Supported by Beam - Case (c)

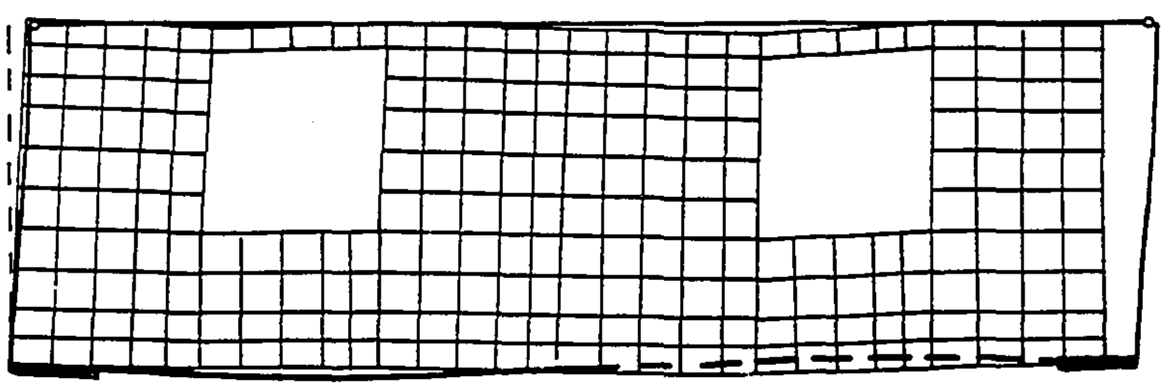

Figure 11.15: Deflected Shape for Complete Module - Case (c)

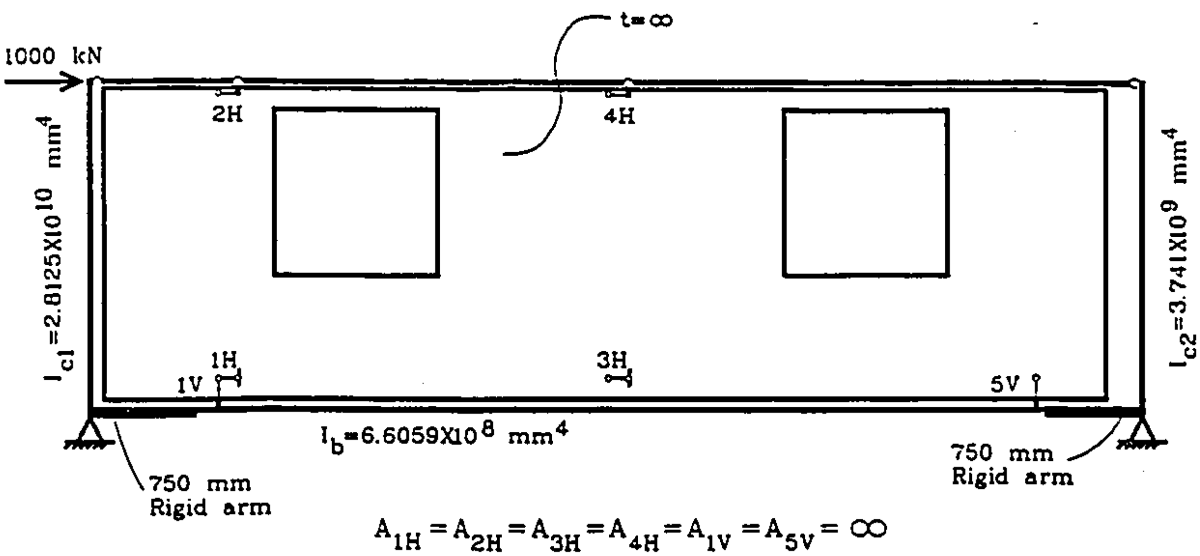

Figure 11.16: Model for Complete Module, but with Panel and Connections Rigid - Case (c)

ment was 17.08 mm, Table 4.3. As in the other cases, the resulting behaviour is due only to the panel's forward rotation causing the beam to bend in 'backward' double curvature, since the moment-resisting frame action was absent, Fig. 5.2b.

From the complete analysis of the panel-clad frame, including the effect of the columns' stiffnesses, and presented in Chapter 4, the top lateral deflection was 3.62 mm, that is, 21 percent of that from the analysis without accounting for the columns' stiffnesses. This places the case of the unequal rigid beam-ends somewhere in between case (b) and case (c), as expected. This, as well as the fact that the longer rigid arm at the windward end imposes on the beam at that end a larger downward displacement than the shorter rigid arm imposes at the leeward end, offers a better explanation for the beam's downwardly biased deflected shape obtained from the complete analysis, Fig. 5.2c.

In Section 5.1.3, the sensitivity of the structure's flexibility to that of the beam and to the flexibility of the panel with its connections were calculated as $2.11X10^{-3}$ mm/kN and $3.10X10^{-3}$ mm/kN, respectively. In this case, the sensitivity of the structure's racking flexibility to the flexibility of the panel with its connections was approximately 50 percent greater than it was to the beam's flexibility. Again, this value places the representative panel-clad frame with unequal rigid beam-ends between cases (b) and (c).

CHAPTER 12

THE STIFFENING EFFECT OF CLADDING: CONCLUSIONS AND RECOMMENDATIONS

12.1 Conclusions

The following conclusions are drawn from the study of the stiffening influence of cladding on the lateral load behaviour of building frames. In cases where specific percentages or factors are given for the effects of the cladding panels, these should be regarded as an indication of the importance in accounting for the panels.

1. Aluminum curtain wall cladding cannot be expected to have a significant stiffening effect on the lateral load behaviour of building structures because of its isolating connection system and its relatively lightweight structural properties.

2. In using the types of connection arrangements prescribed by the CPCI and PCI for "non-loadbearing" precast concrete cladding panels, the panels may be expected to significantly increase the in-plane lateral stiffness of the structural frame. The stiffening is caused by the panels bracing the frame, and increasing its resistance to racking, that is shear, deformation.

3. The interactive behavior of the cladding panel and the moment-resisting frame is a combination of two opposing actions: the unclad frame's 'forward' racking action, and the forward rotation of the panel supported by the beam, which causes an opposing 'backward' racking action of the frame. The net effect tends to be a quadruple-curvature bending deformation of the beam and a shearing deformation of the panel.

4. From finite element analyses of a representative storey-height panel and frame, the racking stiffness of the particular panel-clad frame was found to be 35 times that of the unclad frame.

5. The sensitivity of the structure's racking flexibility to the flexibility of the panel with its connections appears to be of the same order as it is to the flexural flexibility of the beam.

6. The actions that occur when the precast concrete cladding panel interacts with the moment-resisting frame to which it is connected can be, alternatively, and in some respects, better visualized by a proposed analogous spring model.

7. The 'improved', single-diagonal strut model gives a very good representation of the behaviour of a laterally loaded panel connected within a moment-resisting frame. By using this bracing strut model, the analyses of building structures with cladding panels can easily be performed.

8. The effect of including cladding panels as equivalent struts in the analyses of the representative moment-resisting frame and wall-frame structures was to reduce the top deflection of the structures without panels by a significant 68.4 and 36 percent, respectively. The frame-member moments were reduced by approximately 50 to 70 percent in the case of the clad moment-resisting frame structure, and by 25 to 30 percent in the case of the clad wall-frame structure.

9. The displaced shape of the moment-resisting frame structure without the equivalent struts had a predominantly shear configuration, while the deflected shape of the structure with the struts was composed of a larger overall flexural component and a much reduced shear component. In the case of the wall-frame structure, the effect of the cladding panels on the structure's mode of displacement was to lower the point of contraflexure of the deflected shape, corresponding to a relatively greater shear deformation.

10. For the worst loaded panel in the example moment-resisting frame structure, at the fairly representative intensity of wind loading for which the structure was analysed, the connections would not withstand the loads to which they were subjected. The resulting stresses in the panels also indicated that the panels would require additional reinforcement in critical areas. In the case of the wall-frame structure, the connections would require a slight increase in strength to be adequate, while the panels were adequate to withstand the loads to which they would be subjected.

11. The effect of the cladding panels on the dynamic properties of the example moment-resisting frame structure was to reduce its fundamental natural period of vibration by 46 percent, to alter its mode shapes, and to increase its base shear and overturning moment by 117 and 103 percent, respectively. Adding the cladding panels to the wall-frame structure reduced its fundamental period of vibration by approximately 20 percent, but did not significantly alter its mode shapes, and increased its base shear and overturning moment by 15 and 26 percent, respectively.

12. When the connection stiffnesses were reduced by a factor of ten, the shearing stiffness of the single-storey panel-frame module was reduced by a factor of 3.7, that is to being 9.5 times greater than that of the unclad frame. Although the stiffening effect of the panel with its reduced connection stiffnesses was significantly smaller than that of the panel with the original connection stiffnesses, the panel carried as great a proportion of the external load. In the overall static wind load analysis of

the example moment-resisting frame structure with cladding panels, the effect of the reduced connection stiffnesses was to reduce the stiffness by 37 percent from that with the original connection stiffnesses, corresponding to a reduction of the top deflection of the unclad frame structure of 50 percent. In addition, reducing the connection stiffnesses increased the frame-member moments in the bottom storey of the clad frame structure by 10 to 30 percent, but were still a significant 40 percent less than those of the unclad frame structure. Finally, the resulting forces in the connections would still exceed their capacities, while the stresses in the panels were adequate to withstand the induced loads.

13. The effect of the rigid beam-ends on the behaviour of the panel-clad frame is to increase its lateral stiffness, and to increase the 'forward' double-curvature bending of the shorter length beam; therefore, reducing, in a greater proportion, the 'backward' double-curvature bending of the beam caused by the panel's forward rotation. In addition, the sensitivity of the structure's lateral flexibility to that of the beam is reduced more significantly when the effect of the rigid beam-ends is included in the frame.

12.2 Procedure for Analysis of Building Structures Braced by Precast Concrete Cladding Panels

As a result of the investigation described in this first part of the thesis, a practical procedure for the analysis of building structures braced by precast concrete cladding panels is developed. The procedure also includes a description of how to evaluate the loads induced in the panels, their connections and the frame. This analysis procedure would, consequently, allow the engineer to design the frame, panels and panel connections of the building to ensure its adequate lateral stiffness and strength.

The analysis procedure consists of the following major steps:

1. A detailed finite element analysis is made of a single-storey panel-frame module arranged to behave as a typical bay-width storey of a multi-storey multi-bay frame. This includes simulating the effects of panels above and below, and adjacent to the module in question. A description of the special model for a representative panel-clad frame is given in Chapter 4.

2. Using the same model as in Step 1, but effectively without columns by assigning them to have very small inertia, and with the beam assigned to be effectively rigid, a second lateral load analysis of the resulting structure is performed.

3. The improved single-diagonal equivalent strut model described in Chapter 6, Section 6.4, is then used to model the cladding panels in the overall structure analyses. The model is valid for any full-storey, full-bay panel attached to the slab or beam by two loadbearing connections at the bottom and tie-back connections at the top, and

possibly also at the bottom, as recommended by the design manuals. The axial area of the equivalent bracing strut is obtained by equating its horizontal stiffness to the lateral stiffness of the panel and connections supported by a rigid beam, as determined in Step 2.

4. The improved single-diagonal bracing struts are incorporated in the mathematical model of the building structure to allow its structural analysis. The building models with the bracing struts can be used for their static and dynamic linear elastic analyses. Example analyses are presented in Chapters 7 and 9.

5. The forces induced in the panel and its connections are determined and checked against their capacities. First, an estimate of the resulting vertical forces in the bearing connections is made by taking the vertical component of the force in the improved single-diagonal strut of the overall analyses performed in Step 4. The corresponding horizontal forces in the connections restraining lateral movement, are obtained by scaling the horizontal forces resulting from the detailed analysis of the storey-height panel-frame module, Step 1. The scaling factor is equal to the ratio of the vertical forces in the bearing connections determined above to the vertical forces from the detailed analysis (Step 1). The stresses in the panel are scaled similarly. The forces that the connections and the panel must resist are then compared with their capacities, as was done in Chapter 8.

12.3 Further Recommendations

1. The suitability of the presently recommended connection arrangements for panels to be used as bracing should be assessed, and possibly, better alternative connection arrangements considered.

2. Typical connections should be tested for stiffness, strength, and reverse cyclic degradation of strength, and panels should be tested for stiffness. From the results of these tests it may be found necessary to develop new types of connections that can better withstand the loads to which they are subjected when the panels are used as bracing.

3. Detailed finite element models of the connections should be developed and analysed elastically and nonlinearly, and the results compared with the test results obtained above.

4. Using the above results, and the proposed analysis procedure in Chapter 12, a practical procedure for the design of building structures braced by precast concrete cladding panels could be developed.

5. Relatively simple hand methods for determining the effects of the panel's flexibility and the vertical connections' flexibilities on the braced modules shear stiffness should be developed, so that the cladding panels could be accounted for in the overall structure

analyses without having to first perform detailed finite element analyses of a single-storey panel-frame module.

6. Using the algebraic expression for the lateral flexibility of the panel-clad frame developed from the analogous spring model, Appendix A, the sensitivity of the structure's racking flexibility to the flexibilities of the frame, panel, and the connections should be further explored.

7. Although many of the concepts presented in this study apply equally to high-rise and low-rise buildings, a more thorough investigation of the effects of cladding panels on the overall behaviour of low-rise structures should be performed. As a preliminary study, the author has performed some analyses on a five-storey structure whose results are recorded in Appendix C.

PART II

THE STIFFENING EFFECT OF NON-LOADBEARING INFILLS

CHAPTER 13

INTRODUCTION AND LITERATURE REVIEW

13.1 Introduction

13.1.1 General

The possible contribution of internal partitions to the lateral stiffness and strength of building structures is generally neglected in design procedures. Although the partitions are usually assumed as non-structural in function, it has been recognized for many years that some types of partitions can contribute significantly to the lateral stiffness of building structures.

In a report on the damage to buildings during the 1971 San Fernando earthquake (Page et al. 1975), it was noted that there was evidence that the important reserve capacity in non-structural elements such as infill walls and partitions made the difference between survival and collapse of the older buildings. The 1976 Guatemalan earthquake caused considerable damage to partially reinforced masonry partition walls covered with plaster, indicating that they acted as shear walls in taking seismic loads (Engineering News-Record 1976). During the Mexican earthquake of September 19, 1985, masonry infills in many medium- and high-rise buildings suffered severe damages. In many cases the infills prevented structural collapse by sharing the inertial forces acting on the structures. Other reports, also based on experience gained from observations of earthquake damaged buildings, have indicated that non-structural elements, including partitions, are widely appreciated as being a factor in influencing the lateral load behaviour of building structures (McCue et al. 1975, Sharpe 1972).

In one reported case, forced-vibration tests were performed on a twenty-storey building to measure the dynamic structural properties of the building, and to investigate the cause of the development of large diagonal cracks in blockwork partition walls (non-structural) during wind storms (Ellis et al. 1979). A comparison of the test results with those of mathematical models led to the conclusion that additional lateral stiffness, of as much as 75 percent in one direction and 40 percent in another, was provided by the combination of internal partition walls and cladding panels.

In a study of the influence of non-structural partitions on the dynamic response characteristics of four-storey reinforced concrete test structures, it was found that unreinforced masonry infills have an initial extremely high, but short-lived, stiffness under cyclic loading, (Raggett 1972). The effect of the blockwork partitions was, at first, to increase the stiffness of the bare frame by a factor of seven, but after one year of severe ground-motion-induced vibration, the partitions' influence on the stiffness reduced to virtually zero.

As a result of other analytical and experimental investigations of structures, it was found that partition walls other than masonry infills, for example, metal stud and gypsum board walls, can also contribute to the lateral stiffness of buildings (Shepherd et al. 1983, Freeman 1977).

13.1.2 Scope of the Investigation

Non-loadbearing masonry partition walls are often used in buildings around elevator and stair shafts, and are very often used in the lower storeys of tall buildings. Although designers assume these walls to be non-structural in function, it is believed that they can significantly stiffen a structure. The non-loadbearing masonry partitions considered in this study are those commonly used in the Montreal area; that is, they are concrete block partitions which are laid to fit against the columns, but have a gap between the top of the infill and the beam above. The purpose of the gap is to avoid loading the wall as the beam deflects under load or creep. It is usually filled with a compressible filler material to provide acoustic and fire insulation.

When performing an analytical study, the modelling techniques and method of analysis used must be chosen with special care to obtain a close representation of the behaviour of the infilled frame. Important factors that may influence the stiffness response of the infilled frame, and the strength of the infill, should be investigated; these include the stiffness of the beams, the stiffness of the columns, and the aspect ratio of the infill.

From the results and conclusions of detailed analyses of a series of representative single-storey infilled frame modules, a simple and practical method of representing the effects of infills in the overall structure analyses can be developed.

The objectives of this investigation are as follows:

1. To determine the in-plane lateral load mode of behaviour and forces induced in a non-loadbearing infill within a moment-resisting frame, as commonly constructed, by forming and analysing a mathematical model of the problem.

2. To determine the relative influence of the frame's stiffness, and of the infill's properties and dimensions, on the behaviour of the infilled frame.

3. To estimate the magnitude of increase in the racking stiffness of the infilled frame over the stiffness of the bare frame.

4. To compare the various stresses developed in the infill against its respective strengths.

5. To develop a simple model, using the results of detailed analyses, to represent the infill in the overall structure analyses.

6. To examine the influence of the non-loadbearing infilled bents on the static and dynamic responses of the total moment-resisting frame structure.

7. To develop an analysis procedure that will allow for the effects of non-loadbearing masonry infills in the mathematical model of a structure, and that will also allow the strengths of the infills to be compared with the resulting stresses.

13.2 Literature Review

13.2.1 Behaviour of Fully Infilled Frames

The use of a masonry infill to brace a moment-resisting frame combines the rigidity of the infill with the containment of the frame, which restrains the infill from disintegrating after cracking.

The infill braces the frame, partly by its in-plane shear resistance, and partly by its behaving as a diagonal bracing strut in the frame. When the infilled frame is subjected to lateral loading, the frame and infill separate over a large part of the length of each side, and regions of contact remain only adjacent to the corners at the ends of the compression diagonal, Fig. 13.1a. Therefore, the stiffening action of the infill can be conveniently represented by an equivalent strut acting along the compressive paths, Fig. 13.1b.

The behaviour of infilled frames, as described above, has been developed from a combination of results of full-scale and model tests (Polyakov 1956, Benjamin and Williams 1958, Holmes 1961, Stafford Smith 1962, Stafford Smith 1966, Stafford Smith 1967, Esteva 1966, Mainstone and Weeks 1970, Mainstone 1971).

Polyakov (1956) was the first to conclude that an infilled frame behaved as a frame with diagonal bracing, and that the deformations in the brick panels were the greatest near the compression corners.

Benjamin and Williams (1958) reported tests on full-scale single-storey steel and reinforced concrete frames with brickwork infills. They gave tentative formulas for predicting the stiffness and ultimate strength of an infilled frame. Their results indicated that the stiffness of the structure can be derived by considering the stiffness of the wall alone, with a negligible contribution from the frame.

Holmes (1961) tested small two-dimensional square steel frames infilled with brick masonry and concrete walls. Holmes suggested that a suitable cross-sectional area for an equivalent diagonal strut to represent the wall was given by one third of the length of the side of the frame multiplied by the wall thickness.

Stafford Smith (1962, 1966, 1967) showed, through a series of tests, that the stiffness response of an infill and, therefore, of the infilled frame, and the strength of the infill,

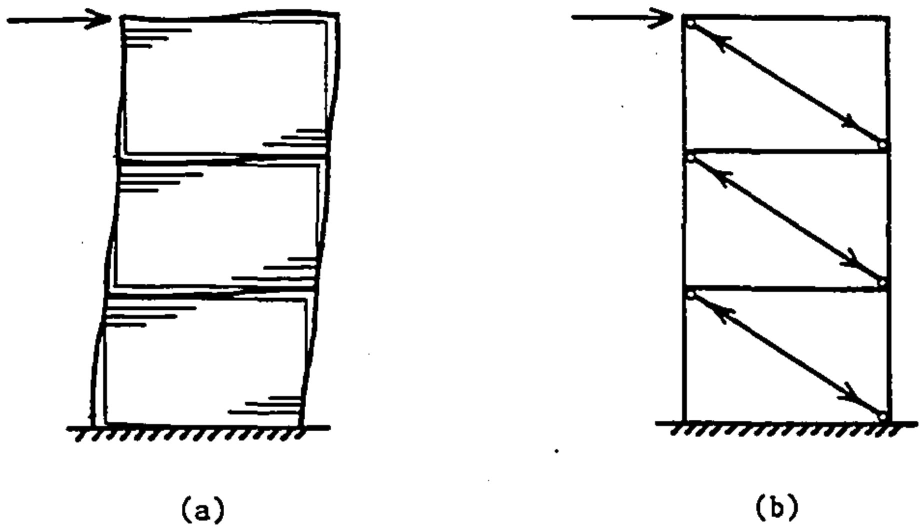

Figure 13.1: Behaviour of Fully Infilled Frames Subjected to In-Plane Lateral Loading

depended not only on the infill's dimensions and physical properties, but also on its length of contact with the surrounding frame. This length of contact was found to be governed by the relative stiffness of the infill and the frame, or to be more specific the relative stiffness of the infill and the column. Stafford Smith also presented a series of graphs to determine the effective width of an equivalent strut as a function of the various influencing parameters.

Esteva (1966) reported experimental investigations into full-scale single-panel reinforced concrete frames with various types of infill. The main purpose of the investigation was to examine the deterioration of diaphragms subjected to cyclic loading.

Mainstone (1970, 1971) also idealized the effect of an infill by an equivalent diagonal strut. He proposed equations for determining the effective width of the equivalent bracing strut.

13.2.2 Infilled Frames with Gaps Between Top of Infill and Beam

The present study is concerned with the effect on the lateral stiffness of a moment-resisting frame of a non-loadbearing masonry infill, as commonly constructed with a gap between the top of the infill and the beam above. The following is a review of research which has been performed in relation to this specific form of infilled frame.

At the University of New Brunswick (Yong 1984, Dawe and Yong 1985, Pook and Dawe 1986), a study was conducted on the shear strength and behaviour of masonry infilled frames subjected to horizontal in-plane loads. Six full-scale, single bay, one-storey, fixed base, concrete block infilled steel frames with five different boundary conditions were investigated. One of the five conditions studied was a 20-mm gap between the infill and the top beam. A finite element program was also developed to analyse the structures.

Two specimens with a 20-mm gap between the wall and the adjacent roof beam were tested: one in which the infill fitted loosely between the column flanges, and the other in which flat bar ties were welded to the columns and embedded in the mortar joints at alternate courses. The resulting crack patterns demonstrated that, for the specimen in which the infill fitted loosely, mostly horizontal cracks with a slight suggestion of diagonal cracking developed; whereas, for that with the infill-to-column ties, more diagonal cracking was induced. However, from the load-deflection curves produced in the study, the overall behaviour and capacity of the two specimens were similar. The ties did not appear to increase the ultimate strength and stiffness of the infill significantly. The ultimate load for an infilled frame in which the infill extended to the beam above was about 63 percent greater than for the similar infilled frame with the 20-mm gap at the top.

The behaviour of semi-confined and fully confined concrete block walls was studied by Wolde-Tinsae and Raj (1986). In-plane cyclic load tests were performed on half-scale, single-storey, fixed base, masonry-infilled steel frames. Five specimens, with and without a 51-mm gap at the top, and with varying amounts of external reinforcement were tested.

It was found that the existence of a gap at the top of the infill greatly reduced the load carrying capacity of the structure, but the gain in lateral strength of the structure over that of the bare frame was still significant. All the infill panels demonstrated the ability to significantly stiffen their frame structure, but as the cyclic loads increased, the strength of the infilled frame subsequently tended to approach that of the corresponding bare frame.

The specimens with gaps at the top developed horizontal cracks along their base from one corner to the other. The specimen with a gap, but no external reinforcement, developed cracks which propagated in a step-wise fashion through the mortar joints and did not pass through the blocks. It was also concluded that the compressive stresses were a maximum at the loaded corners, and the maximum principal tensile stress occurred at the centre of the infill. Furthermore, under cyclic loading, the addition of external reinforcement to the masonry block infills greatly enhanced their strength, resistance to stiffness degradation, and energy dissipation capabilities.

Wolde-Tinsae et al. (1987) also performed a finite element study of the effect of gap sizes between the top of the masonry-infill and the frame beam, on the behaviour of the composite structure under in-plane lateral loading. The structure analysed was a simple one-storey steel frame with a masonry infill.

To determine the influence of gap sizes, Wolde-Tinsae's analyses were performed on a fully confined wall, a wall with 0.17h gap, and a wall with 0.48h gap. In each case, the infill acted as a single diagonal strut after separation. The highest tensile stress occurred at the centre of the infill in all cases. Increasing the gap between the top of the infill and the beam increased the difference between the compressive stresses at the corners, and also increased the compressive stress at the top compressive corner. The shear stress was found to be a maximum at the centre of the infill for the fully infilled frame, and at the loaded corner for the semi-infilled frames. Slip between the infill and the frame in the semi-infilled frame contributed to a significant portion of the total lateral deflection. Furthermore, the effect of the infill on the frame reduced significantly the bending moment in the members in all cases. However, a noticeable increase in the bending moment at the loaded corner of the frame was observed with an increase in gap size.

The equivalent strut analogy was also investigated in Wolde-Tinsae's study. When the gap between the top of infill and the beam was greater than a certain value, which differed from one semi-infilled frame to another, depending on the h/L ratio, the infill tended to transfer the shear from the top of the windward columns to a certain point on the length of contact between the frame and leeward column. It was concluded from this that the equivalent full-diagonal strut analogy is not valid and a possible alternative representation of the structure could be as shown in Fig. 13.2a. When the gap size was equal to 0.17h or smaller, the representation shown in Fig. 13.2b gave results which were close to those obtained using the finite element analyses.

13.2.3 Finite Element Methods of Analysis

To obtain a fair representation of the behaviour of infilled frames, a method of analysis which allows for proper modelling of the elements and of the interaction between the infill and the frame is necessary. In the previous reviews, experimental tests have indicated that

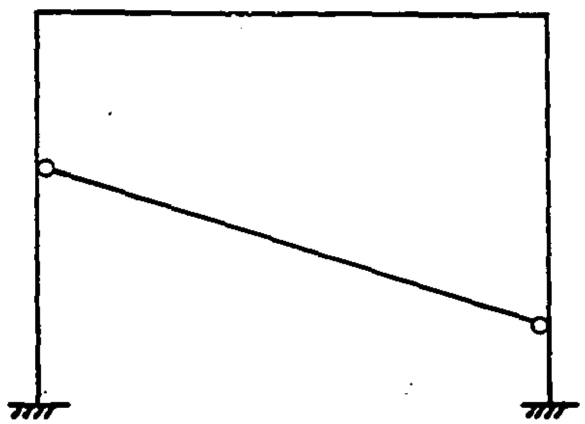

(a) Semi-Infilled Frames with Large Gap

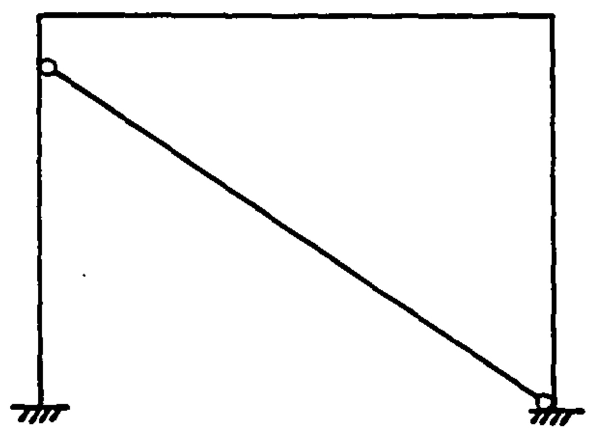

(b) Semi-Infilled Frames with Small Gap

Figure 13.2: Equivalent Strut Models Suggested by Wolde-Tinsae et al. (1987)

the infill separates from the frame when tension develops at the interface, because of the weak tension bond that exists between the two elements. To approach an 'accurate' elastic analysis of an infilled frame, the analysis method must allow for separation cracking between the infill and the frame. The following is a review of the various finite element programs developed for the analysis of infilled frames.

Mallick and Severn (1967) presented a finite element program for the analysis of infilled frames in which the infill was modelled by plane stress rectangular elements and the frame by axially rigid bending elements. Initially, the element stiffness matrices for the infill and frame elements were combined so that the node points were connected to the corresponding nodes of the frame. An iterative process was then used to allow for the interactive behaviour at the interface of the infill and frame. When normal tensile stresses developed at the interface, separation was permitted. Along the interfaces remaining in contact, it was assumed that slip would occur and that shear forces equal to the product of the normal force and the coefficient of friction were applied to the infill. The shear forces were not applied to the frame elements, because these were assumed to be inextensible. Mallick and Garg (1971) later modified this by allowing axial and shear deformations in the girder and leeward column elements. The interaction forces between the infill and frame interface consisted of only normal forces. Rotational displacements of all frame elements were neglected and approximate predetermined contact lengths along the interfaces were assumed.

In Dawson's (1972) study on the influence of unbonded infill walls on the lateral load response of framed structures, the finite element program used a mesh of typical four-node rectangular elements for the infill, traditional beam elements for the frame members, and link elements to allow for separation between the frame and the walls. The link elements were considered to be pin-ended struts of zero length. Each link element had two nodes with one translational degree of freedom at each node. Separation between the frame and the infill was accounted for by using an iterative procedure. Initially a large value was assigned to the stiffness of the link elements. When the structure was loaded the link elements which acted in tension were removed by assigning them to have zero stiffness. The structural matrix was then reassembled and the load reapplied. The iterations proceeded until, ideally, no tension links remained, and compatible nodal displacements existed between the infill and the frame. In addition, a gap element was introduced in the program to account for the lack of tight fit between the walls and the frame. These elements acted in a similar manner to the link elements except that the gap width had to be closed before contact was made between the infill and the frame. The analytical model was found to be 10 percent more flexible than the experimental model.

A method for calculating the dynamic response of a plane moment-resisting frame with infill panels and pre-existent small gaps at the sides and tops of the infills was presented in the following described paper (Kost et al. 1974). All parts of the structure were assumed to be linearly elastic, but the response of the structure was nonlinear because of the opening and closing of gaps. Each infill was modelled by one or more rectangular finite elements having at the most 16 generalized displacements. Modified elements were provided at the infill corners so that the rotation of both edges of the infill element at the corner were identical and equal to the rotation of the frame joint. The beams and columns of the frame were represented by line elements. In addition, a non-friction, sliding link element of zero length and high axial stiffness was inserted or removed whenever a gap closed or opened during the dynamic response of the structure. A static condensation procedure was used in the development of the infill stiffness matrix to eliminate certain nodal displacements.

The finite element program developed by Riddington (1974, 1977) was based on the standard four-node rectangular element with two degrees of freedom per node representing both the infill and the frame members. To simulate the different infill-frame interface conditions, two sets of nodes were generated at each interface. The interface node pairs were connected by a linking matrix which represented a short, very stiff member, forcing the two nodes to have identical displacements. The computerised procedure for the analysis was to first analyse the structure with all the infill-frame interface node pairs linked. These could either be linked by a non-friction sliding connection, in which the nodes were forced to have equal displacements only perpendicular to the interface, or by a shear connection, in which the nodes were forced to have equal displacements in both the horizontal and vertical directions. The infill interface node stresses were then examined automatically for any tension perpendicular to the interface, and where this occurred the node pairs were disconnected. The structure was then automatically re-analysed and the procedure repeated until no further separations occurred. Note that disconnected node pairs were not checked for reconnection, in which case the infill could subsequently overlap the frame. The computer program developed gave a fair representation of the elastic behaviour of the fully infilled frames even after boundary cracking, provided that a tight initial fit of the infill was achieved.

The above program was modified when Riddington (1984) investigated the influence of initial gaps, due to lack of a tight fit, on the infilled frame behaviour. This was achieved by adjusting the stiffness of the linking element to give a difference of displacement of the two interface nodes equal to the initial gap width. Friction was allowed for by applying forces to the frame nodes equal to the product of the coefficient of friction and the normal force acting at the boundary, and equal and opposite forces to the infill nodes.

In the analysis method presented by King and Pandey (1978), the interface between the frame and the infill was modelled using a friction element, which was originally developed by Goodman et al. (1968) and later modified by King and Chandrasekaran (1975). The loads were applied in increments, and an initial lack of tight fit, gap formation, or slip, at the interface between the frame and the infill were readily allowed for by an appropriate initial choice or subsequent automatic adjustment of the modified friction element properties. Nonlinear behaviour of the infill material could also have been considered, if required. The interface elements had three degrees of freedom at the nodes which connected to the frame elements, and two at the nodes which connected to the infill elements. They also took into account the moments produced at the neutral axis of the frame by friction at the interface. In the analyses performed, a close comparison between analytical and experimental results was obtained.

An analytical investigation of the infill-frame system described in Section 13.2.2 was performed by Yong (1984). The program that was developed combined a frame stiffness analysis with a finite element analysis of the infill. Eight-node, plane-stress, rectangular elements were used for the infill analysis, while two-node, traditional beam elements were used for the frame analysis. A shear element and a normal stress element allowed the interface displacements of the infill and the frame to match at a finite number of nodes. These elements had two nodes, each with two degrees of freedom. The stiffness of the friction element was a function of the compressive force in the normal element. The friction force was determined as the product of the normal compressive force and a coefficient of friction. This permitted the infill to slip when the shear force at the interface was greater than the friction force in the friction element. Additionally, the effects of including horizontal joint reinforcement in alternate courses of the blockwork infills, the effects of horizontal bond beam reinforcement at four-course spacings, and the effects of flat bar ties between the infill and the columns were also included in the analyses. The program automatically performed the iterative procedure of analysis. Good correlation was obtained between the experimental and analytical results in the elastic range for a tight initial fit of the infill within the frame.

In a more recent analytical study performed by Wolde-Tinsae et al. (1987) the infill was represented by a mesh of basic four-node rectangular plane stress elements having two degrees of freedom at each node. The frame members were modelled by line elements having three degrees of freedom at each node. The interface between the frame and the infill was represented by a two-node element. Each node had two degrees of freedom. The interface elements had the characteristic of being able to maintain or break physical contact, and permit slip when the shear forces at the boundaries were greater than the friction forces. As in the many other studies described in this section, an iterative process was used to allow the boundary joints to separate.

CHAPTER 14

DESCRIPTION OF MASONRY WALLS

The following discussions on masonry walls is based on information obtained from various sources, including the National Concrete Masonry Association ("Tek-Notes" and "Architectural and Engineering Concrete Masonry Details for Building Construction"), the Ontario Masonry Contractors' Association, the Canadian Standards Association ("Masonry Design for Buildings" (1984), "Masonry Construction for Buildings" (1984), "Concrete Masonry Units" (1985)), "Masonry: Materials, Design, and Construction" by R. C. Smith et al. (1979), and local engineers, masons, and manufacturers.

14.1 Masonry Walls

Masonry walls have the ability to perform several vital building functions simultaneously. They serve as enclosures and sometimes as structure. They also provide a screen against fire, sound, heat transfer, and moisture. Whether of brick, block or stone, masonry units are available in a wide range of types, sizes, shapes, and surface textures. Masonry also has the advantage of offering a finished wall inside and out.

14.1.1 Types of Walls

There are two basic types of masonry walls: loadbearing and non-loadbearing. Loadbearing walls support vertical loads from floors or roofs in addition to their own dead load. Loadbearing walls may also be designed to resist in-plane horizontal forces such as wind and earthquake.. Non-loadbearing walls carry very little vertical load. They can be either exterior walls, where they are primarily subjected to out-of-plane wind pressures, or interior partition walls that carry only their own dead weight.

Masonry walls can also be classified as either single-wythe, composite or cavity walls. The single-wythe wall can be used in either loadbearing or non-loadbearing capacities. The most common type of masonry wall around Montreal used as an infill is the single-wythe wall. Composite walls, in which two or more wythes of masonry of similar or different materials are tied together as a unit, are normally used as loadbearing exterior walls. Cavity walls, in which the two wythes of a wall are laid with a space between the wythes, also serve as loadbearing exterior walls, with the added advantages of protection against rain penetration and of providing greater insulation.

Masonry walls are constructed either of plain masonry, or reinforced masonry. According to the Canadian Standard on "Masonry Design for Buildings" (1984), plain masonry is masonry without steel reinforcement, except that which may be used for bonding or the reduction of the effects of dimensional changes due to variations in the moisture content or temperature. Reinforced masonry is masonry in which steel reinforcement is embedded in such a manner that the two materials act together in resisting forces. Plain masonry has very little strength in tension. The addition of steel reinforcement to masonry introduces tensile strength and ductility, allowing masonry components to withstand tensile stresses with no material failure and to provide resistance to strength degradation under higher loading. Although the Canadian Standard on "Masonry Design for Buildings" (1984) limits the use of plain and partially reinforced masonry to seismic zones 0 and 1, many non-loadbearing interior partition walls are constructed unreinforced and ungrouted (refer to Section 14.2.1 for an explanation of 'grout') in the Montreal region.

14.1.2 Design Methods

The production of sound, durable and relatively inexpensive masonry walls, requires special care in both the design and construction. Two types of masonry design methods have evolved: the empirical type, and a rational type based on engineering analysis.

The empirical design method is the more classical of the two methods. It is based on "rules of thumb", developed by masons through centuries of experience and observation, which have now been standardized in design and construction codes. The empirical rules given in the Canadian Standard on "Masonry Design for Buildings" (1984) can be applied only to the design of plain masonry. They cannot be used in any case if certain height limits are exceeded, or if walls are subjected to very high wind pressures, or in certain other special cases. According to the empirical design method, the wall's stability must be examined as part of the design of all wall types. The stability of a wall depends on its slenderness ratio, that is, the ratio of the wall's effective height to its thickness. Additional stability may be required in the form of lateral supports located at specified distances in either the vertical or horizontal directions. For the design of a loadbearing wall, the wall's compressive load capacity must also be examined. The allowable load capacity of a wall depends upon its cross-sectional area, and the maximum allowable compressive stress of the masonry. In addition to checking the stability of non-loadbearing exterior walls, these shall also be designed for the out-of-plane wind pressures to which they are subjected.

The rational design method in the Canadian Standard on "Masonry Design for Buildings" (1984) applies to the design of plain and reinforced masonry where the design is based on the engineering analysis of the structural effects of the forces acting on the structure. According to this method, masonry walls and columns are designed to have adequate strength to resist the effects of specified loads, by either the coefficient method, or the load deflection method. Allowable stresses in masonry structures must be respected, and as in the empirical design method, stability must also be examined. A working stress design is the basis for both the empirical and the rational design methods.

14.2 Concrete Masonry Walls

The trend towards more efficient lighter construction has led to the development of hollow masonry units, first structural clay tile and later hollow concrete masonry. More than two-thirds of the volume of all masonry walls are constructed of concrete blockwork of one kind or another (Smith et al. 1979). Because of its extensive use, the following discussion will focus on concrete blockwork walls, paying particular attention to the details of non-loadbearing walls.

14.2.1 Basic Components of Concrete Masonry Walls

Concrete Masonry Units:

The concrete masonry units that make up concrete blockwork walls are primarily designed as either hollow or solid. A unit is considered to be hollow if the net concrete cross-sectional area is less than 75 percent of its gross area in any plane parallel to its bearing surface, Fig. 14.1. The solid material in the long face of the units are face shells, while the cross members are webs, and the hollow portions of the units are referred to as cores. Solid units are used mostly for special purposes; for example, in structures that have very high design stresses. Therefore, the majority of the blocks manufactured are of the hollow block category, of which there is a great variety of sizes and shapes. The dimensions and configuration of hollow units have been standardized in North America, so as to have a common comparable product. Fig. 14.2 illustrates the configuration and dimensions of a typical 200 X 200 X 400-mm concrete masonry hollow unit. Also, the dimensions and wall properties for the standard 200 X 200 X 400-mm hollow concrete masonry unit are outlined in Table 14.1.

Concrete masonry units are usually referred to as either normal weight or lightweight, depending on the aggregate from which they are made. Normal weight units are made from aggregates such as sand, gravel, crushed stone and air-cooled blast furnace slag. Aggregates such as expanded shale or clay, expanded blast furnace slag, sintered fly ash, coal cinders, scoria and pumice produce lightweight blocks. The weight-per-unit and the weight of the wall for the standard 200 X 200 X 400-mm hollow concrete block are given in Table 14.1. Lightweight units perform better with respect to sound absorption, and fire and thermal resistance, but are more expensive than normal weight units.

The compressive strength is an important property of concrete masonry units and, in general, the use to which units will be put is related to that strength. Other important physical properties of concrete blocks are their density, water absorption capacity, moisture content, and linear shrinkage potential.

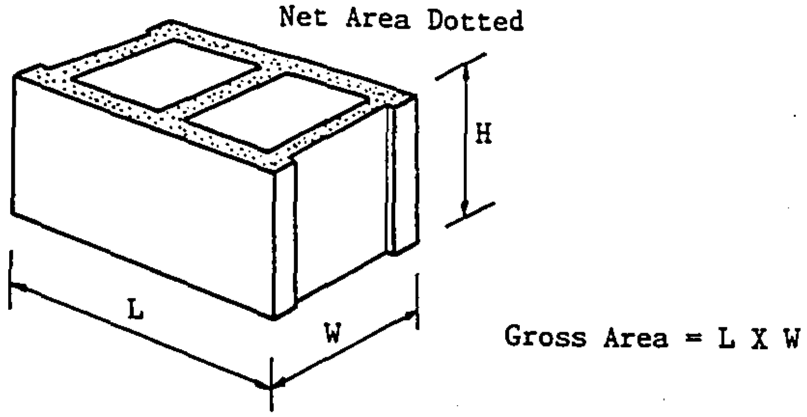

Figure 14.1: Net and Gross Area of a Concrete Block Unit

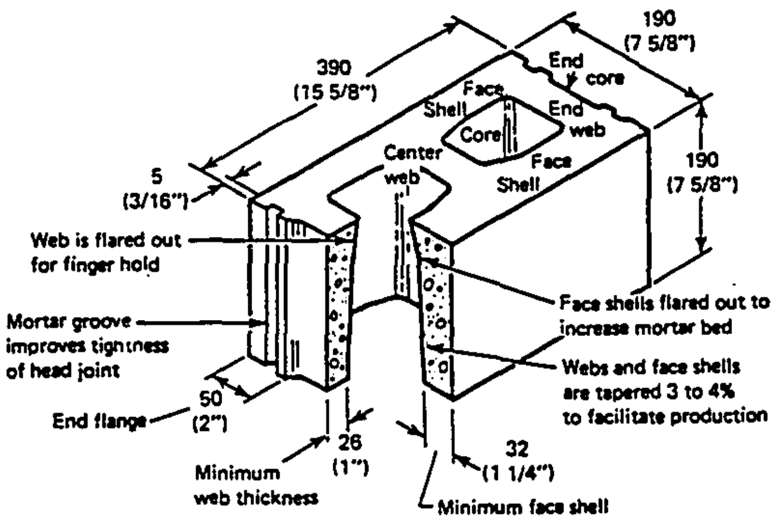

Figure 14.2: Configuration and Dimensions of a Typical 200 X 200 X 400-mm Concrete Masonry Hollow Unit

Properties	Value	
Dimensions per unit (mm)	190X190X390	
Percentage solid (%)	56	
Minimum face shell thickness (mm)	32	
Minimum web thickness (mm)	26	
Gross area (cm^2)	741	
Net area (cm^2)	415	
Gross volume (cm^3)	14079	
Net volume (cm^3)	7889	
Cavities volume (cm^3)	6195	
Equivalent thickness (mm)	106	
Compressive strength (based on gross area) (MPa)	7.5	
	heavy	light
Weight per unit (kg)	16.9	13.8
Weight of wall (kg/mm^2)	211.2	172.5
Density (kg/mm^3)	2100	1600
Water absorption (kg/mm^3)	130	180
Fire resistance (hr) according to:		
-N.S.C.	1.8	2.55
-U.L.C. listed	2.0	4.0
-U.L.C. certificate	2.0	4.0
(on special order only)		
Thermal resistance RSI value ($m^2/^oC/W$)		
-with empty cavities	0.21	0.30
-with filled cavities	0.51	0.81
Sound transmission loss (dB)	49	46
Sound absorption (N.R.C.)	0.27	0.45

Table 14.1: Dimensions and Properties of the Standard 200X200X400-mm Hollow Concrete Block

Mortar:

Mortar serves to bond the masonry units together and to provide an even transfer of stress between them. The basic components of mortar are cement, sand and water. To these are often added hydrated lime, pozzolanic materials, admixtures and color. Mortar must possess a number of important qualities which include workability, water retentivity, consistent rate of hardening, good bond, durability, good compressive strength, and good appearance. Mortar types are specified on the basis of either the proportions of cementatious materials used per batch, or the compressive strength of representative mortar cubes. From the strongest to weakest, the types of mortars used in Canada are M, S, N, O and K. For masonry designed on the basis of engineering analysis, type M, S or N mortar is permitted. For masonry designed by empirical rules, types M, S, N, O and K are permitted, with two exceptions. Types O and K mortar are not allowed where the masonry is to be in direct contact with the soil, or where the masonry is exposed to the weather on all sides. From discussions with local masons, it appears that type M is almost always used, whatever the kind of masonry or whatever the purpose the structure will serve.

Grout:

Another possible component of concrete blockwork walls is grout. Masonry grout is composed of a mixture of cement and fine aggregate, combined with enough water to produce a mix that will flow readily into the cores and cavities without segregation. It is used primarily to bond masonry units and steel together in reinforced masonry walls, so that they act in combination to resist imposed loads. It is usual to place grout in only those cells containing steel reinforcement, but in some loadbearing reinforced masonry walls all cells will be filled with grout.

14.2.2 Concrete Masonry Wall Construction

Bonds and Patterns:

The techniques for building with concrete masonry have, for the most part, followed quite closely those used with brick, tile or stone. A concrete masonry wall is constructed by laying the concrete units in courses. A great variety of wall patterns are possible with concrete block. Fig. 14.3 illustrates just a few of these. The half-block running bond, Fig. 14.3a is the most popular type of bond and pattern.

Mortar Joints:

Bed joints, the horizontal layer of mortar on which the unit is laid, and head joints, the vertical mortar joint between the ends of units, are used with concrete block. Two types of bed joints are used with concrete units: full-mortar bedding, and face-shell bedding. In the former, the webs, as well as the face shells, are bedded in mortar, while with the latter,

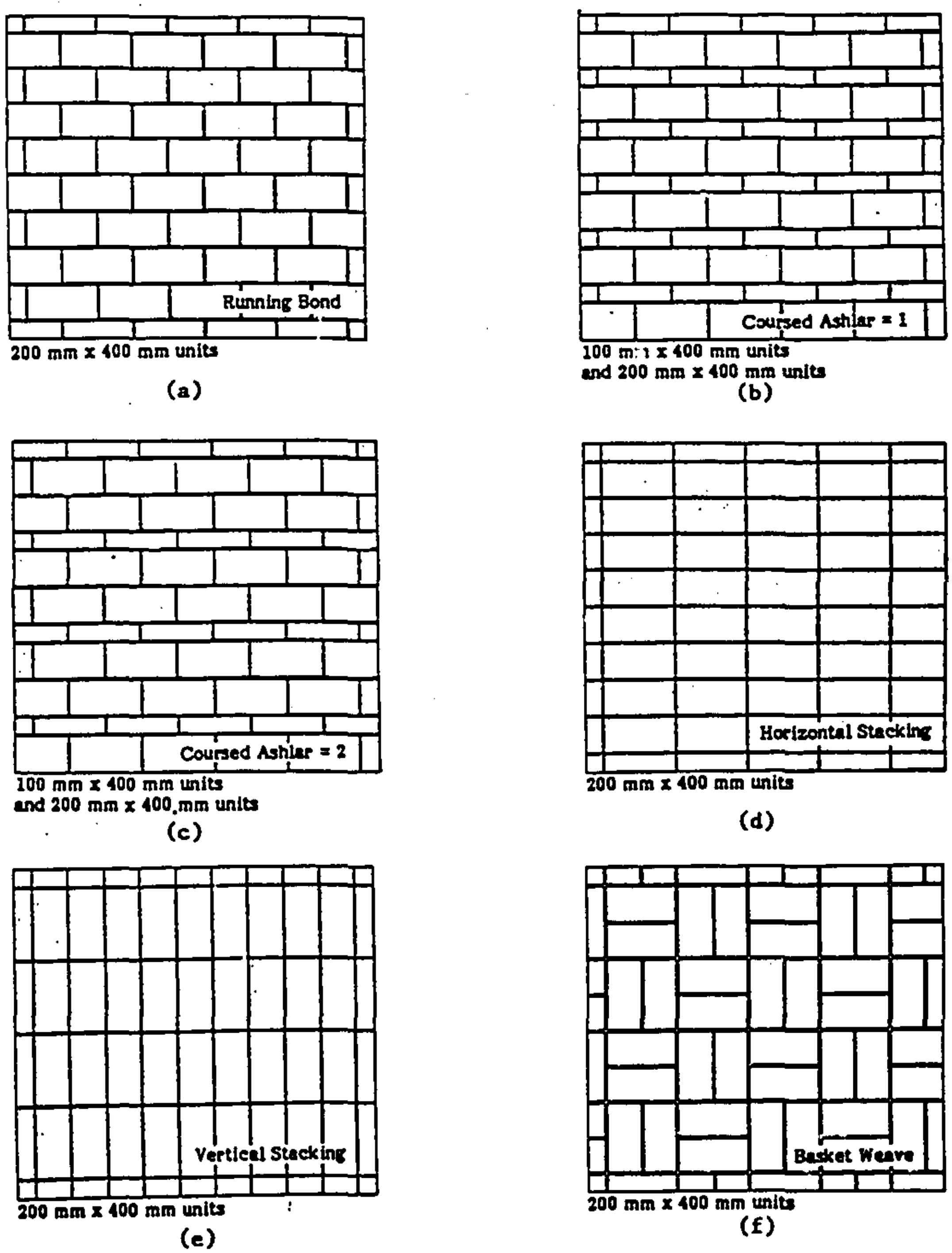

Figure 14.3: Concrete Blockwork Wall Patterns

only the face shells are "buttered". Full mortar bedding is used when laying the starter course of blockwork on a footing or foundation, when laying solid units, or for the webs on either side of grouted cores in partially grouted walls. For all other concrete masonry work with hollow units, it is common practice to use face-shell bedding only.

Horizontal Joint Reinforcement:

Horizontal joint reinforcement laid in the bed joints, as shown in Fig. 14.4, must be provided in walls primarily to control cracking associated with thermal or moisture expansions or contractions. It also serves, together with overlapping the blocks, as structural bonding in single-wythe concrete masonry walls. For non-loadbearing walls, these are usually placed in alternate courses. It should be noted that the horizontal joint reinforcement just described is not considered as reinforcement against imposed forces (see the definition of plain masonry, Section 14.1.1).

Gaps:

Infill panels which are not expected to contribute to the strength and stiffness of the frame, that is, they serve as non- loadbearing interior partitions, are normally isolated from the frame at the top by a gap of up to 25 mm. This avoids the beam above applying load to the infill, as the beam deflects due to loading or creep.

Lateral Support:

Masonry walls must be transversely supported or braced at certain intervals. Transverse support may be provided either by vertical or horizontal elements, or both. The anchorage between walls and supports should be designed to resist the assumed wind, earthquake or blast forces acting either inward or outward. Typical connections at vertical and horizontal supports for non- loadbearing walls are shown in Figs. 14.5 and 14.6, respectively. The flexible ties in Fig. 14.5 also allow for in-plane differential movement between the wall and the frame elements which may be caused by temperature changes, or by loading in the frame.

14.2.3 Some Properties of Concrete Masonry Walls

Compressive Strength:

One of the most important and basic properties used in the design of engineered concrete masonry construction is, the 28-day ultimate compressive strength of concrete masonry, f'_m. A number of factors affect the compressive strength of concrete masonry walls: compressive strength of individual units, eccentricity of vertical load, slenderness of the wall, mortar bedding, workmanship, mortar strength and reinforcing. Results of structural testing seem

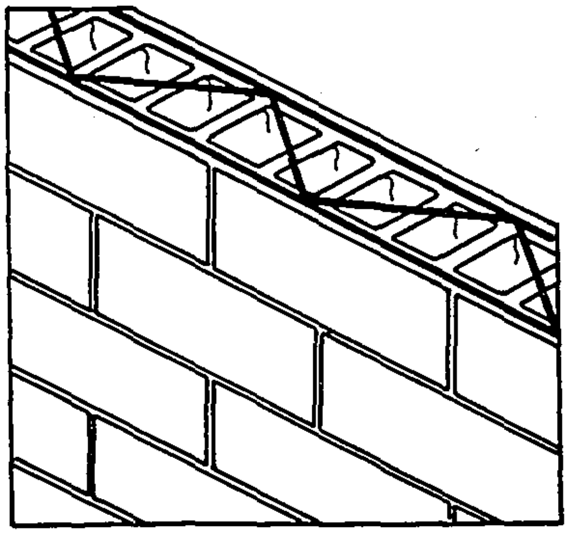

(a) Horizontal Joint Reinforcement
laid in Bed Joints

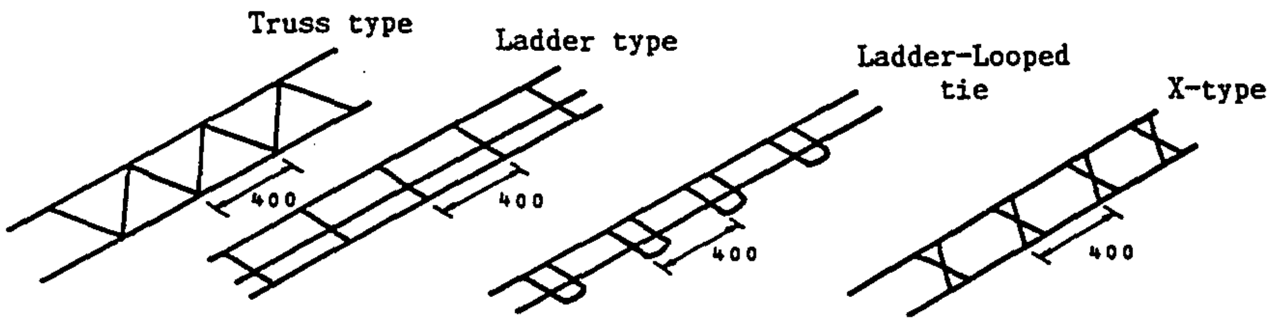

(b) Various Types of Joint Reinforcement

Figure 14.4: Horizontal Joint Reinforcement

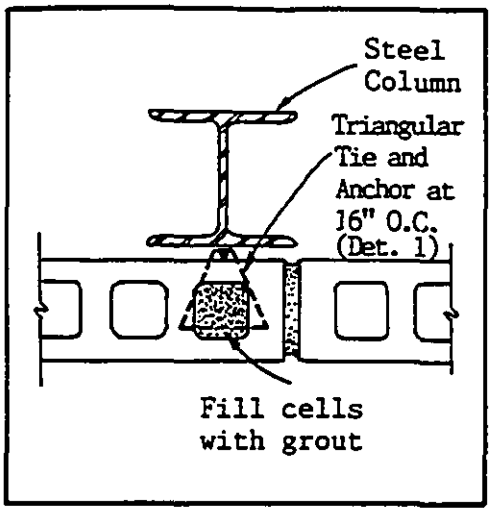

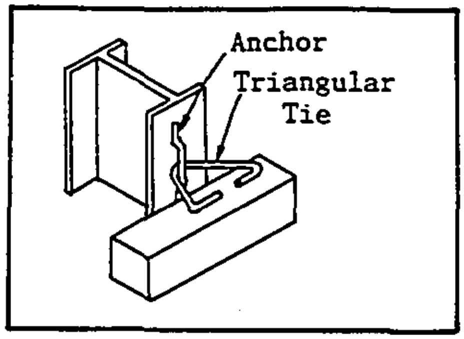

Detail 1

(a) Connection to Steel Column

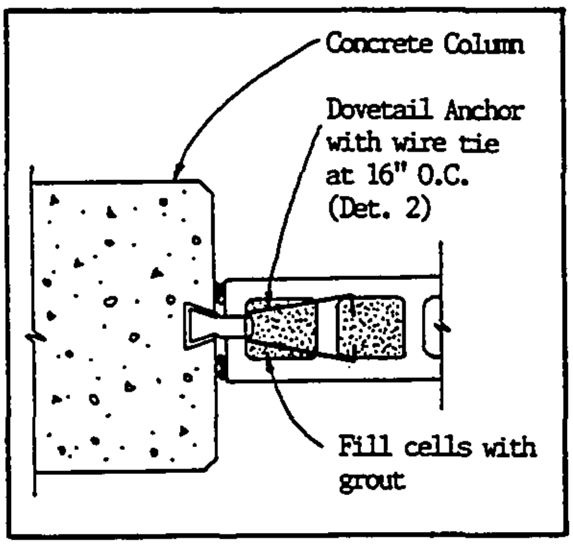

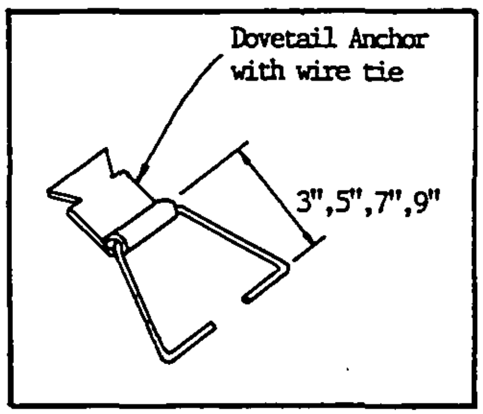

Detail 2

(b) Connection to Concrete Column

Figure 14.5: Details of Some Typical Connections at Vertical Supports

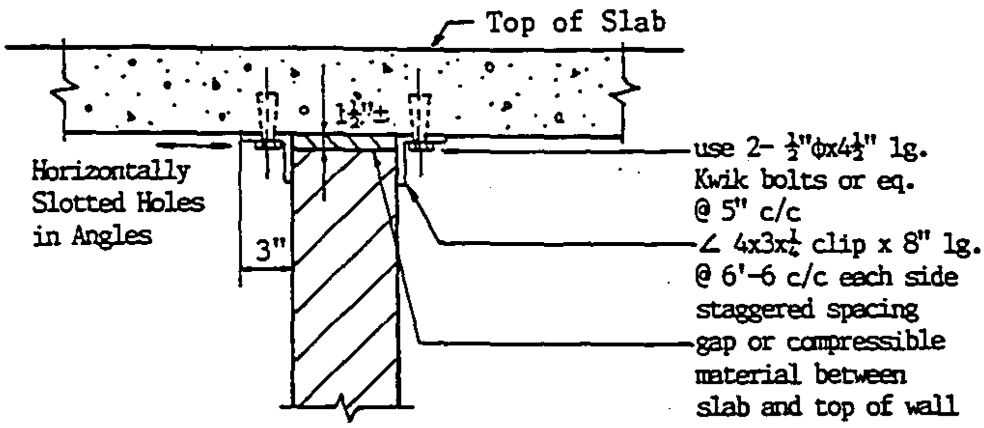

(a) Connection to Concrete Slab

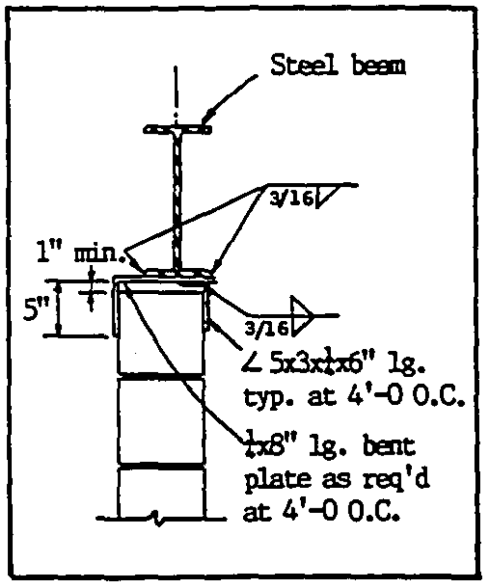

(b) Connection to Steel Beam

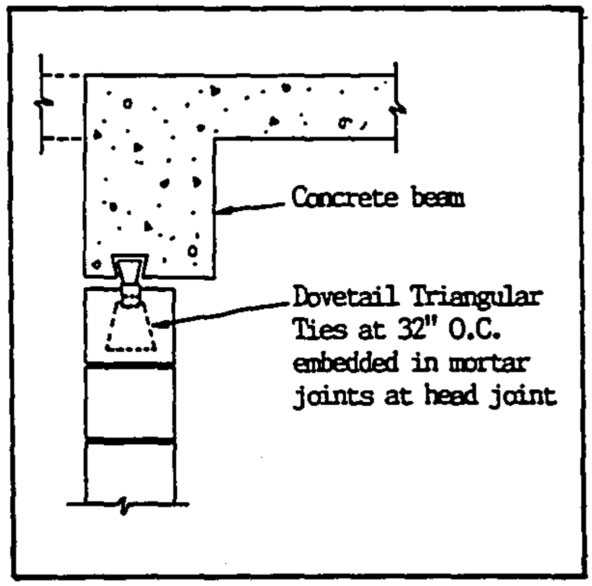

(c) Connection to Concrete Beam

Figure 14.6: Details of Some Typical Connections at Horizontal Supports

to indicate that the compressive strength of the unit is the most important variable for a given situation. The strength of a bearing wall that is fixed at the bottom and supported at the top is not affected by the slenderness up to and beyond the limits set by design criteria. Full mortar bedding will increase the strength of a wall by only 10 to 20 percent over face-shell bedding. The mortar strength has very little influence on the compressive strength of the wall, especially with the stronger mortars such as types M, S, and N.

The value of the compressive strength, f'_m, to be used in the design of masonry constructed with solid or hollow concrete blocks, or hollow concrete blocks filled with grout, having a compressive strength at least equal to that of the block, must conform to Table 2 of the Canadian Standard on "Masonry Design for Buildings" (1984), which is reproduced in Table 17.1 of this thesis.

Modulus of Elasticity:

The modulus of elasticity, which represents the stiffness of the masonry, is an important factor in the analysis and design of composite masonry structures. It is a vital factor in affecting the load distribution between the various structural elements. It is usual to express the modulus of elasticity as a function of the masonry compressive strength, f'_m. For plain and reinforced concrete block masonry, current North American codes specify a value of the modulus of elasticity equal to 1000 f'_m, but not greater than 20000 MPa.

CHAPTER 15

ANALYSIS OF A SINGLE-STOREY INFILLED FRAME WITH A GAP AT THE TOP

In this chapter, a method of analysing an infilled frame is proposed. To perform a detailed finite element analysis of an infilled frame, with a gap between the top of the infill and the frame, a mathematical model representing with reasonable accuracy the frame, the infill, and the interface properties, was required. The effect of the following modelling techniques on the calculated stiffness response of the infilled frame were investigated and will be described in this chapter. These include: the finite element mesh for the infill, the type of element for the frame members, and the weight of the infill. As a result, a single-storey module representing a typical storey of a multi-storey moment-resisting frame, and simulating the effect of infills above and below was developed for a representative infilled frame. The description and purposes of a series of lateral load analyses of the infilled frame is also given.

15.1 Description of Program

The main obstacle to overcome in performing an 'accurate' elastic analysis of an infilled frame is that of allowing for the separation cracks which develop on the boundaries between the infill and frame. Because the tensile bond between the infill and the frame is usually weak and uncertain, cracks are assumed to form wherever there are tensile stresses across the infill-frame boundaries. In Chapter 13, a review of the various programs used previously for the detailed, elastic finite element analyses of infilled frames was presented. In general, in each of the methods of analysis, the infill was represented by rectangular elements, the frame members by the standard prismatic beam-column elements, and the interface by pin-jointed, zero-length, very rigid members. The interface elements maintained or broke physical contact between the infill and the frame. An iterative process was used to allow boundary joints to separate. Comparisons of analytical and experimental results, have shown that in general the computer programs developed gave a fair representation of the elastic behaviour of the infilled frames, even after boundary cracking, provided that a tight initial fit of the infills was achieved in the experimental tests.

In each of the methods presented in the literature, there were differing assumptions and variations from the general method of analysis described above. These will be briefly summarized here. Mallick and Severn (1967) assumed slip would occur along the boundaries remaining in contact, and shear forces equal to the product of the normal force and the coefficient of friction were applied to the infill only. The shear forces were not applied to the frame elements because these were assumed to be inextensible. Dawson's (1972) interface element was a non-friction, sliding connection between the infill and the frame. In addition, he introduced a gap element to account for a lack of tight fit between the wall and the frame. He also checked that the displacements of the nodes on the frame and the corresponding nodes on the wall were compatible. In the method presented by King and Pandey (1978), the interface between the frame and the infill was modelled using the friction element originally developed by Goodman et al. (1968) and modified by King and Chandrasekaran (1975). An initial lack of tight fit, gap formation, and slip at the interface between the frame and the infill were taken into account by a suitable selection and subsequent adjustment of the friction element properties. Yong (1984) represented the infill by 8-noded rectangular elements, and the interface by a normal stress element, as well as a friction element. The wall slipped when the shear force at the interface was greater than the friction force in the friction element. This program also allowed for the interface to reconnect when the infill overlapped with the frame. In Riddington's program (1974), the basic 4-node rectangular element was used to model both the infill and the frame. Two sets of nodes were generated in each interface and were connected by a linking matrix, which represented a short, very stiff member.

A listing of Riddington's program was available in his thesis (1974). The present author ran it on the McGill mainframe computer, but decided not to use it for this study due to its limited number of options. Options such as joint displacement constraints are required in this study, because a single-storey module, representing a typical storey of a moment-resisting frame structure, will be analysed similarly to the frame with cladding, in Part I of this thesis. Having the possibility of using SAP80 (1986), a commercial finite element program with many modelling options, it was decided to combine it with a post-processing program, developed by the Author, that would allow for the boundary joints to separate in an iterative process.

SAP80 (1986) has the advantage of being designed to run on a personal computer. The program has static and dynamic analyses options. Generation options are also available. Plotting capabilities exist for both the undeformed and deformed shapes of a structure. The finite element library consists of the three-dimensional frame element, a three-dimensional shell element, a two-dimensional asolid element, and a three-dimensional solid element. Various modelling options are available, such as the joint constraints option which enable the user to selectively equate displacements of global degrees of freedom, rigid beam-ends, and rigid floor diaphragm modelling.

The Author proposes the following method of analysis for infilled frames. Consider the simple mathematical model of the infilled frame with a gap at the top, shown in Fig. 15.1. A SAP80 input data file must be prepared for the problem. The infill is represented by 4-node quadrilateral membrane elements (shell element option), and the frame members by the standard prismatic beam-column elements. The frame members could have been modelled

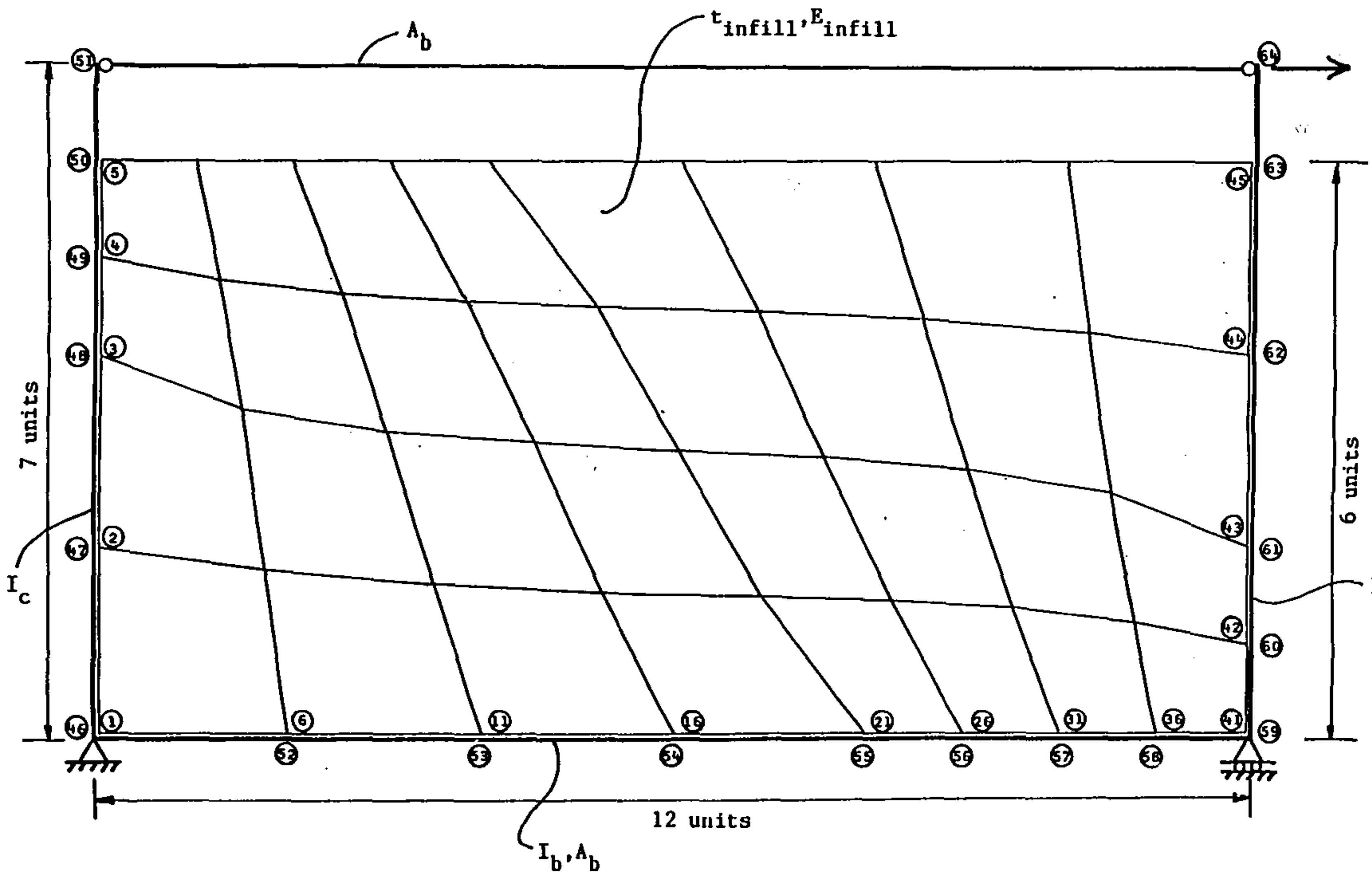

○ = Joint Numbers

Figure 15.1: Mathematical Model of a Simple Example Infilled Frame With a Gap at the Top

alternatively by any type of planar element offered in SAP80 (1986) provided the nodes along the frame are defined at locations corresponding to the nodes on the infill periphery. Initially all the nodes on the infill's boundary in contact with the frame are constrained to displace in the vertical and horizontal directions identically to the corresponding nodes of the frame. The structure is analysed for a lateral load, then the post-processing (or update) program developed by the Author is run. It creates a new SAP80 input file in which appropriate constraints on the infill-frame interface are removed when tensile stresses develop on the infill boundaries, and when shear forces exceed friction forces. The friction forces are taken as equal to the product of the coefficient of friction and the compressive normal forces. The structure is then reanalysed, and the process repeated until the constrained conditions are stable. The update program was also written to reconnect the boundaries if, in an iteration, the displacements of the infill overlap the frame, or if the shear forces become less than the friction forces. A flow-chart of the update program is shown in Fig. 15.2. By estimating the number of iterations required to solve a problem, a batch file could be prepared with the necessary commands that performed all the iterations automatically. It is interesting to note that in the development of this finite element analysis, although an iterative procedure is necessary to obtain the solution, the problem is in fact linear, since the displacements and the stresses are linearly related to the applied load.

The simple infill-frame model shown in Fig. 15.1 was one of several problems analysed to test the method of analysis proposed by the Author. The units used in the analysis do not have any physical significance. Fig. 15.3 shows the results through the various iterations before reaching a stable condition. The same result was obtained for the eleventh iteration, as for the sixth iteration. That is, the unique solution was not obtained, but a correct state of equilibrium must exist between the states of cycles 6 and 10. In Fig. 15.4, the deformed shape for cycle 8 is shown. The infill pushes against the frame at the top-left corner, and near the bottom-right corner. In this iteration the infill was allowed to slip at the bottom-right corner, because the shear force was greater than the friction force. Its displacement, however, was greater than that of the frame. Consequently the corner was reconnected in the next iteration.

There are two main reasons why the problem did not reach a unique equilibrium condition. Firstly, the mesh is discrete with the boundary represented by a finite number of nodes, rather than an infinite number. In all probability, for equilibrium, the end of a length of contact on a boundary does not coincide with one of the defined nodes. Secondly, there are many variables which must reach equilibrium concurrently, such as the lengths of contact and the slip conditions for each of the three boundaries. With so many variables, a slight change in condition at one node, will subsequently cause changes at other nodes in the next iteration. The more refined the mesh, the closer should the results approach the 'exact' solution.

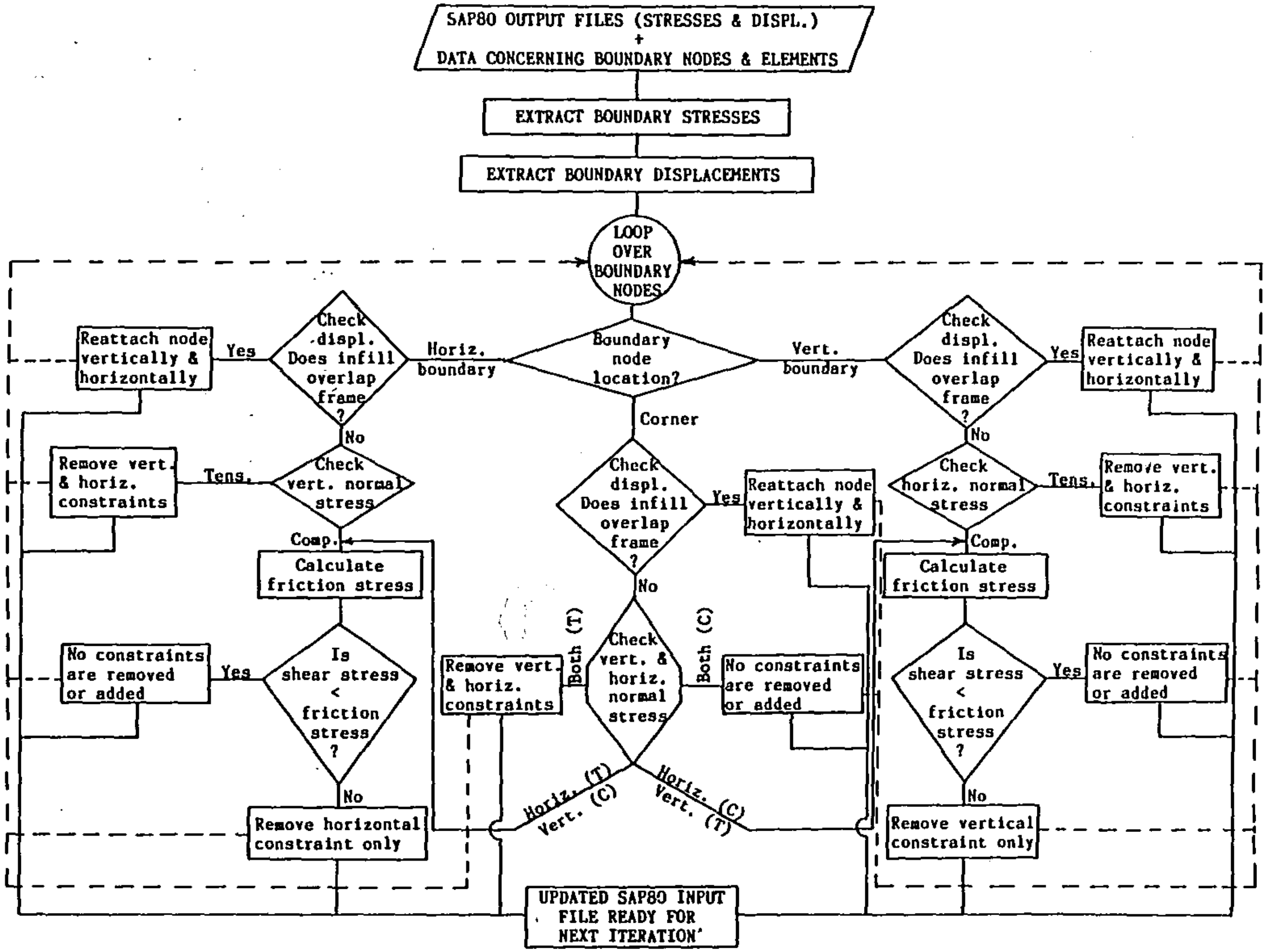

Figure 15.2: Flow Chart of the Update Program

Cycle 1 – Infill completely attached to frame: I.D. = $.1005\times10^{-4}$

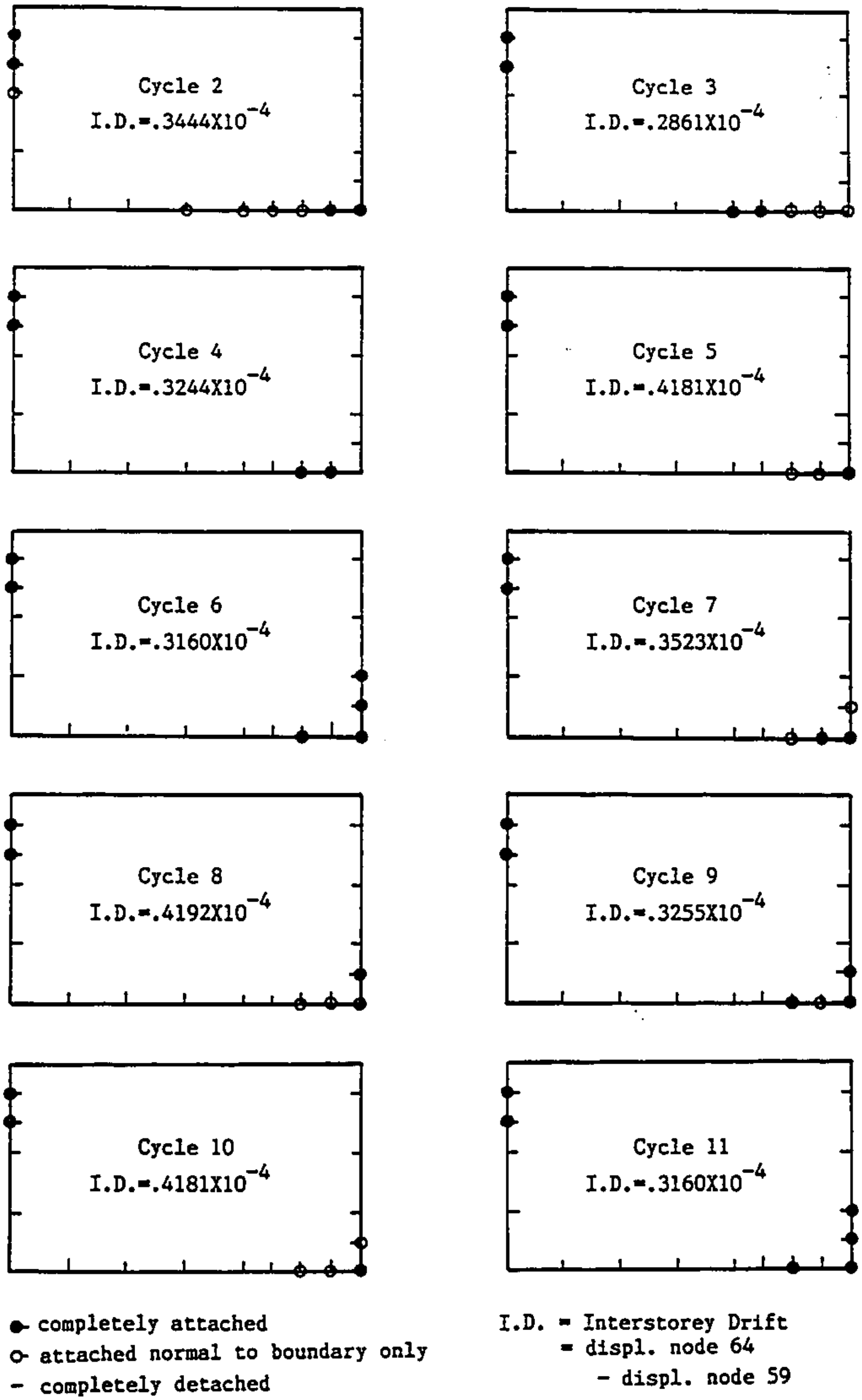

Figure 15.3: Analysis Results of the Simple Example Infilled Frame

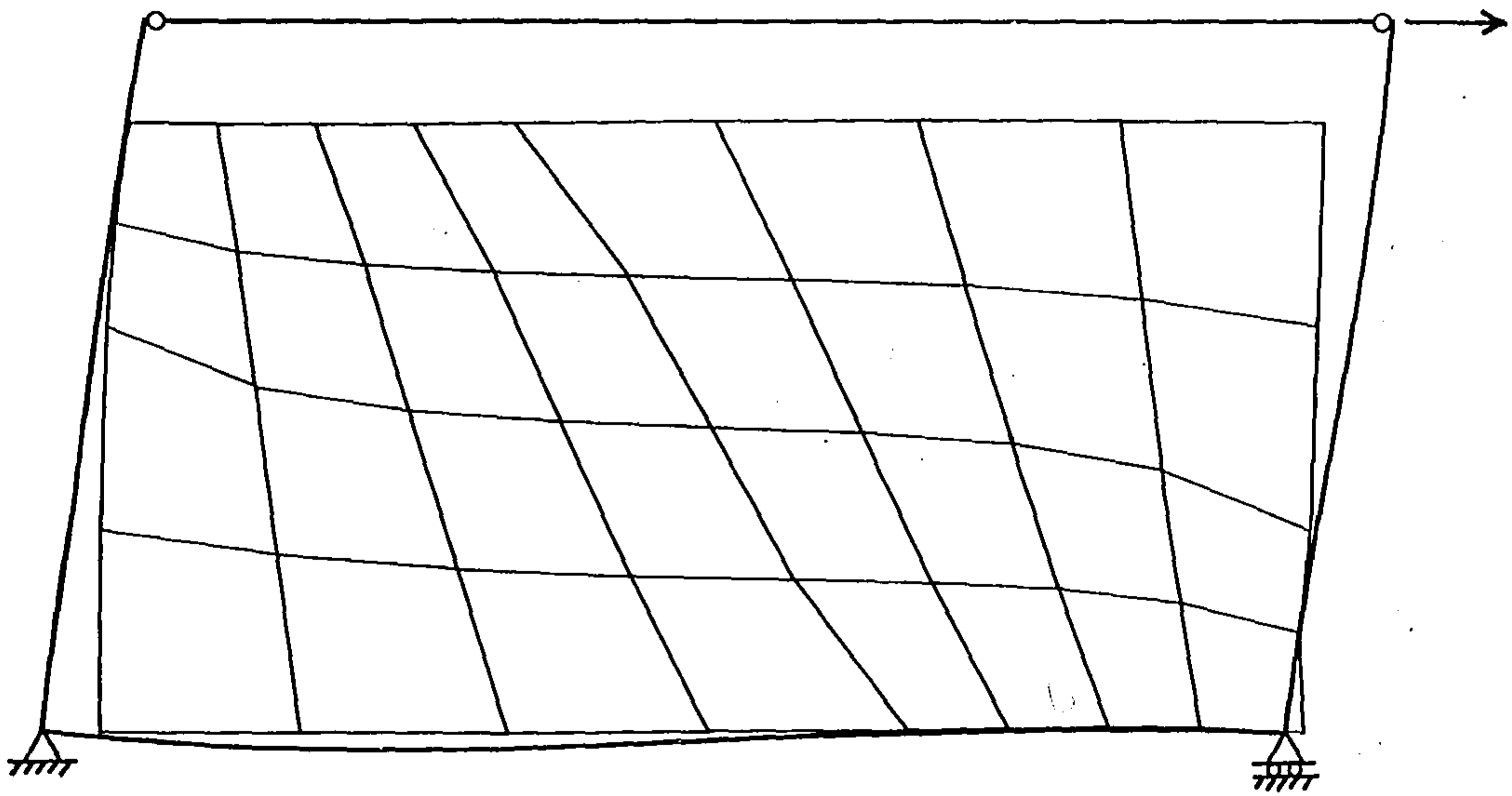

Figure 15.4: Deformed Shape for Cycle 8 of the Simple Example Infilled Frame

15.2 Modelling the Representative Infill

15.2.1 Description of the Representative Infilled Frame

The representative infill partition is of 200 X 200 X 400 mm 2- core concrete block units laid in running bond using type M mortar. All mortar joints are face shell mortar bedding. The wall is assumed to be built up against the vertical structural members with no attempt to integrate it with the frame or to prevent mortar bonding to the concrete members. Standard truss type joint reinforcement is usually placed in alternate courses.

The blockwork partition wall is 5500 mm wide by 2750 mm high, and it is built up to within 25 mm of the underside of the reinforced concrete structural frame, Fig. 15.5. The gap is usually filled with a compressible filler, which will allow the beam above to deflect without imposing vertical loads on the infill below. The filler also acts as a fire and acoustic barrier. Normally, lateral support in the form of staggered angles, as described in Chapter 14, are provided at the top of the wall to prevent it from falling out of its plane during very high wind and seismic loadings. The reinforced concrete frame consists of 300 X 450 mm columns and 300 X 600 mm beams.

15.2.2 Modelling the Infill

To perform the lateral load analyses, a two-dimensional plane stress element model was required to represent the infill. The grading of the finite element mesh was selected to obtain a refined, but efficient, representation of the infill's behaviour.

Stafford Smith (1966) showed that when a fully infilled frame, without gaps, is subjected to a racking load, the frame and infill separate over a large part of the length of each side, and regions of contact remain only adjacent to the corners at the ends of the compression diagonal, Fig. 13.1. A similar type of behaviour was expected for the infill with the gap at the top. Also, it was concluded in Section 15.1 that for the infilled frame analysis to approach the 'exact' solution, a more refined mesh would be required around the contact endpoints. Therefore, to properly model the infill's behaviour, and at the same time obtain a solution efficiently, a finite element mesh with the compression corners having a greater refinement was decided upon.

In Fig. 15.6, four possible mesh grading patterns are presented. It is assumed that the concrete block infill is of a reasonable homogeneous and isotropic material. In Fig. 15.6a, a mesh *using* rectangular elements only, which was also adopted in Riddington's studies (1974, 1977, 1984), is shown. The mesh is refined at the compressive corners as required, but there is an unnecessary refinement in the tension corners. Some of the elements have aspect ratios greater than 2:1, which is usually not desirable in an analysis; however, in this problem these do not occur in critical areas.

The Author developed the mesh grading patterns shown in Figs. 15.6b, c and d. In Fig. 15.6b, the techniques for mesh refinement suggested by Irons and Ahmad (1980), in which triangular shaped elements are avoided, were followed to refine the compression corners

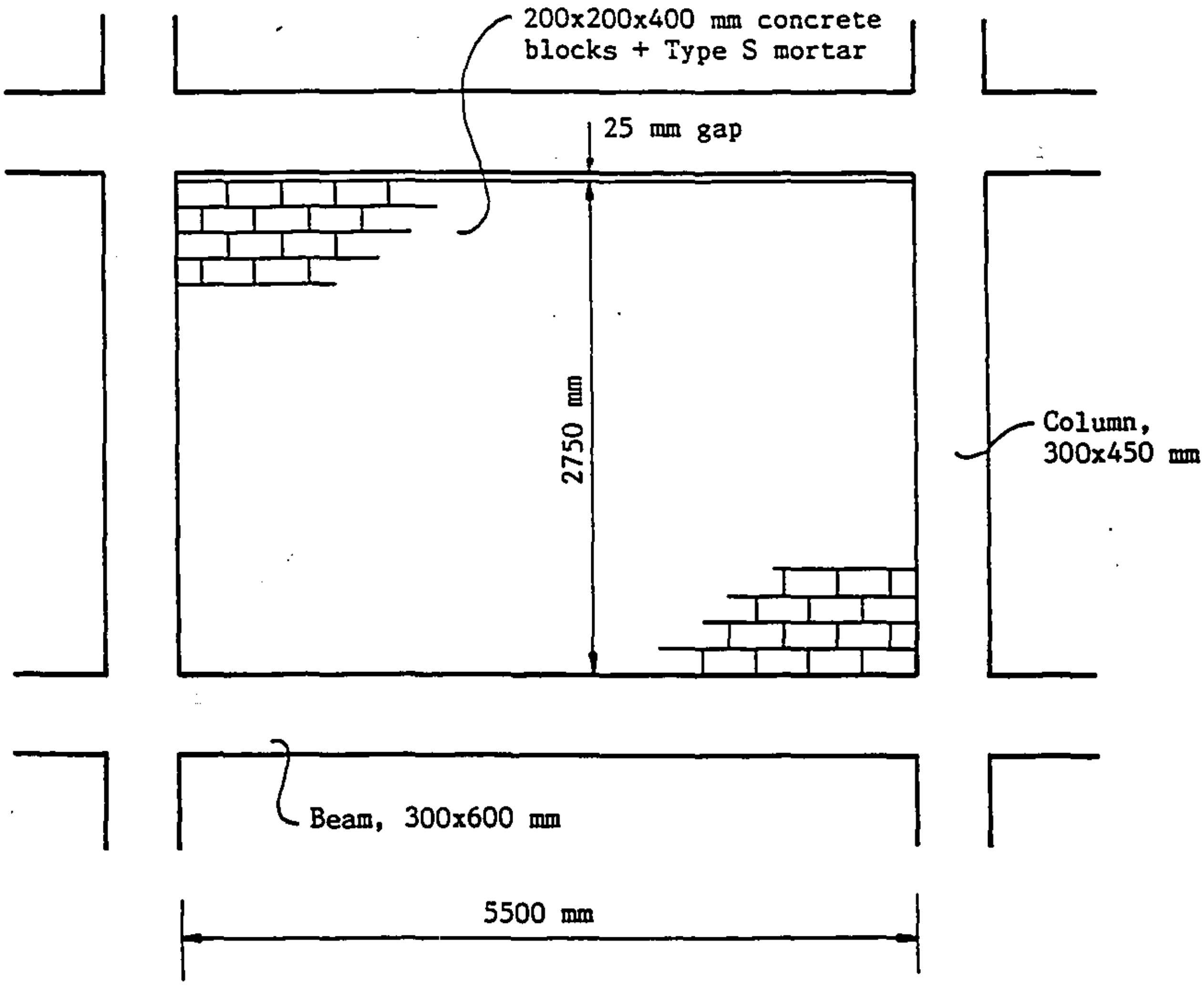

Figure 15.5: Representative Infilled Frame

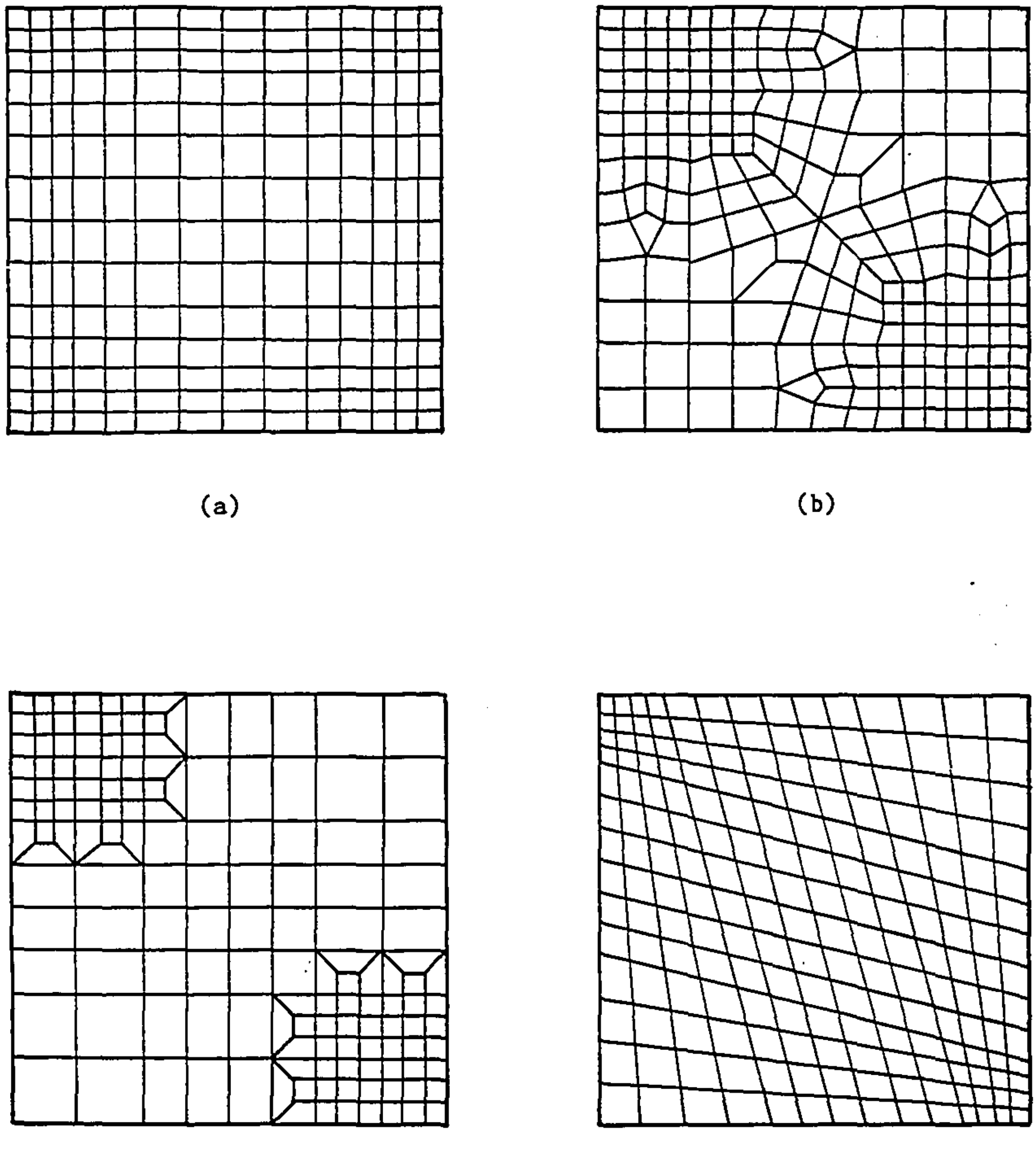

Figure 15.6: Various Mesh Grading Patterns

without needlessly refining the tension corners. Also, the guideline that, for accuracy, the quadrilateral elements should be as nearly as possible parallelograms, with equal sides (Irons and Ahmad 1980) was followed. The mesh shown in Fig. 15.6b was easy to develop for the square infill, however it would be more difficult to devise such a mesh for a rectangular infill. While the mesh grading pattern in Fig. 15.6c could be more easily adapted to a rectangular infill, the transition from an element that is one unit square, to one that is three units by two units, is not as gradual as desirable. On the other hand, the pattern shown in Fig. 15.6d, provides a gradual transition from the refined compressive corners to the coarse tensile corners. The pattern can easily be used for both square and rectangular infills. Furthermore, the mesh can easily be generated by defining the joints along the periphery and using SAP80's Lagrangian joint generation option for all the interior joints. Of all the patterns presented, the pattern in Fig. 15.6d was the best suited for the present study.

Once the mesh grading pattern had been chosen, the degree to which the mesh should be refined for the representative infill had to be decided. To do so, a lateral load analysis of the representative infilled frame which was described in Fig. 15.5 was performed.

The infill was represented by a mesh of 364 membrane plane stress elements, Fig. 15.7. The thickness and modulus of elasticity assigned to the elements was that of the concrete blockwork wall, that is, 200 mm and 10 kN/mm^2, respectively. The frame model consisted of a series of beam elements at each side of the infill, and a series of beam elements at the bottom of the infill, whose joint locations corresponded to those along the infill periphery. The beam elements were assigned the full flexural inertia and axial area of the storey beam, that is, $5.4X10^9$ mm^4 and 180000 mm^2, respectively. The column elements were assigned the full actual flexural inertia, that is, $2.278X10^9$ mm^4. To neglect axial deformations in the columns, the column elements were assigned very large sectional areas. At the top, a link with an axial area equal to that of the storey beam joined the tops of the columns. The frame members were assigned a modulus of elasticity of 20 kN/mm^2. The structure was supported by a pin at the bottom-left corner, and a roller at the bottom-right corner. The horizontal load was applied at the top-right corner. The interstorey drift was calculated as the difference between the displacements of the top-right corner and the bottom-right corner. The frame deformations contributing to this drift are the shear and bending of two full-length full-stiffness columns, and the axial, shear, and bending deformations of one full-sized beam. The infill deformation contributing to this same drift is the shear of one infill. By applying the rotational constraints to opposite ends of the columns of this model, in a similar way to that for the panel-clad frame model, a typical storey of a multi-storey infilled frame was represented by the single-storey module.

The structure, Fig. 15.7, was analysed for a 130 kN lateral load. This is the approximate lateral load to cause an approximate interstorey drift index of 1:400 for the bare frame. A more complete explanation of the magnitude of the lateral load is given later in this chapter. At the 32^{nd} iteration the results obtained were the same as for the 17^{th} iteration. That is, a unique solution was not obtained, and equilibrium must exist at some intermediate position between cycles 17 to 32. The interstorey drifts obtained for the most flexible and most rigid cycles, within the 17^{th} and 32^{nd} iterations were 1.4525 mm and 0.9740 mm, respectively.

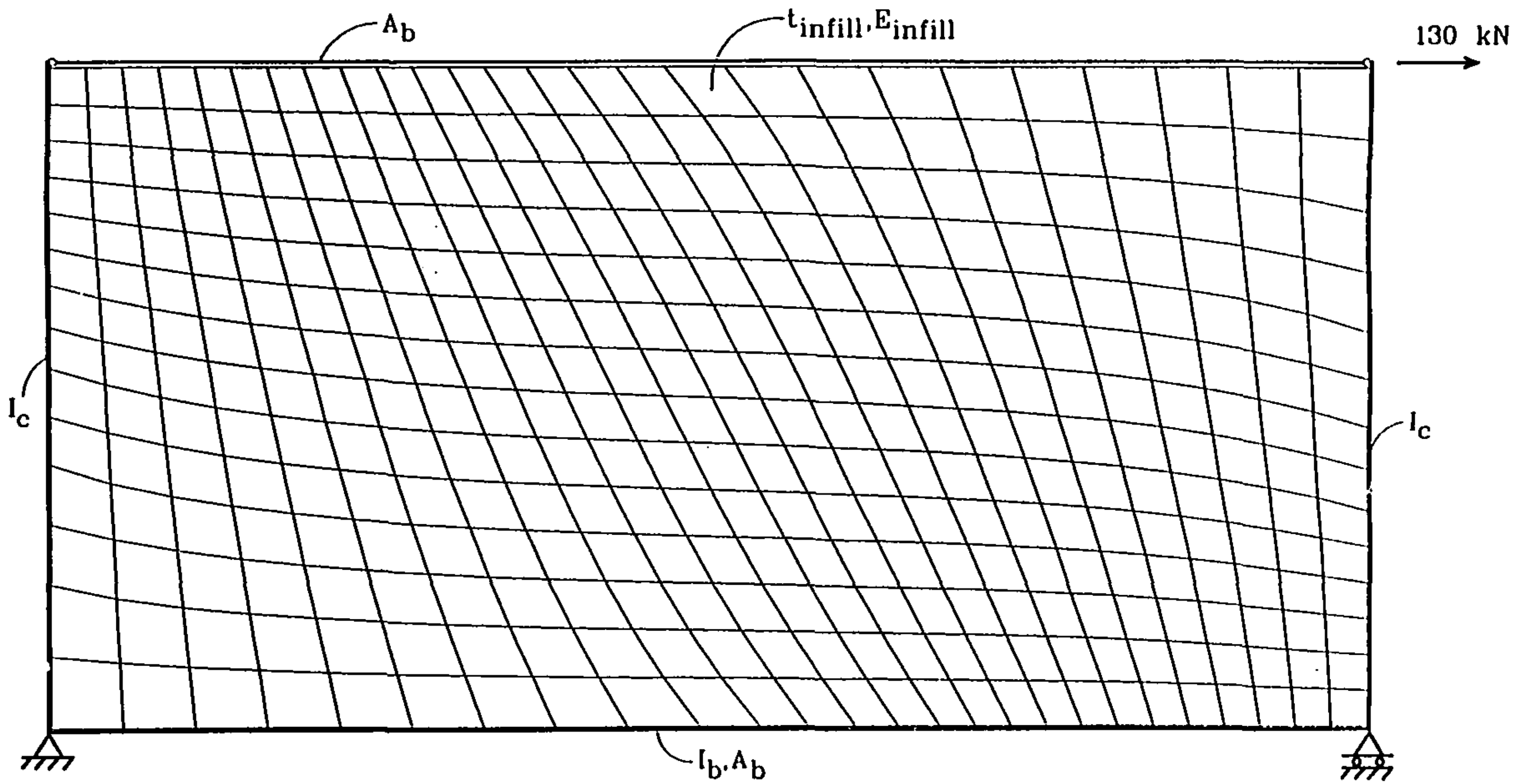

Figure 15.7: Mathematical Model of the Representative Infilled Frame Using a Coarse Mesh

Because of the large number of iterations required to reach a stable condition, and the large difference between the drifts of the most flexible and most rigid cycles, a more refined mesh was devised.

In the more refined model, the infill was represented by a mesh of 684 elements, Fig. 15.8. This structure was also analysed for a lateral load of 130 kN. In this case, identical results were obtained at the 15^{th} and 11^{th} iterations. The interstorey drifts for the most flexible and most rigid cycles, within cycles 11 to 15, were 1.4239 mm and 1.0646 mm, respectively. By refining the mesh, the number of iterations was reduced by half, and the difference between the results of the most flexible and most rigid cycles, within the repeating cycle of iterations, reduced significantly. As expected, the results obtained for the refined mesh analysis lie within the range of those obtained from the coarse mesh analysis. The time required to perform the 15 iterations was acceptable for practical purposes; therefore further refinement was not warranted due to the generalized nature of this study.

15.3 Effect of Different Modelling Techniques for the Moment-Resisting Frame

Three different techniques to model the moment-resisting frame were tested.

In the first case, the frame members were modelled by the conventional line elements, Fig. 15.8, Section 15.2. In so doing, the effect of the column widths and the beam depths were not accounted for. Therefore, the infill forces along the contact lengths were acting at the centrelines of the model members, rather than being offset by half the width of the column or half the depth of the beam, as in the real structure. In addition, the effective moment on the structure was reduced because the storey height and the bay width of the model were less than the actual.

In the second technique, the frame members were represented by a wide-column analogous frame, Fig. 15.9. For this the column was represented by a line element located at its centroidal axis, and assigned to have the flexural inertia of the column. Rigid arms attached perpendicularly to the column and extending to its external fibres were located at the levels of contact between the column and the infill. The beam was modelled in the same way.

In the third technique of modelling the frame, the frame members were modelled using conventional plane stress rectangular or quadrilateral elements, Fig. 15.10. In this technique, the elements were typically assigned thicknesses and a modulus of elasticity equal to those of the actual members, while the sixteen elements at each of the bottom corners were assigned a very high modulus of elasticity to simulate a rigid joint. To provide a representation of the effects of the storeys above and below on each of the considered structures, the top and bottom of the left column, and separately, the top and bottom of the right column, were constrained to rotate identically. For this technique it was additionally necessary to insert rigid arms across the tops of the columns, and at the ends of the columns and beam, Fig. 15.10, to maintain the same rotation across the column widths and beam depth at these locations.

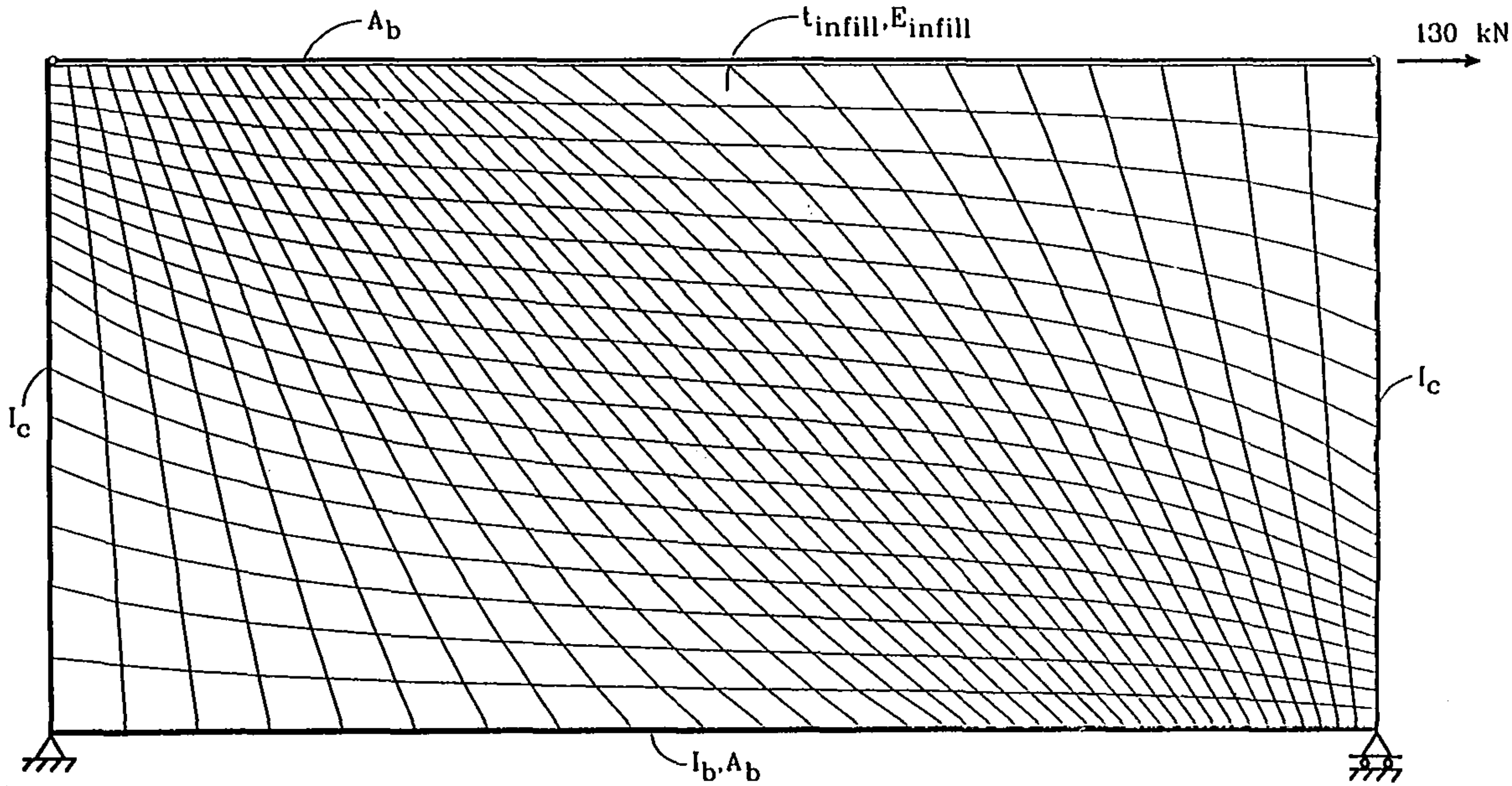

Figure 15.8: Mathematical Model of the Representative Infilled Frame Using a Refined Mesh

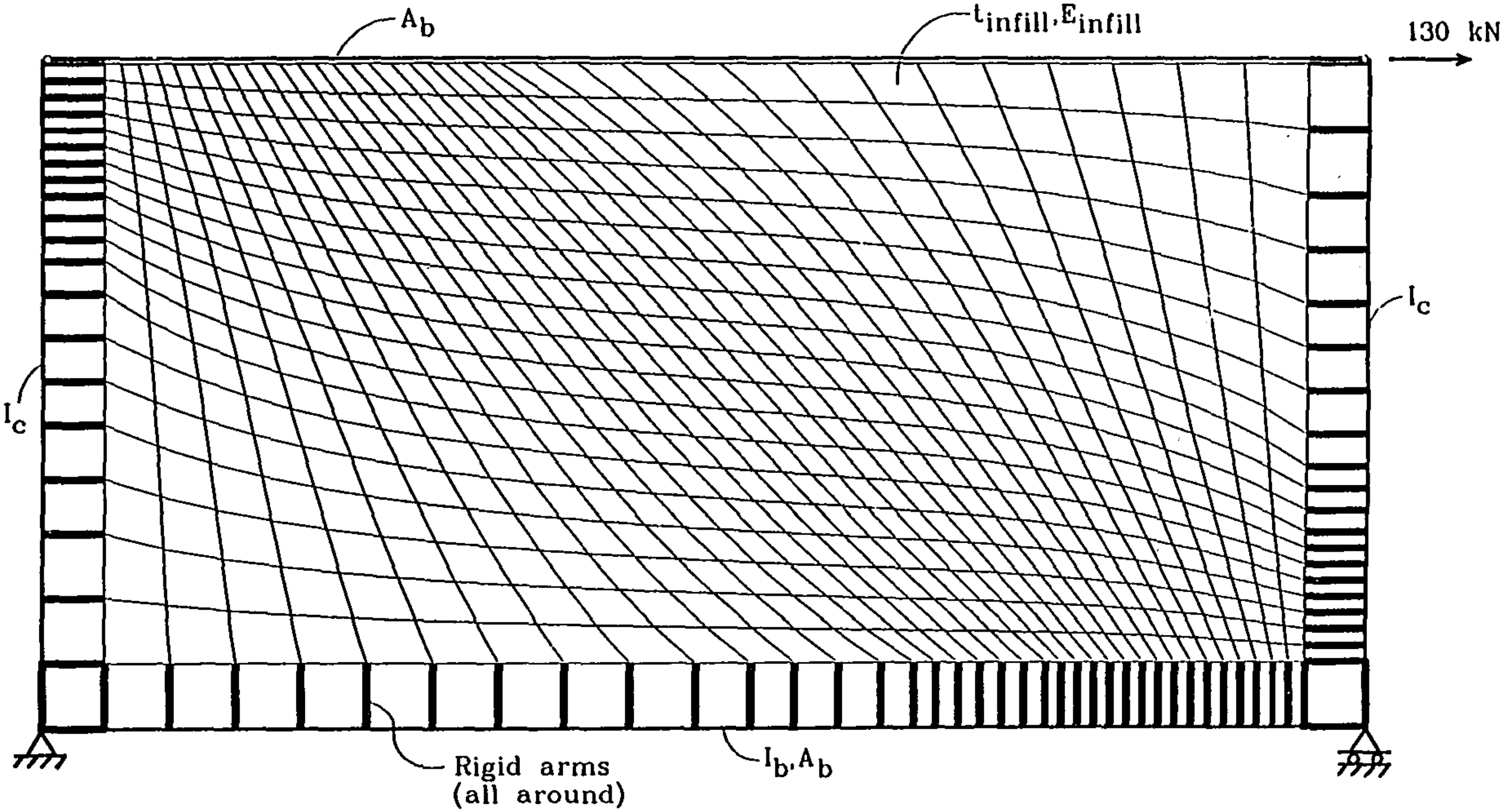

Figure 15.9: Mathematical Model of the Representative Infilled Frame Using a Wide-Column Analogous Frame for the Frame Members

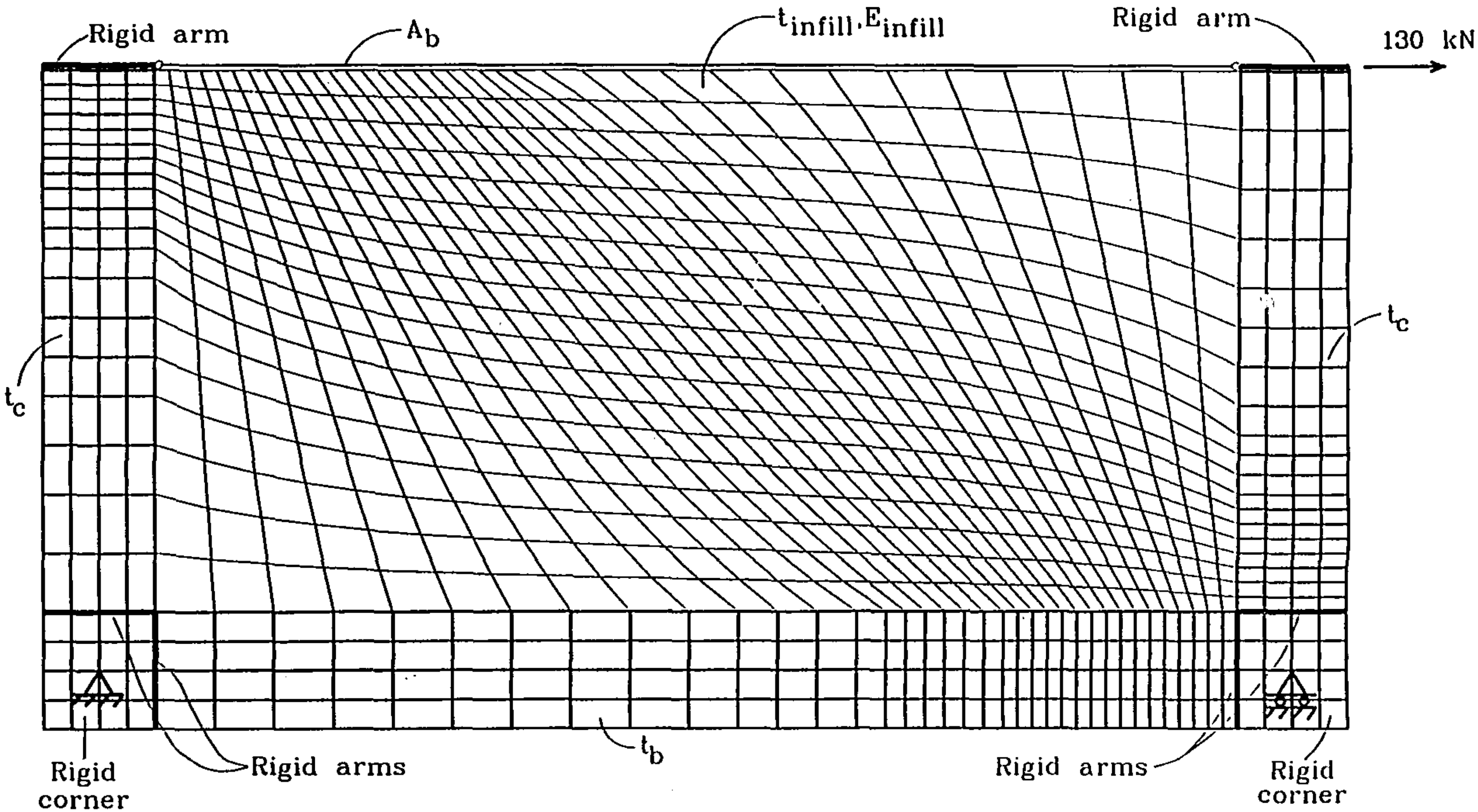

Figure 15.10: Mathematical Model of the Representative Infilled Frame Using Rectangular Plane Stress Elements for the Frame Members

All three models were analysed for a racking load of 130 kN. In the first model, in which the frame members were modelled as line elements, the analysis produced identical results at four-cycle intervals. The most flexible of these was cycle 14 with an interstorey drift of 1.4239 mm, and the stiffest was cycle 11 with an interstorey drift of 1.0646 mm, as reported in Section 15.2. For the wide-column and membrane element analyses, thirty iterations were performed and in neither case was equilibrium reached or did any of the cycles repeat themselves. The reasons for this are uncertain, but it may be that in the case of the full-width columns and full-depth beam, the longitudinal deformations of the columns and the beam are more sensitive to the stresses in the infill; therefore making it difficult to achieve compatibility between the displacements of the frame-members with those of the infill. Nevertheless, a standard of comparison between the three methods was required; therefore, the most flexible iteration was chosen. The reason for choosing the most flexible cycle for comparison is that, in terms of stiffness, the results are conservative. Neglecting the results of the first few cycles in each case, which are greatly affected by the initial condition of complete attachment, the interstorey drifts for the most flexible cycles, that is cycle 13 in the case of the wide-column analysis, and cycle 27 for the membrane element analysis, were 1.2421 mm and 1.7215 mm, respectively. The deflected shapes showing the contact regions between the infill and the frame are presented for the line element, wide-column, and membrane element models in Figs. 15.11, 15.12, and 15.13, respectively.

Table 15.1 provides comparisons between the three analyses for the interstorey drifts, contact lengths, stiffnesses, loading, member forces, and stresses. The contact lengths were smaller for the membrane element analysis than for the other analyses, and the effective loading acting on this model was greater than for the line element analysis due to the effective increase in storey height; therefore, the membrane element model was more flexible than the other two models. As a result, the moments in the frame members of the membrane element analysis were greater than those of the line element analysis. The moments in the frame members of the wide-column analysis were less than those of the line element analysis, because the wide-column model was not as flexible as the line element model. It should be noted that for the membrane element analysis, the moments obtained for the frame members were not very accurate, because of inaccuracies in the analysed stresses due to some of the elements' large aspect ratios and to the abrupt transition regions at the ends of the columns. To maintain the refined mesh in the compressive corners of the infill, more extensive transition regions would be required in the frame members. It was also found that in regions well away from the load injection points, the stresses in the infill were not significantly affected by differences in modelling the frame members.

Although the line element analysis was not conservative with respect to the other analyses for all the response quantities, it was the most suitable technique for modelling the frame because of its simplicity, and, more importantly, because the analysis stabilized around a few cycles. It is estimated that the other analyses would require much more carefully refined models to achieve a similar efficiency.

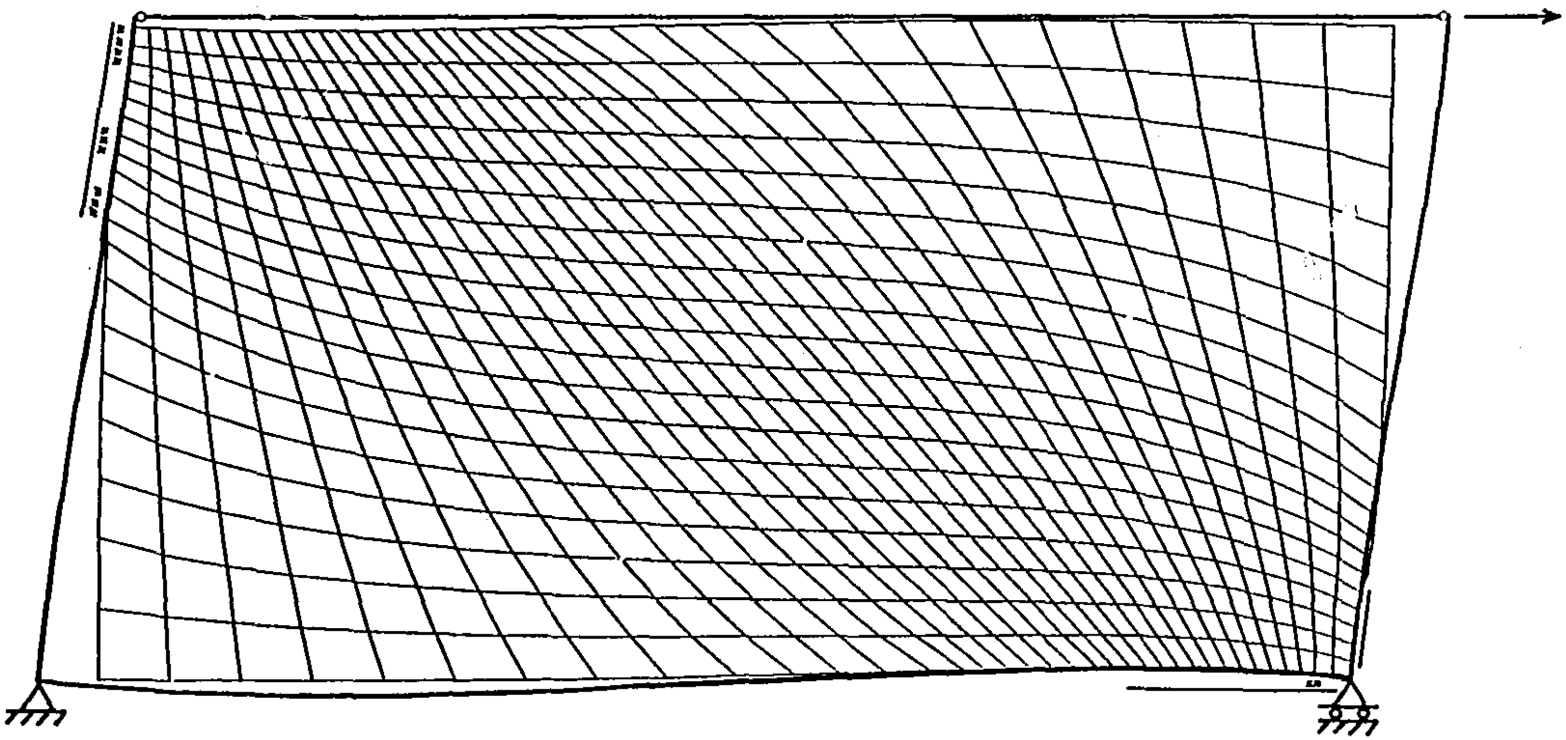

——— connection in normal direction
xxxxxxx connection in tangent direction

Figure 15.11: Deflected Shape for Model Using Line Element Representation of Frame Members

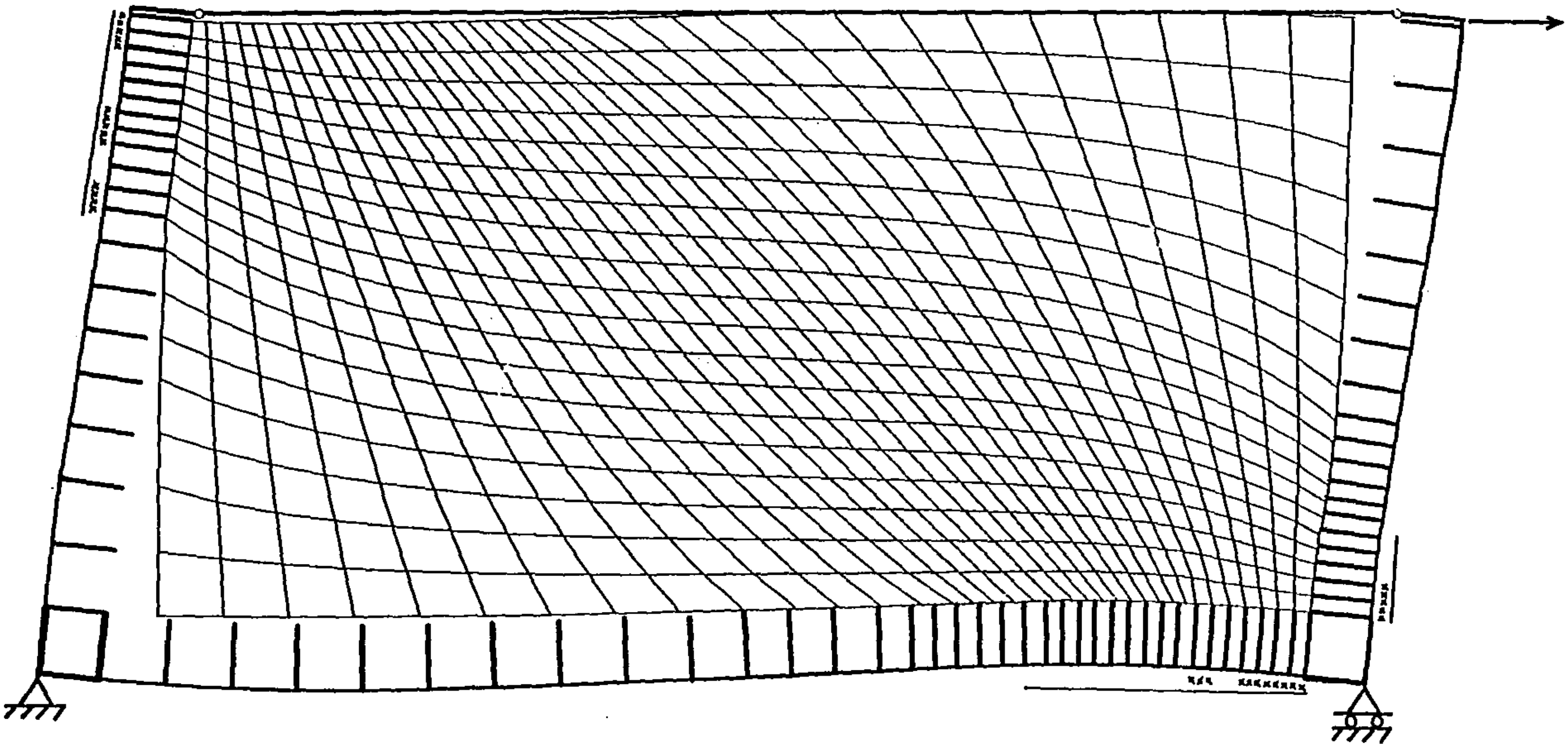

Figure 15.12: Deflected Shape for Model Using Wide-Column Representation of Frame Members

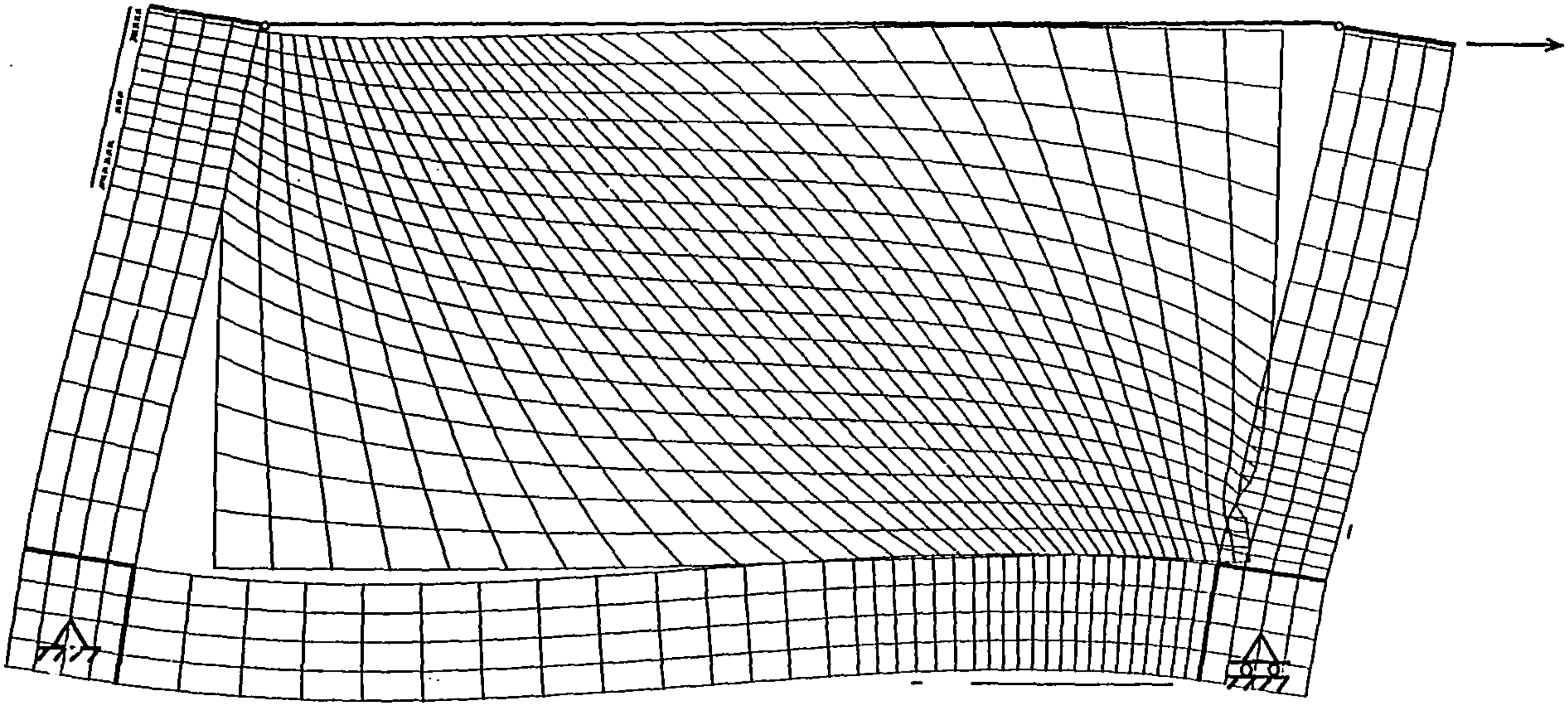

——— connection in normal direction
xxxxxxx connection in tangent direction

Figure 15.13: Deflected Shape for Model Using Membrane Element Representation of Frame Members

RESULTS FOR MOST FLEXIBLE CYCLE	TYPE OF MODEL		
	LINE	WIDE-COLUMN	MEMBRANE
Interstorey drift	1.42 mm	1.24 mm	1.72 mm
Deviation from line element model	—	-13%	+21%
Contact lengths (wrt line element model)	—	greater	less
Stiffness (wrt line element model)	uncons. & cons.	greater	less
Effective loading (wrt line element model)	uncons.	greater	greater
Moments in frame members (wrt line element model)	cons. & uncons.	less	greater
Shear stresses (wrt line element model)	no diff.	similar	similar
Corner compressive stresses (wrt line element model)	uncons.	slightly less	similar
No. of iterations to reach equilibrium	equilibrium exists bet. iterations 11 & 14	no definite equilibrium point or region	no definite equilibrium point or region

wrt: with respect to
uncons.: unconservative wrt other analyses
cons.: conservative wrt other analyses

Table 15.1: Comparison Between Results of Line Element, Wide-Column and Membrane Element Models

15.4 Effect of Including Weight of Infill in Mathematical Model

Before proceeding with the series of lateral load analyses of the infilled frame, the effect of the weight of the wall on the horizontal stiffness of the infilled frame was investigated. The effects of combined vertical and horizontal loading are dependent on the magnitude of the weight of the wall relative to that of the lateral load. Therefore, realistic working loads were used in the combined loading analysis to make a valid comparison.

The weight of the representative infill was obtained from the local manufacturer's specifications, Chapter 14. The weight was given as 172.5 kg/m^2 based on an equivalent thickness of 106 mm. Although in the lateral load analysis the thickness of the infill is taken as the sum of the two face shell thicknesses, that is 60 mm, to obtain the actual axial stresses in the blocks' face shells, the following weight based on the equivalent thickness was used for the infill in the analysis

$$\frac{172.5\ kg/m^2}{0.106\ m} = 1627.4\ kg/m^3 \ \text{ or } \ 16\ kN/m^3 \tag{15.1}$$

The magnitude of the horizontal load has been selected very conservatively so that the interstorey drift of the frame alone does not exceed the interstorey drift index of 1:400. Based on the shear stiffness of the bare frame

$$GA = \frac{Qh}{\delta} = \frac{12E}{h\left[\frac{1}{G} + \frac{1}{C}\right]} \tag{15.2}$$

where Q = horizontal shear,
h = storey height,
δ = interstorey drift,
E = modulus of elasticity,
G = $\sum \frac{I_G}{\ell}$ for which the summation includes all the girders (of length ℓ) in the storey, and
C = $\sum \frac{I_C}{h}$ for which the summation is carried out over all columns in the storey.

A value of 130 kN was determined as the value of the lateral load.

The infilled frame, with the refined mesh as presented in Section 15.2, was analysed for a combined vertical and horizontal load, Fig. 15.14. The results of the combined load analysis were compared with those of the lateral load only analysis. For the combined load analysis, identical results were obtained at the 13^{th} and 9^{th} iterations. Within the repeating cycle of iterations, the interstorey drift for the most rigid cycle was 0.9431 mm, and for the most flexible cycle, 1.3821 mm. For the lateral load only case, the analysis produced identical results at four-cycle intervals, Sections 15.2 and 15.3. Within the repeating cycle of iterations, the infilled frame subjected to vertical and horizontal loading was stiffer, by

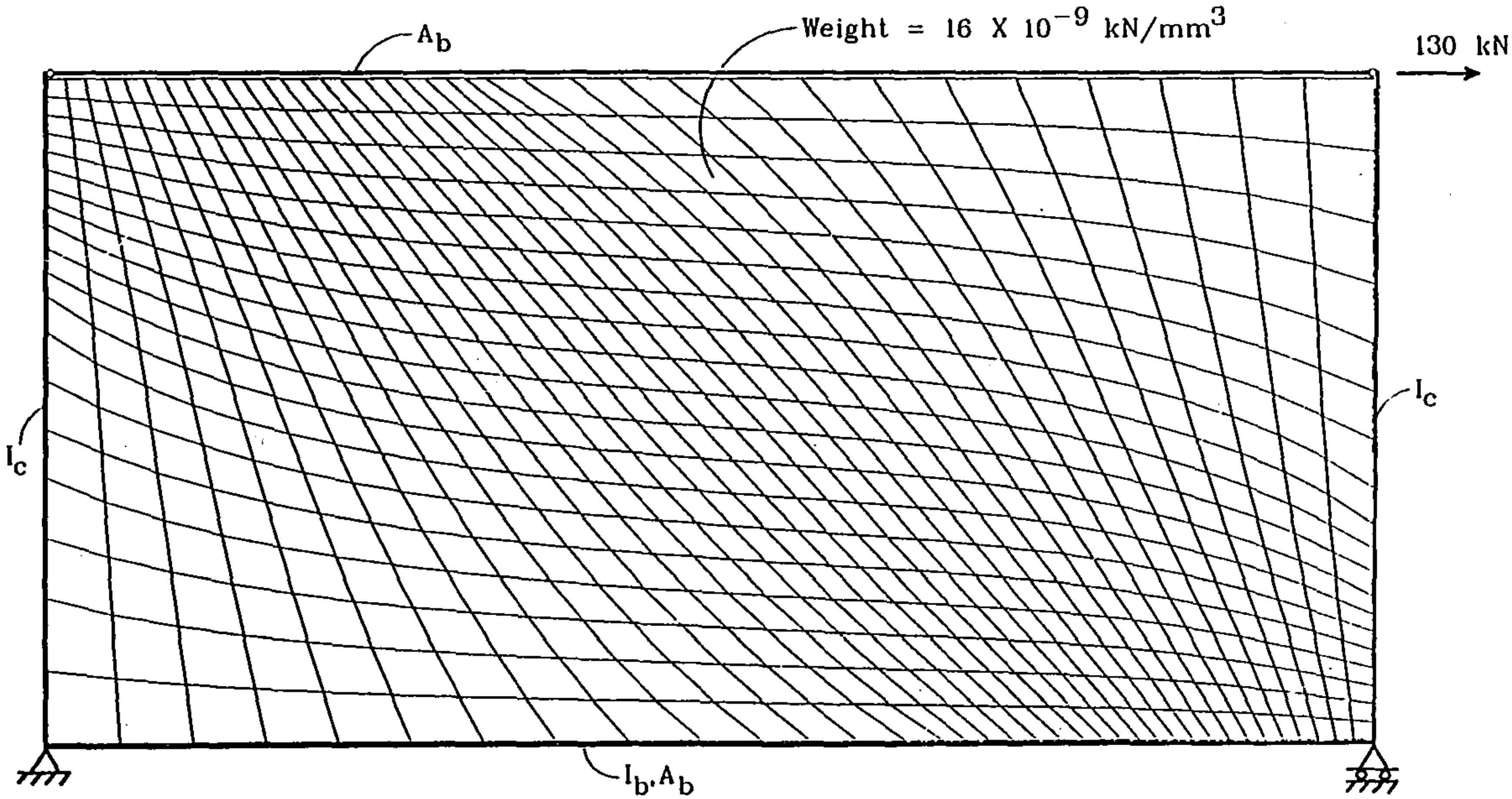

Figure 15.14: Mathematical Model for Combined Load Analysis

approximately 11 percent in the stiffest cycle and 3 percent in the most flexible cycle, than when there was no weight acting on the structure.

Fig. 15.15 shows the displaced shape with the contact regions for the most flexible cycle of the combined load analysis. The contact lengths are slightly longer in the combined load analysis than in the lateral load only analysis, Fig. 15.11. The slight increase in horizontal stiffness that results when the weight of the wall is included is probably caused by the increased length of contact between the infill and the frame, and the consequent more even distribution of the lateral load stresses in the infill.

Contour plots of the vertical, shear, maximum principal and minimum principal stresses are shown for the most flexible cycle of each analysis, in Figs. 15.16, 15.17, 15.18, and 15.19, respectively. As expected, the vertical stresses, Fig. 15.16, are greater in the combined load analysis than in the lateral load only analysis, because of the weight of the infill. The vertical stress at the middle of the panel for the combined load analysis is 14 percent greater than for the lateral load only analysis.

Away from regions of load application, the shear stresses for both load cases, Fig. 15.17, are very similar. The shear stress at the middle of the panel for the combined load analysis is only 2 percent greater than for the lateral load only analysis. Near the compressive corners, the shear stresses are slightly greater for the horizontal load only analysis than for the combined load analysis.

The effect of including the infill's weight does not significantly affect the maximum principal (maximum tensile) stresses, Fig. 15.18. The stress at the middle of the panel for the combined load analysis is 9 percent greater than for the lateral load only analysis. It could have been expected that the maximum tensile stresses in the middle region of the infill would be smaller for the combined load analysis than for the lateral load only analysis, since the compressive stress from the weight of the infill tends to reduce the maximum tensile stress. However, because the horizontal stress in the combined load analysis is reduced by a proportionately larger amount, the maximum principal stresses at the middle region of the infill increase at the level of loading for which the infilled frame was analysed.

The minimum principal stresses, or maximum compressive stresses, Fig. 15.19, have a similar distribution in both load cases. The stress at the middle of the infill in the combined load analysis is 4 percent smaller than that of the lateral load only analysis.

The disadvantage of performing a combined vertical and lateral load analysis is that the effects of the combined loads will be dependent on the magnitude of the weight of the wall relative to that of the lateral load; therefore, deflections and stresses cannot be scaled for different lateral loads. This will be necessary when determining the failing loads of the infill. The results and the conclusions drawn from these will be correct only for that level of loading analysed. Therefore, in the lateral load analyses of the infilled frames to follow, the weight of the infill will be neglected, since the difference between the results obtained from the combined load analysis and those from the horizontal load only analysis is not very significant, and the lateral load only analysis gives conservative results. If the need arises, the effect of the weight of the infill will be accounted for in critical cases.

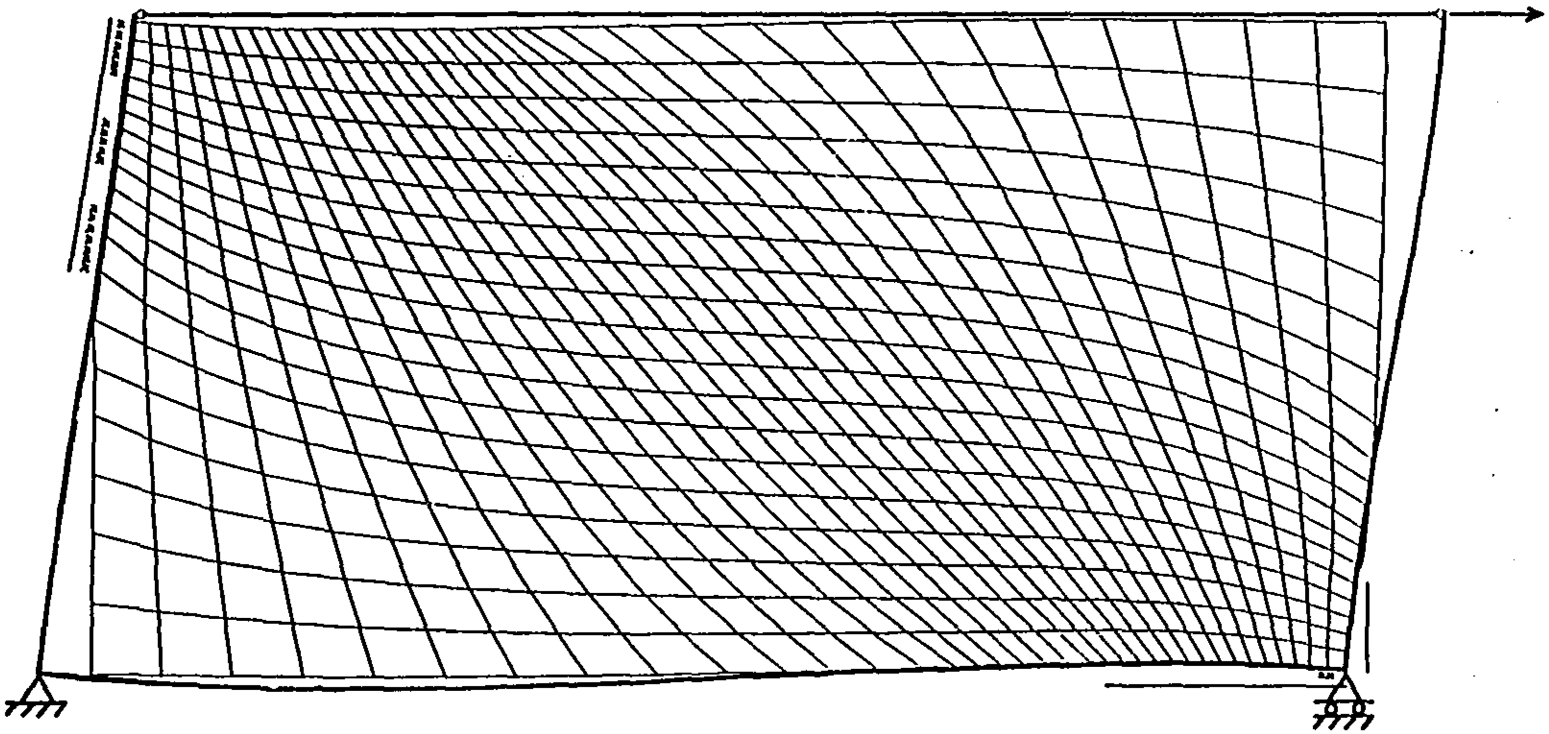

—— connection in normal direction

xxxxxxx connection in tangent direction

Figure 15.15: Deflected Shape for Combined Load Analysis

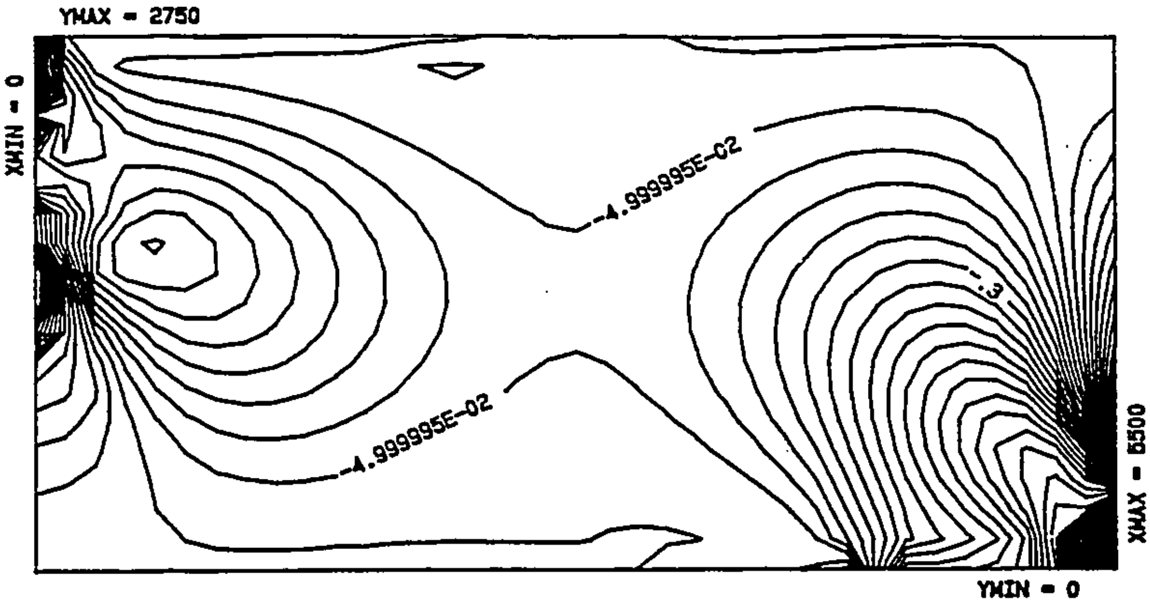

(a) Combined Loads

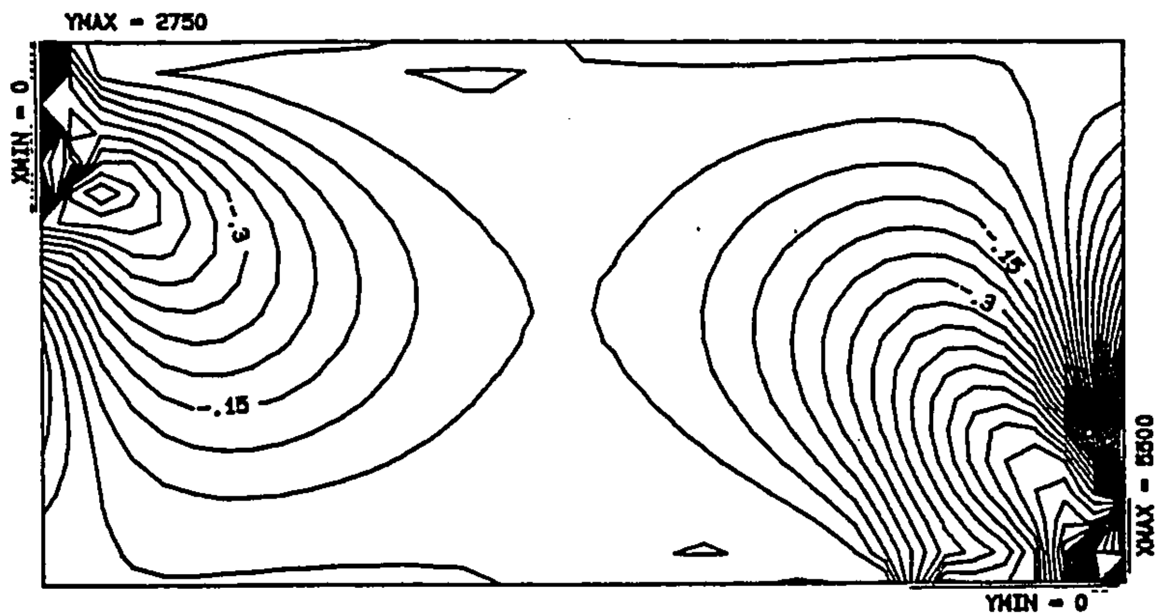

(b) Lateral Load only

All stresses in MPa
Contour Interval = 0.05 MPa

Figure 15.16: Vertical Stresses for Most Flexible Cycle

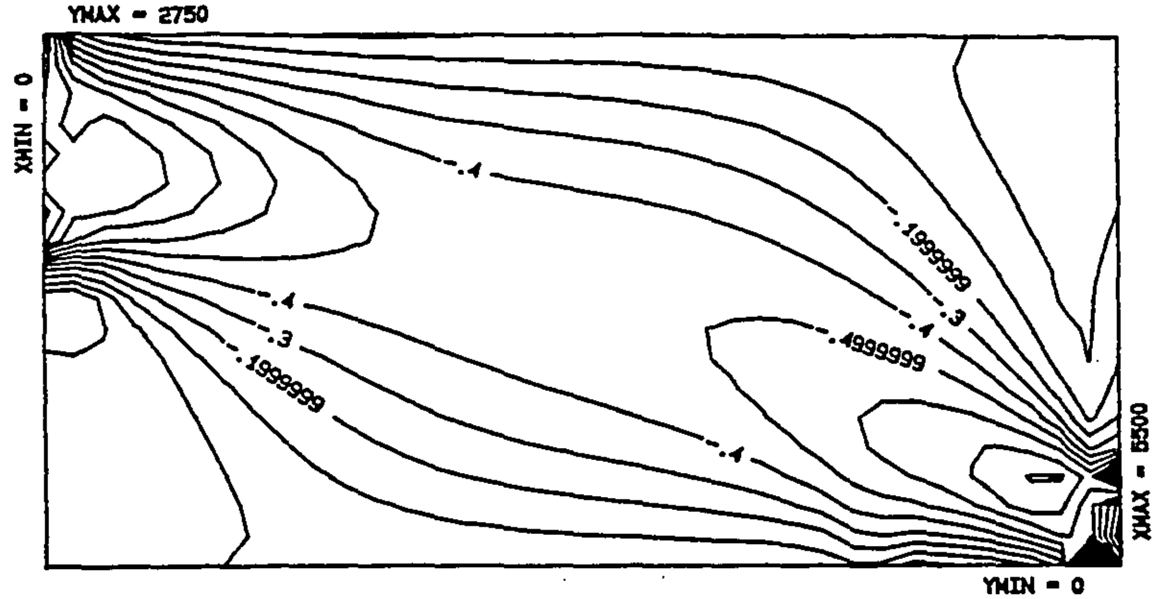

(a) Combined Loads

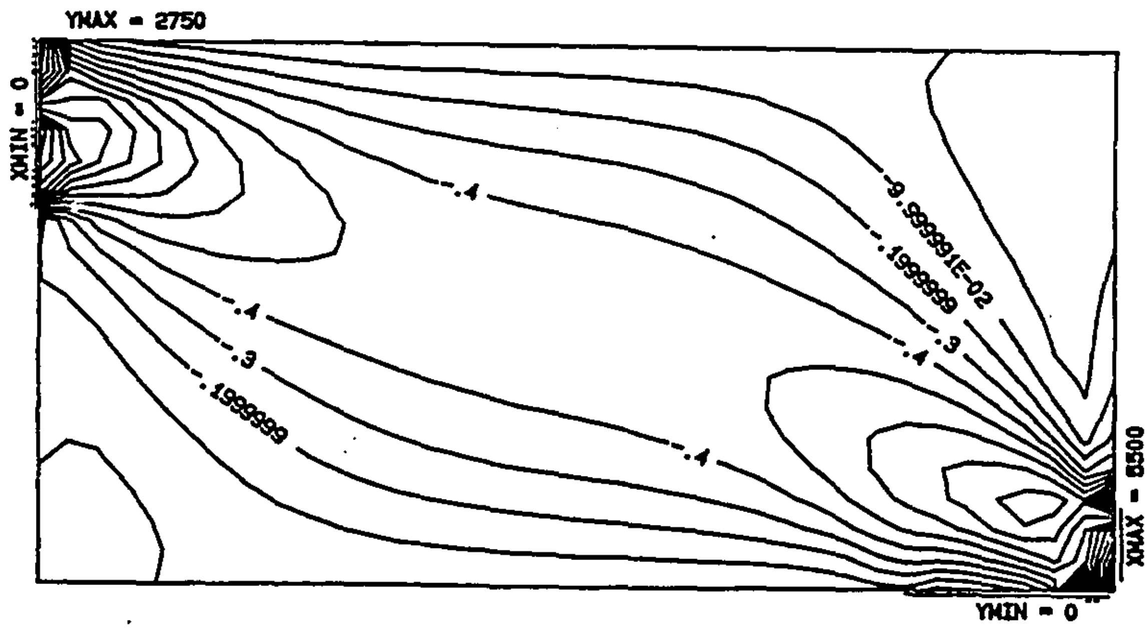

(b) Lateral Load only

All stresses in MPa
Contour Interval = 0.1 MPa

Figure 15.17: Shear Stresses for Most Flexible Cycle

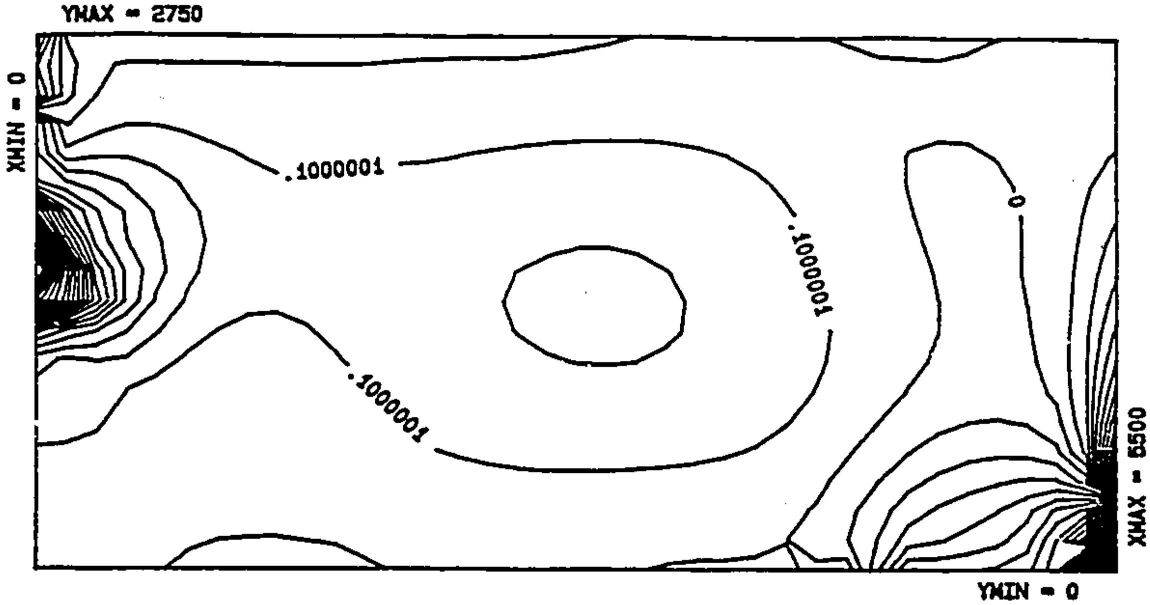

(a) Combined Loads

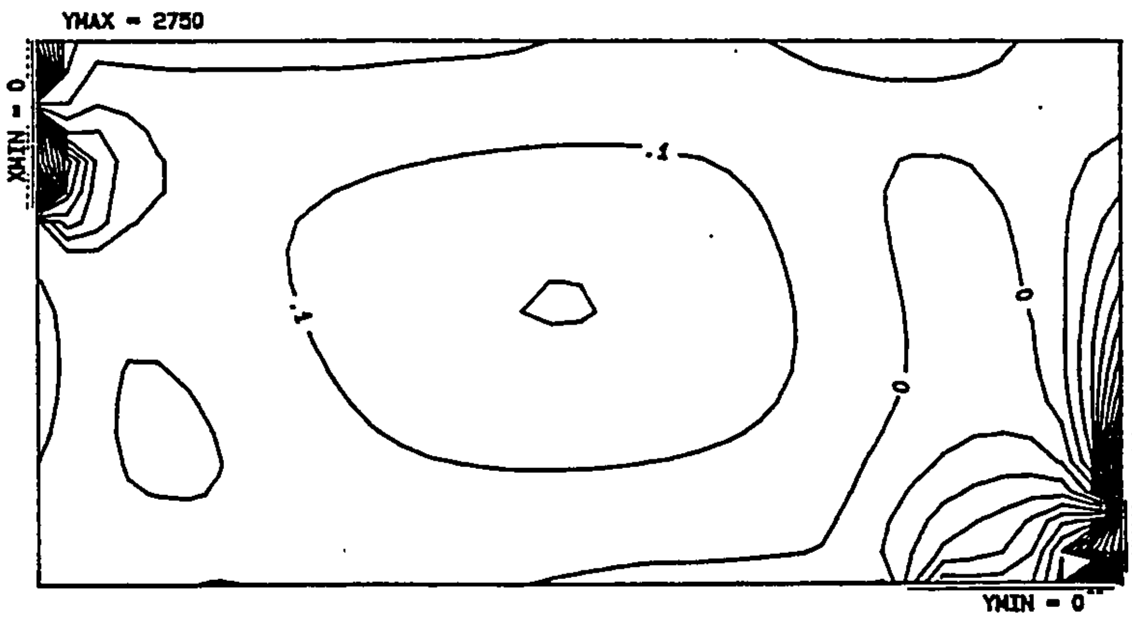

(b) Lateral Load only

All stresses in MPa
Contour Interval = 0.1 MPa

Figure 15.18: Maximum Principal Stresses for Most Flexible Cycle

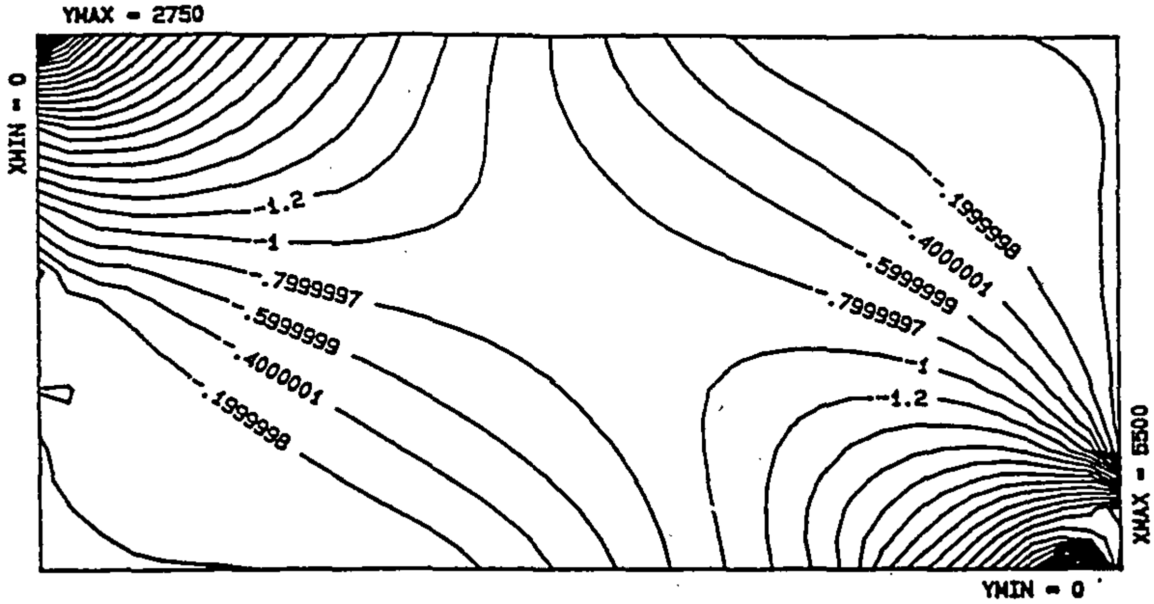

(a) Combined Loads

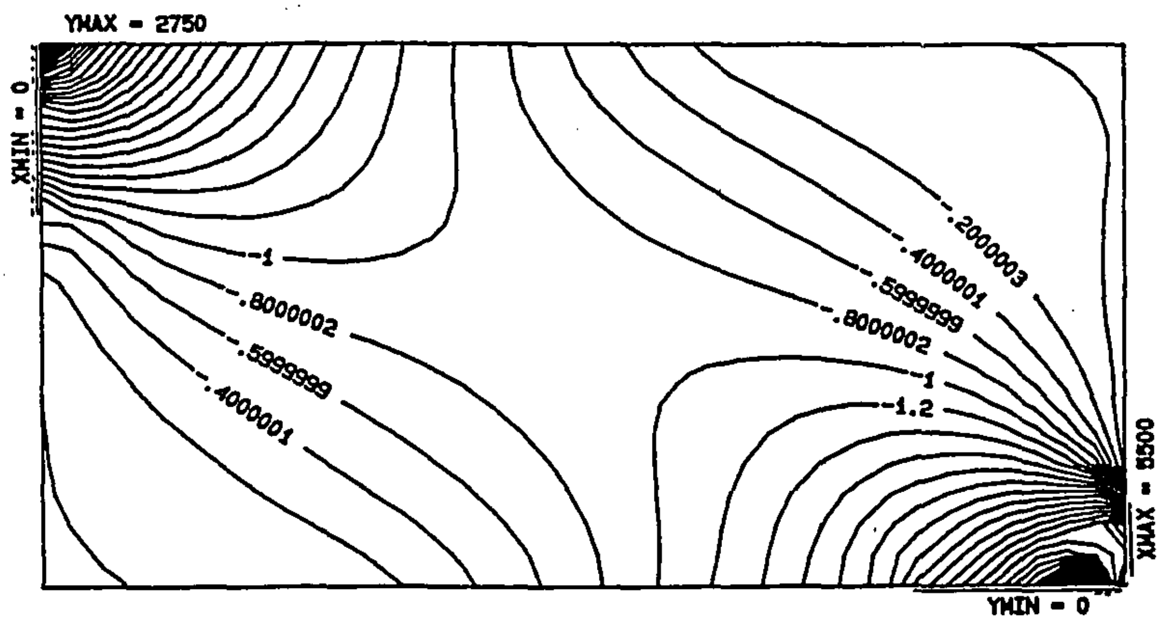

(b) Lateral Load only

All stresses in MPa
Contour Interval = 0.2 MPa

Figure 15.19: Minimum Principal Stresses for Most Flexible Cycle

15.5 Description of Lateral Load Analyses

A series of lateral load analyses of infilled frames, with a gap between the tops of the infills and the frames, was performed. The purposes of the analyses are as follows:

(a) to study the effect of parameters which are considered to be significant in influencing the behaviour of the representative infilled frame. The parameters include:

   i. the stiffness of the beam,
   ii. the stiffness of the column, and
   iii. the aspect ratio of the infilled panels; and

(b) to determine the order of the increase in stiffness of the infilled frame, with a gap between the top of the infill and the frame, over that of the bare moment-resisting frame.

The parameters to be investigated were chosen on the basis that the stiffness response of an infill, and therefore of the infilled frame, is related to the length of contact over which the load is applied to it. Experimental investigations performed by Stafford Smith (1962) have shown that the length of contact is a function of the relative stiffnesses of the frame members in flexure to the infill in diagonal compression; hence the effect of the beam and column stiffnesses were studied, and the stiffness of the infill. The infill's stiffness is dependent on its physical properties and its dimensions; hence the effect of the infill's aspect ratio was studied.

The analysis performed on the representative infilled frame, Sections 15.2 and 15.3, in which the infill, with a height-to-length (h:L) ratio of 1:2, was modelled by a mesh of 684 membrane elements, and the frame members were modelled by line elements, constitutes the standard model. The results of all other analyses will be compared with those of the standard model. To investigate the influence of the beam stiffness on the infilled frame's lateral stiffness, two additional analyses were performed. In one the flexural inertia of the beam of the standard model is halved and in the other doubled, with otherwise identical infilled frames. The influence of the column stiffnesses was investigated similarly. To determine the effect of the infill's aspect ratio (h:L), two further analyses were performed. In one case the aspect ratio was 1:1.5, Fig. 15.20, and in the other 1:2.5, Fig. 15.21, with all other parameters being the same as in the standard model. A diagram depicting the various analyses performed is shown in Fig. 15.22. For all the analyses, the contact lengths, interstorey drifts, bending moment diagrams of the frame members, and stresses in the infills will be studied and compared.

To determine the magnitude of stiffening that an infill, with a gap at the top, contributes to a moment-resisting frame, the interstorey drifts and the frame-member moments obtained from the described infilled frame analyses will be compared with the results from the analyses of the corresponding bare frames.

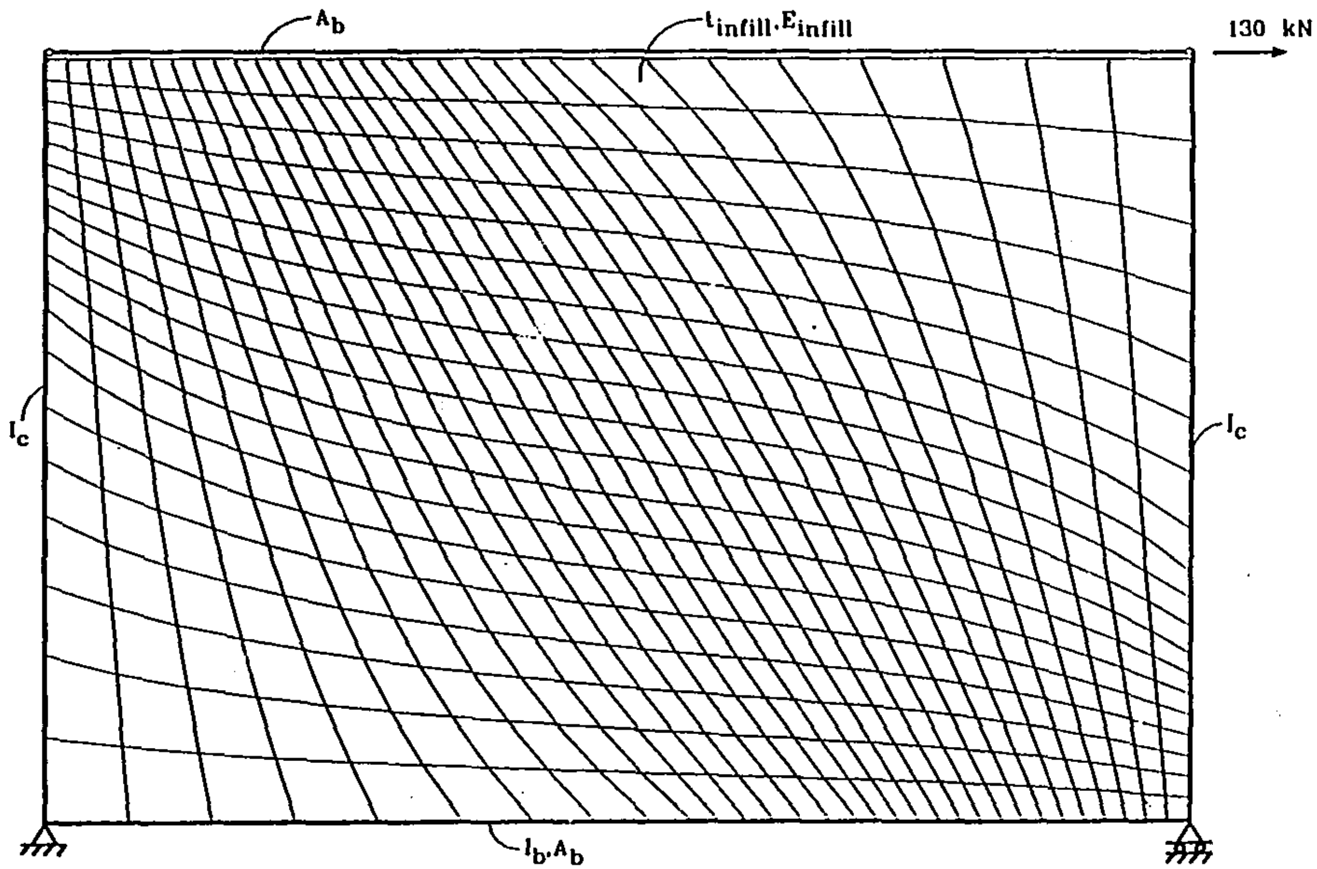

Figure 15.20: Mathematical Model for Representative Infilled Frame With Aspect Ratio of 1:1.5

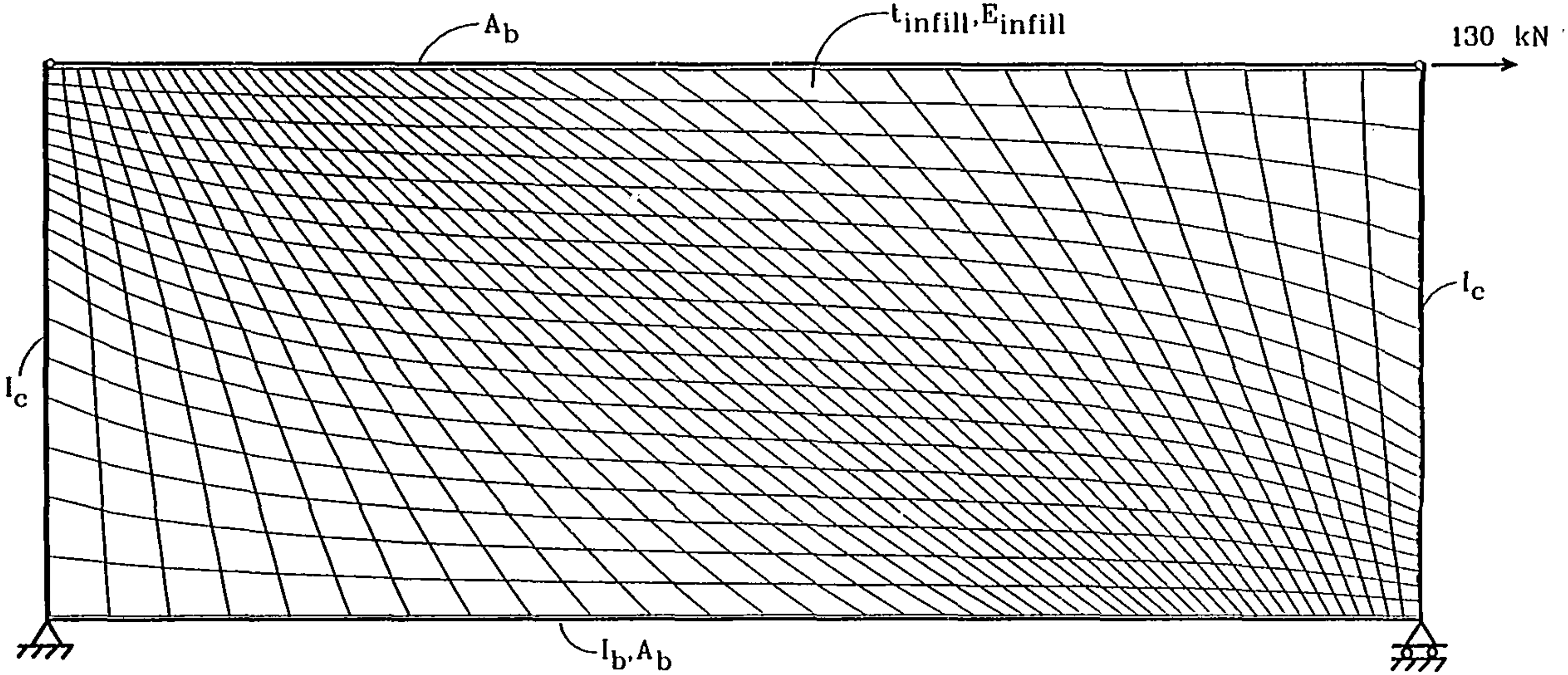

Figure 15.21: Mathematical Model for Representative Infilled Frame With Aspect Ratio of 1:2.5

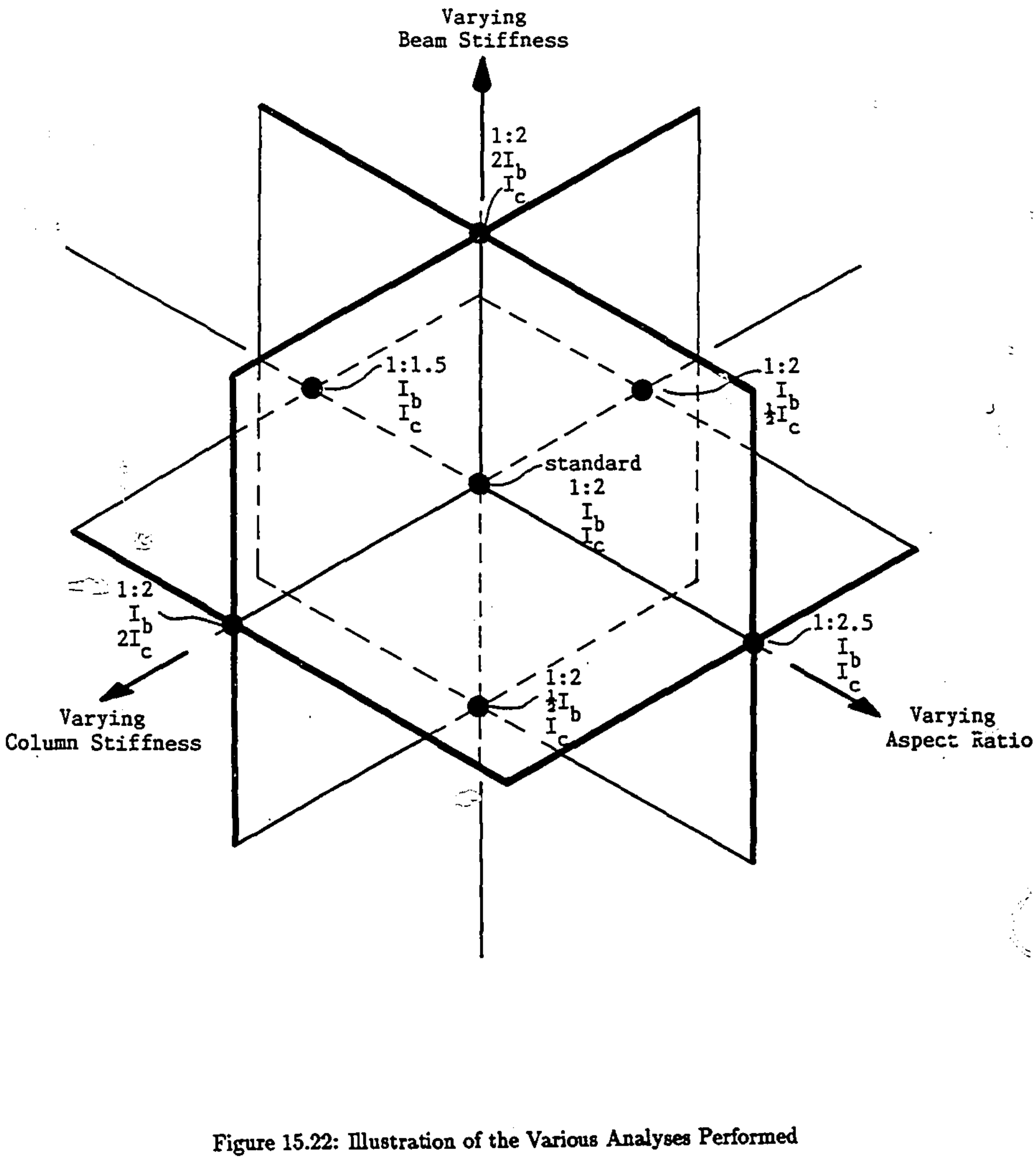

Figure 15.22: Illustration of the Various Analyses Performed

CHAPTER 16

DISCUSSION OF RESULTS FROM ANALYSES OF INFILLED FRAMES

The results obtained from the lateral load analyses described in the previous Chapter are studied in detail to determine the effect of the frame's stiffness and the infill's aspect ratio on the behaviour of the representative infilled frame, with a gap between the top of the infill and the beam above. The interstorey drifts, the deflected shapes, the contact lengths, the bending moment diagrams for the frame members, and the stresses in the infills are examined. The stiffening effect and the interaction of the representative infill with the moment-resisting frame are also discussed.

16.1 Effect of Beam Stiffness

To determine the influence of the beam stiffness on the behaviour of the representative infilled frame with a gap between the top of the infill and the beam above, the flexural inertia of the beam of the standard model was varied in otherwise identical infilled frames. In one case, the flexural inertia of the beam of the standard model was halved, and in the other doubled.

The analysis of the half-inertia beam model stabilized around iterations 13 to 16, while the analysis of the double-inertia beam model stabilized around cycles 9 to 12. Recalling that the standard analysis stabilized around iterations 11 to 14, it was concluded that, for the same degree of mesh refinement, the more flexible the structure, the greater the number of iterations required for the analysis to stabilize around a few cycles. The interstorey drifts for the most flexible cycle, within the four-cycle interval, for each of the three cases are presented and compared in Table 16.1. Varying the beam stiffness by a factor of 0.5 or 2 seems to have affected the calculated stiffness response of the infilled frame by approximately 10 percent. The deflected shapes of the half-inertia beam and double-inertia beam models are shown for the most flexible iteration within the repeating cycle of iterations, in Figs. 16.1 and 16.2, respectively. Comparing these with the deflected shape of the standard model, Fig. 15.11, it was observed that the lengths of contact at the infill-frame interface did not differ significantly between the three analyses. In fact, for the most flexible of the three structures, that is, the half-inertia beam model, the total contact length was greater than

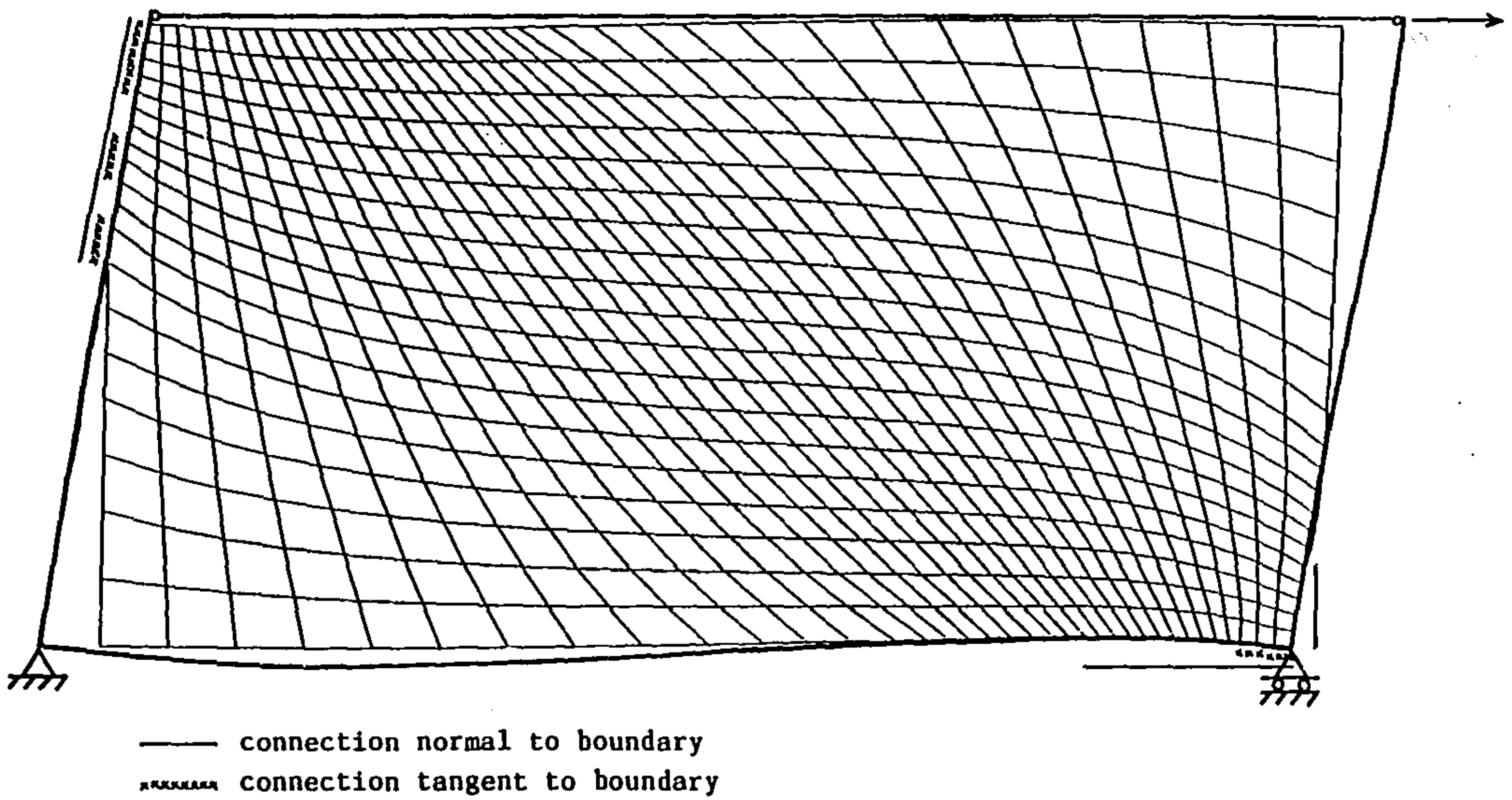

Figure 16.1: Deflected Shape for the Half-Inertia Beam Model

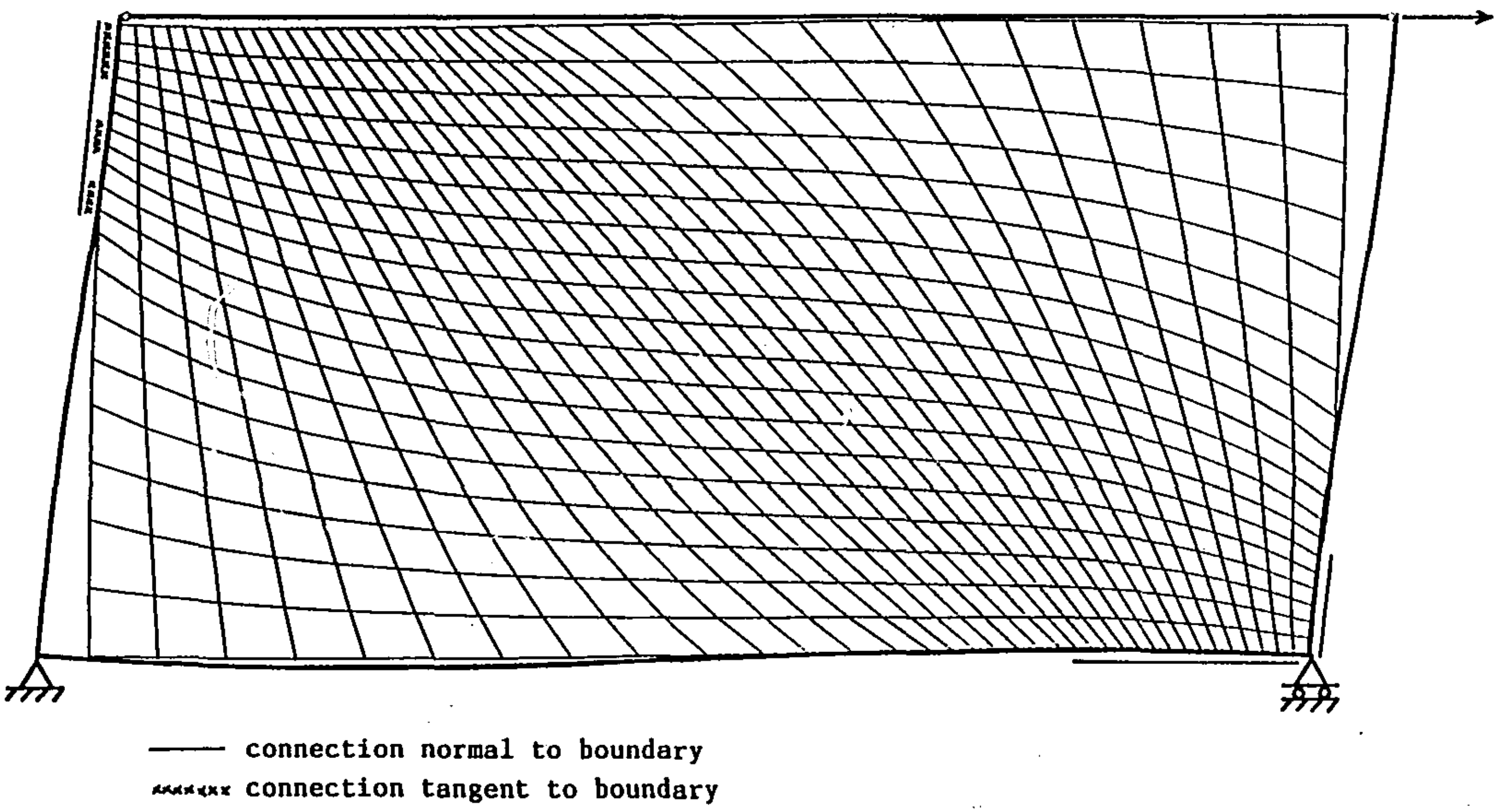

Figure 16.2: Deflected Shape for the Double-Inertia Beam Model

for the other two models. Therefore, the change in stiffness response of the representative infilled frame resulting from the change in the beam's flexural inertia was probably due to the change in the frame's flexibility, rather than to the change in interaction between the infill and the beam. This will be further examined in Section 16.4. The length of contact between the bottom of the infill and the beam was approximately 0.2 times the length of the beam. This is significantly less than the half beam length deduced in Stafford Smith's study (1962, 1966) of fully infilled frames, presumably because of the gap between the top of the infill and the beam.

The frame-member moments obtained from the analyses with varying beam stiffness are presented in Fig. 16.3. The resulting frame-member moments can be simply perceived as the superposition of two actions. As an example, consider first the left column subjected to drift and without the infill's contact at the top. The column bends in double curvature due to racking of the frame, Fig. 16.4a. Note that the effect of constraining the rotation at the top of the column to be the same as that at the bottom, causes the column to bend as though part of a typical intermediate storey. The effect of introducing the infill is to apply normal forces to the column along the length of contact, Fig. 16.4b, which, superposed with the effect in Fig. 16.4a, gives the resulting bending moment diagram shown in Fig. 16.4c.

The second action, that is, the forces applied to the column by the infill, causes the moments at the top and at the bottom of the column, resulting from the first action, to increase and to decrease, respectively. The frame-member moments of the infilled frame, however, are smaller than those of the bare frame because, for the same horizontal load, the frame of the infilled frame deflects much less than the bare frame. This will also be further examined in Section 16.4.

The behaviour described for the left column also applies to the other frame members that are in contact with the infill. In the type of model used in this particular study, the tangential forces which the infill applies to the frame members do not change their moments, because they are applied at the centroidal axes of the members.

A comparison of the moment diagrams for the three cases, Fig. 16.3, indicates, as expected, that the greater the beam stiffness, the greater the frame-member moments, since the frame carries a greater proportion of the external lateral load. The lengths of contact do not differ significantly from one case to the other; consequently, the moment distribution due to the second action is similar in all three cases. Hence, the difference in bending moments from one case to the other arises from the difference in the first, frame racking, action which is a function of the frame stiffness.

Contour plots of the vertical, shear, maximum principal and minimum principal stresses are shown for the most flexible iteration of the four-cycle interval for each analysis, in Figs. 16.5, 16.6, 16.7, and 16.8, respectively. As expected, the trend is the same for each type of stress; that is, the greater the beam stiffness, the greater the proportion of the external load carried by the frame. Therefore, the smaller the proportion carried by the infill, the smaller the infill stresses. For each type of stress, and in each of the cases, the maximum stress occurs at the top-left corner. Whereas, for the fully infilled frames analysed by previous researchers, the maximum shear stress and maximum tensile stress occurred at the centre

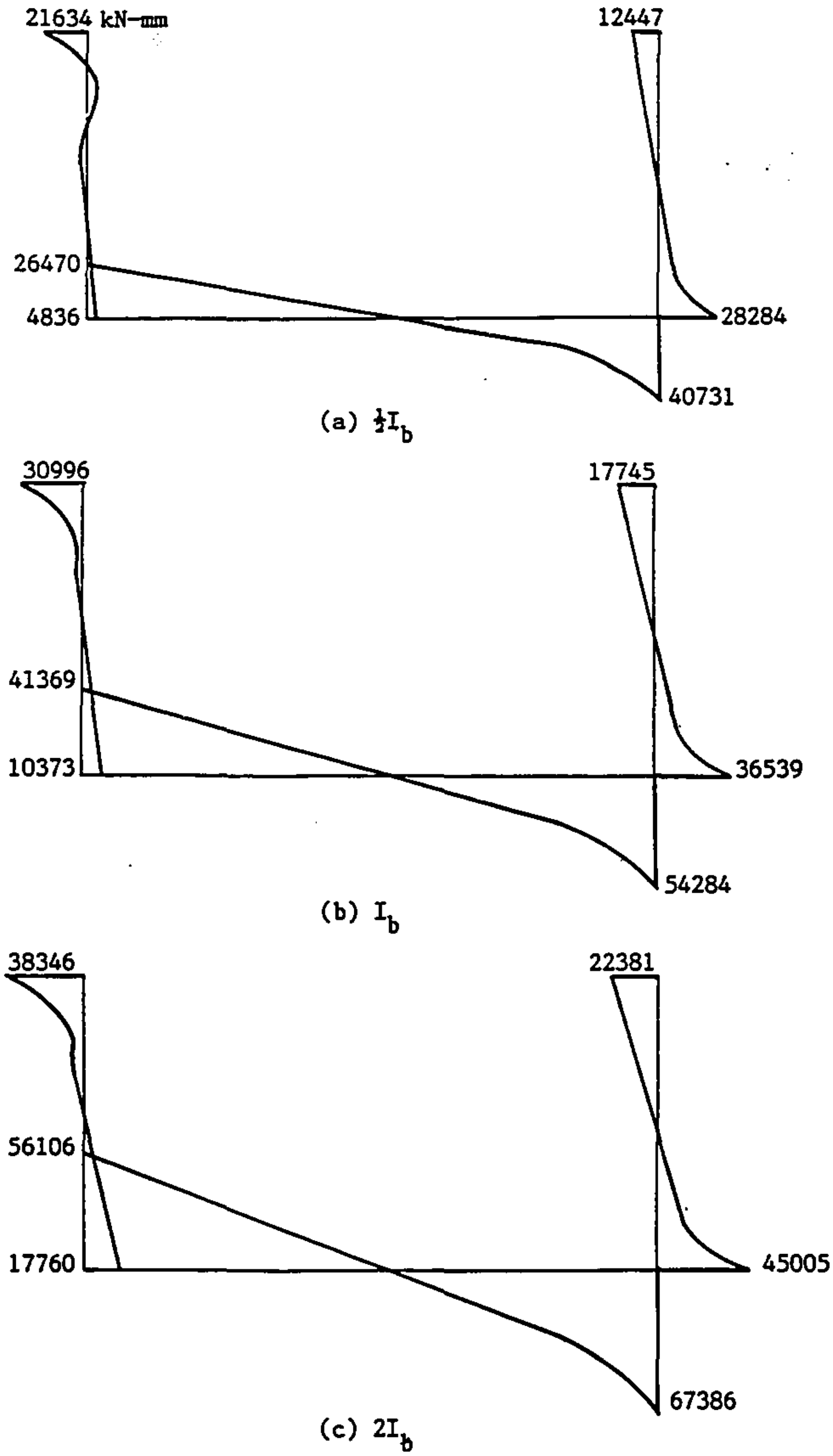

Figure 16.3: Frame-Member Moments for Models with Varying Beam Stiffness

ANALYSIS	INTERSTOREY DRIFT (mm)	DEVIATION FROM STANDARD MODEL
$1/2I_b$	1.5330	8%
I_b	1.4239	—
$2I_b$	1.2827	-10%

Table 16.1: Interstorey Drifts for Most Flexible Cycle (Varying Beam Stiffness Analyses)

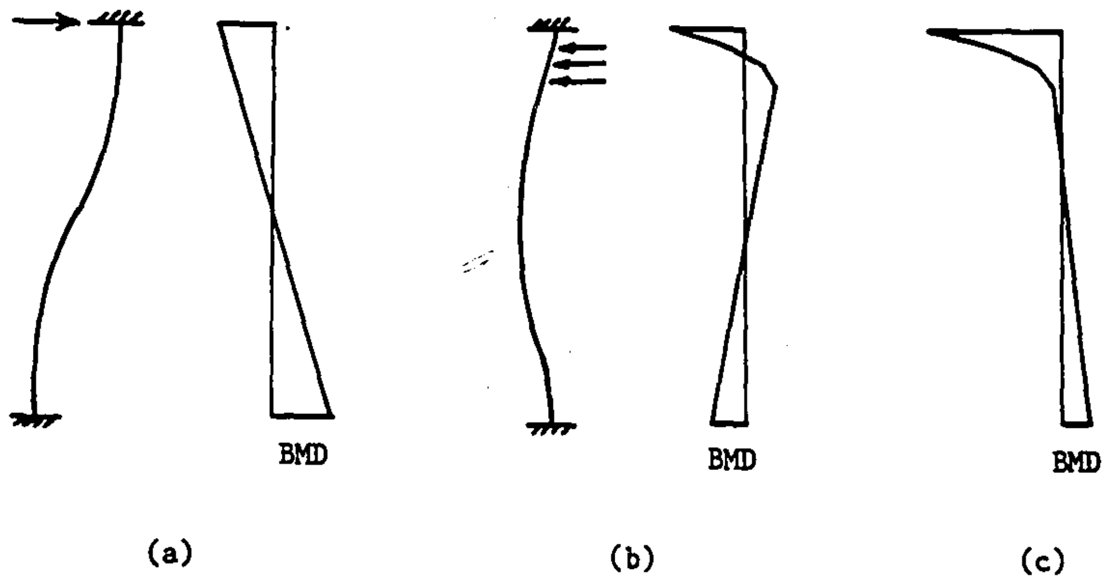

Figure 16.4: Forces Acting on the Frame Members

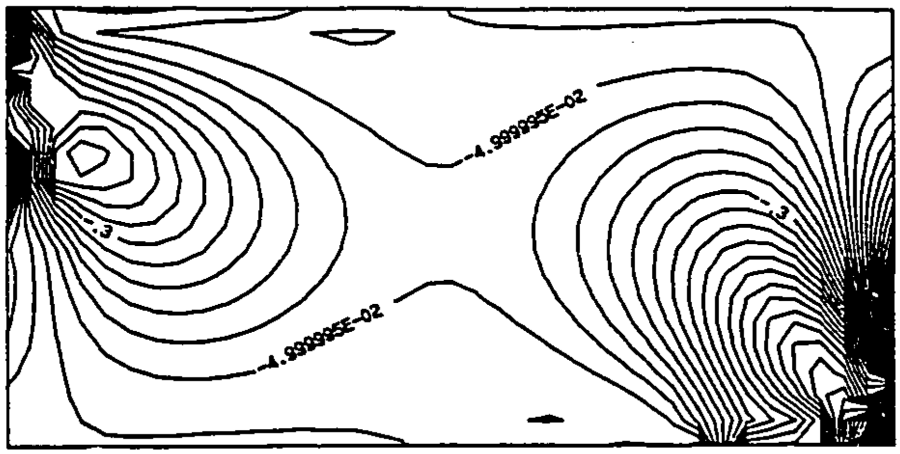

(a) $\frac{1}{2}I_b$

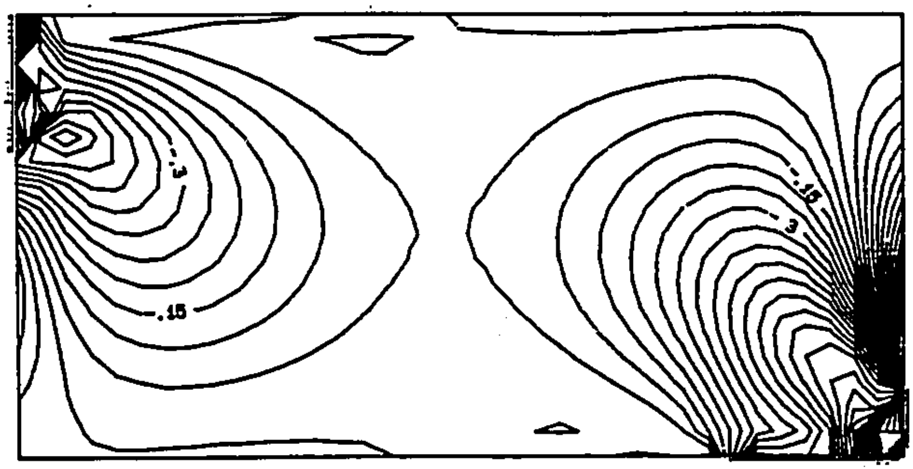

(b) I_b

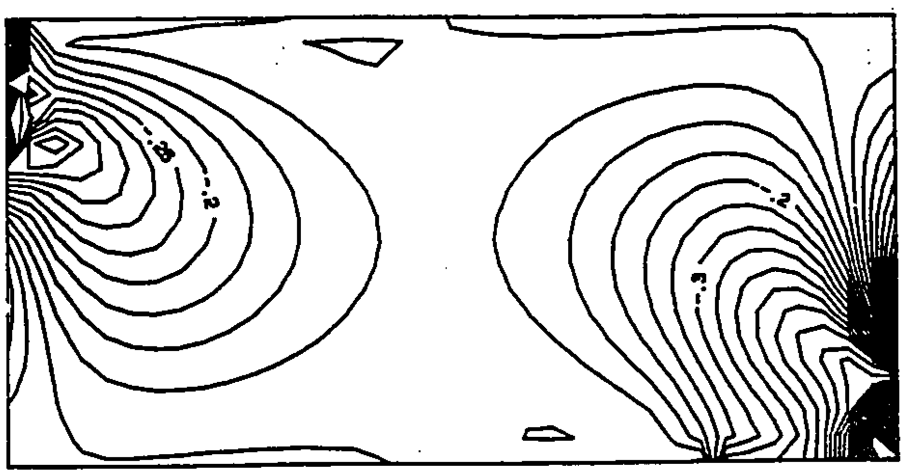

(c) $2I_b$

All stresses in MPa

Figure 16.5: Vertical Stresses for Models with Varying Beam Stiffness

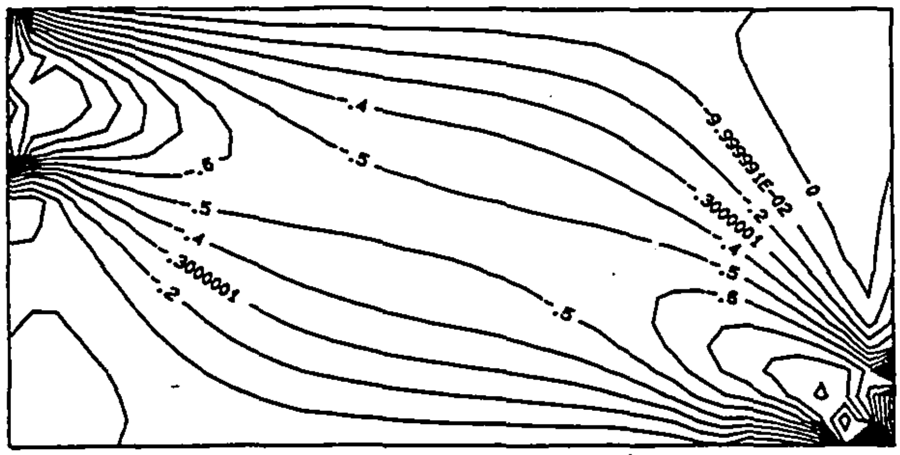

(a) $\frac{1}{2}I_b$

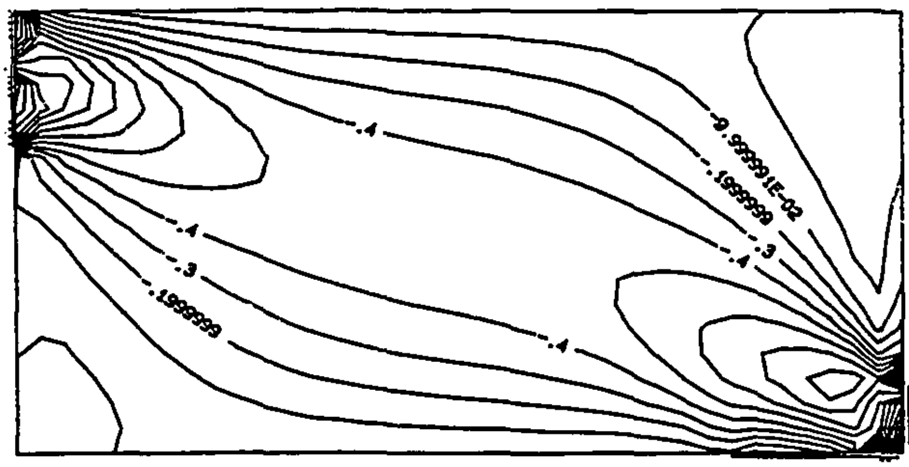

(b) I_b

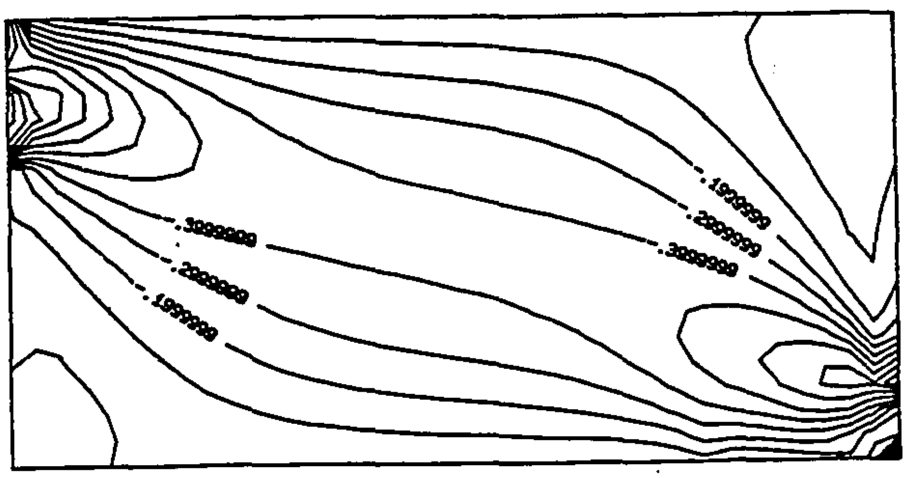

(c) $2I_b$

All stresses in MPa

Figure 16.6: Shear Stresses for Models with Varying Beam Stiffness

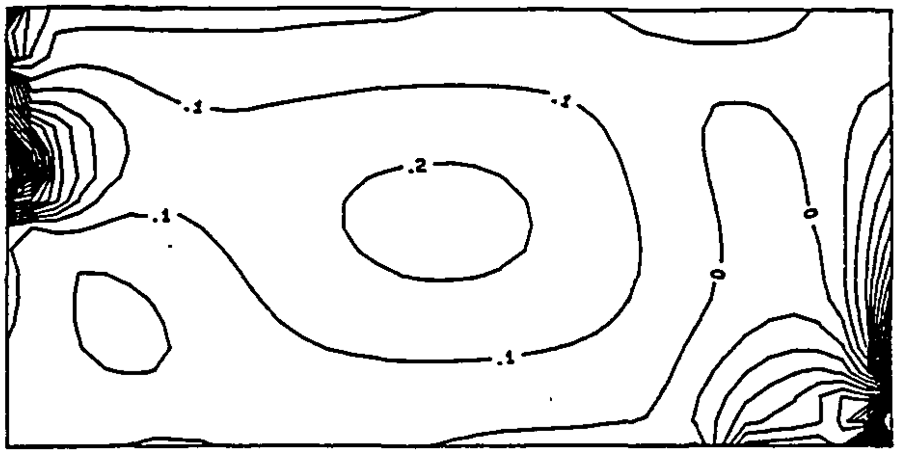

(a) $\frac{1}{2}I_b$

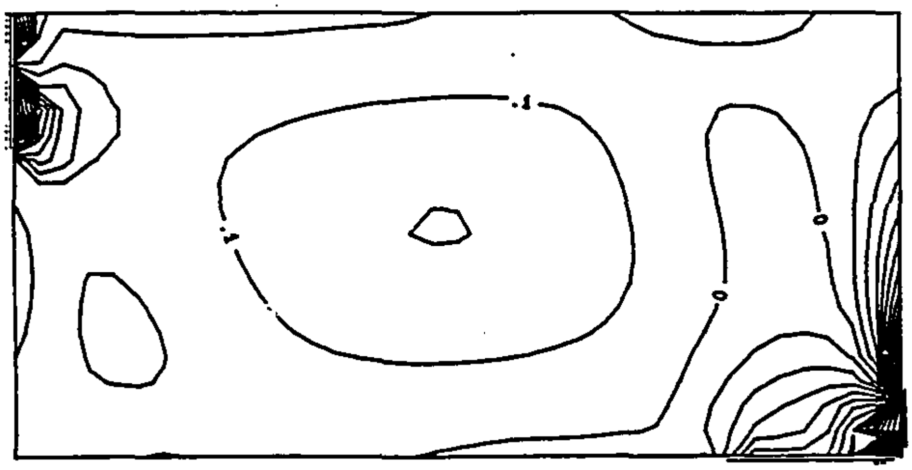

(b) I_b

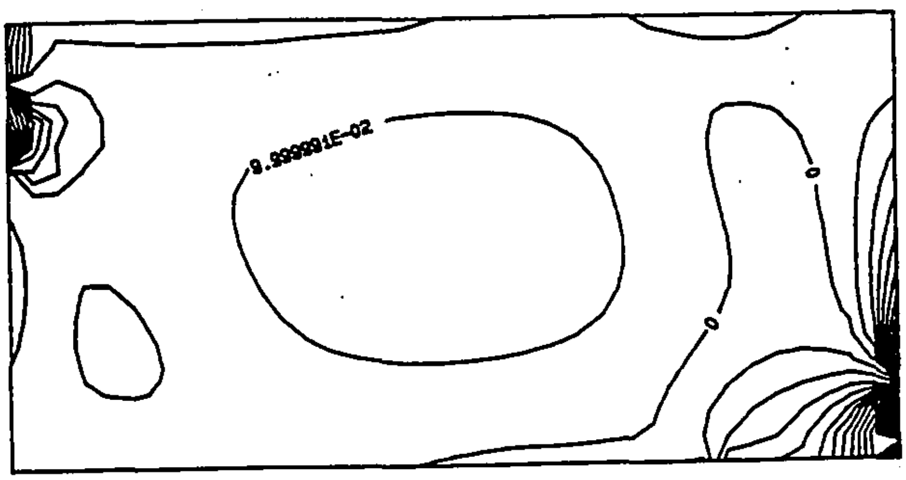

(c) $2I_b$

All stresses in MPa

Figure 16.7: Maximum Principal Stresses for Models with Varying Beam Stiffness

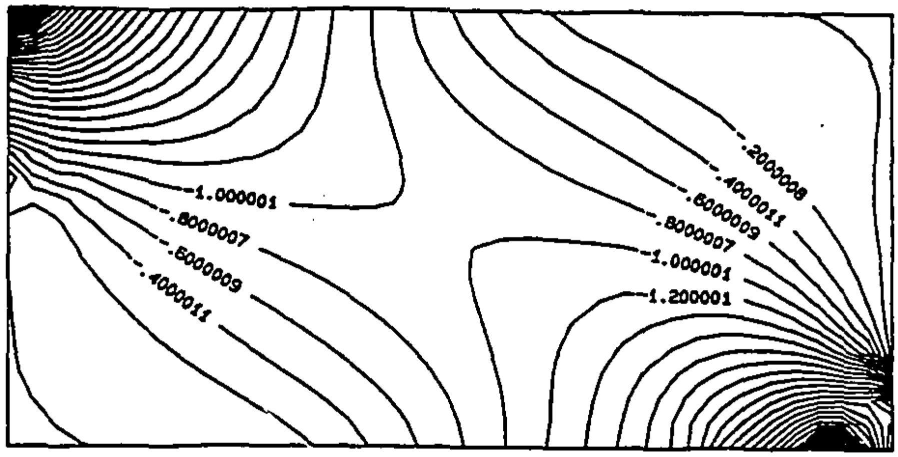

(a) $\frac{1}{2}I_b$

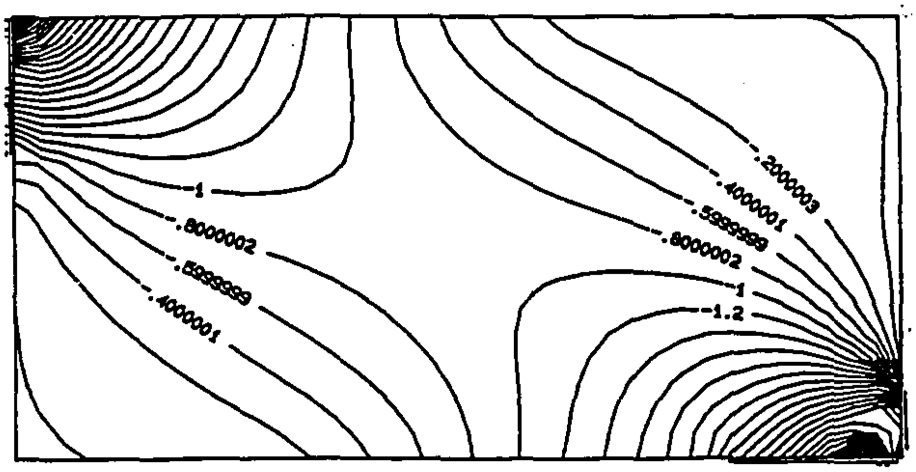

(b) I_b

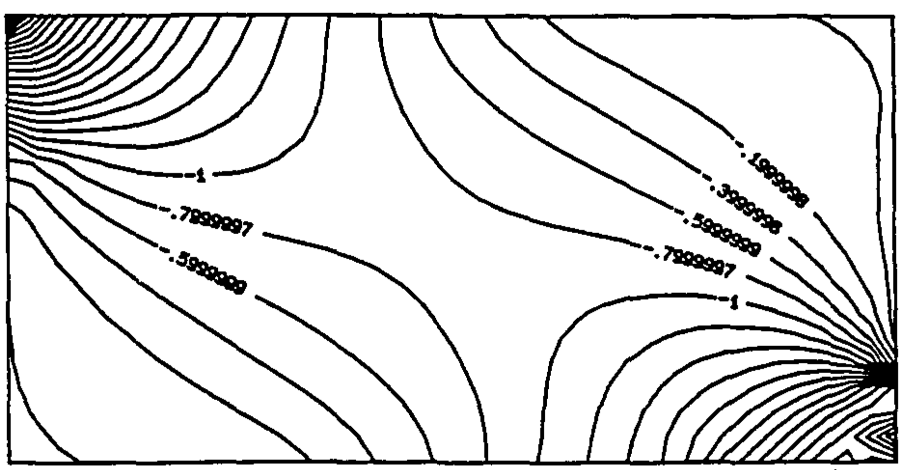

(c) $2I_b$

All stresses in MPa

Figure 16.8: Minimum Principal Stresses for Models with Varying Beam Stiffness

of the infill, Wolde-Tinsae et al. (1987), as the present author, found the shear stress to be maximum at the loaded corner for the semi-infilled frames. Away from regions of contact, where concentrated loads were applied to the infill, the stress distributions were very similar for each of the cases, as a result of the St. Venant effect. The magnitude of the variations in the stresses near the centre of the infill as a result of varying the beam stiffness, Table 16.2, were similar to the variations in the interstorey drifts.

16.2 Effect of Column Stiffnesses

Similarly to when studying the effect of the beam stiffness, the influence of the column stiffnesses on the behaviour of the representative infilled frame was studied by varying the columns' flexural inertias of the standard model. In one analysis, the flexural inertias of the columns of the standard model were halved, and in the other analysis doubled.

In the analysis of the half-inertia column model, identical results were obtained at the 12^{th} and 16^{th} iterations, while for the double-inertia column model, the analysis stabilized around cycles 8 to 11. As was the case when varying the beam stiffness, for the same degree of mesh refinement, the more flexible the structure, the greater the number of iterations required before the analysis stabilized around a few iterations. A comparison of the interstorey drifts obtained from the most flexible iterations, within the repeating cycles of iterations, for the three cases, Table 16.3, indicates that factoring the columns' flexural inertias by 0.5 or 2 varied the calculated stiffness response of the infilled frame by 5 to 7 percent. The deflected shapes of the half- and double-inertia column models are presented for the most flexible iterations, within the four-cycle intervals, in Figs. 16.9 and 16.10, respectively. Comparing these with the deflected shape of the standard model, Fig. 15.11, it was observed that the lengths of contact between the infill and the frame did not differ significantly between the standard model and the half-inertia column model, but the lengths of contact along the left column and the beam were noticeably greater for the double-inertia column model than for the other two models. From the results of the double-inertia column analysis, it may be concluded that the slight increase in lateral stiffness of the infilled frame was due to the increase in the stiffness response of the infills resulting from the increased length of contact against the left column, which were, in turn, due to the increased column stiffnesses. However, the effect of the column stiffnesses for the infilled frames with the gap does not seem to be as important as for the fully infilled frames (Stafford Smith 1966).

The frame-member moments obtained from the analyses with varying column stiffnesses are shown in Fig. 16.11. The distribution of the frame-member moments in all three cases correspond to the combined actions described in the previous section. In general, an increase in the column stiffnesses produced, as expected, greater frame-member moments, since the moment-resisting frame carried a greater proportion of the racking load as its stiffness increased. However, for the double-inertia column model, the moments at the top of the left column, and at the bottom of the right column decreased with the increase in frame stiffness. This resulted because the contact lengths were greater for the double-inertia column model, causing the resultant of the normal forces applied by the infill to the

Analysis	Vertical Stress		Shear Stress		Max. Princ. Stress		Min. Princ. Stress	
	Stress (MPa)	%Dev. from Stand.	Stress (MPa)	%Dev. from Stand.	Stress (MPa)	%Dev. from Stand.	Stress (MPa)	%Dev. from Stand.
$1/2I_b$	-.061	+22%	-.515	+10%	.223	+12%	-.994	+7%
I_b	-.050	—	-.468	—	.199	—	-.929	—
$2I_b$	-.041	-18%	-.421	-10%	.178	-11%	-.849	-9%

Table 16.2: Stresses Near Centre of Infill (Varying Beam Stiffness Analyses)

ANALYSIS	INTERSTOREY DRIFT (mm)	DEVIATION FROM STANDARD MODEL
$1/2I_c$	1.4963	5%
I_c	1.4239	—
$2I_c$	1.3290	-7%

Table 16.3: Interstorey Drifts for Most Flexible Cycle (Varying Column Stiffness Analyses)

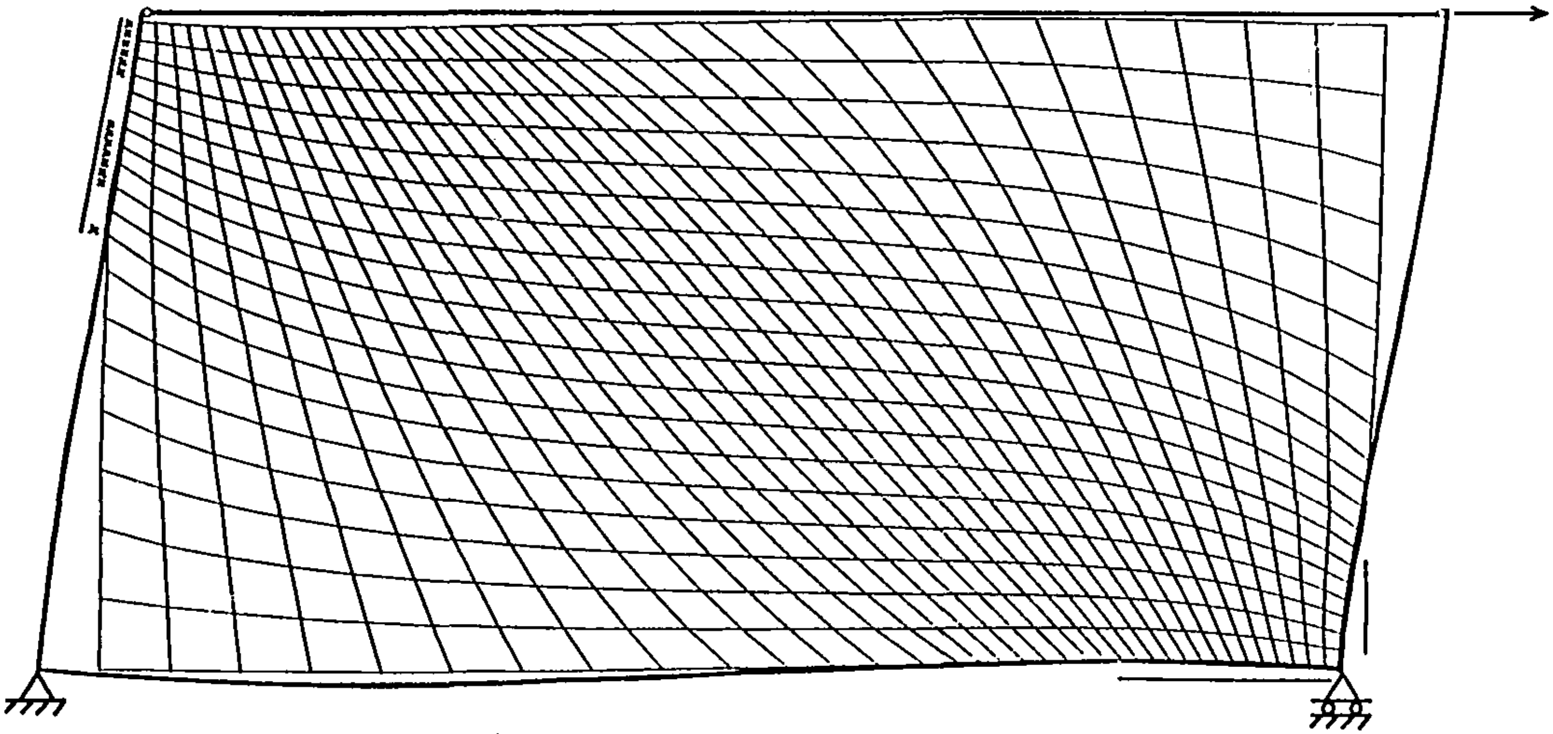

—— connection normal to boundary

xxxxxxx connection tangent to boundary

Figure 16.9: Deflected Shape for the Half-Inertia Column Model

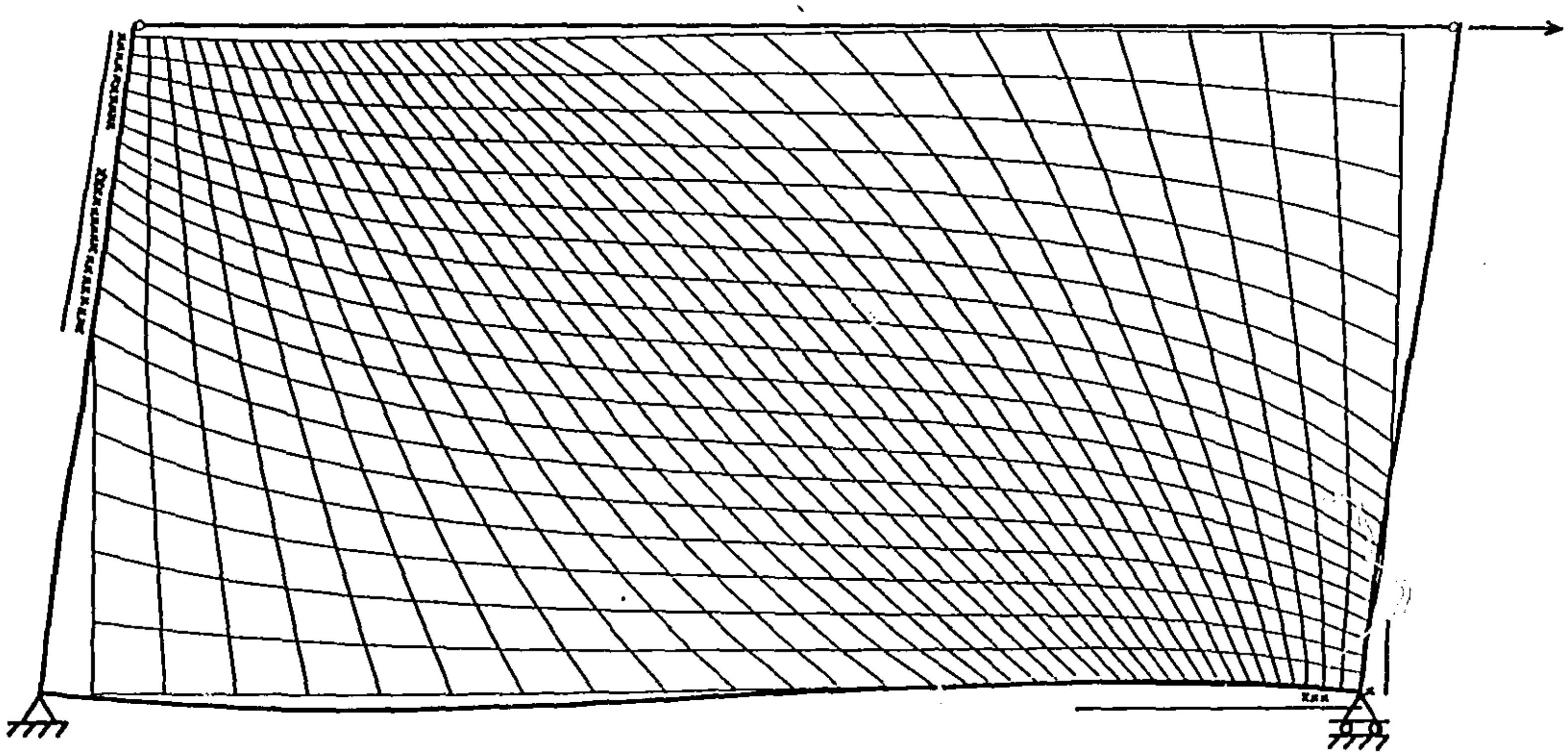

—— connection normal to boundary

xxxxxxx connection tangent to boundary

Figure 16.10: Deflected Shape for the Double-Inertia Column Model

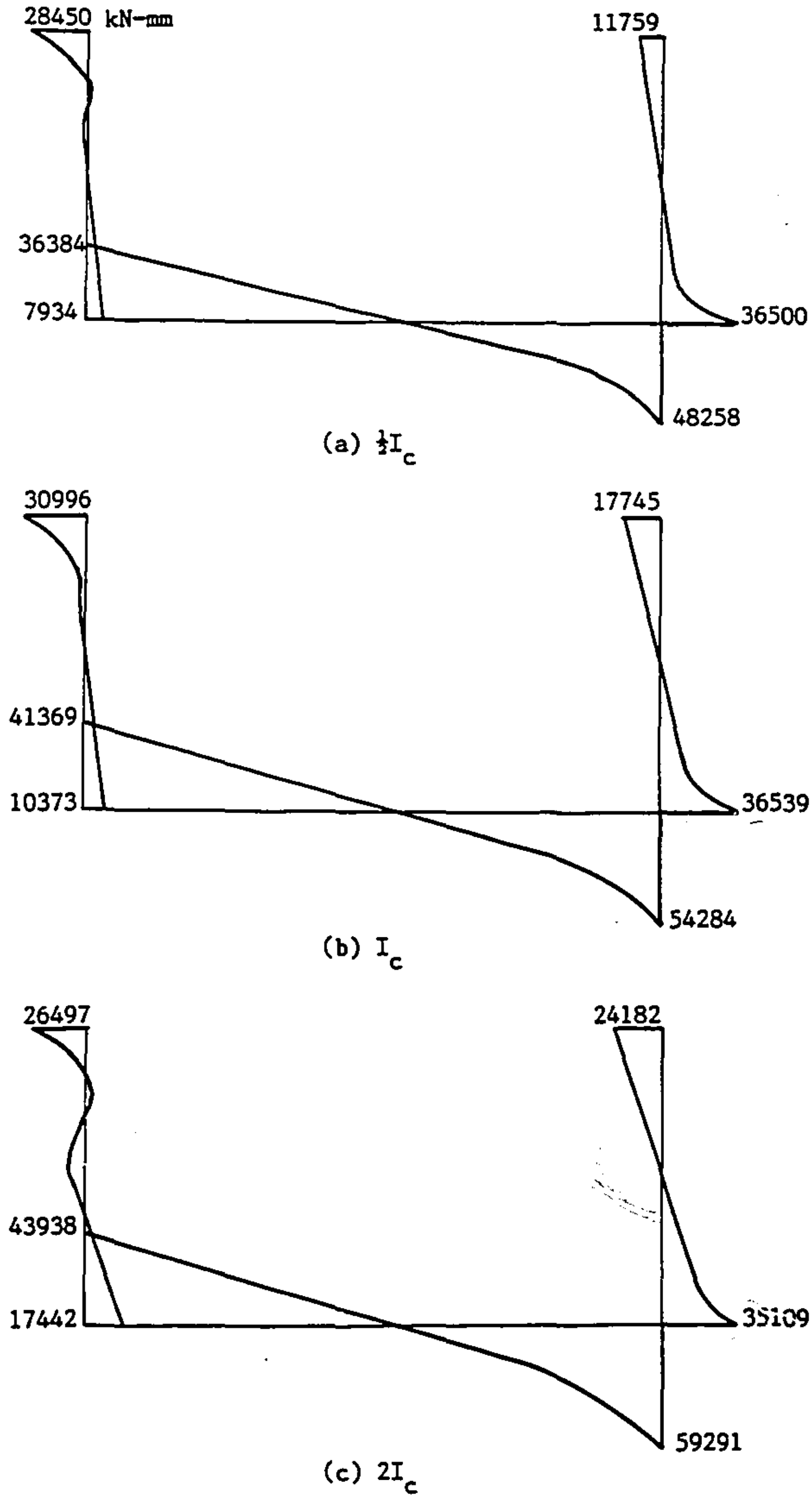

Figure 16.11: Frame-Member Moments for Models with Varying Column Stiffness

members to be at a greater distance from the corner than in the other models. Thus, in turn, reducing the moments at the top of the left column and at the bottom of the right column, and increasing the moments at the bottom of the left column, and at the top of the right column.

Contour plots of the vertical, shear, maximum principal and minimum principal stresses are presented in Figs. 16.12, 16.13, 16.14, and 16.15, respectively. A slight decrease in the shear and maximum compressive stresses was observed as the column stiffnesses increased. However, no noticeable trend was apparent for the vertical and maximum tensile stresses. In general, the stresses in the infills, away from regions of contact with the frame, were not greatly affected by varying the column stiffnesses, as can also be seen from Table 16.4.

16.3 Effect of Aspect Ratio of Infill

To determine the effect of the infill's aspect ratio on the behaviour of the representative infilled frame, the length, L, of the infilled frame was varied, while its height, h, was kept constant. In one analysis, the aspect ratio, h:L, of the infilled frame was 1:1.5, and in the other 1:2.5. Both models were compared with the standard model which had an aspect ratio of 1:2. Except for the change in aspect ratio of the infilled frames, all other parameters were the same as in the standard model.

In the analysis of the 1:1.5 aspect ratio model, identical results were obtained at the 13^{th} and 19^{th} iterations, while for the 1:2.5 aspect ratio model, the analysis stabilized around iterations 11 to 14. The interstorey drifts for the most flexible iteration, within the repeating cycle of iterations, are shown and compared for the varying aspect ratio analyses in Table 16.5. A ± 25 percent deviation in aspect ratio affected the calculated stiffness response of the infilled frame by an average of ± 10 percent. The greater the length-to-height ratio, the more flexible the infilled frame. Reasons to account for this are that as the ratio increases the following parameters are affected:

(a) the frame is more flexible; therefore, it carries a proportionately smaller racking load,

(b) the lengths of contact are proportionately shorter because of the more flexible frame; hence greater strains occur in the compressive regions of the infill which causes it and the structure to be more flexible, and

(c) the inclination of the infill's strut action is smaller which would tend to reduce its axial force, however, the strut and the beam are longer, and their axial deformations would tend to be greater for a given cross-sectional area of strut. The net result of these combined effects would be to cause a more flexible structure.

The displaced shapes of the 1:1.5 and 1:2.5 models are presented in Figs. 16.16 and 16.17, respectively. The absolute values of the lengths of contact between the infill and the beam for the 1:1.5, 1:2, 1:2.5 models were 900 mm, 990 mm, and 1375 mm, respectively. The greater the length-to-height ratio, the greater the absolute length of contact between

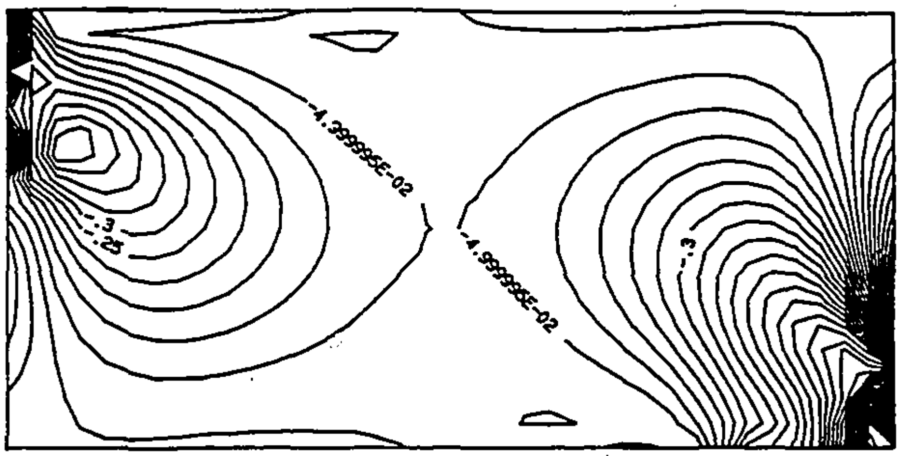

(a) $\frac{1}{2}I_c$

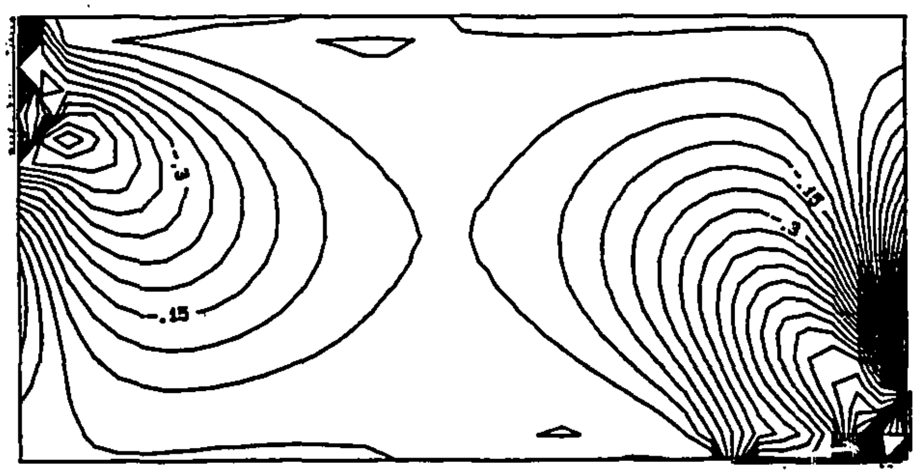

(b) I_c

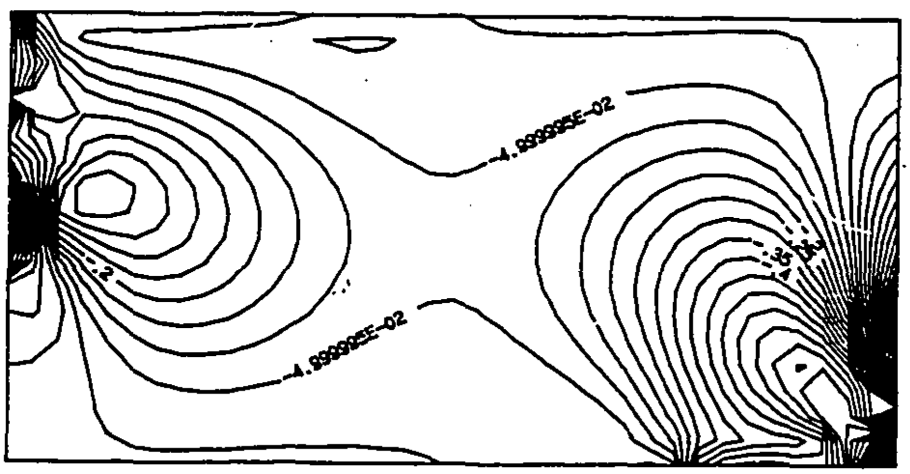

(c) $2I_c$

All stresses in MPa

Figure 16.12: Vertical Stresses for Models with Varying Column Stiffness

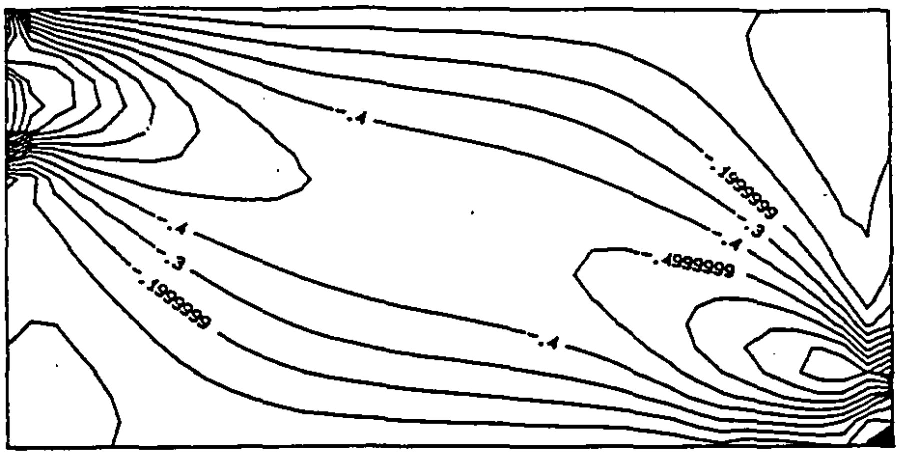

(a) $\frac{1}{2}I_c$

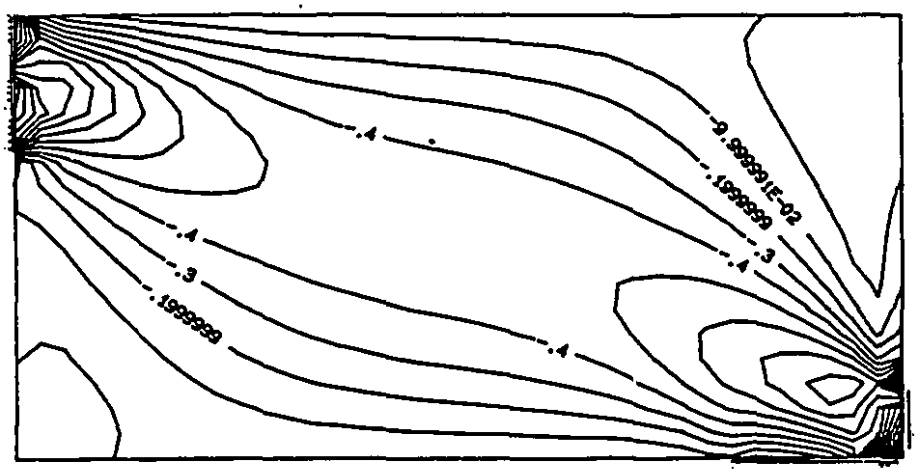

(b) I_c

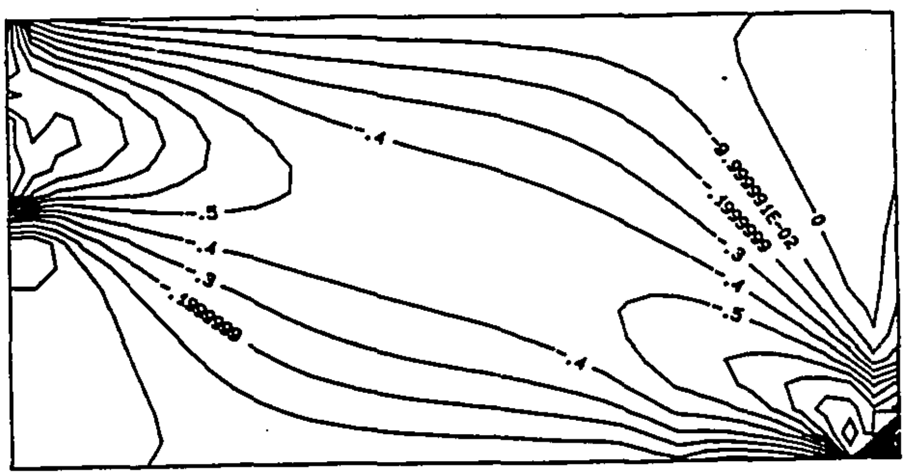

(c) $2I_c$

All stresses in MPa

Figure 16.13: Shear Stresses for Models with Varying Column Stiffness

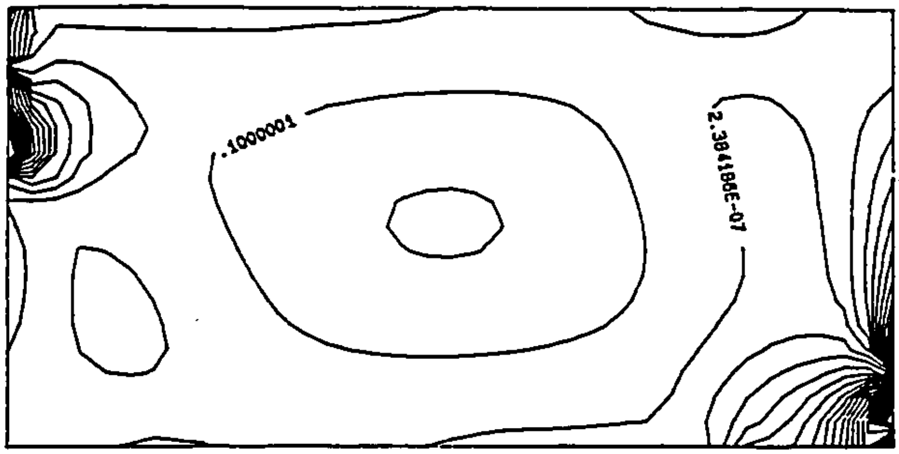

(a) $\frac{1}{2}I_c$

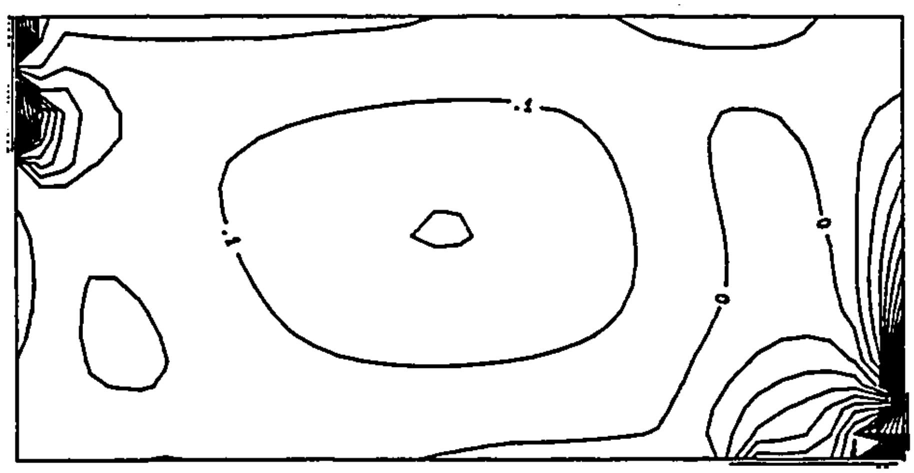

(b) I_c

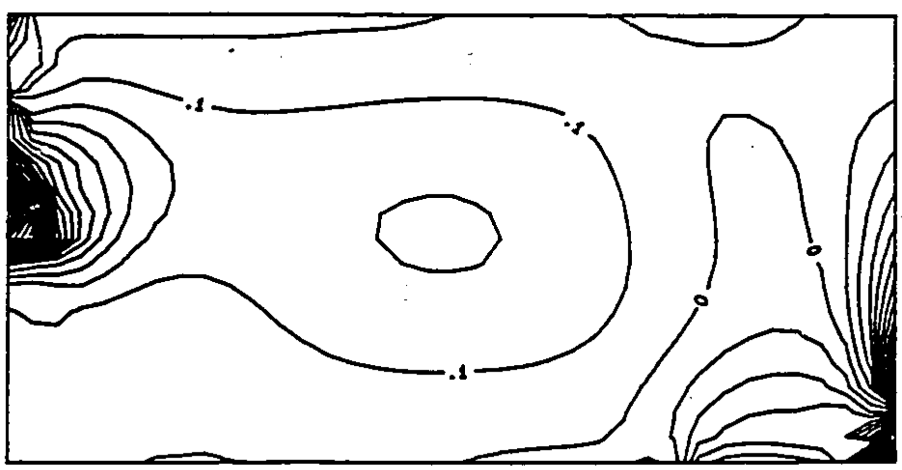

(c) $2I_c$

All stresses in MPa

Figure 16.14: Maximum Principal Stresses for Models with Varying Column Stiffness

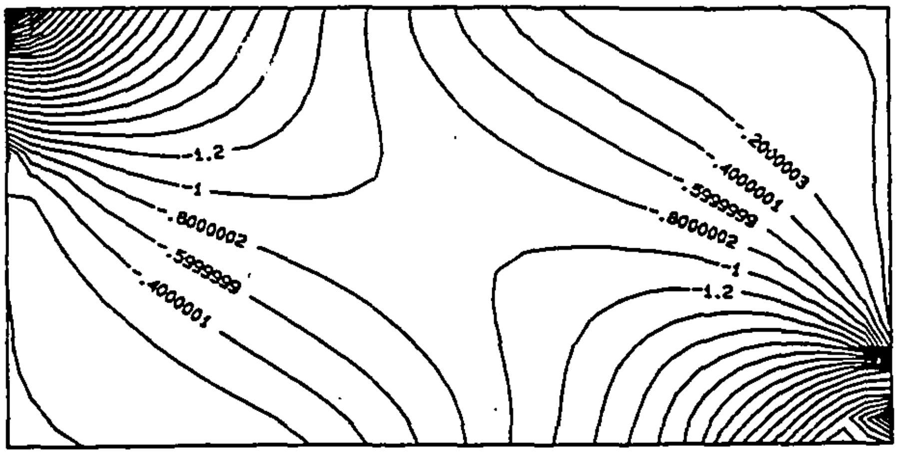

(a) $\frac{1}{2}I_c$

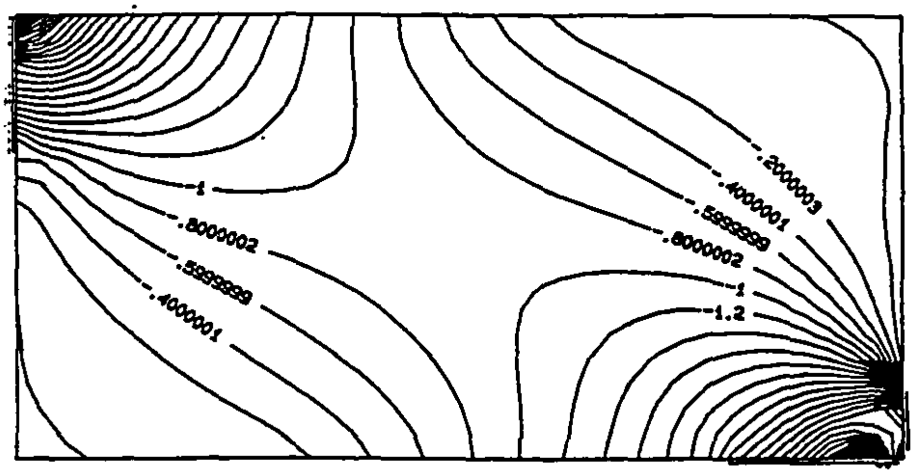

(b) I_c

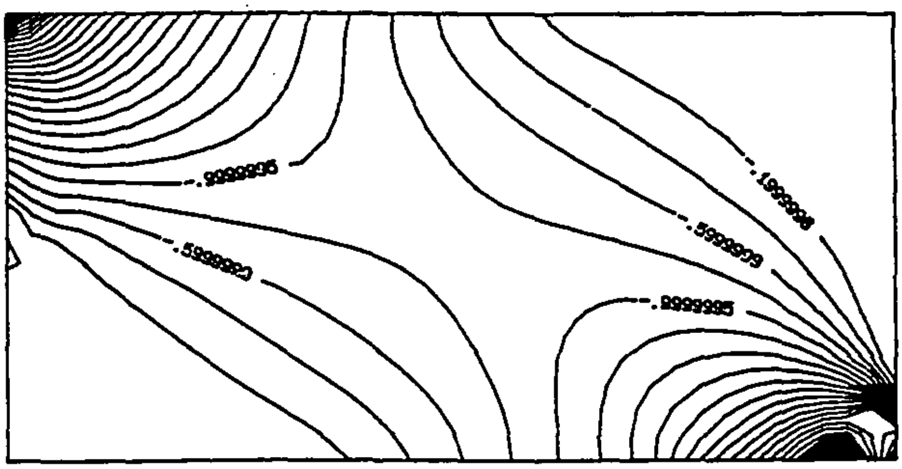

(c) $2I_c$

All stresses in MPa

Figure 16.15: Minimum Principal Stresses for Models with Varying Column Stiffness

Analysis	Vertical Stress		Shear Stress		Max. Princ. Stress		Min. Princ. Stress	
	Stress (MPa)	%Dev. from Stand.	Stress (MPa)	%Dev. from Stand.	Stress (MPa)	%Dev. from Stand.	Stress (MPa)	%Dev. from Stand.
$1/2I_c$	-.050	0%	-.486	+4%	.207	+4%	-.969	+4%
I_c	-.050	—	-.468	—	.199	—	-.929	—
$2I_c$	-.062	+24%	-.460	-2%	.208	+5%	-.847	-9%

Table 16.4: Stresses Near Centre of Infill (Varying Column Stiffness Analyses)

ANALYSIS	INTERSTOREY DRIFT (mm)	DEVIATION FROM STANDARD MODEL
1:1.5	1.2467	-12%
1:2	1.4239	—
1:2.5	1.5348	+8%

Table 16.5: Interstorey Drifts for Most Flexible Cycle (Varying Aspect Ratio Analyses)

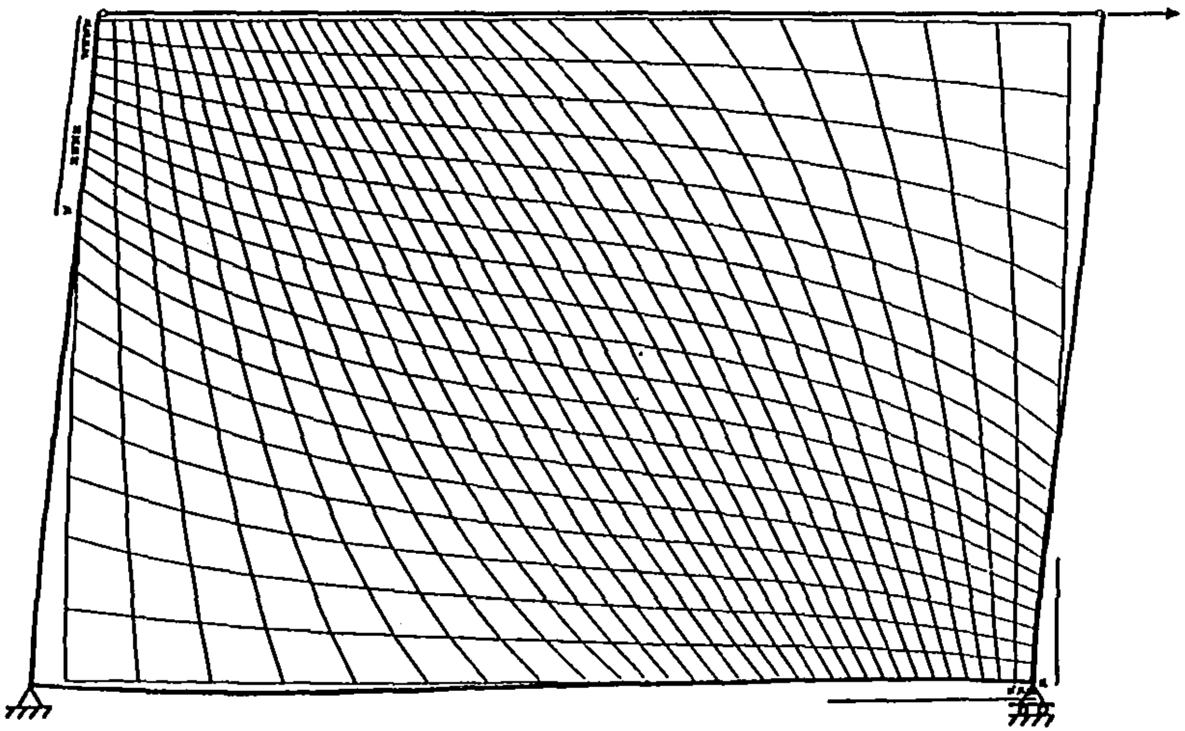

——— connection normal to boundary

xxxxxxx connection tangent to boundary

Figure 16.16: Deflected Shape for the 1:1.5 Model

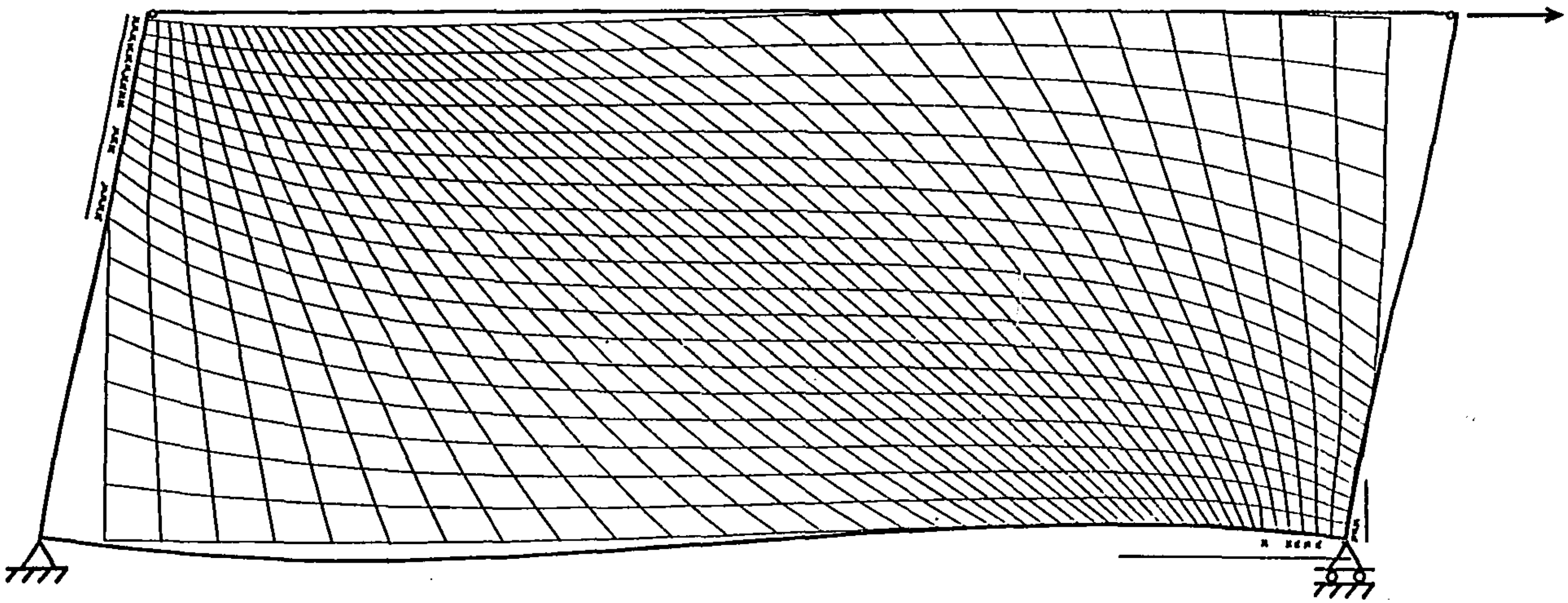

—— connection normal to boundary

xxxxxxx connection tangent to boundary

Figure 16.17: Deflected Shape for the 1:2.5 Model

the infill and the beam. This causes a greater distribution of the stresses which, would tend to increase the stiffness response of the structure. However, the previously described factors are predominant, giving a more flexible infilled frame with increasing length-to-height ratio. In terms of the normalized values, the length of contact between the infill and the beam was 0.22 times the length of the beam, L, for the 1:1.5 analysis, which is slightly greater than the 0.18L and 0.20L obtained for the 1:2 and 1:2.5 analyses, respectively. The length of contact between the infill and the right column was also greater for the 1:1.5 model than for the other two models. While the lengths of contact between the infill and the left column were approximately the same for the 1:1.5 and 1:2 models, they were, unexpectedly, less than that for the 1:2.5 model. Although in general the lengths of contact were proportionately greater for the 1:1.5 analysis than for the 1:2 and 1:2.5 analyses, the lengths of contact for the 1:2 model were not found to be proportionately greater than that of the 1:2.5 model. In fact, the proportionate lengths of contact did not vary significantly between one and the other. This may have resulted because the analyses did not reach a unique equilibrium condition; therefore, an exact comparison was not possible.

A comparison of the frame-member moments in the infilled frames of varying aspect ratios are presented in Fig. 16.18. It is evident that the distribution of the moments in the frame members were dominated by the decrease in frame stiffness due to the increased length-to-height ratio, causing the moments to decrease as a result of the smaller proportion of external lateral load carried by the frame.

Contour diagrams of the vertical, shear, maximum principal and minimum principal stresses are shown for the analyses with varying aspect ratios in Figs. 16.19, 16.20, 16.21, and 16.22, respectively. Away from regions of contact with the frame, the stress distributions in the infills for each analysis were similar, but with the magnitudes of the stresses greatest for the 1:1.5 model, and those for the 1:2 model greater than those for the 1:2.5 model. The values of the stresses near the centres of the infills are shown and compared in Table 16.6. Even though the frame for the 1:1.5 model was stiffer than those for the other models, which meant that the infill carried a smaller horizontal load than in the other cases, the infill stresses were greatest for that model mainly because of the infill's diagonal force being greater, as a result of its greater inclination.

16.4 Infilled Frames vs. Bare Frames

To estimate the lateral stiffening effect of the representative infill, an additional lateral load analysis, of the structural frame without infills, was performed. The standard moment-resisting frame was analysed for a lateral load of 130 kN, Fig. 16.23. The resulting deflected shape of the bare frame is shown in Fig. 16.24 with an interstorey drift of 6.7890 mm. The shearing stiffness of the standard storey-height module with the infill was, therefore, 4.8 times that of the bare frame. Although, the stiffening effect of the infill on the storey-height module was not as great as that of the precast concrete cladding panel, which was 35 times that of the bare frame (Chapter 5), it is still significant. It is of interest to mention that in the studies performed by Stafford Smith (1966), the effect of a fully infilled

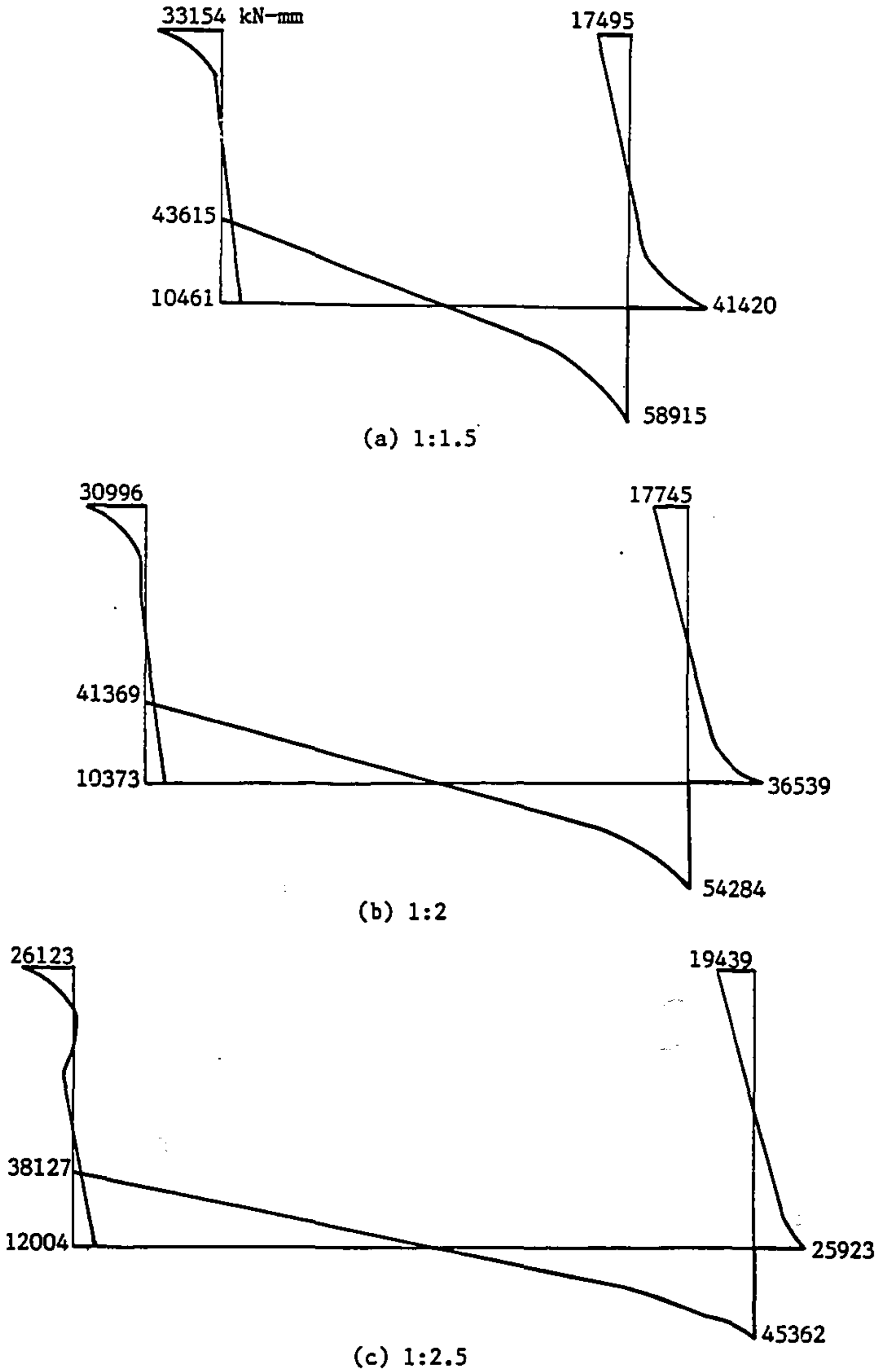

Figure 16.18: Frame-Member Moments for Models with Varying Aspect Ratio

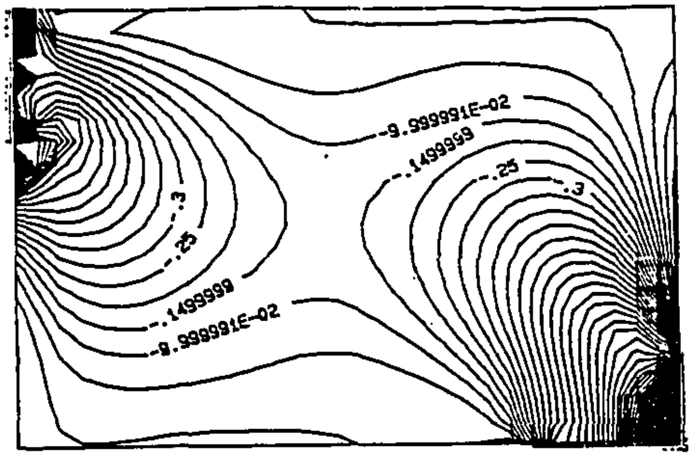

(a) 1:1.5

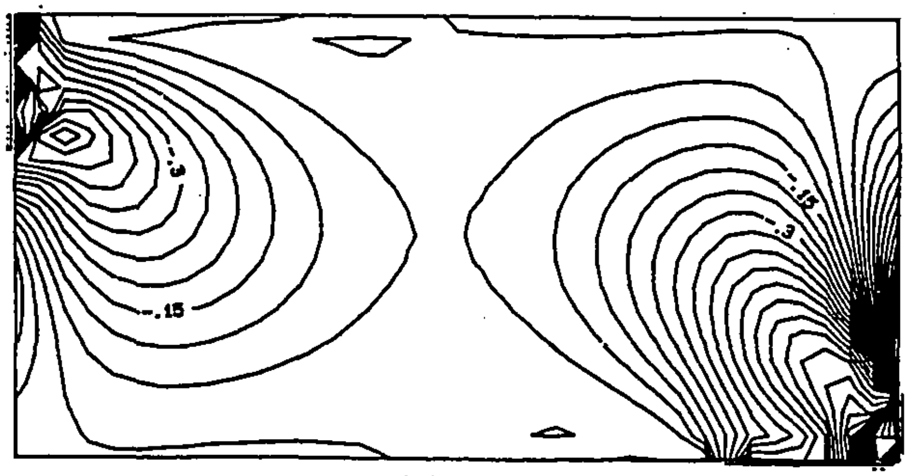

(b) 1:2

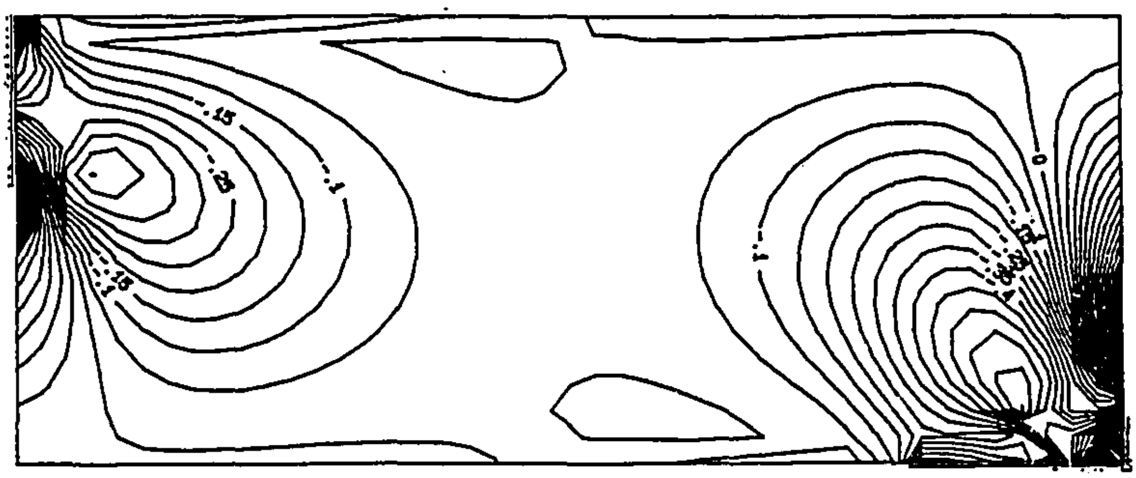

(c) 1:2.5

All stresses in MPa

Figure 16.19: Vertical Stresses for Models with Varying Aspect Ratio

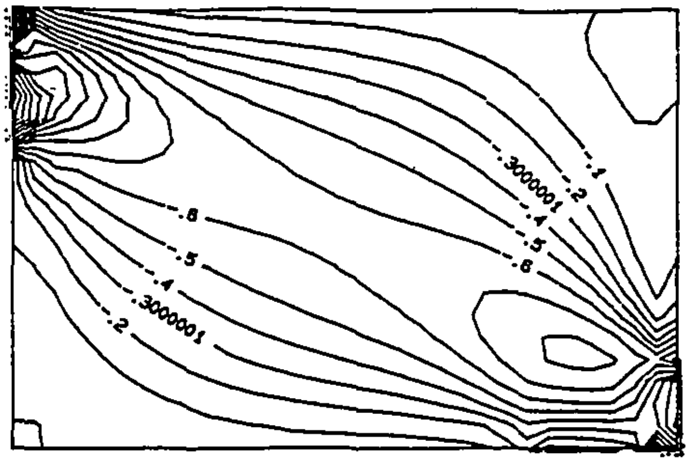

(a) 1:1.5

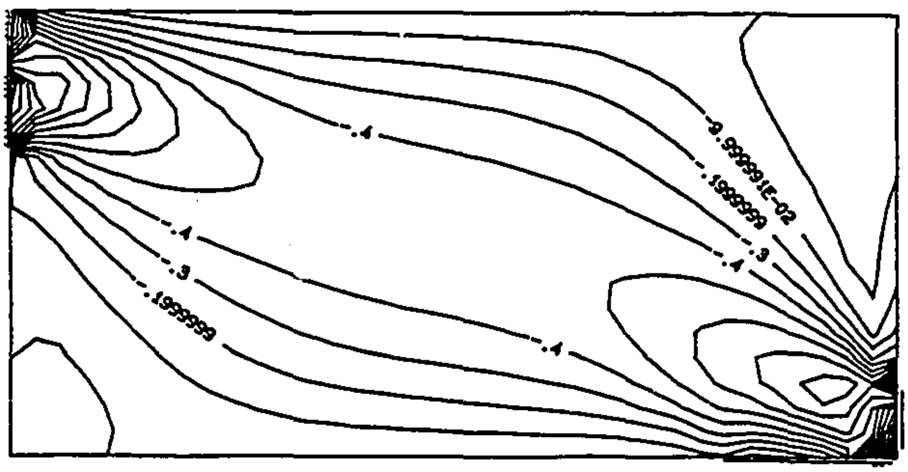

(b) 1:2

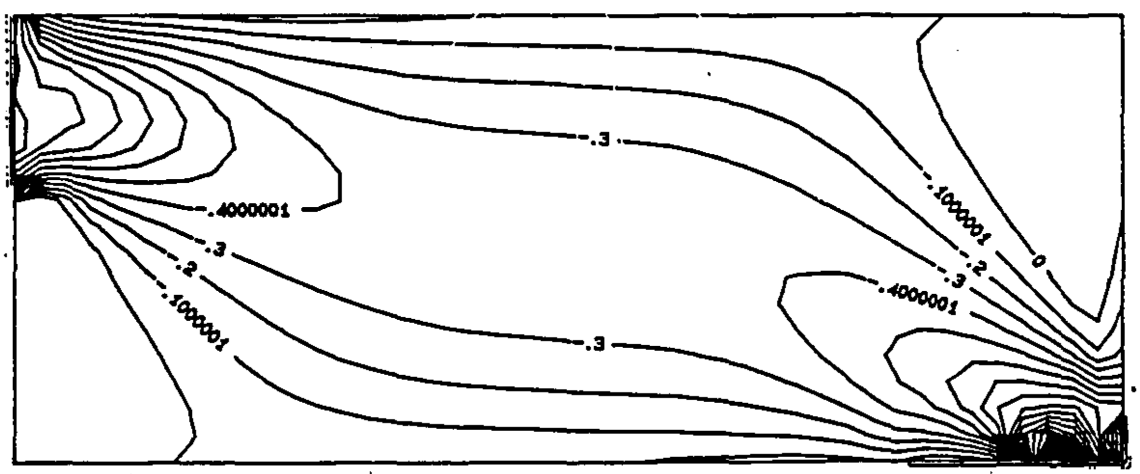

(c) 1:2.5

All stresses in MPa

Figure 16.20: Shear Stresses for Models with Varying Aspect Ratio

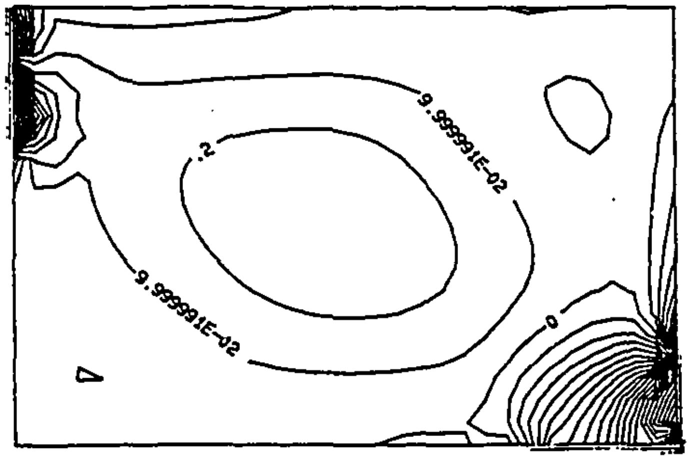

(a) 1:1.5

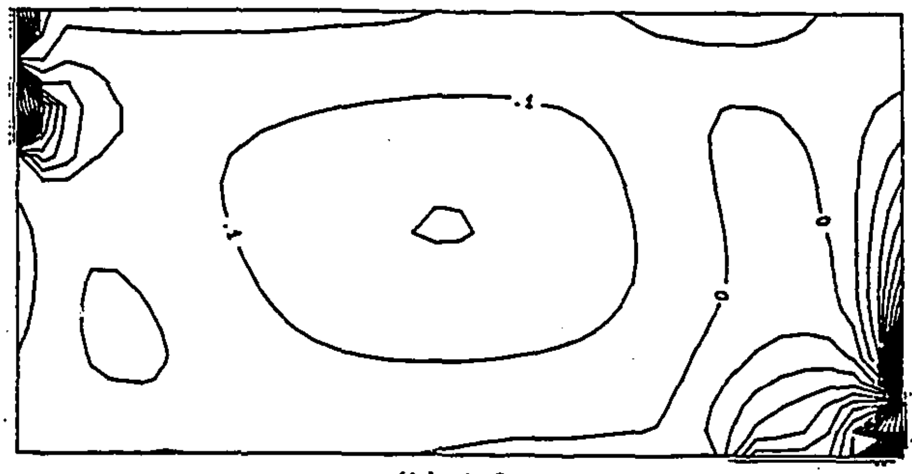

(b) 1:2

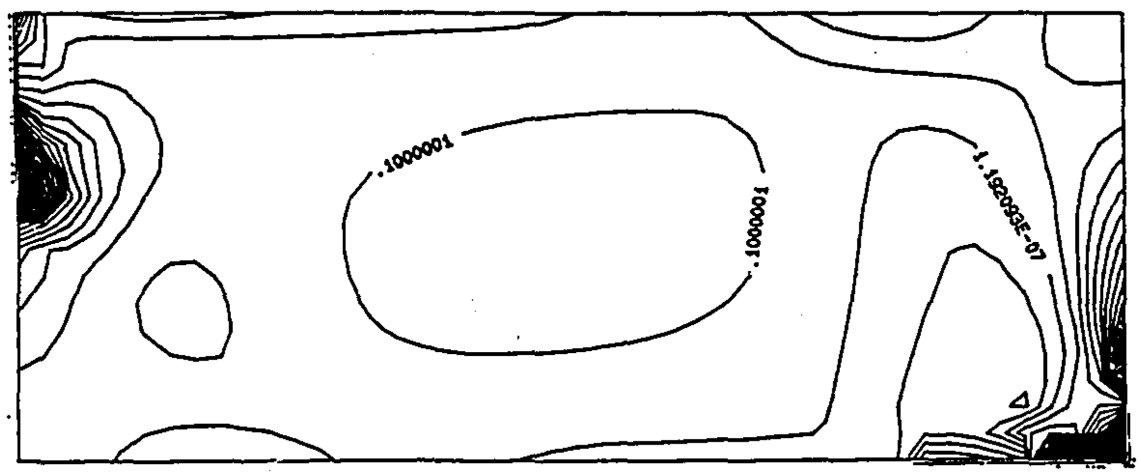

(c) 1:2.5

All stresses in MPa

Figure 16.21: Maximum Principal Stresses for Models with Varying Aspect Ratio

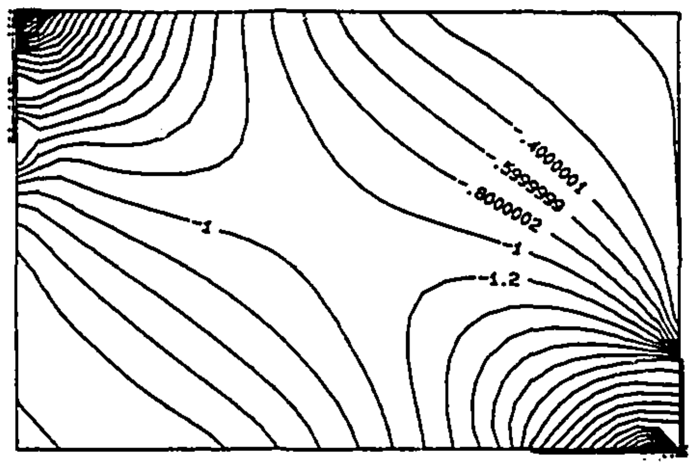

(a) 1:1.5

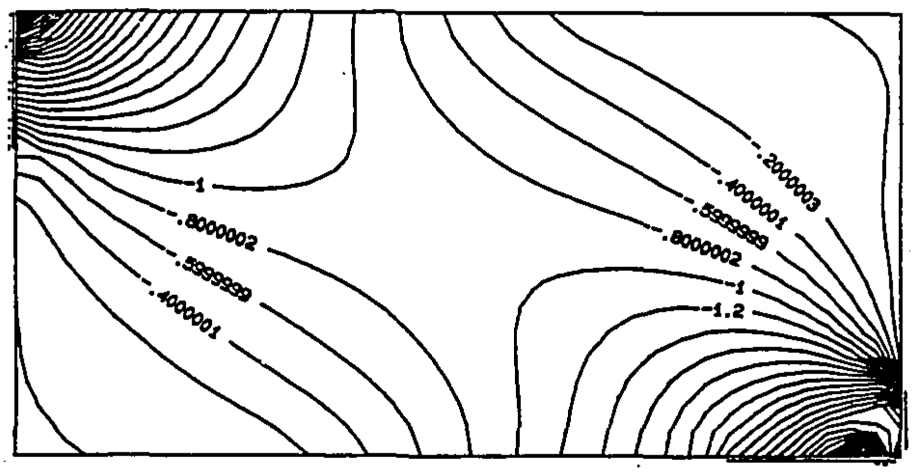

(b) 1:2

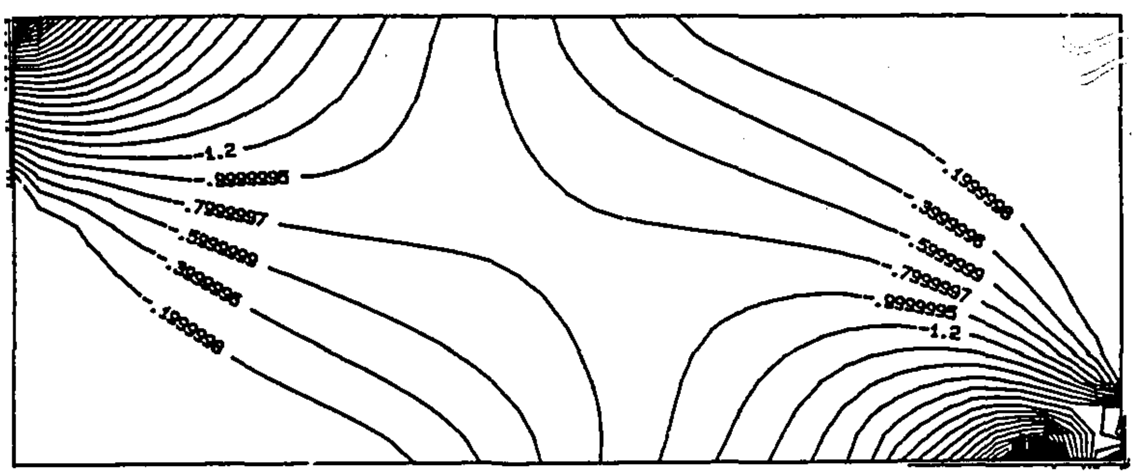

(c) 1:2.5

All stresses in MPa

Figure 16.22: Minimum Principal Stresses for Models with Varying Aspect Ratio

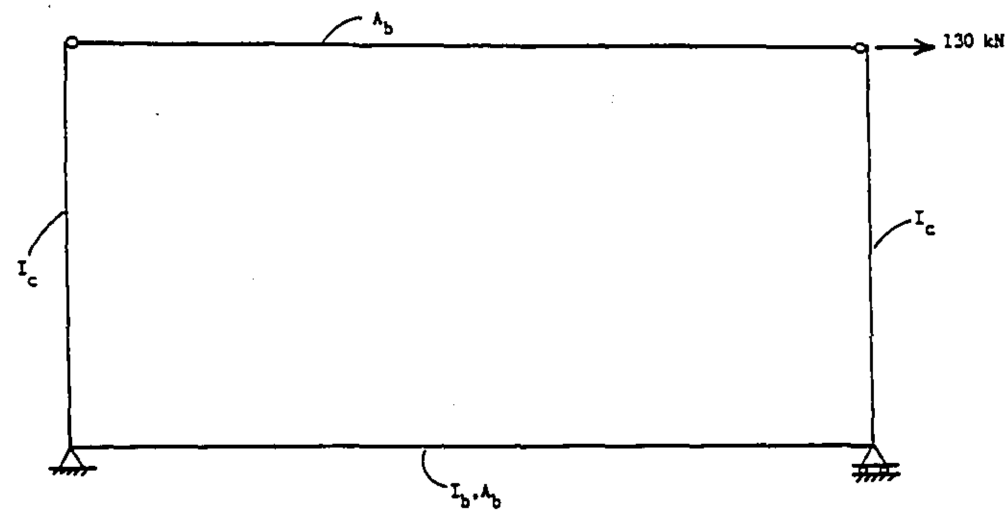

Figure 16.23: Mathematical Model for the Standard Moment-Resisting Frame

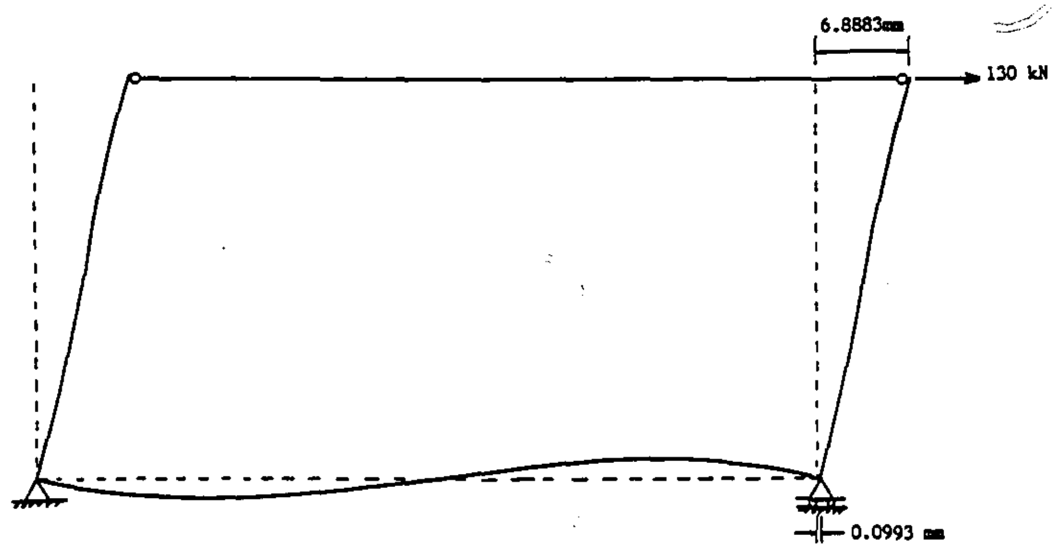

Figure 16.24: Deflected Shape for the Standard Moment-Resisting Frame

frame was to increase the stiffness of the bare frame by as much as 200 to 300 times. As for the fully infilled frame, the stiffening effect of the infill with a gap at the top can be attributed to its action as a diagonal strut in bracing. The regions of contact between the infill and the frame when laterally loaded differ, however, for the two cases. For the fully infilled frame, the regions of contact are adjacent to both the columns and beams at the ends of the compression diagonal, while for the infilled frame with the gap, the regions of contact are adjacent to only the column at the upper end of the compression diagonal and to the column and beam at the lower end. Therefore, in the fully infilled frame the upper compressive corner of the infill is more closely contained, because of the biaxial compressive state of stress, and consequently less strained. Also, while the stiffening action of the fully infilled frame can be reasonably approximated by just one diagonal bracing strut from corner to corner, along the compressive path; the stiffening action of the infilled frame with the gap, is more comparable to the strut model in Fig. 18.11, which allows for greater deformations of the frame. The models shown in Figs. 18.3 and 18.9 provide, however, a crude representation. The above models will be described in greater detail in Chapter 18.

The stiffnesses of the infilled frames analysed in the previous sections are compared with the stiffnesses of their corresponding bare frames in Table 16.7. The increase in stiffness due to the infill was of the same order for all cases. The stiffnesses of the infilled frames were from 3.6 to 7.2 times that of their corresponding bare frames. The effect of the stiffness of the infill, also shown in Table 16.7 for each of the cases, is computed by subtracting the stiffness of the bare frame from the stiffness of the infilled frame, since these act in parallel. The greatest variation occurred with the variation of the aspect ratio, as was determined in Section 16.3. The effect of the stiffness of the infill for the 1:2.5 model is 6 percent less than that of the standard model, and for the 1:1.5 model 13 percent greater. In terms of the effect of the stiffness of the infill, there was not a distinct pattern of variation for the other two parameters. When the stiffness of the beam was varied, the effect of the stiffness of the infill deviated by 1 to 2 percent from that of the infill in the standard model, which leads to conclude that the effect of the beam stiffness does not significantly change the interactive behaviour between the infill and the frame. When the column stiffnesses were varied, the difference between the effect of the infill stiffness for the half-inertia column model and that of the standard model was negligible. For the double-inertia column model, it was only 3 percent greater. This small effect was probably due to the increase in contact lengths which were indicated in the analysis.

The frame-member moments for the bare frames are the same for each model, since the columns carry all the external load, Fig. 16.25. Comparing these with those of the standard infilled model, Fig. 16.25, it can be concluded that the effect of the infill is to reduce the moments in the frame members by approximately 70 percent and more. Deviations of similar magnitudes were also obtained for the other cases.

Analysis	Vertical Stress		Shear Stress		Max. Princ. Stress		Min. Princ. Stress	
	Stress (MPa)	%Dev. from Stand.	Stress (MPa)	%Dev. from Stand.	Stress (MPa)	%Dev. from Stand.	Stress (MPa)	%Dev. from Stand.
1:1.5	-.142	+184%	-.615	+31%	.272	+37%	-1.054	+13%
1:2	-.050	—	-.468	—	.199	—	-.929	—
1:2.5	-.012	-76%	-.382	-18%	.166	-17%	-.831	-11%

Table 16.6: Stresses Near Centre of Infill (Varying Aspect Ratio Analyses)

Analysis Type	Stiffness of Infilled Fr. (kN/mm)	Stiffness of Bare Fr. (kN/mm)	$\frac{\text{Stiff. Inf. Fr.}}{\text{Stiff. Bare Fr.}}$	Stiff. Inf. Fr. - Stiff. Bare Fr. (kN/mm)
STANDARD	91.30	19.15	4.8	72.15
1:1.5	104.28	22.70	4.6	81.58
1:2.5	84.70	16.57	5.1	68.13
$1/2I_b$	84.80	11.78	7.2	73.02
$2I_b$	101.35	27.87	3.6	73.48
$1/2I_c$	86.88	13.93	6.2	72.95
$2I_c$	97.82	23.56	4.2	74.26

Table 16.7: Comparison of Stiffness Response Between Infilled Frames and Corresponding Bare Frames

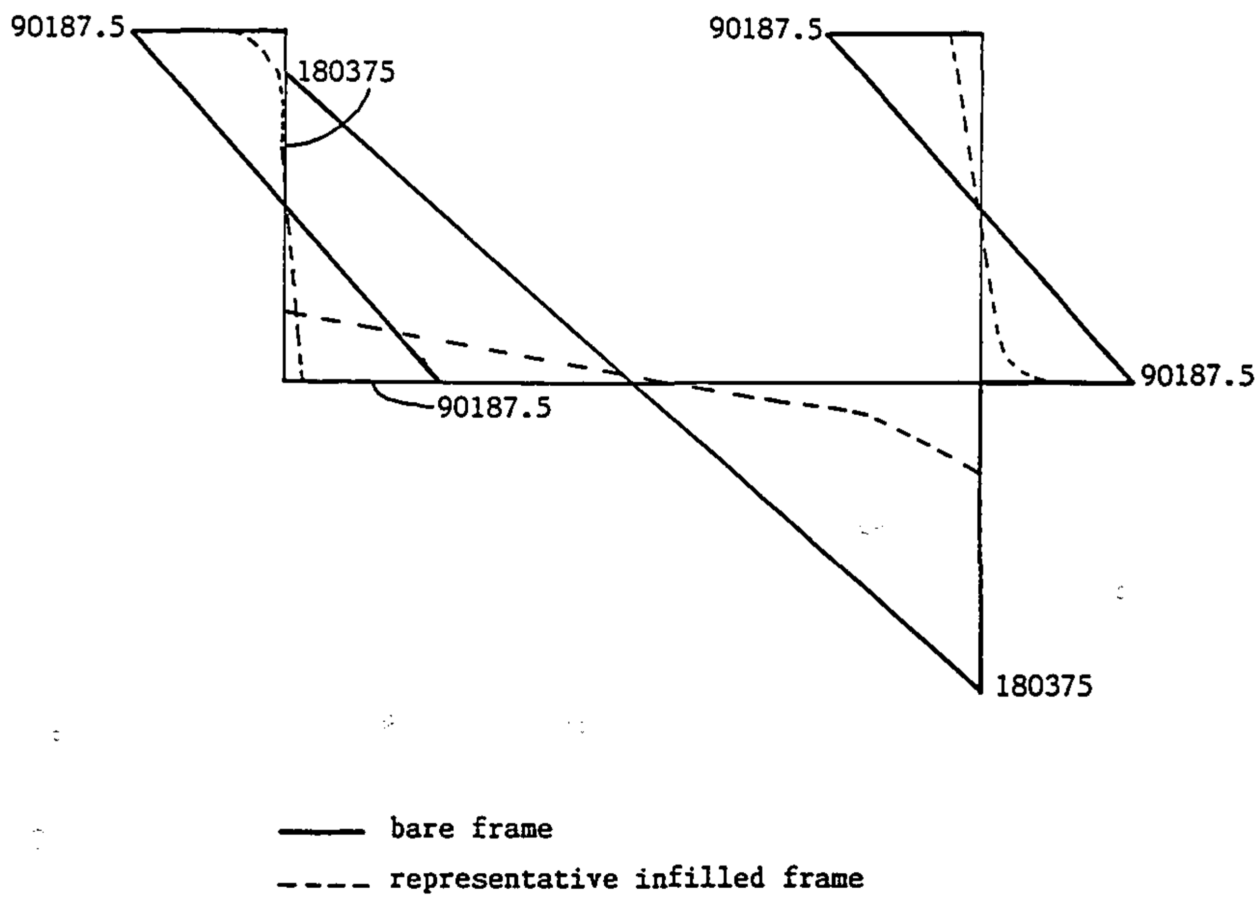

Figure 16.25: Frame-Member Moments for Bare Moment-Resisting Frame

16.5 Summary of Results

The parametric study of the single-storey module was carried out using the analytical technique developed. The parameters investigated included: (i) the beam stiffness, (ii) the column stiffnesses, and (iii) the aspect ratio of the infilled frames. In addition, analyses of the moment-resisting frames without infills were performed to determine the magnitude of the stiffening effect of an infill with a 25-mm gap at the top. It should be noted that exact comparisons of the results were not possible because the discrete method of analysis was inherently incapable of producing a unique solution for the continuously variable length of contact problem. Nevertheless, a good understanding of the behaviour of the infilled frame was obtained.

Varying the beam stiffness by a factor of 0.5 or 2 produced a difference in the calculated stiffness response of the infilled frame of approximately ± 10 percent. The lengths of contact, however, between the infill and the frame were not significantly affected by the change in beam stiffness. The difference in the calculated stiffness response of the infilled frame as a result of varying the beam stiffness, was due to the decrease or increase in the frame's flexibility. The length of contact between the infill and the lower beam was approximately 0.2L compared with 0.5L for a fully infilled frame.

When the column stiffnesses were varied by a factor of 0.5 and 2, the difference in the infilled frame's stiffness response was of +5 and -7 percent, respectively. A significant increase in the length of contact against the left column was observed when the stiffnesses of the columns were doubled. Although part of the increase in the infilled frame's stiffness response, for the double-inertia column model, was due to the increase in the frame's stiffness, it is believed that part of the increase was also due to the more broadly distributed interaction between the infill and the frame.

Varying the aspect ratio of the infilled frame from 1:1.5 to 1:2, and to 1:2.5, resulted in successive reductions of approximately 10 percent in the infilled frames' calculated stiffness responses. The greater the length-to-height ratio, the more flexible the infilled frame. In general, normalized values of the contact lengths were proportionately greater for the 1:1.5 analyses than for the other cases, but the normalized values of the contact lengths for the 1:2 model were not significantly different from those of 1:2.5 model.

The vertical, shear, tensile, and compressive stresses were maximum near the top-left corner of the single-storey module. This is different from the fully infilled frames previously studied (Stafford Smith 1967) in which the maximum shear stress and maximum tensile stress occurred at the centre of the infill.

The stiffnesses of the representative infilled frames with a gap at the top were 3.6 to 7.2 times greater than those of their corresponding bare moment-resisting frames. The effect of the infill on the frame-member moments was to reduce them by approximately 70 percent or more.

CHAPTER 17

RESULTING STRESSES IN INFILLS VS. STRENGTH OF INFILLS

It was deduced in the previous chapter that non-loadbearing infill walls attract significant bracing loads. Therefore, in this chapter the walls are to be checked for possible excessive stress due to the interaction forces. Three potential modes of failure for plain hollow concrete block walls subjected to in-plane lateral loads are described, and the estimated strengths of the three modes of failure for the previously analysed infilled frames are examined. On the basis of existing theories for the failure of masonry as a composite anisotropic material, the calculated strengths of the infills are compared with the resulting analytical stresses, and predicted failure loads are compared with existing experimental evidence.

17.1 Failure Criteria for Blockwork Infills

The possible modes of failure of an infill subjected to in-plane lateral loads include shear failure along the critical bed and head joints, tension failure through the block, mortar and grout (Hamid and Drysdale 1981), and crushing of a corner of the infill against a column (Stafford Smith 1966). It has been shown experimentally that the shear of in-plane laterally loaded infills is a very important failure criterion, particularly for plain hollow concrete block walls.

17.1.1 Shear Strength

To study the shear strength of masonry, experimental tests on masonry wall models and full-scale walls, in particular plain hollow concrete block walls, subject to in-plane forces have demonstrated that failure is characterized by a step-like diagonal cracking through the bed and head joints due to debonding between the blocks and the mortar. This is liable to occur especially when the joints are subjected to low levels of transverse compression (Simms 1964, Scrivener 1969, Fattal 1977, Drysdale et al. 1983, Woodward and Rankin 1985). Tests on masonry assemblages and prisms under combined shear and compression loading have also indicated shear-slip failure of the joints at low normal compressive stresses (Hamid et al. 1979, Hamid and Drysdale 1980a, Hamid and Drysdale 1980b, Atkinson et al. 1989).

Experiments have been performed elsewhere to study the interface conditions between an infilled concrete block wall and its surrounding steel frame (Pook and Dawe 1986). They also studied the effect of a 20-mm gap between the wall and the roof beam. Cracks occurred along the horizontal joints, and there was slight evidence of diagonal cracking for these specimens. In another study, reverse cyclic in-plane shear tests were performed on masonry-infilled steel frames with and without a gap at the top. The plain concrete blockwork infill with a 2 in. (50.8 mm) gap between the top of the wall and frame developed cracks which propagated in a step-wise fashion through the mortar joints.

The failure load of the infill for the above described shear mode of failure is related to the simultaneous combination of shear and compressive stresses induced at all positions in the infill, as a result of the frame leaning on it when the structure is subjected to the external lateral loading. It has been shown experimentally that, it most cases, Coulomb's theory of internal friction can reasonably predict the joint shear strength of masonry walls (Mayes and Clough 1975, Hegemier et al. 1978, Hamid et al. 1979, Hamid and Drysdale 1981, Drysdale et al. 1983, Woodward 1984, Wan Qinglin and Yi Wenzong 1986, Pook et al. 1986, Essawy and Drysdale 1986, Atkinson et al. 1989).

Coulomb's theory of internal friction can be expressed as

$$\tau = \tau_o + \mu\sigma_n \tag{17.1}$$

where τ = shear bond strength on the mortar bed joint,
τ_o = pure shear bond strength of the bed joint when no normal compressive stress is present,
μ = coefficient of friction between the mortar and the masonry units, and
σ_n = normal compressive stress on the mortar joints at failure.

17.1.2 Tensile Capacity

Failure criteria for the tensile strength of ungrouted and grouted unreinforced concrete masonry have been developed by Drysdale and Hamid (1984). These criteria account for the variation in strength due to the anisotropic nature of masonry, and have been shown to compare well with experimental results from splitting tests of ungrouted and grouted masonry disks. The diagonal tensile strength is described as a function of the strengths normal and parallel to the bed joints, which in turn are a function of the strength and geometric characteristics of the block, mortar and grout. Two possible failure modes were considered in the development of the failure criteria for diagonal cracking. For failure mode I, which is splitting failure along a plane passing through the head joints and the blocks' face shells, the strength for <u>ungrouted</u> masonry is given as

$$f_{td} = \frac{2}{3}\left[\left(\frac{1}{2}\eta_{vm} + \eta_h\right)\sigma_{tbm} + \frac{1}{2}\eta_{vb}\sigma_{tbl}\right] \tag{17.2}$$

where f_{td} = diagonal tensile strength of masonry,
η_{vm} = ratio of mortared area of head joint to gross area,
η_h = net-to-gross area ratio of block,
σ_{tbm} = tensile bond strength of mortar,
η_{vb} = net-to-gross area ratio of block in a vertical cross section crossing face shells just beside intermediate web, and
σ_{tbl} = splitting tensile strength of block.

For failure mode II, which for ungrouted masonry occurs at the block-mortar interfaces by tensile bond failure along the head joints and shear bond failure along the bed joints, the strength (ungrouted) is given as

$$f_{td} = \frac{2}{3}\left[(\eta_{vm} + \eta_h)\,\sigma_{tbm} + \left(\frac{a}{b}\right)\eta_h \tau\right] \tag{17.3}$$

where $2a$ = nominal length of block,
b = nominal height of block, and
τ = bond shear strength of mortar bed joints.

The minimum of the strengths calculated from the above two equations, 17.2 and 17.3, governs.

17.1.3 Compressive Strength

For most practical ranges of masonry unit and mortar strengths, the previously described 'stepping' shear and diagonal cracking failure modes will normally control. Therefore, the compressive failure load will be estimated very roughly by comparing the maximum compressive stress with the ultimate compressive strength of the masonry. It is a crude means of determining the compressive failure load, because the ultimate compressive strength of masonry varies with direction due to its anisotropic nature.

The ultimate compressive strength of masonry, denoted as f'_m, is tabulated in the Canadian Standard on "Masonry Design for Buildings" (1984). For hollow concrete blockwork, the values reported in the most recent edition of this design standard, (1984), are based on a mortar-bedded area instead of a net area. The mortar-bedded area is defined as the horizontal area of mortar in a bed joint in full contact with both the masonry unit above and the masonry unit below, and includes the horizontal area of the voids in solid units and grouted voids in hollow units. As explained by Maurenbrecher (1986), since in nearly all cases mortar is laid on the face shells of the block, the use of the mortar-bedded area is more conservative and, therefore, more logical because it is often considerably smaller than the net area of the block. As a result, the ultimate axial load capacity for face-shell bedded blockwork is significantly reduced. The ultimate compressive strength, f'_m, for concrete blockwork, as given in the most recent edition of the Canadian standard on "Masonry Design for Buildings" (1984), is presented in Table 17.1.

Compressive strength of block, MPa (net area)*	Ultimate compressive strength of concrete block masonry			
	Types M and S mortar		Type N mortar	
	Hollow	Solid and grouted	Hollow	Solid and grouted
40 plus	22	17	14	10.5
30	17.5	13.5	12	9
20	13	10	10	7.5
15	9.8	7.5	8	6
10	6.5	5	6	4.5

**Linear interpolation is permitted.*

Note: *Requirements for concrete block masonry units are included in CSA Standards A165.1-M and A165.3-M.*

Table 17.1: CSA Code Values of f'_m for Concrete Block Masonry (Masonry Design for Buildings 1984)

17.2 Checking Strengths of the Representative Infills Against Analysed Lateral Load Stresses

17.2.1 Checking Shear Strength of Infills Against Shear Failure

To calculate the masonry shear strength, Eq. 17.1, of the representative infills, the coefficient of friction between the mortar and masonry units, and the pure bond shear strength of the bed joints, when no compressive normal stress is present, are required.

In a paper on the shear strength of concrete masonry joints (Hamid et al. 1979), the following equation was deduced from experimental tests on ungrouted masonry (6 in. (150-mm) blocks with type S mortar)

$$\tau = 76 + 1.07\sigma_n \text{ (psi)}$$

$$\text{or} \quad \tau = 0.524 + 1.07\sigma_n \text{ (MPa)} \tag{17.4}$$

Therefore, referring to the expression reported in the Canadian Standard on "Masonry Design for Buildings" (1984), that is,

$$v = v_m + 0.3f_{cs} \tag{17.5}$$

where $v \quad = \tau \quad$ = shear bond strength of mortar bed joint,
$v_m \quad = \tau_o \quad$ = pure shear bond strength of the bed joint when no normal compressive stress is present,
$f_{cs} \quad = \sigma_n \quad$ = normal compressive stress on the mortar joints at failure,

and comparing it with Eq. 17.4 for the ungrouted specimens under precompression between 0 - 200 psi (0 - 1.4 MPa), indicates that a safety factor ranging from 2 to 3 is applied.

In another study by Pook et al. (1986), it was found experimentally that the initial ultimate shear strength of masonry joints subjected to compressive stress was

$$\tau = 753 + 0.7\sigma_n \text{ (kPa)} \tag{17.6}$$

and for specimens subjected to cyclic loads, the ultimate shear strength was

$$\tau = 430 + 0.7\sigma_n \text{ (kPa)} \tag{17.7}$$

The authors also mentioned that the expression stated in the 1978 Canadian Standard on "Masonry Design and Construction for Buildings", which is also repeated in the most recent edition of the Canadian Standard on "Masonry Design for Buildings" (1984), Eq. 17.5, incorporates a safety factor of 3 to 4. The results from this study do not differ significantly from other studies (Hamid et al. 1979, Arya and Hegemier 1982).

On the basis of the experimental results reported above, a safety factor of 2 was used in this study, and was applied to the values of the coefficient of friction and the pure shear bond strength reported in the Canadian Standard "Masonry Design for Buildings" (1984). The Code suggests Eq. 17.5 for the design of shear walls with v_m, the pure shear bond strength, equal to 0.23 MPa. Therefore, the ultimate shear strength in this study was taken as

$$\tau = 0.46 + 0.6\sigma_n \text{ (MPa)} \tag{17.8}$$

To check the shear stresses in the representative infills analysed in Chapter 16, the shear and vertical compressive stresses at each node of each element in the infills were extracted. These were entered in a Lotus (1986) spreadsheet, and the joint shear strength was calculated using Eq. 17.8 for each node. The shear stress at each node was then checked against the corresponding joint shear strength. Critical regions, that is where the shear stress exceeded the shear strength, for each of the infilled frames analysed in Chapter 16 were determined, Fig. 17.1. Then, from a drawing of the mesh with the arrangement of the blocks superimposed, the values for the shear strength and stress along the joints were obtained by interpolation. This is shown in Fig. 17.2 for the standard infilled frame analysis as an example. The average shear strength and stress over a block length was then found. From these, the loads to initiate joint shear failure were calculated for different critical joint locations, and a worst load was chosen for each analysis, Table 17.2.

17.2.2 Checking Tensile Strength of Infills Against Tensile Failure

The diagonal tensile strength was calculated using Eqs. 17.2 and 17.3. For the representative infills analysed, the following property values are appropriate:

$$\begin{aligned}
\eta_{vm} &= 1.0 \\
\eta_h &= 0.56 \text{ (Table 14.1)} \\
\eta_{vb} &= 0.61 \\
\sigma_{tbl} &= 1.9 \text{ MPa (Drysdale and Hamid 1982)} \\
\sigma_{tbm} &= 0.59 \text{ MPa (Drysdale and Hamid 1984)} \\
\frac{a}{b} &= 1
\end{aligned}$$

Substituting into Eqs. 17.2, and 17.3 respectively, and using $\tau = .46$ MPa for Eq. 17.3, the following diagonal tensile strengths are obtained

$$\begin{aligned}
\text{Failure Mode I:}\quad f_{td} &= \frac{2}{3}\left[\left(\frac{1}{2}(1.0) + 0.56\right)0.59 + \frac{1}{2}(0.61)(1.9)\right] \\
&= 0.80 \text{ MPa}
\end{aligned} \tag{17.9}$$

On the basis of the experimental results reported above, a safety factor of 2 was used in this study, and was applied to the values of the coefficient of friction and the pure shear bond strength reported in the Canadian Standard "Masonry Design for Buildings" (1984). The Code suggests Eq. 17.5 for the design of shear walls with v_m, the pure shear bond strength, equal to 0.23 MPa. Therefore, the ultimate shear strength in this study was taken as

$$\tau = 0.46 + 0.6\sigma_n \text{ (MPa)} \tag{17.8}$$

To check the shear stresses in the representative infills analysed in Chapter 16, the shear and vertical compressive stresses at each node of each element in the infills were extracted. These were entered in a Lotus (1986) spreadsheet, and the joint shear strength was calculated using Eq. 17.8 for each node. The shear stress at each node was then checked against the corresponding joint shear strength. Critical regions, that is where the shear stress exceeded the shear strength, for each of the infilled frames analysed in Chapter 16 were determined, Fig. 17.1. Then, from a drawing of the mesh with the arrangement of the blocks superimposed, the values for the shear strength and stress along the joints were obtained by interpolation. This is shown in Fig. 17.2 for the standard infilled frame analysis as an example. The average shear strength and stress over a block length was then found. From these, the loads to initiate joint shear failure were calculated for different critical joint locations, and a worst load was chosen for each analysis, Table 17.2.

17.2.2 Checking Tensile Strength of Infills Against Tensile Failure

The diagonal tensile strength was calculated using Eqs. 17.2 and 17.3. For the representative infills analysed, the following property values are appropriate:

$$\begin{aligned}
\eta_{vm} &= 1.0 \\
\eta_h &= 0.56 \text{ (Table 14.1)} \\
\eta_{vb} &= 0.61 \\
\sigma_{tbl} &= 1.9 \text{ MPa (Drysdale and Hamid 1982)} \\
\sigma_{tbm} &= 0.59 \text{ MPa (Drysdale and Hamid 1984)} \\
\frac{a}{b} &= 1
\end{aligned}$$

Substituting into Eqs. 17.2, and 17.3 respectively, and using $\tau = .46$ MPa for Eq. 17.3, the following diagonal tensile strengths are obtained

$$\text{Failure Mode I:} \quad f_{td} = \frac{2}{3}\left[\left(\frac{1}{2}(1.0) + 0.56\right)0.59 + \frac{1}{2}(0.61)(1.9)\right] = 0.80 \text{ MPa} \tag{17.9}$$

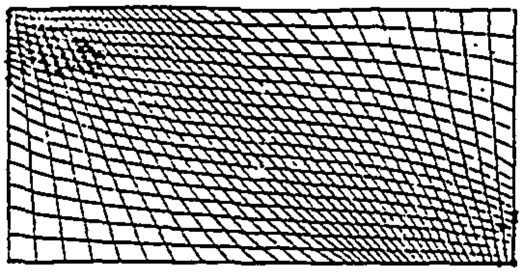

(a) standard

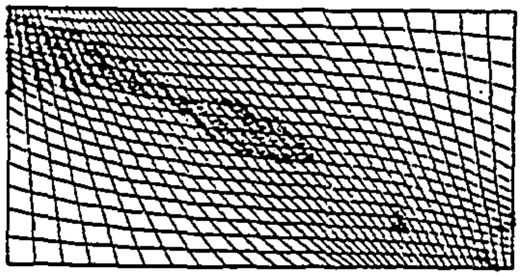

(b) $\frac{1}{2}I_b$

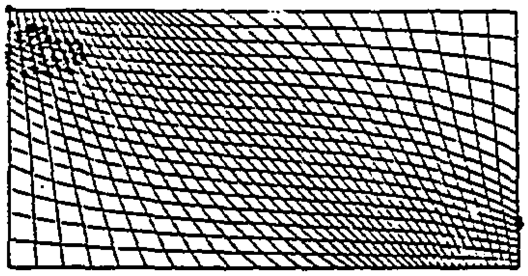

(c) $2I_b$

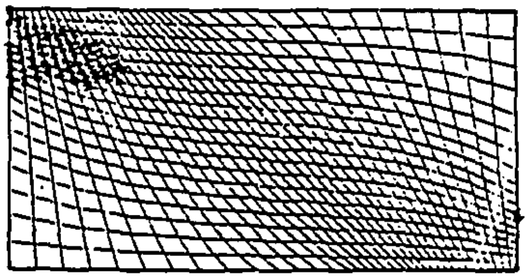

(d) $\frac{1}{2}I_c$

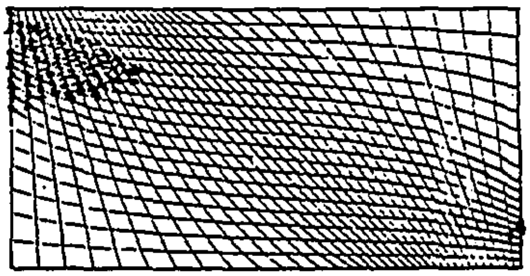

(e) $2I_c$

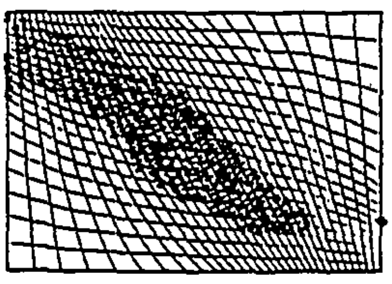

(f) 1:1.5

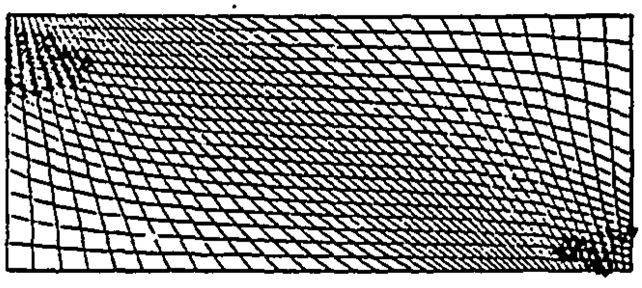

(g) 1:2.5

Note: shading indicates critical regions where shear stress exceeded shear strength

Figure 17.1: Regions Where Shear Stress Exceeded Shear Strength

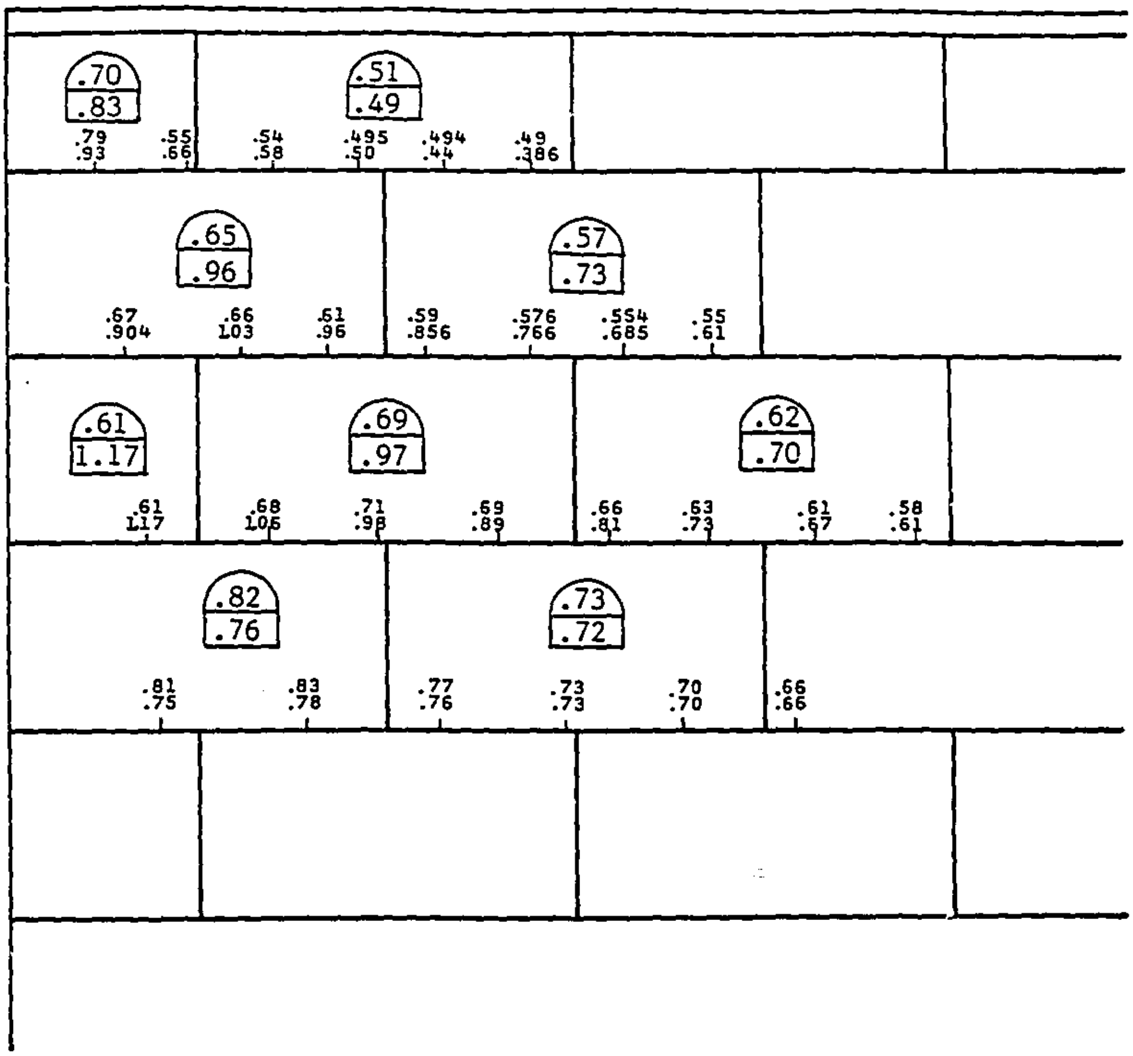

average shear strength over block length
average shear stress over block length

Figure 17.2: Average Shear Stresses and Strengths

ANALYSIS	SHEAR FAILURE			TENSILE FAILURE			COMPRESSIVE FAILURE		
	SHEAR STRENGTH (MPa)	SHEAR STRESS (MPa)	FAILURE LOAD (kN)	TENSILE STRENGTH (MPa)	TENSILE STRESS (MPa)	FAILURE LOAD (kN)	COMPRESSIVE STRENGTH (MPa)	COMPRESSIVE STRESS (MPa)	FAILURE LOAD (kN)
Standard	0.65	0.96	77.7	0.78	0.68	149	10	6.2	210
$1/2I_b$	0.64	1.04	69.5	0.78	1.0	101	10	7.1	183
$2I_b$	0.61	0.84	86.7	0.78	0.55	184	10	5.1	255
$1/2I_c$	0.64	0.99	73.8	0.78	0.73	139	10	6.3	206
$2I_c$	0.59	0.90	77.7	0.78	1.6	63	10	5.8	224
1:1.5	0.67	1.05	71.2	0.78	0.80	127	10	6.0	217
1:2.5	0.75	1.17	68.0	0.78	1.2	85	10	6.2	210

Table 17.2: Loads to Initiate Failure for Various Modes of Failure

$$\text{Failure Mode II:} \quad f_{td} = \frac{2}{3}[(1.0 + 0.56)0.59 + (1)(0.56)(0.46)]$$
$$= 0.78 \text{ MPa} \qquad (17.10)$$

For the representative examples studied, Eqs. 17.2 and 17.3 gave similar values. Although failure mode II (debonding failure), Eq. 17.3, is more critical than Mode I (splitting failure), Eq. 17.2, because of the variability of the properties of the materials involved, the tensile failure mode for the infills in this study could essentially have been I or II.

To determine the loads at which tension failure would occur in the representative infills, the diagonal tensile capacity calculated in Eq. 17.10 was checked against the maximum principal (tensile) stresses.

From the contour plots of the maximum principal stresses presented in Chapter 16, it was observed in all the analyses that high tensile stresses occurred near the boundaries. Away from the boundaries the tensile stresses decreased, to increase again slightly near the centre of the infill. At the boundaries very high tensile stresses, ranging from 2.2 to 3.8 MPa, occurred. These, however, were discarded for comparison purposes, since at the boundaries the concentrated applied loads would tend to cause areas of very high stress concentration. Adjacent to the boundaries, the tensile stresses were also high, but they decreased gradually as the distance from the boundary increased. Therefore, for comparison purposes, the stress at the first nodes in from a boundary was chosen as the maximum tensile stress in the infill. In all the analyses this occurred near the upper-left boundary. The resulting tension failure loads for each of the analyses are also recorded in Table 17.2.

17.2.3 Checking Compressive Strength of Infills Against Compressive Failure

To determine the ultimate compressive strength of masonry based on the Canadian Standard for "Masonry Design for Buildings" (1984), from which the relevant table for concrete block masonry is reproduced in Table 17.1, the compressive strength of a unit block based on its net area is required. Smith et al. (1979) reported a value for the net-area compressive strength for regular strength blocks, based on studies performed by the Portland Cement Association, of approximately 14 MPa. Therefore, the ultimate compressive strength for the representative hollow concrete block infills assumed in this study is approximately 10 MPa, Table 17.1.

To determine the loads at which compressive failure occurred in the representative infills, the 10 MPa ultimate compressive strength of the masonry was checked against the maximum compressive stresses in the infills.

It is evident from the contour plots presented in Chapter 16 that, as expected (Stafford Smith 1966), the maximum compressive stresses occurred along the boundaries of the compressive corners. Similarly to the values adopted for the maximum tensile stresses, the values of maximum compressive stresses at the first nodes in from the boundaries were used for the strength assessment, because of the high stress concentrations occurring on the boundaries. On this basis, the absolutely maximum compressive stress occurred just next to the upper-left boundary for all of the analyses. The resulting loads to cause compressive failure near the top compressive corner are shown in Table 17.2.

17.2.4 Summary of Results

Referring to Table 17.2, in all the analyses except one, a joint shear failure occurred, under a state of shear-compressive stress. The loads at which this occurred ranged between 68 kN and 87 kN. It should be noted that the effect of the infill weight, which was not included in the analyses, would have increased the shear strength by only two percent. The only case in which the infill did not fail due to a joint shear failure, was the double-inertia column analysis. In this case, the failure mode was a tension-shear debonding failure; that is, tensile bond failure along the head joints and shear bond failure along the bed joints. The failure load for the double-inertia column case was 63 kN. From the comparisons of ultimate strengths with the states of stress obtained from the analyses, in none of the cases could compressive failure have occurred, since the loads corresponding to this mode of failure were much greater than the debonding failure loads.

The conclusion that the shear debonding mode of failure would occur for all the cases of the representative infills is supported by experimental studies performed by other researchers on similar types of infilled frames. In a study in which cyclic in-plane shear tests were performed on a semi-confined steel frame with a concrete block infill, it was observed that the specimen with a two-inch (50-mm) gap at the top developed cracks which propagated in a step-wise pattern through mortar joints (Wolde-Tinsae and Raj 1986). In another study (Dawe and Yong 1985) in which the effects of interface conditions between a concrete blockwork infilled steel frame were studied, crack patterns in experimental tests of a frame with a 20-mm gap at the top of the infill showed that a great number of cracks occurred along the horizontal joints, with some diagonal cracking and a very slight suggestion of tensile splitting failure starting in the blocks' face shells.

Table 17.3 presents failure and cracking loads obtained in some experimental investigations of frames infilled with concrete blockwork masonry. Although the sizes of the specimens tested were not the same as the infilled frames analysed in this study, a comparison of the failure loads reported in Table 17.3 with those determined for the representative infills, Table 17.2, demonstrate that the latter are of realistic magnitude.

Tests have indicated that even after sustaining severe diagonal cracking damage, some masonry walls are capable of carrying increased lateral loading due to the redirection of the stress trajectories resulting in a multiple strut action of the infill (Scrivener 1969, Pook et al. 1986, Pook and Dawe 1986, Shing et al. 1987).

As a final note, it should be mentioned that although failure loads in masonry are, in most cases, obtained on the basis of a strength criterion, a serviceability criterion could also be determined on the basis of an allowable interstorey drift.

Source	Wall Type	Mortar	Failure Load (kN)	Crack Load (kN)
Simms (1964)	150-mm hollow clay block (square)	1 : 1 : 6*	127-167	
Fattal (1977)	200-mm hollow concrete block	Type S		
	h/L = 1		72.5-139.5	
	h/L = 2		77.5-97.1	
	h/L = 0.5		86.1-101.4	
Pook & Dawe (1986)	200-mm hollow concrete block (infilled frame with gap)	Type S		
	without col. ties			169
	with col. ties			200

* (cement : lime : sand) by volume

Table 17.3: Failure or Crack Loads for Hollow Block Specimens

CHAPTER 18

MODELLING THE INFILL IN THE OVERALL STRUCTURE ANALYSES

Having established that the non-loadbearing blockwork infills, as they are designed in practice, have a significant stiffening effect, it was necessary to develop simple techniques to model these in the analyses of the total structure. Several equivalent strut models were developed and evaluated on the basis of their accuracy in correctly representing the interactive behaviour of a moment-resisting frame and a masonry infill wall with a gap at the top.

18.1 Simple, Single-Diagonal Strut Model

In the simple, single-diagonal strut model, Fig. 18.1, the diagonal bracing strut is assigned a cross-sectional area to give a horizontal stiffness equivalent to the effect of the infill within the frame. To obtain the effect of the stiffness of the infill within the frame, the lateral stiffness of the bare moment-resisting frame was subtracted from the lateral stiffness of the corresponding infilled frame. The accuracy of this model, and the other models to follow, was checked by comparing the interstorey drifts and the frame-member moments obtained from the lateral load analyses of single-storey representations of the modelled frames, with those obtained from the detailed lateral load analyses of the single-storey representative infilled frames.

The horizontal stiffness of a single-diagonal braced frame, taking into account the axial deformations of the beam, is given as

$$k = \frac{1}{\left[\frac{L}{EA_b} + \frac{d^3}{L^2 E_d A_d}\right]} \tag{18.1}$$

where L = length of beam,
d = length of diagonal,
E = modulus of elasticity of frame members,
E_d = modulus of elasticity of diagonal (infill),
A_b = cross-sectional area of beam, and

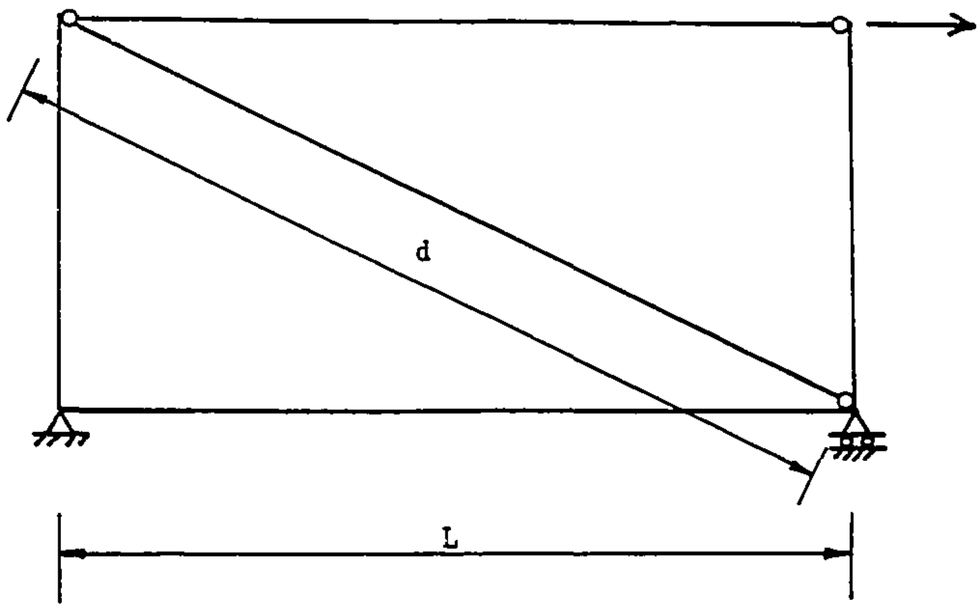

Figure 18.1: Simple, Single-Diagonal Strut Model

A_d = cross-sectional area of diagonal.

The stiffening effect of the infill was calculated for each of the case models analysed in Section 16.4 and the results are presented in Table 16.7. By equating the expression in Eq. 18.1 to the stiffness values for the effect of the infill reported in Table 16.7, and substituting the appropriate properties of the beam and the diagonal, the sectional area of the diagonal was obtained for each of the cases, Table 18.1.

As a check, a lateral load analysis was performed on the simple diagonal braced frame model for each representative infilled frame. The interstorey drifts are presented for each analysis in Table 18.1. The deviations from the detailed finite element analyses of the representative infilled frames are also recorded in Table 18.1. The interstorey drifts of the single-diagonal braced models agree very closely with those of the detailed analyses, having an error of approximately 1 percent due to rounding off the values of the diagonals' sectional areas.

The resulting frame-member moments are compared with those obtained from the detailed infilled frame analysis of the standard model in Fig. 18.2. The maximum moments in the left column, right column, and beam were grossly underestimated, by as much as 48 percent. Similarly large deviations, of up to -60 percent, occurred in the frame-member moments of the other models. The errors in the member moments were of this magnitude because the model does not account for the forces that the infill applies transversely to the frame members over their lengths of contact with the infill; hence the second action contributing to the distribution of the frame-member moments, which was described in Section 16.1, is neglected in this model.

Therefore, the single-diagonal strut model gives "correct" interstorey drifts, provided that a detailed finite element analysis of the infilled frame has been performed first to obtain the correct sectional area of the diagonal. It has the advantages of extreme simplicity in concept and in its use for analysis. It has a major disadvantage, however, in that it does not produce the correct frame-member moments.

18.2 Column-to-Column Strut Model

The more sophisticated column-to-column strut model, Fig. 18.3, consists of a diagonal bracing strut, extending from a point near the top of the left column, a distance m_1 from the top left corner, and ending near the bottom of the right column, a distance m_2 from the bottom right corner. By this arrangement, the horizontal component of the force in the strut acts transversely to the columns, causing them to bend similarly to those in the actual infilled frame.

The infilled frame's interstorey drift and the moments at the ends of the columns, resulting from a detailed finite element analysis of the infilled frame module, were used in combination with an energy analysis of the equivalent column-to-column frame model to obtain the values of the sectional area of the strut, and its locations m_1 and m_2 on the

Analysis	Area of Strut (mm^2)	Interstorey Drift from Detailed Anal. (mm)	Interstorey Drift from Strut Model (mm)	Deviation of Strut Model from Detailed Analysis
STANDARD	62670	1.4239	1.4406	1.2%
$1/2I_b$	63521	1.5330	1.5450	0.8%
$2I_b$	63972	1.2827	1.3028	1.6%
$1/2I_c$	63452	1.4963	1.5097	0.9%
$2I_c$	64737	1.3290	1.3474	1.4%
1:1.5	64970	1.2467	1.2597	1.0%
1:2.5	67538	1.5348	1.5546	1.3%

Table 18.1: Resulting Interstorey Drifts for Simple Diagonal Strut Model

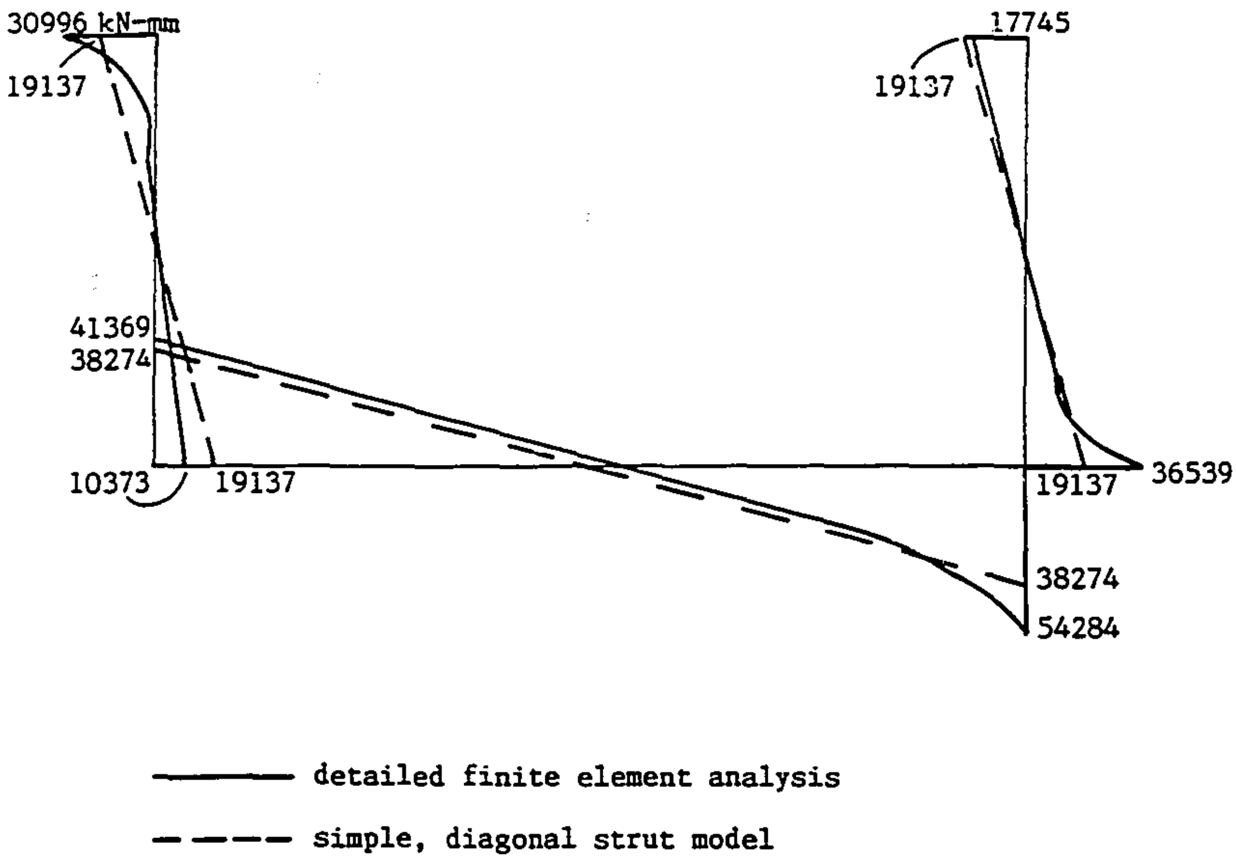

Figure 18.2: Frame-Member Moments for Simple Diagonal Braced Frame Model of the Standard Analysis

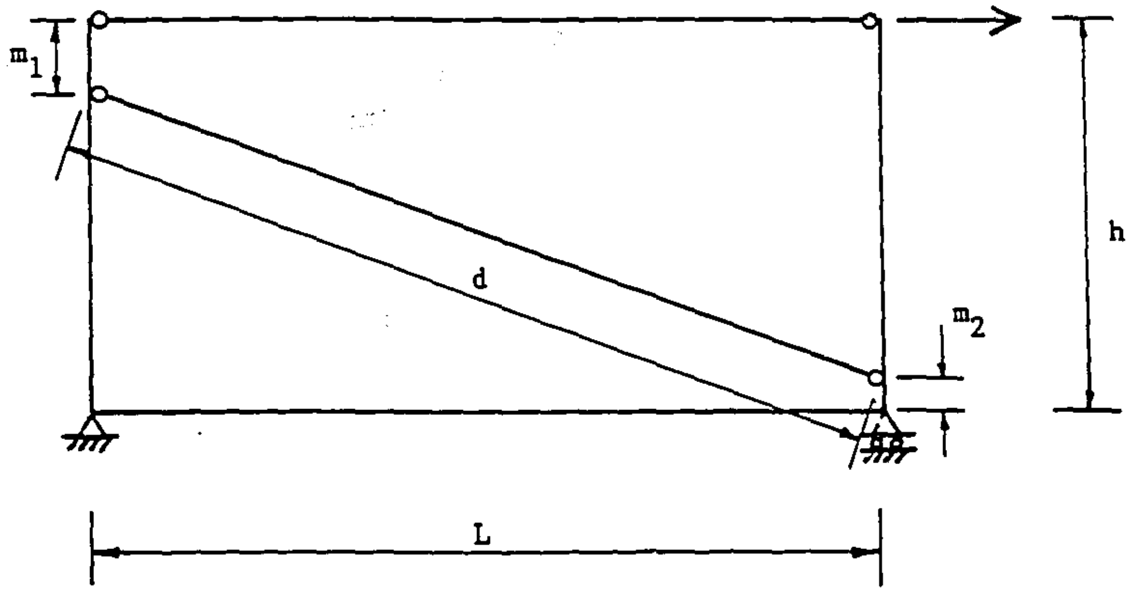

Figure 18.3: Column-to-Column Strut Model

columns. The energy analysis of the module, for a given lateral displacement, consisted of equating the strain energy of the braced frame model to the external work done. Bending in the columns and the beam, and axial deformations in the diagonal bracing strut and the beam all contribute to the internal strain energy of a single-storey representation of the modelled frame. The bending moment diagrams are shown for each of the columns and the beam in Figs. 18.4, 18.5, and 18.6, respectively. The bending moment diagrams for the left and right columns are presented as the superposition of the bending moment diagram due to racking of the frame, Figs. 18.4a and 18.5a, respectively, and of the bending moment diagram due to the horizontal component, P, of the force in the bracing strut, Figs. 18.4b and 18.5b, respectively. The resulting bending moment diagrams are shown for each of the columns in Figs. 18.4c and 18.5c. The bending moment diagram for the beam, Fig. 18.6, corresponds to that of a typical beam of a multi-storey structure bending in double curvature, with the moments at each end equal to the sum of the moments at the bottom and top of the corresponding connecting column.

Before the cross-sectional area of the bracing could be obtained from the energy analysis, five other unknowns had to be solved: the vertical distances, m_1 and m_2, of the ends of the strut from the corners, the values of the moments due to racking of the frame for each of the columns, x and y, and the force in the strut. Four equations can be written relating the unknowns to the moments at the ends of the columns (M_A, M_B, M_C, and M_D) resulting from the detailed finite element analyses of the infilled frames, Figs. 18.4 and 18.5,

$$\frac{Pm_1(h-m_1)^2}{h^2} + x = M_A \tag{18.2}$$

$$x - \frac{Pm_1^2(h-m_1)}{h^2} = M_B \tag{18.3}$$

$$\frac{Pm_2(h-m_2)^2}{h^2} + y = M_D \tag{18.4}$$

$$y - \frac{Pm_2^2(h-m_2)}{h^2} = M_C \tag{18.5}$$

The fifth equation represents the equilibrium of the horizontal forces acting on the free-body diagram of the strut model shown in Fig. 18.7, that is

$$P = Q - V_1 - V_2 \tag{18.6}$$

where Q = external lateral load,
P = horizontal component of the force in the strut,
V_1 = shear in left column between location of strut and bottom corner, and
V_2 = shear in right column between location of strut and top corner

V_1 and V_2 were calculated from the known moments in the columns.

Solving Eqs. 18.2 and 18.3 simultaneously, the horizontal component, P, of the force in the strut can be expressed in terms of m_1 as

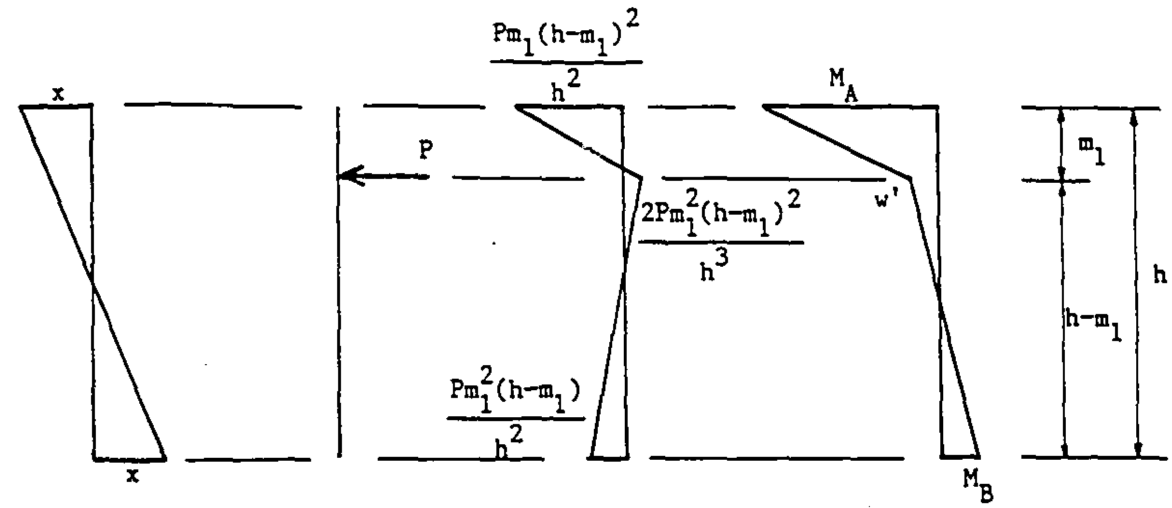

(a) First action (b) Second action (c) Resulting BMD

Figure 18.4: Resulting Bending Moment Diagram for Left Column

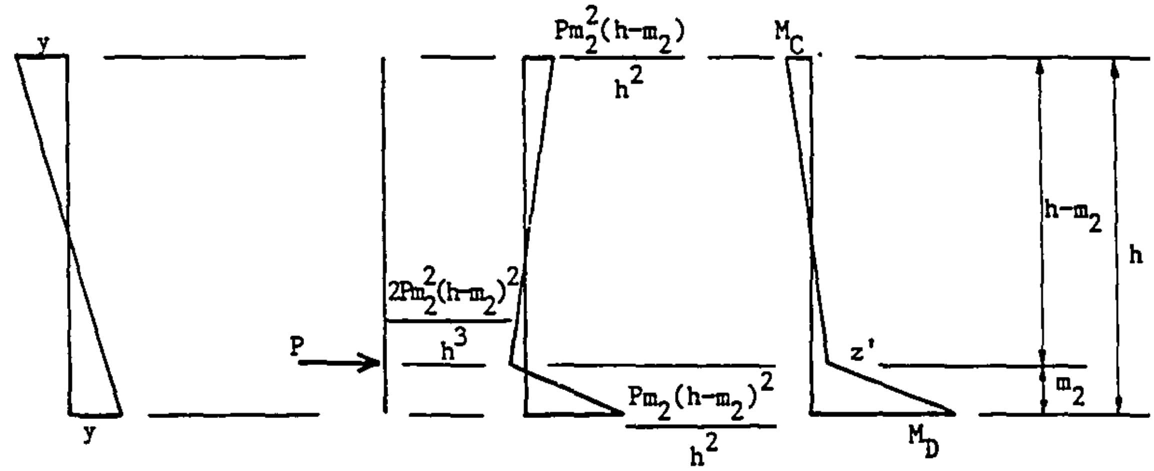

(a) First action (b) Second action (c) Resulting BMD

Figure 18.5: Resulting Bending Moment Diagram for Right Column

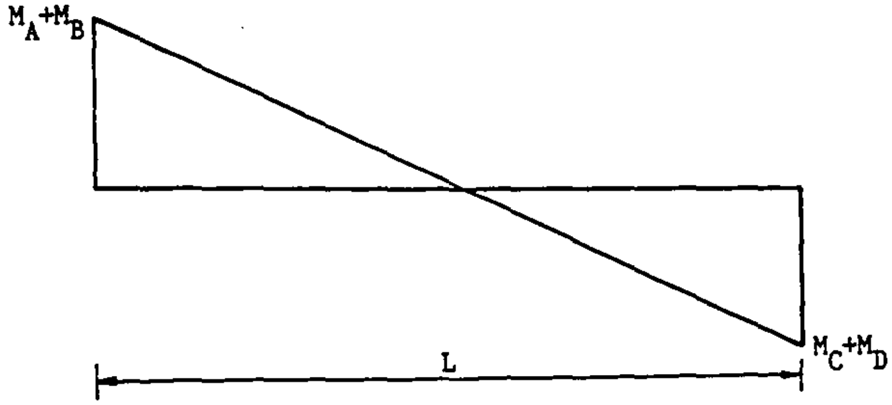

Figure 18.6: Bending Moment Diagram for Beam

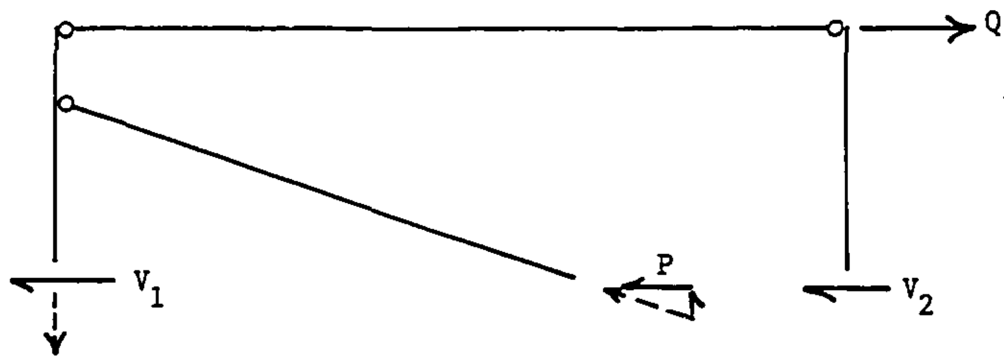

Figure 18.7: Free-Body Diagram of the Column-to-Column Strut Model

$$P = \frac{(M_A - M_B)h}{m_1(h - m_1)} \tag{18.7}$$

The shear, V_1, in the left column between the location of the strut and the bottom corner is given by

$$V_1 = \frac{w' + M_B}{(h - m_1)} \tag{18.8}$$

Using Eq. 18.7 and referring to Fig. 18.4 gives

$$w' = \frac{M_B h - (M_A + M_B)m_1}{h} \tag{18.9}$$

Substituting this into Eq. 18.8 yields

$$V_1 = \frac{2M_B h - (M_A + M_B)m_1}{h(h - m_1)} \tag{18.10}$$

Similarly, an expression for the shear, V_2, in the right column between the location of the strut and the bottom corner can be obtained

$$V_2 = \frac{2M_C h - (M_C + M_D)m_2}{h(h - m_2)} \tag{18.11}$$

Substituting Eqs. 18.7, 18.10, and 18.11 into Eq. 18.6 gives

$$Q - \frac{1}{h}\left[\frac{2M_B m_1 h - (M_A + M_B)m_1^2 + (M_A - M_B)h^2}{m_1(h - m_1)} + \frac{2M_C h - (M_C + M_D)m_2}{(h - m_2)}\right] = 0 \tag{18.12}$$

Solving simultaneously Eqs. 18.4, 18.5, and 18.7 yields

$$m_2 = \frac{h - \sqrt{h^2 - 4\left[\frac{m_1(h-m_1)(M_D-M_C)}{(M_A-M_B)}\right]}}{2} \tag{18.13}$$

Eqs. 18.12 and 18.13 are a function of the unknowns m_1 and m_2. Using these equations, m_1 and m_2 can be solved by trial and error.

The total strain energy, U, for the structure can be expressed as

$$U = \left(\frac{T^2L}{2EA}\right)_{diag.} + \left(\frac{T^2L}{2EA}\right)_{beam} + \left(\int_L \frac{M^2}{2EI}dx\right)_{left\ col.} + \left(\int_L \frac{M^2}{2EI}dx\right)_{right\ col.} + \left(\int_L \frac{M^2}{2EI}dx\right)_{beam} \tag{18.14}$$

Substituting for the appropriate variables, and equating the strain energy, U, to the external work, W, the following expression is obtained

$$W = \frac{P^2d^3}{2L^2A_dE_d} + \frac{R^2L}{2EA_b} + \left(\frac{1}{2EI_c}\right)(f_1 + f_2) + \left(\frac{1}{6EI_b}\right)(f_3) \tag{18.15}$$

where $f_1 = \left(\frac{m_1}{3}\right)(M_A^2 + M_Aw' + w'^2) + \frac{(M_B^3+w'^3)(h-m_1)}{3(M_B+w')}$,

$f_2 = \left(\frac{m_2}{3}\right)(M_D^2 + M_Dz' + z'^2) + \frac{(M_C^3+z'^3)(h-m_2)}{3(M_C+z')}$, and

$f_3 = \frac{L}{(M_A+M_B+M_C+M_D)}[(M_C + M_D)^3 + (M_A + M_B)^3]$

In Eq. 18.15, R is the axial force in the beam, w' and z' are the moments as defined in Figs. 18.4 and 18.5, and I_c and I_b are the moments of inertia of the columns and the beam, respectively. Rearranging Eq. 18.15 yields the following expression for the sectional area of the strut

$$A_d = \frac{P^2d^3}{2L^2E_d\left\{W - \frac{R^2L}{2EA_b} - \left(\frac{1}{2EI_c}\right)(f_1+f_2) - \left(\frac{1}{6EI_b}\right)(f_3)\right\}} \tag{18.16}$$

where $W = \frac{1}{2}Q\delta$ and $\delta =$ the interstorey drift,

$P = \frac{(M_A-M_B)h}{m_1(h-m_1)}$,

$R = Q - \left[\frac{2M_Ch-(M_D+M_C)m_2}{h(h-m_2)}\right]$,

$w' = \frac{M_Bh-(M_A+M_B)m_1}{h}$, and

$z' = \frac{M_Ch-(M_C+M_D)m_2}{h}$.

To summarize, by using the interstorey drift and the moments at the ends of the columns resulting from the detailed analysis of the infilled frame, m_1 and m_2 are first solved using Eqs. 18.12 and 18.13, and finally the cross-sectional area of the diagonal strut is obtained by solving Eq. 18.16.

The values of m_1, m_2, and the cross-sectional areas of the equivalent diagonal struts were computed for each model, Table 18.2. Generally, the stiffer the frame, the larger the values of m_1 and m_2 except for the cases in which the column stiffnesses were varied. That is, the greater the moments at the ends of the frame members, the greater are the lengths m_1 and m_2. In the case of the varying column stiffnesses analyses, however, the frame-member moments decreased with increasing column stiffnesses, for the reason explained in Section 16.2, thus m_1 and m_2 decreased as the column stiffnesses increased. The sectional areas of the struts were not significantly affected by the changes in the stiffnesses of the frame members and the aspect ratios of the infilled frame, while the values of m_1 and m_2 were.

To check the accuracy of the model, a lateral load analysis was performed on the column-to-column strut model for each representative infilled frame. The interstorey drifts are presented and compared with the results of the detailed finite element analyses for each model in Table 18.2. The interstorey drifts of the column-to-column model compare well with those of the detailed analyses, with deviations of 1.8 to 4.2 percent.

The frame-member moments from the strut model are compared with those obtained from the detailed finite element analysis of the standard model in Fig. 18.8. The maximum moment in the left column was closely approximated, while the maximum moments in the right column and the beam were underestimated by 14 and 20 percent, respectively. For the other models, the moments in the left column were also closely represented, but the maximum moments in the right column and the beam were underestimated by 9 to 33 percent. Although this model accounts for the forces that the infill applies transversely to the lengths of contact between the columns and the infill, it does not account for the force that the infill applies to the beam; therefore, the moments at the bottom-right corner were underestimated, in both the beam and the column at that corner.

The column-to-column strut model predicts the interstorey drifts well, again provided that a detailed finite element analysis of a single-storey infilled frame module has been performed first to obtain the sectional area and position of the diagonal. It also gives a very good estimate of the moments in the left column, but underestimates the maximum moments in the right column and the beam by as much as 33 percent.

18.3 Column-to-Beam Strut Model

The alternative column-to-beam strut model in Fig. 18.9 consists of a diagonal bracing strut, which extends from near the top of the left column at a distance m_1' from the top-left corner, to near the right end of the beam, at a distance m_3 from the bottom-right corner. By this arrangement, the horizontal component of the force in the strut acts on the left column, and the vertical component on the beam, causing the left column and the beam to bend similarly to those in the detailed finite element analyses.

The sectional area of the diagonal bracing strut for this model was determined similarly to that of the column-to-column strut model on the basis of a prior detailed finite element

Analysis	m_1 (mm)	m_2 (mm)	Area of Strut (mm^2)	I.D. from Detailed Analysis (mm)	I.D. from Strut Model (mm)	Deviation of Strut Model from Detailed Analysis
STANDARD	200.664	181.511	78306	1.4239	1.3890	-2.5%
$1/2I_b$	150.260	141.166	78979	1.5330	1.4691	-4.2%
$2I_b$	218.006	241.849	79856	1.2827	1.2564	-2.0%
$1/2I_c$	187.841	230.301	77631	1.4963	1.4688	-1.8%
$2I_c$	93.442	113.611	77693	1.3290	1.2728	-4.2%
1:1.5	221.451	234.704	78871	1.2467	1.2148	-2.6%
1:2.5	138.017	61.596	77796	1.5348	1.5053	-1.9%

Table 18.2: Resulting Interstorey Drifts for Column-to-Column Strut Model

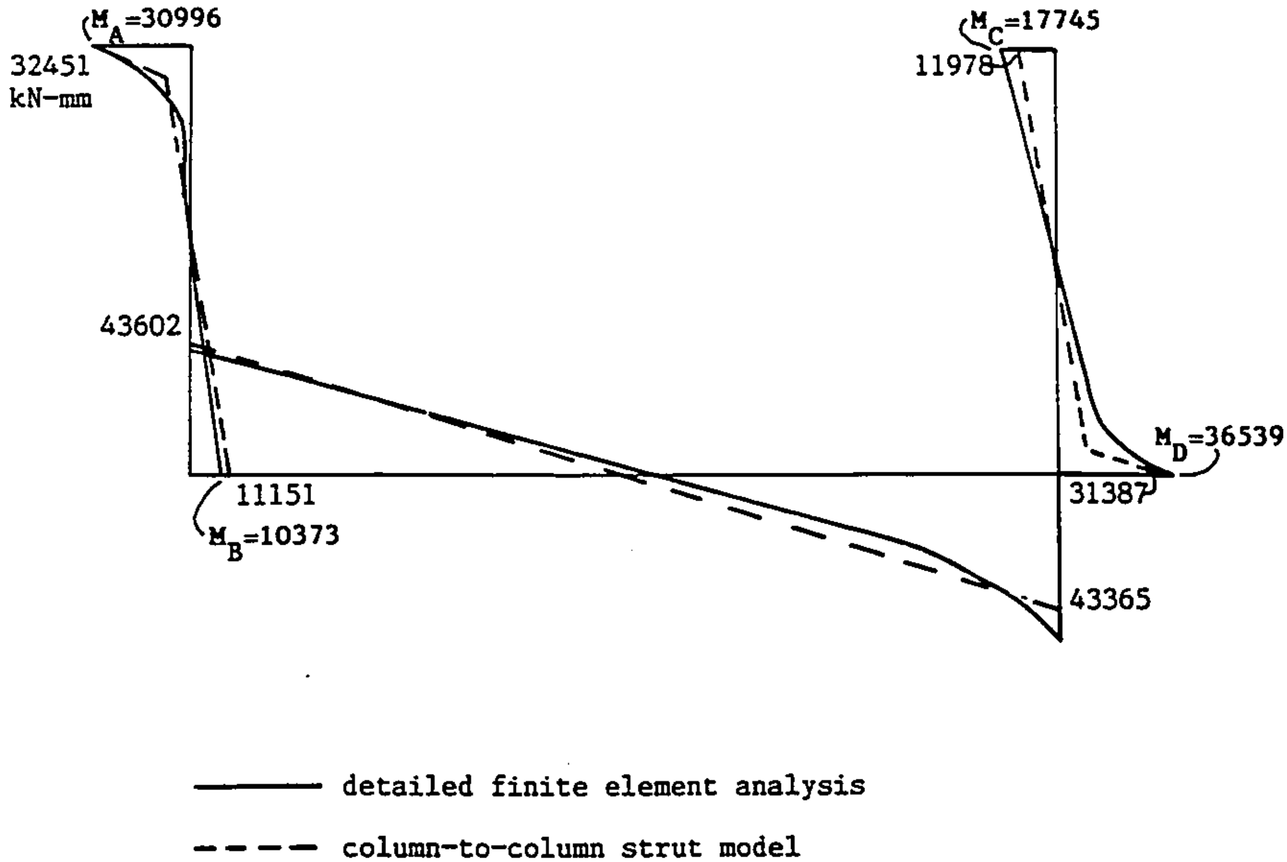

Figure 18.8: Frame-Member Moments for Column-to-Column Braced Frame Model of the Standard Analysis

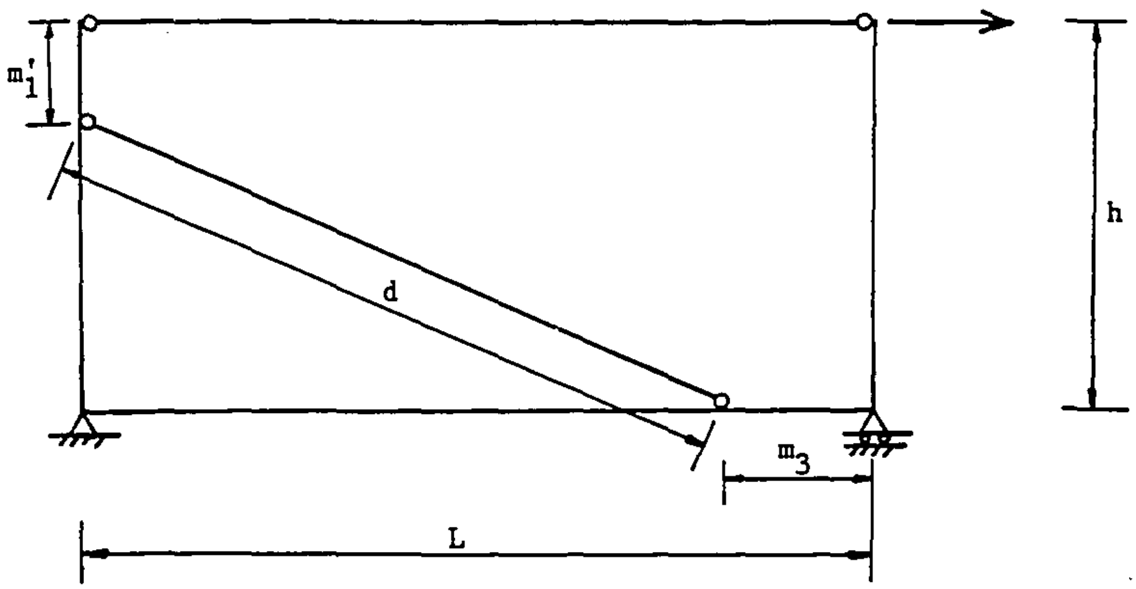

Figure 18.9: Column-to-Beam Strut Model

analysis of a single infilled frame module. Using a procedure similar to that used in the development of the column-to-column strut model, m_1' and m_3 are solved using the following expressions

$$Q - \left[\frac{2M_B h m_1' - (M_A + M_B)m_1'^2 + (M_C + M_D)m_1'(h - m_1') + (M_A - M_B)h^2}{m_1' h(h - m_1')}\right] = 0 \qquad (18.17)$$

and

$$m_3 = \frac{[(M_C + M_D) - (M_A + M_B)]Lm_1'}{(M_A - M_B)h} \qquad (18.18)$$

Then the cross-sectional area of the strut is given by

$$A_d = \frac{P^2 d^3}{2(L - m_3)^2 E_d \left\{W - \frac{R^2 L}{2EA_b} - \left(\frac{1}{2EI_c}\right)(g_1 + g_2) - \left(\frac{1}{2EI_b}\right)(g_3)\right\}} \qquad (18.19)$$

where $P = \frac{(M_A - M_B)h}{m_1'(h - m_1')}$,

$R = Q - \left(\frac{M_D + M_C}{h}\right)$,

$w' = \frac{M_B(h - m_1') - M_A m_1'}{h}$,

$t' = \frac{(M_A + M_B)(L - 2m_3)Lm_1' - (M_A - M_B)hm_3^2}{m_1' L^2}$,

$g_1 = \left(\frac{m_1'}{3}\right)(M_A^2 + M_A w' + w'^2) + \frac{(M_B^3 + w'^3)(h - m_1')}{3(M_B + w')}$,

$g_2 = \frac{(M_C^3 + M_D^3)h}{3(M_C + M_D)}$, and

$g_3 = \frac{m_3}{3}[(M_C + M_D)^2 + (M_C + M_D)t' + t'^2] + \frac{(L - m_3)}{3(M_A + M_B + t')}[(M_A + M_B)^3 + t'^3]$

The values of m_1' and m_3 were calculated for the standard model to be 215.886 mm and 267.952 mm, respectively. While the cross-sectional area was 79336 mm^2. From a lateral load analysis of the column-to-beam strut model for the representative standard infilled frame, the interstorey drift was 1.3322 mm, which deviates by -6.4 percent from the detailed finite element analysis.

The frame-member moments from the column-to-beam strut model are compared with those obtained from the detailed finite element analysis of the infilled frame in Fig. 18.10. The maximum moments in each of the frame members are underestimated by as much as 30 to 53 percent. This model is arranged to account for the forces applied by the infill to the left column and the beam, but does not account for the force applied by the infill to the right column, which is evidently of great importance.

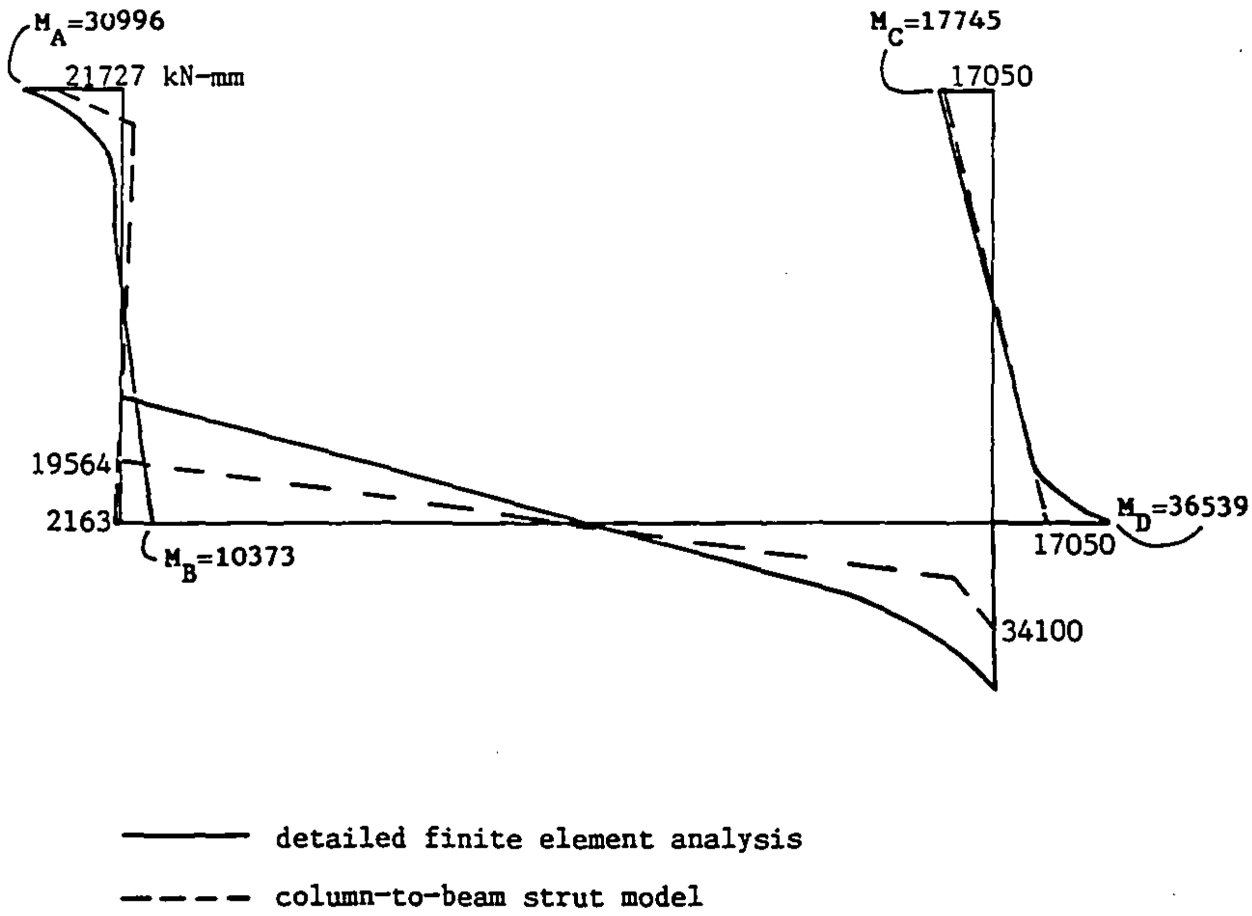

Figure 18.10: Frame-Member Moments for Column-to-Beam Braced Frame Model of the Standard Analysis

It was concluded that the column-to-beam strut model was not successful in correctly representing the behaviour of the example infilled frame. The interstorey drifts and the frame-member moments were not as well predicted as they were by the column-to-column strut model.

18.4 Summary of Results

The simple, single-diagonal strut model, Fig. 18.1, correctly represents the interstorey drifts of the infilled frames with a gap at the top, but grossly underestimates the frame-member moments. The column-to-column strut model, Fig. 18.3, predicts well the interstorey drifts and the moments in the left column and at the left end of the beam, but underestimates the maximum moments in the right column and in the beam. While the column-to-beam strut model, Fig. 18.9, estimates reasonably well the interstorey drifts, but does not predict the frame-member moments as well as the column-to-column strut model.

A model which might better represent the behaviour of the infilled frame with a gap at the top of the infill is shown in Fig. 18.11. It consists of a strut, which extends from near the top of the left column, a distance m_1 from the top-left corner as in the column-to-column strut model, and has a slope equal to that of the strut for the column-to-column strut model. At a distance m_4 from the right column the strut divides into two struts. One strut extends to the right column, a distance m_2' from the bottom-right corner, where m_2' is greater than m_2 in the column-to-column strut model. The other strut extends to the beam, a distance m_3' from the bottom-right corner, where m_3' is also probably greater than m_3 in the column-to-beam model. This arrangement should yield a larger moment at the bottom of the right column and a larger moment at the left end of the beam than in the column-to-beam and column-to-column strut models. Although with such a proposed model, the behaviour of an infilled frame with a gap at the top of the infill would probably be better represented, the large number of variables required to solve it makes it impractical. The Author suggests, therefore, that the column-to-column strut model be used to obtain the correct interstorey drifts and moments in the left column, and that the moments obtained at the bottom of the right column and at the right end of the beam be increased conservatively by 50 percent.

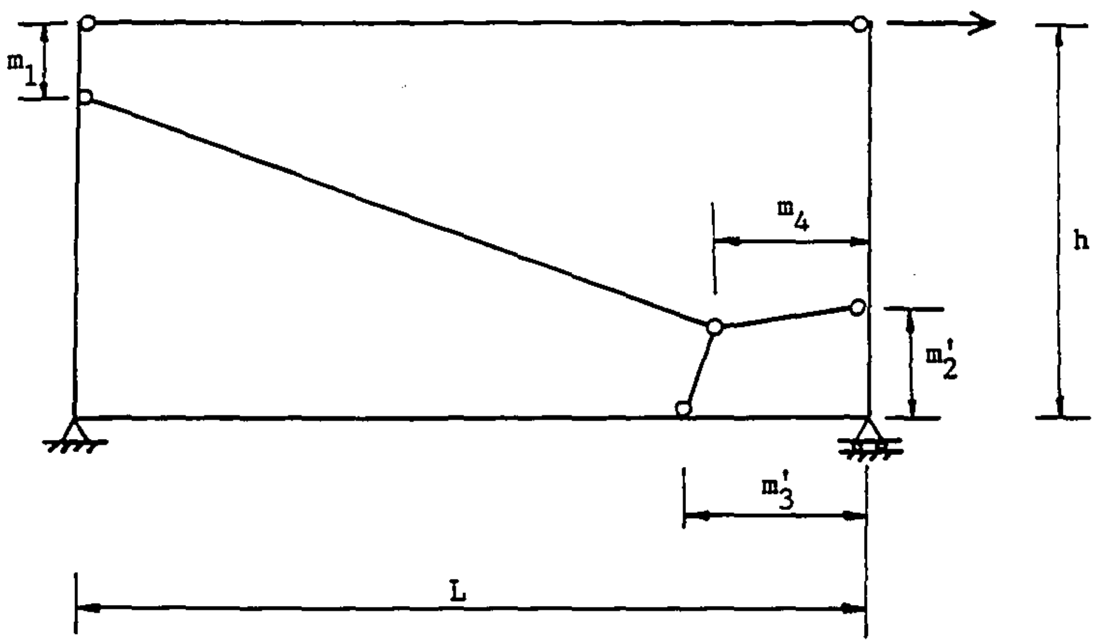

Figure 18.11: Probably More Accurate Equivalent Strut Model

CHAPTER 19

THE EFFECT OF INFILLS ON THE STATIC WIND LOAD RESPONSE OF AN EXAMPLE STRUCTURE

The effect of the non-loadbearing infills on the static wind load response of a modified version of the moment-resisting frame structure described in Part I was investigated. The effects of the infills in the overall structure were simulated by using the column-to-column equivalent strut model described in the previous chapter. To use the equivalent strut, a detailed finite element analysis of a typical intermediate storey of the infilled frame in the example structure was required first. Having determined the size of the equivalent strut, static wind load analyses of the moment-resisting structure, with and without the equivalent diagonal struts, that is, with and without the effects of the infills, were performed and the results compared.

19.1 Modelling the Example Structure

The modified moment-resisting frame structure, Fig. 19.1, differs from the representative moment-resisting frame structure of Part I in the locations, number, and sizes of the columns around the core, and in the beam on which the blockwork infills rest. The core is constructed of 200X200X400 mm blockwork infill walls, with a 25-mm gap at the top of the infill, similar to those of the representative infilled frames analysed in the previous chapters.

To study the building's static response, a three-dimensional analysis of the example moment-resisting frame structure was required. Because the blockwork infills between the corner columns of the core, that is, along axes 4 and 6, were represented by equivalent struts, a half-plan model, rather than a quarter-plan model as in Part I, subjected to half the loading, was analysed. A plan view of the computer model is shown in Fig. 19.2. The columns were represented by beam-type elements. They were assigned their corresponding flexural inertias and sectional areas. The rigid joint zone of the columns on the exterior faces of the building were represented by rigid arms. The slabs were replaced by equivalent beams with effective widths determined from the equations developed by Coull and Wong (1981). On the basis of these effective widths and the thickness of the slab, a horizontal axis of inertia and a sectional area were evaluated and assigned to the beams. A realistic value for the sectional area of the beams was important since the axial deformations of the beam were

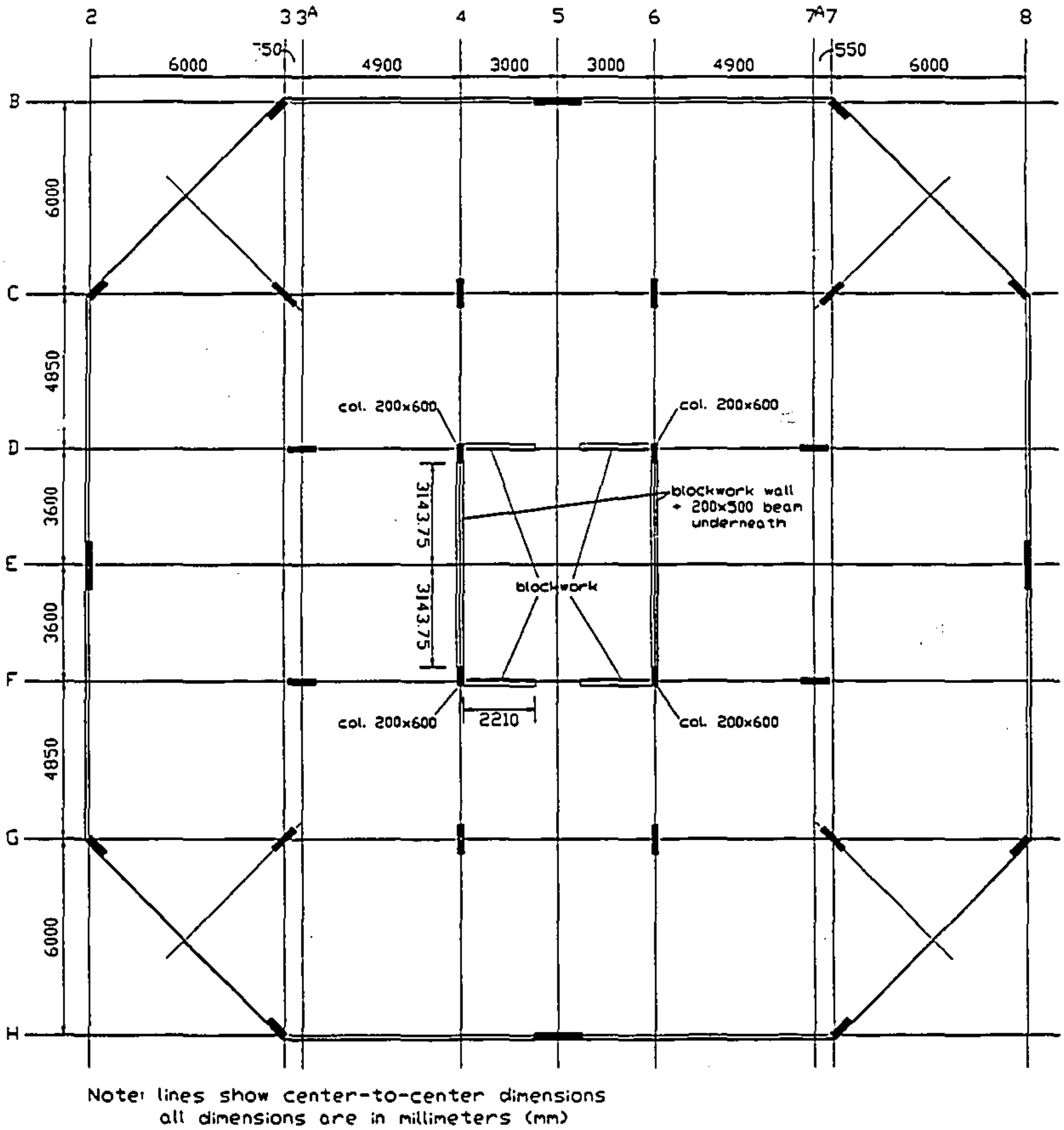

Figure 19.1: Floor Plan of Modified Example Moment-Resisting Frame Structure

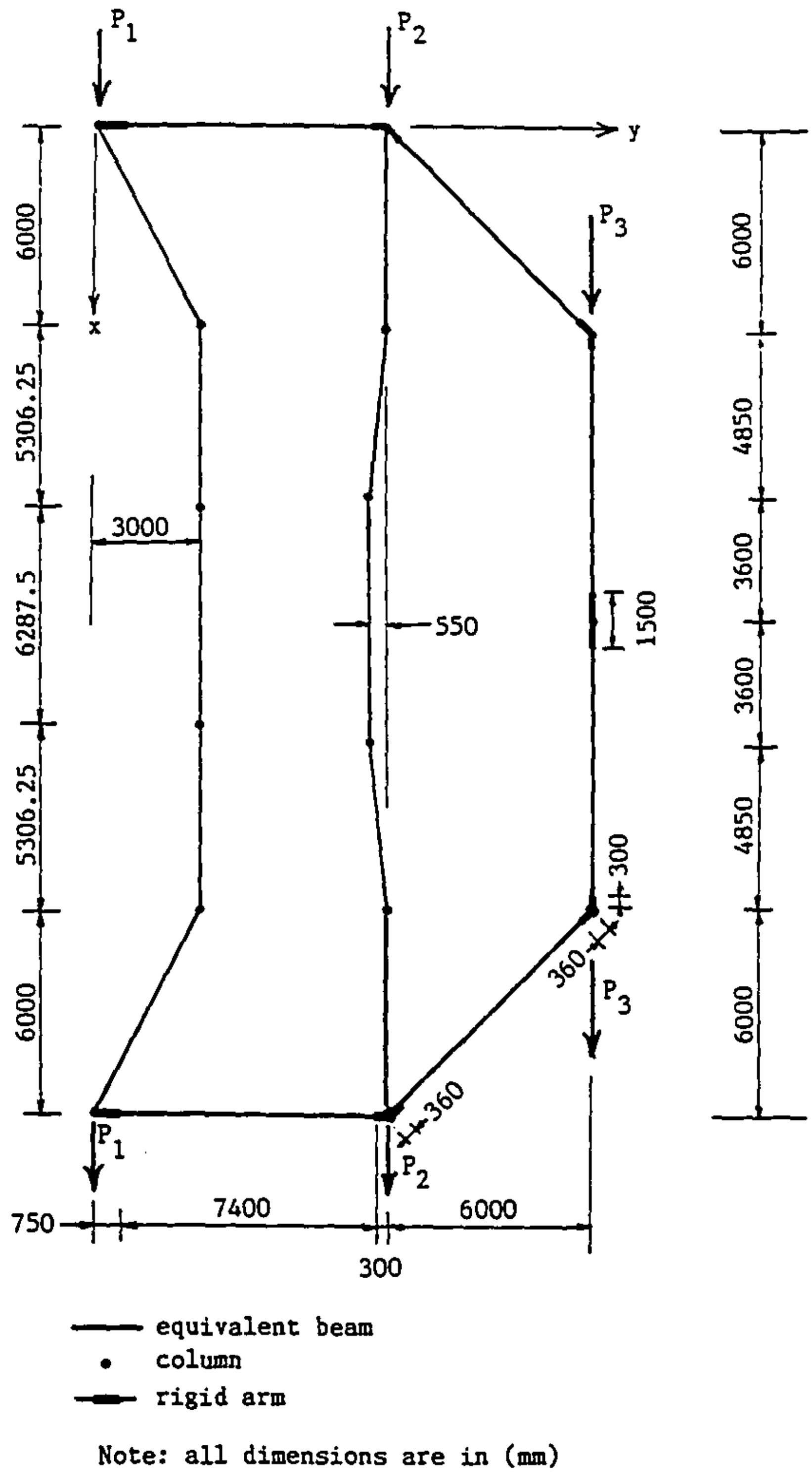

Figure 19.2: Typical Floor Level of the Mathematical Model for the Modified Example Moment-Resisting Frame Structure

significant in the analyses of the representative infilled frames. To establish the conditions of symmetry required for use of the half-plan model of the structure, the horizontal translation of all the nodes in the plane perpendicular to the direction of the loading was restrained, and the ends of the columns on the line of symmetry were restrained against rotation about the axis of loading. The uniformly distributed lateral load of 1.268 kN/m^2 simulating the wind load was applied as equivalent concentrated loads, Fig. 19.2, at the floor levels.

19.2 Modelling the Infills

The blockwork walls between the columns at the corners of the core were modelled by the column-to-column diagonal bracing struts described in Section 18.2. However, the infill and the frame in the example structure did not have exactly the same dimensions and member properties as any of the representative infilled frames already analysed. Therefore, to assign a size to the equivalent strut for the infill in the example structure, it was necessary to first perform a detailed analysis of a single-storey infilled frame using the particular infill size and frame members of the example frame structure.

19.2.1 Detailed Analysis of Example Single-Storey Infilled Frame

The mathematical model of the infilled frame for the detailed finite element analysis is shown in Fig. 19.3. The height-to-length ratio for the infill was 1:2.5, and it was represented by a mesh of 836 membrane plane stress elements, as was the representative 1:2.5 model analysed in Chapter 16. The thickness and modulus of elasticity assigned to the elements were those of the concrete blockwork wall, that is, 200 mm and 10 kN/mm^2 (10000 MPa), respectively. The column elements were assigned the full flexural inertia, since there were no infills in the adjacent bays, that is, $3.6X10^9$ mm^4. To eliminate axial deformations in the columns, the column elements were assigned very large sectional areas. The beam elements were assigned the full flexural inertia and axial area of the storey beam, that is, $2.0833X10^9$ mm^4 and 100000 mm^2, respectively. At the top, a link with an axial area equal to that of the storey beam joined the tops of the columns. The frame members were assigned a modulus of elasticity of 20 kN/mm^2 (20000MPa).

The structure, Fig. 19.3, was analysed for a 130 kN lateral load, as were the representative infilled frames in Chapter 16. Identical results were obtained at the 12^{th} and 14^{th} iterations. That is, equilibrium must exist at some intermediate position between cycles 12 and 13. The interstorey drifts for cycles 12 and 13 were 1.8229 mm and 1.1830 mm, respectively. The contact regions between the infill and the frame are presented for cycles 12 and 13 in Fig. 19.4, and the deflected shape is shown for the most flexible cycle of the two-cycle interval in Fig. 19.5. The frame-member moments are shown in the diagram in Fig. 19.6.

Digressing briefly, the results obtained from the above analysis will be discussed. The analysis differs from the representative 1:2.5 model analysed in Chapter 16 in that it has a smaller storey height, increased column stiffnesses and reduced beam stiffness. Although

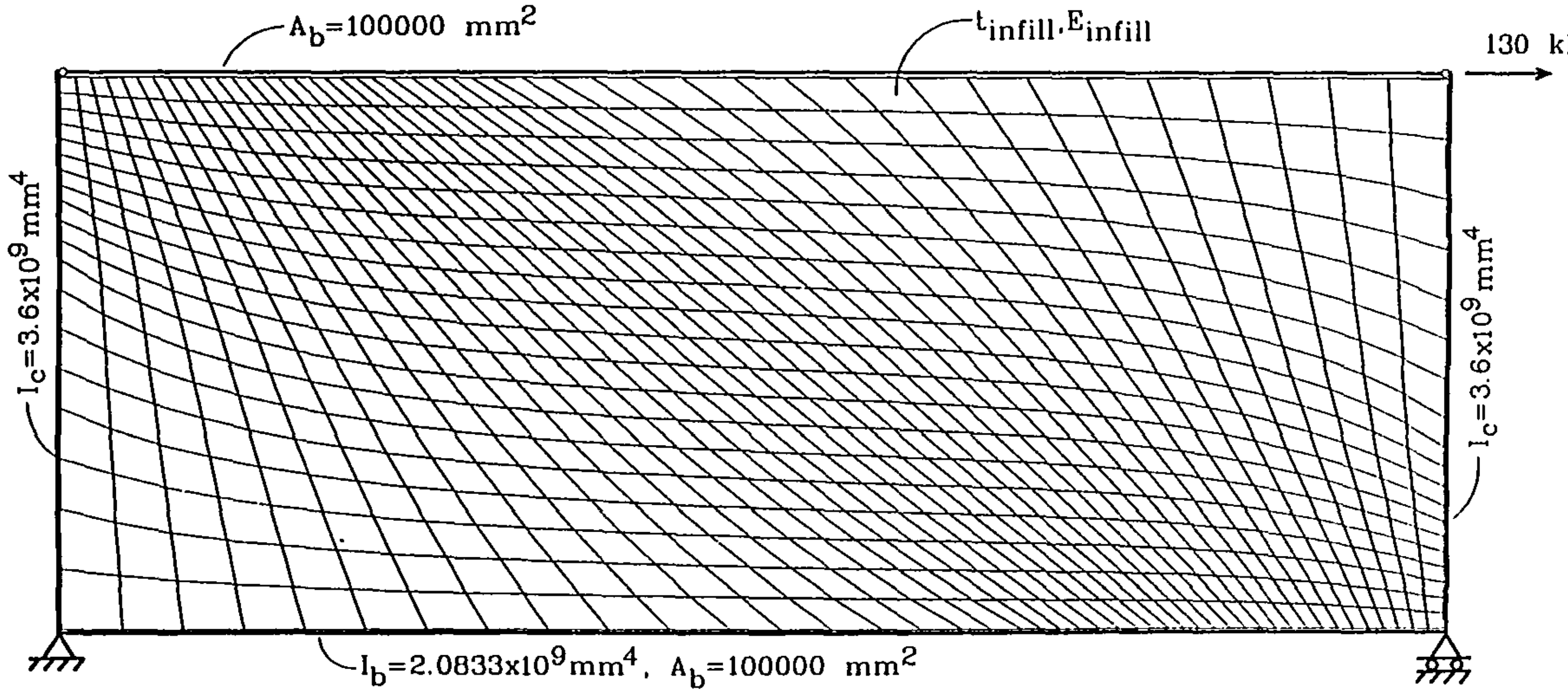

Figure 19.3: Mathematical Model for Example Single-Storey Infilled Frame

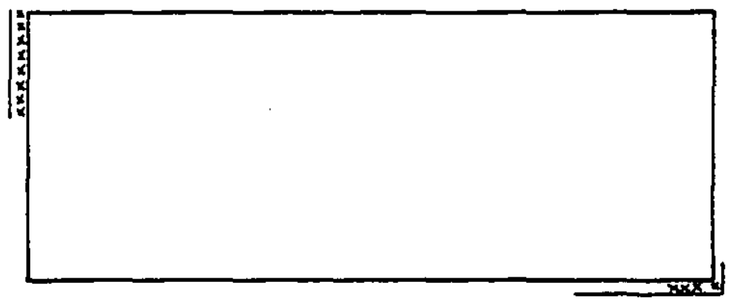

(a) Cycle 12 - Interstorey drift = 1.8229 mm

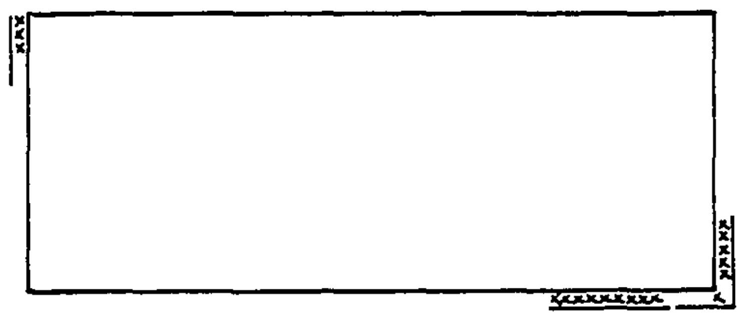

(b) Cycle 13 - Interstorey drift = 1.1830 mm

——— connection normal to boundary

xxxxxxxxx connection tangent to boundary

Figure 19.4: Resulting Contact Regions of the Example Single-Storey Infilled Frame

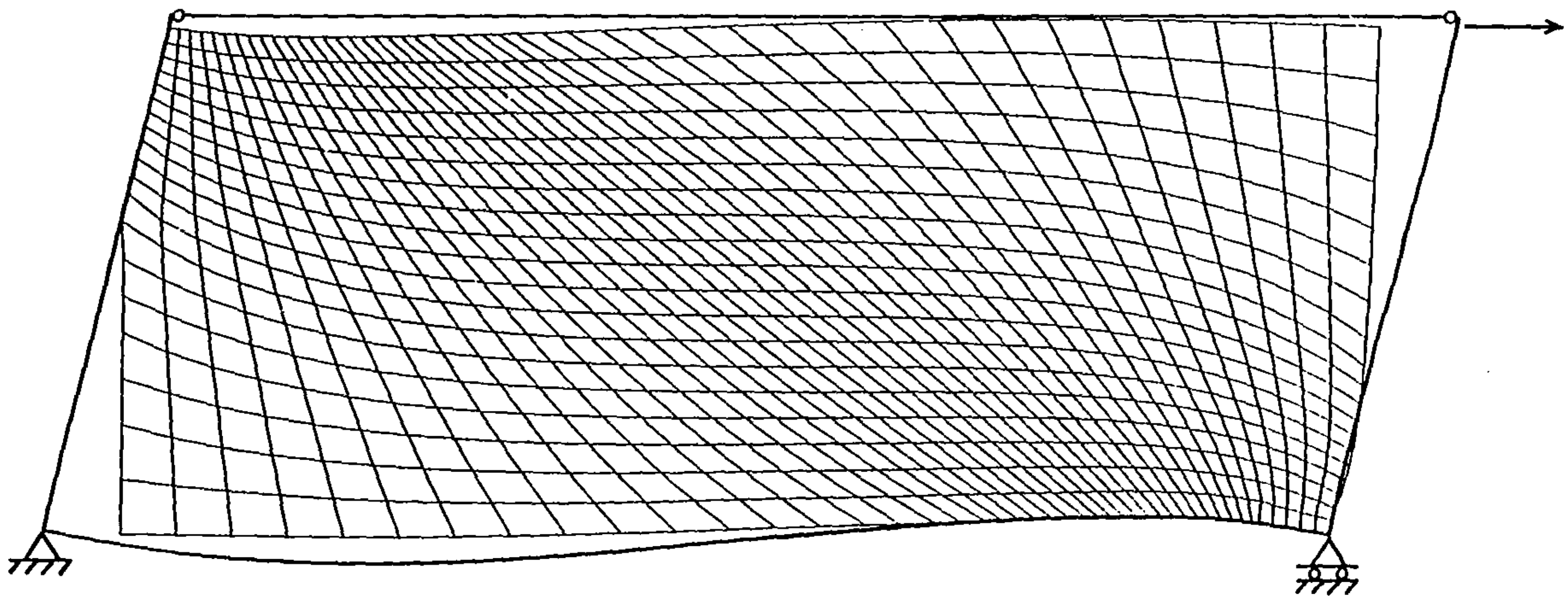

Figure 19.5: Deflected Shape of the Example Single-Storey Infilled Frame

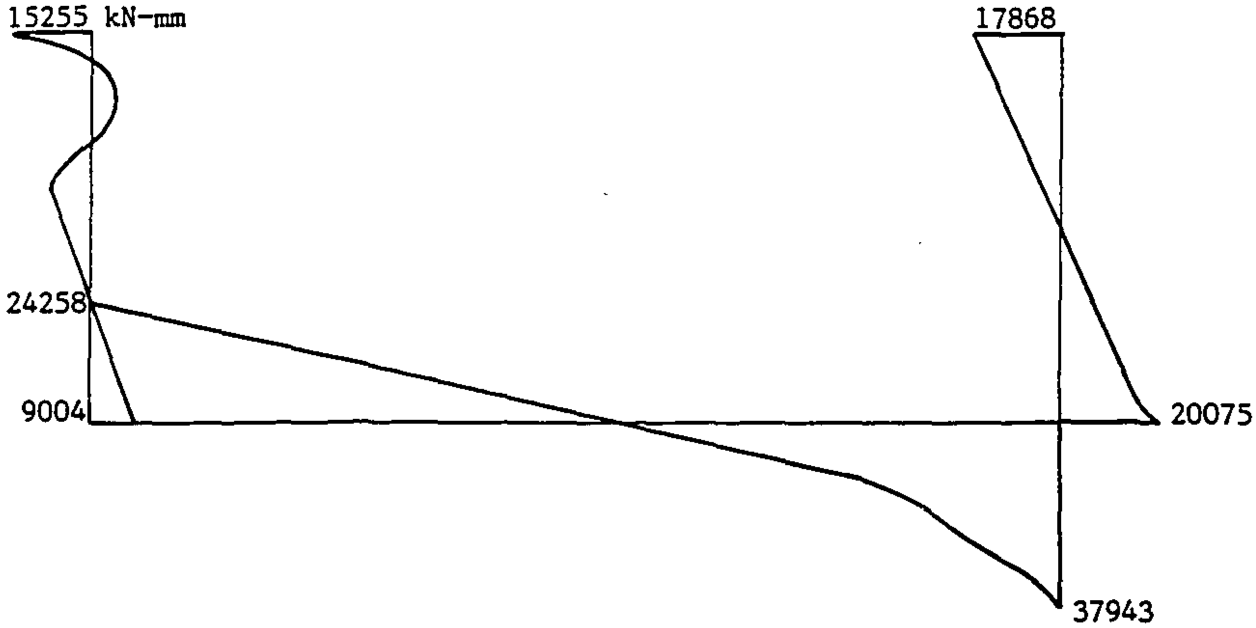

M_A= 15255 kN-mm
M_B= 9004
M_C= 17868
M_D= 20075

Figure 19.6: Frame-Member Moments for the Example Single-Storey Infilled Frame

the number of membrane elements used in this analysis was identical to that of the representative 1:2.5 model analysed in Chapter 16, the smaller storey-height caused the mesh to be comparatively more refined. It was for this reason that the analysis stabilized around two iterations rather than four as in the representative 1:2.5 model. The interstorey drift from this analysis, for the most flexible iteration of the two-cycle interval, is 19 percent greater than that of the representative 1:2.5 model. The combination of the differences of this model from the representative 1:2.5 model caused the former to be a more flexible structure. Consequently, in this analysis the frame-member moments were less than and the infill stresses greater than those in the representative 1:2.5 model.

19.2.2 Equivalent Strut Model

To include the effect of the infills in the three-dimensional analysis of the example moment-resisting frame structure, the column-to-column strut model was chosen.

Substituting the properties of the infilled frame and the frame-member moments obtained from the detailed finite element analysis into Eqs. 18.12 and 18.13, the values of m_1 and m_2 were calculated to be 58.757 mm and 20.431 mm, respectively. Using the resulting interstorey drift from the detailed analysis also, the cross-sectional area of the diagonal strut, was computed as 68791 mm^2, Eq. 18.16. As a check, a lateral load analysis of the single-storey representation of the modelled frame, Fig. 19.7, was performed, and the results compared with those of the detailed finite element analysis. The interstorey drift for the strut model was 5.5 percent less than that of the detailed analysis. The frame-member moments were predicted within 2.5 percent in the left column and at the left end of the beam, but were underestimated by approximately 35 percent in the right column and at the right end of the beam.

To summarize, at every storey the infill extending between columns D6 and F6 in the one-half structure model was represented by a diagonal strut beginning at one column, at a distance of 58.757 mm from the floor above and ending at the other column at a distance of 20.431 mm from the floor below. The diagonal struts were assigned a sectional area of 68791 mm^2.

19.3 Analyses and Results

The moment-resisting frame structure was analysed first without infills, that is without the equivalent diagonal struts. The resulting top deflection of 84.98 mm, gave a drift index of 1/598 which is well within the acceptable limit. The overall displaced shape of the structure, Fig. 19.8, depicts the predominantly shear mode of displacement present in a moment-resisting frame, and the small flexural component of displacement due to the axial deformations in the columns and to their moment fixity at the base.

The structure with infills, that is including the equivalent diagonal struts, was then analysed. The resulting top displacement was 63.58 mm, corresponding to a drift index of

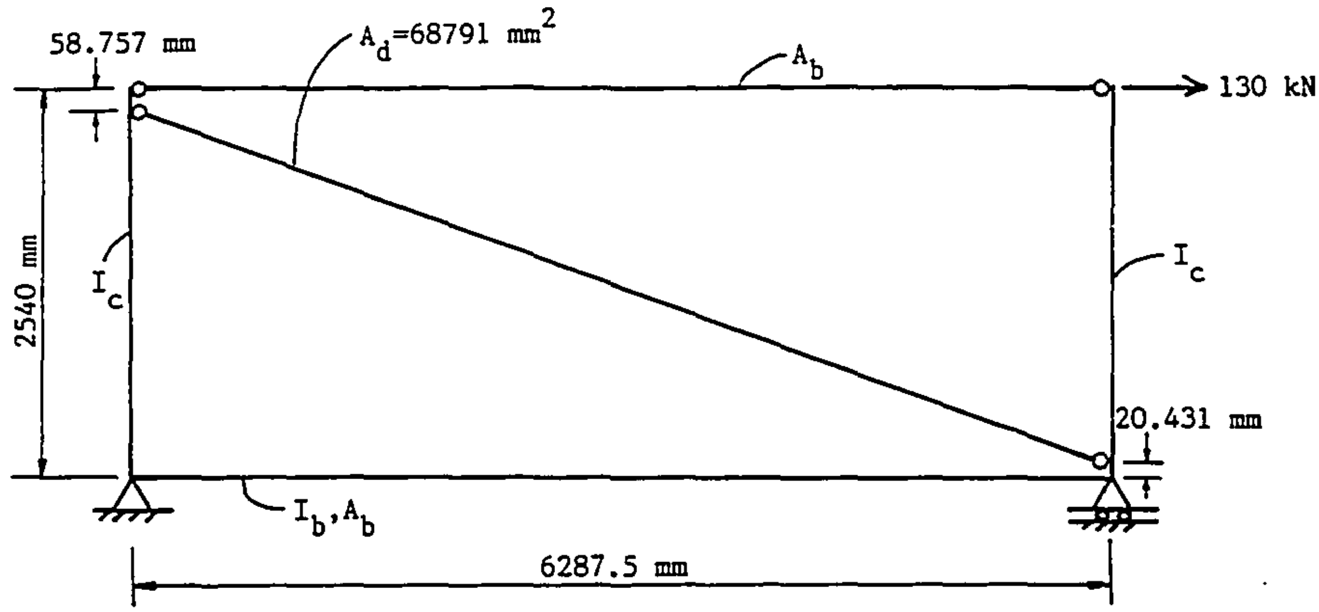

Figure 19.7: Single-Storey Representation of the Equivalent Strut Braced Frame Model

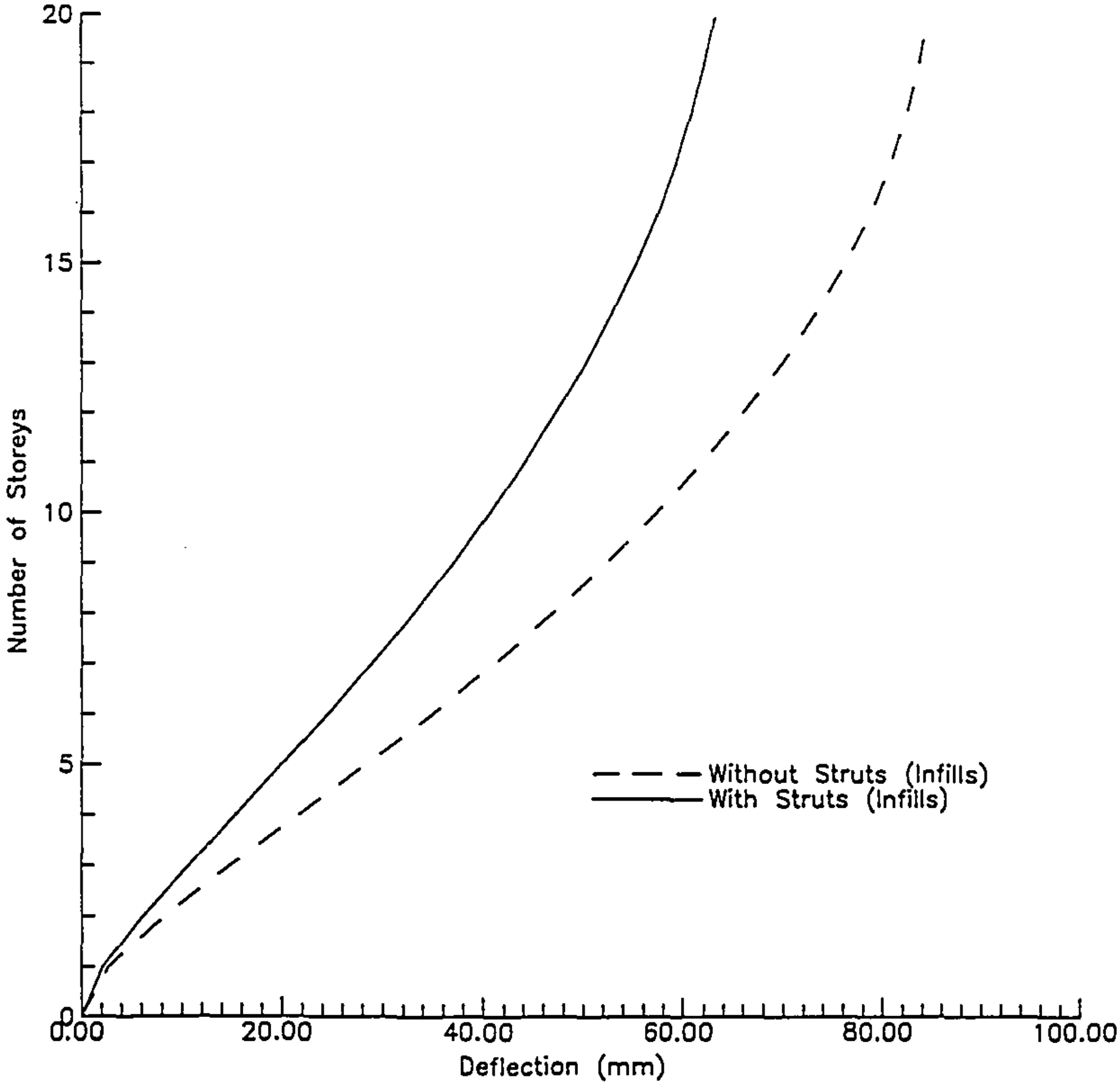

Figure 19.8: Deflected Shapes of the Modified Example Moment-Resisting Frame Structure

1/799. The effect of the infills in one bay of the half-plan model of the structure was to decrease the top displacement of the structure without infills by 25 percent. The stiffening effect of the non-loadbearing infills in this example structure was not as great as that of the cladding panels in Chapter 7. In the half-plan of the structure with the cladding panels, however, two bays were 'braced' in the direction of the wind loading, while in that with the infills, only one bay was 'braced'.

The deflected shape of the moment-resisting frame structure with the infills is also illustrated in Fig. 19.8. This structure also exhibited a predominantly shear behaviour with some flexural behaviour. To better understand the modes of deformations of the structures with and without the infills' effect, the resulting deformations are separated into their components in Figs. 19.9 and 19.10. The deflected shape of the example moment-resisting structure without bracing consisted of a very small flexural component and a larger shear component, giving a predominantly shear configuration, Fig. 19.9. The deflected shape of the example moment-resisting frame structure with bracing, however, was composed of a larger flexural component and a smaller shear component, but still resulting in a predominantly shear behaviour. Fig. 19.11, in which the displaced shape of the structure without infills is normalized to have a top deflection equal to that of the structure with infills, supports the conclusion that the structure with the effect of the infills included had relatively greater flexural deformations than without the infills. By adding the struts, the shear rigidity of the frame structure was increased, while its overall flexural rigidity was reduced. This reduction was due to the significantly increased axial deformations in the columns adjacent to the infill arising from the vertical components of the forces in the struts. Fig. 19.12 shows the distribution of the axial stresses in the columns along axis 6 of the bottom storey for the analyses of the example structure with and without infills. In the case without the infills, the outer bays tended to act as independent frames because the beam of the middle bay was significantly more flexible than those of the outer bays. When the struts were added to represent the infills, the middle infilled bay was significantly stiffened in shear, making it act almostly independently of the outer bays. The effect of the struts was to significantly increase the axial stresses and strains in the middle-bay columns.

The effect of the infills was also to reduce the moments in all the columns and beams in the bottom stories of the structure by approximately 25 to 30 percent. These values, however, neglect the recommended conservative increase of 50 percent in the moments of the column and beam in the lower compressive corner of the infill to allow for their usual underestimate by the analysis.

19.4 Checking Capacity of Infills to Withstand Interaction Forces

Having analysed the overall moment-resisting frame structure for wind loading, with the effect of the infills included, it was of concern to check the interaction forces induced in the infills and compare these with the infills' strengths. The shear carried by the infilled bay at every storey was taken as the sum of the shears in the columns adjacent to the infill just

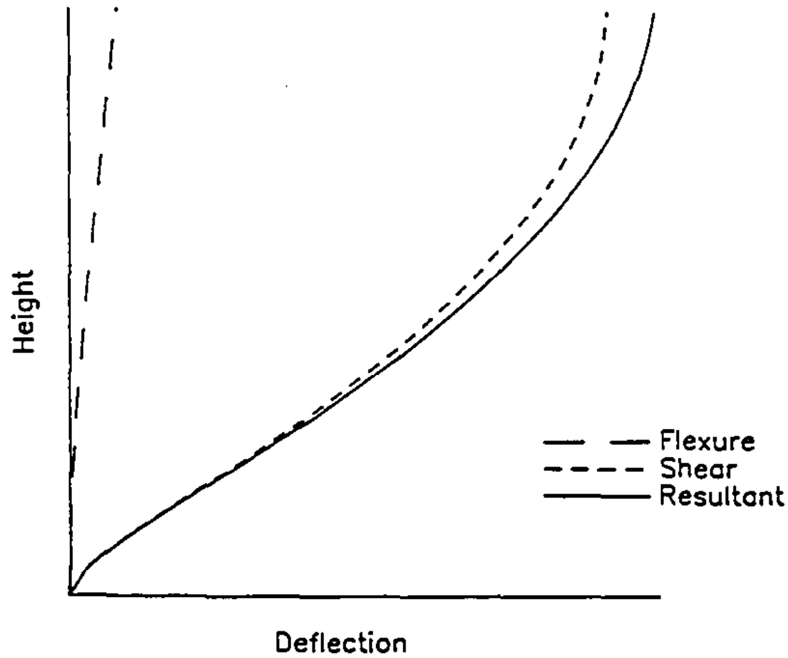

Figure 19.9: Deflected Shapes of the Modified Example Moment-Resisting Frame Structure Without Bracing

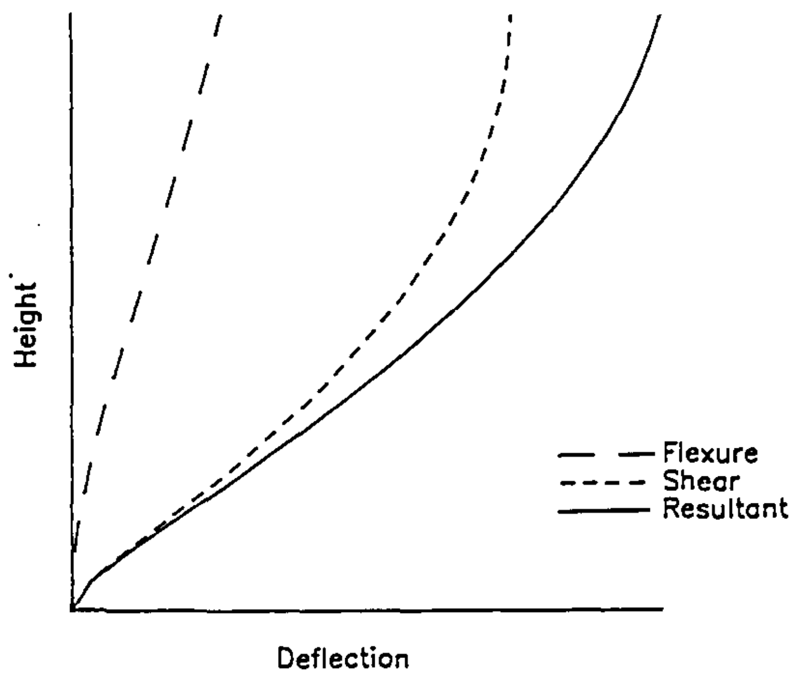

Figure 19.10: Deflected Shapes of the Modified Example Moment-Resisting Frame Structure With Bracing

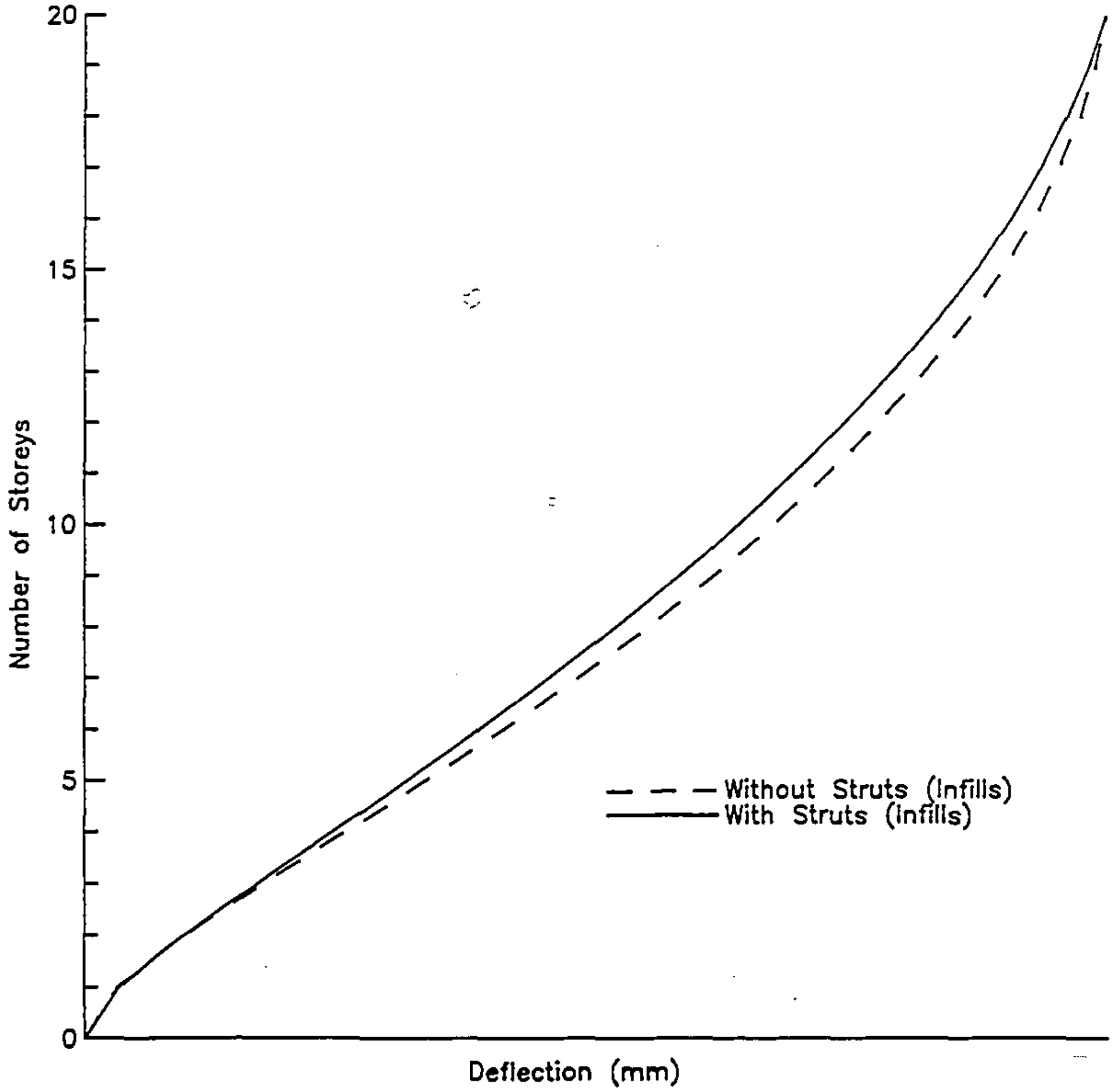

Figure 19.11: Normalized Deflected Shapes of the Modified Example Moment-Resisting Frame Structure

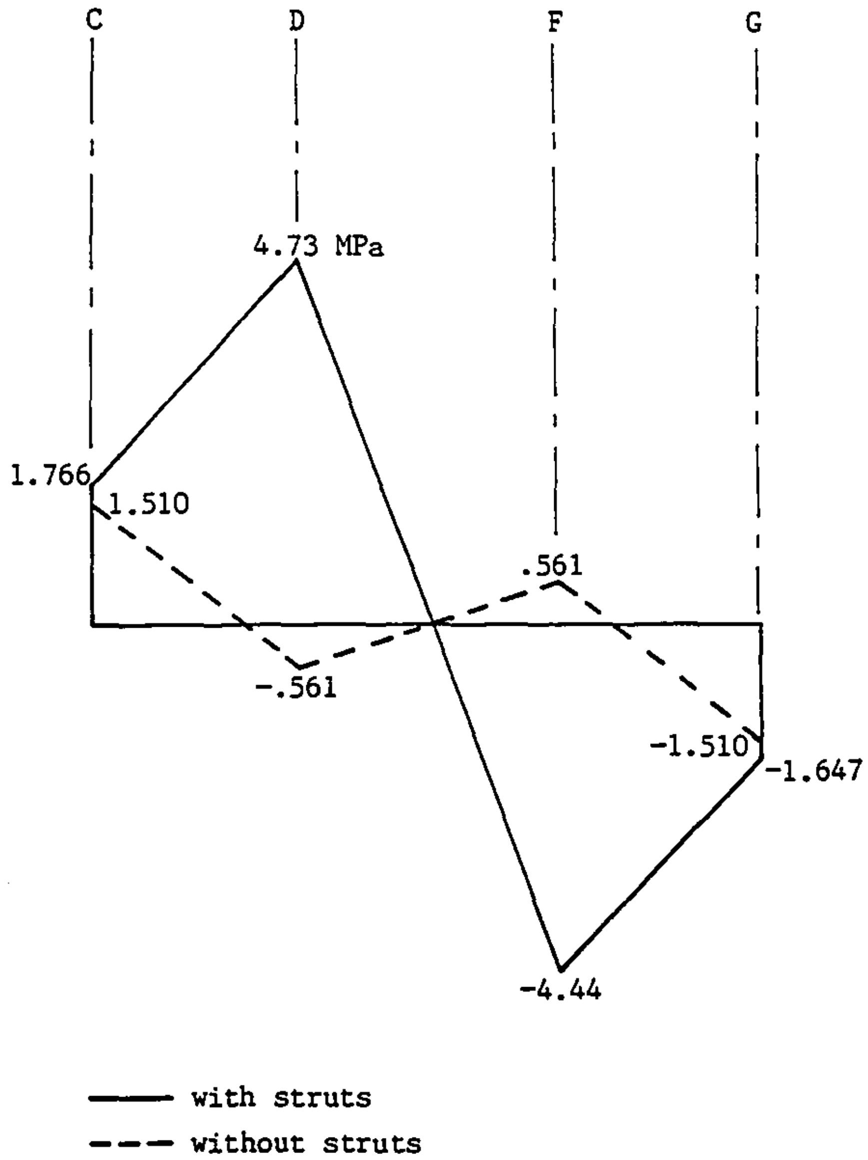

Figure 19.12: Distribution of Axial Stresses in Columns on the Line of the Infill

above the top of the infill. The maximum shear carried by the infilled frame occurred at the third floor level and was equal to 357.1 kN. The total external shear at the third storey was 767.9 kN; therefore, the infilled bay attracted more than 50 percent of the total external load due to its great stiffness.

As a crude approximation, the load carried by the infilled bay in the third storey was compared with the load calculated to cause failure of the infill in the representative 1:2.5 model, Chapter 17. In Table 17.2, the external load required to initiate (cracking) failure of the infill in the representative 1:2.5 model was 68.0 kN, which corresponded to a joint shear failure. Comparing the failure load (68.0 kN) determined in Chapter 17 with the maximum shear (357.1 kN) carried by the infilled frame, it is obvious that at the magnitude of loading analysed, the infills would not be able to withstand the loads which they attract. Only the infills in storeys 16 and above would be capable of carrying the induced loads. On this basis, cracks in non-loadbearing infills should often be found, but in practice the buildings in Montreal are rarely, if ever, subjected to as great a wind load as used in design and in this study. In addition, building structures usually include multi-bay infilled frames and other non-structural elements that would participate in the lateral load resisting system of the structure, as a result the infills would be subjected to smaller loads than those computed in this analysis. As mentioned in Chapter 17, tests have also shown (Scrivener 1969, Pook et al. 1986, Pook and Dawe 1986, Shing et al. 1987) that even after sustaining severe diagonal cracking damage, a masonry wall is capable of carrying an even larger in-plane lateral load due to the redirection of the stress trajectories resulting in a multiple strut action of the infill.

CHAPTER 20

THE EFFECT OF INFILLS ON THE SEISMIC RESPONSE OF THE EXAMPLE STRUCTURE

The effect of the infills on the seismic response of the example moment-resisting frame structure described in Chapter 19 was investigated. A condensed description of the background required and the approach used for the seismic analyses is presented in Chapter 9. Eigenvalue analyses and linear elastic response spectrum analyses of the example structure, with and without the effects of the infills, were performed and the results compared. It should be emphasized that the purpose of these dynamic analyses was to make a comparison between the resulting dynamic properties and design quantities of the example structure, with and without the stiffening effect of the infills, rather than an investigation of their absolute values. As in the static wind load analysis, the infills were modelled by column-to-column bracing struts with appropriate properties.

20.1 The Influence of Infills on the Dynamic Properties

Using the same mathematical model as for the case of the static wind load analysis, except having mass values assigned at every floor level, the natural periods of vibration and mode shapes for the example moment-resisting frame structure, with and without the stiffening effect of the infills, were obtained from an eigenvalue analysis using the SAP80 program. At a typical floor, a mass was assigned to the translational degree of freedom in the direction of the seismic loading, corresponding to the mass of one-half of the structure at that level (without the mass of precast concrete cladding panels), that is, 0.1994 $kN \cdot s^2/mm$. At the top, the mass was assigned a value of only one-half of the mass of the slab, that is, 0.1789 $kN \cdot s^2/mm$.

The first four translational mode shapes are presented in Fig. 20.1 for the cases with and without the stiffening effect of the infills, as represented by bracing struts. The difference between the two cases is not very significant. In the case without bracing, the first mode shape verifies the predominantly shear mode of deformation of the moment-resisting frame structure; while, in the case with the bracing, the first mode shape depicts a greater flexural profile in the lower part of the structure with a reduced shear profile in the upper part. In adding the struts, as was explained for the static wind load analysis, the shear rigidity of

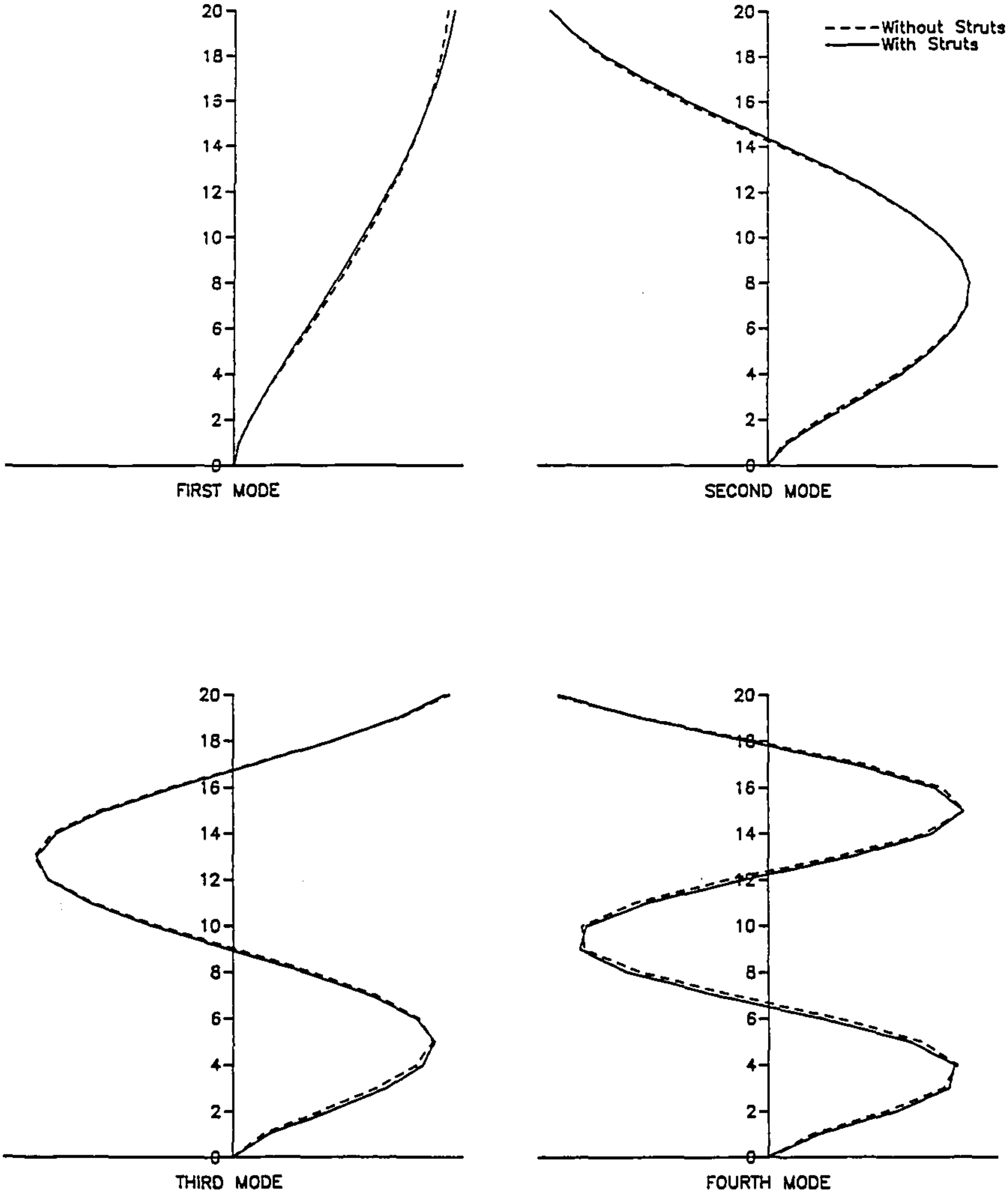

Figure 20.1: Mode Shapes for the Example Frame Structure

the moment-resisting frame structure was increased, its flexural rigidity was simultaneously reduced due to the increased axial deformations in the columns of the braced bay, arising from the vertical components of the forces in the struts. In both cases, the first mode shape is comparable to the deflected shape obtained from the static analysis. The second, third, and fourth mode shapes changed only slightly when the effect of the infills was added. The nodes and anti-nodes occur at similar locations and have approximately the same values for both cases.

The natural periods of vibration for the two models are presented and compared in Table 20.1. The natural periods reduced by 15 to 18 percent when the stiffening effect of the infills was added. The fundamental period for the case with the bracing was 2.94 sec, or 15 percent smaller than the fundamental period of 3.44 sec for the case without the bracing. The deviation was due to the increase in stiffness, since the mass was constant for both cases. The higher modes showed a slightly greater variation; that is, a greater stiffening effect, with the largest difference resulting in the third mode. The infills had a significant stiffening effect on the example structure, but not as great as the effect of the cladding panels, as described in Chapter 9, since the panels were included in twice the number of bays that were infilled.

20.2 The Influence of Infills on the Response Quantities

To determine the effect of the infills on the overall design forces and displacements resulting from seismic excitation, response spectrum analyses were performed on the example moment-resisting frame structure, with and without the stiffening effect of the infills. Similarly to Part I, Chapter 9, the Newmark response spectrum, for 5 percent damping, scaled to 0.04g, was used as the earthquake motion. The cumulative effective modal mass percentages for the example structure, with and without the bracing struts, are shown in Table 20.2. For each model, the SRSS (Square-Root-of-the-Sum-of-the-Squares) combination of four analytical modes, which account for approximately 94 percent of the total effective mass, was used to calculate the peak storey shears, peak storey overturning moments, peak storey deflections, and peak interstorey drifts.

The peak storey shears for the example moment-resisting frame structure, with and without the stiffening effect of the infills, are presented in Fig. 20.2a. The shape of the shear envelope is similar for both cases. However, as the lateral stiffness was increased by including the effect of the infills, and the mass was kept constant, the natural periods decreased. This produced larger spectral accelerations, since for the example structure the modes lay in the region of increasing acceleration with decreasing periods of the Newmark response spectrum. The larger inertial forces resulted in larger storey forces. The value of base shear for the moment-resisting frame structure (half-structure) without struts was 574.5 kN. When the effect of the infills was added, the resulting base shear was 704.7 kN, representing a significant increase of 23 percent over the model without the stiffening effect of the infills.

The peak storey overturning moments for the models with and without bracing struts

Mode Shape	Period Without Effect of Infills (s)	Period With Effect of Infills (s)	Deviation
1	3.4363	2.9364	-15%
2	1.1263	0.9437	-16%
3	0.6381	0.5241	-18%
4	0.4336	0.3587	-17%

Table 20.1: Natural Periods of Vibration for the Example Frame Structure

No. of Modes	Without Effect of Infills	With Effect of Infills
1	77.62%	72.80%
2	87.92%	88.28%
3	91.74%	92.28%
4	93.82%	94.26%

Table 20.2: Effective Modal Mass for the Example Frame Structure

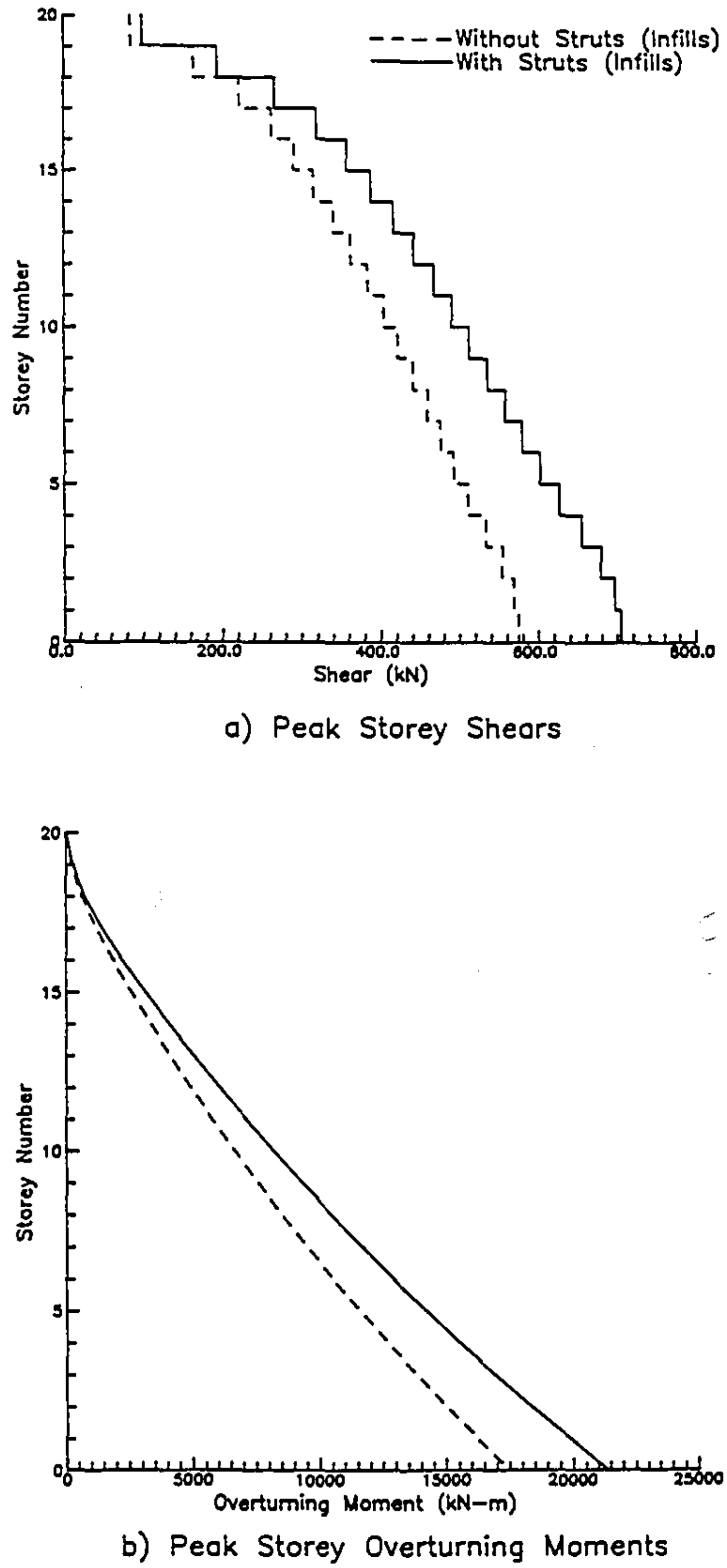

Figure 20.2: Influence of Infills on Storey Force Quantities for the Example Frame Structure

are shown in Fig. 20.2b. The overturning moments exhibited trends similar to those for the storey shears, because of the increased spectral accelerations due to the decreased natural periods of vibration. The base overturning moment for the case in which the stiffening effect of the infills was not included was 17491 kN-m, while for the case in which the stiffening effect of the infills was included it was 21406 kN-m, representing an increase of 22 percent.

In Fig. 20.3a, the peak storey deflections for the example moment-resisting frame structure, with and without the stiffening effect of the infills, are presented. As expected, smaller deflections resulted with the stiffer, but constant mass, model. As was noted in the fundamental mode shape response, the deflected shape of the structure without the struts representing the infills exhibited primarily a shear mode configuration, while the deflected shape of the structure with the bracing struts illustrated a slightly greater overall flexural response with a shear response in the upper part of the structure. The first mode shape contributed significantly to the overall combined response, since the deflected profile of the structure closely resembles the fundamental mode shape. The top displacement for the model with the stiffening effect of the infills included was 60.2 mm, which is 8 percent less than the top displacement of 65.5 mm for the model without the infills. The deflections were not as significantly affected by the stiffening influence of the infills as the design forces were.

The peak interstorey drift response is shown in Fig. 20.3b. When the stiffness of the infills was neglected, the interstorey drift increased with increasing height until the seventh storey, indicating a flexural response due to the fixity of the base and to some axial deformations in the columns. From the seventh storey to the top of the structure, the interstorey drift decreased with increasing height, due to shear deformations. For the structure with the stiffening effect of the infills included, the change in slope occurred at approximately the same level. This indicates that the increase in flexural response due to the stiffening influence of the infills was not significant enough to raise the point of contraflexure. The maximum interstorey drift for the structure with the bracing struts was 4.03 mm; that is, 15 percent less than the interstorey drift of 4.73 mm for the structure without the bracing struts. In both cases, the maximum interstorey drifts occurred at the sixth floor.

The interstorey drift in the top two stories was greater for the structure with the infills than for the structure without the infills. A purely shear-deforming fixed-base structure subjected to a distributed lateral loading is characterized by a small interstorey drift at the top. When the effect of the infills was included, however, an additional flexural component was added to the deflected shape of the structure, thus increasing the interstorey drift in the top part of the structure. Since the deflected shape of the structure without the infills already had a small flexural component due to the axial deformations in the columns, this effect was limited to only the very top floors.

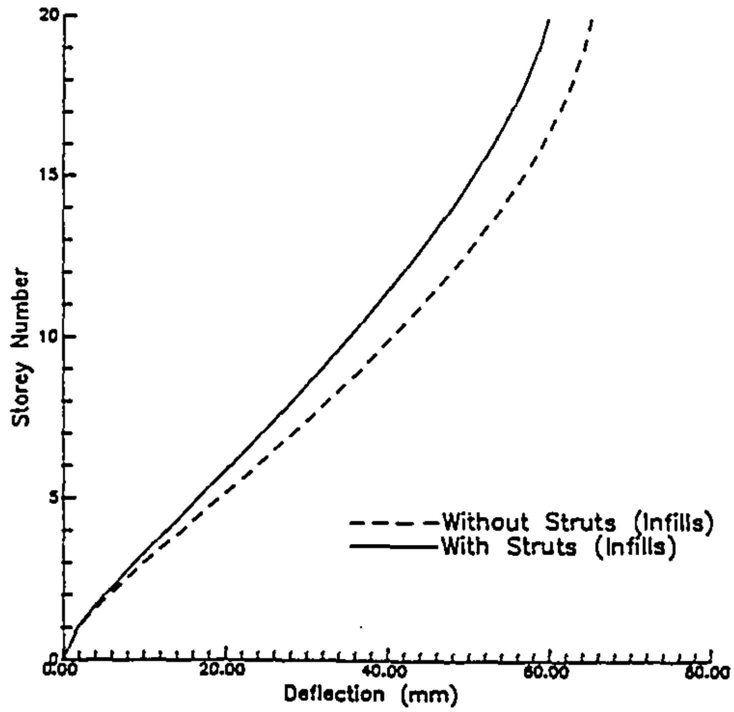

a) Peak Storey Deflections

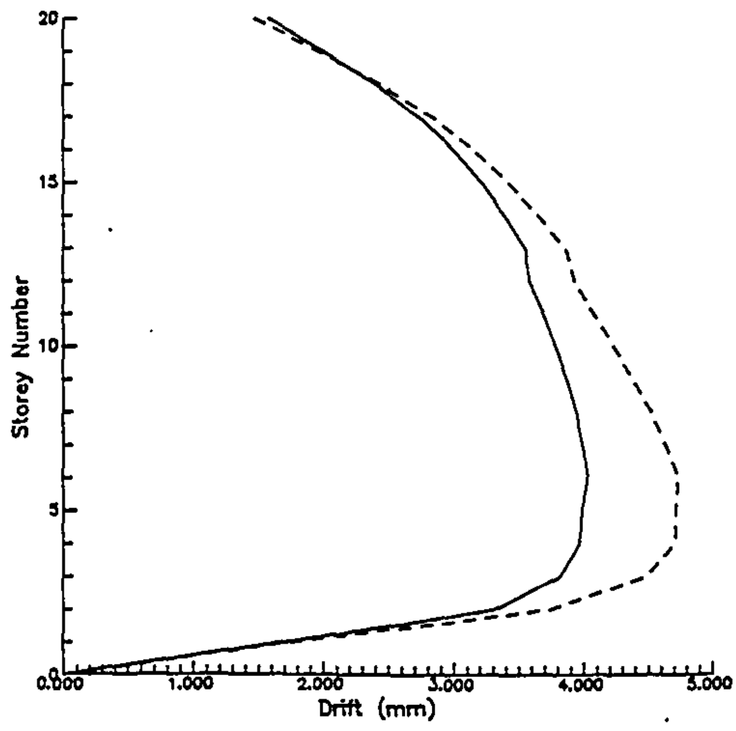

b) Peak Interstorey Drifts

Figure 20.3: Influence of Infills on Storey Displacement Quantities for the Example Frame Structure

20.3 The Relative Influence of Various Modes of Vibration on the Seismic Response

To illustrate the relative influence of the various modes on the total combined response, the modal contributions of the first four modes to the total response (twenty modes) are shown in Fig. 20.4 for the structure without the stiffening effect of the infills, and in Fig. 20.5 for the structure with the effect of the infills. At any storey level, the relative contribution is represented as the square of the individual modal contribution divided by the total sum of the squares of all twenty modal contributions, as explained in Chapter 9. The modal contribution ratios for the forces at the base, the top deflections, and the maximum interstorey drifts are also recorded for the structures without and with the bracing struts in Tables 20.3 and 20.4, respectively.

The effect of the infills did not significantly affect the relative influence of the various modes on the total combined response, as can be seen from Figs. 20.4 and 20.5, and Tables 20.3 and 20.4. The figures indicate that the higher, second, third, and fourth, translational modes contributed relatively more to the peak storey shears and the peak storey overturning moments in the upper six stories of the building. Near the building's mid-height, the peak shear response was dominated by the fundamental mode, but the peak overturning moment still had a significant contribution from the second mode, 25 percent. At the base, the second mode contributed 16 and 14 percent to the total sum of the squares of the base shear values for the structures with and without bracing struts, respectively, Tables 20.3 and 20.4. The first mode dominated the base peak overturning moment, with its contribution being 99 percent. The higher modes generally contributed negligibly to the peak storey deflections except near the base, where the second mode contributed 15 and 13 percent to the total sum of the squares of the deflections, for the structures with and without the stiffening effect of the infills, respectively. The modal contributions to the interstorey drifts resembled those to the shear response except that for the interstorey drifts the fundamental mode contributed more than each of the higher modes. Similar to the shear response, the greatest influence of the higher modes was near the top and the base of the structure.

20.4 Qualitative Comments on the Seismic Capacity of Infills

Considering that the above dynamic analyses were performed to obtain a comparison between the responses of the example structure with and without the stiffening effect of the infills, it would not be meaningful to compare the resulting dynamic forces in the struts with the strength capacity of the infills. However, a qualitative conclusion can be drawn with regard to the infills' capacity to withstand the lateral forces based on the behaviour of an infilled frame with a gap at the top and the calculated dynamic response. Non-loadbearing infills as they are constructed today will inevitably participate in the lateral load resisting

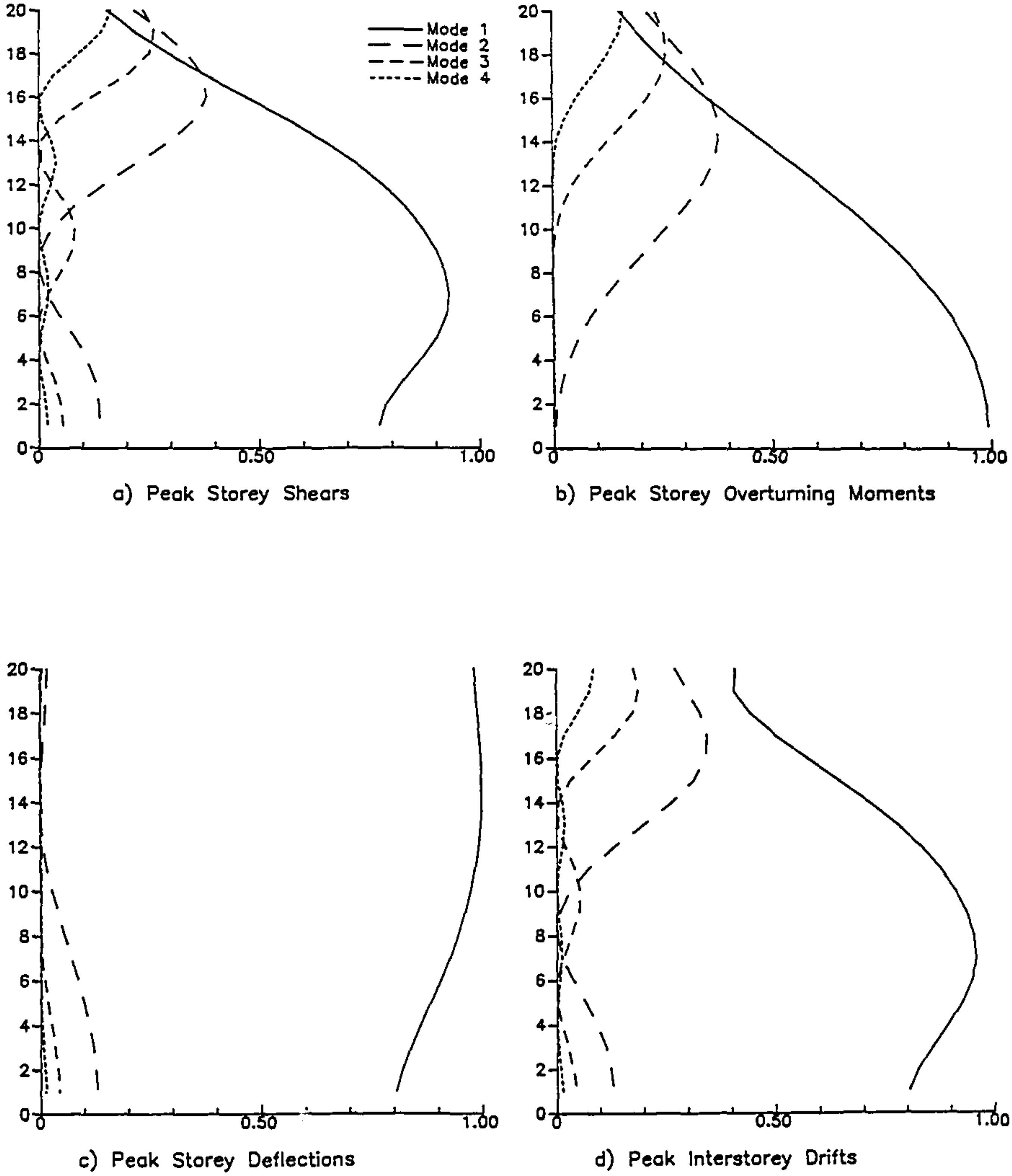

Figure 20.4: Modal Contributions to Response Quantities for Example Frame Structure Without the Effect of Infills

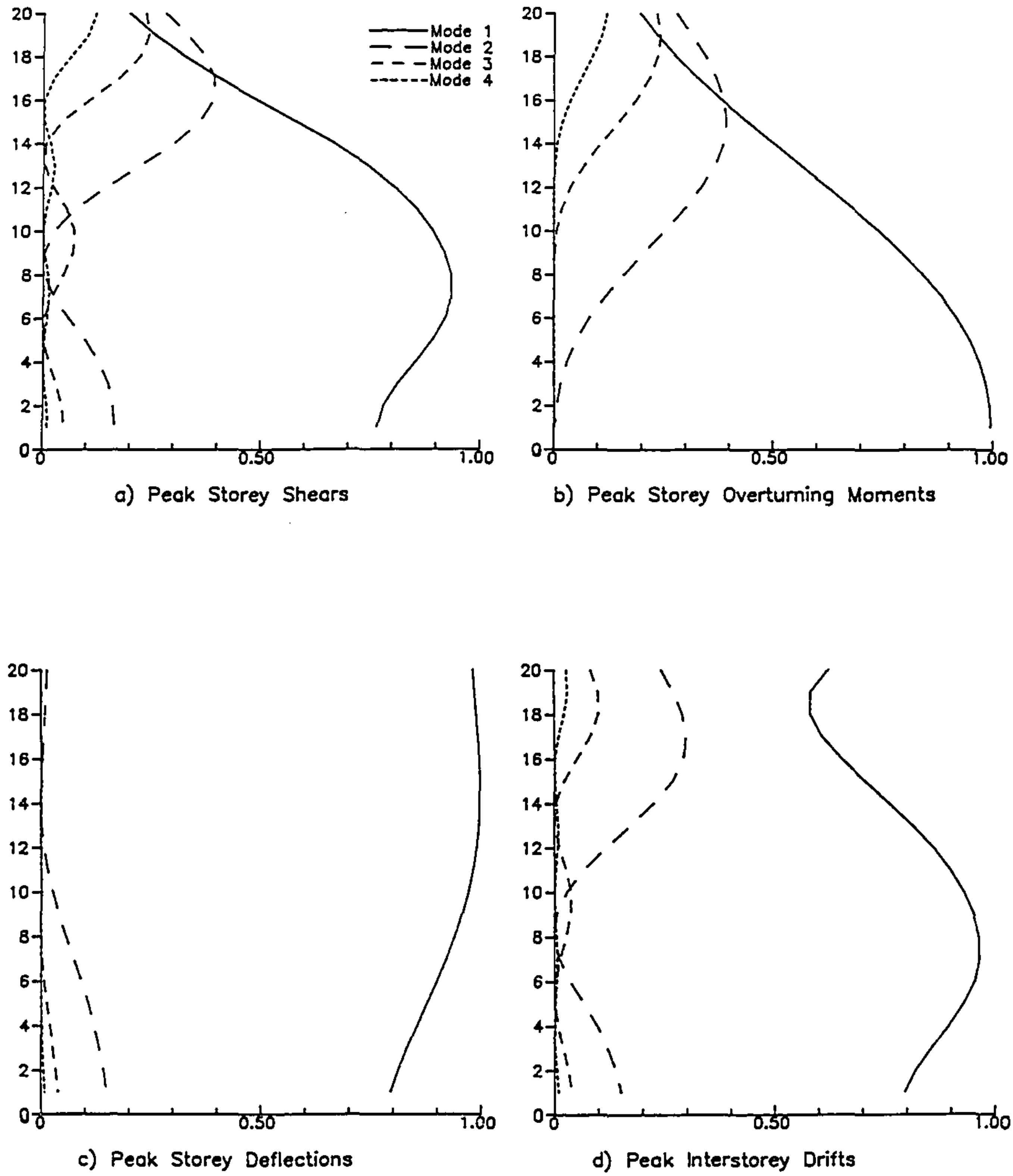

Figure 20.5: Modal Contributions to Response Quantities for Example Frame Structure With the Effect of Infills

Response Quantity	Modal Contribution Ratios					
	Mode 1	Mode 2	Mode 3	Mode 4	Higher Modes	Total
Base Shear	.771	.139	.055	.020	.015	1.000
Base O.M.	.993	.003	.003	.000	.001	1.000
Top Defl.	.982	.016	.002	.000	.000	1.000
Max. I.D.	.949	.038	.001	.007	.005	1.000

O.M. = Overturning Moment
Defl. = Deflection
I.D. = Interstorey Drift

Table 20.3: Modal Contribution Ratios for the Example Frame Structure Without Effect of Infills

Response Quantity	Modal Contribution Ratios					
	Mode 1	Mode 2	Mode 3	Mode 4	Higher Modes	Total
Base Shear	.765	.164	.050	.012	.009	1.000
Base O.M.	.995	.002	.003	.000	.000	1.000
Top Defl.	.984	.015	.001	.000	.000	1.000
Max. I.D.	.954	.036	.002	.005	.003	1.000

Table 20.4: Modal Contribution Ratios for the Example Frame Structure With Effect of Infills

system of a building structure; therefore, their design for strength and ductility must be considered so that they can contribute in resisting the induced earthquake loads.

CHAPTER 21

THE STIFFENING EFFECT OF NON-LOADBEARING INFILLS: CONCLUSIONS AND RECOMMENDATIONS

21.1 Conclusions

As a result of the investigation performed on moment-resisting frames infilled with non-loadbearing masonry walls having a gap at the top of the infill, the following conclusions are drawn. As in the conclusions of the first part, specific percentages or factors given for the effects of the non-loadbearing concrete blockwork infills should be regarded as an indication of the importance in accounting for the infills.

1. By writing a short program to pre- and post-process results given by a commercial finite element program, such as SAP80, the iterative analysis of an infilled frame with a gap at the top of the infill can be performed. A properly conceived mathematical model of a single-storey module of an infilled frame, representing the behaviour of the frame, the infill, and the interaction between them realistically is required.

2. The effect of including the weight of the infill in the mathematical model of the single-storey module is negligible. Its inclusion is not advisable since it would prevent the deflections and stresses being scaled for different values of lateral loads.

3. It is deduced from the results of analyses of representative infilled frames that the effect of an infill, with a gap at the top, on the structural response of a moment-resisting frame is to increase the racking stiffness of the frame by approximately 300 to 800 percent, and to reduce the frame-member moments by approximately 70 percent or more.

4. The difference in the calculated stiffness response of the infilled frame as a result of varying the beam stiffness, from -10 to +10 percent for beam stiffness variations of 50 and 200 percent, respectively, is believed to be due to the change in the frame's flexibility. The lengths of contact between the infill and the frame, and therefore the stiffness of the infill's equivalent strut, were not significantly affected by the change in beam stiffness.

5. There is evidence that doubling the column stiffnesses of the infilled frame increases the length of contact between the infill and the column near the top end of the compression diagonal. This causes a more broadly distributed interaction between the infill and the frame, resulting in an increase in the stiffness of the equivalent strut and in the overall stiffness response.
6. The length-to-height ratio affects the behaviour of the infilled frame. The greater the ratio, the more flexible the infilled frame. This is due to the more flexible frame, the proportionately shorter contact lengths between the frame and infill giving greater strains in the compressive regions, and the greater axial deformations in the beam and the equivalent strut for a given sectional area of the strut.
7. The vertical, shear, tensile and compressive stresses resulting in the infills are maximum near the top loaded corner of the infilled frame.
8. The lateral stiffness of an infilled frame with a gap at the top is significantly less than that of a fully infilled frame due to the reduced regions of contact between the infill and the frame in the former case, and the biaxial compressive state of stress of the upper compressive corner in the latter case.
9. In general, cracking in the infills is initiated by a bed joint shear failure which can be reasonably predicted by Coulomb's theory of internal friction.
10. The best model to represent the interaction between the infill and the frame includes a three-member strut as shown in Fig. 18.11. However, because of its impracticality for analysis, the simpler column-to-column strut model, Fig. 18.3, is recommended as giving a reasonably fair and accurate representation of the infill's effect on the frame stiffness and member moments.
11. The effect on the static wind load response of two-bays of non-loadbearing infills per storey of an example moment-resisting frame structure, is to reduce the top deflection of the structure without infills by 25 percent, and to reduce the moments in the structure's columns and beams in the lower stories by 25 to 30 percent.
12. The overall flexural mode of deformation of a moment-resisting frame structure increases when the effect of the infills is incorporated in the structure. This is a result of the increased axial deformations in the columns adjacent to the infill arising from the vertical components of the infills' diagonal bracing action.
13. As a result of the forces induced in the non-loadbearing masonry walls of the example moment-resisting frame structure, the infills would need to be strengthened if they were to be designed to brace the building against wind loading.
14. The addition of bracing struts, representing the infills, did not significantly affect the mode shapes of the example moment-resisting frame structure, but the natural periods of vibration were 15 to 18 percent smaller than those of the structure without the struts. The base shear and overturning moment were increased by approximately

23 percent when the stiffening effect of the infills was added. The deflections were not as significantly affected.

15. It can be stated as a qualitative deduction that non-loadbearing infills should be strengthened and their ductility improved if they are to be used to resist seismic loads.

21.2 Procedure for Analysis of Building Structures Braced by Non-Loadbearing Infills

On the basis of the study described in Part II of this thesis, a practical procedure for the analysis of building structures braced by "non-loadbearing" infills is developed. This also includes a brief description of how to evaluate the loads induced in the infills and in the moment-resisting frame. Consequently, the engineer can design the frame and the infills of the building to ensure the adequacy of its lateral stiffness and strength.

The analysis procedure is summarized as follows:

1. A detailed finite element analysis of a single-storey module representing a typical storey of the building's infilled frame subjected to a lateral load is performed. The single-storey model must be carefully devised, as described in Section 15.2, to obtain a proper representation of the behaviour of the infilled frame with a gap at the top of the infill.

2. From the results of the detailed analysis, the vertical, shear, and maximum tensile and compressive stresses in the infill are extracted. The loads to initiate failure are calculated as explained in Chapter 17.

3. The section and placement of the equivalent column-to-column strut, which is used to represent the infills in the overall structure analyses, is determined using the inter-storey drift and the moments at the ends of the columns that result from the detailed analysis. A description of the equivalent strut is given in Section 18.2.

4. The equivalent column-to-column struts representing the infills are then incorporated in the mathematical model of the building structure to allow its structural analysis. The building models with the bracing struts can be easily analysed for wind and earthquake loadings. Examples are given in Chapters 19 and 20.

5. The forces shown to be induced in the infills by the overall structure's wind or earthquake analysis are checked against their strengths. The shear carried by the infilled frame in each storey is taken as the sum of the shears in the columns adjacent to and immediately above the top of the infill. The calculated load carried by the infilled frame is then compared with the load to initiate failure of the infill determined in Step 2. This is demonstrated by an example in Section 19.4. The columns and beams

at the bottom-right corner of the infilled frame may require to be designed to carry greater shear and moment imposed on them.

21.3 Further Recommendations

1. A more extensive study should be made of the relationship between the stiffness response of an infilled frame with a gap at the top of the infill and the frame member's stiffnesses, and the infilled frame's aspect ratio.
2. It would be of value to test models, a few storeys high, of infilled frames with gaps at the top of the infill subjected to lateral loads to experimentally confirm the predicted behaviour of a typical storey of the infilled frame.
3. The effect of adjacent-bay infills on the behaviour of an infilled frame with a gap at the top of the infill should be investigated.
4. In considering masonry infills as bracing components, engineers and constructors should respect the requirement in the Canadian Standard on Masonry Design for Buildings (1984) that masonry walls should be reinforced in seismic zones 2 and greater.
5. As an extension to this initial study on the effects of infilled frames with gaps at the top of the infills, a program of experimental testing for the reverse cyclic degradation of the infill's strength should be performed, and the tests results compared with the results from nonlinear analyses.

CHAPTER 22

GENERAL CONCLUSIONS

This study of the lateral stiffening contributed to building structures by non-structural components, and in particular by precast concrete cladding panels and non-loadbearing masonry infill walls, has made a number of original contributions to structural engineering knowledge. In general terms, as opposed to the more specific conclusions in Part 1 and 2, these may be described as follows.

A new understanding has been gained of the interaction between the non-structural elements studied and the primary structure.

The nature and magnitude of the forces induced in the components by their interaction with the frame have been determined.

New, practically useful, modelling techniques for representing the non-structural elements in total building structures have been developed.

The effects of the non-structural components on the static wind load and seismic responses of representative types of tall building structures have been revealed.

Procedures for analysing the total building structures braced by the non-structural elements have been proposed.

In closing, it is necessary for the author to comment that, beyond this contribution to the knowledge in this field, much further work remains to be done to obtain a full understanding of the interaction of cladding panels and non-loadbearing infill walls with their supporting frames. The influences of the many concerned parameters must be more extensively pursued, while the prospect of investigating non-linear behaviour and reverse cyclic loading effects may well involve a study of an order greater in magnitude.

REFERENCES

1. *Aluminum Curtain Wall Design Guide Manual* (1979). Architectural Aluminum Manufacturers Association, Chicago, Illinois, Vols. 1-9.

2. American Petroleum Institute (1981). "API Recommended Practice for Planning, Designing and Constructing Fixed Offshore Platforms," API-RP-2A, 12th Ed.

3. Arya, S. K., and Hegemier, G. A. (1982). "Finite Element Method for Interface Problems," *J. Struct. Div., ASCE*, Vol. 108, No. ST2, pp. 327-342.

4. Atkinson, R. H. et al. (1989). "Response of Masonry Bed Joints in Direct Shear," *J. Struct. Div., ASCE*, Vol. 115, No. 9, pp. 2276-2296.

5. Benjamin, J. R., and Williams, H. A. (1958). "The Behavior of One Storey Brick Shear Walls," *J. Struct. Div., ASCE*, Vol. 84, No. ST4, pp. 1723-1730.

6. Brookes, A. J. (1983). *Cladding of Buildings*, Construction Press, London, England.

7. Clough, R.W., and Penzien, J. (1975). *Dynamics of Structures*, McGraw-Hill Inc., USA.

8. Collins, M. P., and Mitchell, D. (1987). *Prestressed Concrete Basics*, Chapter 3, Canadian Prestressed Concrete Institute, Ottawa, Ontario.

9. *Concrete Masonry Units* (1985). CAN3-A165.1-M85, Canadian Standards Association, Rexdale, Ontario.

10. Coull, A., and Wong, Y. C. (1981). "Bending Stiffness of Floor Slabs in Cross-Wall Structures," *Proc. Instn. Civ. Engrs.*, Part 2, Vol. 71, pp. 17-35.

11. *CPCI Metric Design Manual (Precast and Prestressed Concrete)* (1987). Canadian Prestressed Concrete Institute, Ottawa, Ontario.

12. Craig, J. I., Leistikow, R., and Fennell, C. J. (1988). "Experimental Studies of the Performance of Precast Cladding Connections," *Proc. of the 9th World Conf. Earthquake Engrg.*, Tokyo, Japan, Vol. VI, VI-201 - VI-206.

13. Crawford, R. and Ward, H.S. (1964). "Determination of the Natural Periods of Buildings," *Bull. Seismological Soc. of Am.*, Vol. 54, No. 6, pp. 1743-1756.

14. Dawe, J. L., and Yong, T. C. (1985). "An Investigation of Factors Influencing the Behaviour of Masonry Infill in Steel Frames Subjected to In-Plane Shear," *Proc. of* 7^{th} *Int. Brick Masonry Conf.*, Melbourne, Australia, Vol. 2, pp. 803-814.

15. Dawson, R. V. (1972). "An Analytical and Experimental Study of the Lateral Load Response of Framed Structures Before and After the Inclusion of Infill Walls," thesis submitted to the University of Calgary, Alberta, Canada, in partial fulfillment of the requirements for the degree of Doctor of Philosophy of Engineering.

16. *Design of Concrete Structures for Buildings* (1984). CAN3-A23.3- M84, Canadian Standards Association, Rexdale, Ontario.

17. Drysdale, R. G., and Hamid, A. A. (1982). "In-Plane Tensile Strength of Concrete Masonry," *Can. J. Civ. Engrg.*, Vol. 9, No. 3, pp. 413-421.

18. Drysdale, R. G., and Hamid, A. A. (1984). "Tension Failure Criteria for Plain Concrete Masonry," *J. Struct. Div., ASCE*, Vol. 110, No. 2, pp. 228-244.

19. Drysdale, R. G. et al. (1983). "Comments on Block Masonry Design Code Provisions for Allowable Stresses," *Proc. of* 3^{rd} *Canadian Masonry Symposium.*

20. El-Gazairly, L. F., and Goodno, B. J. (1989). "Dynamic Analysis of a Highrise Building Damaged in the Mexico Earthquake including Cladding-Structure Interaction," *Proc. of the Int. Symposium on Architectural Precast Concrete Cladding - Its Contribution to Lateral Resistance of Buildings*, Chicago, Illinois.

21. Ellis, B. R. (1980). "An Assessment of the Accuracy of Predicting the Fundamental Natural Frequencies of Buildings and the Implications Concerning the Dynamic Analysis of Structures," *Proc. Instn. Civ. Engrs.*, Vol. 69, Part 2, pp. 763-776.

22. Ellis, B. R., Evans, R. A., Jeary, A. P., and Lee, B. E. (1979). "The Wind-Induced Vibration of a Tall Building," *Proc. Int. Symposium Practical Experiences with Flow Induced Vibrations*, Karlsruhe, pp. 747-752.

23. Elmiger, A. (1976). *Architectural and Engineering Concrete Masonry Details for Building Construction*, National Concrete Masonry Association, Virginia, USA.

24. *Engineering News-Record* (1976). "Guatemala Digs Out After Quake; Lessons Bode Well for California," Vol. 196, No. 11, pp. 8-9.

25. *Engineering News-Record* (1980). "Facades: Errors Can Be Expensive," Vol. 204, No. 4, pp. 30-34.

26. Essawy, A. S., and Drysdale, R. G. (1986). "Macroscopic Failure Criterion for Masonry Assemblages," *Proc. of* 4^{th} *Canadian Masonry Symposium*, University of New Brunswick, Canada, pp. 263-277.

27. Esteva, L. (1966). "Behaviour Under Alternating Loads of Masonry Diaphragms Framed by Reinforced Concrete Memb ..s," *Proc. of Int. Symposium on Effects of Repeated Loading of Materials and Structural Elements*, RILEM, Mexico.

28. Fattal, S. G. (1977). "The Capacity of Unreinforced Masonry Shear Walls Under Membrane Loads," National Bureau of Standards, NBS Building Science Series 106, pp. 177-197.

29. Freeman, S. A. (1977). "Racking Tests of High-Rise Building Partitions," *J. Struct. Div., ASCE*, Vol. 103, No. ST8, pp. 1673-1685.

30. Gjelsvik, A. (1974). "Interaction Between Frames and Precast Panel Walls," *J. Struct. Div., ASCE*, Vol. 100, No. ST2, pp. 405-426.

31. Goodman, R. et al. (1968). "A Model for the Mechanics of Jointed Rock," *J. Soil Mech. Foundation Div., ASCE*, Vol. 94, pp. 637-659.

32. Goodno, B. J., Meyyappa, M., and Nagarajaiah, S. (1988). "A Refined Model for Precast Cladding and Connections," *Proc. of the 9th World Conf. on Earthquake Engrg.*, Tokyo, Japan, Vol. VI, VI-195 - VI-200.

33. Goodno, B. J., and Palsson, H. (1986). "Analytical Studies of Building Cladding," *J. Struct. Div., ASCE*, Vol. 112, No. 4, pp. 665-676.

34. Goodno, B. J., and Will, K. M. (1978). "Dynamic Analysis of a High-Rise Building Including Cladding-Structure Interaction Effects," *Proc. Conf. on Computers in Civ. Engrg.*, 1st, Atlanta, Ga., pp. 623-638.

35. Green, R. (1982). "Building Skins: An Overview of Today's Technology," *The Canadian Architect*, Vol. 27, No. 8, pp. 14- 34.

36. Hamid, A. A., and Drysdale, R. G. (1980a). "Behaviour of Brick Masonry Under Combined Shear and Compression Loading," *Proc. of 2nd Canadian Masonry Symposium*, Ottawa, Canada, pp. 51-64.

37. Hamid, A. A., and Drysdale, R. G. (1980b). "Concrete Masonry Under Combined Shear and Compression Along the Mortar Joints," *J. of ACI*, Vol. 77, No. 5, pp. 314-320.

38. Hamid, A. A., and Drysdale, R. G. (1981). "Proposed Failure Criteria for Concrete Block Masonry Under Biaxial Stresses," *J. Struct. Div., ASCE*, Vol. 107, No. ST8, pp. 1675-1687.

39. Hamid, A. A., Drysdale, R. G., and Heidebrecht, A. C. (1979). "Shear Strength of Concrete Masonry Joints," *J. Struct. Div., ASCE*, Vol. 105, No. ST7, pp. 1227-1240.

40. *Handbook of Steel Construction* (1982). 3rd Ed., Canadian Institute of Steel Construction, Willowdale, Ontario.

41. Hegemier, G. A., Nunn, R. O., and Arya, S. K. (1978). "Behavior of Concrete Masonry Under Biaxial Stresses," *Proc. of the North American Masonry Conf.*, University of Colorado, pp. 1-1 - 1-28.

42. Heidebrecht, A. C., and Stafford Smith, B. (1973). "Approximate Analysis of Tall Wall-Frame Structures," *J. Struct. Div., ASCE*, Vol. 99, No. ST2, pp. 199-221.

43. Henry, R. M., Kennedy, D., and Goodspeed, C. H. (1989). "A Simplified Box- Frame Model for Structural Cladding Panels," *Proc. of the Int. Symposium on Architectural Precast Concrete Cladding - Its Contribution to Lateral Resistance of Buildings*, Chicago, Illinois.

44. Henry, R. M., and Roll, F. (1986). "Cladding-Frame Interaction," *J. Struct. Div., ASCE*, Vol. 112, ST4, pp. 815-834.

45. Holmes, M. (1961). "Steel Frame with Brickwork and Concrete Infilling," *Proc. Instn. Civ. Engrs.*, Vol. 19, pp. 473-478.

46. Irons, B., and Ahmad, S. (1980). *Techniques of Finite Elements*, Ellis Horwood Limited, Chichester, England.

47. King, G. J. W., and Chandrasekaran, V. S. (1975). "An Assessment of the Effects of Interaction Between a Structure and its Foundation in Settlement of Structures," Pentech, London, pp. 368-383.

48. King, G. J. W., and Pandey, P. C. (1978). "Analysis of Infilled Frames Using Finite Elements," *Proc. Instn. Civ. Engrs.*, Vol. 65, Part 2, pp. 749-760.

49. Kost, G., Weaver, W., Jr., and Barber, R. (1974). "Nonlinear Dynamic Analysis of Frames with Filler Panels," *J. Struct. Div., ASCE*, Vol. 100, No. ST4, pp. 743-757.

50. *Lotus - 123* (1986). Release 2.01, Lotus Development Corporation, Cambridge, Massachussetts.

51. Mainstone, R. J. (1971). "On the Stiffness and Strength of Infilled Frames," *Proc. Instn. Civ. Engrs.*, Vol. 48, pp. 57-90.

52. Mainstone, R. J., and Weeks, G. (1970). "The Influence of a Bounding Frame on the Racking Stiffnesses and Strengths of Brick Walls," *Proc. of 2nd Int. Brick Masonry Conf.*, SIBMAC, Stoke-on-Trent, pp. 165-171.

53. Maison, B.F., Neuss, C.F., and Kasai, K. (1983). "The Comparative Performance of Seismic Response Spectrum Combination Rules in Building Analysis," *Earthquake Engrg. and Struct. Dynamics*, John Wiley & Sons Ltd., Vol. 11, No. 5.

54. Mallick, D. V., and Garg, R. P. (1971). "Effect of Openings on the Lateral Stiffness of Infilled Frames," *Proc. Instn. Civ. Engrs.*, Vol. 49, pp. 193-209.

55. Mallick, D. V., and Severn, R. T. (1967). "The Behaviour of Infilled Frames Under Static Loading," *Proc. Instn. Civ. Engrs.*, Vol. 3, pp. 639-656.

56. Marcakis, K., and Mitchell, D. (1980). "Precast Concrete Connections With Embedded Steel Members," *PCI Journal*, Vol. 25, No. 4, pp. 88-116.

57. Martineau, R. (1989). "Case Study of a Precast Cladding Interacting with a 15-Story Steel Frame to Provide Lateral Resistance," *Proc. of the Int. Symposium on Architectural Precast Concrete Cladding - Its Contribution to Lateral Resistance of Buildings*, Chicago, Illinois.

58. *Masonry Construction for Buildings* (1984). CAN3-A371-M84, Canadian Standards Association, Rexdale, Ontario.

59. *Masonry Design for Buildings* (1984). CAN3-S304-M84, Canadian Standards Association, Rexdale, Ontario.

60. Maurenbrecher, A. H. P. (1986). "Compressive Strength of Hollow Concrete Blockwork," *Proc. of* 4^{th} *Canadian Masonry Symposium*, University of New Brunswick, Canada, pp. 997-1009.

61. Mayes, R. L., and Clough, R. W. (1975). "A Literature Survey - Compressive, Tensile, Bond and Shear Strength of Masonry," Earthquake Engrg. Research Center, EERC 75-15, University of California, Berkeley.

62. McCue, G. M. et al. (1975). "Building Enclosure and Finish Systems: Their Interaction with the Primary Structure During Seismic Action," *U.S. National Conf. on Earthquake Engrg.*, Ann Arbor, Michigan, pp. 235-244.

63. *National Building Code of Canada* (1980). NRCC No. 17303, National Research Council of Canada, Ottawa, Ontario.

64. *National Building Code of Canada* (1985). NRCC No. 23174, National Research Council of Canada, Ottawa, Ontario.

65. National Concrete Masonry Association (1969). "Compressive Strength of Concrete Masonry," Tek 15, Virginia, USA.

66. National Concrete Masonry Association (1972). "Control of Wall Movement with Concrete Masonry," Tek 3, Virginia, USA.

67. National Concrete Masonry Association (1973). "Design of Concrete Masonry for Crack Control," Tek 53, Virginia, USA.

68. National Concrete Masonry Association (1975). "Empirical Design of Concrete Masonry Walls," Tek 73, Virginia, USA.

69. National Concrete Masonry Association (1975). "Joint Reinforcement and Other Metal Ties for Concrete Masonry Walls," Tek 64, Virginia, USA.

70. National Concrete Masonry Association (1980). "Lateral Support of Concrete Masonry Walls," Tek 111, Virginia, USA.

71. National Concrete Masonry Association (1977). "Metal Anchors for Concrete Masonry Walls," Tek 21A, Virginia, USA.

72. National Concrete Masonry Association (1984). "Mortars for Concrete Masonry," Tek 20A, Virginia, USA.

73. National Concrete Masonry Association (1976). "Sizes and Shapes of Concrete Masonry Units," Tek 2A, Virginia, USA.

74. Neuss, C.F., Maison, B.F., and Bouwkamp, J.G. (1983). "A Study of Computer Modeling Formulation and Special Analytical Procedures for Earthquake Response of Multistory Buildings," A Report to the National Science Foundation, J.G. Bouwkamp, Inc.

75. Newmark, N.M., and Hall, W.J. (1973). "Procedures and Criteria for Earthquake Resistant Design," *Building Practices for Disaster Mitigation*, National Bureau of Standards, Building Science Series 46.

76. Newmark, N.M., Blume, J.A., and Kapur, K.K. (1973). "Seismic Design Spectra for Nuclear Power Plants," *J. Power Div., ASCE*, Vol. 99, No. PO2, pp. 287-304.

77. Nuclear Regulatory Commission (1973). "Design Response Spectra for Seismic Design of Nuclear Power Plants," Regulatory Guide 1.60, Directorate of Regulatory Standards, Washington, D.C., USA.

78. Ontario Masonry Contractors' Association. "4C - Capsule Comments about Common Concerns," Ontario, Canada.

79. Page, R. A. et al. (1975). "Earthquake Shaking and Damage to Buildings," *Science*, Vol. 189, No. 4203, pp. 601-608.

80. Palsson, H., and Goodno, B. J. (1988). "Influence of Interstory Drift on Cladding Panels and Connections," *Proc. of the 9th World Conf. on Earthquake Engrg.*, Tokyo, Japan, Vol. VI, VI-213 - VI-218.

81. Palsson, H., Goodno, B.J., Craig, J.I. and Will, K.M. (1984). "Cladding Influence on Dynamics Response of Tall Buildings," *Earthquake Engrg. and Struct. Dynamics*, Vol. 12, pp. 215-228.

82. *PCI Design Handbook Precast and Prestressed Concrete* (1985). Prestressed Concrete Institute, Chicago, Illinois.

83. *PCI Manual for Structural Design of Architectural Precast Concrete* (1977). Prestressed Concrete Institute, Chicago, Illinois.

84. Pinelli, J. P., and Craig, J. I. (1989). "Experimental Studies of the Performance of Mexican Precast Cladding Connections," *Proc. of the Int. Symposium on Architectural Precast Concrete Cladding - Its Contribution to Lateral Resistance of Buildings*, Chicago, Illinois.

85. Polyakov, S. V. (1956). "Masonry in Framed Buildings: An Investigation into the Strength and Stiffness of Masonry Infilling," State Publishing House of Literature on Building and Architecture, (English Translation), Moscow.

86. Pook, L. L., and Dawe, J. L. (1986). "Effects of Interface Conditions Between a Masonry Shear Panel and Surrounding Steel Frame," *Proc. of* 4^{th} *Canadian Masonry Symposium*, University of New Brunswick, Canada.

87. Pook, L. L., Stylianou, M. A., and Dawe, J. L. (1986). "Experimental Investigation of the Influence of Compression on the Shear Strength of Masonry Joints," *Proc. of* 4^{th} *Canadian Masonry Symposium*, University of New Brunswick, Canada, pp. 1053-1062.

88. Raggett, J. D. (1972). "Influence of Nonstructural Partitions on the Dynamic Response Characteristics of Structures," Report No. JAB-99-94, John A. Blume and Associates Research Division, San Francisco, California.

89. Rathbun, J. C. (1938). "Wind Forces on a Tall Building," *ASCE, Transactions*, Paper No. 2056, pp. 1-82.

90. *Recommended Lateral Force Requirements and Tentative Commentary* (1988). SEAOC Seismology Committee, San Francisco, California.

91. Riddington, J. R. (1974). "The Composite Behaviour of Walls Interacting with Flexural Members," thesis submitted to the University of Southampton, England, in partial fulfillment of the requirements for the degree of Doctor of Philosophy of Engineering.

92. Riddington, J. R. (1984). "The Influence of Initial Gaps on Infilled Frame Behaviour," *Proc. Instn. Civ. Engrs.*, Vol. 77, Part 2, pp. 295-310.

93. Riddington, J. R., and Stafford Smith, B. (1977). "Analysis of Infilled Frames Subject to Racking with Design Recommendations," *The Structural Engineer*, Vol. 52, No. 6, pp. 263-268.

94. Rihal, S. S. (1989). "Earthquake Resistance and Behavior of APCC and Connections," *Proc. of the Int. Symposium on Architectural Precast Concrete Cladding - Its Contribution to Lateral Resistance of Buildings*, Chicago, Illinois.

95. Sack, R. L., Beers, R. J., and Thomas, D. L. (1989). "Seismic Behavior of Architectural Precast Concrete Cladding," *Proc. of the Int. Symposium on Architectural Precast Concrete Cladding - Its Contribution to Lateral Resistance of Buildings*, Chicago, Illinois.

96. *SAP80 Structural Analysis Programs* (1986). Computers & Structures Inc., Berkeley, California.

97. Scrivener, J. C. (1969). "Static Racking Tests on Concrete Masonry Walls," *Designing, Engrg. & Constructing with Masonry Products, Proc. Int. Conf. on Masonry Structural Systems*, University of Texas, pp. 185-191.

98. Sharpe, R. (1972). "Seismic Design of Nonstructural Elements," *ASCE-IABSE Conf. on Planning & Design of Tall Bldgs.*, Discussion No. 2, Vol. 1a-12, Lehigh University, pp. 1143-1148.

99. Shepherd, R., Pardoen, G. C., and Burridge, P. B. (1983). "Analytical and Experimental Dynamic Analyses of a Ten Story Building," *Proc. of* 4^{th} *Canadian Conf. on Earthquake Engrg.*, Vancouver, pp. 362-371.

100. Shing, P. B., Noland, J. L., Spaeh, H., and Klamerus, E. (1987). "Inelastic Behavior of Masonry Wall Panels Under In-Plane Cyclic Loads," *Proc. of* 4^{th} *North American Masonry Conference*, University of California, Los Angeles, Calif., pp. 42-1 - 42-14.

101. Simms, L. G. (1964). "The Shear Strength of Some Storey-Height Brickwork and Blockwork Walls," *CPTB Technical Note*, Clay Products Technical Bureau, London, Vol. 1, No. 5, pp. 1-8.

102. Smith, R. C. et al. (1979). *Masonry: Materials, Design, Construction*, Reston Publishing Co., Inc., Virginia, USA.

103. Stafford Smith, B. (1962). "Lateral Stiffness of Infilled Frames," *J. Struct. Div., ASCE*, Vol. 88, No. ST6, pp. 183-199.

104. Stafford Smith, B. (1966). "The Composite Behavior of Infilled Frames," *Tall Buildings*, Pergamon, Oxford, pp. 481-492.

105. Stafford Smith, B. (1967). "Methods for Predicting the Lateral Stiffness and Strength of Multi-Storey Infilled Frames," *Building Science*, 2, pp.247-257.

106. Stephen, R.M., et al. (1974). "The Dynamic Behavior of a Multi-storey Pyramid-Shaped Building," Earthquake Engrg. Research Centre, Report EERC 73-17, Berkeley, California.

107. Tomasetti, R.L., et al. (1986). "A Stressed-Skin Tube Tower: One Mellon Bank Centre," *Advances in Tall Buildings*, Council on Tall Buildings & Urban Habitat, Van Nostrand Reinhold Co., N.Y., pp. 573-605.

108. Veterans Administration (1973). "Earthquake Resistant Design Requirements for VA Hospital Favilities," Office of Construction, Handbook H-08-8.

109. Wan Qinglin and Yi Wenzong (1986). "The Shear Strength of Masonry Wall Under Combined Stresses," *Proc. of* 4^{th} *Canadian Masonry Symposium*, University of New Brunswick, Canada, pp. 596-608.

110. Ward, H.S., and Crawford, R. (1966). "Wind-Induced Vibrations and Building Modes," *Bull. of the Seisomological Soc. of Am.*, Vol. 56, No. 4, pp. 793-813.

111. Weidlinger, P. (1973). "Shear Field Panel Bracing," *J. Struc. Div., ASCE*, Vol. 99, No. ST7, Paper 9870, pp. 1615-1631.

112. Wilson, E. L., Der Kiureghian, A., and Bayo, E. P. (1981). "A Replacement for the SRSS Method in Seismic Analyses," *Earthquake Engrg. and Struct. Dynamics*, Short Communications, Vol. 9, pp. 187-194.

113. Wiss, J. F., and Curth, O. E. (1970). "Wind Deflections of Tall Concrete Frame Buildings," *J. Struct. Div., ASCE*, Vol. 96, No. ST7, pp. 1461-1480.

114. Wolde-Tinsae, A. M., and Raj, B. (1986). "Behavior of Semi-Confined and Fully Confined Externally Reinforced Masonry Walls," *Proc. of* 4^{th} *Canadian Masonry Symposium*, University of New Brunswick, Canada, pp. 1038-1052.

115. Wolde-Tinsae, A. M. et al. (1987). "Finite Element Study of Semi-Confined Masonry Walls," *Proc. of* 4^{th} *North American Masonry Conf.*, University of California, Los Angeles, USA, pp. 19-1 - 19-15.

116. Woodward, K., and Rankin, F. (1984). "Influence of Vertical Compressive Stress on Shear Resistance of Concrete Block Masonry Walls," National Bureau of Standards, U.S. Dept. of Commerce, Report No. NBSIR 84-2929, Gaithersburg, Md.

117. Woodward, K., and Rankin, F. (1985). "Influence of Aspect Ratio on Shear Resistance of Concrete Block Masonry Walls," National Bureau of Standards, U.S. Dept. of Commerce, Report No. NBSIR 84-2993, Gaithersburg, Md.

118. Yong, T. C. (1984). "Shear Strength of Masonry Infilled Panels in Steel Frames," thesis submitted to the University of New Brunswick, Canada, in partial fulfillment of the requirements for the degree of Master of Science in Engineering.

APPENDIX A

THE FLEXIBILITY OF THE PANEL-CLAD FRAME'S ANALOGOUS SPRING MODEL IN ALGEBRAIC TERMS

In this appendix, the analogous spring model described in Chapter 5, Section 5.2, is used to develop an expression for the flexibility of the complete panel-clad frame module in algebraic terms, as a function of the flexural inertias of the frame members, the flexibilities of the panel and its connections, the storey height, and the relative distance of the bearing connections from the column-beam joint to the length of the beam. Using this algebraic expression, the sensitivity of the structure's lateral flexibility to the flexibilities of the frame, panel and connections can be deduced.

As was explained in Section 5.2, the flexibilities representing the behaviour of the beam, f_{b1}, f_{b2} and f_{b3}, are unknown; therefore, three equations are required to solve for these. Consider first the flexibility of the beam bending in 'forward' double curvature. This is equivalent to finding the lateral flexibility of the frame in Fig. A.1, which consists of a flexible beam with a flexural rigidity of EI_b, very rigid columns, and a rigid link at the top to constrain the tops of the columns to translate identically. From Fig. A.1, the flexibility of the beam bending in 'forward' double curvature is given as

$$\frac{\Delta_1}{Q} = \frac{h^2 L}{12EI_b} \tag{A.1}$$

In terms of the analogous spring model, the flexibility of the beam bending in 'forward' double curvature was given in Eq. 5.3. Substituting the left side of Eq. 5.3 into Eq. A.1 yields

$$f_{b1} + f_{b3} = \frac{h^2 L}{12EI_b} \tag{A.2}$$

Eq. A.2 is valid for a beam of length L, flexural inertia I_b, and no rigid beam-ends.

Consider next the flexibility of the beam bending in 'backward' double curvature. This is equivalent to finding the lateral flexibility of the frame in Fig. A.2, which consists of a rigid frame supported by a flexible beam. Referring to Fig. A.2, the flexibility of the beam

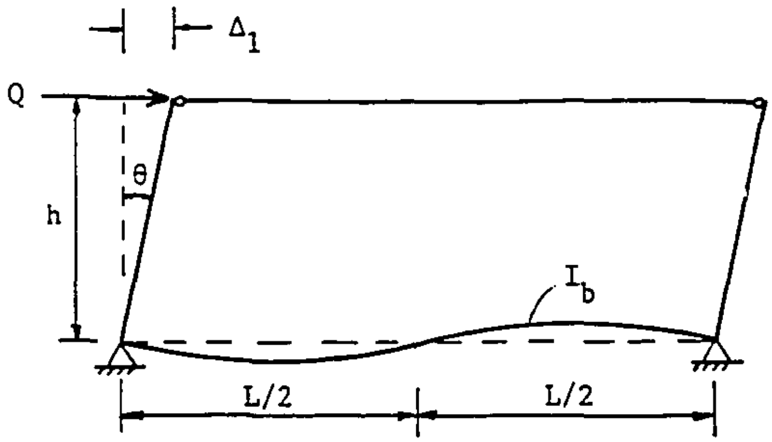

$$\theta = \frac{\Delta_1}{h}$$

Moment at the end of the beam $= \frac{Qh}{2}$

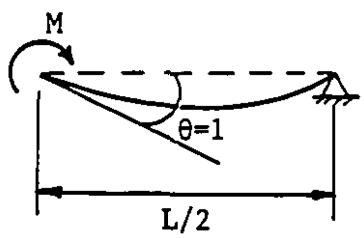

$$\text{Rot. Stiff.} = \frac{M}{\theta} = \frac{3EI_b}{L/2} = \frac{6EI_b}{L}$$

Figure A.1: Flexibility of Beam Bending in 'Forward' Double Curvature

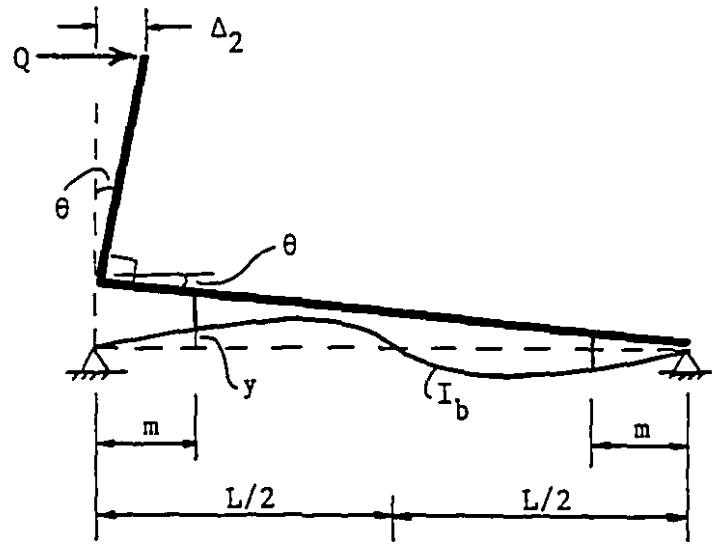

$$\theta = \frac{y}{\frac{L}{2} - m} = \frac{\Delta_2}{h-s}$$

Vert. Force in bearing conn.
$= P = \frac{Q(h-s)}{L-2m}$

where s = location of bearing conn. above beam level
= length of vert. links

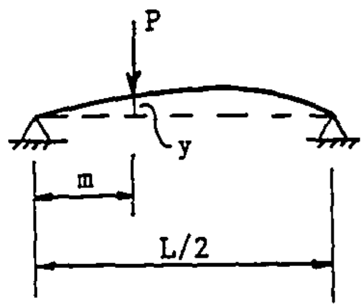

$$y = \frac{2Pm^2\left(\frac{L}{2} - m\right)^2}{3EI_bL}$$

Figure A.2: Flexibility of Beam Bending in 'Backward' Double Curvature bending in 'backward' double curvature is given by

$$\frac{\Delta_2}{Q} = \frac{(h-s)^2 m^2}{3EI_b L} \tag{A.3}$$

In terms of the analogous spring model, the flexibility of the beam bending in 'backward' double curvature was given in Eq. 5.5. Substituting the left side of Eq. 5.5 into Eq. A.3 gives

$$f_{b2} + f_{b3} = \frac{(h-s)^2 m^2}{3EI_b L} \tag{A.4}$$

Having found Eqs. A.2 and A.4, a third equation is required to solve for the three unknowns. Consider the lateral flexibility of the structure shown in Fig. A.3, consisting of a flexible beam, rigid columns, and a rigid panel with rigid connecitons. Referring to Fig. A.3, the rotation at A is given by

$$\theta = \frac{\Delta_4}{h} \tag{A.5}$$

and the deflection of the beam at B is

$$\left(\frac{L}{2} - m\right)\frac{\Delta_4}{h-s} \tag{A.6}$$

The behaviour of the beam ABC can be considered as a superposition of the beam fixed at A, and subjected to a vertical force, P, resulting in the bearing connection at B, Fig. A.4a. and of the beam subjected to a moment M_2 to allow for the rotation θ, Fig. A.4b.

The external lateral load, Q, is shared between the panel and its connections, Q_1, and the columns, Q_2, that is,

$$Q = Q_1 + Q_2 \tag{A.7}$$

Therefore, the force in the bearing connections is given by

$$P = \frac{Q_1(h-s)}{2(\frac{L}{2} - m)} \tag{A.8}$$

Referring to Fig. A.4a, the following expressions are obtained

$$M_1 = \frac{Pm\left(\frac{L}{2} - m\right)(L-m)}{2\left(\frac{L}{2}\right)^2} \tag{A.9}$$

and

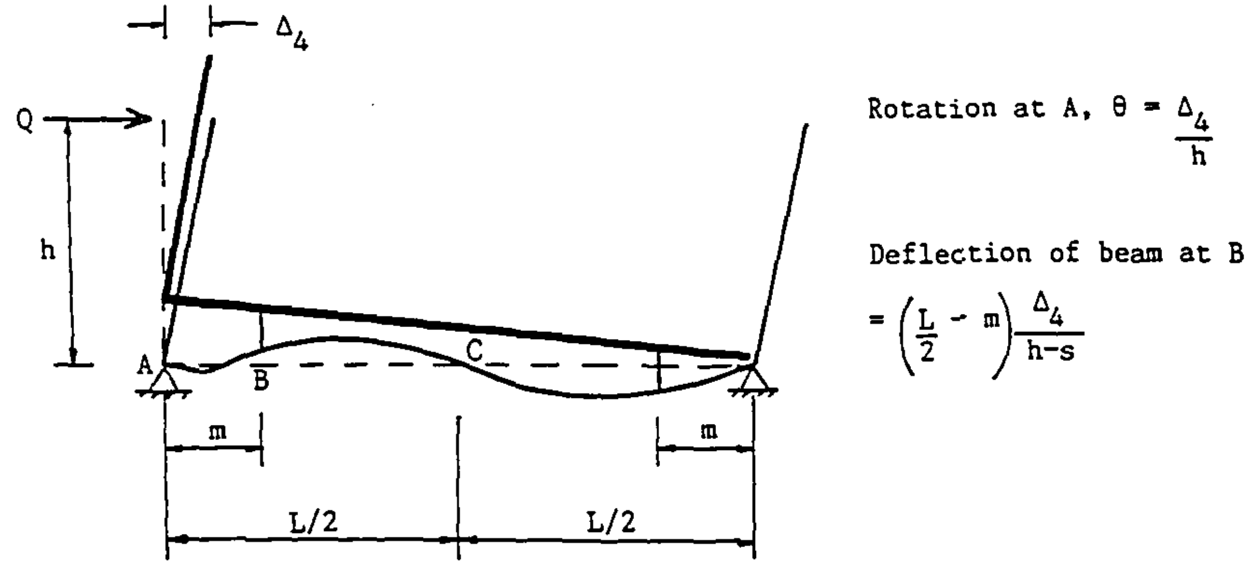

Figure A.3: Flexibility of Clad Frame with Beam Flexible, Columns Rigid, and Panel Rigid with Rigid Connections

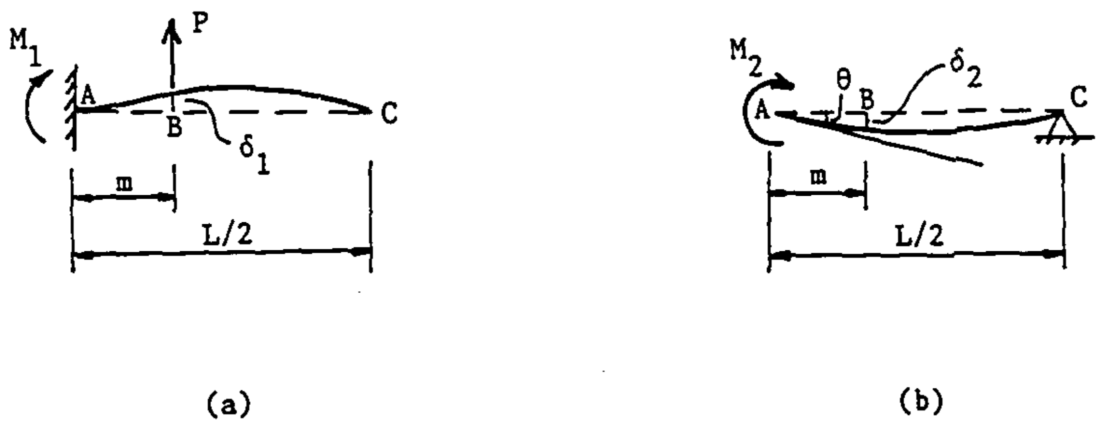

Figure A.4: Behaviour of the Beam ABC

$$\delta_1 = \frac{Pm^3\left(\frac{L}{2}-m\right)^2(2L-m)}{12EI_b\left(\frac{L}{2}\right)^3} \tag{A.10}$$

Substituting Eq. A.8 into Eqs. A.9 and A.10 yields

$$M_1 = \frac{Q_1(h-s)m(L-m)}{4\left(\frac{L}{2}\right)^2} \tag{A.11}$$

and

$$\delta_1 = \frac{Q_1(h-s)m^3(2L-m)\left(\frac{L}{2}-m\right)}{24EI_b\left(\frac{L}{2}\right)^3} \tag{A.12}$$

Referring to Fig. A.4b, and using the moment area method, the following expressions are found

$$\theta = \frac{M_2\left(\frac{L}{2}\right)}{3EI_b} \tag{A.13}$$

$$\delta_2 = \frac{M_2 m(L-m)\left(\frac{L}{2}-m\right)}{6EI_b\left(\frac{L}{2}\right)} \tag{A.14}$$

By taking the sum of the deflections of the beam at B from Figs. A.4a and A.4b, that is, Eqs. A.12 and A.14, the total deflection of the beam at B in Fig. A.3, Eq. A.6, is determined to be

$$\delta_1 - \delta_2 = \left(\frac{L}{2}-m\right)\frac{\Delta_4}{h-s}$$

$$\frac{Q_1(h-s)m^3(2L-m)}{24EI_b\left(\frac{L}{2}\right)^3} - \frac{M_2 m(L-m)}{6EI_b\left(\frac{L}{2}\right)} = \frac{\Delta_4}{h-s} \tag{A.15}$$

The moment at the end of the beam in the complete structure, Fig. A.3, is given by the superposition of the moments in Figs. A.4a and A.4b, that is,

$$\frac{Q_1(h-s)m(L-m)}{4\left(\frac{L}{2}\right)^2} + M_2 = \frac{Q_2 h}{2} \tag{A.16}$$

By equating Eq. A.5 to Eq. A.13. and rearranging, an expression for M_2 in terms of the lateral flexibility of the structure in Fig. A.3 is found

$$M_2 = \frac{\Delta_4}{h}\left(\frac{3EI_b}{\left(\frac{L}{2}\right)}\right) \tag{A.17}$$

Solving Eqs. A.7, A.15, A.16, and A.17 simultaneously, the following expression for the lateral flexibility of the structure in Fig. A.3 is obtained

$$\frac{\Delta_4}{Q} = \frac{m^3(h-s)^2(2L-m)}{3EI_bL\left\{L^2 + 4\left(\frac{h-s}{h}\right)mL - 4m^2\left(\frac{h-s}{h}\right)\left[1-\left(\frac{h-s}{h}\right)\right]\right\}} \tag{A.18}$$

Denoting the flexibility of the beam bending in 'forward' double curvature, Eq. A.2, by A, that is,

$$f_{b1} + f_{b3} = \frac{h^2L}{12EI_b} = A \tag{A.19}$$

and setting

$$\frac{h-s}{h} = \alpha \tag{A.20}$$

and

$$\frac{m}{L} = \beta \tag{A.21}$$

the flexibility of the beam bending in 'backward' double curvature, Eq. A.4, can be rewritten as

$$f_{b2} + f_{b3} = 4\alpha^2\beta^2 A \tag{A.22}$$

and the lateral flexibility of the structure in Fig. A.3, Eq. A.18, can be taken as

$$\frac{\Delta_4}{Q} = \frac{4\beta^3(2-\beta)\alpha^2}{[1+4\alpha\beta-4\beta^2\alpha(1-\alpha)]}\cdot A \tag{A.23}$$

In terms of the analogous spring model, the lateral flexibility of the structure in Fig. A.3, can be obtained by assigning a zero flexibility to the springs f_c, f_{hc}, f_p, and f_{vc} in Eq. 5.11, that is

$$\frac{\Delta_4}{Q} = \frac{f_{b1}(f_{b2}+f_{b3}) + f_{b2}f_{b3}}{(f_{b1}+f_{b3}) + (f_{b2}+f_{b3}) + 2f_{b3}} \tag{A.24}$$

Substituting Eqs. A.19, A.22, and A.23 into Eq. A.24 yields the following equation for f_{b3}

$$
\begin{aligned}
f_{b3} &= [\sqrt{k^2 - k(1 + 4\alpha^2\beta^2) + 4\alpha^2\beta^2} - k] \cdot A \\
&= p \cdot A
\end{aligned}
\tag{A.25}
$$

where

$$
k = \frac{4\beta^3(2-\beta)\alpha^2}{[1 + 4\alpha\beta - 4\beta^2\alpha(1-\alpha)]}
\tag{A.26}
$$

and

$$
p = \sqrt{k^2 - k(1 + 4\alpha^2\beta^2) + 4\alpha^2\beta^2} - k
\tag{A.27}
$$

Substituting Eqs. A.19, A.22, and A.25 into Eq. 5.11, and setting

$$
f_{hc} + f_p + f_{vc} = f_{pc}
\tag{A.28}
$$

an expression for the flexibility of the complete panel-clad frame module is determined to be

$$
\frac{\Delta_3}{Q} = \frac{f_{pc}f_c + (f_{pc} + 4\alpha^2\beta^2 f_c)A + (4\alpha^2\beta^2 - p^2)A}{f_c + f_{pc} + (1 + 4\alpha^2\beta^2 + 2p)A}
\tag{A.29}
$$

Note that the above equations are valid only for a beam which does not have rigid arms at its ends.

APPENDIX B

STIFFENING EFFECT OF THE PANEL AND CONNECTIONS ON A RIGID BEAM AND ON A FLEXIBLE FRAME

In Chapter 6, the cross-sectional areas of the diagonal bracing struts in models 2 through 4 were obtained by equating the bracing strut(s) horizontal stiffness(es) to the lateral stiffness of the panel and connections supported by a rigid beam. That is, it was assumed that the stiffening effect of the panel and its connections on a rigid beam is equal to the stiffening effect of the panel and its connections within a flexible frame. This results, as was explained in Chapter 6, because the lateral stiffening effect of the panel and its connections, thus the stiffness of the diagonal strut, is dependent on the lateral displacement of the panel, and on the vertical forces in the bearing connections. Therefore, provided that the diagonal strut(s) has the correct axial area to give the correct lateral displacement, by equilibrium the vertical forces acting transversely to the beam will be the same whether the beam is rigid or flexible. An analytical proof of the above statement follows.

First consider the panel rigidly supported and laterally loaded in its plane. This is analogous to representing the panel by a pin-jointed frame and rigidly supporting it at the same locations of the panel connections, Fig. B.1. The pin support at 1 represents the vertical and horizontal restraint provided by the windward bearing connection, the roller at 5 represents the vertical restraint provided by the leeward bearing connection, the lateral restraint at 3 represents that provided by the tie-back connection near the bottom of the panel, and the lateral load is transferred at the locations of the top tie-back connections, 2 and 4. The frame was analysed by computer, since the structure was statically indeterminate, for the loading and frame member properties shown in Fig. B.1. The resulting relative lateral displacement between the top and bottom of the frame was determined to be 64.9264 units, giving a corresponding lateral stiffness for the structure of 0.7701.

In order to claim that the stiffening effect of the panel and its connections on a rigid beam is identical to the stiffening effect of the panel and its connections within a flexible frame, the diagonal stiffness of the panel's analogous frame, Fig. B.2, converted to a horizontal stiffness must be identical to that computed above from Fig. B.1. Using the method of virtual work, the diagonal stiffness of the frame, Fig. B.2, was found to be 0.9626. The lateral stiffness is equal to the product of the diagonal stiffness and $\cos^2\theta$, Eq. 6.1, where θ is the angle of the diagonal to the horizontal. Therefore, for the frame in Fig. B.2,

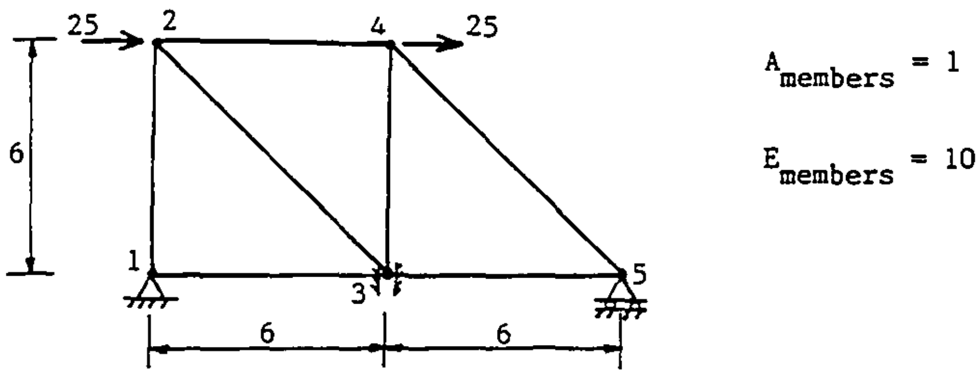

Figure B.1: Mathematical Model of Frame Representing Panel Supported by a Rigid Beam

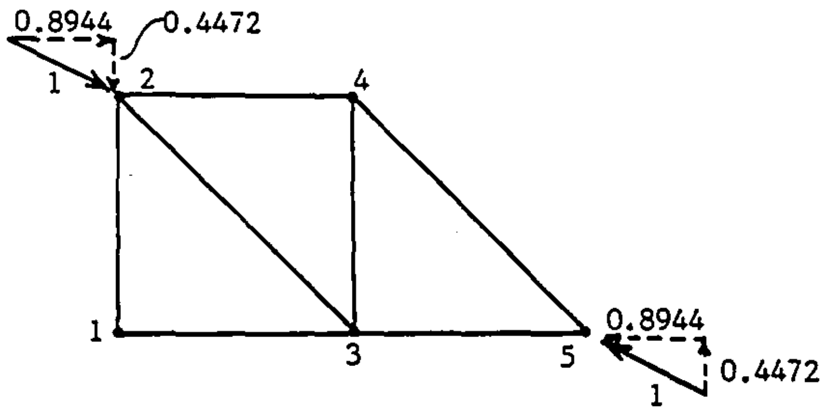

Figure B.2: Model Used to Compute Diagonal Stiffness of the Panel's Analogous Frame

$\theta = 26.565°$, and the resulting lateral stiffness is computed to be 0.7701, which is identical to that obtained for the rigidly supported frame in Fig. B.1.

APPENDIX C

THE EFFECT OF PRECAST CONCRETE CLADDING PANELS ON A LOW-RISE MOMENT-RESISTING FRAME STRUCTURE

The influence of the precast concrete cladding panels on the lateral stiffness of a five-storey moment-resisting frame structure was studied. The representative building used for the five-storey structure is similar to the example twenty-storey moment-resisting frame building presented in Chapter 4, except that it is five stories high, and has column sections that do not change throughout the height of the structure. The sizes of the columns are the same as those of the middle region of the twenty-storey structure. The cladding panels were modelled by the improved single-diagonal bracing struts, with the same axial stiffness as in the case of the example twenty-storey structures. Static wind load analyses as well as eigenvalue analyses of the structure, with and without the effects of the cladding panels, were performed and the results compared.

It was decided to study the stiffening effect of the cladding panels on a low-rise structure, rather than on a structure taller than the twenty-storey structures already explored, because a taller structure would behave similarly to the twenty-storey buildings except that the dominant flexural component of the deflected shape, due to the columns' axial deformations, would be even more dominant. A low-rise structure, on the other hand, behaves differently, since the axial deformations of the columns are negligible and the moment-resisting frame structure deforms primarily in a shear mode.

C.1 The Effect of Panels on the Static Wind Load Analysis of a Low-Rise Structure

Initially, the example five-storey structure was analysed without the cladding panels, that is without the equivalent diagonal struts. The resulting top displacement was 4.011 mm corresponding to a drift index of 1/3166. The overall deflected shape of the structure, Fig. C.1, is typical of a low-rise moment-resisting frame structure, that is, with a predominantly shear profile, and a very small flexural component in the lowest region due to the fixity of the base. The structure with cladding panels, that is including the diagonal bracing struts, was then analysed. The resulting deflection at the top of the structure was 0.824 mm giving

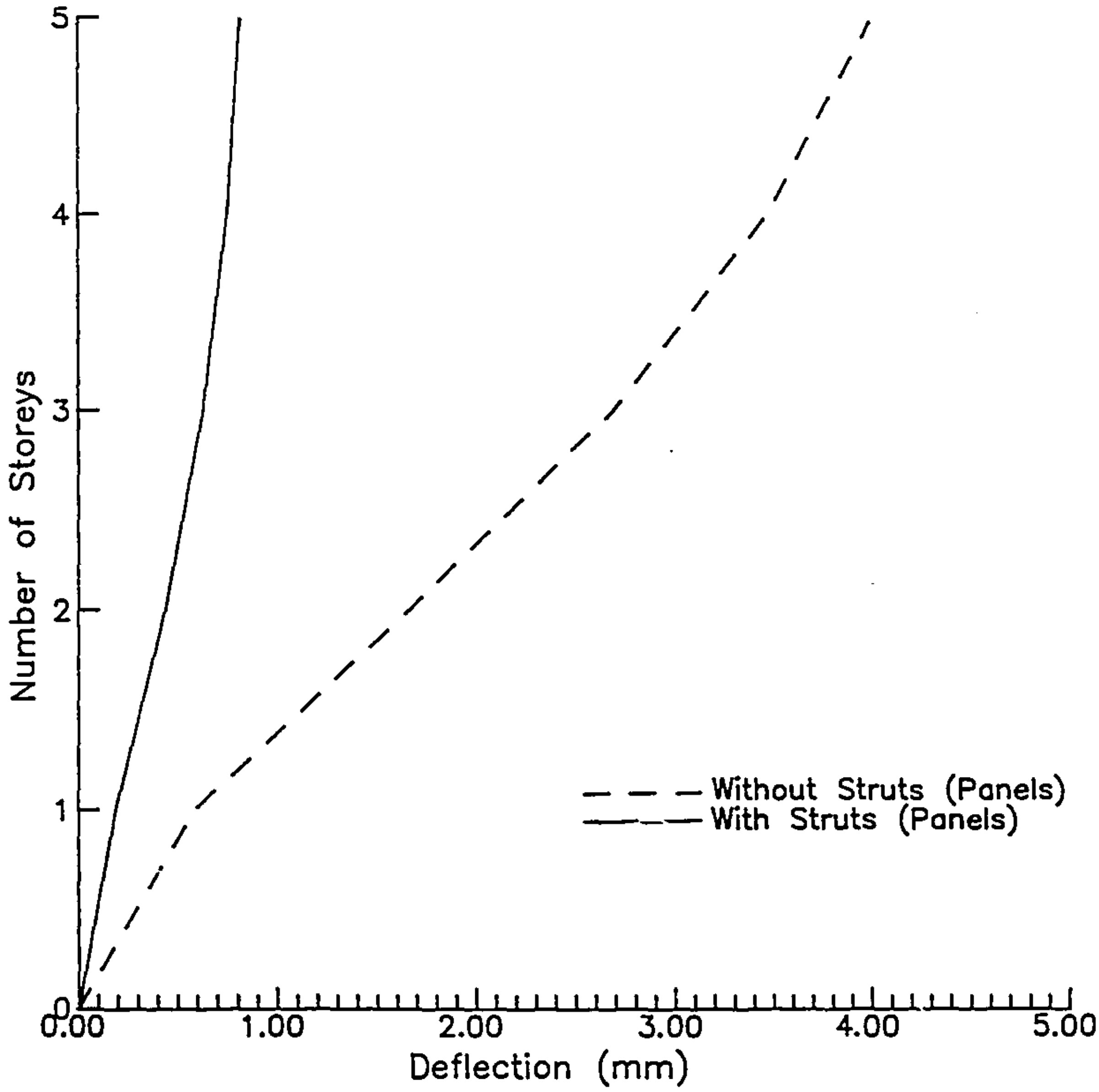

Figure C.1: Deflected Shapes of the Low-Rise Example Moment-Resisting Frame Structure a drift index of 1/15400, which was 79 percent less than that of the structure without cladding panels. The panels evidently had a very significant stiffening influence on the lateral stiffness of the five-storey moment-resisting frame structure. The effect was greater than for the twenty-storey structure of Chapter 7. This can be explained by the fact that in a taller frame there is a component of deflection due to the overall bending of the frame resulting from the axial deformations of the columns, while in a low-rise moment-resisting frame structure the overall flexural component is negligible. Therefore, even though the amount of pull-back on the racking of the frames is approximately the same for both the low-rise and high-rise frames, because of the negligible magnitude of the bending component in the deflection of the low-rise frame a proportionately greater reduction in deflection is caused by the panels.

The deflected shape of the five-storey structure with cladding panels is also shown in Fig. C.1. The shear mode of deformation is evident. To obtain a better comparison of the deflected shapes of the structures with and without the panels, the deflected shape of the five-storey structure without struts is normalized to have a top displacement equal to that of the structure with struts, Fig. C.2. It can be observed that relatively greater shear deformation is present in the structure with the bracing. This can be attributed to the fact that the stiffness of the bottom storey in the braced structure relative to the total stiffness of the braced structure was smaller than the ratio of the stiffness of the bottom storey in the unbraced structure to the total stiffness of the unbraced structure. Therefore, relative to the displacements in the other storeys, the displacement in the first storey was greater for the braced structure than for the unbraced structure. This corresponded with the greater shear configuration of the clad structure.

As for the twenty-storey structure, the frame-member moments in the lower storeys of the clad five-storey structure, except for the beam supporting the cladding panel, were approximately 50 to 70 percent less than those of the unclad five-storey structure.

From the results obtained in the previous analysis it was found that the largest diagonal force occurred in the second storey. However, its value was only 19 percent of that obtained from the analysis of the twenty-storey moment-resisting frame structure. Therefore, the resulting forces in the connections of the panel and the resulting stresses in the panel were also 19 percent of those obtained for the twenty-storey structure, which is within the capacities of all the connections, except the unfactored shear resistance in the bolt of the worst loaded tie-back connection, and the allowable stresses of the panel computed in Chapter 8.

C.2 The Effect of Panels on the Fundamental Period of Vibration

As for the case of the twenty-storey structures, the fundamental periods of vibration for the five-storey structure, with and without the effect of the cladding panels, were found from an eigenvalue analysis. The values of the mass per floor used for the five-storey structures

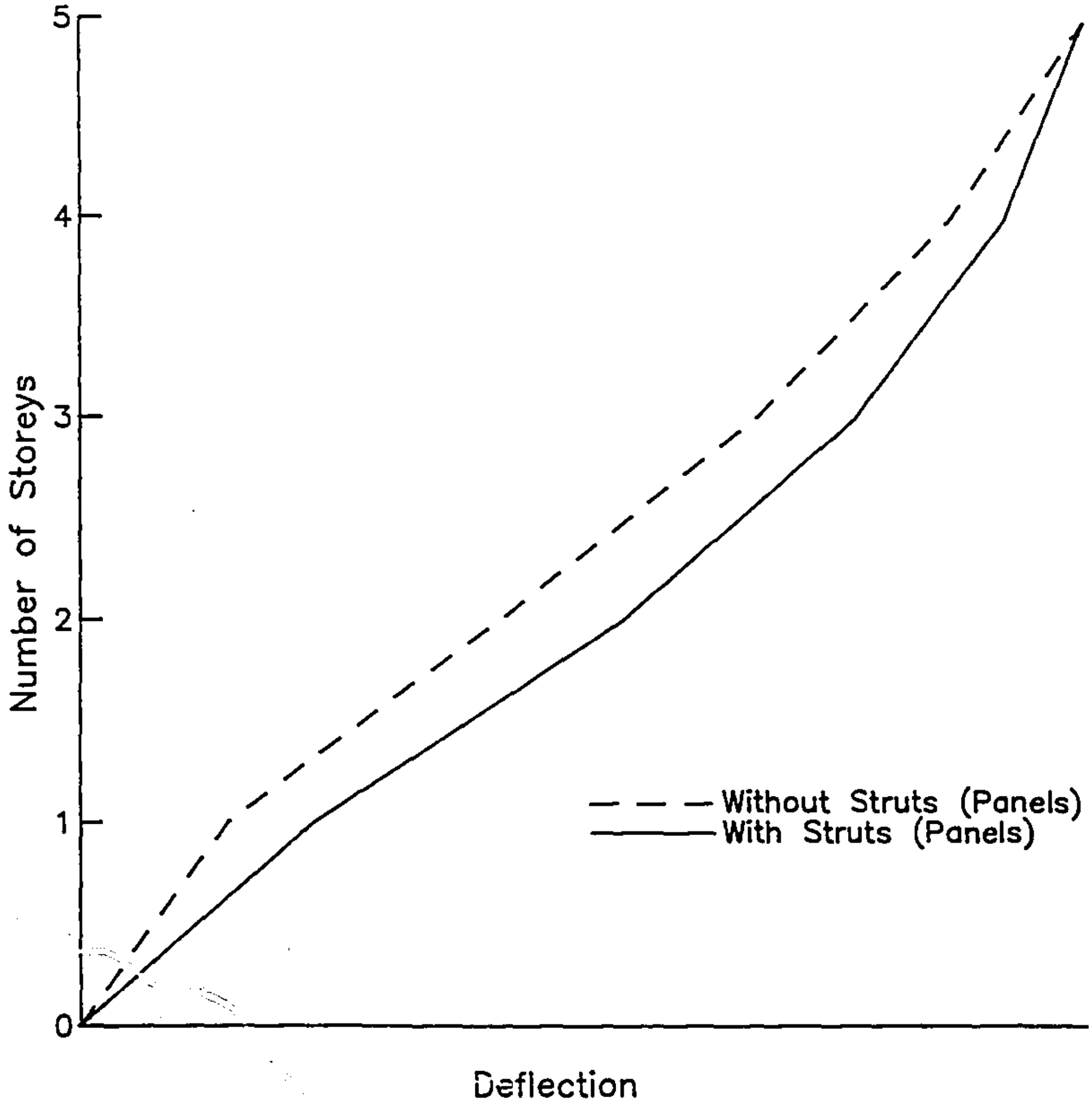

Figure C.2: Normalized Deflected Shapes of the Low-Rise Example Moment-Resisting Frame Structure were identical to those used for the twenty-storey building structures. The fundamental period of vibration obtained for the structure without the stiffening effect of the panels, but including their mass, was 0.814 sec, while that of the structure accounting for the panels was 0.375 sec. The fundamental period for the latter case was 46 percent of that for the former; hence, indicating a significant influence of the cladding on the lateral stiffness of the five-storey structure.

APPENDIX D

UPDATE PROGRAM TO ALLOW ANALYSIS OF INFILLED FRAMES

The update program was written to remove constraints at the infill-frame interfaces when tensile stresses develop on the infill boundaries and when shear forces exceed friction forces, and to reassign constraints (i.e reattach the boundary) in the case of the infill subsequently overlapping the frame and when the shear forces reduce to less than the friction forces. This version of the program applies only to the analysis of infilled-frames with gaps at the top of the infill. For the analysis, the infill must be represented by a mesh of shell elements (membrane type) and must lie in the x-y plane, whiie the frame members may be represented by any type of element. The program has been successfully checked for a number of lateral load analyses of single-storey infilled frame modules.

For the program to run successfully, the data must be prepared according to the following instructions:

1. Prepare a SAP80 input file, called INFILL, for the infilled frame as usual, except for the following:
   (a) the first line of the file must be blank
   (b) the second line of the file must be the filename, INFILL
   (c) in the constraints block first present the constraint data for the boundary nodes that will be considered for separation in the following manner:
      - supply one constraint condition per line per node,
      - node numbers must be written in 'I3' format in ascending order,
      - only one blank space must follow the constrained node number,
      - supply two constraint conditions for each boundary node, first the x-constraint, then the y-constraint,

        e.g. constraints
        1 c=26,0,0,0,0,0
        1 c=0,26,0,0,0,0
        2 c=27,0,0,0,0,0
        2 c=0,27,0,0,0,0

3 c=28,0,0,0,0,0
3 c=0,28,0,0,0,0
4 c=29,0,0,0,0,0
4 c=0,29,0,0,0,0
⋮

- if the user does not wish to constrain a boundary node in a particular direction, constraint data must still be supplied for it. For example, if node 1 is to be constrained only in the y-direction, supply data as follows for node 1:

  1 c=0,0,0,0,0,0
  1 c=0,26,0,0,0,0

(d) other constraint data may follow

2. Prepare a data file called INFILL.DAT which will contain data for the nodes to be considered for separation. The data should be prepared in the following manner:

   (a) the first line contains the number of nodes which will be considered for separation at the start of the analysis (MJ), the total number of shell elements on the boundaries (MK), and the coefficient of friction using the following format:
   Format: 2I3,F4.2

   (b) the subsequent MJ lines should each contain a boundary node number, a flag, and the frame node number to which the infill node is constrained.

   flag = 1 if nodes are along horizontal boundary,
   = 2 if nodes are along the left vertical boundary,
   = 3 if node is at the bottom left corner,
   = 4 if nodes are along the right vertical boundary, and
   = 5 if node is at the bottom right corner.

   The node numbers must be in ascending order, and the corresponding frame nodes must also be in ascending order; therefore, node numbering should be carefully chosen.
   Format: 3I3

   (c) the subsequent MK lines should each contain a boundary element number. Element numbers must also be in ascending order.
   Format: I3

The program will create an output file called INFILL.OUT in which the average stresses at the boundary nodes, and statements indicating which nodes have been unconstrained or reattached, are presented. The program will also state the number of constraints which were removed in the iteration.

Once the data file and the SAP80 input file have been prepared, the user should prepare a batch file for the iterative analysis of the infilled frame. This batch file should contain the statements to allow SAP80 to perform the analysis and calculate the stresses, and UPDATE5 to remove constraints where tensile stresses have developed or to reattach nodes. These two steps are repeated over again for the successive constraint conditions, for as many iterations as desired. After each iteration only the necessary files, under different filenames, should be retained.

The listing of the update program is provided below:

```
$LARGE
      PROGRAM UPDATES
      DOUBLE PRECISION S1T,S2T,S3T,CF,DIV,DX,DY,XX,YY
      INTEGER NMJ(120,3),IDNO(900),IDEL(900)
      DOUBLE PRECISION S11(900,2),S22(900,2),S12(900,2),SUM(3),
     $                 SIGMA(120,3),DI(120,2),DF(120,2)
      CHARACTER*80 LINE,LINE9,LINE3,LINE4
      CHARACTER*4 KEY,KEY2
      CHARACTER*6 KEY3
C
C---  INITIALIZE  ---
C
      NTM=0
      NI1=11
      NI2=12
      NOT=6
      NI3=13
      NI4=14
      NI5=15
C
      WRITE (NTM,1000)
1000  FORMAT (/,
     $' ┌──────────────────────────────────────────┐',/,
     $' │   PROGRAM TO REMOVE CONSTRAINTS ON INFILL │',/,
     $' │   BOUNDARIES WHEN TENSILE STRESSES DEVELOP│',/,
     $' │   AND WHEN SHEAR STRESSES EXCEED FRICTION │',/,
     $' │     1) Extract S11, S22 & S12 from SAP80  │',/,
     $' │        shell elements results & compute   │',/,
     $' │        average at the nodes               │',/,
     $' │     2) Extract displ. from SAP80 results  │',/,
     $' │     3) Check for tensile stresses & shear │',/,
     $' │        stresses exceeding friction & remove│',/,
     $' │        constraints from SAP80 input file  │',/,
     $' │        (check displ. for overlap & reattach)│',/,
     $' │                                           │',/,
     $' │   CURRENT CAPACITY:                       │',/,
     $' │   900 NODES, 900 ELEM., 120 BOUNDARY NODES│',/,
     $' │                                           │',/,
     $' │   BY  REGINA GAIOTTI  (MARCH 14, 1989)    │',/,
     $' │                       THANKS TO PROF. LEGER│',/,
     $' └──────────────────────────────────────────┘',/)
C
      OPEN (NI1,FILE='INFILL.DAT',STATUS='OLD',FORM='FORMATTED')
      REWIND NI1
      OPEN (NI2,FILE='INFILL.F4F',STATUS='OLD',FORM='FORMATTED')
      REWIND NI2
      OPEN (NOT,FILE='INFILL.OUT',STATUS='NEW',FORM='FORMATTED')
      OPEN (NI3,FILE='INFILL',STATUS='OLD')
      REWIND NI3
      OPEN (NI4,FILE='INFILLUP',STATUS='NEW')
      OPEN (NI5,FILE='INFILL.SOL',STATUS='OLD',FORM='FORMATTED')
      REWIND NI5
C
C---  PUT IDENTIFIER IN OUTPUT FILE ---
C
      WRITE (NOT,901)
      WRITE (NTM,901)
901   FORMAT (/,
     $' SUMMARY OF DATA FILES:',/,
```

```
     $' ————————————————————',/,
     $' SAP80 INPUT FILE NAME               ——> INFILL    ',/,
     $' DATA FOR BOUNDARY NODES FILE NAME ——> INFILL.DAT',/,
     $' SAP80 SHELL FORCES FILE NAME        ——> INFILL.F4F',/,
     $' SAP80 DISPLACEMENTS FILE NAME       ——> INFILL.SOL',/,
     $' RESULTS FROM UPDATES FILE NAME      ——> INFILL*.OUT',/)
C
C---  READ DATA FILE NAME AND INITIALIZE ---
C
C      ┌────────────────────────────────────┐
C      │  PHASE I - EXTRACT BOUNDARY STRESSES │
C      └────────────────────────────────────┘
C
      WRITE (NTM,11)
      WRITE (NOT,11)
11    FORMAT (//,' —— PHASE I - EXTRACT BOUNDARY STRESSES ——',/)
      DO 1 I=1,900
      IDNO(I)=0
      DO 2 J=1,2
      S11(I,J)=0.0
      S22(I,J)=0.0
      S12(I,J)=0.0
2     CONTINUE
1     CONTINUE
      DO 3 K=1,120
      DO 4 L=1,2
      DI(K,L)=0.0
      DF(K,L)=0.0
4     CONTINUE
3     CONTINUE
      DO 10 I=1,900
10    IDEL(I)=0
      DO 611 M=1,120
      DO 612 N=1,3
      SIGMA(M,N)=0.0
      NMJ(M,N)=0
612   CONTINUE
611   CONTINUE
      WRITE (NTM,12)
12    FORMAT (/,' READING THE INFILL.DAT FILE',//)
      READ (NI1,1010) MJ,MK,CF
1010  FORMAT (2I3,F4.2)
      DO 20 I=1,MJ
      READ (NI1,2010) NMJ(I,1),NMJ(I,2),NMJ(I,3)
2010  FORMAT (3I3)
      NN=NMJ(I,1)
      IDNO(NN)=1
20    CONTINUE
      DO 30 I=1,MK
      READ (NI1,1030) NEL
1030  FORMAT (I3)
30    IDEL(NEL)=1
C
C---  LOOP OVER ELEMENTS ---
C
      WRITE (NTM,31)
31    FORMAT (/,' READING SAP80 SHELL FORCES FILE ... PLEASE WAIT',//)
35    CONTINUE
      ID=0
C
```

```
C---  FIND ELEMENT ID ---
C
40    READ (NI2,41) LINE
41    FORMAT (A80)
      READ (LINE,42) KEY
42    FORMAT (A4)
      IF (KEY.EQ.' ELE') READ (LINE,2020) ID
2020  FORMAT (11X,I6)
C
      IF (IDEL(ID).NE.1) GO TO 40
      WRITE (NTM,1040) ID
1040  FORMAT ('+PROCESSING ELEMENT NO. :',I5)
C
C---  PULL OUT S11, S22 AND S12 AND PUT IN A TABLE ---
C
      DO 60 I=1,2
60    READ (NI2,65)
65    FORMAT (A1)
C
      DO 70 I=1,4
      READ (NI2,75) IDN,S1T,S2T,S3T
75    FORMAT (I6,3F12.0)
      IF (IDNO(IDN).EQ.0) GO TO 70
      IC=IDNO(IDN)
      S11(IDN,IC)=S1T
      S22(IDN,IC)=S2T
      S12(IDN,IC)=S3T
      IDNO(IDN)=IDNO(IDN)+1
70    CONTINUE
C
C---  CHECK FOR LAST ELEMENT TO PROCESS ---
C
      IF (ID.LT.NEL) GO TO 35
C
C---  PRINT RESULTS ---
C
      WRITE (NOT,3000)
3000  FORMAT (' NODE        S11(A)           S22(A)           S12(A)')
C
C---  LOOP OVER BOUNDARY NODES ---
C
      DO 600 I=1,MJ
      NI=NMJ(I,1)
C
C---  COMPUTE AVERAGE VALUE ---
C
      DIV=2.
      IF (DABS(S11(NI,2)).LE.1.D-05 .AND.
     $    DABS(S22(NI,2)).LE.1.D-05 .AND.
     $    DABS(S12(NI,2)).LE.1.D-05) DIV=1.
      DO 610 K=1,3
610   SUM(K)=0.0
      DO 620 K=1,2
      SUM(1)=SUM(1)+S11(NI,K)
      SUM(2)=SUM(2)+S22(NI,K)
      SUM(3)=SUM(3)+S12(NI,K)
620   CONTINUE
      DO 625 K=1,3
625   SIGMA(I,K)=SUM(K)/DIV
C
```

```
      WRITE (NOT,3010) NI,(SIGMA(I,K),K=1,3)
3010  FORMAT (I4,3X,E14.7,2X,E14.7,2X,E14.7)
C
600   CONTINUE
C
C     ┌──────────────────────────────────────────┐
C     | PHASE II - EXTRACT BOUNDARY DISPLACEMENTS |
C     └──────────────────────────────────────────┘
C
      WRITE (NTM,21)
      WRITE (NOT,21)
21    FORMAT (//,' ── PHASE II - EXTRACT BOUNDARY DISPLACEMENTS ──',/)
      WRITE (NTM,22)
22    FORMAT (/,' READING SAP80 DISPLACEMENTS FILE ... PLEASE WAIT',//)
C
      KK=1
61    READ (NI5,41) LINE3
      READ (LINE3,43) KEY3
43    FORMAT (A6)
      IF (KEY3.NE.' J O I') GO TO 61
      DO 59 L1=1,4
59    READ (NI5,65)
C
      DO 62 I=1,51
      READ (NI5,63) JJ,DX,DY
63    FORMAT (I6,2F12.0)
      IF (JJ.GT.NMJ(MJ,3)) GO TO 46
      IF (NMJ(KK,1).NE.JJ .AND. NMJ(KK,3).NE.JJ) GO TO 62
      IF (NMJ(KK,3).EQ.JJ) GO TO 64
      DI(KK,1)=DX
      DI(KK,2)=DY
      KK=KK+1
      IF (KK.GT.MJ) KK=1
      GO TO 62
64    DF(KK,1)=DX
      DF(KK,2)=DY
      KK=KK+1
62    CONTINUE
      IF (KK.LE.MJ) GO TO 61
C
46    WRITE (NOT,4000)
4000  FORMAT (' I-NODE       I-D(X)          I-D(Y)     F-NODE
     $'F-D(X)          F-D(Y)')
C
      DO 57 I1=1,MJ
      WRITE (NOT,4010) NMJ(I1,1),DI(I1,1),DI(I1,2),NMJ(I1,3),DF(I1,1),
     $                 DF(I1,2)
4010  FORMAT (I6,3X,E14.6,2X,E14.6,2X,I6,3X,E14.6,2X,E14.6)
57    CONTINUE
C
      WRITE (NTM,3030) CF
      WRITE (NOT,3030) CF
3030  FORMAT (/,' THE COEFFICIENT OF FRICTION IS ',F4.2)
C
C     ┌──────────────────────────────────────────────────────────┐
C     | PHASE III - SCAN FOR TENSILE STRESSES, CHECK SHEAR STRESSES |
C     |             AND REMOVE APPROPRIATE CONSTRAINTS FROM SAP80   |
C     |             INPUT FILE (CHECK DISPLACEMENTS IN CASE OF OVER- |
C     |             LAP AND REATTACH)                               |
C     └──────────────────────────────────────────────────────────┘
```

```
C
      WRITE (NTM,701)
      WRITE (NOT,701)
701   FORMAT (//,' --- PHASE III - SCANNING FOR TENSILE STRESSES,',/,
     $'                  CHECKING SHEAR STRESSES AND REMOVING',/,
     $'                  CONSTRAINTS FROM SAP80 INPUT FILE, ALSO',/,
     $'                  CHECKING DISPLACEMENTS AND REATTACHING',//)
C
C---  FIND CONSTRAINTS DATA BLOCK IN SAP80 INPUT FILE ---
C
502   READ (NI3,500) LINE
500   FORMAT (A80)
      WRITE (NI4,500) LINE
      READ (LINE,501) KEY
501   FORMAT (A4)
      IF (KEY.NE.'cons') GO TO 502
C
C---  LOOP OVER BOUNDARY NODES ---
C
      ICOUNT=0
C
      DO 80 I=1,MJ
      IF (NMJ(I,2).EQ.3 .OR. NMJ(I,2).EQ.5) GO TO 85
      IF (NMJ(I,2).EQ.2 .OR. NMJ(I,2).EQ.4) GO TO 86
C
C---  IF NODE IS ALONG A HORIZONTAL BOUNDARY ---
C
      YY=DF(I,2)-DI(I,2)
      IF (YY.GE.1.D-06) GO TO 230
C
      IF (SIGMA(I,2).LE.1.D-05) GO TO 79
C
C---  REMOVE VERTICAL CONSTRAINT AND HORIZONTAL CONSTRAINT ---
C
      CALL RMVHV (NI3,NI4,NOT,NMJ(I,1),ICOUNT)
C
      GO TO 80
C
C---  IF NODE IS ALONG A VERTICAL BOUNDARY ---
C
86    IF (NMJ(I,2).EQ.2) XX=DF(I,1)-DI(I,1)
      IF (NMJ(I,2).EQ.4) XX=DI(I,1)-DF(I,1)
      IF (XX.GE.1.D-06) GO TO 230
C
      IF (SIGMA(I,1).LE.1.D-05) GO TO 78
C
C---  REMOVE HORIZONTAL CONSTRAINT AND VERTICAL CONSTRAINT ---
C
      CALL RMVHV (NI3,NI4,NOT,NMJ(I,1),ICOUNT)
C
      GO TO 80
C
C---  IF NODE IS AT A CORNER ---
C
85    IF (NMJ(I,2).EQ.3) XX=DF(I,1)-DI(I,1)
      IF (NMJ(I,2).EQ.5) XX=DI(I,1)-DF(I,1)
      YY=DF(I,2)-DI(I,2)
      IF (XX.GE.1.D-06 .OR. YY.GE.1.D-06) GO TO 230
C
      IF (SIGMA(I,1).LE.1.D-05 .AND. SIGMA(I,2).LE.1.D-05) GO TO 80
```

```
      IF (SIGMA(I,1).LE.1.D-05 .OR. SIGMA(I,2).LE.1.D-05) GO TO 77
C
C---  REMOVE HORIZONTAL AND VERTICAL CONSTRAINTS ---
C
      CALL RMVHV (NI3,NI4,NOT,NMJ(I,1),ICOUNT)
C
      GO TO 80
C
79    FRICTION=CF*DABS(SIGMA(I,2))
      IF (DABS(SIGMA(I,3)).GT.FRICTION) GO TO 9001
      CALL CHECK2 (NI3,NI4,NMJ(I,1),L)
      CALL CHECK1 (NI3,NI4,NMJ(I,1),M)
      IF (L.EQ.1 .AND. M.EQ.0) GO TO 230
      GO TO 80
C
C---  REMOVE HORIZONTAL CONSTRAINT ONLY ---
C
9001  CALL RMVH (NI3,NI4,NOT,NMJ(I,1),ICOUNT)
C
      GO TO 80
C
78    FRICTION=CF*DABS(SIGMA(I,1))
      IF (DABS(SIGMA(I,3)).GT.FRICTION) GO TO 9002
      CALL CHECK2 (NI3,NI4,NMJ(I,1),M)
      CALL CHECK1 (NI3,NI4,NMJ(I,1),L)
      IF (L.EQ.1 .AND. M.EQ.0) GO TO 230
      GO TO 80
C
C---  REMOVE VERTICAL CONSTRAINT ONLY ---
C
9002  CALL RMVV (NI3,NI4,NOT,NMJ(I,1),ICOUNT)
C
      GO TO 80
C
77    IF (SIGMA(I,1).LE.1.D-05) GO TO 76
      CALL CHECK1 (NI3,NI4,NMJ(I,1),L)
      IF (L.EQ.1) GO TO 311
      FRICTION=CF*DABS(SIGMA(I,2))
      IF(DABS(SIGMA(I,3)).LE.FRICTION) GO TO 80
C
C---  REMOVE HORIZONTAL CONSTRAINT ONLY ---
C
311   CALL RMVH (NI3,NI4,NOT,NMJ(I,1),ICOUNT)
C
      GO TO 80
C
76    CALL CHECK2 (NI3,NI4,NMJ(I,1),L)
      IF (L.EQ.1) GO TO 312
      FRICTION=CF*DABS(SIGMA(I,1))
      IF (DABS(SIGMA(I,3)).LE.FRICTION) GO TO 80
C
C---  REMOVE VERTICAL CONSTRAINT ONLY ---
C
312   CALL RMVV (NI3,NI4,NOT,NMJ(I,1),ICOUNT)
C
      GO TO 80
C
C---  REATTACH NODE ---
C
230   READ (NI3,41) LINE4
```

```
      WRITE (NI4,41) LINE4
      READ (LINE4,235) NN1
235   FORMAT (I3)
      IF (NN1.NE.NMJ(I,1)) GO TO 230
      BACKSPACE NI4
      WRITE (NI4,238) NN1,NMJ(I,3)
238   FORMAT (I3,' c=',I3,',0,0,0,0,0')
      WRITE (NI4,239) NN1,NMJ(I,3)
239   FORMAT (I3,' c=0,',I3,',0,0,0,0')
      READ (NI3,65)
      WRITE (NOT,237) NN1
237   FORMAT (' NODE NO.  ',I3,' HAS BEEN REATTACHED',/)
C
      GO TO 80
C
80    CONTINUE
C
C---  PRINT NUMBER OF CONSTRAINTS REMOVED IN THIS ITERATION ---
C
      WRITE (NTM,509) ICOUNT
      WRITE (NOT,509) ICOUNT
509   FORMAT (//,' THE NUMBER OF CONSTRAINTS REMOVED IN THIS'
     $' ITERATION IS ',I3)
C
      DO 222 I=1,100
      READ (NI3,500,END=990) LINE9
      WRITE (NI4,500) LINE9
222   CONTINUE
990   CLOSE (NI4)
      END
C
C
      SUBROUTINE RMVHV (NI3,NI4,NOT,NMJ,ICOUNT)
C
C     The following subroutine will remove the horizontal and vertical
C     constraints of a boundary node.
C
      CHARACTER*80 LINE2,LINE2B
      CHARACTER*17 CONS,CHK1,CHK1B
      DATA CONS/' c=0,0,0,0,0,0   '/
C
505   READ (NI3,500) LINE2
      WRITE (NI4,500) LINE2
500   FORMAT (A80)
      READ (LINE2,650) NNN,CHK1
650   FORMAT (I3,A17)
      IF (NNN.NE.NMJ) GO TO 505
      IF (CHK1.EQ.CONS) GO TO 605
      BACKSPACE NI4
      WRITE (NI4,700) NNN,CONS
700   FORMAT (I3,A17)
C
605   READ (NI3,500) LINE2B
      WRITE (NI4,500) LINE2B
      READ (LINE2B,650) NNN2,CHK1B
      IF (NNN2.NE.NMJ) GO TO 605
      IF (CHK1B.EQ.CONS .AND. CHK1.EQ.CONS) GO TO 81
      IF (CHK1B.EQ.CONS .AND. CHK1.NE.CONS) GO TO 82
      BACKSPACE NI4
      WRITE (NI4,700) NNN2,CONS
```

```
      IF (CHK1.EQ.CONS) GO TO 83
C
      ICOUNT=ICOUNT+2
      WRITE (NOT,507) NMJ
507   FORMAT (' THE VERT. & HORIZ. CONSTRAINTS FOR NODE  ',I3,' HAVE'
     $' BEEN REMOVED',/)
      GO TO 81
C
82    ICOUNT=ICOUNT+1
      WRITE (NOT,508) NMJ
508   FORMAT (' THE HORIZ. CONSTRAINT FOR NODE  ',I3,' HAS BEEN'
     $' REMOVED',/)
      GO TO 81
C
83    ICOUNT=ICOUNT+1
      WRITE (NOT,509) NMJ
509   FORMAT (' THE VERT.  CONSTRAINT FOR NODE  ',I3,' HAS BEEN'
     $' REMOVED',/)
81    RETURN
      END
C
C
      SUBROUTINE RMVH (NI3,NI4,NOT,NMJ,ICOUNT)
C
C     The following subroutine will only remove the horizontal
C     constraint of a boundary node.
C
      CHARACTER*80 LINE2,LINE2B
      CHARACTER*17 CONS,CHK1
      DATA CONS/' c=0,0,0,0,0,0   '/

505   READ (NI3,500) LINE2
      WRITE (NI4,500) LINE2
500   FORMAT (A80)
      READ (LINE2,650) NNN,CHK1
650   FORMAT (I3,A17)
      IF (NNN.NE.NMJ) GO TO 505
      IF (CHK1.EQ.CONS) GO TO 81
      BACKSPACE NI4
      WRITE (NI4,700) NNN,CONS
700   FORMAT (I3,A17)
C
      READ (NI3,500) LINE2B
      WRITE (NI4,500) LINE2B
C
      ICOUNT=ICOUNT+1
      WRITE (NOT,507) NMJ
507   FORMAT (' THE HORIZ. CONSTRAINT FOR NODE  ',I3,' HAS BEEN'
     $' REMOVED',/)
81    RETURN
      END
C
C
      SUBROUTINE RMVV (NI3,NI4,NOT,NMJ,ICOUNT)
C
C     The following subroutine will only remove the vertical
C     constraint of a boundary node.
C
      CHARACTER*80 LINE2,LINE2B
      CHARACTER*17 CONS,CHK1
```

```
      DATA CONS/' c=0,0,0,0,0,0   '/
C
505   READ (NI3,500) LINE2
      WRITE (NI4,500) LINE2
500   FORMAT (A80)
      READ (LINE2,650) NNN
650   FORMAT (I3,A17)
      IF (NNN.NE.NMJ) GO TO 505
      READ (NI3,500) LINE2B
      WRITE (NI4,500) LINE2B
      READ (LINE2B,650) NNN2,CHK1
      IF (CHK1.EQ.CONS) GO TO 81
      BACKSPACE NI4
      WRITE (NI4,700) NNN2,CONS
700   FORMAT (I3,A17)
C
      ICOUNT=ICOUNT+1
      WRITE (NOT,507) NMJ
507   FORMAT (' THE VERT.  CONSTRAINT FOR NODE  ',I3,' HAS BEEN'
     $' REMOVED',/)
81    RETURN
      END
C
C
      SUBROUTINE CHECK1 (NI3,NI4,NMJ,L)
C
C     The following subroutine will check if the vertical constraint
C     has been removed.
C
      CHARACTER*80 LINE2,LINE2B
      CHARACTER*17 CONS,CHK1
      DATA CONS/' c=0,0,0,0,0,0   '/
C
      L=0
505   READ (NI3,500) LINE2
      WRITE (NI4,500) LINE2
500   FORMAT (A80)
      READ (LINE2,650) NNN
650   FORMAT (I3,A17)
      IF (NNN.NE.NMJ) GO TO 505
      READ (NI3,500) LINE2B
      WRITE (NI4,500) LINE2B
      READ (LINE2B,650) NNN2,CHK1
      IF (CHK1.EQ.CONS) L=1
      BACKSPACE NI3
      BACKSPACE NI3
      BACKSPACE NI4
      BACKSPACE NI4
      RETURN
      END
C
C
      SUBROUTINE CHECK2 (NI3,NI4,NMJ,L)
C
C     The following subroutine will check if the horizontal constraint
C     has been removed.
C
      CHARACTER*80 LINE2
      CHARACTER*17 CONS,CHK1
      DATA CONS/' c=0,0,0,0,0,0   '/
```

```
C
      L=0
505   READ (NI3,500) LINE2
      WRITE (NI4,500) LINE2
500   FORMAT (A80)
      READ (LINE2,650) NNN,CHK1
650   FORMAT (I3,A17)
      IF (NNN.NE.NMJ) GO TO 505
      IF (CHK1.EQ.CONS) L=1
      BACKSPACE NI3
      BACKSPACE NI4
      RETURN
      END
```